Development of stabilized NTS_1R and CXCR4 PET ligands using N^{ω}-carbamoylated arginines for label attachment

Dissertation

zur Erlangung des Doktorgrades der Naturwissenschaften

(Dr. rer. nat.)

an der Fakultät für Chemie und Pharmazie

der Universität Regensburg

vorgelegt von

Lisa Schindler

aus Passau

im Jahr 2022

Die vorliegende Arbeit entstand im Zeitraum von Februar 2017 bis Dezember 2022 unter der Anleitung von Prof. Dr. Günther Bernhardt und PD Dr. Max Keller an der Fakultät für Chemie und Pharmazie der Universität Regensburg.

Das Promotionsgesuch wurde eingereicht im November 2022.

Tag der mündlichen Prüfung:	23.12.2022
Vorsitzender des Prüfungsausschusses:	Prof. Dr. Rainer Müller
Erstgutachter:	PD Dr. Max Keller
Zweitgutachter:	Prof. Dr. Olaf Prante
Drittprüfer:	Prof. Dr. Pierre Koch

für Susi

Danke, dass Du alles auf den Kopf und wieder zurück gestellt hast.

Acknowledgements

An dieser Stelle möchte ich mich herzlich bedanken bei allen, die diese Arbeit ermöglicht und zu ihrem Gelingen beigetragen haben.

Allen voran danke ich Herrn PD Dr. Max Keller ausdrücklich für die viele, viele Zeit, die er sich immer für meine Forschung genommen hat, sowohl im Rahmen von fachlichen Gesprächen als auch bei den PET-Versuchen am Klinikum. Ohne Deine Unterstützung und den tatkräftigen Einsatz wäre die Umsetzung des Projektes nicht möglich gewesen. Danke, dass Du immer mit Geduld, Aufmerksamkeit und „Herzblut" ans Werk gehst und ich eine strukturierte und zielorientierte Arbeitsweise von Dir lernen durfte.

Ein großer Dank geht ebenso an Herrn Prof. Dr. Olaf Prante, der meine Arbeit sowohl durch die Kooperation bei den ^{18}F-markierten PET-Liganden als auch durch die Übernahme des Zweitgutachtens unterstützt hat. Vielen Dank für die unkomplizierte und gute Zusammenarbeit!

Ich danke Herrn Prof. Dr. Pierre Koch dafür, dass er meine Arbeit immer nach Kräften unterstützt hat. Ein großes Dankeschön auch, Pierre, für die Übernahme der Rolle des Drittprüfers und die vielen Süßigkeiten in der Küche.

Herrn Prof. Dr. Rainer Müller danke ich für seine freundliche Bereitschaft, den Vorsitz des Prüfungskomitees zu übernehmen.

Bezüglich der Entwicklung von ^{68}Ga-markierten PET-Liganden und der Kooperation bei den Tierversuchen bedanke ich mich für die Unterstützung durch Herrn Prof. Dr. Dirk Hellwig. Danke für Ihr stetes Interesse am Projekt und die motivierte Zusammenarbeit!

Herr Prof. Dr. Günther Bernhardt hat insbesondere zu Beginn meiner Arbeit durch seine fachlichen Anregungen und sein kritisches Hinterfragen die Projekte mitgestaltet, wofür ich mich herzlich bedanke.

Ein großes, großes Dankeschön geht an Frau Dr. Jutta Moosbauer, für ihre unermüdliche Motivation und das Bewahren eines kühlen Kopfes bei oftmals hetzigen Versuchsabläufen. Ich danke Dir, liebe Jutta, für Deinen Einsatz bei der Durchführung der Radiosynthesen und den zahlreichen Besprechungen, sowie für die manchmal komplexe Koordination der Versuchstermine. Du bist a Scharnierl!

Bei den weiteren Co-Autoren der Publikationen zu ^{18}F- und ^{68}Ga-markierten PET-Liganden, Frau PD Dr. Simone Maschauer, Herrn Dr. Daniel Schmidt, Herrn Dr. Thilo Spruss, Herrn PD Dr. Steffen Lüdeke, Herrn Dr. Frank Hofheinz, Herrn Sebastian Meister, Herrn Dr. Bernd Echtenacher und Herrn Prof. Dr. Jens Pietzsch, bedanke ich mich für die konstruktive Zusammenarbeit.

Ich danke außerdem der Deutschen Forschungsgemeinschaft für die finanzielle Unterstützung meines Promotionsprojektes und der Konferenzbeiträge (KE 1857/1-2 und KE 1857/1-3).

Für die Hilfe bei der Zellkultur und der Durchführung der Assays danke ich Frau Brigitte Wenzl, Frau Susanne Bollwein, Frau Lydia Schneider, und besonders Frau Maria Beer-Krön, die auch an den schwierigen Tagen immer ein freundliches Wort und ein offenes Ohr für mich hatte. Danke auch für die gelegentlichen Chauffeur-Dienste zum

frühmorgendlichen Beginn! Herrn Peter Richthammer (meinem Herzibobberl) und seinen goldenen Händen danke ich für die häufige technische Unterstützung und vor allem dafür, dass er mich so oft mit seinen Sprüchen zum Lachen gebracht hat. Herrn Franz Wiesenmayer danke ich für seine viele Hilfe im Tierstall und bei einigen unserer Versuche. An dieser Stelle geht mein Dank auch an alle MTAs am Uniklinikum, die unsere Experimente durch das Bedienen des PET-Scanners unterstützt haben.

Herrn Josef Kiermaier und Herrn Fritz Kastner möchte ich für ihre Hilfe bei den HRMS- und NMR-Messungen danken.

Meinen Wahlpflichtpraktikantinnen Frau Maria Pfaffinger, Frau Christina Gromes, Frau Denise Rautenstrauch, Frau Sandra Krogner und Frau Elena Schmid danke ich für ihren jeweiligen Beitrag zu meinen Forschungsprojekten.

Von allen Doktoranden möchte ich mich am meisten und ausdrücklich bei Herrn Christoph Müller bedanken. Die Gespräche mit Dir waren eine Bereicherung für mich. Danke Christoph, für Deine absolute Authentizität, Dein Verständnis, und dass Du die Dinge siehst, die sonst keiner sieht.

Frau Ulla Seibel-Ehlert danke ich für ihre verständnisvolle und vertrauenswürdige Art – Du hattest immer ein offenes Ohr, und ich habe viel von Dir gelernt. Danke Ulla, dass Du Dir insbesondere in den schweren Phasen Zeit für mich genommen hast.

Frau Denise Mönnich, meiner Koch-Kumpanin: mit Deiner quirligen Art und positiven Ausstrahlung hast Du mich so oft wieder zum Lächeln gebracht, wenn es schwierig war. Danke für die Spätzle-Abende; das gemeinsame Kichern mit Dir werde ich vermissen.

Frau Dr. Lisa Forster, Frau Dr. Carina Höring und Frau Franziska Schettler, meine drei wunderbaren Mitbetreuerinnen im Biochemie-Praktikum: ich danke Euch für die unkomplizierte und reibungslose Organisation, und dafür, dass Ihr sogar diesen Nachmittagen einen spaßigen Charakter verliehen habt.

Frau Dr. Frauke Antoni, Frau Dr. Corinna Weinhart und Herrn Fabian Ertl, mit denen ich die Freude hatte, das Labor zu teilen, danke ich für unzählige hilfreiche fachliche sowie persönliche Gespräche und das viele Lachen, das mir immer gut getan hat.

Allen aktuellen und ehemaligen Kollegen vom Lehrstuhl Koch (ehem. Buschauer) danke ich dafür, dass sie dazu beigetragen haben, dass meine Zeit an der Uni bereichernd und lebendig war.

Der bunten Truppe aus der KHG rund um Herrn Hermann-Josef Eckl und Frau Rena Kagerer bin ich tief verbunden; Ihr habt mich all die Zeit über herzlich und *freund*lich begleitet, mich zum Nachdenken angeregt und mir an so manchem schweren Tag geholfen, wieder freier zu atmen. Ich danke Euch! Der Abschied von der Blauen Stunde wird mir mit am schwersten fallen.

Ich danke all den Verrückten aus dem Sportzentrum, die die Zeit beim Bogenschießen, Vertikaltuch und Klettern zum Teil zu den witzigsten Stunden am Tag gemacht haben. Dieser Dank geht natürlich auch an meine Mitstreiter bei den Hindernisläufen. Aroo! Sensei Manfred Gell vom Karate in Passau danke ich für alles, was er mir mit auf den Weg gegeben hat, und dass wir immer noch verbunden sind.

Insbesondere seien an dieser Stelle meine wunderbaren Wegbegleiterinnen Frau Katrin Abstreiter, Frau Uschi Schmidl und Frau Sophia Weigert genannt, die mich durch ihren Beistand und das gemeinsame Reflektieren so weit *voran* gebracht haben. Danke, dass Ihr mir mit Eurer aufrichtigen, zugewandten und empathischen Art helft, nicht stehen zu bleiben, und mir neue Sichtweisen aufzeigt. Ihr seid mir ein wertvoller Schatz, für den ich sehr dankbar bin.

[illegible]

Jag tackar mitt kära får uttryckligt för hans stora, stora hjärta full av empati. Du är alltid så omhändertagande och lyssnar väldigt omtänksamt, och du fanns där för mig när som helst. Ditt stöd och din oförtröttlig uppmuntran på krångliga dagar har hjälpt mig varje gång, även om jag inte har kunnit visa det alltid. Tack även för de otaliga roliga matlagningskvällarna, och för att du har „motiverat" mig att springa igen och igen.

Ein großer und aufrichtiger Dank gilt Frau Dr. Stefanie Wolkerstorfer. Dich an meiner Seite zu haben ist ein Geschenk – insbesondere in diesen spannenden Jahren. Ich bin sehr dankbar für unser Vertrauen und unseren Zusammenhalt: Du warst und bist mir eine verlässliche Stütze in jeder denkbaren Situation, und auch viele Kilometer zwischen uns ändern daran nichts. Danke Steffi, eine Freundin wie Dich kann man sich nur wünschen.

Meinem lieben (jungen!) Fräulein Christa Heigl danke ich von Herzen für ihre Begleitung mein Leben lang. Danke Christa, dass Du so liebevoll und fürsorglich bist, und dass ich die Verbundenheit mit Dir immer spüren durfte.

Meinen größten Dank jedoch schulde ich meiner Familie; meinen Geschwistern Flo, Andi und Lena, sowie meinen Eltern Franz und Evelin. Ihr habt mich all die Zeit über mit Liebe und Rückhalt unterstützt, ermutigt und an mich geglaubt. Danke, dass wir immer zusammenhalten, wenn es darauf ankommt, und ich mich so oft von Eurer Hilfe und Eurem Beistand aufgefangen fühlen durfte. Ich bin so dankbar, dass ich Euch hab, und dass Ihr alle meine Wege, insbesondere in den schweren Zeiten, begleitet habt und weiter begleitet. Ohne Euch hätte ich so Vieles nicht gewagt.

Publications, presentations and professional training

Publications (peer-reviewed articles)

(published prior to the submission of this thesis)

Grätz, L.; Müller, C.; Pegoli, A.; Schindler, L.; Bernhardt, G.; Littmann, T. Insertion of Nanoluc into the extracellular loops as a complementary method to establish BRET-based binding assays for GPCRs. *ACS Pharmacol Transl Sci* **2022**, *5*, 1142-1155, doi: 10.1021/acsptsci.2c00162.

Schindler, L.; Moosbauer, J.; Schmidt, D.; Spruss, T.; Grätz, L.; Lüdeke, S.; Hofheinz, F.; Meister, S.; Echtenacher, B.; Bernhardt, G.; et al. Development of a neurotensin-derived ^{68}Ga-labeled PET ligand with high in vivo stability for imaging of NTS_1 receptor-expressing tumors. *Cancers (Basel)* **2022**, *14*, 4922, doi:10.3390/cancers14194922.

Schindler, L.; Wohlfahrt, K.; Gluhacevic von Krüchten, L.; Prante, O.; Keller, M.; Maschauer, S. Neurotensin analogs by fluoroglycosylation at N^{ω}-carbamoylated arginines for PET imaging of NTS1-positive tumors. *Sci Rep* **2022**, *12*, 15028, doi:10.1038/s41598-022-19296-0.

Spinnler, K.; von Krüchten, L.; Konieczny, A.; Schindler, L.; Bernhardt, G.; Keller, M. An alkyne-functionalized arginine for solid-phase synthesis enabling "bioorthogonal" peptide conjugation. *ACS Med Chem Lett* **2020**, *11*, 334-339, doi:10.1021/acsmedchemlett.9b00388.

Keller, M.; Mahuroof, S.A.; Hong Yee, V.; Carpenter, J.; Schindler, L.; Littmann, T.; Pegoli, A.; Hübner, H.; Bernhardt, G.; Gmeiner, P.; et al. Fluorescence labeling of neurotensin(8-13) via arginine residues gives molecular tools with high receptor affinity. *ACS Med Chem Lett* **2020**, *11*, 16-22, doi:10.1021/acsmedchemlett.9b00462.

Schindler, L.; Bernhardt, G.; Keller, M. Modifications at Arg and Ile give neurotensin(8-13) derivatives with high stability and retained NTS_1 receptor affinity. *ACS Med Chem Lett* **2019**, *10*, 960-965, doi:10.1021/acsmedchemlett.9b00122.

Keller, M.; Weiss, S.; Hutzler, C.; Kuhn, K.K.; Mollereau, C.; Dukorn, S.; Schindler, L.; Bernhardt, G.; König, B.; Buschauer, A. N^{ω}-Carbamoylation of the argininamide moiety: an avenue to insurmountable NPY Y_1 receptor antagonists and a radiolabeled selective high-affinity molecular tool ([^{3}H]UR-MK299) with extended residence time. *J Med Chem* **2015**, *58*, 8834-8849, doi:10.1021/acs.jmedchem.5b00925.

Keller, M.; Schindler, L.; Bernhardt, G.; Buschauer, A. Toward labeled argininamide-type NPY Y_1 receptor antagonists: identification of a favorable propionylation site in BIBO3304. *Arch Pharm (Weinheim)* **2015**, *348*, 390-398, doi:10.1002/ardp.201400427.

Oral presentation

Metabolically stabilized neurotensin(8-13) derivatives: ^{68}Ga-labeling via carbamoylated arginines gives NTS_1R PET ligands with high receptor affinity. *9th Austrian Peptide Symposium* (2019, Vienna, Austria).

Poster presentations

(only contributions as presenting author are listed)

Schindler, L.; Moosbauer, J.; Schmidt, D.; Spruss, T.; Grätz, L.; Hofheinz, F.; Meister, S.; Bernhardt, G.; Pietzsch, J.; Hellwig, D.; Keller, M. Development of a peptidic ^{68}Ga-labeled PET ligand with high in vivo stability for NTS_1R-mediated tumor imaging. *Annual Meeting of the German Pharmaceutical Society - DPhG* (2022, Marburg, Germany).

Schindler, L.; Moosbauer, J.; Bernhardt, G.; Hellwig, D.; Keller, M. Metabolically stabilized neurotensin(8-13) derivatives: ^{68}Ga-labeling via carbamoylated arginines gives NTS_1R PET ligands with high receptor affinity. *58th annual meeting of the German Society for Nuclear Medicine* (2020, online).

Schindler, L.; Bernhardt, G.; Keller, M. Metabolically stabilized neurotensin(8-13) derivatives: ^{68}Ga-labeling via carbamoylated arginines gives NTS_1R PET ligands with high receptor affinity. *9th Austrian Peptide Symposium* (2019, Vienna, Austria).

Schindler, L.; Bernhardt, G.; Keller, M. Structural modifications of NT(8-13) to increase metabolic stability: N-methylation, N-terminal acylation and Ile/Tle exchange. *8th Austrian Peptide Symposium* (2018, Salzburg, Austria).

Professional training

Fortbildung für Projektleiter und Beauftragte für Biologische Sicherheit (§§ 15 und 17 Gentechniksicherheitsverordnung) (March 2018, Regensburg).

Seminar: Radioanalytische Arbeitsmethoden für Naturwissenschaftler und Pharmazeuten (February 2018, Regensburg).

Contents

Chapter 1

General introduction

1.1 Neurotensin and the neurotensin receptor family

1.1.1 Neurotensin and NT(8-13)

Neurotensin (NT) is an endogenous linear peptide of 13 amino acids (*cf.* Figure 1.1) which was first isolated from bovine hypothalami in 1973[1] followed by the identification of the amino acid sequence in 1975[2]. Intestinal bovine NT was isolated[3] and sequenced[4] shortly after, and in the following time sequence analogy of the bovine, canine, murine and human ortholog was reported[5,6]. Processing of its biological precursor proneurotensin (also referred to as proneuromedin N) by endopeptidases leads to the release of tissue-specific levels of NT and other bioactive cleavage products[7-9]. NT is found in the central nervous system[10-13] as well as in the periphery, mainly in the gastrointestinal tract[8,14-17]. Centrally, NT acts as a neurotransmitter and neuromodulator, being involved in, e.g., modulation of pain and hormone secretion, regulation of feeding, body temperature and blood pressure as well as in memory and cognition[6,9,12,18-23]. The peripheral effects of NT include, among other things, a paracrine and endocrine hormonal modulation of the gastrointestinal and the cardiovascular system and proinflammatory responses[8,12,16,24-26]. Moreover, NT was reported to stimulate the proliferation of healthy and tumor cells by triggering and amplifying the effects of different endogenous growth factors[6,8,9,17,18,25,27-33].

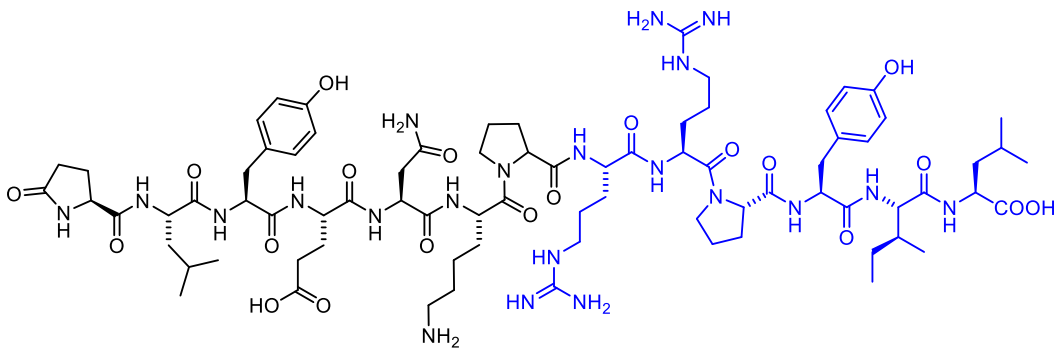

Figure 1.1. Structure of the neurotransmitter and neuromodulator neurotensin (NT), and amino acid sequences of NT and (in blue) of its equi-potent carboxy-terminal fragment NT(8-13).

Structure-activity relationship studies revealed that the carboxy-terminal hexapeptide in NT, also referred to as NT(8-13) (*cf.* Figure 1.1) represents the biologically active fragment of the peptide and displays the potency of full-length NT[2,8,12,25,34]. Therefore, NT(8-13) has been used extensively as a lead structure for the development of imaging and therapeutic agents derived from NT[35-41].

1.1.2 The neurotensin NTS_1, NTS_2 and NTS_3 receptor

The biological targets of NT are neurotensin receptors, of which three subtypes have been isolated, i.e., the NTS_1R, NTS_2R and NTS_3R[42-48]. Both the NTS_1R and the NTS_2R are located at the cell surface and were identified as members of the superfamily of G-protein coupled receptors (GPCRs) containing seven trans-membrane (TM) domains[43-46,48], whereas the NTS_3R revealed a 100% homology with the 1 TM domain glycoprotein gp95/sortilin[49,50] mainly located in intracellular compartments[8,50,51]. The NTS_1R is often

referred to as the high-affinity binding site for NT, characterized by subnanomolar binding constants[43,44,52], while NT displays lower (nanomolar) affinity towards the NTS_2R[45,46,48]. Interestingly, in contrast to the NTS_1R, the NTS_2R recognizes the structurally unrelated histamine receptor antagonist levocabastine, which initially enabled the differentiation between the two receptor subtypes[9,25,43,45,46,48,52-54]. Expression of the NTS_1R was reported for the brain and gastrointestinal tissues[43,44,55], whereas the NTS_2R subtype is almost exclusively located in the brain[8,45,46,48,56]. Evidence for NTS_3R expression was described for, e.g., the brain, spinal cord, thyroid, skeletal muscle and testis[8,42,47,49,57].

Upon receptor activation by binding of, e.g., NT, the NTS_1R was shown to initiate G-protein-dependent signaling via different Gα subunits[58]. For instance, NT-mediated activation of $G\alpha_q$ leads to an increase in phospholipase C (PLC) activity, resulting in the generation of inositol triphosphate (IP_3) and diacylglycerol (DAG). This is followed by an increase in intracellular Ca^{2+}-concentrations and the activation of protein kinase C (PKC), which eventually triggers cell proliferation, survival, migration and invasion[9,32,33]. NTS_1R activation was also reported to enhance the intracellular production of cyclic adenosine monophosphate (cAMP)[9,58]. The signaling pathway of the NTS_2R however is still only poorly understood. Depending on the receptor-expressing cell system used for evaluation (e.g., CHO, COS-7 or HEK293 cells) and the species the NTS_2R was isolated from, NT, NT derivatives and levocabastine were found to act as agonists, antagonists or inverse agonists[9,33,59,60].

1.1.3 NT receptor expression in cancer tissues

Lately, NT receptors have increasingly gained interest due to reports on the expression of these receptors in various types of cancer and their involvement in tumor growth. Elevated levels of the NTS_2R were found in patients suffering from chronic B cell leukemia[61] and prostate cancer[62], and NTS_2R-mediated activation of signaling cascades by NT was described for glioma cells[63]. With respect to the NTS_3R, overexpression was reported in human cancer cell lines like, among others, breast cancer, thyroid cancer or glioma[33,57,64], and interaction of the NTS_3R with the other two receptor subtypes was observed in pancreas, colon and prostate cancer cells[57,64]. However, the involvement of the NT-NTS_1R axis in cancer has been studied most intensively. Increased expression of the NTS_1R, compared to the corresponding healthy tissues, was reported for a variety of clinically relevant tumors such as breast cancer, small cell lung cancer, colorectal and inflammatory bowel disease-related carcinoma, Ewing's sarcoma and the prognostically poor pancreatic adenocarcinoma[31,44,65-68]. The above-mentioned stimulation of tumor cell proliferation by NT is accomplished by the secretion of NT from the neoplastic cells combined with their expression of NT receptors. Thereby, the cells can autocrinely trigger their own growth and, paracrinely, the growth of adjacent tumor cells[25,29,32,33,64]. Hence, the development of visually detectable (e.g., radiolabeled) ligands for NT receptors, especially for the NTS_1R, is considered a promising approach aiming at potential radiopharmaceuticals for the diagnosis and/or treatment of NT receptor-positive tumors[69,70].

1.2 The CXC-motif chemokine receptor CXCR4

1.2.1 Chemokines and chemokine receptors

Chemokines are members of the cytokine peptide family, comprising chemotactic function and thus activating and directing leukocytes[71,72] along chemotactic gradients. A common structural feature of these intercrines are four conserved cysteines which form two disulfide bonds[73] and constitute the basis for the family member classification. Depending on the number of amino acids separating the first two N-terminal cysteines, the chemokines are divided into four subgroups: CXC, CC, CX3C and C (the latter one containing only the second and the fourth cysteine residue)[74,75]. In the late 80s and early 90s, an 89 amino acid peptide was initially identified by molecular cloning from a murine bone marrow stromal cell line, therefore named stromal cell derived factor (SDF-1α, see Figure 1.2)[76-78], and it was classified as a member of the CXC intercrine family[79]. The homeostatic chemokine SDF-1α (also referred to as CXCL12) is the endogenous ligand[74,80-82] of the class A-type GPCR CXCR4, and the SDF-1α-CXCR4 axis was reported to be involved, amongst other things, in homing or retention of stem cells and organogenesis during embryonal development[75,83-86], B-lymphopoiesis[87-89], vascularization[74,90,91] and mobilization and trafficking of stem and progenitor cells[86,92].

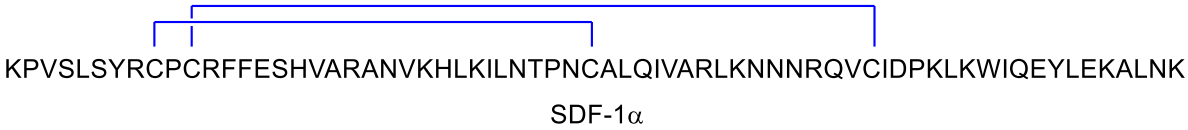

Figure 1.2. Amino acid sequence of the endogenous CXCR4 ligand SDF-1α (CXCL12). The blue lines indicate the disulfide bridges.

On the cellular level, the CXCR4 couples predominantly to G_i-proteins transducing the stimulus of extracellular SDF-1α receptor binding to intracellular signaling cascades. This results in the activation of effector proteins, in the inhibition of adenylyl cyclase activity, but also in increased cytosolic Ca^{2+}-levels[75,86,91,93-96]. In humans, SDF-1α is secreted in several organs or tissues, such as bone marrow, lymph nodes, lungs and liver[82,86,91], whereas the chemokine receptor CXCR4 is ubiquitously present on the surface of embryonic and adult tissue cells including leukocytes[96,97], progenitor or stem cells[86,98-100] and in bone marrow[82,98].

1.2.2 The SDF-1α-CXCR4 axis in human malignancies

Notably, overexpression of the CXCR4 was reported for a variety of tumors, among them breast cancer[91,101], prostate cancer[102,103] and leukemia[91,104,105]. Data indicate that chemokine receptor expression in certain tumors further contributes to site-specific metastasis, as some tissue-specific chemokines act as attractants for tumor cells expressing their respective receptor counterpart[96,104,106,107]. This was initially suggested after investigations on CXCR4-positive breast cancer cells that underwent chemotactic migration towards tissues expressing the chemokine SDF-1α, e.g., lymph nodes and bone marrow, which also correspond to the most common metastasis sites for breast cancer[101]. Moreover, some chemokines, including SDF-1α, are able to procure tumor cell survival grown under adverse conditions[82,108,109].

Besides its involvement in cancer progression, the CXCR4 was found to act as a cofactor for the fusion of the human immunodeficiency virus (HIV) with human T-cells and its

subsequent entry into the cells[110]. Additional studies reported that SDF-1α serves as an efficient inhibitor of HIV infection of cells expressing both the CXCR4 and CD4 (cluster of differentiation 4), the primary receptor for HIV-1, by T-cell-tropic HIV-1 strains[80,81].

Currently, the CXCR4 is more intensively under investigation with respect to the potential treatment of the coronavirus disease 2019 (COVID-19)[111,112]. Reports on amplified CXCR4-positive T-cell proportions in the lungs of patients suffering from a severe COVID-19 infection compared to patients with mild disease progression or unexposed individuals[111,113] suggest a role of the CXCR4 in the homing of T-cells to inflamed tissues like the lungs, which finally results in a poor outcome of the disease[111,114,115].

Considering the involvement of the CXCL12-CXCR4 axis in the above-mentioned malignancies, the exploration of CXCR4 antagonists is of particular interest with regard to clinical imaging and treatment of these diseases.

1.3 Peptidic receptor ligands – challenges and benefits

1.3.1 Comparative overview of peptidic and non-peptidic ligands used as radiopharmaceuticals

In general, addressing a peptide receptor via ligand-receptor-interaction can be pursued by two main strategies, i.e., application of a peptidic or a non-peptidic ligand. Depending on the intended purpose, the development of either type of ligand may implicate both advantages and disadvantages.

Non-peptidic ligands often act as antagonists at their target receptor; thus, they do not elicit a cellular response. Receptor subtype selective antagonists represent useful tools with regard to elucidating the physiologic or pathologic role of the receptor under investigation[6,9,12,25,116]. Besides, for some peptide receptors a higher number of binding sites within a receptor population, i.e., recognition of more conformational receptor states, was reported for antagonistic ligands compared to peptide ligand binding[6,117-120], which can result in higher accumulation of, e.g., radiolabeled antagonistic imaging tracers in target tissues and organs expressing the corresponding receptor, and consequently higher tissue-to-background ratios[121]. Furthermore, non-peptidic compounds display different pharmacokinetic properties in comparison to peptides, resulting in altered biodistribution profiles with often lower tracer uptake in dose-limiting organs like the kidneys[122-125]. Imaging of receptors expressed in the brain is often unfeasible with peptidic ligands as they barely pass the blood-brain-barrier in sufficient amounts[126,127], but it has successfully been performed using non-peptidic tracers[128,129]. However, the most crucial advantage of non-peptidic over peptidic pharmaceuticals is their - in the majority of cases - higher in vitro and in vivo stability[9,121,123,130], potentially enabling longer circulation times and higher specific binding at the target tissue.

Peptidic ligands, mainly acting as agonists, hold the advantage of stimulating cellular internalization after binding to a surface receptor[17,121,131,132]. This can result in higher accumulation and prolonged retention of the compound in the target tissue, and, in the case of radiolabeled compounds, lead to high tissue-to-background ratios for receptor imaging[121,123]. As synthetic peptidic ligands are often derived from the corresponding endogenous peptides, these compounds often display high target binding affinity (which can be beneficial for the tracer accumulation in target tissues in the case of peptidic radiopharmaceuticals[123,133]) and provoke only minor adverse reactions in vivo[123,134,135]. Peptides are synthetically easily accessible by solid-phase peptide synthesis offering a broad range of possible modifications, e.g., replacement of natural by non-natural amino acids, attachment of labels and chelating agents or conjugation to biomodifying moieties in order to alter the peptide's stability and pharmacokinetic properties[121,123,133]. In vivo, radiolabeled peptidic tracers often show a rapid clearance from blood and non-target compartments[123,133] and, compared to some antagonistic tracers, faster elimination kinetics, which is favorable with respect to an application of radioligands labeled with short-lived radionuclides[123,136].

1.3.2 Clinically investigated or established antagonists at the NTS_1R and the CXCR4

Considering the characteristics of both agonistic and antagonistic peptide receptor ligands, certain compromises may have to be tolerated during the development of a new radiopharmaceutical. However, high target affinity combined with sufficient compound stability is a key for the preparation of promising candidates for, e.g., in vivo receptor imaging. The vast majority of ligands developed for targeting NT receptors are peptides derived from NT(8-13)[35-41,70], but the discovery of the non-peptidic high-affinity NTS_1R antagonist SR48692[137] (see Figure 1.3) paved the way for a more intense exploration of antagonistic radiolabeled NT receptor ligands[124,130,138-141]. To date, the NTS_1R antagonist [^{177}Lu]Lu-3BP-227 (now IPN01087, for structure see Figure 1.3) is under investigation in stage I/II-clinical trials with regard to endoradiotherapy of patients diagnosed with NTS_1R-positive tumors[142]. Despite of its peptidic nature, the cyclic compound FC131 (see Figure 1.3) was the first described high-affinity antagonist for the CXCR4[143] and subsequent structural modifications led to the development of the cyclic antagonist [^{68}Ga]Ga-Pentixafor (see Figure 1.3)[144-146], which was subject of several clinical tumor imaging studies[146-152]. The non-peptidic CXCR4 antagonist Plerixafor (AMD3100, Mozobil™, for structure see Figure 1.3), initially developed in order to be used for the treatment of HIV infections, obtained the approval as stem cell mobilizing drug for patients with lymphoma or multiple myeloma in the United States and in Europe in 2008 and 2009, respectively[153,154].

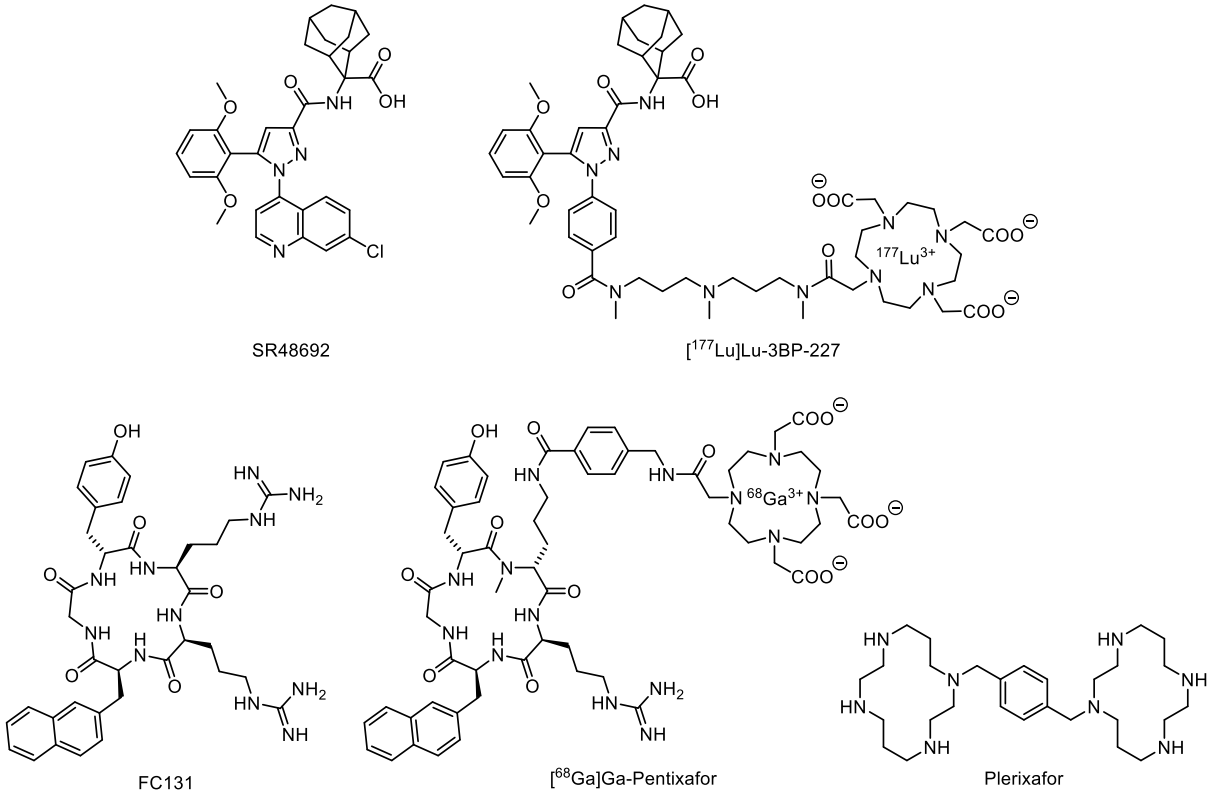

Figure 1.3. Structures of the NTS_1R antagonists SR48692[137] and [^{177}Lu]Lu-3BP-227 (IPN01087)[139], and of the CXCR4 antagonists FC131[143], [^{68}Ga]Ga-Pentixafor[144] and Plerixafor (AMD3100, Mozobil™)[155].

1.3.3 Proteolytic degradation in plasma

As mentioned above, one of the major drawbacks of peptidic ligands is their short plasma half-life owing to proteolytic degradation, which often limits their applicability for, e.g., in vivo receptor imaging, as proteolysis may impede the access of sufficient amounts of the intact peptide-derived pharmaceutical to the target tissues[123,134,135,156,157]. Degradation by exo- or endopeptidases occurs via the hydrolysis of amide bonds in the amino acid chain[135,157], thereby strongly diminishing the in vivo bioavailability of peptidic compounds. For NT and its bioactive carboxyterminal fragment, NT(8-13), distinct cleavage sites in the peptide backbone have been reported: degradation by metalloendopeptidase 24.15 (EC 3.4.24.15) takes place at the bond between Arg^{8} and Arg^{9}, the Pro^{10}-Tyr^{11}-bond is cleaved by metalloendopeptidase 24.16 (EC 3.4.24.16) and neutral endopeptidase 24.11 (EC 3.4.24.11), while cleavage of the bond between Tyr^{11} and Ile^{12} occurs via EC 3.4.24.11 or the angiotensin converting enzyme (EC 3.4.15.1)[25,158,159]. The three NT inactivating peptidases EC 3.4.24.15, EC 3.4.24.16 and EC 3.4.24.11 are widely distributed in the brain as well as in the periphery; thus, proteolytic degradation of NT in plasma proceeds very rapidly, thereby terminating the biological activity of the neuropeptide[9]. Investigations on the in vitro stability of NT(8-13) revealed a plasma half-life of only a few minutes[160,161]. Therefore, modification of the NT(8-13) core structure is necessary in order to develop stable NT-receptor ligands useful for in vivo applications.

1.3.4 Structural modifications for peptide stabilization

To date, many different strategies to enhance the metabolic stability of peptidic compounds have been pursued; the most frequently used approaches will be discussed in more detail in the following paragraph, focusing on modifications of ligands targeting the NTS_1R, NTS_2R or the CXCR4.

The replacement of amino acids in the P1, P2, P1' or P2' position is one of the most frequently used alterations in peptidic drug development and is often conducted by applying (in part non-natural) amino acids which are structurally related to the respective native amino acid in order to minimize the impairment of the ligand's receptor binding properties[12,162-165]. However, even minor changes in an amino acid side chain can result in a substantial shift of proteolytic stability and receptor affinity[37,162,165-167]. A prominent example of such a structural sensitivity is the replacement of Ile^{12} in NT receptor ligands derived from NT(8-13) by α-*tert*-butylglycine (*tert*-leucine, Tle), which currently represents the state of the art to stabilize the C-terminus of NT(8-13) derivatives[35,37-39,161,163,164,167-171]. The sole shift of one methyl-group from the γ-position in Ile to the ß-carbon atom in Tle was reported to procure enhanced peptide stability; however, in many cases the receptor affinity of Tle^{12}-containing ligands is markedly decreased as compared to their Ile^{12}-containing analogs[35,70,169,172-175]. The exchange of either Arg^{8}, Arg^{9} or both arginines in NT(8-13) by lysine also represents a commonly used modification for NT receptor ligands[37-39,161,162,164-168,170,171,176], thereby retaining the basic character of the N-terminal residues, which is important for the interaction with the NTS_1R[177,178]. The described CXCR4 ligand [^{68}Ga]Ga-Pentixafor[144] (for structure see Figure 1.3) comprises three frequently used modifications which can enhance peptide stability against proteolytic degradation: firstly, the compound contains two D-configured amino acids. The replacement of naturally occurring L-amino acids by their D-configured congeners can potentially impair the cleavage site recognition by peptidases, resulting in a reduced

degree of degradation[176,179,180]. However, this modification is also prone to affect binding affinity and/or subtype selectivity as it was described, e.g., for NT(8-13) analogs that underwent a shift from NTS_1R- to NTS_2R-selectivity after incorporation of D-Tyr or derivatives thereof in position 11[164,165,176]. Secondly, [^{68}Ga]Ga-Pentixafor, like many of the currently reported CXCR4 ligands and numerous compounds targeting other peptide receptors[39,149,176,181-183], is a cyclic peptide. Although it can largely influence the binding properties, cyclization inevitably rigidifies the molecule's conformation and thereby hampers the access of endo- and exopeptidases to specific cleavage sites[179-181,183-185]. Lastly, the α-nitrogen of D-ornithine in [^{68}Ga]Ga-Pentixafor is methylated, and this modification was also applied to several reported NT(8-13) analogs, as N^{α}-methylation or -alkylation was found to prevent cleavage of the respective amide bond[36,161,174,179,180,186-188]. Other structural variations applied to peptide amide bonds in order to prohibit proteolytic degradation include bond reduction[35,160,161,168,173,179,189], the use of triazole amide bond surrogates[169] or the incorporation of peptoid structures, i.e., glycines bearing the side chain of the native amino acid at the α-nitrogen[37,38,165,166,168,170,190]. Furthermore, to prevent decomposition by exopeptidases, many reported acyclic peptidic ligands were N- or C-terminally acylated or alkylated[161,164,166,167,169,171,190-193].

1.4 Tumor imaging and therapy via non-invasive methods

1.4.1 Positron emission tomography

In the past decades, substantial advancements have been made with regard to non-invasive in vivo imaging modalities. Based on the injection of a detectable tracer addressing a target of interest, several molecular imaging techniques enable, e.g., the visualization of a biochemical pathway, substrate conversion or the expression pattern and density of a specific cellular structure such as a receptor or transporter[194,195]. The detection of the distribution and, depending on the type of imaging technique, the quantification of the tracer provides valuable physiologic and/or pathologic information for disease diagnosis, staging, planning of treatment, therapy control, prognosis and surveillance[194,195]. Advantage of these imaging methods is taken in clinical examinations as well as in pre-clinical small animal studies for research purposes dealing with indications in oncology, cardiology or neurology[195,196]. Besides visualization modalities such as single-photon emission computed tomography (SPECT) or magnetic resonance imaging (MRI), positron emission tomography (PET), often coupled with computed tomography (PET-CT), has emerged as one of the most powerful imaging techniques because of superior sensitivity, high spatial resolution and the potential for quantification of the applied tracer[194,195,197-199]. A schematic illustration of the measurement principle of PET is depicted in Figure 1.4.

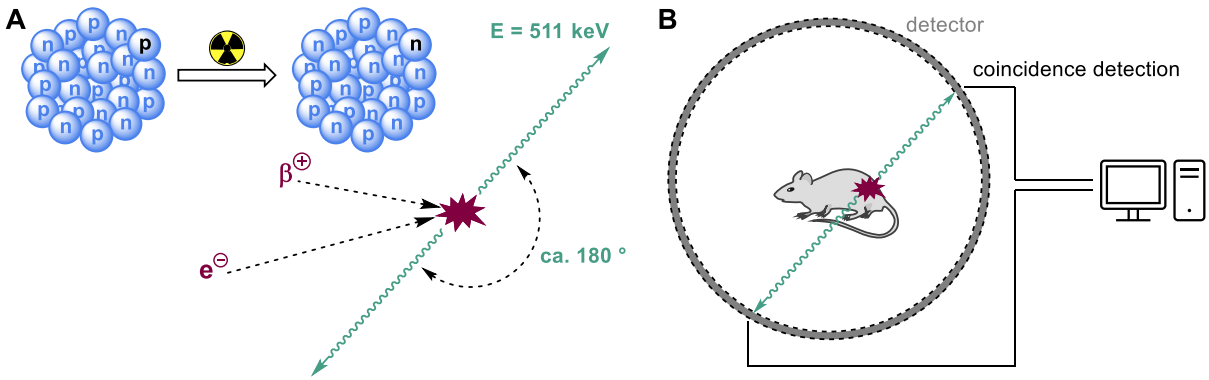

Figure 1.4. Schematic illustration of positron decay and PET imaging, based on Vaquero et al.[195]. (A) A positron-emitting radionuclide reaches a stable state by release of a positron, which collides with an electron in an event called annihilation, resulting in the emission of two photons with an energy of 511 keV each[196,200]. (B) During the PET scan, true-incident events of photons impinging simultaneously on the circular detector are used to recalculate the position of the source of the photons[195,196].

PET imaging is based on the use of a tracer which is labeled with a positron-emitting radionuclide and displays high affinity to the target structure of interest[194]. Commonly used radionuclides for PET imaging and the corresponding labeling methods for tracer preparation are described in more detail below. Positron emission occurs in isotopes that are neutron-deficient and hence reach a more stable state by converting a proton inside their nucleus into a neutron[195,196]. This nuclear transmutation can be described with the general equations (1) and (2), whereby A represents the atomic mass number, Z is the nuclear charge number (atomic number), and ν is a neutrino compensating for the difference between the energy of the respective emitted ß-particle and the maximum energy of the emitted positrons[196]:

$$ {}^{1}_{1}p^{+} \rightarrow {}^{1}_{0}n + {}^{0}_{1}\beta^{+} + \nu \quad (1) $$

$$ {}^{A}_{Z}X \rightarrow {}^{A}_{Z-1}Y + {}^{0}_{1}\beta^{+} + \nu \quad (2) $$

The energy of the emitted positron, typically ranging between 0.5-2 MeV (E_{max})[196,201], is successively transferred onto other atoms the positron collides with while it passes through the surrounding matter (e.g., organs or tissues of the patient examined). Eventually, the positron combines with an electron in an event called annihilation, thereby producing two gamma ray-photons with an energy of 511 keV moving in opposite directions (note: the mass energies of a positron and an electron correspond to 511 keV each according to $E = m \times c^2$)[195,196,198,200]. If the PET scanner, circularly surrounding the examined patient or object, detects the impingement of two photons approximately 180 ° to each other within a short time frame (1-10 ns), this will be considered a true-coincidence event, and can be used to determine the spatial origin of the radiation[195,196]. As the applied radiopharmaceutical ideally accumulates specifically in the target tissue, the distribution of activity allows, by section-wise scanning of the patient or laboratory animal and accumulation of true-coincidence signals, the reconstruction of a three-dimensional image of organs or tissues of interest[196,198].

1.4.2 Radionuclides for endoradiotherapy and diagnosis

Ionizing radiation emitted by radionuclides has been used in clinical applications for many decades now; however, depending on the type of objective (i.e., diagnosis or therapy), the choice of an appropriate nuclide is crucial. Table 1.1 gives an overview of the most commonly used radionuclides together with their physical properties and the field of clinical application.

Table 1.1. Physical properties, fields of application and sources of the clinically most commonly used radioisotopes[196,198,200,202-206].

radionuclide	$t_{1/2}$	decay mode[a]	application	source
^{18}F	110 min	β⁺ (97%) EC (3%)	PET	cyclotron
^{64}Cu	12.7 h	β⁺ (19%) β⁻ (40%) EC (41%)	PET, therapy	cyclotron
^{67}Ga	3.3 d	EC (100%) γ	SPECT	cyclotron
^{67}Cu	2.6 d	β⁻ (100%) γ	therapy	accelerator
^{68}Ga	68 min	β⁺ (89%) EC (11%)	PET	^{68}Ge/^{68}Ga generator
^{86}Y	14.7 h	β⁺ (33%) EC (66%)	PET	cyclotron
^{90}Y	2.7 d	β⁻ (100%)	therapy	^{90}Sr/^{90}Y generator
^{99m}Tc	6.0 h	IT (100%) γ	SPECT	^{99}Mo/^{99m}Tc generator
^{111}In	2.8 d	EC (100%) γ	SPECT	cyclotron
^{177}Lu	6.7 d	β⁻ (100%) γ	therapy	reactor
^{225}Ac	9.9 d	α (100%)	therapy	radiochemical extraction from ^{229}Th

[a]The portion of the respective mode of decay is given in parentheses. EC = electron capture. IT = isomeric transition.

Decisive for the type of application a radionuclide is suitable for is the mode of its decay. Therapeutically usable nuclides are emitters of α- or β⁻-particles which transfer their energy onto the surrounding atoms within only short distances of traveling (below one micrometer up to a few millimeters, depending on their energy)[205]. Therefore, the intended biological effect, the irreversible damage and subsequent death of cells in, e.g., tumor tissue, is restricted to the matter closely surrounding the site of decay and does not affect more distant organs and tissues. Commonly used isotopes for endoradiotherapy comprise, among others, the β⁻-emitters ^{67}Cu, ^{90}Y and ^{177}Lu, and recent investigations suggest the α-emitter ^{225}Ac as an appropriate surrogate of the former for the therapy of patients with contraindications or resistance to radiopharmaceuticals labeled with β⁻-emitting nuclides[123,203-205]. Radioisotopes appropriate for diagnostic purposes generally emit β⁺- or γ-radiation, the former one producing high-energy photons which can - like γ-radiation - be detected outside of the patient's body due to a longer traveling distance[205]. SPECT imaging is performed using single-photon emitting radionuclides like ^{67}Ga, ^{111}In and, most frequently, ^{99m}Tc, emitting γ-radiation with an energy (140 keV) favorable for the detection by gamma cameras[203,206].

The range of positron-emitters frequently used in the clinic comprises the metal isotopes ^{64}Cu, ^{68}Ga and ^{86}Y as well as the non-metal nuclide ^{18}F[200,202,203]. The physical properties of these isotopes are critical with regard to PET image quality: the higher the initial energy of the positron, the further it travels in the surrounding matter until the annihilation event takes place. As PET image construction is based on the recalculation of the position of the source of the gamma-photons (i.e., not the site of origin of the β⁺-emitter itself), the uncertainty correlates with the initial β⁺-energy[196]. As ^{18}F emits β⁺-particles with a maximum energy of 635 keV, this nuclide is often preferred over ^{68}Ga emitting higher-energetic positrons (E_{max} = 1900 keV)[198,200].

Another crucial aspect is the physical half-life of the nuclide of interest: long-lived radioisotopes such as ^{177}Lu ($t_{1/2}$ = 6.7 d) or ^{67}Ga ($t_{1/2}$ = 3.3 d) enable the expansion of the therapeutic effect or the observation of a pathologic state over time; however, the prolonged radiation exposure for the patient is considerable. Short-lived radionuclides like ^{68}Ga ($t_{1/2}$ = 68 min) or ^{18}F ($t_{1/2}$ = 110 min) are easier to handle in that respect. However, a transfer of ^{68}Ga- and ^{18}F-labeled radiopharmaceuticals between clinics is limited or not feasible, though[200]. In practice, the choice of a certain isotope also strongly depends on the technical equipment available for manufacturing of the radionuclide. While some commonly used radionuclides such as ^{68}Ga, ^{90}Y and ^{99m}Tc can easily be eluted from a generator containing their respective parent nuclide (*cf.* Table 1.1), the generation of, e.g., ^{18}F, ^{64}Cu and ^{111}In requires a cyclotron[200,203].

1.4.3 Current status of clinically used PET tracers targeting the NTS_1R and the CXCR4

Prompted by its overexpression in a variety of tumors as mentioned above, the NTS_1R is considered a promising target for diagnostic purposes in the field of oncology[33,207], and a vast number of ligands labeled with radionuclides suitable for PET imaging were investigated in pre-clinical studies[70]. However, mostly due to stability issues of peptidic NTS_1R ligands or unfavorable biodistribution patterns, no radiolabeled peptidic NTS_1R ligand was successfully transferred to the clinic so far[33,70].

With regard to the CXCR4, its pivotal role in a range of malignancies such as cancer or infections with HIV has inspired the development and pre-clinical investigation of numerus CXCR4 PET ligands. The most promising candidate, the diagnostically interesting peptidic PET tracer [^{68}Ga]Ga-Pentixafor is currently intensively studied in several clinical examinations[146,151,152,208]. Interestingly, no ^{18}F-labeled CXCR4 PET ligand has so far reached the clinical trial stage.

As becomes obvious from this overview involving also antagonistic receptor ligands under clinical investigation or already approved for applications other than PET, peptidic compounds have so far been inferior to non-peptidic compounds with respect to a successful translation to the clinic. Further improvement of the many currently available peptidic structures is necessary, especially regarding in vivo stability, to render those ligands suitable for in vivo PET imaging, thus allowing an exploitation of the advantages of peptides described above. Moreover, in order to broaden the range of options for labeling a peptidic core structure with a radionuclide of interest, alternatives to the so far reported strategies of conjugation of the radiolabel, which will be discussed in more detail in the next section, need to be explored.

1.5 Strategies for the radiolabeling of peptides with clinically relevant nuclides

1.5.1 Covalently bound radionuclides or -labels

The attachment of some clinically relevant radionuclides can be based on covalent binding. Two main strategies have been pursued in this regard: direct labeling and indirect labeling by means of a prosthetic group[203]. The clinically most frequently used nuclides which can be covalently bound to a compound are radioiodine (^{123}I is used for SPECT imaging, ^{124}I is appropriate for PET imaging and ^{131}I is applied for radiotherapy) and ^{18}F. Direct iodination mostly occurs via electrophilic substitution on a peptide's Tyr or His side chain under mild conditions (pH 7-8, aqueous buffer)[200,203]. Contrary to this, direct radiofluorination via nucleophilic substitution requires harsh conditions (often strong bases) which might not be compatible with peptides[198,203]. An alternative strategy for covalent labeling of a compound is provided by the use of prosthetic groups which are labeled with the radionuclide of choice beforehand and subsequently conjugated under mild conditions to, e.g., an amine, hydroxyl or carboxyl functional group available in the precursor peptide[200,203]. For example, the *N*-hydroxy-succinimidyl ester (NHS) moiety of *N*-succinimidyl-3-[*I]iodobenzoate ([*I]SIB) and *N*-succinimidyl-4-[^{18}F]fluorobenzoate ([^{18}F]SFB) (for structures see Figure 1.5) allows the conjugation to amine groups by amide bond formation[198,203].

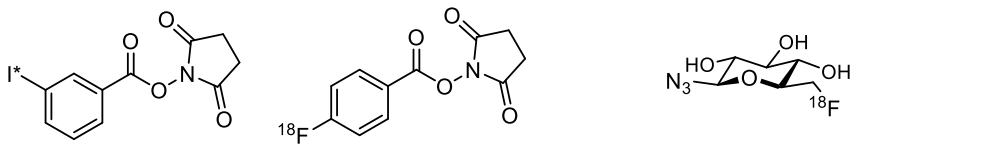

Figure 1.5. Structures of the prosthetic groups [*I]SIB, [^{18}F]SFB and a [^{18}F]fluoroglucosyl azide applied as labeling agents for radioiodination or -fluorination reactions[203,209].

A broader range of labeling options was made available by the introduction of "click chemistry", whereby the conjugation of the pre-labeled synthon to the peptidic core structure occurs via a 1,3-dipolar copper(I)-catalyzed cycloaddition between an azide and an alkyne functionality[198,203]. The click reaction of, e.g., azido-functionalized ^{18}F-labeled sugar building blocks such as the 6-deoxy-6-fluoro-ß-D-glucosyl azide[209] shown in Figure 1.5 with alkyne-functionalized peptides leads to the formation of a triazole moiety under mild conditions[198,203].

However, in the case of covalent binding of the radionuclide or -label to the target compound, chemoselectivity issues may have to be considered, and the synthetic procedures often require two or more reaction steps[198,210]. For labeling with short-lived radioisotopes like ^{18}F, a time-consuming preparation of the tracer can be limiting with respect to sample activity available for the in vivo application. Regarding this, a more straight-forward way of peptide labeling is provided by chelation of the radionuclide.

1.5.2 Labeling via chelation

The preparation of a tracer labeled with a radiometal can be accomplished very easily in a one-step procedure by incorporation the respective metal ion in an appropriate chelating moiety conjugated to the tracer pharmacophore. A variety of chelators suitable for the

insertion of different ions have been developed so far, a selection of which is depicted in Figure 1.6. In general, these chelators are composed of a cyclic or acyclic multidentate structure capable of forming complexes with the inserted ions, whereby one of the dentate arms is often used for attachment to the peptide of interest. In most cases, this attachment occurs via amide bond formation with, e.g., lysine residues or the N-terminus, or, quite frequently, to an additional spacer moiety linked to the peptide[123,200,202,203].

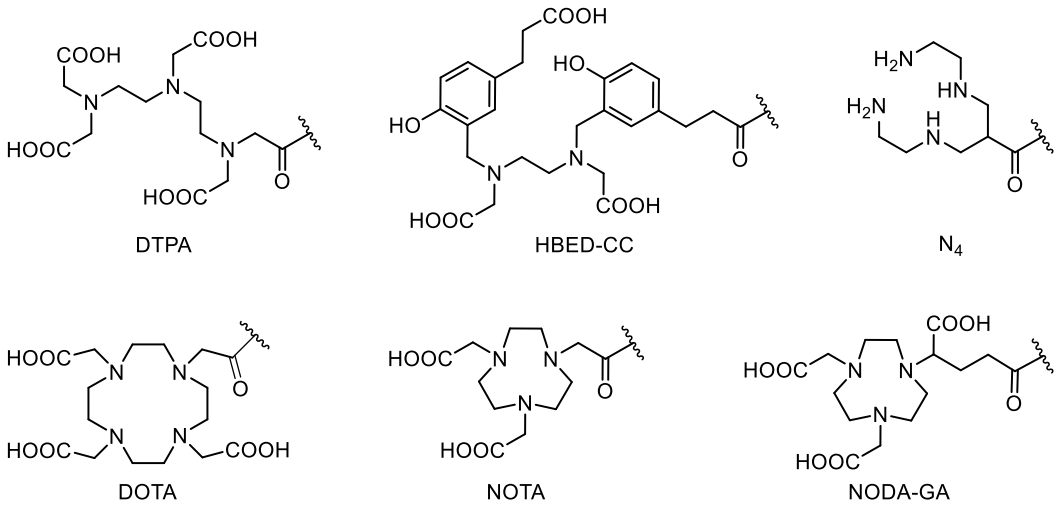

Figure 1.6. Structures of the radiometal ion chelators DTPA, HBED-CC, N_4, DOTA, NOTA and NODA-GA commonly used for clinical applications[203,211]. The wavy line represents the site of attachment to the target structure, e.g., a peptide.

The most crucial feature of a chelator is its ability to form chemically and physiologically stable complexes with the metal ion because a release of the radiometal after injection of the tracer would lead to an unspecific accumulation of the radionuclide in off-target tissues and, subsequently, to undesired side effects or false positive results, e.g., of a PET scan[123,203,212]. For instance, the release of $^{177}Lu^{3+}$ or $^{90}Y^{3+}$ causes their accumulation in bones and can result in bone marrow damage[203]. Thus, depending on the physical properties of the radiometal of interest (e.g., its ionic radius, its commonly occurring oxidation state and the preferred geometry of coordination (i.e., tetrahedral, octahedral etc.)), the most suitable chelator has to be chosen to achieve thermodynamic stability of the metal complex[202]. Table 1.2 gives an overview of chelators appropriate for complexation of the clinically most relevant radiometal ions[121,123,202,203], together with the respective association constants.

Table 1.2. Suitable chelators for the complexation of (radio)metal ions relevant for nuclear medicine, and corresponding association constants.

Chelator[a]	complexed metal ion	logK[b]
DTPA	Cu^{2+}	21.5[c]
	Ga^{3+}	25.5[c]
	Y^{3+}	22.5[c]
	In^{3+}	29.5[c]
	Lu^{3+}	22.4[d]
HBED-CC	Ga^{3+}	n.r.[e]
N_4	Tc^{5+} [f]	n.r.[e]
DOTA	Cu^{2+}	22.3[c] / 22.7[d]
	Ga^{3+}	21.3[c] / 26.1[g]
	Y^{3+}	24.3[c]
	In^{3+}	23.9[c]
	Lu^{3+}	25.5[c]
NOTA	Cu^{2+}	21.6[c] / 19.8[d]
	Ga^{3+}	31.0[c]
	In^{3+}	26.2[c]
NODA-GA	Cu^{2+}	n.r.[e]
	Ga^{3+}	n.r.[e]
	In^{3+}	n.r.[e]

[a]For structures of the chelators see Figure 1.6. [b]Logarithm of the association constant K (K = [ML]/[M][L], where [ML] is the concentration of the metal ion complex, [M] is the concentration of the free metal ion and [L] is the concentration of metal-free chelator). [c]Correia et al.[202]. [d]Martell et al.[213]. [e]The formation of stable complexes was reported (Eder et al.[211], Correia et al.[202], Gourni et al.[214], Makarem et al.[215]), but logK values were not provided. n.r. = not reported. [f]The metal core corresponds to TcO_2^+ [173,202]. [g]Kubíček et al.[212].

Acyclic chelators such as diethylenetriaminepentaacetic acid (DTPA), *N*,*N*′-bis[2-hydroxy-5(carboxyethyl)benzyl]ethylenediamine-*N*,*N*′-diacetic acid (HBED-CC) or 6-carboxy-1,4,8,11-tetraazaundecane (N_4) often show faster labeling kinetics as compared to cyclic chelators, resulting from their less rigid linear structure and more flexible "arms", which allow a conformational adaption necessary for ion complexation[203,216]. However, they are usually inferior with respect to stability; for instance, insertion of metals other than In^{3+} into DTPA is unsuitable due to loss of the metal ion in vivo[203]. The slow labeling kinetics of cyclic chelators like 1,4,7,10-tetraazacyclododecane-1,4,7,10-tetraacetic acid (DOTA), 1,4,7-triazacyclononane-1,4,7-triacetic acid (NOTA) or 1,4,7-triazacyclononane-1-glutaric acid-4,7-acetic acid (NODA-GA), which form much more stable metal complexes, can be overcome by heating the reaction mixture[203,217,218]. N_4 and other acyclic chelators are often applied for labeling with ^{99m}Tc, whereas DOTA and NOTA represent the most frequently used chelators for metal ion insertion of In^{3+}, Y^{3+}, Ga^{3+} and Lu^{3+} [121,203,212].

Notably, in order to make use of the physical nature of ^{18}F convenient for PET imaging, attempts were made to enable the simple chelation of this non-metal as well[219]. By exploiting the strong association between fluoride and aluminum, several chelators were investigated with respect to their ability to form stable complexes with AlF^{2+}-ions, or, regarding the development of PET tracers, [^{18}F]AlF^{2+}-ions[219-223]. The most widely investigated chelators capable of chelating AlF^{2+} are NOTA and HBED-CC[220,224-237]; however, the chemical and physiological stability of these complexes are controversially

discussed after reports on observed in vivo defluorination and, connected to this, accumulation of $^{18}F^-$ in the bones[219,229,232,233,235,238-240].

In addition to the convenient and timesaving labeling procedure, radiolabeling of a tracer via chelation is also considered a useful approach with respect to the preparation of theranostic compounds. By application of the same precursor or a congener conjugated to a different chelator, labeling with different radionuclides allows the use of the radiopharmaceutical for either diagnostic or therapeutic purposes. The highly comparable binding properties and biodistribution profiles of the corresponding pair of tracers enables a more reliable decision (based on the diagnostic imaging data) on whether a patient can benefit from a treatment with the respective therapeutic tracer or not[241-244]. The aforementioned NTS_1R antagonist [^{177}Lu]Lu-3BP-227 (for structure see Figure 1.3), investigated in HT-29 tumor-bearing mice in terms of a therapeutic effect, had initially successfully been applied for ^{111}In-labeling and subsequent SPECT/CT imaging of HT-29 tumors[138,139]. In vivo PET imaging of the CXCR4 with the tracer [^{68}Ga]Ga-Pentixafor (structure shown in Figure 1.3) is often complemented by its structurally very closely related congener Pentixather ([3-iodo-D-Tyr^1]Pentixafor) after labeling with ^{177}Lu or ^{90}Y[245]. Notably, the theranostic approach was already transferred to the clinic, e.g., with the approval of the diagnostic somatostatin receptor ligand [^{68}Ga]Ga-DOTA-TOC and its therapeutic counterpart [^{177}Lu]Lu-DOTA-TATE by the European Medicines Agency (EMA) in 2016 and 2017, respectively[246,247].

1.6 Objectives and scope of the thesis

The neurotensin NTS_1R, belonging to the superfamily of G-protein coupled receptors, represents an interesting target for cancer diagnosis and treatment by radiotherapy due to its (over)expression in a variety of malignant tumors[31,44,65-68]. Numerous peptidic NTS_1R ligands, labeled with the positron-emitting radionuclides ^{18}F or ^{68}Ga for PET imaging purposes, have been developed so far. Most of them are structurally derived from the lead compound NT(8-13), the biologically active fragment of neurotensin. However, not least owing to insufficient stability (in vitro or in vivo), none of these peptidic tracers has yet been transferred to the clinics[33,70].

Similarly, the development of radiolabeled compounds targeting the chemokine receptor CXCR4 is considered a promising approach towards diagnostic imaging of CXCR4-expressing tumors and endoradiotherapy[144,150,248-254]. Although clinical trials have already been conducted with a ^{68}Ga-labeled CXCR4 antagonist[146,151,152,208], clinical data on ^{18}F-labeled CXCR4 PET ligands are still lacking.

Therefore, the primary aim of the present work was the development of proteolytically stable high-affinity ligands for the NTS_1R and CXCR4 including potential PET ligands. In an initial study, an N^{α}-methyl scan had to be performed for NT(8-13) and in some of these methylated analogs, Ile^{12} had to be additionally replaced by Tle^{12}. The in vitro plasma stabilities and NTS_1R affinities of these NT(8-13) derivatives had to be determined.

For the preparation of PET ligand candidates, a recently introduced labeling strategy for peptides, based on the bioisosteric replacement of arginine by an N^{ω}-carbamoylated arginine containing an amino-functionalized linker for peptide conjugation, had to be applied throughout. In the case of NT(8-13) derivatives, the modified arginine had to be incorporated in position 8 or 9 of the most promising candidates identified in the initial study on stabilized NT(8-13) analogs in order to obtain precursor compounds for the synthesis of (potential) NTS_1R PET ligands. One part of this project had to deal with the preparation of ^{18}F-labeled NTS_1R ligands. For this purpose, the amine-functionalized NT(8-13) derivatives had to be alkynylated to enable a conjugation to a fluorinated azido sugar by copper(I)-catalyzed azide-alkyne cycloaddition. The second part of the project aimed at ^{68}Ga-labeled PET tracers targeting the NTS_1R. For this approach, the amino-functionalized N^{ω}-carbamoylated arginine residue had to be used for the attachment of a metal ion chelator followed by insertion of Ga^{3+}. To identify a structural modification at the C-terminus of the hexapeptides being superior to the Ile^{12}/Tle^{12} exchange with respect to a stabilization against proteolytic degradation and impairment of NTS_1R binding, various unnatural amino acids had to be incorporated in position 11, 12 or 13 of N-terminally methylated NT(8-13). All prepared NT(8-13) analogs, including the "cold" forms of NTS_1R PET ligands, had to be investigated with respect to NTS_1R affinity and, in part, also NTS_2R binding, as well as in terms of in vitro plasma stability. For the most promising candidates, the respective ^{18}F- or ^{68}Ga-labeled congeners had to be prepared and examined in vivo in biodistribution studies and PET imaging experiments using HT-29 tumor-bearing mice.

Moreover, cyclic peptidic CXCR4 ligands derived from the cyclic pentapeptide FC131 had to be prepared. Either arginine in FC131, Arg^2 or Arg^3, had to be replaced by an N^{ω}-carbamoylated arginine. After alkyne-functionalization, the "cold" forms of CXCR4 PET

ligands had to be prepared by azide-alkyne cycloaddition using the same fluorinated glycosyl azide as for the synthesis of the fluorinated NTS_1R PET ligand candidates. The in vitro plasma stability had to be determined and the CXCR4 binding affinities had to be estimated by the determination of the antagonistic activities in a functional CXCR4 assay.

1.7 References

1. Carraway, R.; Leeman, S.E. The isolation of a new hypotensive peptide, neurotensin, from bovine hypothalami. *J Biol Chem* **1973**, *248*, 6854-6861.
2. Carraway, R.; Leeman, S.E. The amino acid sequence of a hypothalamic peptide, neurotensin. *J Biol Chem* **1975**, *250*, 1907-1911.
3. Kitabgi, P.; Carraway, R.; Leeman, S.E. Isolation of a tridecapeptide from bovine intestinal tissue and its partial characterization as neurotensin. *J Biol Chem* **1976**, *251*, 7053-7058.
4. Carraway, R.; Kitabgi, P.; Leeman, S.E. The amino acid sequence of radioimmunoassayable neurotensin from bovine intestine. *J Biol Chem* **1978**, *253*, 7996-7998.
5. Hammer, R.A.; Leeman, S.E.; Carraway, R.; Williams, R.H. Isolation of human intestinal neurotensin. *J Biol Chem* **1980**, *255*, 2476-2480.
6. Rostène, W.H.; Alexander, M.J. Neurotensin and neuroendocrine regulation. *Front Neuroendocrinol* **1997**, *18*, 115-173, doi:10.1006/frne.1996.0146.
7. Carraway, R.E.; Mitra, S.P.; Spaulding, G. Posttranslational processing of the neurotensin neuromedin-N precursor. *Ann Ny Acad Sci* **1992**, *668*, 1-16, doi:DOI 10.1111/j.1749-6632.1992.tb27335.x.
8. Vincent, J.P.; Mazella, J.; Kitabgi, P. Neurotensin and neurotensin receptors. *Trends Pharmacol Sci* **1999**, *20*, 302-309, doi:10.1016/s0165-6147(99)01357-7.
9. Sarret, P.; Cavelier, F. Neurotensin and its receptors. In *Reference Module in Neuroscience and Biobehavioral Psychology*; Elsevier: Amsterdam, the Netherlands, 2017.
10. Nemeroff, C.B.; Luttinger, D.; Prange, A.J. Neurotensin - Central nervous system effects of a neuropeptide. *Trends Neurosci* **1980**, *3*, 212-215, doi:Doi 10.1016/0166-2236(80)90080-6.
11. Manberg, P.J.; Youngblood, W.W.; Nemeroff, C.B.; Rossor, M.N.; Iversen, L.L.; Prange, A.J., Jr.; Kizer, J.S. Regional distribution of neurotensin in human brain. *J Neurochem* **1982**, *38*, 1777-1780, doi:10.1111/j.1471-4159.1982.tb06664.x.
12. Tyler-McMahon, B.M.; Boules, M.; Richelson, E. Neurotensin: Peptide for the next millennium. *Regul Pept* **2000**, *93*, 125-136, doi:10.1016/s0167-0115(00)00183-x.
13. Binder, E.B.; Kinkead, B.; Owens, M.J.; Nemeroff, C.B. Neurotensin and dopamine interactions. *Pharmacol Rev* **2001**, *53*, 453-486.
14. Orci, L.; Baetens, O.; Rufener, C.; Brown, M.; Vale, W.; Guillemin, R. Evidence for immunoreactive neurotensin in dog intestinal mucosa. *Life Sci* **1976**, *19*, 559-561, doi:10.1016/0024-3205(76)90236-8.
15. Helmstaedter, V.; Feurle, G.E.; Forssmann, W.G. Ultrastructural identification of a new cell type--the N-cell as the source of neurotensin in the gut mucosa. *Cell Tissue Res* **1977**, *184*, 445-452, doi:10.1007/BF00220968.

16. Kitabgi, P. Effects of neurotensin on intestinal smooth muscle: Application to the study of structure-activity relationships. *Ann N Y Acad Sci* **1982**, *400*, 37-55, doi:10.1111/j.1749-6632.1982.tb31559.x.

17. Sarret, P.; Kitabgi, P. Neurotensin and receptors. In *Encyclopedia of neuroscience*, Squire, L.R., Ed.; Elsevier: 2009; pp. 1021-1034.

18. Mazella, J.; Vincent, J.P. Functional roles of the NTS2 and NTS3 receptors. *Peptides* **2006**, *27*, 2469-2475, doi:10.1016/j.peptides.2006.04.026.

19. St-Gelais, F.; Jomphe, C.; Trudeau, L.E. The role of neurotensin in central nervous system pathophysiology: What is the evidence? *J Psychiatr Neurosci* **2006**, *31*, 229-245.

20. Boules, M.; Li, Z.; Smith, K.; Fredrickson, P.; Richelson, E. Diverse roles of neurotensin agonists in the central nervous system. *Front Endocrinol (Lausanne)* **2013**, *4*, 36, doi:10.3389/fendo.2013.00036.

21. Xiao, Z.Y.; Cilz, N.I.; Kurada, L.; Hu, B.Q.; Yang, C.X.; Wada, E.; Combs, C.K.; Porter, J.E.; Lesage, F.; Lei, S.B. Activation of neurotensin receptor 1 facilitates neuronal excitability and spatial learning and memory in the entorhinal cortex: beneficial actions in an Alzheimer's disease model. *J Neurosci* **2014**, *34*, 7027-7042, doi:10.1523/Jneurosci.0408-14.2014.

22. Schroeder, L.E.; Leinninger, G.M. Role of central neurotensin in regulating feeding: Implications for the development and treatment of body weight disorders. *Bba-Mol Basis Dis* **2018**, *1864*, 900-916, doi:10.1016/j.bbadis.2017.12.036.

23. Furlan, A.; Corona, A.; Boyle, S.; Sharma, R.; Rubino, R.; Habel, J.; Gablenz, E.C.; Giovanniello, J.; Beyaz, S.; Janowitz, T.; et al. Neurotensin neurons in the extended amygdala control dietary choice and energy homeostasis. *Nat Neurosci* **2022**, *25*, 1470-1480, doi:10.1038/s41593-022-01178-3.

24. Castagliuolo, I.; Wang, C.C.; Valenick, L.; Pasha, A.; Nikulasson, S.; Carraway, R.E.; Pothoulakis, C. Neurotensin is a proinflammatory neuropeptide in colonic inflammation. *J Clin Invest* **1999**, *103*, 843-849, doi:10.1172/JCI4217.

25. Myers, R.M.; Shearman, J.W.; Kitching, M.O.; Ramos-Montoya, A.; Neal, D.E.; Ley, S.V. Cancer, chemistry, and the cell: Molecules that interact with the neurotensin receptors. *ACS Chem Biol* **2009**, *4*, 503-525, doi:10.1021/cb900038e.

26. Bugni, J.M.; Pothoulakis, C. Neurotensin. In *Handbook of biologically active peptides (section XIII: Gastrointestinal peptides)*, 2nd ed.; Kastin, A.J., Ed.; Academic press: 2013; pp. 1265-1270.

27. Wood, J.G.; Hoang, H.D.; Bussjaeger, L.J.; Solomon, T.E. Neurotensin stimulates growth of small intestine in rats. *Am J Physiol* **1988**, *255*, G813-G817, doi:DOI 10.1152/ajpgi.1988.255.6.G813.

28. Hasegawa, K.; Kar, S.; Carr, B.I. Stimulation of hepatocyte DNA synthesis by neurotensin. *J Cell Physiol* **1994**, *158*, 215-222, doi:10.1002/jcp.1041580202.

29. Thomas, R.P.; Hellmich, M.R.; Townsend, C.M., Jr.; Evers, B.M. Role of gastrointestinal hormones in the proliferation of normal and neoplastic tissues. *Endocr Rev* **2003**, *24*, 571-599, doi:10.1210/er.2002-0028.

30. Carraway, R.E.; Plona, A.M. Involvement of neurotensin in cancer growth: Evidence, mechanisms and development of diagnostic tools. *Peptides* **2006**, *27*, 2445-2460, doi:10.1016/j.peptides.2006.04.030.

31. Souazé, F.; Dupouy, S.; Viardot-Foucault, V.; Bruyneel, E.; Attoub, S.; Gespach, C.; Gompel, A.; Forgez, P. Expression of neurotensin and NT1 receptor in human breast cancer: A potential role in tumor progression. *Cancer Res* **2006**, *66*, 6243-6249, doi:10.1158/0008-5472.CAN-06-0450.

32. Wu, Z.; Martinez-Fong, D.; Trédaniel, J.; Forgez, P. Neurotensin and its high affinity receptor 1 as a potential pharmacological target in cancer therapy. *Front Endocrinol (Lausanne)* **2012**, *3*, 184, doi:10.3389/fendo.2012.00184.

33. Nikolaou, S.; Qiu, S.; Fiorentino, F.; Simillis, C.; Rasheed, S.; Tekkis, P.; Kontovounisios, C. The role of neurotensin and its receptors in non-gastrointestinal cancers: A review. *Cell Commun Signal* **2020**, *18*, 68, doi:10.1186/s12964-020-00569-y.

34. Granier, C.; Vanrietschoten, J.; Kitabgi, P.; Poustis, C.; Freychet, P. Synthesis and characterization of neurotensin analogs for structure/activity relationship studies - Acetyl-neurotensin-(8-13) is the shortest analog with full binding and pharmacological activities. *Eur J Biochem* **1982**, *124*, 117-124, doi:DOI 10.1111/j.1432-1033.1982.tb05913.x.

35. Bergmann, R.; Scheunemann, M.; Heichert, C.; Mäding, P.; Wittrisch, H.; Kretzschmar, M.; Rodig, H.; Tourwé, D.; Iterbeke, K.; Chavatte, K.; et al. Biodistribution and catabolism of ^{18}F-labeled neurotensin(8-13) analogs. *Nucl Med Biol* **2002**, *29*, 61-72, doi:10.1016/s0969-8051(01)00284-0.

36. García-Garayoa, E.; Bläuenstein, P.; Blanc, A.; Maes, V.; Tourwé, D.; Schubiger, P.A. A stable neurotensin-based radiopharmaceutical for targeted imaging and therapy of neurotensin receptor-positive tumours. *Eur J Nucl Med Mol Imaging* **2009**, *36*, 37-47, doi:10.1007/s00259-008-0894-y.

37. Maschauer, S.; Einsiedel, J.; Haubner, R.; Hocke, C.; Ocker, M.; Hübner, H.; Kuwert, T.; Gmeiner, P.; Prante, O. Labeling and glycosylation of peptides using click chemistry: A general approach to ^{18}F-glycopeptides as effective imaging probes for positron emission tomography. *Angew Chem Int Ed Engl* **2010**, *49*, 976-979, doi:10.1002/anie.200904137.

38. Maschauer, S.; Einsiedel, J.; Hocke, C.; Hübner, H.; Kuwert, T.; Gmeiner, P.; Prante, O. Synthesis of a ^{68}Ga-labeled peptoid-peptide hybrid for imaging of neurotensin receptor expression in vivo. *ACS Med Chem Lett* **2010**, *1*, 224-228, doi:10.1021/ml1000728.

39. Maschauer, S.; Ruckdeschel, T.; Tripal, P.; Haubner, R.; Einsiedel, J.; Hübner, H.; Gmeiner, P.; Kuwert, T.; Prante, O. *In vivo* monitoring of the antiangiogenic effect of neurotensin receptor-mediated radiotherapy by small-animal positron emission

tomography: A pilot study. *Pharmaceuticals (Basel)* **2014**, *7*, 464-481, doi:10.3390/ph7040464.

40. Jia, Y.; Shi, W.; Zhou, Z.; Wagh, N.K.; Fan, W.; Brusnahan, S.K.; Garrison, J.C. Evaluation of DOTA-chelated neurotensin analogs with spacer-enhanced biological performance for neurotensin-receptor-1-positive tumor targeting. *Nucl Med Biol* **2015**, *42*, 816-823, doi:10.1016/j.nucmedbio.2015.07.010.

41. Deng, H.; Wang, H.; Zhang, H.; Wang, M.; Giglio, B.; Ma, X.; Jiang, G.; Yuan, H.; Wu, Z.; Li, Z. Imaging neurotensin receptor in prostate cancer with ^{64}Cu-labeled neurotensin analogs. *Mol Imaging* **2017**, *16*, 1-11, doi:10.1177/1536012117711369.

42. Mazella, J.; Chabry, J.; Kitabgi, P.; Vincent, J.P. Solubilization and characterization of active neurotensin receptors from mouse-brain. *J Biol Chem* **1988**, *263*, 144-149.

43. Tanaka, K.; Masu, M.; Nakanishi, S. Structure and functional expression of the cloned rat neurotensin receptor. *Neuron* **1990**, *4*, 847-854, doi:10.1016/0896-6273(90)90137-5.

44. Vita, N.; Laurent, P.; Lefort, S.; Chalon, P.; Dumont, X.; Kaghad, M.; Gully, D.; Le Fur, G.; Ferrara, P.; Caput, D. Cloning and expression of a complementary DNA encoding a high affinity human neurotensin receptor. *FEBS Lett* **1993**, *317*, 139-142, doi:10.1016/0014-5793(93)81509-x.

45. Chalon, P.; Vita, N.; Kaghad, M.; Guillemot, M.; Bonnin, J.; Delpech, B.; Le Fur, G.; Ferrara, P.; Caput, D. Molecular cloning of a levocabastine-sensitive neurotensin binding site. *FEBS Lett* **1996**, *386*, 91-94, doi:10.1016/0014-5793(96)00397-3.

46. Mazella, J.; Botto, J.M.; Guillemare, E.; Coppola, T.; Sarret, P.; Vincent, J.P. Structure, functional expression, and cerebral localization of the levocabastine-sensitive neurotensin/neuromedin N receptor from mouse brain. *J Neurosci* **1996**, *16*, 5613-5620.

47. Zsürger, N.; Mazella, J.; Vincent, J.P. Solubilization and purification of a high-affinity neurotensin receptor from newborn human brain. *Brain Res* **1994**, *639*, 245-252, doi:Doi 10.1016/0006-8993(94)91737-X.

48. Vita, N.; Oury-Donat, F.; Chalon, P.; Guillemot, M.; Kaghad, M.; Bachy, A.; Thurneyssen, O.; Garcia, S.; Poinot-Chazel, C.; Casellas, P.; et al. Neurotensin is an antagonist of the human neurotensin NT_2 receptor expressed in Chinese hamster ovary cells. *Eur J Pharmacol* **1998**, *360*, 265-272, doi:10.1016/s0014-2999(98)00678-5.

49. Petersen, C.M.; Nielsen, M.S.; Nykjær, A.; Jacobsen, L.; Tommerup, N.; Rasmussen, H.H.; Røigaard, H.; Gliemann, J.; Madsen, P.; Moestrup, S.K. Molecular identification of a novel candidate sorting receptor purified from human brain by receptor-associated protein affinity chromatography. *J Biol Chem* **1997**, *272*, 3599-3605, doi:10.1074/jbc.272.6.3599.

50. Mazella, J.; Zsürger, N.; Navarro, V.; Chabry, J.; Kaghad, M.; Caput, D.; Ferrara, P.; Vita, N.; Gully, D.; Maffrand, J.P.; et al. The 100-kDa neurotensin receptor is

gp95/sortilin, a non-G-protein-coupled receptor. *J Biol Chem* **1998**, *273*, 26273-26276, doi:10.1074/jbc.273.41.26273.

51. Nielsen, M.S.; Jacobsen, C.; Olivecrona, G.; Gliemann, J.; Petersen, C.M. Sortilin/neurotensin receptor-3 binds and mediates degradation of lipoprotein lipase. *J Biol Chem* **1999**, *274*, 8832-8836, doi:10.1074/jbc.274.13.8832.

52. Vincent, J.P. Neurotensin receptors: Binding properties, transduction pathways, and structure. *Cell Mol Neurobiol* **1995**, *15*, 501-512, doi:10.1007/BF02071313.

53. Schotte, A.; Leysen, J.E.; Laduron, P.M. Evidence for a displaceable non-specific [^{3}H]neurotensin binding site in rat brain. *Naunyn Schmiedebergs Arch Pharmacol* **1986**, *333*, 400-405, doi:10.1007/BF00500016.

54. Kitabgi, P.; Rostène, W.; Dussaillant, M.; Schotte, A.; Laduron, P.M.; Vincent, J.P. Two populations of neurotensin binding sites in murine brain - Discrimination by the antihistamine levocabastine reveals markedly different autoradiographic distribution. *Eur J Pharmacol* **1987**, *140*, 285-293, doi:Doi 10.1016/0014-2999(87)90285-8.

55. Kitabgi, P.; Kwan, C.Y.; Fox, J.E.T.; Vincent, J.P. Characterization of neurotensin binding to rat gastric smooth-muscle receptor-sites. *Peptides* **1984**, *5*, 917-923, doi:Doi 10.1016/0196-9781(84)90117-7.

56. The human protein atlas: NTSR2. Available online: https://www.proteinatlas.org/ENSG00000169006-NTSR2/tissue (accessed on November 3, 2022).

57. Ghaemimanesh, F.; Mehravar, M.; Milani, S.; Poursani, E.M.; Saliminejad, K. The multifaceted role of sortilin/neurotensin receptor 3 in human cancer development. *J Cell Physiol* **2021**, *236*, 6271-6281, doi:10.1002/jcp.30344.

58. Besserer-Offroy, E.; Brouillette, R.L.; Lavenus, S.; Froehlich, U.; Brumwell, A.; Murza, A.; Longpré, J.M.; Marsault, E.; Grandbois, M.; Sarret, P.; et al. The signaling signature of the neurotensin type 1 receptor with endogenous ligands. *Eur J Pharmacol* **2017**, *805*, 1-13, doi:10.1016/j.ejphar.2017.03.046.

59. Pelaprat, D. Interactions between neurotensin receptors and G proteins. *Peptides* **2006**, *27*, 2476-2487, doi:10.1016/j.peptides.2006.04.027.

60. Kleczkowska, P.; Lipkowski, A.W. Neurotensin and neurotensin receptors: Characteristic, structure-activity relationship and pain modulation-A review. *Eur J Pharmacol* **2013**, *716*, 54-60, doi:10.1016/j.ejphar.2013.03.004.

61. Saada, S.; Marget, P.; Fauchais, A.L.; Lise, M.C.; Chemin, G.; Sindou, P.; Martel, C.; Delpy, L.; Vidal, E.; Jaccard, A.; et al. Differential expression of neurotensin and specific receptors, NTSR1 and NTSR2, in normal and malignant human B lymphocytes. *J Immunol* **2012**, *189*, 5293-5303, doi:10.4049/jimmunol.1102937.

62. Swift, S.L.; Burns, J.E.; Maitland, N.J. Altered expression of neurotensin receptors is associated with the differentiation state of prostate cancer. *Cancer Res* **2010**, *70*, 347-356, doi:10.1158/0008-5472.Can-09-1252.

63. Ayala-Sarmiento, A.E.; Martinez-Fong, D.; Segovia, J. The internalization of neurotensin by the low-affinity neurotensin receptors (NTSR2 and vNTSR2) activates ERK 1/2 in glioma cells and allows neurotensin-polyplex transfection of tGAS1. *Cell Mol Neurobiol* **2015**, *35*, 785-795, doi:10.1007/s10571-015-0172-z.

64. Ouyang, Q.; Zhou, J.; Yang, W.; Cui, H.J.; Xu, M.H.; Yi, L. Oncogenic role of neurotensin and neurotensin receptors in various cancers. *Clin Exp Pharmacol P* **2017**, *44*, 841-846, doi:10.1111/1440-1681.12787.

65. Maoret, J.J.; Pospai, D.; Rouyer-Fessard, C.; Couvineau, A.; Laboisse, C.; Voisin, T.; Laburthe, M. Neurotensin receptor and its mRNA are expressed in many human colon cancer cell lines but not in normal colonic epithelium: Binding studies and RT-PCR experiments. *Biochem Biophys Res Commun* **1994**, *203*, 465-471, doi:10.1006/bbrc.1994.2205.

66. Reubi, J.C.; Waser, B.; Friess, H.; Büchler, M.; Laissue, J. Neurotensin receptors: A new marker for human ductal pancreatic adenocarcinoma. *Gut* **1998**, *42*, 546-550, doi:10.1136/gut.42.4.546.

67. Reubi, J.C.; Waser, B.; Schaer, J.C.; Laissue, J.A. Neurotensin receptors in human neoplasms: High incidence in Ewing's sarcomas. *Int J Cancer* **1999**, *82*, 213-218, doi:10.1002/(sici)1097-0215(19990719)82:2<213::aid-ijc11>3.0.co;2-8.

68. Bossard, C.; Souazé, F.; Jarry, A.; Bezieau, S.; Mosnier, J.F.; Forgez, P.; Laboisse, C.L. Over-expression of neurotensin high-affinity receptor 1 (NTS1) in relation with its ligand neurotensin (NT) and nuclear b-catenin in inflammatory bowel disease-related oncogenesis. *Peptides* **2007**, *28*, 2030-2035, doi:10.1016/j.peptides.2007.06.030.

69. Dupouy, S.; Mourra, N.; Doan, V.K.; Gompel, A.; Alifano, M.; Forgez, P. The potential use of the neurotensin high affinity receptor 1 as a biomarker for cancer progression and as a component of personalized medicine in selective cancers. *Biochimie* **2011**, *93*, 1369-1378, doi:10.1016/j.biochi.2011.04.024.

70. Maschauer, S.; Prante, O. Radiopharmaceuticals for imaging and endoradiotherapy of neurotensin receptor-positive tumors. *J Labelled Comp Radiopharm* **2018**, *61*, 309-325, doi:10.1002/jlcr.3581.

71. Baggiolini, M.; Dewald, B.; Moser, B. Interleukin-8 and related chemotactic cytokines--CXC and CC chemokines. *Adv Immunol* **1994**, *55*, 97-179.

72. Springer, T.A. Traffic signals on endothelium for lymphocyte recirculation and leukocyte emigration. *Annu Rev Physiol* **1995**, *57*, 827-872, doi:10.1146/annurev.ph.57.030195.004143.

73. Oppenheim, J.J.; Zachariae, C.O.; Mukaida, N.; Matsushima, K. Properties of the novel proinflammatory supergene "intercrine" cytokine family. *Annu Rev Immunol* **1991**, *9*, 617-648, doi:10.1146/annurev.iy.09.040191.003153.

74. Murphy, P.M.; Baggiolini, M.; Charo, I.F.; Hebert, C.A.; Horuk, R.; Matsushima, K.; Miller, L.H.; Oppenheim, J.J.; Power, C.A. International union of pharmacology. XXII. Nomenclature for chemokine receptors. *Pharmacol Rev* **2000**, *52*, 145-176.

75. Zlotnik, A.; Yoshie, O. The chemokine superfamily revisited. *Immunity* **2012**, *36*, 705-716, doi:10.1016/j.immuni.2012.05.008.

76. Nishikawa, S.; Ogawa, M.; Nishikawa, S.; Kunisada, T.; Kodama, H. B lymphopoiesis on stromal cell clone: Stromal cell clones acting on different stages of B cell differentiation. *Eur J Immunol* **1988**, *18*, 1767-1771, doi:10.1002/eji.1830181117.

77. Tashiro, K.; Tada, H.; Heilker, R.; Shirozu, M.; Nakano, T.; Honjo, T. Signal sequence trap: A cloning strategy for secreted proteins and type I membrane proteins. *Science* **1993**, *261*, 600-603, doi:10.1126/science.8342023.

78. Nagasawa, T.; Kikutani, H.; Kishimoto, T. Molecular cloning and structure of a pre-B-cell growth-stimulating factor. *Proc Natl Acad Sci U S A* **1994**, *91*, 2305-2309, doi:10.1073/pnas.91.6.2305.

79. Shirozu, M.; Nakano, T.; Inazawa, J.; Tashiro, K.; Tada, H.; Shinohara, T.; Honjo, T. Structure and chromosomal localization of the human stromal cell-derived factor 1 (SDF1) gene. *Genomics* **1995**, *28*, 495-500, doi:10.1006/geno.1995.1180.

80. Bleul, C.C.; Farzan, M.; Choe, H.; Parolin, C.; Clark-Lewis, I.; Sodroski, J.; Springer, T.A. The lymphocyte chemoattractant SDF-1 is a ligand for LESTR/fusin and blocks HIV-1 entry. *Nature* **1996**, *382*, 829-833, doi:10.1038/382829a0.

81. Oberlin, E.; Amara, A.; Bachelerie, F.; Bessia, C.; Virelizier, J.L.; Arenzana-Seisdedos, F.; Schwartz, O.; Heard, J.M.; Clark-Lewis, I.; Legler, D.F.; et al. The CXC chemokine SDF-1 is the ligand for LESTR/fusin and prevents infection by T-cell-line-adapted HIV-1. *Nature* **1996**, *382*, 833-835, doi:10.1038/382833a0.

82. Balkwill, F. Cancer and the chemokine network. *Nat Rev Cancer* **2004**, *4*, 540-550, doi:10.1038/nrc1388.

83. Nagasawa, T.; Tachibana, K.; Kishimoto, T. A novel CXC chemokine PBSF/SDF-1 and its receptor CXCR4: Their functions in development, hematopoiesis and HIV infection. *Semin Immunol* **1998**, *10*, 179-185, doi:10.1006/smim.1998.0128.

84. McGrath, K.E.; Koniski, A.D.; Maltby, K.M.; McGann, J.K.; Palis, J. Embryonic expression and function of the chemokine SDF-1 and its receptor, CXCR4. *Dev Biol* **1999**, *213*, 442-456, doi:10.1006/dbio.1999.9405.

85. Moepps, B.; Braun, M.; Knöpfle, K.; Dillinger, K.; Knöchel, W.; Gierschik, P. Characterization of a *Xenopus laevis* CXC chemokine receptor 4: Implications for hematopoietic cell development in the vertebrate embryo. *Eur J Immunol* **2000**, *30*, 2924-2934, doi:10.1002/1521-4141(200010)30:10<2924::AID-IMMU2924>3.0.CO;2-Y.

86. Kucia, M.; Jankowski, K.; Reca, R.; Wysoczynski, M.; Bandura, L.; Allendorf, D.J.; Zhang, J.; Ratajczak, J.; Ratajczak, M.Z. CXCR4-SDF-1 signalling, locomotion, chemotaxis and adhesion. *J Mol Histol* **2004**, *35*, 233-245, doi:10.1023/b:hijo.0000032355.66152.b8.

87. Nagasawa, T.; Hirota, S.; Tachibana, K.; Takakura, N.; Nishikawa, S.; Kitamura, Y.; Yoshida, N.; Kikutani, H.; Kishimoto, T. Defects of B-cell lymphopoiesis and

bone-marrow myelopoiesis in mice lacking the CXC chemokine PBSF/SDF-1. *Nature* **1996**, *382*, 635-638, doi:10.1038/382635a0.

88. Ma, Q.; Jones, D.; Borghesani, P.R.; Segal, R.A.; Nagasawa, T.; Kishimoto, T.; Bronson, R.T.; Springer, T.A. Impaired B-lymphopoiesis, myelopoiesis, and derailed cerebellar neuron migration in CXCR4- and SDF-1-deficient mice. *Proc Natl Acad Sci U S A* **1998**, *95*, 9448-9453, doi:10.1073/pnas.95.16.9448.

89. Zou, Y.R.; Kottmann, A.H.; Kuroda, M.; Taniuchi, I.; Littman, D.R. Function of the chemokine receptor CXCR4 in haematopoiesis and in cerebellar development. *Nature* **1998**, *393*, 595-599, doi:10.1038/31269.

90. Tachibana, K.; Hirota, S.; Iizasa, H.; Yoshida, H.; Kawabata, K.; Kataoka, Y.; Kitamura, Y.; Matsushima, K.; Yoshida, N.; Nishikawa, S.; et al. The chemokine receptor CXCR4 is essential for vascularization of the gastrointestinal tract. *Nature* **1998**, *393*, 591-594, doi:10.1038/31261.

91. Teixidó, J.; Martínez-Moreno, M.; Díaz-Martínez, M.; Sevilla-Movilla, S. The good and bad faces of the CXCR4 chemokine receptor. *Int J Biochem Cell Biol* **2018**, *95*, 121-131, doi:10.1016/j.biocel.2017.12.018.

92. Tsutsumi, H.; Tanaka, T.; Ohashi, N.; Masuno, H.; Tamamura, H.; Hiramatsu, K.; Araki, T.; Ueda, S.; Oishi, S.; Fujii, N. Therapeutic potential of the chemokine receptor CXCR4 antagonists as multifunctional agents. *Biopolymers* **2007**, *88*, 279-289, doi:10.1002/bip.20653.

93. Ganju, R.K.; Brubaker, S.A.; Meyer, J.; Dutt, P.; Yang, Y.; Qin, S.; Newman, W.; Groopman, J.E. The a-chemokine, stromal cell-derived factor-1a, binds to the transmembrane G-protein-coupled CXCR-4 receptor and activates multiple signal transduction pathways. *J Biol Chem* **1998**, *273*, 23169-23175, doi:10.1074/jbc.273.36.23169.

94. Horuk, R. Chemokine receptors. *Cytokine Growth Factor Rev* **2001**, *12*, 313-335, doi:10.1016/s1359-6101(01)00014-4.

95. Mellado, M.; Rodríguez-Frade, J.M.; Mañes, S.; Martínez, A.C. Chemokine signaling and functional responses: The role of receptor dimerization and TK pathway activation. *Annu Rev Immunol* **2001**, *19*, 397-421, doi:10.1146/annurev.immunol.19.1.397.

96. Balkwill, F. The significance of cancer cell expression of the chemokine receptor CXCR4. *Semin Cancer Biol* **2004**, *14*, 171-179, doi:10.1016/j.semcancer.2003.10.003.

97. Loetscher, M.; Geiser, T.; O'Reilly, T.; Zwahlen, R.; Baggiolini, M.; Moser, B. Cloning of a human seven-transmembrane domain receptor, LESTR, that is highly expressed in leukocytes. *J Biol Chem* **1994**, *269*, 232-237.

98. Kuil, J.; Buckle, T.; van Leeuwen, F.W. Imaging agents for the chemokine receptor 4 (CXCR4). *Chem Soc Rev* **2012**, *41*, 5239-5261, doi:10.1039/c2cs35085h.

99. Cojoc, M.; Peitzsch, C.; Trautmann, F.; Polishchuk, L.; Telegeev, G.D.; Dubrovska, A. Emerging targets in cancer management: Role of the CXCL12/CXCR4 axis. *Onco Targets Ther* **2013**, *6*, 1347-1361, doi:10.2147/OTT.S36109.

100. Bianchi, M.E.; Mezzapelle, R. The chemokine receptor CXCR4 in cell proliferation and tissue regeneration. *Front Immunol* **2020**, *11*, 2109, doi:10.3389/fimmu.2020.02109.

101. Müller, A.; Homey, B.; Soto, H.; Ge, N.; Catron, D.; Buchanan, M.E.; McClanahan, T.; Murphy, E.; Yuan, W.; Wagner, S.N.; et al. Involvement of chemokine receptors in breast cancer metastasis. *Nature* **2001**, *410*, 50-56, doi:10.1038/35065016.

102. Taichman, R.S.; Cooper, C.; Keller, E.T.; Pienta, K.J.; Taichman, N.S.; McCauley, L.K. Use of the stromal cell-derived factor-1/CXCR4 pathway in prostate cancer metastasis to bone. *Cancer Res* **2002**, *62*, 1832-1837.

103. Sun, Y.X.; Wang, J.; Shelburne, C.E.; Lopatin, D.E.; Chinnaiyan, A.M.; Rubin, M.A.; Pienta, K.J.; Taichman, R.S. Expression of CXCR4 and CXCL12 (SDF-1) in human prostate cancers (PCa) in vivo. *J Cell Biochem* **2003**, *89*, 462-473, doi:10.1002/jcb.10522.

104. Kucia, M.; Reca, R.; Miekus, K.; Wanzeck, J.; Wojakowski, W.; Janowska-Wieczorek, A.; Ratajczak, J.; Ratajczak, M.Z. Trafficking of normal stem cells and metastasis of cancer stem cells involve similar mechanisms: Pivotal role of the SDF-1-CXCR4 axis. *Stem Cells* **2005**, *23*, 879-894, doi:10.1634/stemcells.2004-0342.

105. Furusato, B.; Mohamed, A.; Uhlén, M.; Rhim, J.S. CXCR4 and cancer. *Pathol Int* **2010**, *60*, 497-505, doi:10.1111/j.1440-1827.2010.02548.x.

106. Tanaka, T.; Bai, Z.; Srinoulprasert, Y.; Yang, B.G.; Hayasaka, H.; Miyasaka, M. Chemokines in tumor progression and metastasis. *Cancer Sci* **2005**, *96*, 317-322, doi:10.1111/j.1349-7006.2005.00059.x.

107. Zlotnik, A. Involvement of chemokine receptors in organ-specific metastasis. *Contrib Microbiol* **2006**, *13*, 191-199, doi:10.1159/000092973.

108. Zhou, Y.; Larsen, P.H.; Hao, C.; Yong, V.W. CXCR4 is a major chemokine receptor on glioma cells and mediates their survival. *J Biol Chem* **2002**, *277*, 49481-49487, doi:10.1074/jbc.M206222200.

109. Broxmeyer, H.E.; Cooper, S.; Kohli, L.; Hangoc, G.; Lee, Y.; Mantel, C.; Clapp, D.W.; Kim, C.H. Transgenic expression of stromal cell-derived factor-1/CXC chemokine ligand 12 enhances myeloid progenitor cell survival/antiapoptosis in vitro in response to growth factor withdrawal and enhances myelopoiesis in vivo. *J Immunol* **2003**, *170*, 421-429, doi:10.4049/jimmunol.170.1.421.

110. Feng, Y.; Broder, C.C.; Kennedy, P.E.; Berger, E.A. HIV-1 entry cofactor: Functional cDNA cloning of a seven-transmembrane, G protein-coupled receptor. *Science* **1996**, *272*, 872-877, doi:10.1126/science.272.5263.872.

111. Neidleman, J.; Luo, X.; George, A.F.; McGregor, M.; Yang, J.; Yun, C.; Murray, V.; Gill, G.; Greene, W.C.; Vasquez, J.; et al. Distinctive features of SARS-CoV-2-specific T cells predict recovery from severe COVID-19. *Cell reports* **2021**, *36*, 109414, doi:10.1101/2021.01.22.21250054.

112. Daoud, S.; Taha, M. Ligand-based modeling of CXC chemokine receptor 4 and identification of inhibitors of novel chemotypes as potential leads towards new anti-

COVID-19 treatments. *Med Chem* **2022**, *18*, 871-883, doi:10.2174/1573406418666220118153541.

113. Khalil, B.A.; Elemam, N.M.; Maghazachi, A.A. Chemokines and chemokine receptors during COVID-19 infection. *Comput Struct Biotechnol J* **2021**, *19*, 976-988, doi:10.1016/j.csbj.2021.01.034.

114. Silvin, A.; Chapuis, N.; Dunsmore, G.; Goubet, A.G.; Dubuisson, A.; Derosa, L.; Almire, C.; Hénon, C.; Kosmider, O.; Droin, N.; et al. Elevated calprotectin and abnormal myeloid cell subsets discriminate severe from mild COVID-19. *Cell* **2020**, *182*, 1401-1418, doi:10.1016/j.cell.2020.08.002.

115. Mamazhakypov, A.; Viswanathan, G.; Lawrie, A.; Schermuly, R.T.; Rajagopal, S. The role of chemokines and chemokine receptors in pulmonary arterial hypertension. *Br J Pharmacol* **2021**, *178*, 72-89, doi:10.1111/bph.14826.

116. Freidinger, R.M. Non-peptide ligands for peptide receptors. *Trends Pharmacol Sci* **1989**, *10*, 270-274, doi:10.1016/0165-6147(89)90026-6.

117. Betancur, C.; Canton, M.; Burgos, A.; Labeeuw, B.; Gully, D.; Rostène, W.; Pelaprat, D. Characterization of binding sites of a new neurotensin receptor antagonist, [^{3}H]SR 142948A, in the rat brain. *Eur J Pharmacol* **1998**, *343*, 67-77, doi:10.1016/s0014-2999(97)01510-0.

118. Ginj, M.; Zhang, H.; Waser, B.; Cescato, R.; Wild, D.; Wang, X.; Erchegyi, J.; Rivier, J.; Maecke, H.R.; Reubi, J.C. Radiolabeled somatostatin receptor antagonists are preferable to agonists for *in vivo* peptide receptor targeting of tumors. *Proc Natl Acad Sci U S A* **2006**, *103*, 16436-16441, doi:10.1073/pnas.0607761103.

119. Wild, D.; Fani, M.; Behe, M.; Brink, I.; Rivier, J.E.; Reubi, J.C.; Maecke, H.R.; Weber, W.A. First clinical evidence that imaging with somatostatin receptor antagonists is feasible. *J Nucl Med* **2011**, *52*, 1412-1417, doi:10.2967/jnumed.111.088922.

120. Dash, A.; Chakraborty, S.; Pillai, M.R.; Knapp, F.F., Jr. Peptide receptor radionuclide therapy: An overview. *Cancer Biother Radiopharm* **2015**, *30*, 47-71, doi:10.1089/cbr.2014.1741.

121. Schottelius, M.; Wester, H.J. Molecular imaging targeting peptide receptors. *Methods* **2009**, *48*, 161-177, doi:10.1016/j.ymeth.2009.03.012.

122. Cescato, R.; Maina, T.; Nock, B.; Nikolopoulou, A.; Charalambidis, D.; Piccand, V.; Reubi, J.C. Bombesin receptor antagonists may be preferable to agonists for tumor targeting. *J Nucl Med* **2008**, *49*, 318-326, doi:10.2967/jnumed.107.045054.

123. Fani, M.; Maecke, H.R.; Okarvi, S.M. Radiolabeled peptides: Valuable tools for the detection and treatment of cancer. *Theranostics* **2012**, *2*, 481-501, doi:10.7150/thno.4024.

124. Lang, C.; Maschauer, S.; Hübner, H.; Gmeiner, P.; Prante, O. Synthesis and evaluation of a ^{18}F-labeled diarylpyrazole glycoconjugate for the imaging of NTS1-positive tumors. *J Med Chem* **2013**, *56*, 9361-9365, doi:10.1021/jm401491e.

125. Wild, D.; Fani, M.; Fischer, R.; Del Pozzo, L.; Kaul, F.; Krebs, S.; Fischer, R.; Rivier, J.E.; Reubi, J.C.; Maecke, H.R.; et al. Comparison of somatostatin receptor agonist and antagonist for peptide receptor radionuclide therapy: A pilot study. *J Nucl Med* **2014**, *55*, 1248-1252, doi:10.2967/jnumed.114.138834.

126. Ermisch, A.; Barth, T.; Rühle, H.J.; Skopková, J.; Hrbas, P.; Landgraf, R. On the blood-brain barrier to peptides: Accumulation of labelled vasopressin, DesGlyNH$_2$-vasopressin and oxytocin by brain regions. *Endocrinol Exp* **1985**, *19*, 29-37.

127. Pardridge, W.M. CNS drug design based on principles of blood-brain barrier transport. *J Neurochem* **1998**, *70*, 1781-1792, doi:10.1046/j.1471-4159.1998.70051781.x.

128. Gully, D.; Maffrand, J.P.; Soubrié, P.; Rostène, W.; Kitabgi, P.; Le Fur, G. [Neurotensin receptor antagonists and therapeutical perspectives]. *Therapie* **1995**, *50*, 5-7.

129. Lohith, T.G.; Zoghbi, S.S.; Morse, C.L.; Araneta, M.F.; Barth, V.N.; Gœbl, N.A.; Tauscher, J.T.; Pike, V.W.; Innis, R.B.; Fujita, M. Brain and whole-body imaging of nociceptin/orphanin FQ peptide receptor in humans using the PET ligand ^{11}C-NOP-1A. *J Nucl Med* **2012**, *53*, 385-392, doi:10.2967/jnumed.111.097162.

130. Renard, E.; Moreau, M.; Bellaye, P.S.; Guillemin, M.; Collin, B.; Prignon, A.; Denat, F.; Goncalves, V. Positron emission tomography imaging of neurotensin receptor-positive tumors with ^{68}Ga-labeled antagonists: The chelate makes the difference again. *J Med Chem* **2021**, *64*, 8564-8578, doi:10.1021/acs.jmedchem.1c00523.

131. Bodei, L.; Paganelli, G.; Mariani, G. Receptor radionuclide therapy of tumors: A road from basic research to clinical applications. *J Nucl Med* **2006**, *47*, 375-377.

132. Cescato, R.; Schulz, S.; Waser, B.; Eltschinger, V.; Rivier, J.E.; Wester, H.J.; Culler, M.; Ginj, M.; Liu, Q.; Schonbrunn, A.; et al. Internalization of sst$_2$, sst$_3$, and sst$_5$ receptors: Effects of somatostatin agonists and antagonists. *J Nucl Med* **2006**, *47*, 502-511.

133. Lee, S.; Xie, J.; Chen, X. Peptide-based probes for targeted molecular imaging. *Biochemistry* **2010**, *49*, 1364-1376, doi:10.1021/bi901135x.

134. Jenssen, H.; Aspmo, S.I. Serum stability of peptides. In *Peptide-based drug design*, Otvos, L., Ed.; Methods in molecular biology; Humana Press: New York, NY, 2008; pp. 177-186.

135. Tasdemiroglu, Y.; Gourdie, R.G.; He, J.Q. *In vivo* degradation forms, anti-degradation strategies, and clinical applications of therapeutic peptides in non-infectious chronic diseases. *Eur J Pharmacol* **2022**, *932*, 175192, doi:10.1016/j.ejphar.2022.175192.

136. Fanelli, R.; Chastel, A.; Previti, S.; Hindié, E.; Vimont, D.; Zanotti-Fregonara, P.; Fernandez, P.; Garrigue, P.; Lamare, F.; Schollhammer, R.; et al. Silicon-containing neurotensin analogues as radiopharmaceuticals for NTS$_1$-positive tumors imaging. *Bioconjugate Chem* **2020**, *31*, 2339-2349, doi:10.1021/acs.bioconjchem.0c00419.

137. Gully, D.; Canton, M.; Boigegrain, R.; Jeanjean, F.; Molimard, J.C.; Poncelet, M.; Gueudet, C.; Heaulme, M.; Leyris, R.; Brouard, A.; et al. Biochemical and pharmacological profile of a potent and selective nonpeptide antagonist of the neurotensin receptor. *Proc Natl Acad Sci U S A* **1993**, *90*, 65-69, doi:10.1073/pnas.90.1.65.

138. Schulz, J.; Rohracker, M.; Stiebler, M.; Goldschmidt, J.; Grosser, O.S.; Osterkamp, F.; Pethe, A.; Reineke, U.; Smerling, C.; Amthauer, H. Comparative evaluation of the biodistribution profiles of a series of nonpeptidic neurotensin receptor-1 antagonists reveals a promising candidate for theranostic applications. *J Nucl Med* **2016**, *57*, 1120-1123, doi:10.2967/jnumed.115.170530.

139. Schulz, J.; Rohracker, M.; Stiebler, M.; Goldschmidt, J.; Stöber, F.; Noriega, M.; Pethe, A.; Lukas, M.; Osterkamp, F.; Reineke, U.; et al. Proof of therapeutic efficacy of a ^{177}Lu-labeled neurotensin receptor 1 antagonist in a colon carcinoma xenograft model. *J Nucl Med* **2017**, *58*, 936-941, doi:10.2967/jnumed.116.185140.

140. Baum, R.P.; Singh, A.; Schuchardt, C.; Kulkarni, H.R.; Klette, I.; Wiessalla, S.; Osterkamp, F.; Reineke, U.; Smerling, C. ^{177}Lu-3BP-227 for neurotensin receptor 1-targeted therapy of metastatic pancreatic adenocarcinoma - first clinical results. *J Nucl Med* **2018**, *59*, 809-814, doi:10.2967/jnumed.117.193847.

141. Osterkamp, F.; Smerling, C.; Reineke, U.; Haase, C.; Ungewiss, J. Neurotensin receptor ligands. US10961199B2, March 30 2021.

142. Clinical Trials.gov: Study to evaluate the safety and activity (including distribution) of ^{177}Lu-3BP-227 in subjects with solid tumours expressing neurotensin receptor type 1. Available online: https://clinicaltrials.gov/ct2/show/results/NCT03525392 (accessed on November 3, 2022).

143. Fujii, N.; Oishi, S.; Hiramatsu, K.; Araki, T.; Ueda, S.; Tamamura, H.; Otaka, A.; Kusano, S.; Terakubo, S.; Nakashima, H.; et al. Molecular-size reduction of a potent CXCR4-chemokine antagonist using orthogonal combination of conformation- and sequence-based libraries. *Angew Chem Int Ed Engl* **2003**, *42*, 3251-3253, doi:10.1002/anie.200351024.

144. Demmer, O.; Gourni, E.; Schumacher, U.; Kessler, H.; Wester, H.J. PET imaging of CXCR4 receptors in cancer by a new optimized ligand. *ChemMedChem* **2011**, *6*, 1789-1791, doi:10.1002/cmdc.201100320.

145. Herrmann, K.; Lapa, C.; Wester, H.J.; Schottelius, M.; Schiepers, C.; Eberlein, U.; Bluemel, C.; Keller, U.; Knop, S.; Kropf, S.; et al. Biodistribution and radiation dosimetry for the chemokine receptor CXCR4-targeting probe ^{68}Ga-pentixafor. *J Nucl Med* **2015**, *56*, 410-416, doi:10.2967/jnumed.114.151647.

146. Buck, A.K.; Haug, A.; Dreher, N.; Lambertini, A.; Higuchi, T.; Lapa, C.; Weich, A.; Pomper, M.G.; Wester, H.J.; Zehnder, A.; et al. Imaging of C-X-C motif chemokine receptor 4 expression in 690 patients with solid or hematologic neoplasms using ^{68}Ga-pentixaFor PET. *J Nucl Med* **2022**, *63*, 1687-1692, doi:10.2967/jnumed.121.263693.

147. Lapa, C.; Lückerath, K.; Rudelius, M.; Schmid, J.S.; Schoene, A.; Schirbel, A.; Samnick, S.; Pelzer, T.; Buck, A.K.; Kropf, S.; et al. [^{68}Ga]Pentixafor-PET/CT for imaging of chemokine receptor 4 expression in small cell lung cancer--initial experience. *Oncotarget* **2016**, *7*, 9288-9295, doi:10.18632/oncotarget.7063.

148. Lapa, C.; Schreder, M.; Schirbel, A.; Samnick, S.; Kortüm, K.M.; Herrmann, K.; Kropf, S.; Einsele, H.; Buck, A.K.; Wester, H.J.; et al. [^{68}Ga]Pentixafor-PET/CT for imaging of chemokine receptor CXCR4 expression in multiple myeloma - Comparison to [^{18}F]FDG and laboratory values. *Theranostics* **2017**, *7*, 205-212, doi:10.7150/thno.16576.

149. Walenkamp, A.M.E.; Lapa, C.; Herrmann, K.; Wester, H.J. CXCR4 ligands: The next big hit? *J Nucl Med* **2017**, *58*, 77S-82S, doi:10.2967/jnumed.116.186874.

150. Habringer, S.; Lapa, C.; Herhaus, P.; Schottelius, M.; Istvanffy, R.; Steiger, K.; Slotta-Huspenina, J.; Schirbel, A.; Hänscheid, H.; Kircher, S.; et al. Dual targeting of acute leukemia and supporting niche by CXCR4-directed theranostics. *Theranostics* **2018**, *8*, 369-383, doi:10.7150/thno.21397.

151. Herhaus, P.; Lipkova, J.; Lammer, F.; Yakushev, I.; Vag, T.; Slotta-Huspenina, J.; Habringer, S.; Lapa, C.; Pukrop, T.; Hellwig, D.; et al. CXCR4-targeted PET imaging of central nervous system B-cell lymphoma. *J Nucl Med* **2020**, *61*, 1765-1771, doi:10.2967/jnumed.120.241703.

152. Mayerhoefer, M.E.; Raderer, M.; Lamm, W.; Pichler, V.; Pfaff, S.; Weber, M.; Kiesewetter, B.; Hacker, M.; Kazianka, L.; Staber, P.B.; et al. CXCR4 PET imaging of mantle cell lymphoma using [^{68}Ga]Pentixafor: Comparison with [^{18}F]FDG-PET. *Theranostics* **2021**, *11*, 567-578, doi:10.7150/thno.48620.

153. FDA approval letter for Mozobil (plerixafor). Application numer: 022311. December 15, 2008. Availabe online: https://www.accessdata.fda.gov/drugsatfda_docs/nda/2008/022311s000TOC.cfm (accessed on November 3, 2022).

154. EMA authorization letter for Mozobil (plerixafor). Application number: EMA/254533/2019. July 30, 2009. Available online: https://www.ema.europa.eu/en/medicines/human/EPAR/mozobil#authorisation-details-section (accessed on November 3, 2022).

155. De Clercq, E.; Yamamoto, N.; Pauwels, R.; Balzarini, J.; Witvrouw, M.; Devreese, K.; Debyser, Z.; Rosenwirth, B.; Peichl, P.; Datema, R.; et al. Highly potent and selective inhibition of human immunodeficiency virus by the bicyclam derivative JM3100. *Antimicrob Agents Ch* **1994**, *38*, 668-674, doi:Doi 10.1128/Aac.38.4.668.

156. Werle, M.; Bernkop-Schnürch, A. Strategies to improve plasma half life time of peptide and protein drugs. *Amino Acids* **2006**, *30*, 351-367, doi:10.1007/s00726-005-0289-3.

157. Pernot, M.; Vanderesse, R.; Frochot, C.; Guillemin, F.; Barberi-Heyob, M. Stability of peptides and therapeutic success in cancer. *Expert Opin Drug Metab Toxicol* **2011**, *7*, 793-802, doi:10.1517/17425255.2011.574126.

158. Kitabgi, P.; De Nadai, F.; Rovère, C.; Bidard, J.N. Biosynthesis, maturation, release, and degradation of neurotensin and neuromedin N. *Ann N Y Acad Sci* **1992**, *668*, 30-42, doi:10.1111/j.1749-6632.1992.tb27337.x.

159. Davis, T.P.; Konings, P.N. Peptidases in the CNS: Formation of biologically active, receptor-specific peptide fragments. *Crit Rev Neurobiol* **1993**, *7*, 163-174.

160. García-Garayoa, E.; Allemann-Tannahill, L.; Bläuenstein, P.; Willmann, M.; Carrel-Rémy, N.; Tourwé, D.; Iterbeke, K.; Conrath, P.; Schubiger, P.A. *In vitro* and *in vivo* evaluation of new radiolabeled neurotensin(8-13) analogues with high affinity for NT1 receptors. *Nucl Med Biol* **2001**, *28*, 75-84, doi:10.1016/s0969-8051(00)00190-6.

161. Bläuenstein, P.; García-Garayoa, E.; Rüegg, D.; Blanc, A.; Tourwé, D.; Beck-Sickinger, A.; Schubiger, P.A. Improving the tumor uptake of ^{99m}Tc-labeled neuropeptides using stabilized peptide analogues. *Cancer Biother Radiopharm* **2004**, *19*, 181-188, doi:10.1089/108497804323071959.

162. Cusack, B.; McCormick, D.J.; Pang, Y.P.; Souder, T.; Garcia, R.; Fauq, A.; Richelson, E. Pharmacological and biochemical profiles of unique neurotensin 8-13 analogs exhibiting species selectivity, stereoselectivity, and superagonism. *J Biol Chem* **1995**, *270*, 18359-18366, doi:10.1074/jbc.270.31.18359.

163. Maina, T.; Nikolopoulou, A.; Stathopoulou, E.; Galanis, A.S.; Cordopatis, P.; Nock, B.A. [^{99m}Tc]Demotensin 5 and 6 in the NTS1-R-targeted imaging of tumours: Synthesis and preclinical results. *Eur J Nucl Med Mol Imaging* **2007**, *34*, 1804-1814, doi:10.1007/s00259-007-0489-z.

164. Boules, M.; Liang, Y.; Briody, S.; Miura, T.; Fauq, I.; Oliveros, A.; Wilson, M.; Khaniyev, S.; Williams, K.; Li, Z.; et al. NT79: A novel neurotensin analog with selective behavioral effects. *Brain Res* **2010**, *1308*, 35-46, doi:10.1016/j.brainres.2009.10.050.

165. Einsiedel, J.; Held, C.; Hervet, M.; Plomer, M.; Tschammer, N.; Hübner, H.; Gmeiner, P. Discovery of highly potent and neurotensin receptor 2 selective neurotensin mimetics. *J Med Chem* **2011**, *54*, 2915-2923, doi:10.1021/jm200006c.

166. Held, C.; Plomer, M.; Hübner, H.; Meltretter, J.; Pischetsrieder, M.; Gmeiner, P. Development of a metabolically stable neurotensin receptor 2 (NTS2) ligand. *ChemMedChem* **2013**, *8*, 75-81, doi:10.1002/cmdc.201200376.

167. Maschauer, S.; Greff, C.; Einsiedel, J.; Ott, J.; Tripal, P.; Hübner, H.; Gmeiner, P.; Prante, O. Improved radiosynthesis and preliminary in vivo evaluation of a ^{18}F-labeled glycopeptide-peptoid hybrid for PET imaging of neurotensin receptor 2. *Bioorgan Med Chem* **2015**, *23*, 4026-4033, doi:10.1016/j.bmc.2015.01.053.

168. Bruehlmeier, M.; García-Garayoa, E.; Blanc, A.; Holzer, B.; Gergely, S.; Tourwé, D.; Schubiger, P.A.; Bläuenstein, P. Stabilization of neurotensin analogues: Effect on peptide catabolism, biodistribution and tumor binding. *Nucl Med Biol* **2002**, *29*, 321-327, doi:10.1016/s0969-8051(01)00304-3.

169. Mascarin, A.; Valverde, I.E.; Vomstein, S.; Mindt, T.L. 1,2,3-Triazole stabilized neurotensin-based radiopeptidomimetics for improved tumor targeting. *Bioconjugate Chem* **2015**, *26*, 2143-2152, doi:10.1021/acs.bioconjchem.5b00444.

170. Maschauer, S.; Einsiedel, J.; Hübner, H.; Gmeiner, P.; Prante, O. ^{18}F- and ^{68}Ga-labeled neurotensin peptides for PET imaging of neurotensin receptor 1. *J Med Chem* **2016**, *59*, 6480-6492, doi:10.1021/acs.jmedchem.6b00675.

171. Mascarin, A.; Valverde, I.E.; Mindt, T.L. Structure-activity relationship studies of amino acid substitutions in radiolabeled neurotensin conjugates. *ChemMedChem* **2016**, *11*, 102-107, doi:10.1002/cmdc.201500468.

172. Kokko, K.P.; Hadden, M.K.; Orwig, K.S.; Mazella, J.; Dix, T.A. In vitro analysis of stable, receptor-selective neurotensin[8-13] analogues. *J Med Chem* **2003**, *46*, 4141-4148, doi:10.1021/jm0300633.

173. Nock, B.A.; Nikolopoulou, A.; Reubi, J.C.; Maes, V.; Conrath, P.; Tourwé, D.; Maina, T. Toward stable N_4-modified neurotensins for NTS1-receptor-targeted tumor imaging with ^{99m}Tc. *J Med Chem* **2006**, *49*, 4767-4776, doi:10.1021/jm060415g.

174. Alshoukr, F.; Rosant, C.; Maes, V.; Abdelhak, J.; Raguin, O.; Burg, S.; Sarda, L.; Barbet, J.; Tourwé, D.; Pelaprat, D.; et al. Novel neurotensin analogues for radioisotope targeting to neurotensin receptor-positive tumors. *Bioconjug Chem* **2009**, *20*, 1602-1610, doi:10.1021/bc900151z.

175. Richelson, E.; McCormick, D.J.; Pang, Y.P.; Phillips, K.S. Peptide analogs that are potent and selective for human neurotensin receptor subtype 2. US2009/0062212A1, March 5 2009.

176. Magafa, V.; Matsoukas, M.T.; Karageorgos, V.; Dermitzaki, E.; Exarchakou, R.; Stylos, E.K.; Pardalos, M.; Margioris, A.N.; Varvounis, G.; Tzakos, A.G.; et al. Novel stable analogues of the neurotensin C-terminal hexapeptide containing unnatural amino acids. *Amino Acids* **2019**, *51*, 1009-1022, doi:10.1007/s00726-019-02741-2.

177. Pang, Y.P.; Cusack, B.; Groshan, K.; Richelson, E. Proposed ligand binding site of the transmembrane receptor for neurotensin(8-13). *J Biol Chem* **1996**, *271*, 15060-15068, doi:10.1074/jbc.271.25.15060.

178. Barroso, S.; Richard, F.; Nicolas-Ethève, D.; Reversat, J.L.; Bernassau, J.M.; Kitabgi, P.; Labbé-Jullié, C. Identification of residues involved in neurotensin binding and modeling of the agonist binding site in neurotensin receptor 1. *J Biol Chem* **2000**, *275*, 328-336, doi:10.1074/jbc.275.1.328.

179. Adessi, C.; Soto, C. Converting a peptide into a drug: Strategies to improve stability and bioavailability. *Curr Med Chem* **2002**, *9*, 963-978, doi:10.2174/0929867024606731.

180. Räder, A.F.B.; Reichart, F.; Weinmüller, M.; Kessler, H. Improving oral bioavailability of cyclic peptides by *N*-methylation. *Bioorg Med Chem* **2018**, *26*, 2766-2773, doi:10.1016/j.bmc.2017.08.031.

181. Marsault, E.; Peterson, M.L. Macrocycles are great cycles: Applications, opportunities, and challenges of synthetic macrocycles in drug discovery. *J Med Chem* **2011**, *54*, 1961-2004, doi:10.1021/jm1012374.

182. Konieczny, A.; Conrad, M.; Ertl, F.J.; Gleixner, J.; Gattor, A.O.; Grätz, L.; Schmidt, M.F.; Neu, E.; Horn, A.H.C.; Wifling, D.; et al. N-terminus to arginine side-chain cyclization of linear peptidic neuropeptide Y Y_4 receptor ligands results in picomolar binding constants. *J Med Chem* **2021**, *64*, 16746-16769, doi:10.1021/acs.jmedchem.1c01574.

183. Abdalla, M.A.; McGaw, L.J. Natural cyclic peptides as an attractive modality for therapeutics: A mini review. *Molecules* **2018**, *23*, 2080, doi:10.3390/molecules23082080.

184. Price, D.A.; Mathiowetz, A.M.; Liras, S. Designing orally bioavailable peptide and peptoid macrocycles. In *Practical medicinal chemistry with macrocycles: Design, synthesis, and case studies*, 1st ed.; Marsault, E., Peterson, M.L., Eds.; Wiley Online Library: 2017; pp. 59-76.

185. Zorzi, A.; Deyle, K.; Heinis, C. Cyclic peptide therapeutics: Past, present and future. *Curr Opin Chem Biol* **2017**, *38*, 24-29, doi:10.1016/j.cbpa.2017.02.006.

186. García-Garayoa, E.; Maes, V.; Bläuenstein, P.; Blanc, A.; Hohn, A.; Tourwé, D.; Schubiger, P.A. Double-stabilized neurotensin analogues as potential radiopharmaceuticals for NTR-positive tumors. *Nucl Med Biol* **2006**, *33*, 495-503, doi:10.1016/j.nucmedbio.2006.01.007.

187. Maes, V.; García-Garayoa, E.; Bläuenstein, P.; Tourwé, D. Novel ^{99m}Tc-labeled neurotensin analogues with optimized biodistribution properties. *J Med Chem* **2006**, *49*, 1833-1836, doi:10.1021/jm051172f.

188. Alshoukr, F.; Prignon, A.; Brans, L.; Jallane, A.; Mendes, S.; Talbot, J.N.; Tourwé, D.; Barbet, J.; Gruaz-Guyon, A. Novel DOTA-neurotensin analogues for ^{111}In scintigraphy and ^{68}Ga PET imaging of neurotensin receptor-positive tumors. *Bioconjug Chem* **2011**, *22*, 1374-1385, doi:10.1021/bc200078p.

189. Lugrin, D.; Vecchini, F.; Doulut, S.; Rodriguez, M.; Martinez, J.; Kitabgi, P. Reduced peptide bond pseudopeptide analogs of neurotensin: Binding and biological activities, and in vitro metabolic stability. *Eur J Pharmacol* **1991**, *205*, 191-198, doi:Doi 10.1016/0014-2999(91)90819-C.

190. Einsiedel, J.; Hübner, H.; Hervet, M.; Härterich, S.; Koschatzky, S.; Gmeiner, P. Peptide backbone modifications on the C-terminal hexapeptide of neurotensin. *Bioorg Med Chem Lett* **2008**, *18*, 2013-2018, doi:10.1016/j.bmcl.2008.01.110.

191. Henry, J.A.; Horwell, D.C.; Meecham, K.G.; Rees, D.C. A structure-affinity study of the amino acid side-chains in neurotensin: N and C-terminal deletions and Ala-scan. *Bioorg Med Chem Lett* **1993**, *3*, 949-952, doi:Doi 10.1016/S0960-894x(00)80698-8.

192. García-Garayoa, E.; Bläuenstein, P.; Bruehlmeier, M.; Blanc, A.; Iterbeke, K.; Conrath, P.; Tourwé, D.; Schubiger, P.A. Preclinical evaluation of a new, stabilized neurotensin(8-13) pseudopeptide radiolabeled with ^{99m}Tc. *J Nucl Med* **2002**, *43*, 374-383.

193. Orwig, K.S.; Lassetter, M.R.; Hadden, M.K.; Dix, T.A. Comparison of N-terminal modifications on neurotensin(8-13) analogues correlates peptide stability but not

binding affinity with in vivo efficacy. *J Med Chem* **2009**, *52*, 1803-1813, doi:10.1021/jm801072v.

194. Wester, H.J. Nuclear imaging probes: From bench to bedside. *Clin Cancer Res* **2007**, *13*, 3470-3481, doi:10.1158/1078-0432.CCR-07-0264.

195. Vaquero, J.J.; Kinahan, P. Positron emission tomography: Current challenges and opportunities for technological advances in clinical and preclinical imaging systems. *Annu Rev Biomed Eng* **2015**, *17*, 385-414, doi:10.1146/annurev-bioeng-071114-040723.

196. *Positron emission tomography*; Bailey, D.L., Townsend, D.W., Valk, P.E., Maisey, M.N., Eds.; Springer: London, UK, 2005.

197. Heppeler, A.; André, J.P.; Buschmann, I.; Wang, X.; Reubi, J.C.; Hennig, M.; Kaden, T.A.; Maecke, H.R. Metal-ion-dependent biological properties of a chelator-derived somatostatin analogue for tumour targeting. *Chemistry* **2008**, *14*, 3026-3034, doi:10.1002/chem.200701264.

198. Kumar, K.; Ghosh, A. ^{18}F-AlF Labeled peptide and protein conjugates as positron emission tomography imaging pharmaceuticals. *Bioconjug Chem* **2018**, *29*, 953-975, doi:10.1021/acs.bioconjchem.7b00817.

199. Lammertsma, A.A. Essentials of quantitative imaging with PET. In *Nuclear medicine textbook*, Volterrani, D., Ed.; Springer Nature: Switzerland, 2019; pp. 219-233.

200. Salvadori, P.A.; Filidei, E.; Giorgetti, A. Positron-emitting radiopharmaceuticals. In *Nuclear medicine textbook*, Volterrani, D., Ed.; Springer Nature: Switzerland, 2019; pp. 57-98.

201. Ametamey, S.M.; Honer, M.; Schubiger, P.A. Molecular imaging with PET. *Chem Rev* **2008**, *108*, 1501-1516, doi:10.1021/cr0782426.

202. Correia, J.D.; Paulo, A.; Raposinho, P.D.; Santos, I. Radiometallated peptides for molecular imaging and targeted therapy. *Dalton Trans* **2011**, *40*, 6144-6167, doi:10.1039/c0dt01599g.

203. Fani, M.; Maecke, H.R. Radiopharmaceutical development of radiolabelled peptides. *Eur J Nucl Med Mol Imaging* **2012**, *39 Suppl 1*, 11-30, doi:10.1007/s00259-011-2001-z.

204. Kratochwil, C.; Bruchertseifer, F.; Giesel, F.L.; Weis, M.; Verburg, F.A.; Mottaghy, F.; Kopka, K.; Apostolidis, C.; Haberkorn, U.; Morgenstern, A. ^{225}Ac-PSMA-617 for PSMA-targeted a-radiation therapy of metastatic castration-resistant prostate cancer. *J Nucl Med* **2016**, *57*, 1941-1944, doi:10.2967/jnumed.116.178673.

205. Orsini, F.; Guidoccio, F.; Mariani, G. Radiopharmaceuticals for therapy. In *Nuclear medicine textbook*, Volterrani, D., Ed.; Springer Nature: Switzerland, 2019; pp. 99-116.

206. Orsini, F.; Puta, E.; Guidoccio, F.; Mariani, G. Single-photon-emitting radiopharmaceuticals. In *Nuclear medicine textbook*, Volterrani, D., Ed.; Springer Nature: Switzerland, 2019; pp. 21-56.

207. Christou, N.; Blondy, S.; David, V.; Verdier, M.; Lalloué, F.; Jauberteau, M.O.; Mathonnet, M.; Perraud, A. Neurotensin pathway in digestive cancers and clinical applications: An overview. *Cell Death Dis* **2020**, *11*, 1027, doi:10.1038/s41419-020-03245-8.

208. Ferro-Flores, G.; Ocampo-García, B.; Luna-Gutiérrez, M.; Santos-Cuevas, C.; Jiménez-Mancilla, N.; Azorín-Vega, E.; Meléndez-Alafort, L. Radiolabeled protein-inhibitor peptides with rapid clinical translation towards imaging and therapy. *Curr Med Chem* **2020**, *27*, 7032-7047, doi:10.2174/0929867327666191223121211.

209. Maschauer, S.; Haubner, R.; Kuwert, T.; Prante, O. ^{18}F-Glyco-RGD peptides for PET imaging of integrin expression: Efficient radiosynthesis by click chemistry and modulation of biodistribution by glycosylation. *Mol Pharm* **2014**, *11*, 505-515, doi:10.1021/mp4004817.

210. Richter, S.; Wuest, F. ^{18}F-Labeled peptides: The future is bright. *Molecules* **2014**, *19*, 20536-20556, doi:10.3390/molecules191220536.

211. Eder, M.; Wängler, B.; Knackmuss, S.; Le Gall, F.; Little, M.; Haberkorn, U.; Mier, W.; Eisenhut, M. Tetrafluorophenolate of HBED-CC: A versatile conjugation agent for ^{68}Ga-labeled small recombinant antibodies. *Eur J Nucl Med Mol Imaging* **2008**, *35*, 1878-1886, doi:10.1007/s00259-008-0816-z.

212. Kubíček, V.; Havlíčková, J.; Kotek, J.; Tircsó, G.; Hermann, P.; Tóth, E.; Lukeš, I. Gallium(III) complexes of DOTA and DOTA-monoamide: Kinetic and thermodynamic studies. *Inorg Chem* **2010**, *49*, 10960-10969, doi:10.1021/ic101378s.

213. Martell, A.E.; Motekaitis, R.J.; Clarke, E.T.; Delgado, R.; Sun, Y.Z.; Ma, R. Stability constants of metal complexes of macrocyclic ligands with pendant donor groups. *Supramol Chem* **1996**, *6*, 353-363, doi:Doi 10.1080/10610279608032555.

214. Gourni, E.; Canovas, C.; Goncalves, V.; Denat, F.; Meyer, P.T.; Maecke, H.R. (R)-NODAGA-PSMA: A versatile precursor for radiometal labeling and nuclear imaging of PSMA-positive tumors. *PLoS One* **2015**, *10*, e0145755, doi:10.1371/journal.pone.0145755.

215. Makarem, A.; Konrad, M.; Liolios, C.; Kopka, K. A convenient synthesis for HBED-CC-tris(*tert*-butyl ester). *Synlett* **2018**, *29*, 1239-1243, doi:10.1055/s-0036-1591950.

216. Liu, S. Bifunctional coupling agents for radiolabeling of biornolecules and target-specific delivery of metallic radionuclides. *Adv Drug Deliver Rev* **2008**, *60*, 1347-1370, doi:10.1016/j.addr.2008.04.006.

217. Breeman, W.A.P.; de Jong, M.; Visser, T.J.; Erion, J.L.; Krenning, E.P. Optimising conditions for radiolabelling of DOTA-peptides with ^{90}Y, ^{111}In and ^{177}Lu at high specific activities. *Eur J Nucl Med Mol I* **2003**, *30*, 917-920, doi:10.1007/s00259-003-1142-0.

218. Velikyan, I.; Beyer, G.J.; Långström, B. Microwave-supported preparation of ^{68}Ga bioconjugates with high specific radioactivity. *Bioconjugate Chem* **2004**, *15*, 554-560, doi:DOI 10.1021/bc030078f.

219. McBride, W.J.; Sharkey, R.M.; Karacay, H.; D'Souza, C.A.; Rossi, E.A.; Laverman, P.; Chang, C.H.; Boerman, O.C.; Goldenberg, D.M. A novel method of ^{18}F radiolabeling for PET. *J Nucl Med* **2009**, *50*, 991-998, doi:10.2967/jnumed.108.060418.

220. Laverman, P.; McBride, W.J.; Sharkey, R.M.; Eek, A.; Joosten, L.; Oyen, W.J.; Goldenberg, D.M.; Boerman, O.C. A novel facile method of labeling octreotide with ^{18}F-fluorine. *J Nucl Med* **2010**, *51*, 454-461, doi:10.2967/jnumed.109.066902.

221. McBride, W.J.; D'Souza, C.A.; Sharkey, R.M.; Karacay, H.; Rossi, E.A.; Chang, C.H.; Goldenberg, D.M. Improved ^{18}F labeling of peptides with a fluoride-aluminum-chelate complex. *Bioconjug Chem* **2010**, *21*, 1331-1340, doi:10.1021/bc100137x.

222. D'Souza, C.A.; McBride, W.J.; Sharkey, R.M.; Todaro, L.J.; Goldenberg, D.M. High-yielding aqueous ^{18}F-labeling of peptides via Al^{18}F chelation. *Bioconjug Chem* **2011**, *22*, 1793-1803, doi:10.1021/bc200175c.

223. Shetty, D.; Choi, S.Y.; Jeong, J.M.; Lee, J.Y.; Hoigebazar, L.; Lee, Y.S.; Lee, D.S.; Chung, J.K.; Lee, M.C.; Chung, Y.K. Stable aluminium fluoride chelates with triazacyclononane derivatives proved by X-ray crystallography and ^{18}F-labeling study. *Chem Commun (Camb)* **2011**, *47*, 9732-9734, doi:10.1039/c1cc13151f.

224. Lang, L.; Li, W.; Guo, N.; Ma, Y.; Zhu, L.; Kiesewetter, D.O.; Shen, B.; Niu, G.; Chen, X. Comparison study of [^{18}F]FAl-NOTA-PRGD2, [^{18}F]FPPRGD2, and [^{68}Ga]Ga-NOTA-PRGD2 for PET imaging of U87MG tumors in mice. *Bioconjug Chem* **2011**, *22*, 2415-2422, doi:10.1021/bc200197h.

225. Laverman, P.; D'Souza, C.A.; Eek, A.; McBride, W.J.; Sharkey, R.M.; Oyen, W.J.G.; Goldenberg, D.M.; Boerman, O.C. Optimized labeling of NOTA-conjugated octreotide with F-18. *Tumor Biol* **2012**, *33*, 427-434, doi:10.1007/s13277-011-0250-x.

226. Malik, N.; Zlatopolskiy, B.; Machulla, H.J.; Reske, S.N.; Solbach, C. One pot radiofluorination of a new potential PSMA ligand [Al^{18}F]NOTA-DUPA-Pep. *J Labelled Compd Rad* **2012**, *55*, 320-325, doi:10.1002/jlcr.2944.

227. Wan, W.; Guo, N.; Pan, D.; Yu, C.; Weng, Y.; Luo, S.; Ding, H.; Xu, Y.; Wang, L.; Lang, L.; et al. First experience of ^{18}F-alfatide in lung cancer patients using a new lyophilized kit for rapid radiofluorination. *J Nucl Med* **2013**, *54*, 691-698, doi:10.2967/jnumed.112.113563.

228. Malik, N.; Baur, B.; Winter, G.; Reske, S.N.; Beer, A.J.; Solbach, C. Radiofluorination of PSMA-HBED *via* Al^{18}F^{2+} chelation and biological evaluations in vitro. *Mol Imaging Biol* **2015**, *17*, 777-785, doi:10.1007/s11307-015-0844-6.

229. Boschi, S.; Lee, J.T.; Beykan, S.; Slavik, R.; Wei, L.; Spick, C.; Eberlein, U.; Buck, A.K.; Lodi, F.; Cicoria, G.; et al. Synthesis and preclinical evaluation of an Al^{18}F radiofluorinated GLU-UREA-LYS(AHX)-HBED-CC PSMA ligand. *Eur J Nucl Med Mol Imaging* **2016**, *43*, 2122-2130, doi:10.1007/s00259-016-3437-y.

230. Poschenrieder, A.; Osl, T.; Schottelius, M.; Hoffmann, F.; Wirtz, M.; Schwaiger, M.; Wester, H.J. First ^{18}F-labeled Pentixafor-based imaging agent for PET imaging of

CXCR4 expression in vivo. *Tomography* **2016**, *2*, 85-93, doi:10.18383/j.tom.2016.00130.

231. Liu, T.L.; Liu, C.; Xu, X.X.; Liu, F.; Guo, X.Y.; Li, N.; Wang, X.J.; Yang, J.H.; Yang, X.; Zhu, H.; et al. Preclinical evaluation and pilot clinical study of Al^{18}F-PSMA-BCH for prostate cancer PET imaging. *J Nucl Med* **2019**, *60*, 1284-1292, doi:10.2967/jnumed.118.221671.

232. Lütje, S.; Franssen, G.M.; Herrmann, K.; Boerman, O.C.; Rijpkema, M.; Gotthardt, M.; Heskamp, S. In vitro and in vivo characterization of an ^{18}F-AlF-labeled PSMA ligand for imaging of PSMA-expressing xenografts. *J Nucl Med* **2019**, *60*, 1017-1022, doi:10.2967/jnumed.118.218941.

233. Piron, S.; De Man, K.; Van Laeken, N.; D'Asseler, Y.; Bacher, K.; Kersemans, K.; Ost, P.; Decaestecker, K.; Deseyne, P.; Fonteyne, V.; et al. Radiation dosimetry and biodistribution of ^{18}F-PSMA-11 for PET imaging of prostate cancer. *J Nucl Med* **2019**, *60*, 1736-1742, doi:10.2967/jnumed.118.225250.

234. Piron, S.; Verhoeven, J.; Descamps, B.; Kersemans, K.; De Man, K.; Van Laeken, N.; Pieters, L.; Vral, A.; Vanhove, C.; De Vos, F. Intra-individual dynamic comparison of ^{18}F-PSMA-11 and ^{68}Ga-PSMA-11 in LNCaP xenograft bearing mice. *Sci Rep* **2020**, *10*, 21068, doi:10.1038/s41598-020-78273-7.

235. Piron, S.; De Man, K.; Schelfhout, V.; Van Laeken, N.; Kersemans, K.; Achten, E.; De Vos, F.; Ost, P. Optimization of PET protocol and interrater reliability of ^{18}F-PSMA-11 imaging of prostate cancer. *EJNMMI Res* **2020**, *10*, 14, doi:10.1186/s13550-020-0593-7.

236. dos Santos, G.; Taroco, M.R.; Giglio, J.; Savio, E.; Alonso, O. Al^{18}F-PSMA-HBED-CC as a novel tracer for the evaluation of prostate cancer patients with biochemical relapse: Intraindividual comparison with ^{68}Ga-PSMA-HBED-CC. *J Nucl Med* **2020**, *61*, 1268.

237. Piron, S.; Verhoeven, J.; Courtyn, J.; Kersemans, K.; Descamps, B.; Pieters, L.; Vral, A.; Vanhove, C.; De Vos, F. Preclinical comparative study of [^{18}F]AlF-PSMA-11 and [^{18}F]PSMA-1007 in varying PSMA expressing tumors. *Sci Rep* **2022**, *12*, 15744, doi:10.1038/s41598-022-20060-7.

238. Al-Momani, E.; Israel, I.; Samnick, S. Validation of a [Al^{18}F]PSMA-11 preparation for clinical applications. *Appl Radiat Isot* **2017**, *130*, 102-108, doi:10.1016/j.apradiso.2017.09.003.

239. Giglio, J.; Zeni, M.; Savio, E.; Engler, H. Synthesis of an Al^{18}F radiofluorinated GLU-UREA-LYS(AHX)-HBED-CC PSMA ligand in an automated synthesis platform. *EJNMMI Radiopharm Chem* **2018**, *3*, 4, doi:10.1186/s41181-018-0039-y.

240. Ioppolo, J.A.; Nezich, R.A.; Richardson, K.L.; Morandeau, L.; Leedman, P.J.; Price, R.I. Direct *in vivo* comparison of [^{18}F]PSMA-1007 with [^{68}Ga]Ga-PSMA-11 and [^{18}F]AlF-PSMA-11 in mice bearing PSMA-expressing xenografts. *Appl Radiat Isot* **2020**, *161*, 109164, doi:10.1016/j.apradiso.2020.109164.

241. Benešová, M.; Schäfer, M.; Bauder-Wüst, U.; Afshar-Oromieh, A.; Kratochwil, C.; Mier, W.; Haberkorn, U.; Kopka, K.; Eder, M. Preclinical evaluation of a tailor-

made DOTA-conjugated PSMA inhibitor with optimized linker moiety for imaging and endoradiotherapy of prostate cancer. *J Nucl Med* **2015**, *56*, 914-920, doi:10.2967/jnumed.114.147413.

242. Jo, S.D.; Ku, S.H.; Won, Y.Y.; Kim, S.H.; Kwon, I.C. Targeted nanotheranostics for future personalized medicine: Recent progress in cancer therapy. *Theranostics* **2016**, *6*, 1362-1377, doi:10.7150/thno.15335.

243. Turner, J.H. An introduction to the clinical practice of theranostics in oncology. *Brit J Radiol* **2018**, *91*, doi:10.1259/bjr.20180440.

244. Langbein, T.; Weber, W.A.; Eiber, M. Future of theranostics: An outlook on precision oncology in nuclear medicine. *J Nucl Med* **2019**, *60*, 13s-19s, doi:10.2967/jnumed.118.220566.

245. Schottelius, M.; Osl, T.; Poschenrieder, A.; Hoffmann, F.; Beykan, S.; Hänscheid, H.; Schirbel, A.; Buck, A.K.; Kropf, S.; Schwaiger, M.; et al. [^{177}Lu]pentixather: Comprehensive preclinical characterization of a first CXCR4-directed endoradiotherapeutic agent. *Theranostics* **2017**, *7*, 2350-2362, doi:10.7150/thno.19119.

246. EMA authorization letter for SomaKit TOC (edotreotide). Application number: EMA/624039/2016. December 8, 2016. Available online: https://www.ema.europa.eu/en/medicines/human/EPAR/somakit-toc#authorisation-details-section (accessed on November 3, 2022).

247. EMA authorization letter for Lutathera (lutetium (^{177}Lu) oxodotreotide). Application number: EMA/524726/2017. September 26, 2017. Available online: https://www.ema.europa.eu/en/medicines/human/EPAR/lutathera#authorisation-details-section (accessed on November 3, 2022).

248. Jacobson, O.; Weiss, I.D.; Kiesewetter, D.O.; Farber, J.M.; Chen, X. PET of tumor CXCR4 expression with 4-^{18}F-T140. *J Nucl Med* **2010**, *51*, 1796-1804, doi:10.2967/jnumed.110.079418.

249. Gourni, E.; Demmer, O.; Schottelius, M.; D'Alessandria, C.; Schulz, S.; Dijkgraaf, I.; Schumacher, U.; Schwaiger, M.; Kessler, H.; Wester, H.J. PET of CXCR4 expression by a ^{68}Ga-labeled highly specific targeted contrast agent. *J Nucl Med* **2011**, *52*, 1803-1810, doi:10.2967/jnumed.111.098798.

250. Åberg, O.; Pisaneschi, F.; Smith, G.; Nguyen, Q.D.; Stevens, E.; Aboagye, E.O. ^{18}F-labelling of a cyclic pentapeptide inhibitor of the chemokine receptor CXCR4. *J Fluorine Chem* **2012**, *135*, 200-206, doi:10.1016/j.jfluchem.2011.11.003.

251. George, G.P.C.; Pisaneschi, F.; Stevens, E.; Nguyen, Q.D.; Åberg, O.; Spivey, A.C.; Aboagye, E.O. Scavenging strategy for specific activity improvement: Application to a new CXCR4-specific cyclopentapeptide positron emission tomography tracer. *J Labelled Compd Rad* **2013**, *56*, 679-685, doi:10.1002/jlcr.3095.

252. Weiss, I.D.; Jacobson, O. Molecular imaging of chemokine receptor CXCR4. *Theranostics* **2013**, *3*, 76-84, doi:10.7150/thno.4835.

253. Brickute, D.; Braga, M.; Kaliszczak, M.A.; Barnes, C.; Lau, D.; Carroll, L.; Stevens, E.; Trousil, S.; Alam, I.S.; Nguyen, Q.D.; et al. Development and evaluation of an

^{18}F-radiolabeled monocyclam derivative for imaging CXCR4 expression. *Mol Pharm* **2019**, *16*, 2106-2117, doi:10.1021/acs.molpharmaceut.9b00069.

254. Linde, P.; Baues, C.; Wegen, S.; Trommer, M.; Quaas, A.; Rosenbrock, J.; Celik, E.; Marnitz, S.; Bruns, C.J.; Fischer, T.; et al. Pentixafor PET/CT for imaging of chemokine receptor 4 expression in esophageal cancer - a first clinical approach. *Cancer Imaging* **2021**, *21*, 22, doi:10.1186/s40644-021-00391-w.

Chapter 2

Modifications at Arg and Ile give neurotensin(8-13) derivatives with high stability and retained NTS_1R affinity

Prior to the submission of this thesis, the content of this chapter was published as a scientific article:

Schindler, L.; Bernhardt, G.; Keller, M. Modifications at Arg and Ile give neurotensin(8-13) derivatives with high stability and retained NTS_1 receptor affinity. *ACS Med Chem Lett* **2019**, *10*, 960-965, doi:10.1021/acsmedchemlett.9b00122.

2.1 Introduction

The neuromodulator neurotensin (NT), a 13 amino acid peptide (Figure 2.1), is found in the central nervous system (CNS), mediating, e.g., analgesic effects, as well as in the periphery (primarily in the gastrointestinal tract)[1,2]. The carboxy-terminal hexapeptide of NT (NT(8-13) (**2.01**), Figure 2.1), is biologically equi-active to NT[3]. The physiological effects of NT are mediated by three cell-surface receptors: the NT receptors 1 and 2 (NTS_1R, NTS_2R), both G-protein coupled receptors[4], and the NTS_3R, which belongs to the Vps10p-domain receptor family[2,5]. The NTS_1R has increasingly gained interest as a target for tumor diagnosis and therapy, as it was reported to be (over)expressed in a variety of malignancies, among them the prognostically poor pancreatic adenocarcinoma, Ewing's sarcoma, breast cancer, and colorectal carcinoma[6-9]. Thus, radiolabeled NTS_1R ligands harbor the potential of being used as radiopharmaceuticals. The majority of such compounds (e.g., ^{68}Ga- and ^{18}F-labeled for PET diagnostics, ^{177}Lu-labeled for endoradiotherapy) has been derived from the agonist **2.01**[10-19]. Notably, also NTS_1R ligands derived from non-peptidic antagonists have been explored as radiodiagnostics and radiotherapeutics[20,21]. Recently reported data of a clinical trial on the treatment of pancreatic adenocarcinoma in men by ^{177}Lu-labeled NTS_1R antagonists give reason to develop clinical trial candidates with improved properties[22]. Therefore, peptidic NTS_1R ligands, such as radiolabeled derivatives of **2.01**, should be considered for clinical trials.

A major drawback of peptide **2.01** is its rapid degradation in vivo by peptidases (see Figure 2.1)[23,24]. Enzymatic degradation of **2.01** occurs at three major sites: the Arg^8-Arg^9 bond, the Pro^{10}-Tyr^{11} bond and the bond between Tyr^{11} and Ile^{12} (*cf.* Figure 2.1)[24,25]. The predominant approaches to stabilize the backbone of **2.01** are N-methylation of Arg^8 or Arg^9, N-terminal acylation and the exchange of Ile^{12} by *tert*-butylglycine (Tle)[10-15,17,26-38]. However, for some interesting analogs of **2.01**, such as N-methylated derivatives, investigations on the stability are lacking[33,39]. It is worth mentioning that described derivatives of **2.01**, containing Tle^{12} instead of Ile^{12}, include additional structural modifications throughout[10-12,29,31,32,38,40], i.e., [Tle^{12}]NT(8-13) (**2.02**, *cf.* Figure 2.1) has not been reported to date to the best of the authors' knowledge. Therefore, it is difficult to estimate the impact of the Ile^{12}/Tle^{12} exchange on the stability of Tle^{12}-containing derivatives of **2.01**.

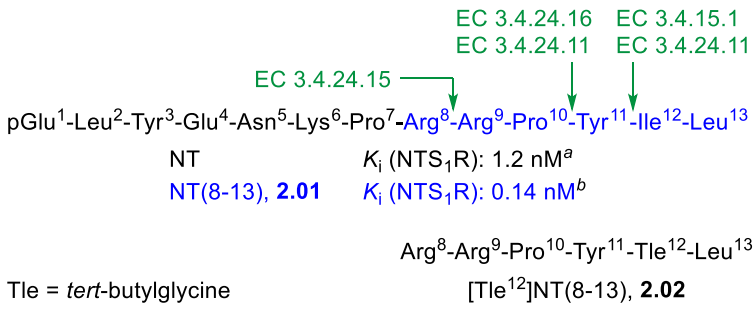

Figure 2.1. Amino acid sequences of neurotensin, **2.01** (NT(8-13), in blue) and **2.02**, as well as major enzymatic cleavage sites (in green) of **2.01**[3,24,25]. EC 3.4.24.15: metalloendopeptidase 24.15, EC 3.4.24.16: metalloendopeptidase 24.16, EC 3.4.24.11: neutral endopeptidase 24.11, EC 3.4.15.1: angiotensin converting enzyme (ACE)[24,25]. [a]Granier et al.[41] [b]Keller et al.[42]

Aiming at a systematic study on the stabilization of the NT(8-13) core structure, we synthesized compound **2.02**, performed an N-methyl scan of **2.01**, combined N-methylation with the Ile^{12}/Tle^{12} exchange and, additionally, prepared N-terminally acylated derivatives of **2.01**. All compounds were studied with respect to NTS_1R binding and plasma stability.

2.2 Results and discussion

2.2.1 Chemistry

Peptides **2.02**, **2.03**[34], **2.04**[33], **2.05**[33,39], **2.06**[33], **2.07**, **2.08** and **2.09**[33] were prepared by solid-phase peptide synthesis (SPPS) according to the 9-fluorenylmethoxycarbonyl (Fmoc) protecting group strategy using 1-hydroxybenzotriazole (HOBt)/*O*-(1*H*-benzotriazol-1-yl)-*N*,*N*,*N*′,*N*′-tetramethyluronium hexafluorophosphate (HBTU) and diisopropylethylamine (DIPEA) for amide bond formation (Scheme 2.1). Coupling of Fmoc-protected amino acids to the secondary amino group of N-methylated amino acids turned out to be the yield limiting factor in case of **2.05**, **2.06** and **2.09** (overall yields: 18%, 15% and 20%, respectively). The N-terminally propionylated derivative **2.11** was obtained by treatment of the respective resin-bound, side chain-protected, but N-terminally deprotected precursor peptide with succinimidyl propionate (**2.10**) followed by cleavage from the resin and side chain deprotection. By contrast, the N-terminally propionylated peptide **2.12** was prepared by solution phase treatment of **2.02** with compound **2.10** (Scheme 2.1).

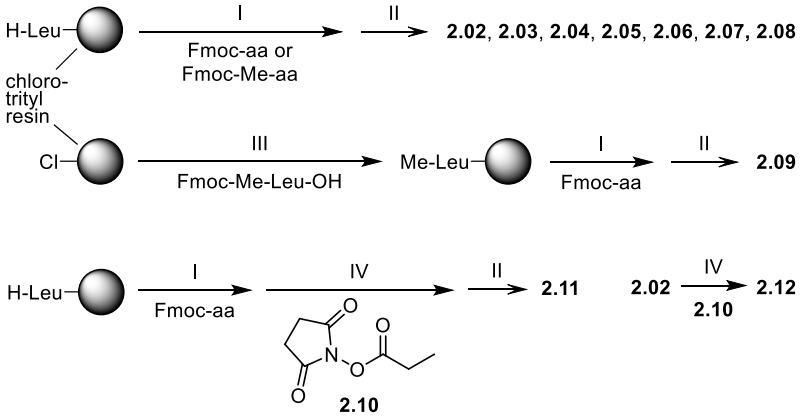

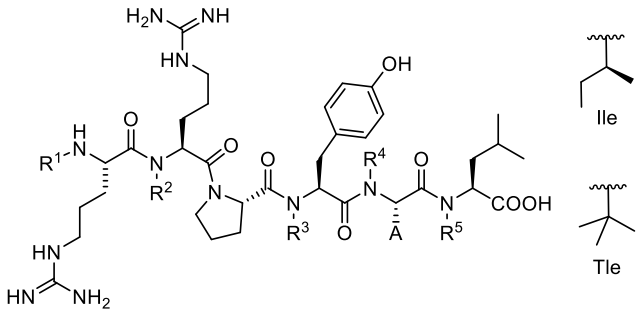

compd.	R^1	R^2	R^3	R^4	R^5	A
2.02	H	H	H	H	H	Tle
2.03	CH_3	H	H	H	H	Ile
2.04	H	CH_3	H	H	H	Ile
2.05	H	H	CH_3	H	H	Ile
2.06	H	H	H	CH_3	H	Ile
2.07	CH_3	H	H	H	H	Tle
2.08	H	CH_3	H	H	H	Tle
2.09	H	H	H	H	CH_3	Ile
2.11	CO-C_2H_5	H	H	H	H	Ile
2.12	CO-C_2H_5	H	H	H	H	Tle

Scheme 2.1. Syntheses of the NT(8-13) derivatives **2.02**-**2.09**, **2.11** and **2.12**. Reagents and conditions: (I) Fmoc strategy SPPS using HBTU/HOBt and DIPEA, DMF/NMP (80:20 v/v), 35 °C, 2 × 1 h or 2 × 2 h, Fmoc-deprotection: 20% piperidine in DMF/NMP (80:20 v/v), rt, 2 × 8-10 min; (II) (1) hexafluoro-2-propanol (HFIP)/CH_2Cl_2 (1:3 v/v), rt, 2 × 20 min, (2) TFA/H_2O (95:5 v/v), rt, 3 h; (III) DIPEA, CH_2Cl_2, 35 °C, 14 h; (IV) DIPEA, DMF/NMP (80:20 v/v), rt, 1 h; overall yields: 77% (**2.02**), 67% (**2.03**), 56% (**2.04**), 18% (**2.05**), 15% (**2.06**), 42% (**2.07**), 38% (**2.08**), 20% (**2.09**), 56% (**2.11**), 85% (**2.12**).

2.2.2 In vitro binding studies at the NTS_1R

NTS_1R binding data (K_i values) were determined for **2.01**-**2.09**, **2.11** and **2.12** by competition binding with [^{3}H]UR-MK300[42] ([^{3}H]**2.13**, for structure see Figure A2.1,

Appendix) at intact hNTS$_1$R-expressing HT-29 colon carcinoma cells (Table 2.1). The replacement of Ile^{12} by Tle^{12} in **2.01** (compound **2.02**) resulted in a minor decrease in NTS$_1$R affinity (K_i values of **2.01** and **2.02**: 0.33 *vs.* 1.2 nM, *cf.* Table 2.1). Regarding the N-methyl scan of **2.01** (peptides **2.03**-**2.06** and **2.09**), methylation at Arg^8 or Arg^9 (**2.03**, **2.04**) did not affect NTS$_1$R affinity (K_i < 0.5 nM, Table 2.1). By contrast, N-methylation of Tyr^{11}, Ile^{12} or Leu^{13} (**2.05**, **2.06**, **2.09**) led to a considerable decrease in NTS$_1$R affinity (K_i values: > 1000 nM, 60 nM and 880 nM, respectively, *cf.* Table 2.1). As expected, the combination of the N-methylation at Arg^8 or Arg^9 with the replacement of Ile^{12} by Tle^{12} (peptides **2.07** and **2.08**) resulted in NTS$_1$R affinities comparable to that of **2.02** (Table 2.1). The N-terminally propionylated analogs of **2.01** and **2.02** (compounds **2.11** and **2.12**) exhibited K_i values (NTS$_1$R) of 1.0 and 18 nM, respectively.

Table 2.1. Peptide sequences and NTS$_1$R affinities of **2.01**-**2.09**, **2.11** and **2.12**, as well as stabilities of **2.01**-**2.09**, **2.11** and **2.12** in human plasma/PBS (1:2 v/v) (37 °C).

cpd.	sequence	pK_i ± SEM/ K_i [nM] NTS$_1$R[a]	% intact peptide in plasma[b] after the specified incubation times:						
			10 min	30 min	1 h	2 h	6 h	24 h	48 h
2.01	Arg-Arg-Pro-Tyr-Ile-Leu	9.49 ± 0.03/0.33 (lit. 0.14[c])	23.1 ± 0.2	n.d.	< 1	n.d.	n.d.	< 1	< 1
2.02	Arg-Arg-Pro-Tyr-Tle-Leu	8.93 ± < 0.01/1.2	10.8 ± 0.5	n.d.	< 1	n.d.	n.d.	< 1	< 1
2.03	Me-Arg-Arg-Pro-Tyr-Ile-Leu	9.65 ± 0.01/0.22 (lit. 0.29[d])	92.1 ± 0.1	88.2 ± 0.2	79.7 ± 0.1	70.8 ± 0.1	n.d.	n.d.	n.d.
2.04	Arg-Me-Arg-Pro-Tyr-Ile-Leu	9.55 ± 0.05/0.29 (lit. 0.51[e])	> 99	93.6 ± 0.1	83.7 ± 0.3	66.4 ± 0.1	n.d.	n.d.	n.d.
2.05	Arg-Arg-Pro-Me-Tyr-Ile-Leu	< 6/> 1000 (lit. 5100[e])	22.9 ± 0.2	< 1	< 1	< 1	n.d.	n.d.	n.d.
2.06	Arg-Arg-Pro-Tyr-Me-Ile-Leu	7.22 ± 0.04/60 (lit. 160[e])	2.6 ± 0.5	< 1	< 1	< 1	n.d.	n.d.	n.d.
2.07	Me-Arg-Arg-Pro-Tyr-Tle-Leu	9.07 ± 0.06/0.88	n.d.	n.d.	> 99	n.d.	> 99	98.3 ± 0.8	86.8 ± 0.3
2.08	Arg-Me-Arg-Pro-Tyr-Tle-Leu	8.79 ± 0.02/1.6	n.d.	n.d.	> 99	n.d.	> 99	> 99	> 99
2.09	Arg-Arg-Pro-Tyr-Ile-Me-Leu	6.12 ± 0.14/880 (lit. 190[e])	39.9 ± 0.9	< 1	< 1	< 1	n.d.	n.d.	n.d.
2.11	Prop-Arg-Arg-Pro-Tyr-Ile-Leu	9.02 ± 0.08/1.0	> 99	84.0 ± 0.1	71.8 ± 0.2	32.4 ± 0.1	n.d.	n.d.	n.d.
2.12	Prop-Arg-Arg-Pro-Tyr-Tle-Leu	7.75 ± 0.04/18	n.d.	n.d.	> 99	n.d.	> 99	> 99	92.5 ± 0.9

[a]Determined by radioligand competition binding with [^{3}H]**2.13** at HT-29 cells; mean values from two (**2.01**, **2.02**), three (**2.03**, **2.04**) or four (**2.06**-**2.09**, **2.11**, **2.12**) independent experiments, each performed in triplicate. Given are mean values ± SEM (pK_i) and mean values (K_i); K_i values from the literature are given in parentheses. [b]The initial concentration of the peptides in plasma/PBS (1:2 v/v) was 100 µM; presented are mean values ± SEM from three independent experiments (SEM not given if no decomposition was observed). [c]Keller et al.[42] [d]Orwig et al.[34] [e]Härterich et al.[33] n.d. = not determined. Prop = propionyl.

Figure 2.2 illustrates a general decrease in NTS_1R affinity caused by the replacement of Ile^{12} by Tle^{12} in **2.01**, **2.03**, **2.04** and **2.11**, giving **2.02**, **2.07**, **2.08** and **2.12**, respectively, and a dependency of the extent of the decrease in affinity on the primary structure of the peptides. This is in agreement with reported NTS_1R binding data of derivatives of **2.01** containing Tle^{12} [10,11,27,31,38,40].

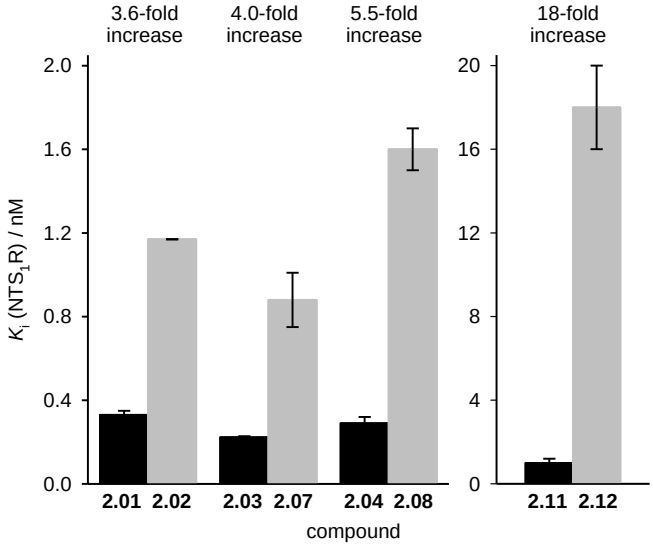

Figure 2.2. Decrease in NTS_1R affinity (increase in K_i) resulting from the exchange of Ile^{12} by Tle^{12} in **2.01**, **2.03**, **2.04** and **2.11** (black bars) giving **2.02**, **2.07**, **2.08** and **2.12** (grey bars), respectively. Note: the scales of the Y-axes are different.

2.2.3 Peptide stability in human plasma

In order to investigate the effect of N-methylation (**2.03**-**2.09**), the Ile^{12}/Tle^{12} exchange (**2.02**, **2.07**, **2.08**, **2.12**) and N-terminal acylation (**2.11**, **2.12**) on the stability of the peptides against enzymatic cleavage, the stability of all compounds was investigated in human plasma at 37 °C for up to 48 h (Figure 2.3, Table 2.1). Whereas N-methylation of Arg^8 or Arg^9 in **2.01** (compounds **2.03** and **2.04**) significantly enhanced the peptide stability in plasma compared to **2.01**, methylation of Tyr^{11}, Ile^{12} and Leu^{13} (**2.05**, **2.06**, **2.09**) did not lead to higher plasma stabilities. Strikingly, peptide **2.02**, which differed from **2.01** only with respect to the replacement of Ile^{12} by Tle^{12}, proved to be as unstable as **2.01** (Figure 2.3, Table 2.1). However, the combination of the Ile^{12}/Tle^{12} exchange with N-methylation of Arg^8 or Arg^9 (**2.07**, **2.08**) resulted in significantly higher plasma stabilities ($t_{1/2}$ > 48 h) compared to **2.03** and **2.04**. These results confirmed that both, N-terminal (cleavage between Arg^8 and Arg^9) and C-terminal (cleavage between Tyr^{11} and Ile^{12}) degradation are highly relevant, and revealed that the former occurs faster than the latter. As in case of N-terminal methylation of **2.01** (peptide **2.03**), N-terminal propionylation of **2.01** (peptide **2.11**) resulted in a moderate increase in enzymatic stability compared to **2.01** ($t_{1/2}$ of **2.11** between 1 h and 2 h, *cf*. Table 2.1). The combination of N-terminal propionylation with an Ile^{12}/Tle^{12} exchange (compound **2.12**) led to an excellent plasma stability as also observed in case of combining N-terminal methylation with an Ile^{12}/Tle^{12} exchange (peptide **2.07**) (Figure 2.3, Table 2.1).

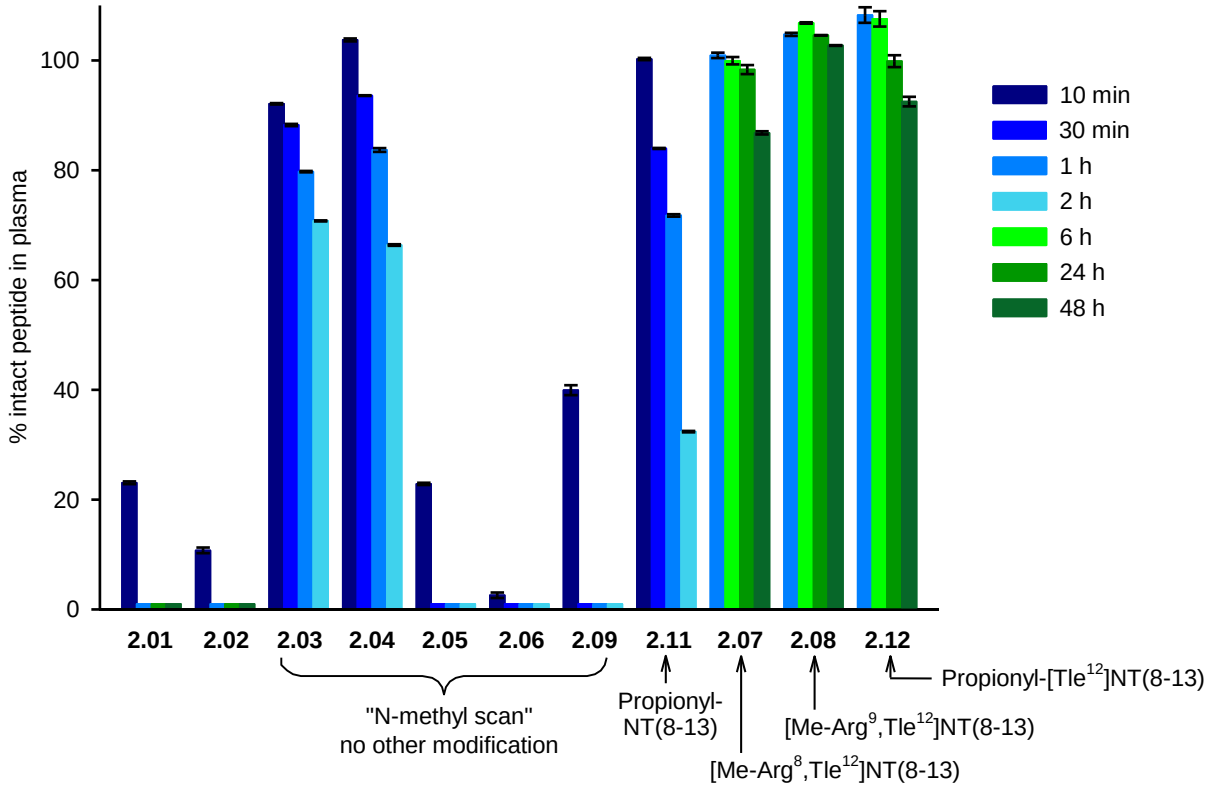

Figure 2.3. Stabilities of **2.01**-**2.09**, **2.11** and **2.12** in human plasma/PBS (1:2 v/v) at 37 °C investigated for up to 48 h. Data represent mean values ± SEM from three independent experiments.

Figure 2.4 provides an overview of the major degradation fragments identified by LC-HRMS. The Arg^{8}-Arg^{9}, Pro^{10}-Tyr^{11} and Tyr^{11}-Ile^{12} bonds were identified as the major cleavage sites (Figure 2.4), being in agreement with reported data on the metabolic stability of **2.01**[24,25]. As outlined above, the present study suggests that cleavage of Arg^{8} in **2.01** occurs faster than its C-terminal degradation. This is, on the one hand, in agreement with reports in the literature[24], on the other hand it is in disagreement with other reports, which suggest an Ile^{12}/Tle^{12} exchange as the most crucial structural modification with respect to metabolic stabilization[27,28].

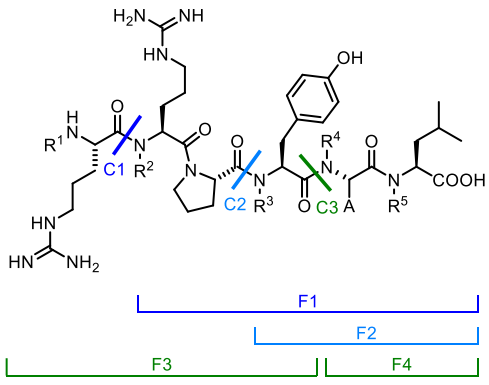

Identified fragments after incubation in human plasma/PBS (1:2 v/v):

compd.	R^1	R^2	R^3	R^4	R^5	A	F1	F2	F3	F4
2.01	H	H	H	H	H	*(S)*-1-methylpropyl	x	x		
2.02	H	H	H	H	H	*tert*-butyl	x	x		
2.03	CH_3	H	H	H	H	*(S)*-1-methylpropyl			x	x
2.04	H	CH_3	H	H	H	*(S)*-1-methylpropyl			x	x
2.05	H	H	CH_3	H	H	*(S)*-1-methylpropyl	x			
2.06	H	H	H	CH_3	H	*(S)*-1-methylpropyl	x	x		
2.07	CH_3	H	H	H	H	*tert*-butyl				
2.08	H	CH_3	H	H	H	*tert*-butyl				
2.09	H	H	H	H	CH_3	*(S)*-1-methylpropyl	x	x		x
2.11	$CO\text{-}C_2H_5$	H	H	H	H	*(S)*-1-methylpropyl			x	x
2.12	$CO\text{-}C_2H_5$	H	H	H	H	*tert*-butyl		x		x

Figure 2.4. Major enzymatic cleavage sites (C1-C3) of compounds **2.01**-**2.09**, **2.11** and **2.12** as well as corresponding fragments F1-F4, identified by LC-HRMS analysis after incubation in human plasma at 37 °C for up to 48 h.

2.3 Conclusion

In conclusion, the synthesis and investigation of N-methylated derivatives of NT(8-13) (**2.01**), N-terminally acylated derivatives of **2.01** and analogs containing Tle^{12} instead of Ile^{12}, revealed that only the combination of appropriate N-terminal (e.g., N-methylation of Arg^8) and C-terminal (replacement of Ile^{12} by Tle^{12}) structural modifications in **2.01** affords highly stable (plasma half-life > 48 h) congeners of **2.01** (compounds **2.07**, **2.08** and **2.12**). Fortunately, two of the most stable compounds (**2.07**, **2.08**) exhibited the highest NTS_1R affinities of the investigated analogs of **2.01**. This work answers open questions concerning the controversially discussed impact of various structural modifications of **2.01** on the enzymatic stability, thus supporting the development of stable radiolabeled derivatives of **2.01**, which harbor the potential of being used as radiopharmaceuticals.

2.4 Experimental section

Additional information on materials, chemicals, protocols and additional analytical data of compounds (HPLC analyses, ^{1}H-NMR spectra) are provided in the Appendix.

2.4.1 General procedure for SPPS

Peptides were synthesized by manual SPPS according to the Fmoc strategy. 5-mL polypropylene/polyethylene syringes from B. Braun Melsungen (Melsungen, Germany) or 5-mL BD Discardit II syringes (Becton Dickinson, Heidelberg, Germany) equipped with a polyethylene frit (pore size 35 µm) served as reaction vessels. Protected standard L-amino acids and protected N-methylated L-amino acids were purchased from Merck Biosciences (Schwalbach am Taunus, Germany) (Fmoc-N-Me-Arg(Pbf)-OH, Fmoc-Ile-OH, Fmoc-N-Me-Ile-OH, Fmoc-N-Me-Leu-OH, Fmoc-Pro-OH, Fmoc-Tle-OH (Fmoc-α-*tert*-butylglycine)) or from Iris Biotech (Fmoc-Arg(Pbf)-OH, Fmoc-Tyr(*t*Bu)-OH, Fmoc-N-Me-Tyr(*t*Bu)-OH). The H-Leu-2-ClTrt resin and the 2-ClTrt-Cl resin were purchased from Merck Biosciences and Iris Biotech, respectively. A mixture of DMF and NMP (80:20 v/v) was used as solvent (ca. 2.2 mL per 1 mmol Fmoc-aa) for the coupling reactions and for Fmoc deprotection. In case of using the H-Leu-2-ClTrt solid support (synthesis of **2.02**-**2.08** and **2.11**), the resin was allowed to swell in the solvent for 45 min before the beginning of the synthesis. Protected standard amino acids (Fmoc-Arg(Pbf)-OH, Fmoc-Ile-OH, Fmoc-Pro-OH, Fmoc-Tyr(*t*Bu)-OH) as well as Fmoc-Tle-OH were used in 5-fold excess, and the protected N-methylated amino acids Fmoc-N-Me-Arg(Pbf)-OH, Fmoc-N-Me-Ile-OH and Fmoc-N-Me-Tyr(*t*Bu)-OH were used in 3.5-fold excess. Amino acid coupling was performed with HBTU/HOBt/DIPEA (standard amino acids and Fmoc-Tle-OH: 4.9/5/10 equiv., N-methylated amino acids: 3.45/3.5/7 equiv.). For the coupling of N-methylated amino acids anhydrous solvents (DMF, NMP) were used. All amino acids were pre-incubated with HBTU/HOBt/DIPEA at rt for 5 min prior to addition to the resin. The coupling reactions were performed under shaking at 35 °C (standard amino acids: 2 × 1 h ("double" coupling), N-methylated amino acids: 2 × 2 h). After coupling, the resin was washed with solvent (4 ×). Fmoc deprotection was performed with piperidine (20% in DMF/NMP (80:20 v/v)) at rt for 2 × 8-10 min. After Fmoc deprotection the resin was washed with solvent (6 ×). The last coupling and Fmoc deprotection step was followed by washing of the resin with solvent (4 ×) and CH_2Cl_2 (treated with K_2CO_3) (6 ×). Peptides were cleaved off the resin with CH_2Cl_2/HFIP (3:1 v/v) (rt, 2 × 20 min). The solutions, containing the crude peptide, were separated from the resin by filtration and the resin was washed with CH_2Cl_2/HFIP (3:1 v/v). The filtrates were combined, the volatiles were evaporated, TFA/water (95:5 v/v) (1-3 mL) was added and the mixture was stirred at rt for 3 h (after 2 h additional TFA (70-300 µL) was added). The mixture was transferred to a 100-mL flask containing water (33-100 mL) followed by lyophilization to obtain the crude peptides, which were purified by preparative HPLC.

2.4.2 Synthesis protocols and analytical data of compounds 2.02-2.09, 2.11 and 2.12

Arg-Arg-Pro-Tyr-2-*tert*-butyl-Gly-Leu tris(hydrotrifluoroacetate) (2.02). Peptide **2.02** was synthesized according to the general procedure using a H-Leu-2-ClTrt resin (loading 0.79 mmol/g) (100 mg, 0.079 mmol). Purification by preparative RP-HPLC (column: Kinetex-XB C18, gradient: 0-35 min: A1/B 92:8-57:43, t_R = 18 min) afforded **2.02**

as white fluffy solid (70.6 mg, 77%). ^{1}H-NMR (600 MHz, DMSO-d_6): δ 0.79-0.95 (m, 15H), 1.43-1.74 (m, 11H), 1.74-1.92 (m, 3H), 1.92-2.06 (m, 1H), 2.63-2.76 (m, 1H), 2.80-2.95 (m, 1H), 3.03-3.17 (m, 4H), 3.48-3.69 (m, 2H), 3.73-3.95 (m, 1H), 4.17-4.25 (m, 1H), 4.25-4.31 (m, 1H), 4.31-4.39 (m, 1H), 4.40-4.57 (m, 2H), 6.56-6.68 (m, 2H), 6.68-7.13 (br s, 4H, interfering with the next listed signal), 6.98-7.01 (m, 2H), 7.13-7.55 (br s, 4H), 7.55-7.73 (m, 3H), 7.98 (d, 1H, *J* 7.9 Hz), 8.02-8.57 (m, 4H), 8.65 (d, 1H, *J* 6.7 Hz), 9.19 (s, 1H), 12.48 (br s, 1H). HRMS (LC method A): *m/z* [*M*+2H]$^{2+}$ calcd. for [$C_{38}H_{66}N_{12}O_8$]$^{2+}$ 409.2558, found 409.2563. RP-HPLC (220 nm): 99% (t_R = 6.3 min, *k* = 7.3). $C_{38}H_{64}N_{12}O_8$ · $C_6H_3F_9O_6$ (817.01 + 342.07).

***N*$^{\alpha}$-Methyl-Arg-Arg-Pro-Tyr-Ile-Leu tris(hydrotrifluoroacetate) (2.03)[34].** Peptide **2.03** was synthesized according to the general procedure using a H-Leu-2-ClTrt resin (loading 0.79 mmol/g) (50 mg, 0.0395 mmol). Purification by preparative RP-HPLC (column: Kinetex-XB C18, gradient: 0-35 min: A1/B 92:8-57:43, t_R = 19 min) afforded **2.03** as white fluffy solid (30.8 mg, 67%). ^{1}H-NMR (600 MHz, DMSO-d_6): δ 0.78-0.92 (m, 12H), 0.99-1.09 (m, 1H), 1.38-1.87 (m, 16H), 1.92-2.06 (m, 1H), 2.41-2.48 (m, 3H), 2.67 (dd, 1H, *J* 8.3, 14.0 Hz), 2.83-2.91 (m, 1H), 3.02-3.21 (m, 4H), 3.48-3.67 (m, 2H), 3.69-3.88 (m, 1H), 4.14-4.29 (m, 2H), 4.29-4.38 (m, 1H), 4.38-4.59 (m, 2H), 6.58-6.64 (m, 2H), 6.64-7.15 (br s, 4H, interfering with the next listed signal), 6.98-7.01 (m, 2H), 7.15-7.59 (br s, 4H), 7.59-7.85 (m, 3H), 7.90 (d, 1H, *J* 7.9 Hz), 8.20 (d, 1H, *J* 7.9 Hz), 8.64-9.29 (m, 4H), 12.39 (br s, 1H). HRMS (LC method A): *m/z* [*M*+2H]$^{2+}$ calcd. for [$C_{39}H_{68}N_{12}O_8$]$^{2+}$ 416.2636, found 416.2645. RP-HPLC (220 nm): > 99% (t_R = 6.6 min, *k* = 7.7). $C_{39}H_{66}N_{12}O_8$ · $C_6H_3F_9O_6$ (831.03 + 342.07).

***N*$^{\alpha}$-Argininyl-*N*$^{\alpha}$-methyl-Arg-Pro-Tyr-Ile-Leu tris(hydrotrifluoroacetate) (2.04)[33].** Peptide **2.04** was synthesized according to the general procedure using a H-Leu-2-ClTrt resin (loading 0.79 mmol/g) (50 mg, 0.0395 mmol). Purification by preparative RP-HPLC (column: Kinetex-XB C18, gradient: 0-35 min: A1/B 92:8-57:43, t_R = 19 min) afforded **2.04** as white fluffy solid (26.0 mg, 56%). ^{1}H-NMR (600 MHz, DMSO-d_6): δ 0.78-0.86 (m, 9H), 0.90 (d, 3H, *J* 6.6 Hz), 1.02-1.10 (m, 1H), 1.37-1.46 (m, 3H), 1.49-1.80 (m, 13H), 1.94-2.02 (m, 1H), 2.68 (dd, 1H, *J* 8.7, 14.1 Hz), 2.85-2.90 (m, 1H), 2.92 (s, 3H), 3.06-3.15 (m, 4H), 3.27-3.29 (m, 1H), 3.42-3.55 (m, 1H), 4.15-4.25 (m, 2H), 4.25-4.33 (m, 1H), 4.33-4.51 (m, 2H), 5.08-5.19 (m, 1H), 6.58-6.67 (m, 2H), 6.67-7.13 (br s, 4H, interfering with the next listed signal), 6.99-7.02 (m, 2H), 7.13-7.61 (br s, 4H, interfering with the next listed signal), 7.52-7.56 (m, 1H), 7.63-7.77 (m, 2H), 7.91 (d, 1H, *J* 7.8 Hz), 7.99-8.36 (m, 4H), 9.17 (s, 1H), 12.49 (br s, 1H). HRMS (LC method A): *m/z* [*M*+H]$^+$ calcd. for [$C_{39}H_{67}N_{12}O_8$]$^+$ 831.5199, found 831.5202. RP-HPLC (220 nm): > 99% (t_R = 6.7 min, *k* = 7.8). $C_{39}H_{66}N_{12}O_8$ · $C_6H_3F_9O_6$ (831.03 + 342.07).

Arg-Arg-Pro-*N*$^{\alpha}$-methyl-Tyr-Ile-Leu tris(hydroacetate) (2.05)[33,39]. Peptide **2.05** was synthesized according to the general procedure using a H-Leu-2-ClTrt resin (loading 0.79 mmol/g) (100 mg, 0.079 mmol). Purification by preparative RP-HPLC (column: YMC-Actus Triart C8, gradient: 0-30 min: A2/B 90:10-65:35, t_R = 17 min) afforded **2.05** as white solid (14.6 mg, 18%). ^{1}H-NMR (600 MHz, DMSO-d_6): δ 0.74-0.89 (m, 13H), 0.97-1.08 (m, 1H), 1.11-1.19 (m, 1H), 1.24-1.32 (m, 1H), 1.33-1.66 (m, 12H), 1.79-1.85 (m, 11H), 2.63-2.72 (m, 3H), 2.74-2.79 (m, 1H), 2.88-2.92 (m, 1H), 2.99-3.05 (m, 2H), 3.11-3.15 (m, 3H), 3.44-3.46 (m, 2H), 3.97-4.00 (m, 1H), 4.21-4.27 (m, 1H), 4.40-4.47 (m, 1H), 4.53-4.60 (m, 1H), 4.95-5.04 (m, 1H), 6.60-6.67 (m, 2H), 6.99-7.08 (m, 2H), 7.27-7.81 (m, 9H), 8.41-8.52 (m,

1H), 8.58-8.74 (m, 2H), 9.19 (s, 1H). Note: five exchangeable protons (NH, OH) of the 3-fold protonated molecule were not apparent. HRMS (LC method A): *m/z* [*M*+H]$^+$ calcd. for [$C_{39}H_{67}N_{12}O_8$]$^+$ 831.5199, found 831.5194. RP-HPLC (220 nm): 99% (t_R = 7.6 min, *k* = 9.0). $C_{39}H_{66}N_{12}O_8$ · $C_6H_{12}O_6$ (831.03 + 180.16).

Arg-Arg-Pro-Tyr-*N*$^{\alpha}$-methyl-Ile-Leu tris(hydrotrifluoroacetate) (2.06)[33]. Peptide **2.06** was synthesized according to the general procedure using a H-Leu-2-ClTrt resin (loading 0.79 mmol/g) (50 mg, 0.0395 mmol). Purification by preparative RP-HPLC (column: Kinetex-XB C18, gradient: 0-35 min: A1/B 92:8-57:43, t_R = 20 min) afforded **2.06** as white fluffy solid (6.7 mg, 15%). ^{1}H-NMR (600 MHz, DMSO-d_6): δ 0.72-0.93 (m, 13H), 1.17-1.25 (m, 1H), 1.40-1.76 (m, 12H), 1.78-1.92 (m, 3H), 1.96-2.12 (m, 1H), 2.61-2.98 (m, 5H), 2.98-3.27 (m, 4H), 3.52-3.73 (m, 2H), 3.74-3.89 (m, 1H), 4.04-4.22 (m, 1H), 4.31-4.39 (m, 1H), 4.43-4.52 (m, 1H), 4.68-5.07 (m, 2H), 6.57-6.68 (m, 2H), 6.68-7.13 (br s, 4H, interfering with the next listed signal), 6.94-6.99 (m, 2H), 7.13-7.56 (br s, 4H), 7.56-7.78 (m, 2H), 7.86-8.90 (m, 6H), 9.24 (s, 1H), 12.38 (br s, 1H). HRMS (LC method A): *m/z* [*M*+2H]$^{2+}$ calcd. for [$C_{39}H_{68}N_{12}O_8$]$^{2+}$ 416.2636, found 416.2643. RP-HPLC (220 nm): > 99% (t_R = 7.0 min, *k* = 8.2). $C_{39}H_{66}N_{12}O_8$ · $C_6H_3F_9O_6$ (831.03 + 342.07).

***N*$^{\alpha}$-Methyl-Arg-Arg-Pro-Tyr-2-*tert*-butyl-Gly-Leu tris(hydrotrifluoroacetate) (2.07).** Peptide **2.07** was synthesized according to the general procedure using a H-Leu-2-ClTrt resin (loading 0.79 mmol/g) (45 mg, 0.0356 mmol). Purification by preparative RP-HPLC (column: Kinetex-XB C18, gradient: 0-35 min: A1/B 92:8-57:43, t_R = 17 min) afforded **2.07** as white fluffy solid (17.7 mg, 42%). ^{1}H-NMR (600 MHz, DMSO-d_6): δ 0.83 (d, 3H, *J* 6.5 Hz), 0.85-0.94 (m, 12H), 1.41-1.87 (m, 14H), 1.93-2.05 (m, 1H), 2.46-2.48 (m, 3H), 2.68 (dd, 1H, *J* 8.4, 14.1 Hz), 2.85-2.91 (m, 1H), 3.05-3.14 (m, 4H), 3.54-3.57 (m, 1H), 3.59-3.61 (m, 1H), 3.75-3.80 (m, 1H), 4.18-4.24 (m, 1H), 4.26-4.30 (m, 1H), 4.32-4.38 (m, 1H), 4.43-4.60 (m, 2H), 6.61 (d, 2H, *J* 8.5 Hz), 6.64-7.12 (br s, 4H, interfering with the next listed signal), 6.98-7.00 (m, 2H), 7.12-7.55 (br s, 4H), 7.55-7.67 (m, 3H), 7.89-8.09 (m, 1H), 8.15-8.30 (m, 1H), 8.72-9.07 (m, 3H), 9.10-9.27 (m, 1H), 12.48 (br s, 1H). HRMS (LC method A): *m/z* [*M*+2H]$^{2+}$ calcd. for [$C_{39}H_{68}N_{12}O_8$]$^{2+}$ 416.2636, found 416.2644. RP-HPLC (220 nm): > 99% (t_R = 6.3 min, *k* = 7.3). $C_{39}H_{66}N_{12}O_8$ · $C_6H_3F_9O_6$ (831.03 + 342.07).

***N*$^{\alpha}$-Argininyl-*N*$^{\alpha}$-methyl-Arg-Pro-Tyr-2-*tert*-butyl-Gly-Leu tris(hydrotrifluoroacetate) (2.08).** Peptide **2.08** was synthesized according to the general procedure using a H-Leu-2-ClTrt resin (loading 0.79 mmol/g) (45 mg, 0.0356 mmol). Purification by preparative RP-HPLC (column: Kinetex-XB C18, gradient: 0-35 min: A1/B 92:8-57:43, t_R = 18 min) afforded **2.08** as white fluffy solid (15.9 mg, 38%). ^{1}H-NMR (600 MHz, DMSO-d_6): δ 0.81-0.85 (m, 3H), 0.87-0.93 (m, 12H), 1.40-1.79 (m, 14H), 1.93-2.02 (m, 1H), 2.64-2.72 (m, 1H), 2.85-2.96 (m, 4H), 3.08-3.15 (m, 4H), 3.30-3.32 (m, 1H), 3.50-3.52 (m, 1H), 4.18-4.24 (m, 1H), 4.25-4.32 (m, 2H), 4.32-4.39 (m, 1H), 4.41-4.49 (m, 1H), 5.09-5.16 (m, 1H), 6.59-6.64 (m, 2H), 6.64-7.12 (br s, 4H, interfering with the next listed signal), 6.99-7.02 (m, 2H), 7.12-7.52 (br s, 4H), 7.52-7.61 (m, 2H), 7.69-7.73 (m, 1H), 7.95-8.01 (m, 1H), 8.06-8.29 (m, 4H), 9.17 (s, 1H), 12.47 (br s, 1H). HRMS (LC method A): *m/z* [*M*+2H]$^{2+}$ calcd. for [$C_{39}H_{68}N_{12}O_8$]$^{2+}$ 416.2636, found 416.2646. RP-HPLC (220 nm): > 99% (t_R = 6.3 min, *k* = 7.3). $C_{39}H_{66}N_{12}O_8$ · $C_6H_3F_9O_6$ (831.03 + 342.07).

Arg-Arg-Pro-Tyr-Ile-*N*$^{\alpha}$-methyl-Leu tris(hydrotrifluoroacetate) (2.09)[33]. Peptide **2.09** was synthesized on a 2-ClTrt-Cl resin (loading 1.6 mmol/g) (50 mg, 0.08 mmol). The

resin was treated with a solution of Fmoc-N-Me-Leu-OH (29.4 mg, 0.08 mmol) and DIPEA (34.8 µL, 0.2 mmol) in CH_2Cl_2 (0.5 mL) at 35 °C for 14 h. MeOH (50 µL) and CH_2Cl_2 (100 µL) were added and shaking was continued at rt for 15 min. The liquid was removed by filtration and the resin was washed with CH_2Cl_2 (3 ×), MeOH (3 ×) and DMF/NMP (80:20 v/v) (4 ×). The loading of the resin with Fmoc-N-Me-Leu was estimated to amount to 0.8 mmol/g (50 mg, 0.04 mmol) (basis for the calculation of the yield). Fmoc-deprotection of N-Me-Leu and further SPPS was performed according to the general procedure. Purification by preparative RP-HPLC (column: Kinetex-XB C18, gradient: 0-20 min: A1/B 92:8-72:28, 20-42 min: A1/B 72:28-35:65, t_R = 22 min) afforded **2.09** as white fluffy solid (9.1 mg, 20%). ^{1}H-NMR (600 MHz, DMSO-d_6): δ 0.73-0.90 (m, 12H), 1.01-1.12 (m, 1H), 1.30-1.38 (m, 1H), 1.44-1.60 (m, 7H), 1.62-1.73 (m, 4H), 1.75-1.87 (m, 4H), 1.95-2.03 (m, 1H), 2.56-2.62 (m, 1H), 2.75-2.80 (m, 1H), 2.95 (s, 3H), 3.05-3.12 (m, 4H), 3.54-3.56 (m, 1H), 3.58-3.60 (m, 1H), 3.78-3.82 (m, 1H), 4.29-4.34 (m, 1H), 4.38-4.52 (m, 2H), 4.54-4.64 (m, 1H), 5.05-5.17 (m, 1H), 6.59-6.66 (m, 2H), 6.68-7.13 (br s, 4H, interfering with the next listed signal), 7.00-7.03 (m, 2H), 7.13-7.56 (br s, 4H), 7.56-7.67 (m, 2H), 7.81-8.04 (m, 1H), 8.06-8.30 (m, 4H), 8.48-8.70 (m, 1H), 9.20 (s, 1H), 12.71 (br s, 1H). HRMS (LC method A): *m/z* $[M+2H]^{2+}$ calcd. for $[C_{39}H_{68}N_{12}O_8]^{2+}$ 416.2636, found 416.2644. RP-HPLC (220 nm): > 99% (t_R = 8.2 min, k = 9.8). $C_{39}H_{66}N_{12}O_8 \cdot C_6H_3F_9O_6$ (831.03 + 342.07).

***N*$^{\alpha}$-Propanoyl-Arg-Arg-Pro-Tyr-Ile-Leu bis(hydrotrifluoroacetate) (2.11).** Peptide **2.11** was synthesized according to the general procedure using a H-Leu-2-ClTrt resin (loading 0.79 mmol/g) (50 mg, 0.0395 mmol). After the last amino acid coupling and Fmoc deprotection step, the resin was treated with a solution of **2.10** (20.3 mg, 0.119 mmol, 3 equiv.) and DIPEA (20.6 µL, 0.119 mmol, 3 equiv.) in DMF/NMP (80:20 v/v) (2 mL) under shaking at rt for 1 h. The resin was washed with DMF/NMP (80:20 v/v) (6 ×) and the peptide was cleaved off the resin as described in the general procedure. Purification by preparative RP-HPLC (column: Kinetex-XB C18, gradient: 0-35 min: A1/B 92:8-57:43, t_R = 21 min) afforded **2.11** as white fluffy solid (24.5 mg, 56%). ^{1}H-NMR (600 MHz, DMSO-d_6): δ 0.76-0.81 (m, 3H), 0.84 (d, 6H, *J* 6.4 Hz), 0.90 (d, 3H, *J* 6.6 Hz), 0.94-1.01 (m, 3H), 1.01-1.10 (m, 1H), 1.39-1.57 (m, 9H), 1.59-1.72 (m, 4H), 1.72-1.87 (m, 3H), 1.95-2.02 (m, 1H), 2.08-2.18 (m, 2H), 2.68 (dd, 1H, *J* 8.2, 14.0 Hz), 2.86 (dd, 1H, *J* 5.1, 14.0 Hz), 3.03-3.12 (m, 4H), 3.57-3.58 (m, 1H), 3.60-3.61 (m, 1H), 4.17-4.24 (m, 2H), 4.24-4.30 (m, 1H), 4.30-4.36 (m, 1H), 4.36-4.43 (m, 1H), 4.43-4.50 (m, 1H), 6.52-6.62 (m, 2H), 6.62-7.06 (br s, 4H, interfering with the next listed signal), 6.98-7.01 (m, 2H), 7.06-7.62 (br s, 4H, interfering with the next listed signal), 7.43-7.50 (m, 2H), 7.69-7.79 (m, 1H), 7.79-8.02 (m, 2H), 8.02-8.16 (m, 1H), 8.16-8.30 (m, 1H), 9.01-9.29 (m, 1H), 12.49 (br s, 1H). HRMS (LC method A): *m/z* $[M+2H]^{2+}$ calcd. for $[C_{41}H_{70}N_{12}O_9]^{2+}$ 437.2689, found 437.2697. RP-HPLC (220 nm): > 98% (t_R = 8.1 min, k = 9.7). $C_{41}H_{68}N_{12}O_9 \cdot C_4H_2F_6O_4$ (873.07 + 228.05).

***N*$^{\alpha}$-Propanoyl-Arg-Arg-Pro-Tyr-2-*tert*-butyl-Gly-Leu bis(hydrotrifluoroacetate) (2.12).** Peptide **2.02** (22.2 mg, 0.0191 mmol) was dissolved in DMF/NMP (75:25 v/v) (180 µL). A solution of DIPEA (10 µL, 0.057 mmol) and **2.10** (9.8 mg, 0.057 mmol) in anhydrous DMF (23 µL) was added and the mixture was stirred at rt for 1 h followed by the addition of TFA/H_2O (1:9 v/v) (ca 0.06 mmol TFA). Purification by preparative RP-HPLC (column: Kinetex-XB C18, gradient: 0-35 min: A1/B 92:8-57:43, t_R = 20 min) afforded **2.12** as white fluffy solid (17.9 mg, 85%). ^{1}H-NMR (600 MHz, DMSO-d_6): δ 0.81-0.92 (m, 15H), 0.97-1.01 (m, 3H), 1.40-1.68 (m, 11H), 1.68-1.86 (m, 3H), 1.93-2.04 (m, 1H), 2.07-2.18

(m, 2H), 2.68 (dd, 1H, *J* 8.2, 13.9 Hz), 2.85-2.90 (m, 1H), 3.03-3.12 (m, 4H), 3.49-3.50 (m, 1H), 3.58-3.61 (m, 1H), 4.18-4.24 (m, 1H), 4.24-4.31 (m, 2H), 4.31-4.38 (m, 1H), 4.41-4.48 (m, 2H), 6.53-6.62 (m, 2H), 6.62-7.04 (br s, 4H, interfering with the next listed signal), 6.98-7.01 (m, 2H), 7.04-7.56 (br s, 4H, interfering with the next listed signal), 7.43-7.49 (m, 2H), 7.56-7.63 (m, 1H), 7.82-7.94 (m, 1H), 7.94-8.02 (m, 1H), 8.02-8.12 (m, 1H), 8.22 (d, 1H, *J* 7.5 Hz), 9.16 (s, 1H), 12.47 (br s, 1H). HRMS (LC method A): *m/z* $[M+2H]^{2+}$ calcd. for $[C_{41}H_{70}N_{12}O_9]^{2+}$ 437.2689, found 437.2706. RP-HPLC (220 nm): > 99% (t_R = 7.7 min, *k* = 9.1). $C_{41}H_{68}N_{12}O_9 \cdot C_4H_2F_6O_4$ (873.07 + 228.05).

2.5 References

1. Myers, R.M.; Shearman, J.W.; Kitching, M.O.; Ramos-Montoya, A.; Neal, D.E.; Ley, S.V. Cancer, chemistry, and the cell: Molecules that interact with the neurotensin receptors. *ACS Chem Biol* **2009**, *4*, 503-525, doi:10.1021/cb900038e.

2. Vincent, J.P.; Mazella, J.; Kitabgi, P. Neurotensin and neurotensin receptors. *Trends Pharmacol Sci* **1999**, *20*, 302-309, doi:10.1016/s0165-6147(99)01357-7.

3. Carraway, R.; Leeman, S.E. The amino acid sequence of a hypothalamic peptide, neurotensin. *J Biol Chem* **1975**, *250*, 1907-1911.

4. Tanaka, K.; Masu, M.; Nakanishi, S. Structure and functional expression of the cloned rat neurotensin receptor. *Neuron* **1990**, *4*, 847-854, doi:10.1016/0896-6273(90)90137-5.

5. Mazella, J.; Zsürger, N.; Navarro, V.; Chabry, J.; Kaghad, M.; Caput, D.; Ferrara, P.; Vita, N.; Gully, D.; Maffrand, J.P.; et al. The 100-kDa neurotensin receptor is gp95/sortilin, a non-G-protein-coupled receptor. *J Biol Chem* **1998**, *273*, 26273-26276, doi:10.1074/jbc.273.41.26273.

6. Maoret, J.J.; Pospai, D.; Rouyer-Fessard, C.; Couvineau, A.; Laboisse, C.; Voisin, T.; Laburthe, M. Neurotensin receptor and its mRNA are expressed in many human colon cancer cell lines but not in normal colonic epithelium: Binding studies and RT-PCR experiments. *Biochem Biophys Res Commun* **1994**, *203*, 465-471, doi:10.1006/bbrc.1994.2205.

7. Reubi, J.C.; Waser, B.; Friess, H.; Büchler, M.; Laissue, J. Neurotensin receptors: A new marker for human ductal pancreatic adenocarcinoma. *Gut* **1998**, *42*, 546-550, doi:10.1136/gut.42.4.546.

8. Reubi, J.C.; Waser, B.; Schaer, J.C.; Laissue, J.A. Neurotensin receptors in human neoplasms: High incidence in Ewing's sarcomas. *Int J Cancer* **1999**, *82*, 213-218, doi:10.1002/(sici)1097-0215(19990719)82:2<213::aid-ijc11>3.0.co;2-8.

9. Souazé, F.; Dupouy, S.; Viardot-Foucault, V.; Bruyneel, E.; Attoub, S.; Gespach, C.; Gompel, A.; Forgez, P. Expression of neurotensin and NT1 receptor in human breast cancer: A potential role in tumor progression. *Cancer Res* **2006**, *66*, 6243-6249, doi:10.1158/0008-5472.CAN-06-0450.

10. Bergmann, R.; Scheunemann, M.; Heichert, C.; Mäding, P.; Wittrisch, H.; Kretzschmar, M.; Rodig, H.; Tourwé, D.; Iterbeke, K.; Chavatte, K.; et al. Biodistribution and catabolism of ^{18}F-labeled neurotensin(8-13) analogs. *Nucl Med Biol* **2002**, *29*, 61-72, doi:10.1016/s0969-8051(01)00284-0.

11. Alshoukr, F.; Rosant, C.; Maes, V.; Abdelhak, J.; Raguin, O.; Burg, S.; Sarda, L.; Barbet, J.; Tourwé, D.; Pelaprat, D.; et al. Novel neurotensin analogues for radioisotope targeting to neurotensin receptor-positive tumors. *Bioconjug Chem* **2009**, *20*, 1602-1610, doi:10.1021/bc900151z.

12. García-Garayoa, E.; Bläuenstein, P.; Blanc, A.; Maes, V.; Tourwé, D.; Schubiger, P.A. A stable neurotensin-based radiopharmaceutical for targeted imaging and

therapy of neurotensin receptor-positive tumours. *Eur J Nucl Med Mol Imaging* **2009**, *36*, 37-47, doi:10.1007/s00259-008-0894-y.

13. Maschauer, S.; Einsiedel, J.; Hocke, C.; Hübner, H.; Kuwert, T.; Gmeiner, P.; Prante, O. Synthesis of a ^{68}Ga-labeled peptoid-peptide hybrid for imaging of neurotensin receptor expression in vivo. *ACS Med Chem Lett* **2010**, *1*, 224-228, doi:10.1021/ml1000728.

14. Maschauer, S.; Einsiedel, J.; Haubner, R.; Hocke, C.; Ocker, M.; Hübner, H.; Kuwert, T.; Gmeiner, P.; Prante, O. Labeling and glycosylation of peptides using click chemistry: A general approach to ^{18}F-glycopeptides as effective imaging probes for positron emission tomography. *Angew Chem Int Ed Engl* **2010**, *49*, 976-979, doi:10.1002/anie.200904137.

15. Alshoukr, F.; Prignon, A.; Brans, L.; Jallane, A.; Mendes, S.; Talbot, J.N.; Tourwé, D.; Barbet, J.; Gruaz-Guyon, A. Novel DOTA-neurotensin analogues for ^{111}In scintigraphy and ^{68}Ga PET imaging of neurotensin receptor-positive tumors. *Bioconjug Chem* **2011**, *22*, 1374-1385, doi:10.1021/bc200078p.

16. Maschauer, S.; Ruckdeschel, T.; Tripal, P.; Haubner, R.; Einsiedel, J.; Hübner, H.; Gmeiner, P.; Kuwert, T.; Prante, O. *In vivo* monitoring of the antiangiogenic effect of neurotensin receptor-mediated radiotherapy by small-animal positron emission tomography: A pilot study. *Pharmaceuticals (Basel)* **2014**, *7*, 464-481, doi:10.3390/ph7040464.

17. Jia, Y.; Shi, W.; Zhou, Z.; Wagh, N.K.; Fan, W.; Brusnahan, S.K.; Garrison, J.C. Evaluation of DOTA-chelated neurotensin analogs with spacer-enhanced biological performance for neurotensin-receptor-1-positive tumor targeting. *Nucl Med Biol* **2015**, *42*, 816-823, doi:10.1016/j.nucmedbio.2015.07.010.

18. Maschauer, S.; Einsiedel, J.; Hübner, H.; Gmeiner, P.; Prante, O. ^{18}F- and ^{68}Ga-labeled neurotensin peptides for PET imaging of neurotensin receptor 1. *J Med Chem* **2016**, *59*, 6480-6492, doi:10.1021/acs.jmedchem.6b00675.

19. Deng, H.; Wang, H.; Zhang, H.; Wang, M.; Giglio, B.; Ma, X.; Jiang, G.; Yuan, H.; Wu, Z.; Li, Z. Imaging neurotensin receptor in prostate cancer with ^{64}Cu-labeled neurotensin analogs. *Mol Imaging* **2017**, *16*, 1-11, doi:10.1177/1536012117711369.

20. Lang, C.; Maschauer, S.; Hübner, H.; Gmeiner, P.; Prante, O. Synthesis and evaluation of a ^{18}F-labeled diarylpyrazole glycoconjugate for the imaging of NTS1-positive tumors. *J Med Chem* **2013**, *56*, 9361-9365, doi:10.1021/jm401491e.

21. Schulz, J.; Rohracker, M.; Stiebler, M.; Goldschmidt, J.; Grosser, O.S.; Osterkamp, F.; Pethe, A.; Reineke, U.; Smerling, C.; Amthauer, H. Comparative evaluation of the biodistribution profiles of a series of nonpeptidic neurotensin receptor-1 antagonists reveals a promising candidate for theranostic applications. *J Nucl Med* **2016**, *57*, 1120-1123, doi:10.2967/jnumed.115.170530.

22. Baum, R.P.; Singh, A.; Schuchardt, C.; Kulkarni, H.R.; Klette, I.; Wiessalla, S.; Osterkamp, F.; Reineke, U.; Smerling, C. ^{177}Lu-3BP-227 for neurotensin receptor 1-targeted therapy of metastatic pancreatic adenocarcinoma - first clinical results. *J Nucl Med* **2018**, *59*, 809-814, doi:10.2967/jnumed.117.193847.

23. Pedersen, J.H.; Beck, H.; Shokouh-Amiri, M.; Fischer, A. Effect of neurotensin in the dumping syndrome. *Scand J Gastroenterol* **1986**, *21*, 478-482, doi:10.3109/00365528609015165.

24. García-Garayoa, E.; Allemann-Tannahill, L.; Bläuenstein, P.; Willmann, M.; Carrel-Rémy, N.; Tourwé, D.; Iterbeke, K.; Conrath, P.; Schubiger, P.A. *In vitro* and *in vivo* evaluation of new radiolabeled neurotensin(8-13) analogues with high affinity for NT1 receptors. *Nucl Med Biol* **2001**, *28*, 75-84, doi:10.1016/s0969-8051(00)00190-6.

25. Kitabgi, P.; De Nadai, F.; Rovère, C.; Bidard, J.N. Biosynthesis, maturation, release, and degradation of neurotensin and neuromedin N. *Ann N Y Acad Sci* **1992**, *668*, 30-42, doi:10.1111/j.1749-6632.1992.tb27337.x.

26. Tyler-McMahon, B.M.; Boules, M.; Richelson, E. Neurotensin: Peptide for the next millennium. *Regul Pept* **2000**, *93*, 125-136, doi:10.1016/s0167-0115(00)00183-x.

27. Bruehlmeier, M.; García-Garayoa, E.; Blanc, A.; Holzer, B.; Gergely, S.; Tourwé, D.; Schubiger, P.A.; Bläuenstein, P. Stabilization of neurotensin analogues: Effect on peptide catabolism, biodistribution and tumor binding. *Nucl Med Biol* **2002**, *29*, 321-327, doi:10.1016/s0969-8051(01)00304-3.

28. García-Garayoa, E.; Bläuenstein, P.; Bruehlmeier, M.; Blanc, A.; Iterbeke, K.; Conrath, P.; Tourwé, D.; Schubiger, P.A. Preclinical evaluation of a new, stabilized neurotensin(8-13) pseudopeptide radiolabeled with ^{99m}Tc. *J Nucl Med* **2002**, *43*, 374-383.

29. Bläuenstein, P.; García-Garayoa, E.; Rüegg, D.; Blanc, A.; Tourwé, D.; Beck-Sickinger, A.; Schubiger, P.A. Improving the tumor uptake of ^{99m}Tc-labeled neuropeptides using stabilized peptide analogues. *Cancer Biother Radiopharm* **2004**, *19*, 181-188, doi:10.1089/108497804323071959.

30. Maes, V.; García-Garayoa, E.; Bläuenstein, P.; Tourwé, D. Novel ^{99m}Tc-labeled neurotensin analogues with optimized biodistribution properties. *J Med Chem* **2006**, *49*, 1833-1836, doi:10.1021/jm051172f.

31. Nock, B.A.; Nikolopoulou, A.; Reubi, J.C.; Maes, V.; Conrath, P.; Tourwé, D.; Maina, T. Toward stable N_4-modified neurotensins for NTS1-receptor-targeted tumor imaging with ^{99m}Tc. *J Med Chem* **2006**, *49*, 4767-4776, doi:10.1021/jm060415g.

32. Maina, T.; Nikolopoulou, A.; Stathopoulou, E.; Galanis, A.S.; Cordopatis, P.; Nock, B.A. [^{99m}Tc]Demotensin 5 and 6 in the NTS1-R-targeted imaging of tumours: Synthesis and preclinical results. *Eur J Nucl Med Mol Imaging* **2007**, *34*, 1804-1814, doi:10.1007/s00259-007-0489-z.

33. Härterich, S.; Koschatzky, S.; Einsiedel, J.; Gmeiner, P. Novel insights into GPCR-peptide interactions: Mutations in extracellular loop 1, ligand backbone methylations and molecular modeling of neurotensin receptor 1. *Bioorg Med Chem* **2008**, *16*, 9359-9368, doi:10.1016/j.bmc.2008.08.051.

34. Orwig, K.S.; Lassetter, M.R.; Hadden, M.K.; Dix, T.A. Comparison of N-terminal modifications on neurotensin(8-13) analogues correlates peptide stability but not

binding affinity with in vivo efficacy. *J Med Chem* **2009**, *52*, 1803-1813, doi:10.1021/jm801072v.

35. Boules, M.; Liang, Y.; Briody, S.; Miura, T.; Fauq, I.; Oliveros, A.; Wilson, M.; Khaniyev, S.; Williams, K.; Li, Z.; et al. NT79: A novel neurotensin analog with selective behavioral effects. *Brain Res* **2010**, *1308*, 35-46, doi:10.1016/j.brainres.2009.10.050.

36. Einsiedel, J.; Held, C.; Hervet, M.; Plomer, M.; Tschammer, N.; Hübner, H.; Gmeiner, P. Discovery of highly potent and neurotensin receptor 2 selective neurotensin mimetics. *J Med Chem* **2011**, *54*, 2915-2923, doi:10.1021/jm200006c.

37. Held, C.; Plomer, M.; Hübner, H.; Meltretter, J.; Pischetsrieder, M.; Gmeiner, P. Development of a metabolically stable neurotensin receptor 2 (NTS2) ligand. *ChemMedChem* **2013**, *8*, 75-81, doi:10.1002/cmdc.201200376.

38. Mascarin, A.; Valverde, I.E.; Mindt, T.L. Structure-activity relationship studies of amino acid substitutions in radiolabeled neurotensin conjugates. *ChemMedChem* **2016**, *11*, 102-107, doi:10.1002/cmdc.201500468.

39. Bittermann, H.; Einsiedel, J.; Hübner, H.; Gmeiner, P. Evaluation of lactam-bridged neurotensin analogues adjusting $\psi(\mathrm{Pro}^{10})$ close to the experimentally derived bioactive conformation of NT(8-13). *J Med Chem* **2004**, *47*, 5587-5590, doi:10.1021/jm049644y.

40. Kokko, K.P.; Hadden, M.K.; Orwig, K.S.; Mazella, J.; Dix, T.A. In vitro analysis of stable, receptor-selective neurotensin[8-13] analogues. *J Med Chem* **2003**, *46*, 4141-4148, doi:10.1021/jm0300633.

41. Granier, C.; Vanrietschoten, J.; Kitabgi, P.; Poustis, C.; Freychet, P. Synthesis and characterization of neurotensin analogs for structure/activity relationship studies - Acetyl-neurotensin-(8-13) is the shortest analog with full binding and pharmacological activities. *Eur J Biochem* **1982**, *124*, 117-124, doi:DOI 10.1111/j.1432-1033.1982.tb05913.x.

42. Keller, M.; Kuhn, K.K.; Einsiedel, J.; Hübner, H.; Biselli, S.; Mollereau, C.; Wifling, D.; Svobodová, J.; Bernhardt, G.; Cabrele, C.; et al. Mimicking of arginine by functionalized N^{ω}-carbamoylated arginine as a new broadly applicable approach to labeled bioactive peptides: High affinity angiotensin, neuropeptide Y, neuropeptide FF, and neurotensin receptor ligands as examples. *J Med Chem* **2016**, *59*, 1925-1945, doi:10.1021/acs.jmedchem.5b01495.

2.6 Appendix

2.6.1 General experimental conditions

If not otherwise stated, solvents and buffer components, purchased from commercial suppliers, were of analytical grade. Gradient grade MeOH for HPLC was obtained from Merck (Darmstadt, Germany) and gradient grade acetonitrile for HPLC was from Sigma-Aldrich (Taufkirchen, Germany). *N*,*N*-Diisopropylethylamine (DIPEA, 99%) was from ABCR (Karlsruhe, Germany). Anhydrous DMF (99.8%), 1,1,1,3,3,3-hexafluoro-2-propanol (HFIP) and 1-Methyl-D-Trp (**2.14**) were purchased from Sigma-Aldrich. DMF (for peptide synthesis, packed under nitrogen, code D/3848/PB17), NMP (for peptide synthesis, nitrogen flushed), anhydrous NMP (99,5%) and HOBt hydrate were obtained from Acros Organics/Fisher Scientific (Nidderau, Germany). Trifluoroacetic acid and absolute EtOH were purchased from Honeywell (Seelze, Germany). Piperidine and HBTU were from Iris Biotech (Marktredwitz, Germany). Bovine serum albumin (BSA) was purchased from Serva (Heidelberg, Germany), and ammonium acetate (98%) was from Merck. Peptide **2.01** (tris(hydrotrifluoroacetate)) was purchased from SynPeptide (Shanghai, China). Succinimidyl propionate (**2.10**) was prepared according to a described procedure[1]. Millipore water was used throughout for the preparation of buffers, stock solutions and HPLC eluents. 1.5- and 2-mL polypropylene reaction vessels with screw cap (in the following referred to as "reaction vessel with screw cap") from Süd-Laborbedarf (Gauting, Germany) were used for the preparation and storage of stock solutions, and for small-scale reactions. 1.5- or 2-mL polypropylene reaction vessels (in the following referred to as "reaction vessel") from Sarstedt (Nümbrecht, Germany) were used for the preparation of dilute solutions, and for the investigation of stabilities in plasma. Reactions under anhydrous conditions were performed under argon atmosphere using anhydrous solvents. For the evaporation of solvents in 1.5- or 2-mL reaction vessels a Savant Speed-Vac Plus SC110A vacuum concentrator (Thermo Fischer Scientific, Waltham, MA) was used. NMR spectra were recorded on a Bruker Avance 600 instrument (^{1}H: 600 MHz, T = 300 K) (Bruker, Karlsruhe, Germany). NMR spectra were calibrated based on the solvent residual peaks (^{1}H-NMR, DMSO-d_6: δ = 2.50 ppm) and data (^{1}H-NMR) are reported as follows: chemical shift δ in ppm (multiplicity (s = singlet, d = doublet, t = triplet, q = quartet, m = multiplet, br s = broad singlet), integral, coupling constant J in Hz). High resolution mass spectra (HRMS) were acquired with an Agilent 6540 UHD Accurate-Mass Q-TOF LC/MS system coupled to an Agilent 1290 HPLC system (Agilent Technologies, Santa Clara, CA), using an ESI source. Analyses were either performed with LC method A or B. Method A: column: Luna Omega C18, 1.6 µm, 50 × 2.1 mm (Phenomenex, Aschaffenburg, Germany), column temperature: 40 °C, flow: 0.6 mL/min, solvent/linear gradient: 0-4 min: 0.1% aq HCOOH/0.1% HCOOH in MeCN 95:5-2:98, 4-5 min: 2:98. Method B: column: YMC Triart C18, 1.9 µm, 75 × 2 mm (YMC Europe, Dinslaken, Germany), column temperature: 40 °C, flow: 0.6 mL/min, solvent/linear gradient: 0-10 min: 0.1% aq HCOOH/0.1% HCOOH in MeCN 100:0-70:30, 10-11 min: 70:30-2:98, 11-12 min: 2:98. Preparative HPLC was performed with a system from Knauer (Berlin, Germany) consisting of two K-1800 pumps and a K-2001 detector. A Kinetex-XB C18, 5 µm, 250 mm × 21 mm (Phenomenex) or a YMC-Actus Triart C8, 5 µm, 250 mm × 20 mm (YMC) served as RP-columns at flow rates of 20 mL/min and 18 mL/min, respectively. Mixtures of 0.2% aq TFA (A1) and acetonitrile (B), or 10 mM ammonium acetate buffer (pH 5) (A2) and B were used as mobile phase. A

detection wavelength of 220 nm was used throughout. Collected fractions were lyophilized using an Alpha 2-4 LD apparatus (Martin Christ, Osterode am Harz, Germany) equipped with a vacuubrand RZ 6 rotary vane vacuum pump. Analytical HPLC analysis of compounds **2.02**-**2.09**, **2.11** and **2.12** was performed with a system from Agilent Technologies consisting of a 1290 Infinity binary pump equipped with a degasser, a 1290 Infinity Autosampler, a 1290 Infinity Thermostated Column Compartment, a 1260 Infinity Diode Array Detector and a 1260 Infinity Fluorescence Detector. A Kinetex-XB C18, 2.6 µm, 100 × 3 mm (Phenomenex) or a YMC Triart C8, S-5µm, 250 × 4.6 mm (YMC) were used as stationary phase at a flow rate of 0.6 mL/min and 1 mL/min, respectively. The oven temperature was set to 25 °C. Mixtures of 0.04% aq TFA (A3) and B, or A2 and B served as mobile phase. The following linear gradients were applied: compounds **2.02**-**2.04**, **2.06**-**2.09**, **2.11** and **2.12** (Kinetex-XB): 0-12 min: A3/B 90:10-70:30, 12-16 min: 70:30-5:95, 16-20 min: 5:95; compound **2.05** (YMC Triart): 0-25 min: A2/B 90:10-65:35, 25-27 min: 65:35-5:95, 27-35 min: 5:95. The injection volume was 20 µL. UV detection was performed at 220 nm and fluorescence detection at 275/305 nm. Retention (capacity) factors k were calculated from the retention times t_R according to $k = (t_R - t_0)/t_0$ (t_0 = dead time). Synthesized peptides were characterized by ^{1}H-NMR spectroscopy, HRMS, and RP-HPLC analysis. Additionally, ^{1}H-COSY NMR spectra were acquired of peptides **2.02**-**2.06**, **2.09** and **2.11**. The purity of all final compounds, determined by RP-HPLC (220 nm), was ≥ 98%.

Annotation concerning the ^{1}H-NMR spectra (solvent: DMSO-d_6) of **2.04**, **2.05**, **2.07**-**2.09**, **2.11** and **2.12**: in order to allow an integration of the signals interfering with the broad water signal at ca 3.5 ppm, ^{1}H-NMR spectra were additionally recorded in DMSO-d_6/D_2O (11:1 or 4:1 v/v).

2.6.2 Radioligand competition binding assay

Competition binding with [^{3}H]UR-MK300 ([^{3}H]**2.13**) at the hNTS$_1$R was performed at 23 ± 1 °C using intact human HT-29 colon carcinoma cells (grown in antibiotic-free McCoy's 5A medium supplemented with 5% FCS) as described previously[2]. Prior to the competition binding experiments, the K_d value of [^{3}H]**2.13** was determined by saturation binding at HT-29 cells as reported previously (data not shown)[2]. The obtained K_d value amounted to 0.55 ± 0.03 nM (mean value ± SEM from two independent determinations performed in triplicate) being in excellent agreement with the reported K_d of [^{3}H]**2.13** (K_d = 0.51 nM)[2]. Binding data were analyzed by plotting % specifically bound radioligand (100% = specifically bound radioligand in the absence of competitor) over log(concentration of competitor) followed by a four-parameter sigmoidal fit (SigmaPlot 11.0, Systat Software). Resulting pIC_{50} values were converted to IC_{50} values and K_i values were calculated from the IC_{50} values according to the Cheng-Prusoff equation[3] using a K_d value of 0.55 nM. The K_i values from individual experiments were transformed to pK_i values, followed by the calculation of mean pK_i values ± SEM.

2.6.3 Experimental protocol for the investigation of the stability of 2.01-2.09, 2.11 and 2.12 in human plasma

The metabolic stabilities of **2.01**-**2.09**, **2.11** and **2.12** were investigated in human blood plasma/PBS, pH 7.4 (1:2 v/v) (in the following referred to as plasma/PBS) at 37 °C using 1.5- or 2-mL polypropylene reaction vessels. The vessels were placed in a Thermocell

mixing block from Bioer (Hangzhou, China). 1-Methyl-D-tryptophan (**2.14**) was used as internal standard. As the RP-HPLC purity of **2.14** was < 95% (data not shown), the compound was purified by preparative HPLC to give a purity of > 99%. Plasma was obtained by the collection of human blood from a healthy donor in 5.5-mL heparinized plasma-monovettes followed by centrifugation at 1,200 × g at 4 °C for 10 min. The supernatants were pooled in two 50-mL Falcon tubes and centrifuged again at 1,200 × g at 4 °C for 10 min. The plasma was aliquoted and stored at −80 °C.

For the addition of the peptides to plasma/PBS, 5 mM stock solutions in EtOH/HCl (20 mM) (50:50 v/v) (**2.01**) or MeCN/0.04% aq TFA (30:70 v/v) (**2.02**-**2.09**, **2.11** and **2.12**) were used. Recoveries were determined for peptide concentrations of 80 µM and 4 µM, and an internal standard concentration of 10 µM. For this purpose, **2.14** and the peptide were added to plasma/PBS (total volume: 70 µL), immediately followed by vortexing (ca 10 s) and precipitation of protein by the addition of ice-cold EtOH/MeCN (50:50 v/v) (140 µL). The mixture was vortexed for 5 min und centrifuged at 16,100 × g at 4 °C for 10 min. Aliquots (180 µL) of the supernatant were transferred to 1.5-mL reaction vessels containing 10% aq TFA (5 µL). The volatiles were removed in a vacuum concentrator under reduced pressure at 40 °C (ca 60 min) and the residue was taken up in MeCN/0.04% aq TFA (10:90 v/v) (90 µL) by vortexing (2 min). The samples were filtrated through a 0.2 µm RC-membrane filter (Phenomenex, Aschaffenburg, Germany) and analyzed by RP-HPLC using the analytical HPLC system and the conditions as for the purity control of **2.02**-**2.04**, **2.06**-**2.09**, **2.11** and **2.12** (general experimental conditions), but applying the following gradient: 0-12 min: A3/B 90:10-73:27, 12-16 min: 73:27-5:95, 16-20 min: 5:95. On the day of an experiment four-point calibrations were performed for the respective peptides and the internal standard. Peak areas representing 100% recovery were obtained by analyzing 53.3 µM and 2.67 µM peptide solutions as well as a 6.67 µM solution of **2.14** (in duplicate each). All peak areas were transformed into concentrations (µM) and percent recoveries of the peptides and the internal standard were calculated based on the average values of the 100% reference samples (see Table A2.1). Recovery ratios were obtained by dividing the recovery of the peptide by the recovery of **2.14** for each individual sample (n = 3-5, *cf.* Table A2.1).

For the investigation of the stabilities in plasma, the peptides and **2.14** were added to plasma/PBS at a concentration of 100 µM and 10 µM, respectively (in triplicate each). After 10 min, 1 h, 24 h and 48 h (**2.01** and **2.02**), 10 min, 30 min, 1 h and 2 h (**2.03**-**2.06**, **2.09** and **2.11**), or 1 h, 6 h, 24 h and 48 h (**2.07**, **2.08** and **2.12**) of incubation under shaking at 37 °C aliquots (70 µL) were taken and processed as described above for the determination of recoveries. On the day of an experiment four-point calibrations were performed for the respective peptides and **2.14**. Peak areas representing 100% recovery were obtained by analyzing 66.7 µM peptide solutions and a 6.67 µM solution of **2.14** (in duplicate).

Based on the calibration, the peak areas of the 100% references and of the samples were transformed into concentrations (µM). Recoveries of **2.01**-**2.09**, **2.11** and **2.12** were calculated by multiplying the recovery of **2.14**, obtained for each individual sample, with the recovery ratio obtained for the concentration of 80 µM (remaining peptide concentration in plasma/PBS > 20 µM) or 4 µM (remaining peptide concentration in

plasma/PBS < 20 µM). The concentrations of the peptides in plasma/PBS were obtained by dividing the determined peptide concentration by the respective recovery. Degradation (%) of **2.01**-**2.09**, **2.11** and **2.12** was calculated based on the average values of the 100% reference samples. Note: Data analysis was based on UV detection at 220 nm (**2.01**, **2.03**-**2.09**, **2.11**, **2.12** and **2.14**) or fluorescence detection at 275/305 nm (**2.02**).

The major degradation fragments of peptides **2.03**-**2.09**, **2.11** and **2.12** were identified by LC-HRMS analysis (LC-MS instrument and conditions see general experimental conditions; LC method A (**2.01**, **2.02**) or B (**2.03**-**2.09**, **2.11**, **2.12**)) using the same samples as used for HPLC analysis described above.

2.6.4 Figures A2.1 and A2.2 and Table A2.1

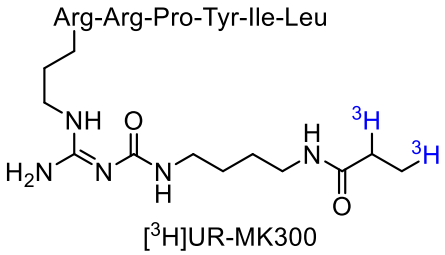

Figure A2.1. Structure of the tritium-labeled NT(8-13) derivative [^{3}H]UR-MK300 ([^{3}H]**2.13**) used as radioligand for NTS_1R competition binding studies (reported K_d = 0.51 nM[2]).

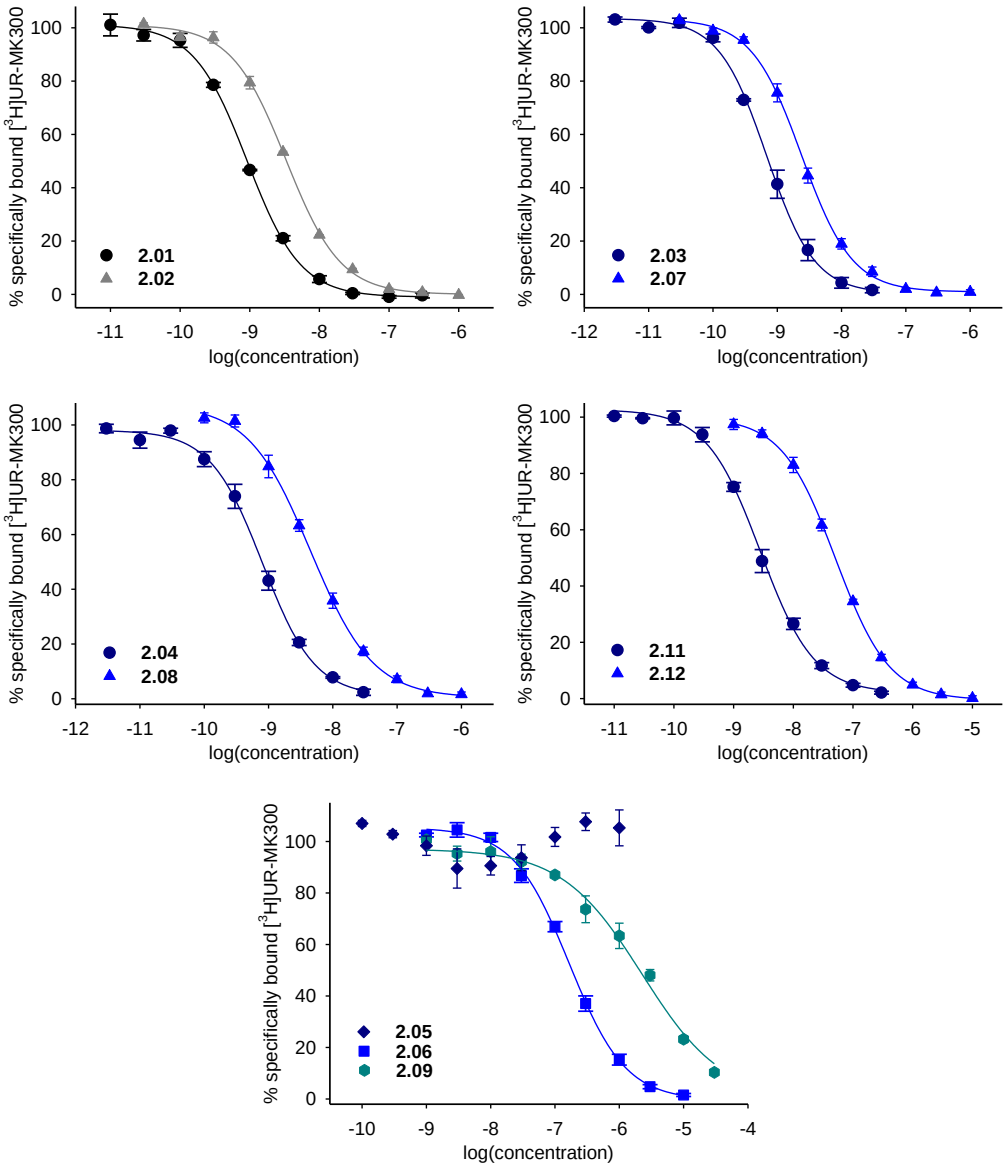

Figure A2.2. Displacement curves of [^{3}H]UR-MK300 ([^{3}H]**2.13**) (K_d = 0.55 nM, c = 1 nM) obtained from competition binding experiments with **2.01**-**2.09**, **2.11** and **2.12** at intact $hNTS_1R$-expressing HT-29 cells. Compounds containing Ile^{12} are represented by circles, compounds containing Tle^{12} are represented by triangles. Data represent mean values ± SEM from at least two independent experiments (performed in triplicate).

Table A2.1. Recoveries of peptides **2.01**-**2.09**, **2.11** and **2.12** from human plasma/PBS (1:2 v/v) for two different concentrations (80 μM and 4 μM), and ratios of peptide-recovery over recovery of internal standard (**2.14**).

Compd.	Peptide concentration 80 μM			Peptide concentration 4 μM		
	recovery peptide (%)[a]	recovery **2.14** (%)[a]	ratio[b]	recovery peptide (%)[a]	recovery **2.14** (%)[a]	ratio[b]
2.01	78	91	0.85	79	92	0.86
	72	83	0.86	82	91	0.90
	80	89	0.90	76	93	0.82
	76	86	0.89	85	95	0.89
				80	95	0.85
			(0.88 ± 0.01)			(0.86 ± 0.01)
2.02	91	99	0.92	88	99	0.89
	90	96	0.93	86	90	0.95
	92	101	0.91	91	99	0.91
	92	103	0.90			
			(0.91 ± 0.01)			(0.92 ± 0.02)
2.03	101	95	1.06	92	94	0.98
	105	96	1.09	85	92	0.92
	100	97	1.03	91	91	1.01
	96	94	1.02	85	90	0.94
	96	93	1.02	93	90	1.04
			(1.04 ± 0.01)			(0.98 ± 0.02)
2.04	84	91	0.93	93	89	1.04
	77	82	0.94	97	93	1.04
	75	83	0.90	92	89	1.03
	92	96	0.96	87	84	1.03
	89	95	0.93	86	85	1.01
			(0.93 ± 0.01)			(1.03 ± 0.01)
2.05	88	95	0.92	96	92	1.05
	88	95	0.93	98	94	1.04
	87	93	0.93	98	94	1.05
	88	96	0.92	101	96	1.05
				97	92	1.06
			(0.92 ± 0.003)			(1.05 ± 0.003)
2.06	76	95	0.81	84	95	0.88
	89	104	0.86	83	98	0.85
	75	90	0.83	84	95	0.88
	82	98	0.84			
	78	99	0.80			
			(0.83 ± 0.01)			(0.87 ± 0.01)
2.07	89	94	0.95	105	98	1.07
	88	96	0.92	103	99	1.04
	93	99	0.94	108	105	1.03
	94	101	0.93	106	99	1.08
				107	106	1.01
			(0.93 ± 0.01)			(1.05 ± 0.01)

Table A2.1 continued

2.08	89	102	0.87	103	105	0.99
	87	98	0.89	103	101	1.02
	92	100	0.92	104	107	0.97
	93	103	0.90	100	100	0.99
	85	97	0.87	101	99	1.02
			(0.89 ± 0.01)			(1.00 ± 0.01)
2.09	90	104	0.87	85	92	0.92
	90	100	0.90	95	101	0.94
	88	98	0.90	90	99	0.91
	90	99	0.91			
			(0.89 ± 0.01)			(0.93 ± 0.01)
2.11	78	93	0.84	97	100	0.97
	89	101	0.88	85	88	0.96
	87	99	0.88	86	87	0.99
	81	93	0.87	101	104	0.97
	73	86	0.84			
			(0.86 ± 0.01)			(0.97 ± 0.005)
2.12	87	99	0.88	95	100	0.95
	86	99	0.87	100	102	0.97
	87	101	0.86	95	94	1.01
	92	101	0.91	103	103	1.00
	83	93	0.89	101	102	0.99
			(0.88 ± 0.01)			(0.98 ± 0.01)

[a]Recoveries of the peptides and of the internal standard (**2.14**) from human plasma/PBS (1:2 v/v) using a peptide concentration of 80 µM or 4 µM and an internal standard concentration of 10 µM (three, four or five independent experiments). [b]Ratios of peptide recovery over recovery of **2.14** calculated for individual experiments, as well as mean recovery ratios ± SEM (given in parenthesis).

2.6.5 RP-HPLC chromatograms of compounds 2.02-2.09, 2.11 and 2.12

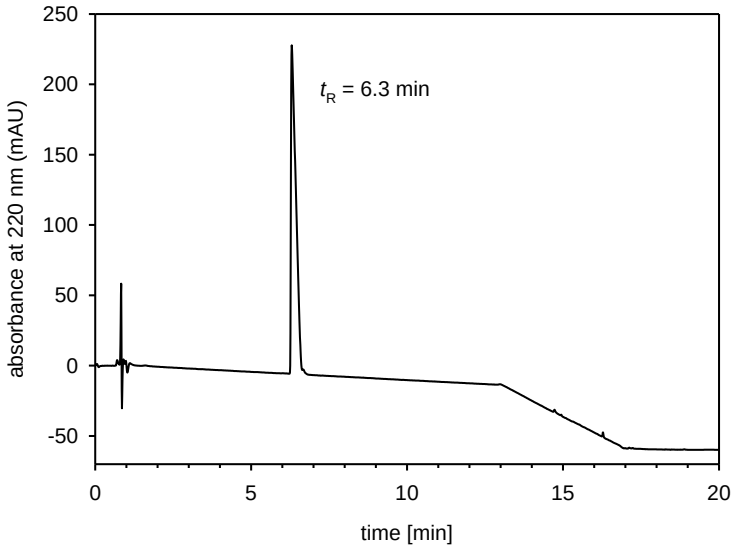

RP-HPLC analysis (purity control) of compound **2.02**

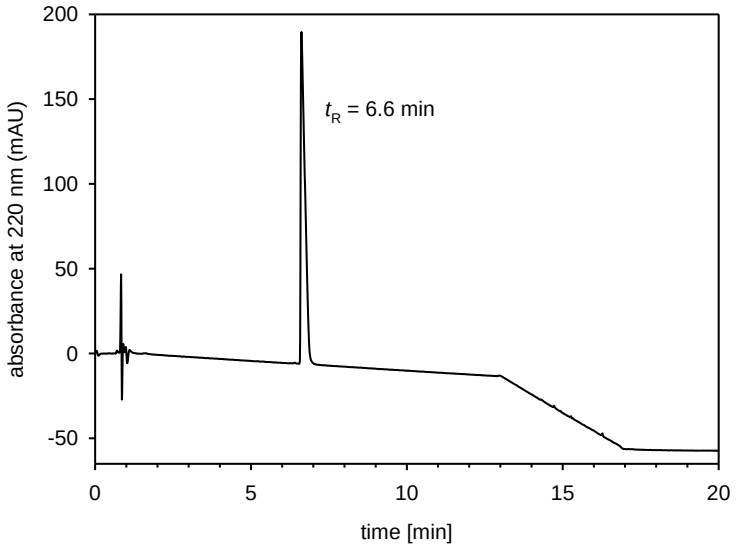

RP-HPLC analysis (purity control) of compound **2.03**

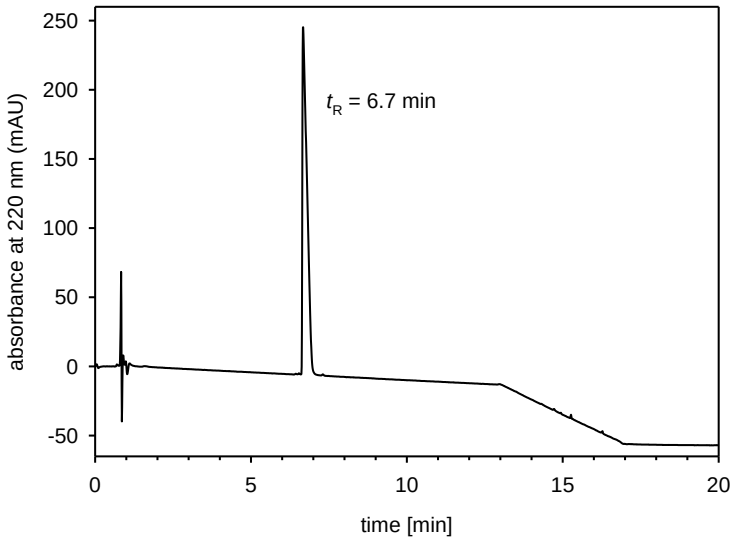

RP-HPLC analysis (purity control) of compound **2.04**

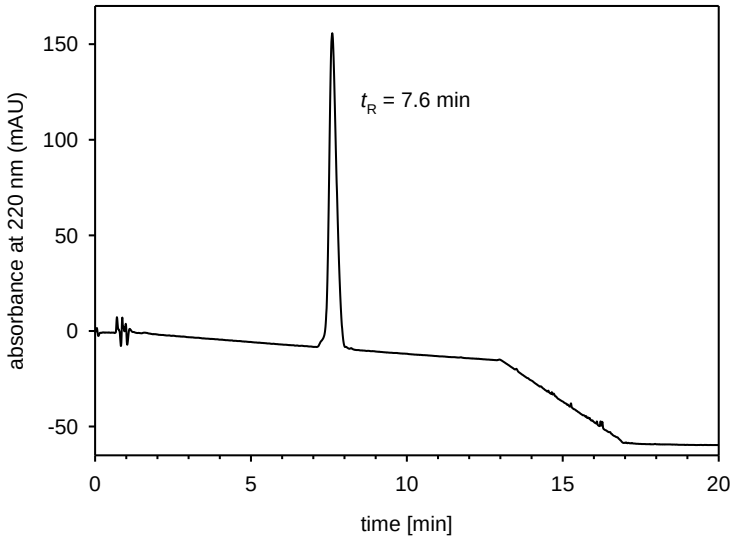

RP-HPLC analysis (purity control) of compound **2.05**

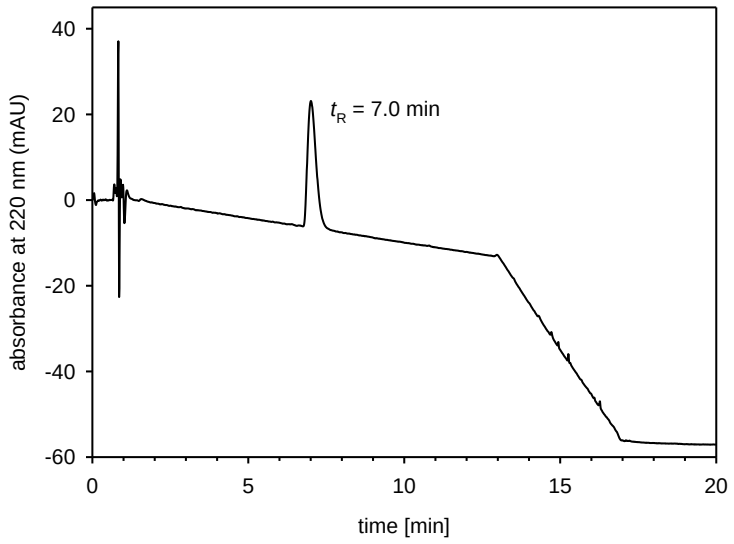

RP-HPLC analysis (purity control) of compound **2.06**

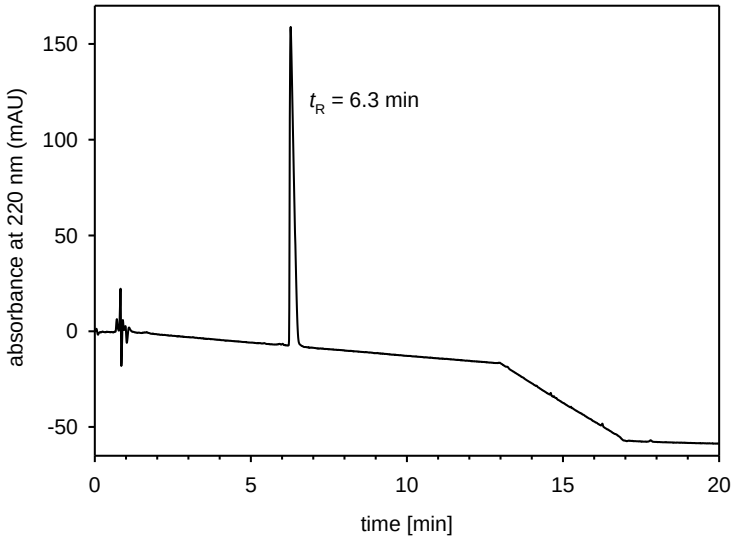

RP-HPLC analysis (purity control) of compound **2.07**

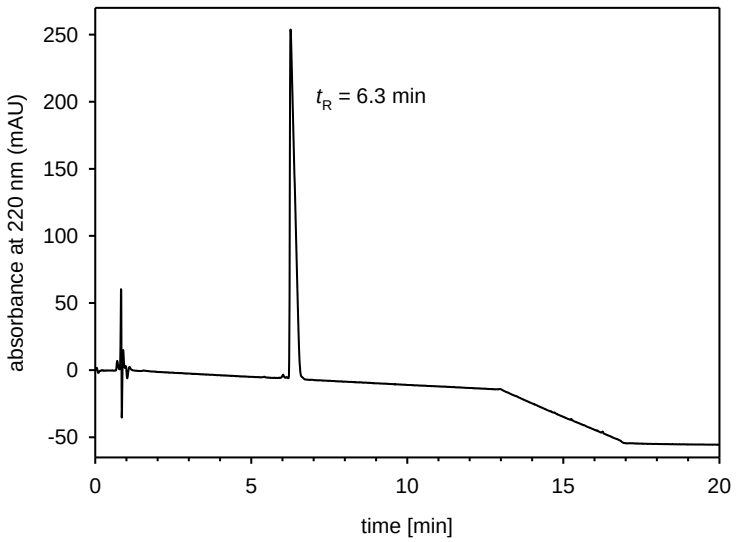

RP-HPLC analysis (purity control) of compound **2.08**

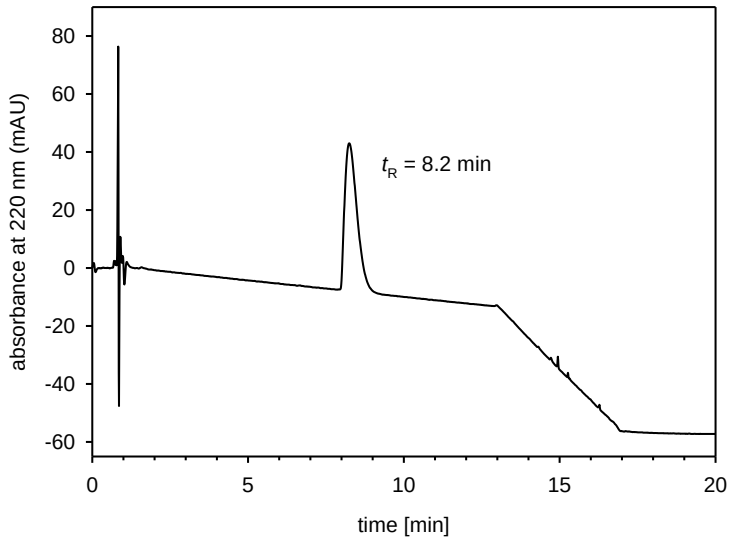

RP-HPLC analysis (purity control) of compound **2.09**

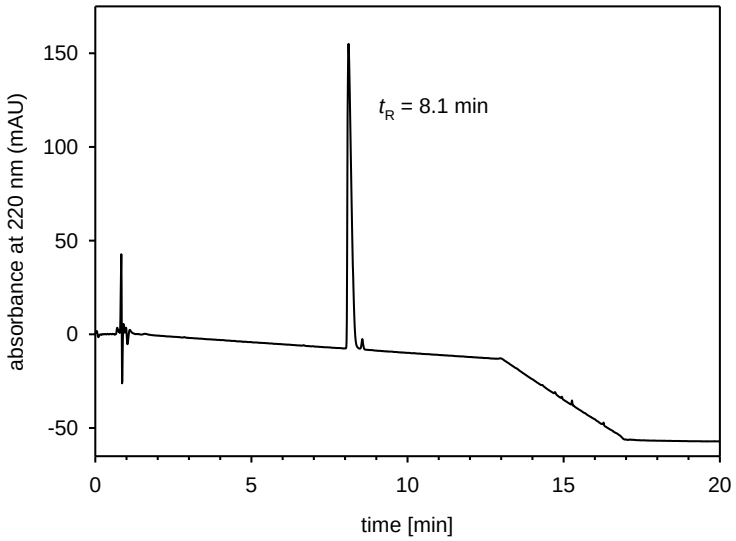

RP-HPLC analysis (purity control) of compound **2.11**

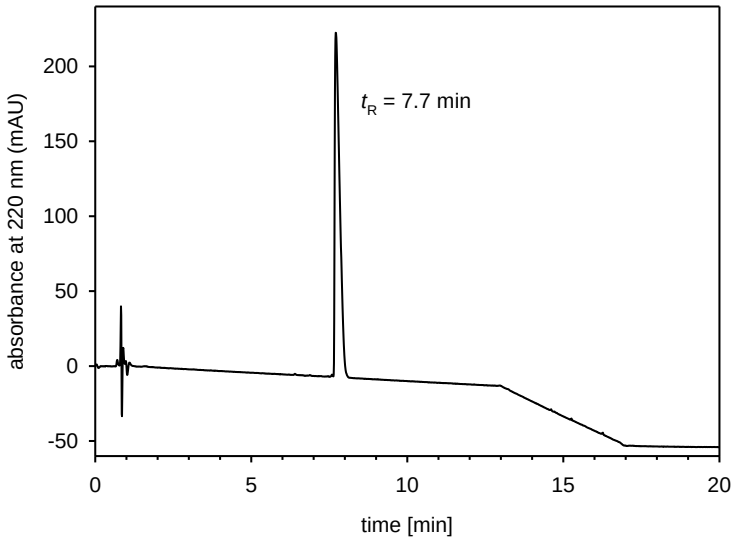

RP-HPLC analysis (purity control) of compound **2.12**

2.6.6 ^{1}H-NMR spectra of compounds 2.02-2.09, 2.11 and 2.12 in DMSO-d_6 and DMSO-d_6/D_2O

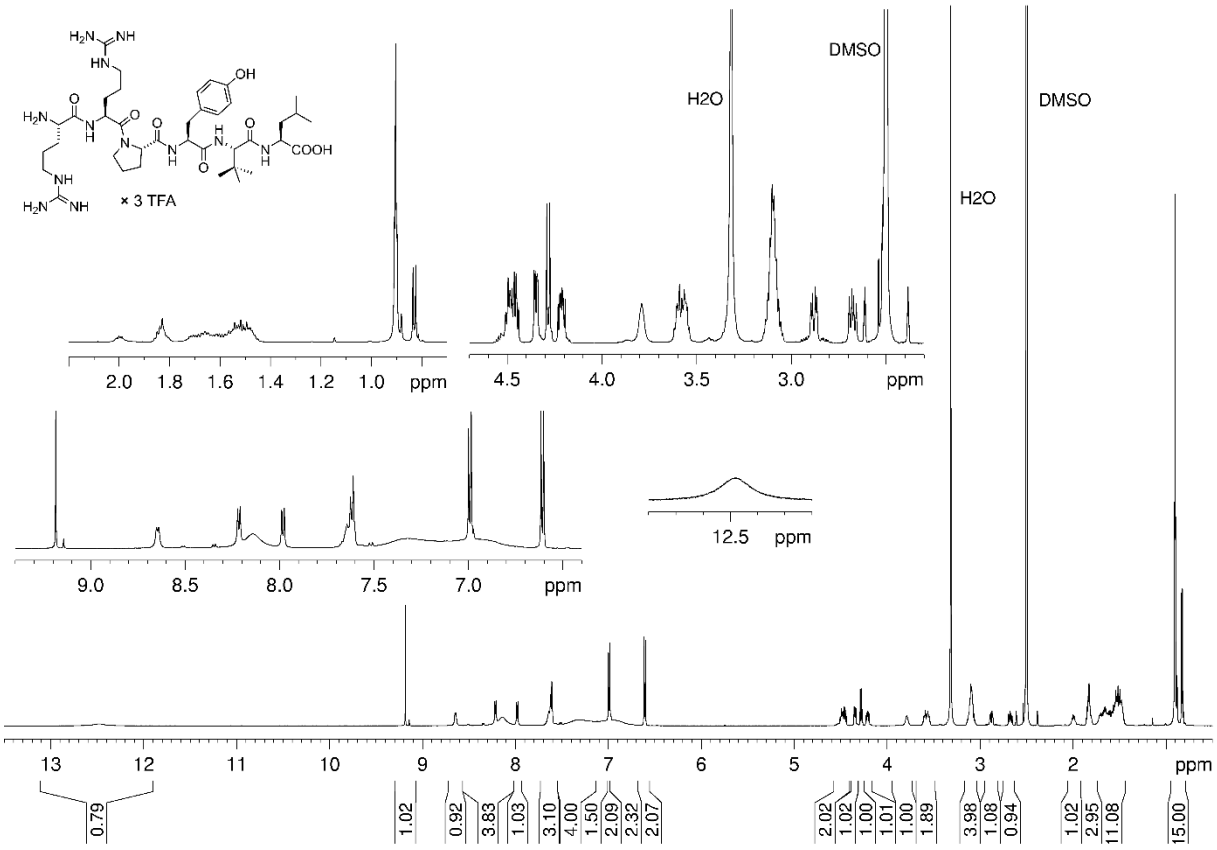

^{1}H-NMR spectrum (600 MHz, DMSO-d_6) of compound **2.02**

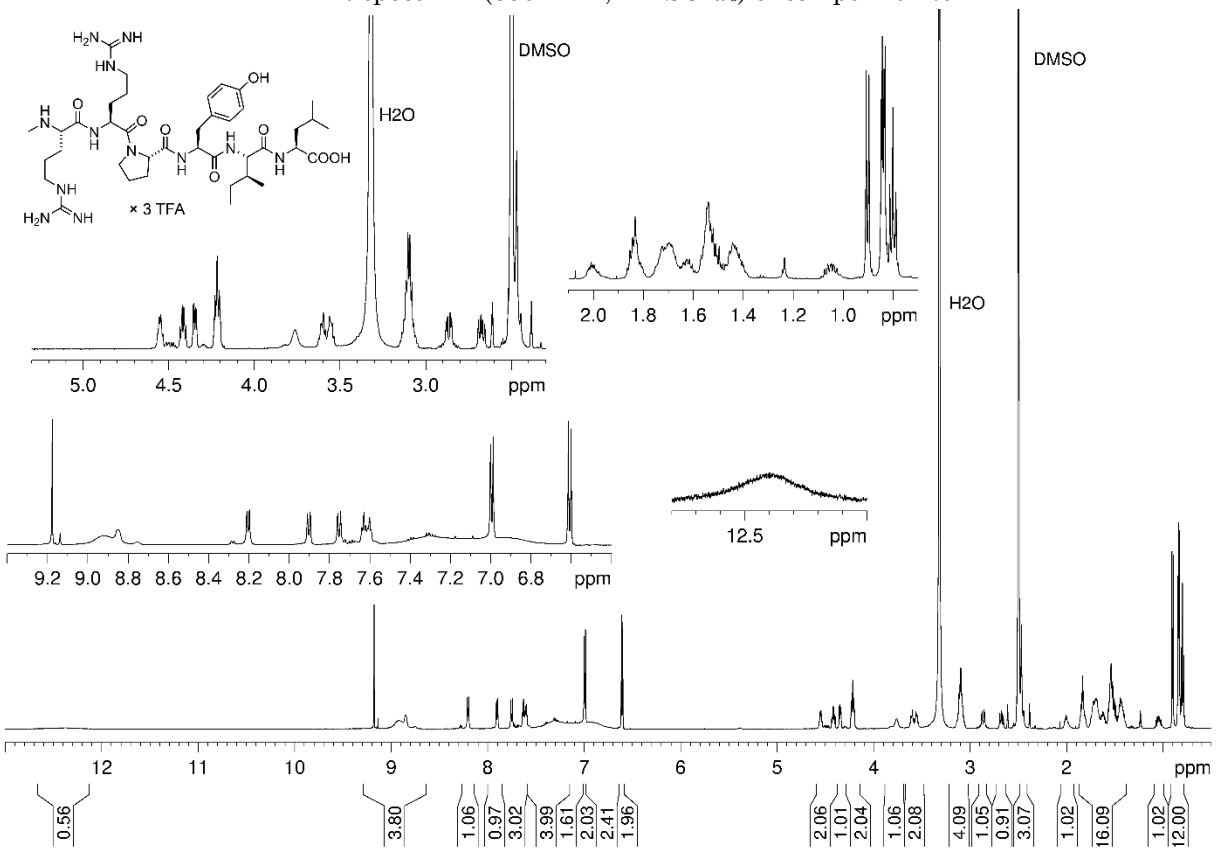

^{1}H-NMR spectrum (600 MHz, DMSO-d_6) of compound **2.03**

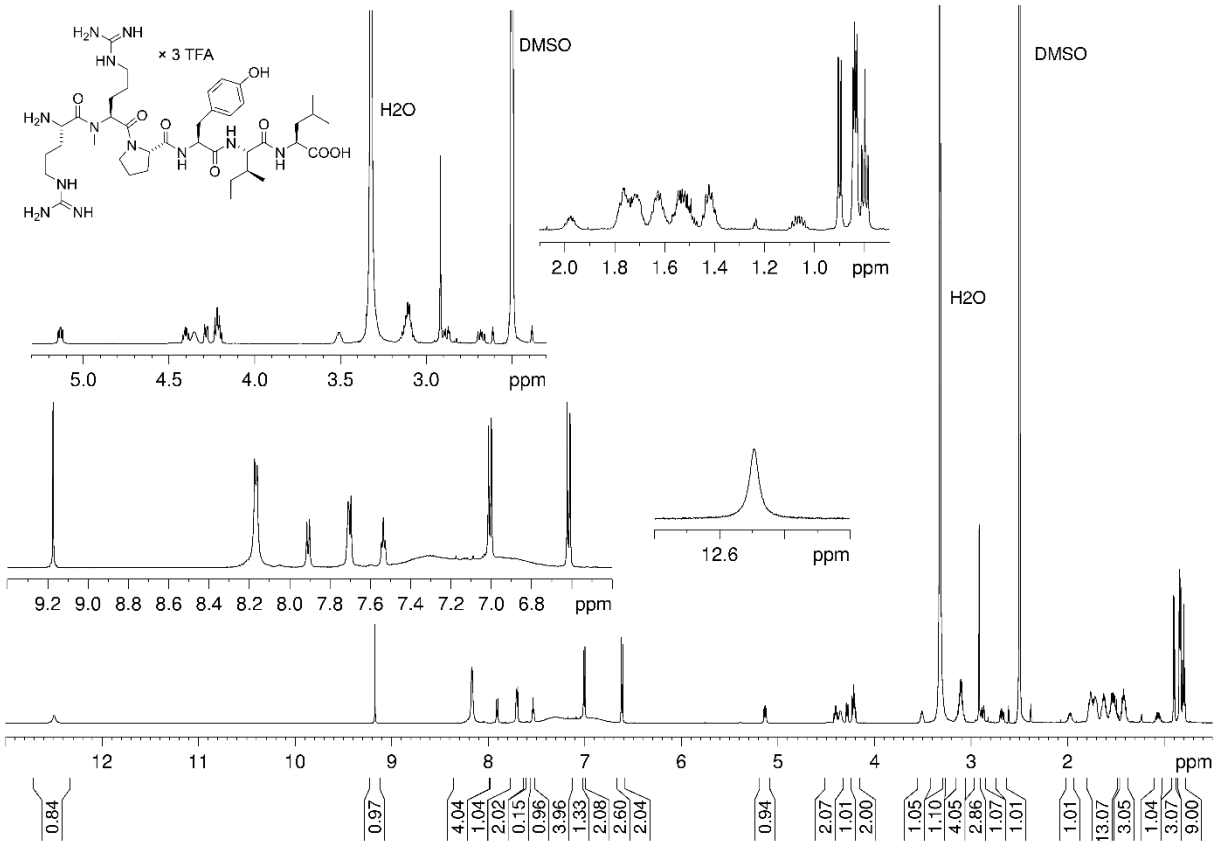

^{1}H-NMR spectrum (600 MHz, DMSO-d_6) of compound **2.04**

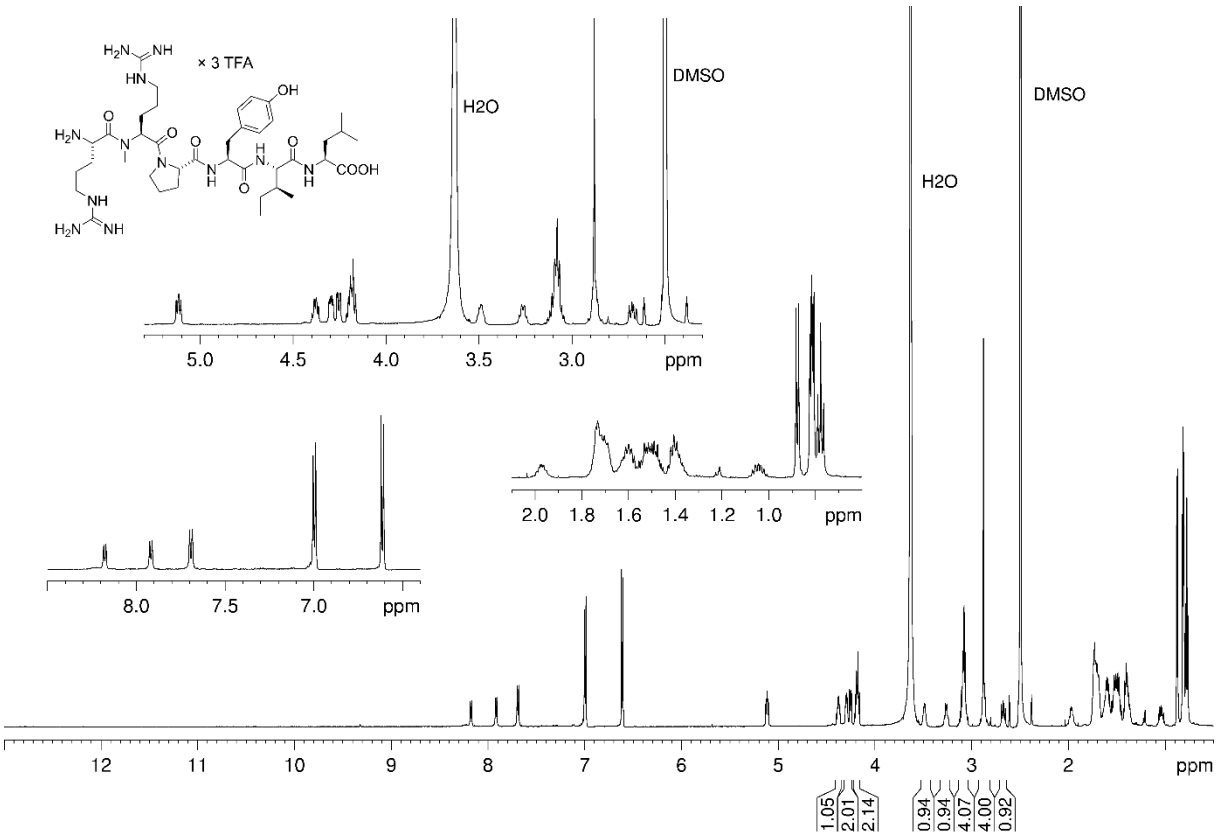

^{1}H-NMR spectrum (600 MHz, DMSO-d_6/D_2O 11:1 v/v) of compound **2.04**

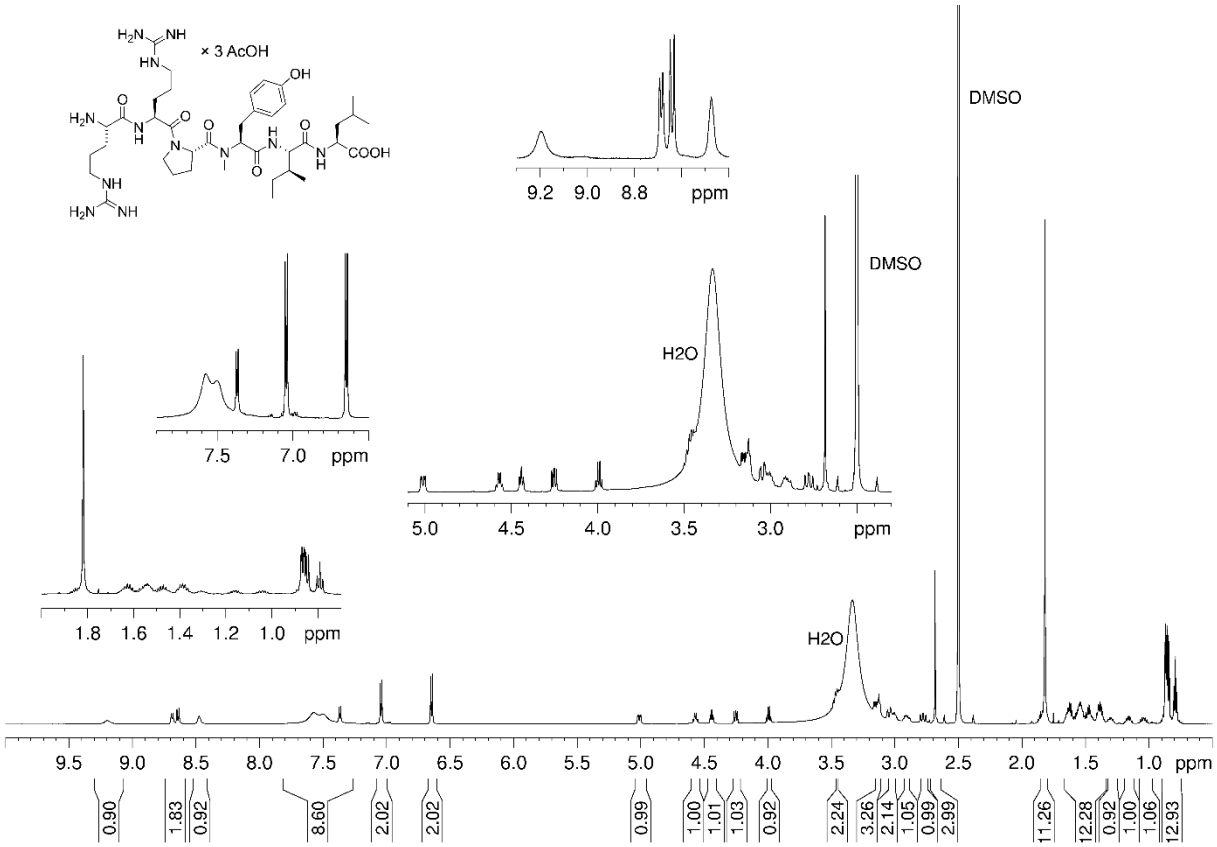

^{1}H-NMR spectrum (600 MHz, DMSO-d_6) of compound **2.05**

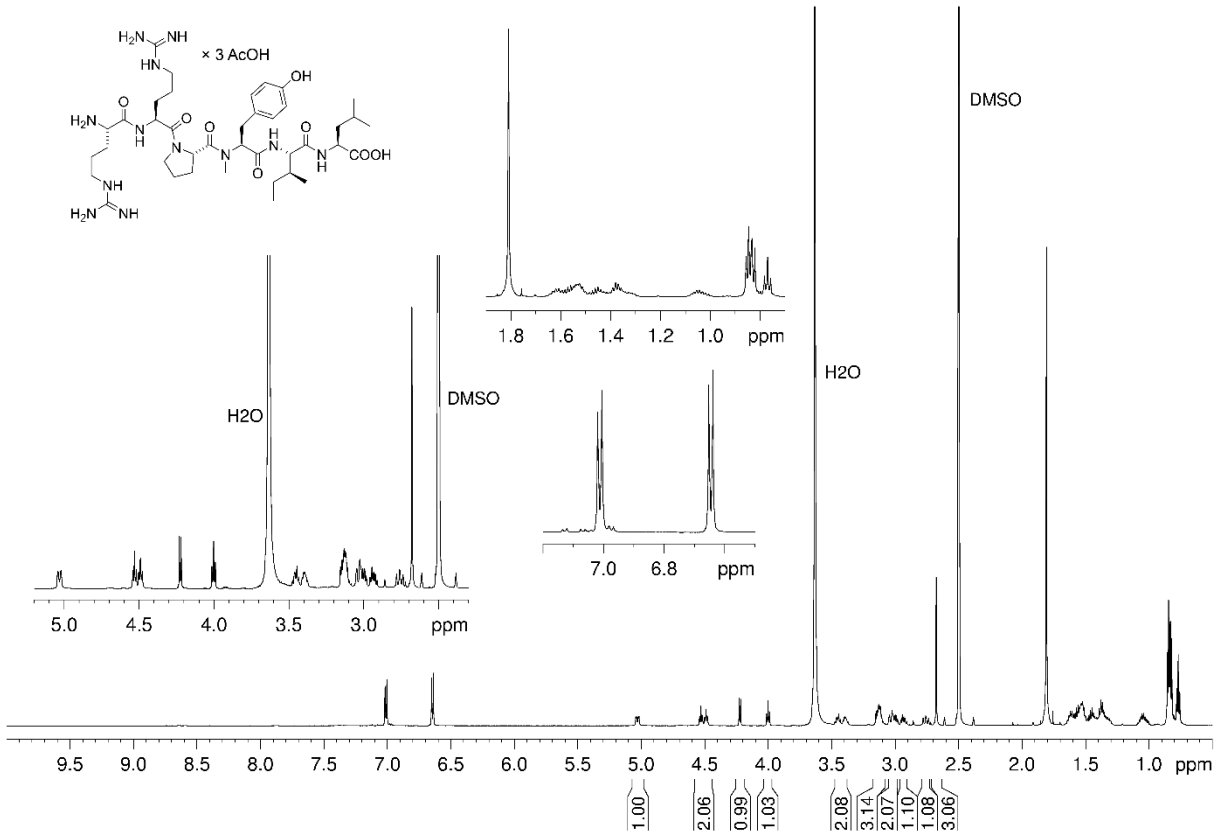

^{1}H-NMR spectrum (600 MHz, DMSO-d_6/D_2O 11:1 v/v) of compound **2.05**

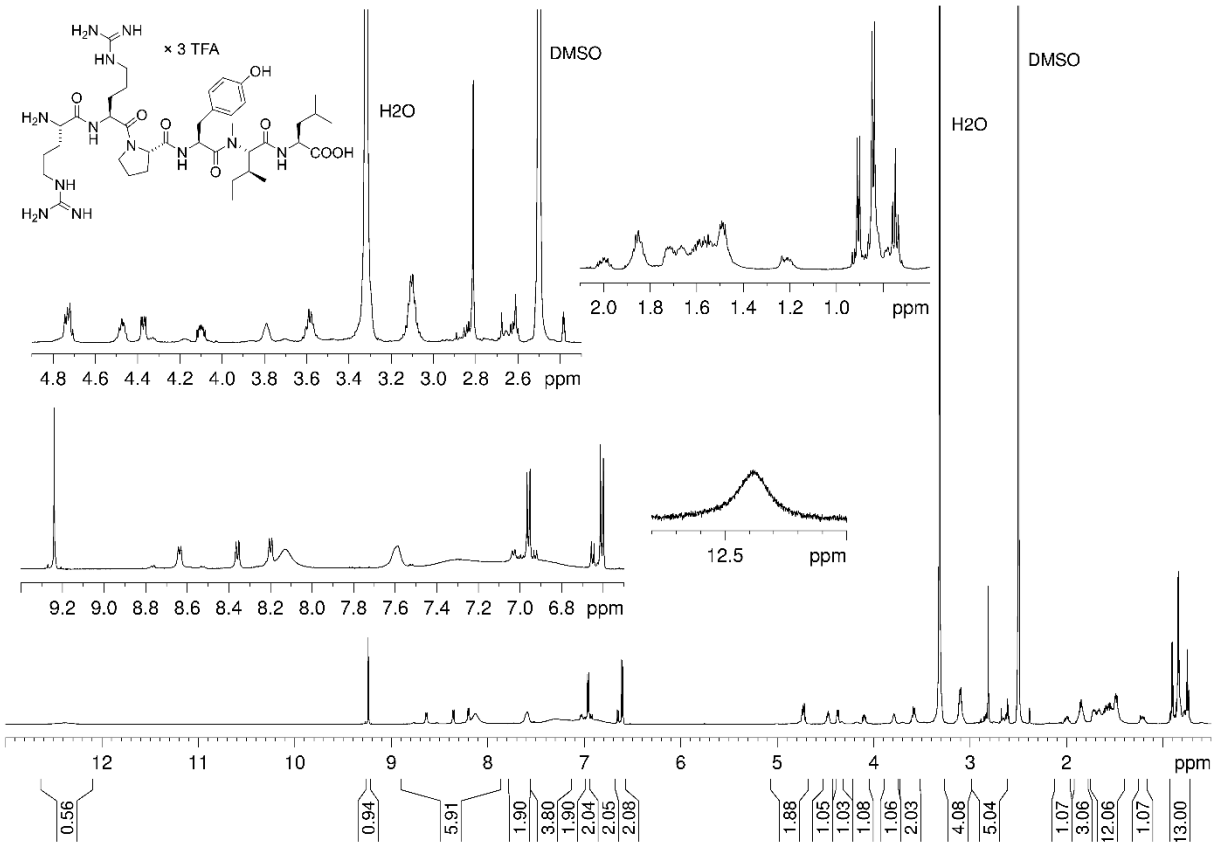

^{1}H-NMR spectrum (600 MHz, DMSO-d_6) of compound **2.06**

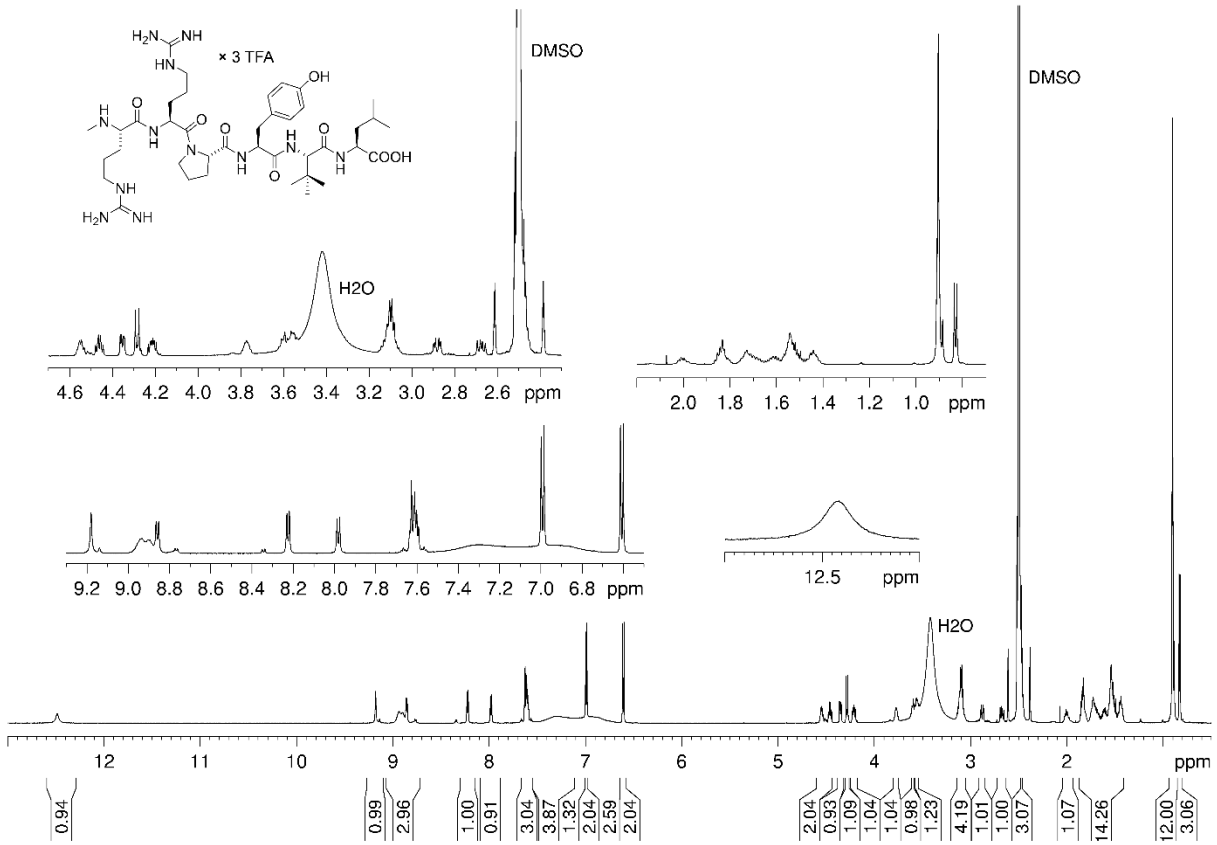

^{1}H-NMR spectrum (600 MHz, DMSO-d_6) of compound **2.07**

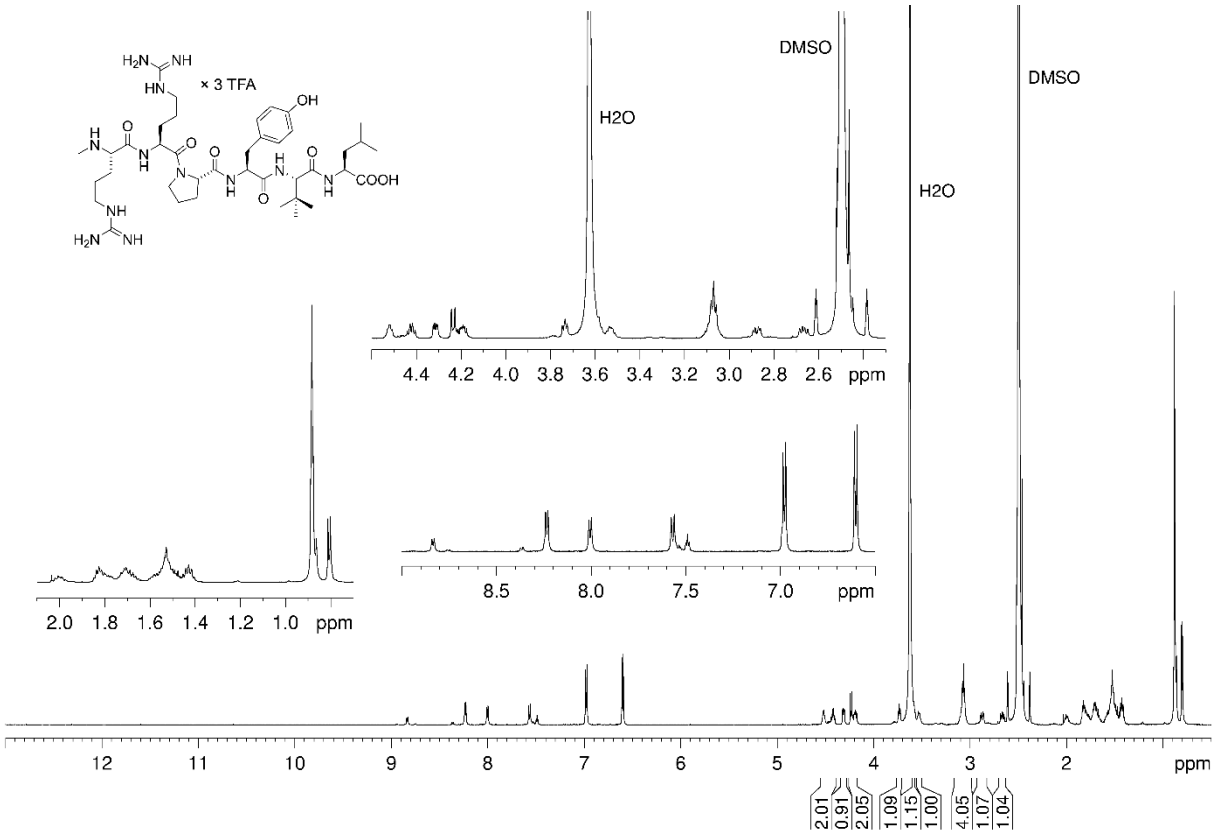

^{1}H-NMR spectrum (600 MHz, DMSO-d_6/D_2O 11:1 v/v) of compound **2.07**

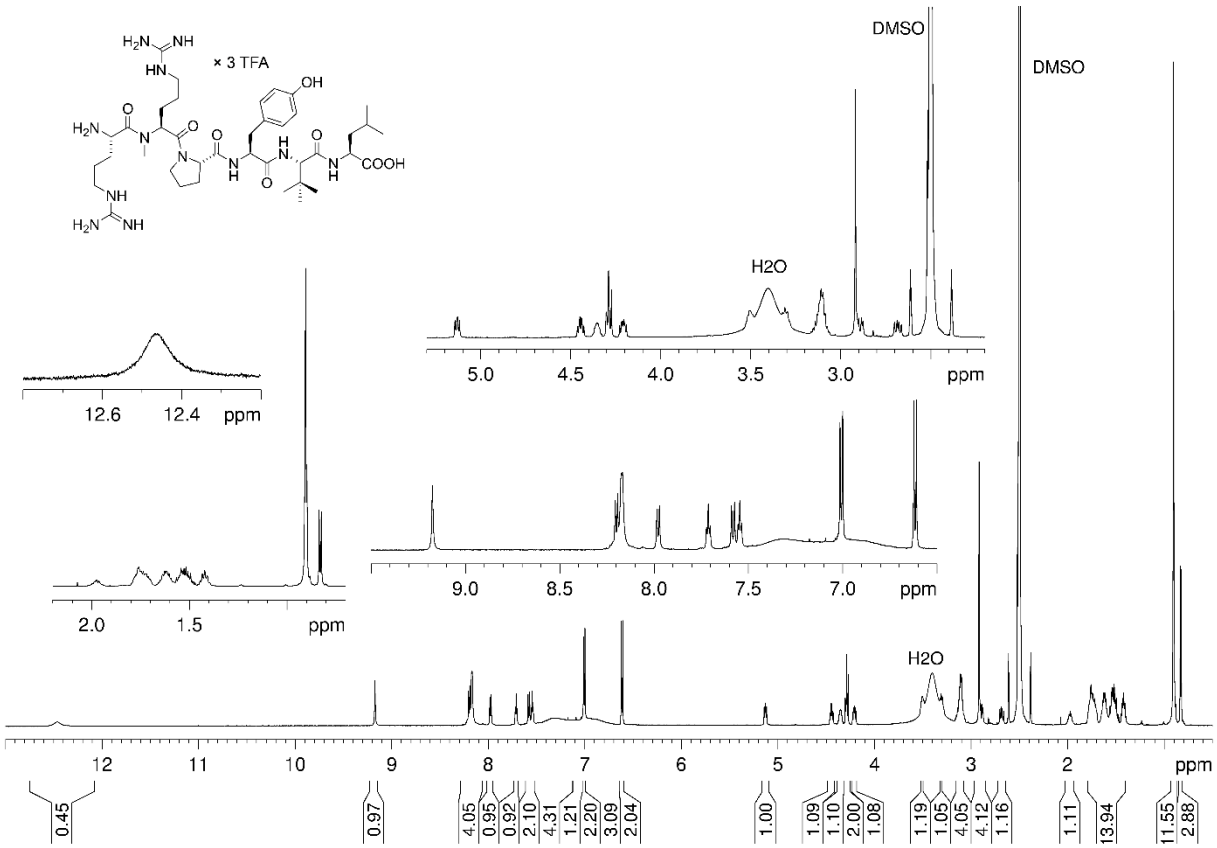

^{1}H-NMR spectrum (600 MHz, DMSO-d_6) of compound **2.08**

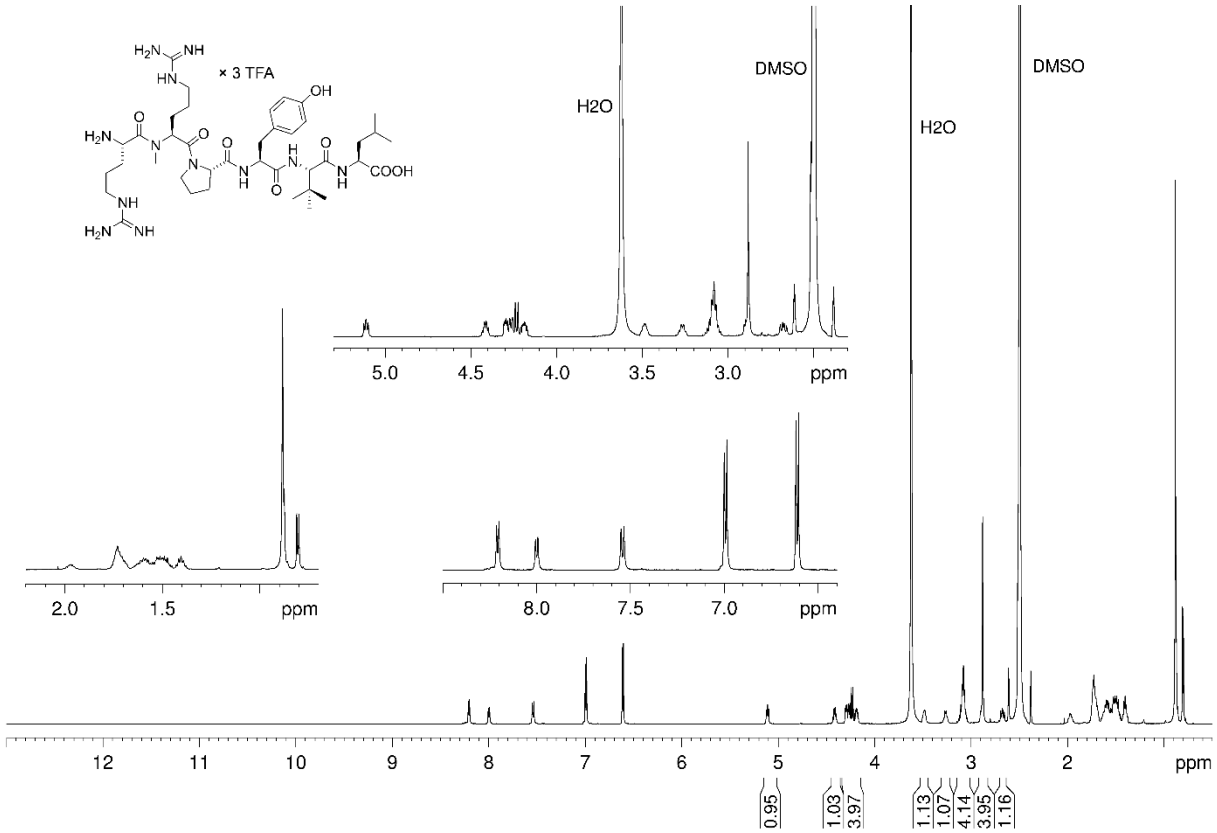

^{1}H-NMR spectrum (600 MHz, DMSO-d_6/D_2O 11:1 v/v) of compound **2.08**

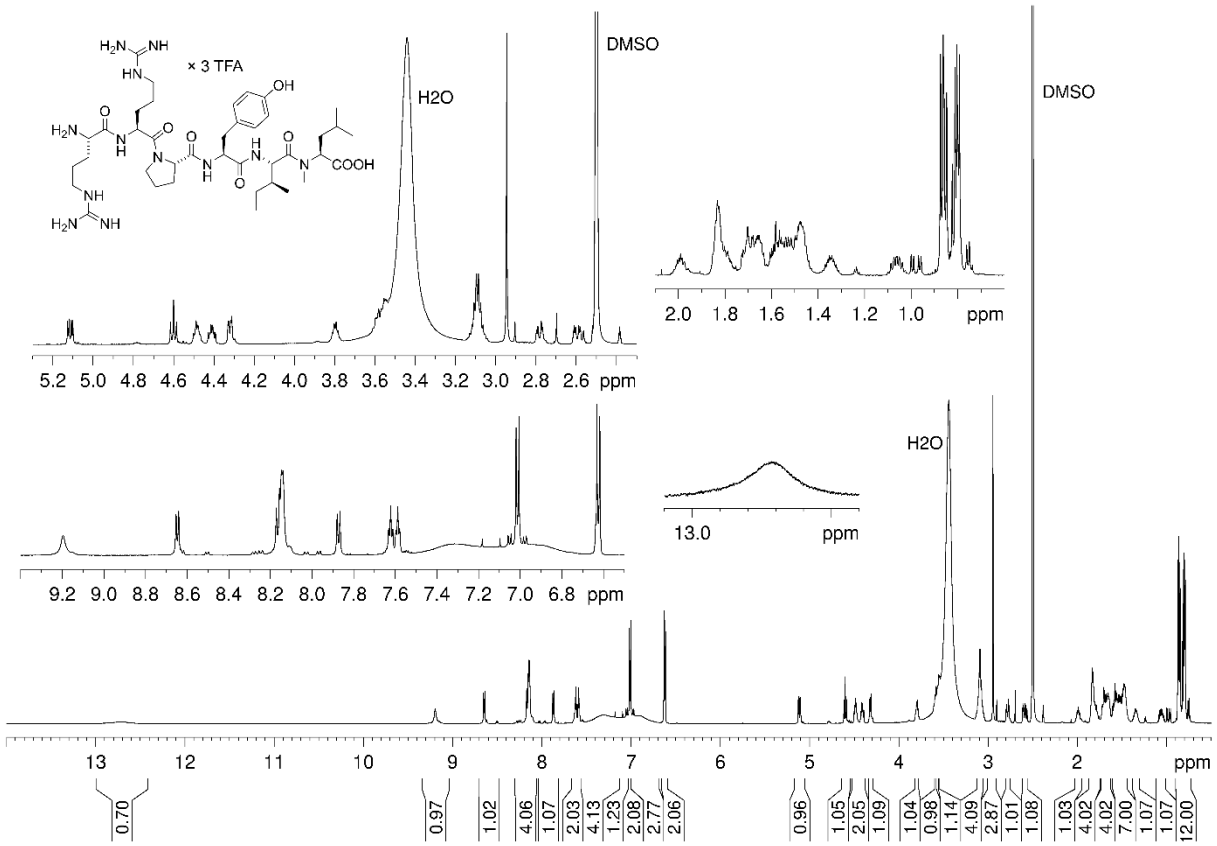

^{1}H-NMR spectrum (600 MHz, DMSO-d_6) of compound **2.09**

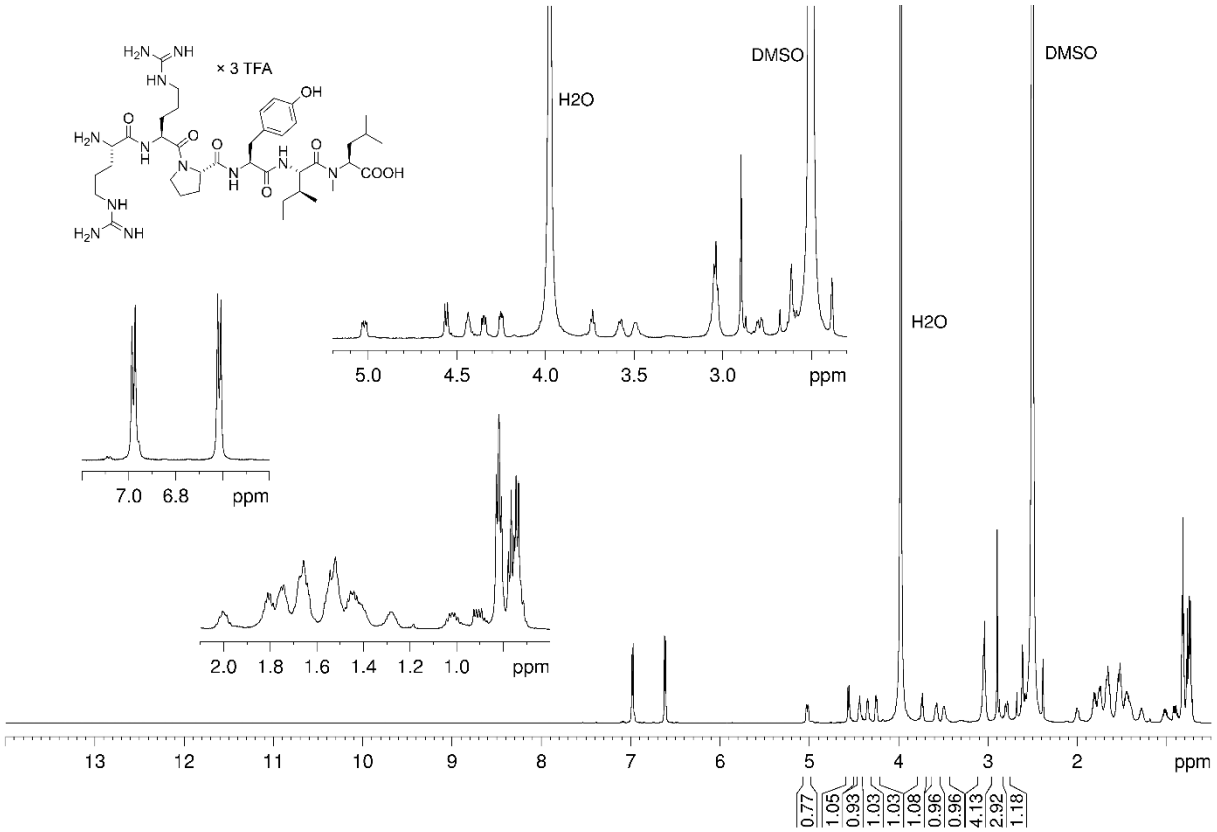

^{1}H-NMR spectrum (600 MHz, DMSO-d_6/D_2O 4:1 v/v) of compound **2.09**

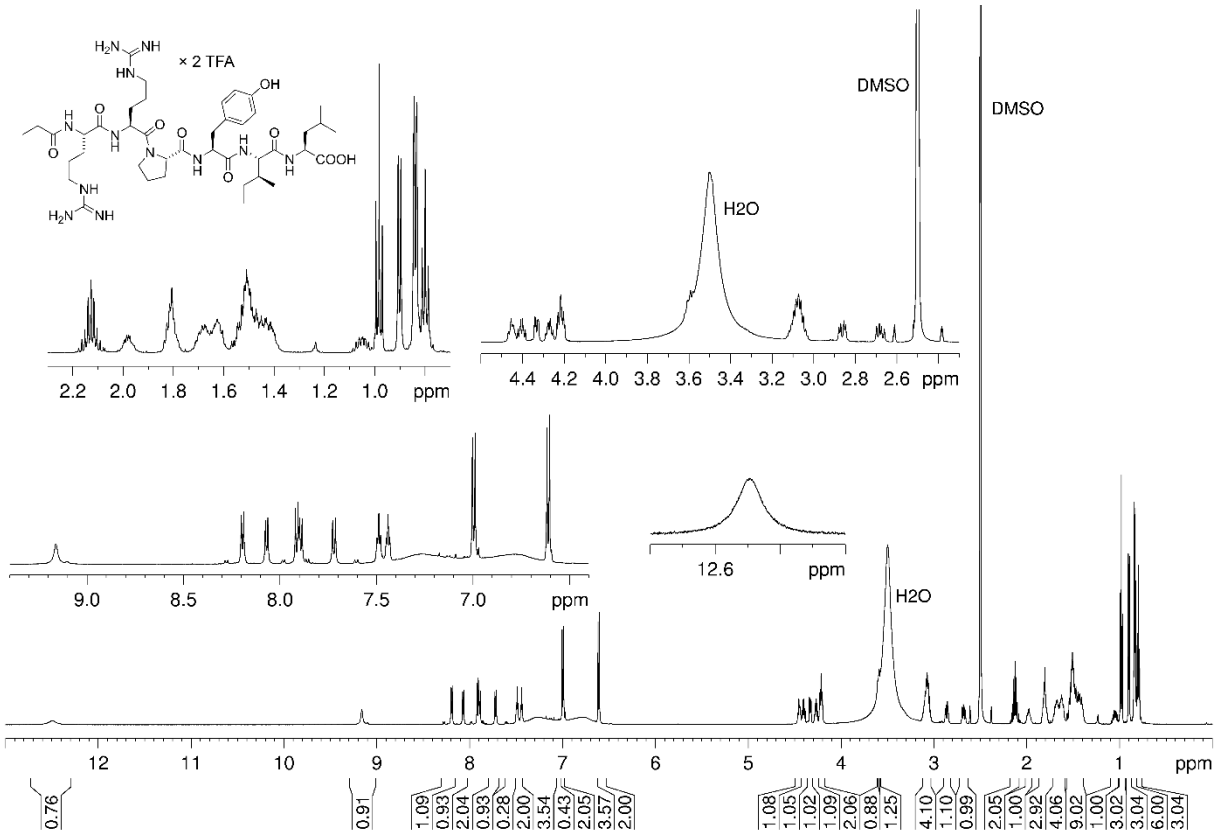

^{1}H-NMR spectrum (600 MHz, DMSO-d_6) of compound **2.11**

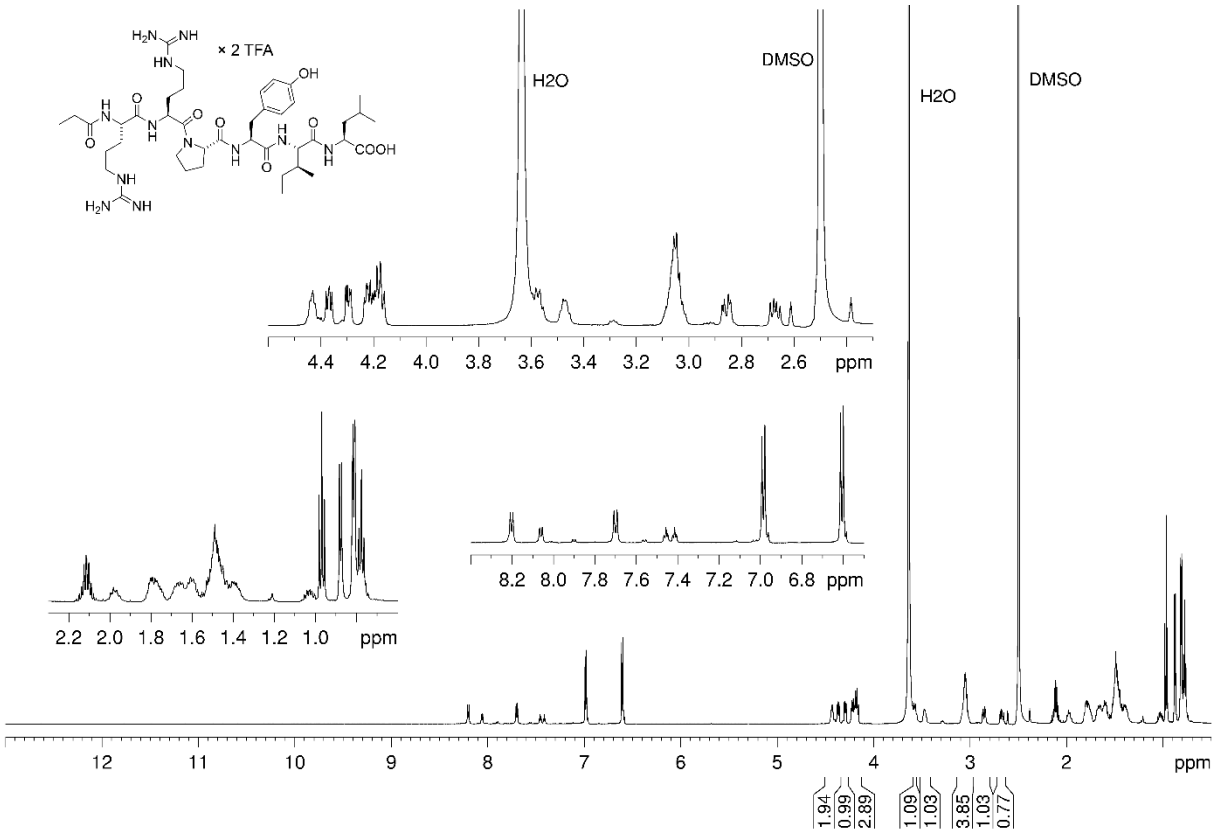

^{1}H-NMR spectrum (600 MHz, DMSO-d_6/D_2O 11:1 v/v) of compound **2.11**

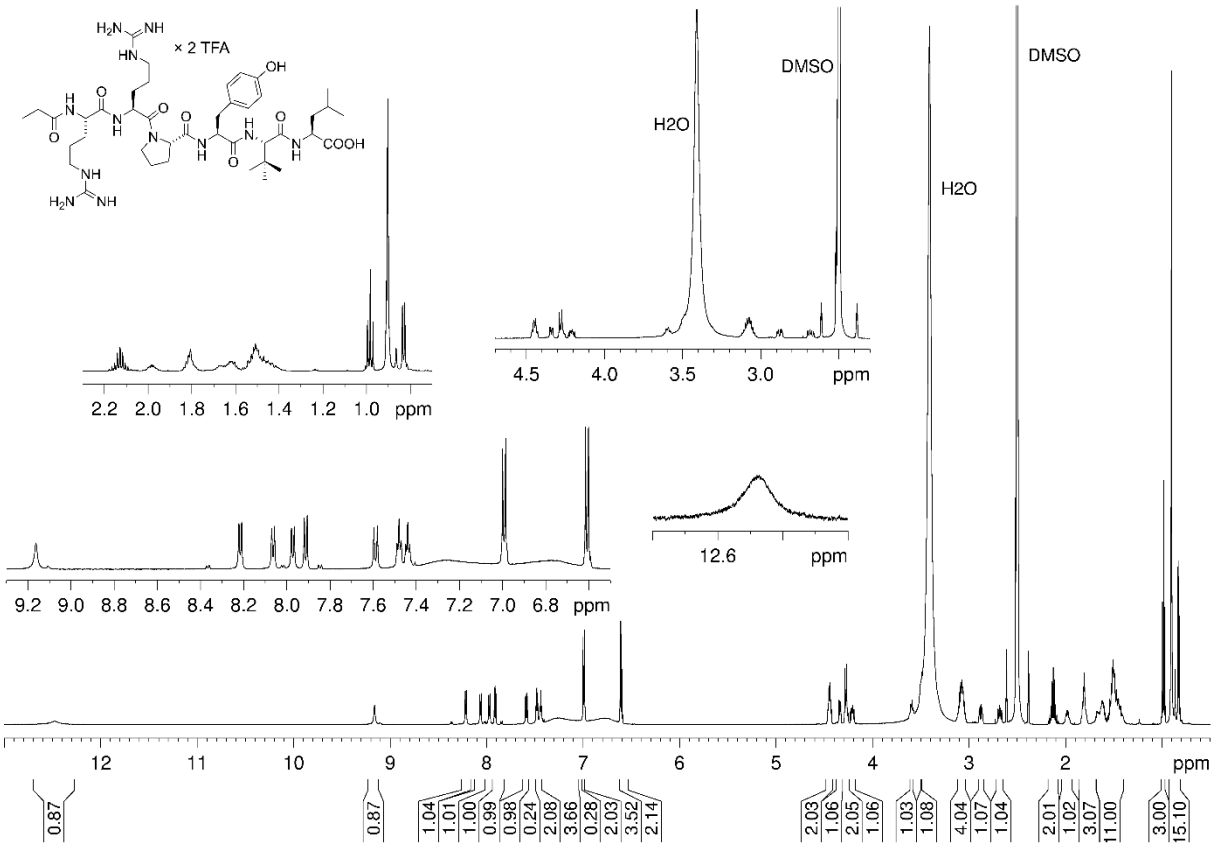

^{1}H-NMR spectrum (600 MHz, DMSO-d_6) of compound **2.12**

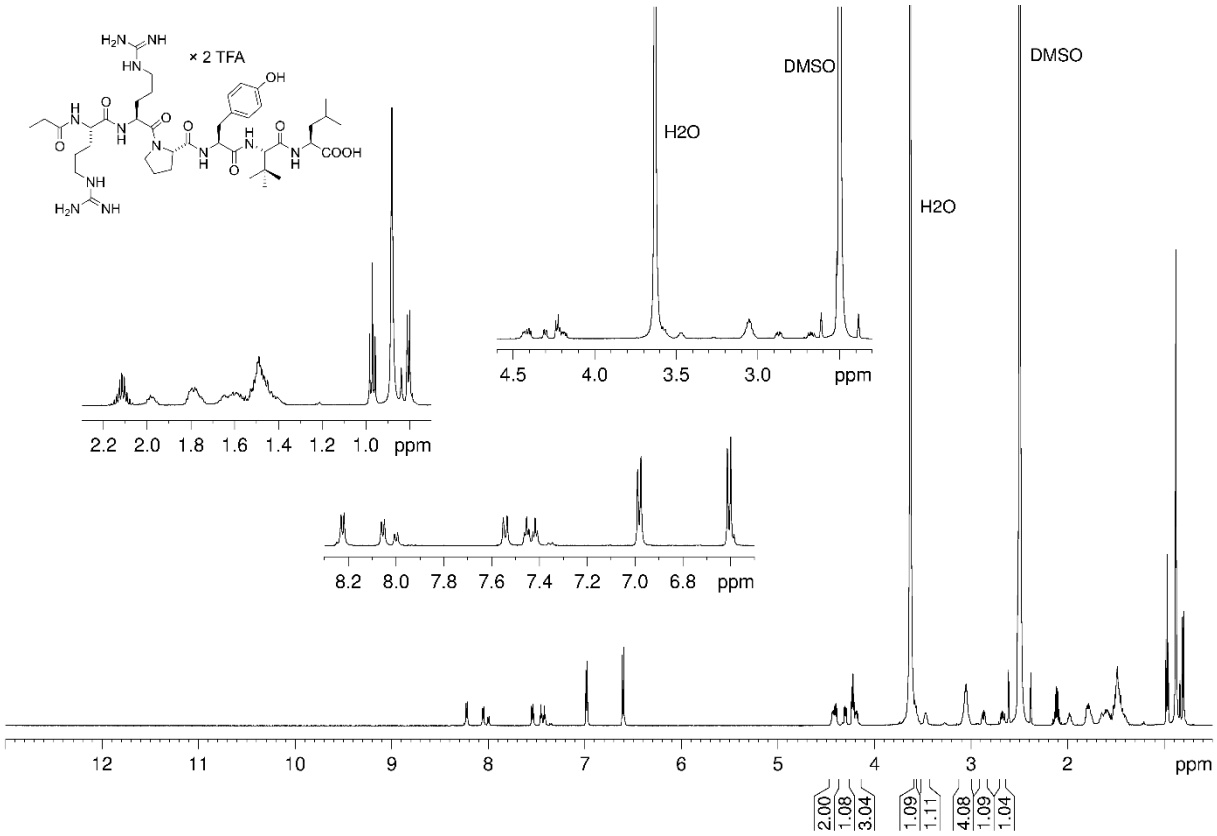

^{1}H-NMR spectrum (600 MHz, DMSO-d_6/D_2O 11:1 v/v) of compound **2.12**

2.6.7 References

1. Keller, M.; Pop, N.; Hutzler, C.; Beck-Sickinger, A.G.; Bernhardt, G.; Buschauer, A. Guanidine-acylguanidine bioisosteric approach in the design of radioligands: Synthesis of a tritium-labeled N^G-propionylargininamide ([^{3}H]-UR-MK114) as a highly potent and selective neuropeptide Y Y_1 receptor antagonist. *J Med Chem* **2008**, *51*, 8168-8172, doi:10.1021/jm801018u.

2. Keller, M.; Kuhn, K.K.; Einsiedel, J.; Hübner, H.; Biselli, S.; Mollereau, C.; Wifling, D.; Svobodová, J.; Bernhardt, G.; Cabrele, C.; et al. Mimicking of arginine by functionalized N^ω-carbamoylated arginine as a new broadly applicable approach to labeled bioactive peptides: High affinity angiotensin, neuropeptide Y, neuropeptide FF, and neurotensin receptor ligands as examples. *J Med Chem* **2016**, *59*, 1925-1945, doi:10.1021/acs.jmedchem.5b01495.

3. Cheng, Y.; Prusoff, W.H. Relationship between the inhibition constant (K_I) and the concentration of inhibitor which causes 50 per cent inhibition (I_{50}) of an enzymatic reaction. *Biochem Pharmacol* **1973**, *22*, 3099-3108, doi:10.1016/0006-2952(73)90196-2.

Chapter 3

Neurotensin analogs by fluoroglycosylation at *N*ω-carbamoylated arginines for PET imaging of NTS_1R-positive tumors

Prior to the submission of this thesis, the content of this chapter was published in collaboration with partners:

Schindler, L.; Wohlfahrt, K.; Gluhacevic von Krüchten, L.; Prante, O.; Keller, M.; Maschauer, S. Neurotensin analogs by fluoroglycosylation at N^{ω}-carbamoylated arginines for PET imaging of NTS1-positive tumors. *Sci Rep* **2022**, *12*, 15028, doi:10.1038/s41598-022-19296-0.

The following experimental work and data processing was performed by co-authors:

Wohlfahrt (née Spinnler), K.:	Synthesis and radioligand competition binding experiments of compounds **3.07**, **3.08**, **3.11**, **3.12**, **3.17**, **3.18** and **3.20**
Gluhacevic von Krüchten (née von Krüchten), L.:	Synthesis and radioligand competition binding experiments of compounds **3.09** and **3.13**, determination of the plasma stability of compounds **3.11**, **3.12** and **3.13**
Maschauer, S.:	Synthesis, in vitro and in vivo studies of [^{18}F]**3.21**
Maschauer, S.; Prante, O.:	Data analysis of in vitro and in vivo studies of [^{18}F]**3.21**

Note: The compounds assigned with **2.01**, **2.02** and **2.07** in Chapter 2 are also part of Chapter 3. To avoid an assignment of several numbers to the same compound, the numbers **2.01**, **2.02** and **2.07** are also used in this chapter, which had been, as mentioned before, published as a scientific article prior to submission of this thesis. Instead of reorganizing the compound numbers, the numbers designating the same compounds as **2.01**, **2.02** and **2.07** in the published article were omitted in Chapter 3 resulting in gaps in compound numbering, i.e., **3.01**, **3.02** and **3.03** are missing.

3.1 Introduction

The neurotensin receptor 1 (NTS_1R), belonging to the class A of G-protein coupled receptors, was reported to be expressed by various types of malignant tumors, including pancreatic adenocarcinoma, colorectal and prostate carcinoma[1-6]. Therefore, the NTS_1R represents an interesting target for tumor imaging by positron emission tomography (PET) and endoradiotherapy. The primary endogenous agonist of the NTS_1R is the tridecapeptide neurotensin, acting as a local hormone in the gastrointestinal tract and as a neurotransmitter and neuromodulator in the central nervous system[7-9]. As the C-terminal hexapeptide sequence of neurotensin (NT(8-13) (**2.01**), Figure 3.1A) exhibits biological activity comparable to that of neurotensin[10], this hexapeptide has served as a lead structure for the development of a large variety of radioligand candidates for PET[11]. For in vivo applications, it is well-known that the peptide backbone of **2.01** needs to be stabilized against proteolytic degradation, occurring at the N-terminal and C-terminal site. Following the strategy of N-methylation of Arg^8 and C-terminal stabilization by the introduction of Tle^{12} instead of Ile^{12} [12], we recently studied the stability of the NT(8-13) derivatives **2.02** and **2.07** (Figure 3.1A), conforming that **2.02** was readily degraded in human plasma by enzymatic cleavage of the Arg^8-Arg^9 bond, whereby **2.07** exhibited high stability[13]. In the case of the previously described NTS_1R PET ligand **3.04** (Figure 3.1A)[14], the N-terminal part of the peptide was stabilized by replacement of Arg^8-Arg^9 with $NLys^8$-Lys^9 and prolongation at the N-terminus by a fluoroglucosyl-triazolylmethyl glycine derivative. However, these structural modifications resulted in a considerable reduction in NTS_1R affinity when compared to **2.02** or **2.07** (Figure 3.1A). The reported NT(8-13)-derived potential PET ligand **3.05** is, like **3.04**, N-terminally fluoroglucosylated, but contains Arg^8-Arg^9 instead of $NLys^8$-Lys^9 and Ile instead of Tle. Compound **3.05** exhibits high NTS_1R affinity, however, it represents no useful PET ligand candidate due to low in vitro stability in human serum[15].

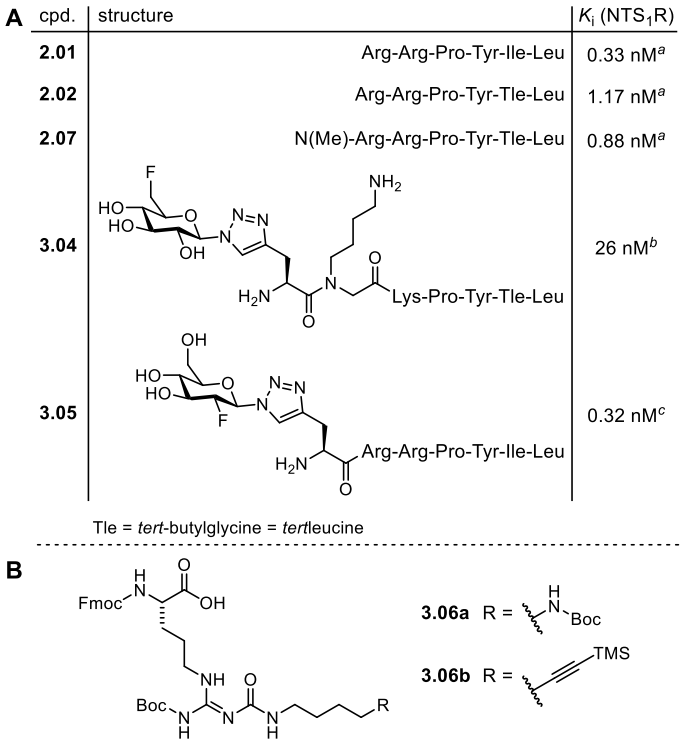

Figure 3.1. (A) Structures and NTS$_1$R affinities of NT(8-13) (**2.01**) and reported NT(8-13) derivatives **2.02**, **2.07**, **3.04** and **3.05**. (B) Structures of the previously reported arginine building blocks **3.06a**[16] and **3.06b**[17] which were used in this work for the synthesis of (potential) PET ligands derived from **2.01**. [a]Schindler et al.[13] [b]Maschauer et al.[14] [c]Maschauer et al.[15]

The vast majority of previously reported neurotensin-derived NTS$_1$R PET ligands (including **3.04**, Figure 3.1A) have in common that the prosthetic group or chelator for radiolabeling with or without a linker was attached to the N-terminus of the respective NT(8-13) peptide analogs, and in most cases, at least one arginine (Arg^8 or Arg^9) was replaced by lysine[14,15,18,19].

Based on our previous work on N^{ω}-carbamoylation of Arg^8 or Arg^9 for the design of fluorescence-labeled NT(8-13) analogs[20], we herein present a series of NT(8-13) analogs containing an N^{ω}-carbamoylated Arg^8 or Arg^9, respectively, to allow for fluoroglycosylation in these positions. We previously demonstrated that ^{18}F-fluoroglycosylation of peptides positively influences their in vivo clearance behaviour[15,21,22], and it has been frequently shown that glycosylation is an effective approach to improve the in vivo blood stability and membrane permeability of peptides[23,24]. With the aim of combining N^{ω}-carbamoylation with subsequent chemoselective fluoroglycosylation, the previously described arginine building blocks **3.06a**[16] or **3.06b**[17] (Figure 3.1B) were incorporated into the NT(8-13) analogs **2.02** and **2.07** instead of Arg^8 or Arg^9. The resulting series of NT(8-13) analogs, containing the fluoroglycosylated peptides **3.11**-**3.13**, **3.20** and **3.21** as NTS$_1$R PET ligand candidates, were studied in vitro regarding their NTS$_1$R affinity as well as stability in blood plasma. Finally, the ^{18}F-labeled glycopeptide [^{18}F]**3.21** was prepared by click chemistry-based ^{18}F-fluoroglycosylation and evaluated in a tumor mouse model by small animal PET imaging studies.

3.2 Results

3.2.1 Chemistry

The synthesis of the potential NTS_1R PET ligands **3.11**-**3.13**, **3.20** and **3.21** is outlined in Scheme 3.1. The alkyne-functionalized precursor peptides **3.07**-**3.09**, containing a modified arginine derived from building block **3.06b**[17] (Figure 3.1B) in position 8 (**3.07**) or 9 (**3.08**, **3.09**), were obtained by the strategy of solid-phase peptide synthesis (SPPS) using Fmoc protecting groups, following a previously described procedure[16]. For the incorporation of the N^{α}-methylated arginine in peptide **3.09**, commercially available Fmoc-N-Me-Arg(Pbf)-OH was used. Conjugation of **3.07**-**3.09** to 6-deoxy-6-fluoro-ß-D-glucosyl azide (**3.10**)[21] by copper(I)-catalyzed azide-alkyne cycloaddition (CuAAC) yielded the potential NTS_1R PET ligands **3.11**-**3.13** (Scheme 3.1). The amino-functionalized precursor peptides **3.14** and **3.16**, both containing a modified arginine derived from **3.06a**[16] (Figure 3.1B) in position 8, but differing with respect to N-terminal methylation (non-methylated: **3.14**, N-terminally methylated: **3.16**), were also prepared by Fmoc SPPS. The N-terminal methyl group in peptide **3.16** was introduced after the coupling and Fmoc deprotection of arginine building block **3.06a** while the peptide was still attached to the solid support, applying a procedure reported by Miller et al.[25] For this purpose, the resin-bound peptide was treated with collidine and 2-nitrobenzenesulfonylchloride followed by treatment with the methylating reagent 4-nitrobenzenesulfonic acid methylester (**3.15**) and the base MTBD. Deprotection of the secondary amine using DBU and 2-mercaptoethanol, and subsequent cleavage from the resin and side chain deprotection yielded **3.16** in an overall yield of 45% (Scheme 3.1).

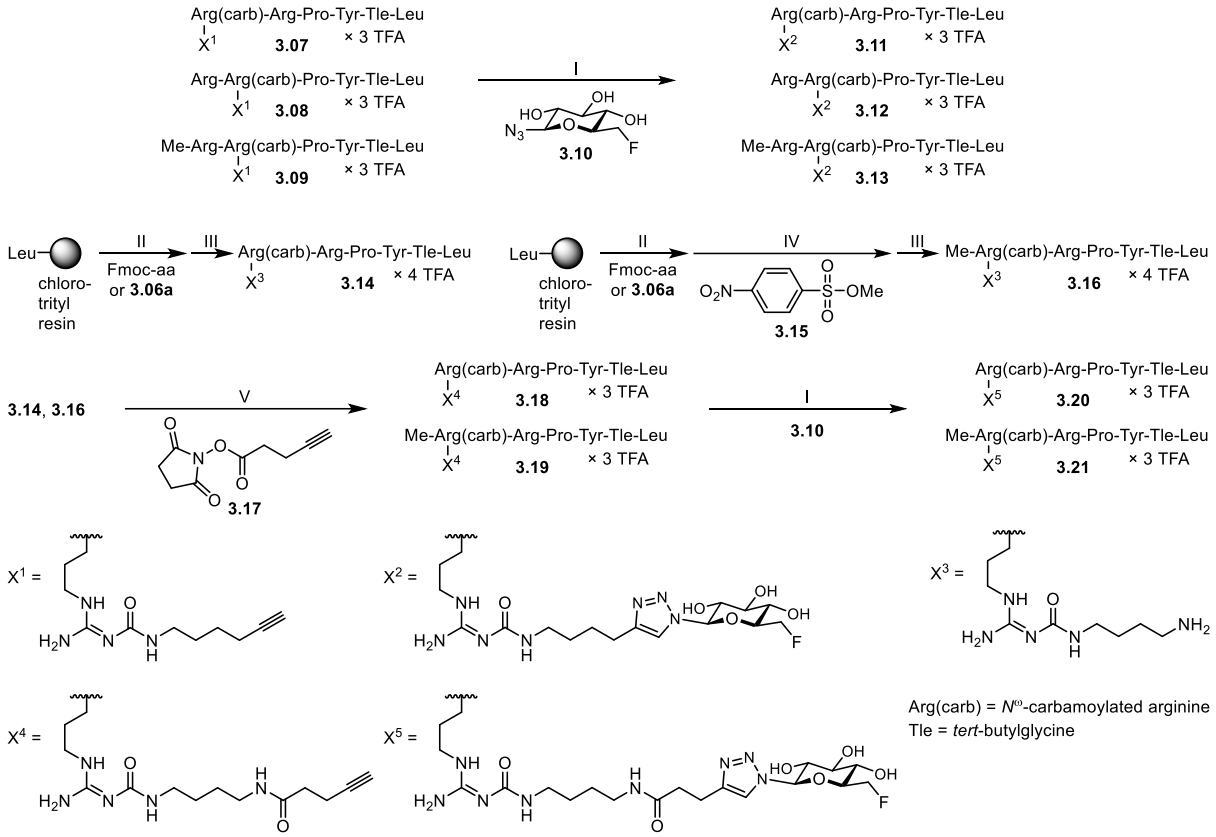

Scheme 3.1. Synthesis of the glycosylated and fluorinated potential NTS_1R PET ligands **3.11**-**3.13**, **3.20** and **3.21**, which were obtained by CuAAC reaction of alkyne-functionalized NT(8-13) derivatives (**3.07**, **3.08**, **3.09**, **3.18**, **3.19**) to 6-deoxy-6-fluoro-ß-D-glucosyl azide **3.10**. Reagents and conditions: (I) $CuSO_4$, sodium ascorbate, PBS/NMP (1:1 v/v) or EtOH/PBS (1:9 v/v), rt, 30 min, 45% (**3.11**), 45% (**3.12**), 68% (**3.13**), 25% (**3.20**), 79% (**3.21**); (II) Fmoc strategy SPPS using HBTU/HOBt and DIPEA, DMF/NMP (80:20 v/v), 35 °C, 2 × 1 h or 2 × 2 h, Fmoc-deprotection: 20% piperidine in DMF/NMP (80:20 v/v), rt, 2 × 8-10 min; (III) (1) hexafluoro-2-propanol (HFIP)/CH_2Cl_2 (1:3 v/v), rt, 2 × 20 min, (2) TFA/H_2O (95:5 v/v), rt, 3 h; (IV) (1) collidine, 2-nitrobenzenesulfonylchloride, CH_2Cl_2, rt, 2 h, (2) MTBD, DMF, rt, 30 min, (3) DBU, 2-mercaptoethanol, DMF, rt, 30 min; (V) DIPEA, DMF/NMP (80:20 v/v), rt, 30-55 min, 59% (**3.18**), 90% (**3.19**); overall yields of **3.14** and **3.16**: 49% and 45%, respectively.

The amino-functionalized precursor peptides **3.14** and **3.16** were transformed to the alkyne-functionalized peptides **3.18** and **3.19**, respectively, by treatment with the succinimidyl ester of pentyn-4-oic acid (**3.17**[26]). Conjugation of **3.18** and **3.19** with glycosyl azide **3.10** by CuAAC afforded the potential NTS_1R PET ligands **3.20** and **3.21**. Purification by preparative reversed-phase HPLC yielded the series of PET ligand candidates (**3.11**-**3.13**, **3.20**, **3.21**) with a purity of ≥ 98% (detection at 220 nm). It should be noted that in all synthesized NT(8-13) derivatives, *tert*-butylglycine (*tert*-leucine, Tle) was incorporated instead of Ile[12], as this modification results in a considerable stabilization of the C-terminus against proteolytic degradation[12,13].

3.2.2 In vitro characterization

NTS_1R affinities of the precursor peptides **3.07**-**3.09**, **3.14**, **3.16**, **3.18** and **3.19** as well as of the potential PET ligands **3.11**-**3.13**, **3.20** and **3.21** were determined by competitive receptor binding experiments on human HT-29 colon carcinoma cells stably expressing the NTS_1R, using the previously reported tritium-labeled NT(8-13) derivative [^{3}H]UR-

MK300[16] as radioligand. All peptides, precursors and potential PET ligands, displayed K_i values in the single-digit nanomolar range (Table 3.1), demonstrating that N^{ω}-carbamoylation at Arg^8 or Arg^9 and conjugation to the sugar moiety reduced the affinity for NTS_1R only slightly, by a factor of 3-7, when compared to the NTS_1R affinities of **2.02** and **2.07**.

Table 3.1. NTS_1R affinities of **2.01**, **2.02**, **2.07**, **3.07**-**3.09**, **3.11**-**3.14**, **3.16** and **3.18**-**3.21**.

cpd.	pK_i ± SEM / K_i [nM][a]	cpd.	pK_i ± SEM / K_i [nM][a]	cpd.	pK_i ± SEM / K_i [nM][a]
2.01	9.49 ± 0.03 / 0.33[13]	**3.09**	8.13 ± 0.13 / 7.7	**3.16**	8.55 ± 0.03 / 2.8
2.02	8.93 ± 0.0002 / 1.2[13]	**3.11**	8.34 ± 0.04 / 4.6	**3.18**	8.37 ± 0.11 / 4.4
2.07	9.07 ± 0.06 / 0.88[13]	**3.12**	8.26 ± 0.10 / 5.8	**3.19**	8.12 ± 0.04 / 7.7
3.07	8.36 ± 0.12 / 4.6	**3.13**	8.21 ± 0.04 / 6.2	**3.20**	8.60 ± 0.01 / 2.5
3.08	8.03 ± 0.03 / 9.4	**3.14**	8.69 ± 0.09 / 2.2	**3.21**	8.39 ± 0.08 / 4.3

[a]Determined by radioligand competition binding with [^{3}H]UR-MK300 at intact HT-29 cells (K_d = 0.55 nM[13], c = 1 nM; see Figures A3.1 and A3.2, Appendix). Data are given as mean values ± SEM (pK_i) or mean values (K_i) from two (**2.01**, **2.02**, **3.07**, **3.09**, **3.11**, **3.13**, **3.18**, **3.20**), three (**3.08**, **3.12**, **3.14**, **3.16**), four (**2.07**, **3.19**) or five (**3.21**) independent experiments, each performed in triplicate.

The stabilities in human plasma of the non-methylated peptides **3.11**, **3.12**, **3.14**, **3.18** and **3.20** were considerably lower compared to the methylated peptides **3.13**, **3.16**, **3.19** and **3.21** (Table 3.2), showing that the proteolytic stability was significantly increased by the introduction of a methyl group at the amino-terminus of the peptides, as expected. The potential PET ligand **3.21**, being most favorable with respect to in vitro stability in human plasma and adequate NTS_1R affinity (Tables 3.1 and 3.2) was chosen as a promising candidate for ^{18}F-labeling and in vivo tumor imaging studies. In this context, it is worth mentioning that the favored peptide **3.21** also showed excellent in vitro stability in mouse plasma (Table 3.2).

Table 3.2. In vitro plasma stabilities of **3.11-3.14, 3.16** and **3.18-3.21** determined at 37 °C.

compd.	% intact peptide in human plasma after the given incubation time[a]						
	10 min	25 min	1 h	2 h	6 h	24 h	48 h
3.11	72 ± 1	24 ± 1	1.1 ± 0.1	< 1	n.d.	n.d.	n.d.
3.12	86 ± 1	28 ± 1	< 1	< 1	n.d.	n.d.	n.d.
3.13	n.d.	n.d.	n.d.	> 99	> 99	> 99	96 ± 1
3.14	50 ± 2	n.d.	< 1	n.d.	< 1	< 1	n.d.
3.16	n.d.	n.d.	> 99	n.d.	> 99	> 99	> 99
3.18	59 ± 1	n.d.	< 1	n.d.	< 1	< 1	n.d.
3.19	n.d.	n.d.	> 99	n.d.	> 99	> 99	99 ± 1
3.20	78 ± 1	n.d.	6.4 ± 0.1	n.d.	n.d.	< 1	n.d.
3.21	n.d.	n.d.	> 99	n.d.	> 99	> 99	99 ± 1
compd.	% intact peptide in mouse plasma after the given incubation time[a]						
	10 min	25 min	1 h	2 h	6 h	24 h	48 h
3.21	> 99	n.d.	> 99	> 99	> 99	> 99	> 99

[a]The initial concentration of each peptide in human or mouse plasma/PBS (1:2 v/v) was 100 µM. Data represent mean values ± SEM from three independent experiments (SEM not given when no decomposition was observed). n.d. = not determined.

3.2.3 Radiosynthesis

The nucleophilic ^{18}F-for-tosylate substitution on triacetylated 6-*O*-tosyl-glucosyl azide with subsequent deacetylation to achieve 6-deoxy-6-[^{18}F]fluoroglucosyl azide [^{18}F]**3.10**[21] (Scheme 3.2) has been proven to be a reliable and robust ^{18}F-synthesis in our laboratory, provided that utmost caution is given to the purity of the tosylate precursor[14,22,27]. The two-step radiosynthesis of [^{18}F]**3.21** required the ^{18}F-synthesis of glycosyl azide [^{18}F]**3.10**, which was obtained in an activity yield (AY) of 40-45% after a total synthesis time of about 30 min, and subsequent use of alkyne **3.19** for CuAAC with [^{18}F]**3.10** in the presence of $Cu(OAc)_2$, tris(3-hydroxypropyltriazolyl)methylamine (THPTA) and sodium ascorbate in phosphate buffer (pH 8) (Scheme 3.2). The radiochemical yield (RCY) of [^{18}F]**3.21** was excellent (92% after 10 min). After isolation by semipreparative HPLC (see Figure A3.4, Appendix), the total radiosynthesis starting from [^{18}F]fluoride gave [^{18}F]**3.21** in high radiochemical purity of > 99%, molar activities of 75-130 GBq/µmol (n = 5), and an activity yield (AY) of 20-23% in a synthesis time of 65-70 min.

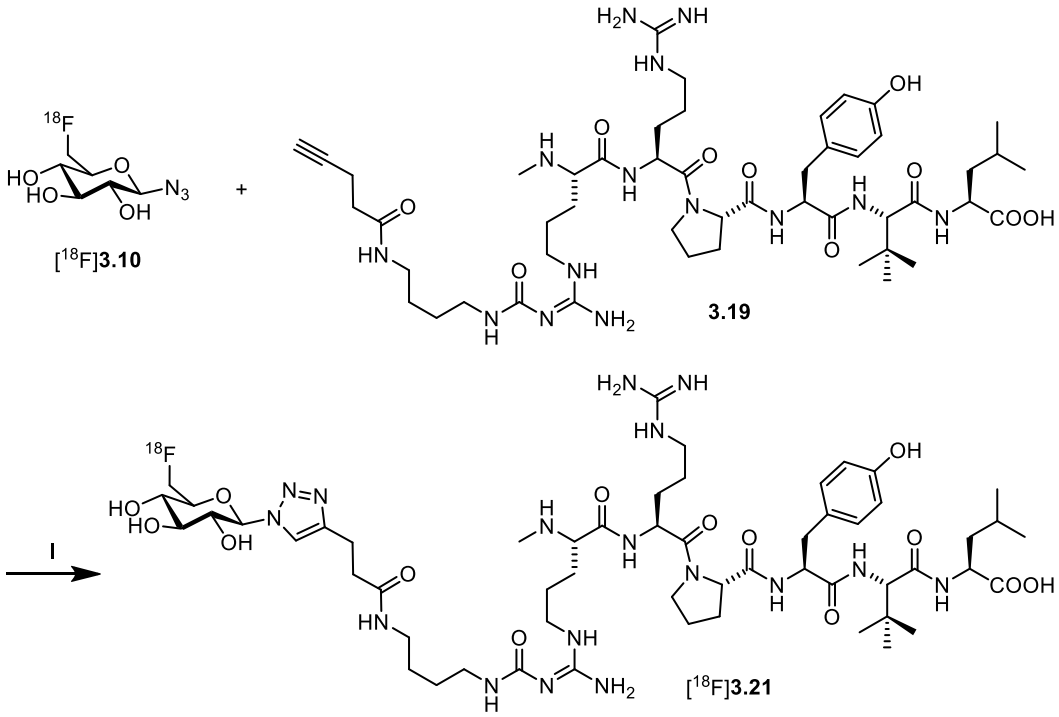

Scheme 3.2. Radiosynthesis of [^{18}F]**3.21.** Reagents and conditions: (I) $Cu(OAc)_2$, THPTA, sodium ascorbate, phosphate buffer pH 8, 60 °C, 10 min, 92% RCY.

3.2.4 In vitro characterization and in vivo stability in blood of [^{18}F]3.21

The $logD_{7.4}$ of [^{18}F]**3.21** was determined to be −3.1, therefore showing high hydrophilicity, as expected. Accordingly, the binding of [^{18}F]**3.21** to plasma proteins in vitro was low with only 10% of the protein-bound fraction (Table 3.3). As determined for reference compound **3.21** (Table 3.2), the stability of the radiotracer [^{18}F]**3.21** in human serum and plasma in vitro was confirmed to be high as well (Table 3.3). After 160 min, the HPLC analysis showed degradation products of only 2% in serum and 3% in plasma (*cf.* Figure A3.5, Appendix). In addition, the HPLC analysis of a blood sample from one mouse, taken at 10 min p.i. of [^{18}F]**3.21**, revealed 30% of intact tracer in the blood (Table 3.3). At 20 min p.i., no intact radiotracer was detectable in the blood anymore (*cf.* Figure A3.5, Appendix).

Table 3.3. Summary of in vitro properties and in vitro and in vivo stability of [^{18}F]**3.21** (see also Figure A3.5, Appendix).

$logD_{7.4}$	Plasma protein binding	Stability in human serum and plasma (in vitro, after 60 min)	Stability in mouse blood (in vivo, 10 min p.i.)
−3.1 ± 0.1 (n = 3)	10%	99%	30%

3.2.5 In vivo characterization of [^{18}F]3.21

The biodistribution of [^{18}F]**3.21** was studied in subcutaneous xenotransplanted HT-29 tumor-bearing mice. Mice were intravenously injected with [^{18}F]**3.21**, dissected at 30, 60 and 90 min p.i. and organs of interest were measured for radioactivity (Figure 3.2 and Table A3.3, Appendix). The highest uptake (12-16 %ID/g) was determined in the kidneys at all time points, indicating predominant renal clearance of [^{18}F]**3.21**. The liver showed moderate uptake values of 4-5 %ID/g with a slow washout. The tumor uptake value was 5 %ID/g at 30 min p.i. and about 2-3 %ID/g at later time points with excellent tumor retention of [^{18}F]**3.21** from 60 to 90 min p.i. The washout from blood was fast (2 %ID/g after 30 min to 0.4 %ID/g after 60 min and 0.1 %ID/g after 90 min) leading to high tumor-to-blood ratios, increasing from 3 (30 min) to 30 at 90 min p.i. The tumor-to-muscle ratios were in the same range as the tumor-to-blood ratios (*cf.* Table A3.3, Appendix).

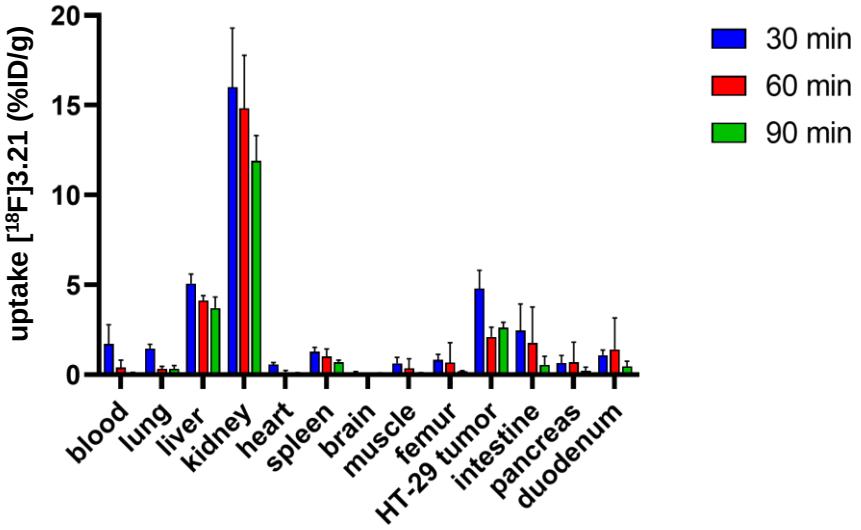

Figure 3.2. Biodistribution of [^{18}F]**3.21** in HT-29-bearing nude mice at 30, 60 and 90 min p.i. Each bar represents the mean value ± SD as determined from four independent animals per studied time point.

3.2.6 PET imaging

HT-29 tumor-bearing mice were injected with [^{18}F]**3.21** and dynamic PET scans from 0-60 min were conducted to verify the specific uptake of [^{18}F]**3.21** in NTS_1R-positive HT-29 tumors in vivo. Co-injections of [^{18}F]**3.21** together with **2.07** as a competitive ligand were performed to define unspecific tumor uptake of [^{18}F]**3.21**. The highly specific uptake of [^{18}F]**3.21** in the tumors could be demonstrated by comparing the mean tumor uptake value of animals at 60 min p.i. of [^{18}F]**3.21** (3.0 ± 0.8 %ID/g, n = 8) to that of co-injected ([^{18}F]**3.21** + **2.07**) animals (1.1 ± 0.3 %ID/g, n = 4), indicating a significant 63% decrease in uptake in the tumor region (Figure 3.3A). The time-activity-curve for tumor uptake of [^{18}F]**3.21** is depicted in Figure 3.3B, showing the highest tumor uptake of [^{18}F]**3.21** of

4.3 ± 1.2 %ID/g at 15-20 min p.i. with a slow washout to 3.0 ± 0.8 %ID/g over time, whereas the unspecific uptake of [^{18}F]**3.21** was 2.5 ± 0.6 %ID/g at 15-20 min p.i. with washout to 1.1 ± 0.3 %ID/g at 60 min p.i. (Figure 3.3B). Non-target organs, such as the kidneys, showed no specific uptake (Figure 3.3C).

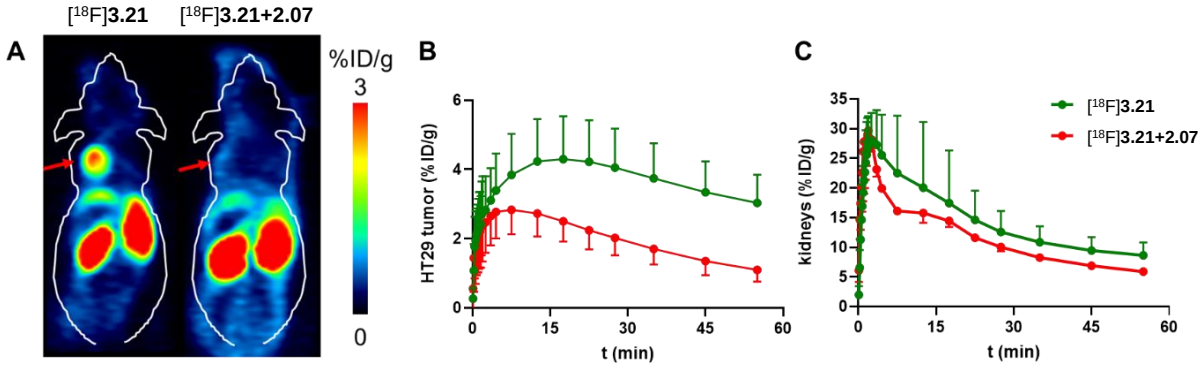

Figure 3.3. (A) Representative coronal PET image 50-60 min p.i. from a HT-29 tumor-bearing mouse injected with [^{18}F]**3.21** (left) and, on the following day, with [^{18}F]**3.21** together with **2.07** (100 nmol, right). Red arrows indicate the tumor. (B), (C) Time-activity-curves of [^{18}F]**3.21** in HT-29 tumors (B) and kidneys (C) in HT-29 tumor-bearing mice as determined by PET. Each point represents the mean ± SD in %ID/g from animals injected with [^{18}F]**3.21** (n = 8) and from animals co-injected with [^{18}F]**3.21** and **2.07** (100 nmol/animal, n = 4).

3.3 Discussion

Neurotensin receptors are expressed on a variety of tumor entities and therefore have been identified as a target for diagnostic imaging as well as therapy of these tumors. Until now, a large variety of neurotensin receptor radioligands were developed, most of them based on the endogenous peptide neurotensin[11]. Among those, the vast majority of peptide tracers for PET were designed by modification and prolongation of the N-terminus of the respective peptide, to introduce a chelator, such as DOTA (1,4,7,10-tetraazacyclododecane-1,4,7,10-tetraacetic acid) or NOTA (1,4,7-triazacyclononane-1,4,7-triacetic acid) for radiolabeling with ^{68}Ga as positron emitter. ^{68}Ga has the advantage of generally easy and fast radiolabeling in high yields and good availability of the radionuclide; however, ^{18}F is superior regarding half-life (110 min for ^{18}F vs. 68 min for ^{68}Ga) and lower radiation exposure for the patient due to lower maximal decay energy also resulting in PET diagnostics with higher spatial resolution and sensitivity. A single batch of an ^{18}F-labeled radiopharmaceutical can be applied to treat more patients than with a single ^{68}Ga production batch. Therefore, the availability of ^{18}F-labeled NTS_1R tracers for diagnostic imaging by PET, especially for patients with pancreatic cancer, is important.

To extend the existing portfolio of NTS_1R ligands for PET, we aimed at developing ^{18}F-labeled NT(8-13) analogs by N^{ω}-carbamoylation of Arg^8 or Arg^9 applying building blocks **3.06a** or **3.06b**, thereby opening the possibility for regiospecific ^{18}F-fluoroglycosylation at Arg^8 or Arg^9. It is well known that carbamoylation contributes to the molecular ageing of proteins in vivo and has important effects on the progression of chronic kidney disease[28]. For example, carbamoylation of albumin resulted in altered albumin transport in rats, leading to significantly increased vascular clearance[29]. Thus, we assumed that carbamoylation together with fluoroglycosylation could be feasible to achieve peptide radiotracers with fast clearance from blood and reduced renal uptake.

From the synthesized series of carbamoylated NTS_1R peptide ligands in this work, the N-terminally methylated (Me-Arg^8-containing) glycopeptides **3.13** and **3.21** showed high affinities towards the NTS_1R in the one-digit nanomolar range together with excellent in vitro stabilities over 48 h. Due to the higher NTS_1R affinity of **3.21** compared to **3.13**, this glycopeptide was chosen for ^{18}F-labeling and further evaluation in vitro and in vivo. The radiosynthesis of [^{18}F]**3.21** by ^{18}F-fluoroglycosylation was straightforward with high yield and provided [^{18}F]**3.21** in high radiochemical purity. In vitro, [^{18}F]**3.21** showed high stability in human serum and plasma with almost no degradation over 160 min. The lipophilicity was very low ($logD_{7.4}$ = −3.1), therefore, renal clearance in vivo could be expected, as it is common for analogs of **2.01**. The binding to plasma proteins in blood was also low (10%), which is also expected for small hydrophilic peptides derived from **2.01**.

To date, there are very few publications on ^{18}F-labeled peptide tracers for the NTS_1R that demonstrate sufficient stability for in vivo experiments. Among them are [^{18}F]**3.04**[14] and its 2-[^{18}F]fluorodeoxy congener[15], both based on the metabolically stable sequence Pra-NLys-Lys-Pro-Tyr-Tle-Leu, as well as the [^{18}F]AlF^{2+}-labeled derivative of **2.01** based on the sequence Ac-Lys(NOTA)-Pro-Me-Arg-Arg-Pro-Tyr-Tle-Leu ([^{18}F]AlF-NOTA-NT)[30] (for comparison see Figure A3.3, Appendix). Due to the use of different animal models with different tumors, it appears difficult to compare the previously published ^{18}F-labeled NTS_1R ligands with [^{18}F]**3.21**. However, the respective tumor-to-blood ratio of the tracers

could be considered for comparison to estimate the signal-to-background ratios of PET images obtained by the respective ^{18}F-labeled NTS$_1$R ligands.

Compared to our previously published peptide [^{18}F]**3.04**[14] (Pra(6-[^{18}F]FGlc)-NLys^8-Lys^9-Pro^{10}-Tyr^{11}-Tle^{12}-Leu^{13}, Figure 3.1A), the tumor uptake of [^{18}F]**3.21** was 3-5-fold higher (5 %ID/g) and [^{18}F]**3.21** revealed improved tumor retention at 60 to 90 min p.i. (2.1-2.6 %ID/g). The initial renal uptake of [^{18}F]**3.21** was significantly reduced, however, only moderate washout from kidneys was observed (16-12 %ID/g from 30-90 min p.i. vs. 31-19 %ID/g from 10-60 min p.i. for [^{18}F]**3.04**[14]). The relatively low uptake in kidneys at late time points after injection is similar for both 6-deoxy-6-[^{18}F]fluoroglycosyl compounds. This observation could be related to a role of the sodium-dependent glucose transporter (SGLT) in the kidney, as also described for 6-deoxy-6-fluoroglucose[31]. A large number of other published 6-deoxy-6-[^{18}F]fluoroglycosylated tracers show equally low uptake in kidneys[32], however, the role of SGLT for the clearance of 6-deoxy-6-[^{18}F]fluoroglycosyl conjugates through kidneys remains to be elucidated.

In contrast to [^{18}F]**3.04**[14], very high tumor-to-blood and tumor-to-muscle ratios were obtained by [^{18}F]**3.21**, increasing over time after tracer injection to reach a ratio of 30 at 90 min p.i., suggesting excellent signal-to-background ratios in PET imaging studies. It should be mentioned that, to our knowledge, a tumor-to-blood ratio of 30 has not been previously achieved with any other published ^{18}F-labeled peptide ligand for the NTS$_1$R. The PET scans of mice injected with [^{18}F]**3.21** confirmed the high-contrast tumor imaging, in which the tumor is very clearly delineated from the background (Figure 3.3A). The specificity of the tumor uptake of [^{18}F]**3.21** was proven by displacement studies with co-injection of high-affinity and metabolically stable NTS$_1$R ligand **2.07** together with [^{18}F]**3.21**, demonstrating that unspecific binding of [^{18}F]**3.21** in the tumor is negligible.

Recently, Wang et al. reported on the synthesis of [^{18}F]AlF-NOTA-NT[30]. They introduced the chelator NOTA to the formerly published "NT20.3" sequence (Ac-Lys(NOTA)-Pro-Me-Arg-Arg-Pro-Tyr-Tle-Leu) and radiolabeled it with [^{18}F]AlF^{2+}. The resulting [^{18}F]AlF-NOTA-NT showed high NTS$_1$R affinity (IC_{50} = 2.6 nM). PET scans of AsPC-1 and Panc-1 tumor-bearing mice at 1 h p.i. demonstrated specific tumor uptake with 3-4 %ID/g and tumor-to-muscle ratios of 7-8, which slightly decreased over 4 hours to 5-6. As mentioned above, a direct comparison between [^{18}F]AlF-NOTA-NT and [^{18}F]**3.21** is difficult due to the use of different animal models, however, the main feature of carbamoylated peptide [^{18}F]**3.21** is the very high tumor-to-blood ratio of 30 at 90 min p.i., whereas the radiosynthesis of [^{18}F]AlF-NOTA-NT is more straightforward.

3.4 Conclusion

Taken together, we here describe the strategy to combine N^{ω}-carbamoylation with ^{18}F-fluoroglycosylation for the development of new ^{18}F-labeled NT(8-13) analogs with high affinity to the NTS_1R, sufficient metabolic stability and high and specific uptake in NTS_1R-positive HT-29 tumors in vivo. The PET tracer [^{18}F]**3.21** has the potential to be used as molecular probe for PET imaging of other NTS_1R-expressing tumors such as pancreatic adenocarcinoma. Moreover, the present study suggests that N^{ω}-carbamoylated arginines, such as **3.06a**, might be useful for the preparation of chelator-conjugated, ^{68}Ga- or ^{177}Lu-labeled NT(8-13) analogs with higher NTS_1R affinity compared to reported chelator-bearing NTS_1R ligands.

3.5 Experimental section

Additional information on materials, chemicals, and additional analytical data of compounds (HPLC analyses, ^{1}H- and ^{13}C-NMR spectra) are provided in the Appendix.

3.5.1 General procedure for SPPS

Peptides were synthesized by manual SPPS according to a reported procedure[16] with the following modifications: The resin was allowed to swell in the solvent for 45 min before the beginning of the synthesis. Protected standard amino acids (Fmoc-Arg(Pbf)-OH, Fmoc-Pro-OH, Fmoc-Tyr(*t*Bu)-OH) were used in 5-fold excess, Fmoc-N-Me-Arg(Pbf)-OH was used in 3.5-fold excess, and Fmoc-Tle-OH was used in 5-fold excess (**3.07**, **3.08**), 4-fold excess (**3.09**, **3.16**) or 4.4-fold excess (**3.14**). The arginine building block **3.06a** was used in 3-fold excess and the arginine building block **3.06b** was used in 2.45-fold (**3.07**, **3.08**) or 3-fold (**3.09**) excess. Amino acid coupling was performed with HBTU/HOBt/DIPEA (Fmoc-Arg(Pbf)-OH, Fmoc-Pro-OH, Fmoc-Tyr(*t*Bu)-OH: 4.9/5/10 equiv., Fmoc-N-Me-Arg(Pbf)-OH: 3.45/3.5/7 equiv., Fmoc-Tle-OH: 4.9/5/10 (**3.07**, **3.08**), 3.95/4/8 (**3.09**, **3.16**) or 4.35/4.4/8.8 (**3.14**) equiv., **3.06a**: 3/3/6 equiv., **3.06b**: 2.2/2.2/4.4 (**3.07**, **3.08**) or 2.95/3/6 (**3.09**) equiv.). For the coupling of Fmoc-N-Me-Arg(Pbf)-OH and the arginine building blocks **3.06a** and **3.06b**, anhydrous solvents (DMF, NMP) were used. Except for the arginine building blocks **3.06a** and **3.06b**, "double coupling" was performed (2 × 45 min or 60 min at 35 °C). In the case of the arginine derivatives **3.06a** and **3.06b**, "single coupling" was performed with a longer reaction time (16 h at 35 °C). Peptides were cleaved off the resin with CH_2Cl_2/HFIP (4:1 v/v) (**3.07**, **3.08**) or CH_2Cl_2/HFIP (3:1 v/v) (**3.09**, **3.14**, **3.16**) (rt, 2 × 20 min).

3.5.2 Synthesis protocols and analytical data of compounds 3.07-3.09, 3.11-3.14 and 3.16-3.21

(*N*$^{\omega}$-5-Hexynylaminocarbonyl)Arg-Arg-Pro-Tyr-2-*tert*-butyl-Gly-Leu tris(hydrotrifluoroacetate) (3.07). The peptide was synthesized according to the general procedure (resin**:** 43.8 mg, 0.034 mmol). The product was purified by preparative RP-HPLC (column: Kinetex-XB C18; gradient: 0-35 min: A2/B 92:8-47:53, t_R = 22 min). Lyophilization of the eluate afforded peptide **3.07** as white fluffy solid (16.9 mg, 39%). ^{1}H-NMR (600 MHz, DMSO-d_6): δ 0.81-0.95 (m, 15H), 1.40-1.65 (m, 12H), 1.65-1.77 (m, 3H), 1.77-1.88 (m, 3H), 1.88-2.03 (m, 1H), 2.14-2.23 (td, 2H, *J* 6.9, 2.6 Hz), 2.64-2.73 (m, 1H), 2.77 (t, 1H, *J* 2.6 Hz), 2.82-2.93 (m, 1H), 3.02-3.16 (m, 4H), 3.20-3.29 (m, 2H), 3.52-3.66 (m, 2H), 3.78-3.94 (m, 1H), 4.16-4.25 (m, 1H), 4.28 (d, 1H, *J* 9.8 Hz), 4.32-4.40 (m, 1H), 4.40-4.59 (m, 2H), 6.58-6.62 (m, 2H), 6.62-7.18 (br s, 2H, interfering with the next listed signal), 6.97-7.01 (m, 2H), 7.18-7.49 (br s, 2H), 7.49-7.57 (br s, 1H), 7.61 (d, 1H, *J* 9.3 Hz), 7.65-7.72 (m, 1H), 7.97 (d, 1H, *J* 8.1 Hz), 8.03-8.30 (m, 4H), 8.30-8.56 (m, 2H), 8.67 (d, 1H, *J* 7.5 Hz), 8.96-9.18 (br s, 1H), 9.20 (s, 1H), 10.07-10.51 (br s, 1H), 12.23-12.75 (br s, 1 H). ^{13}C-NMR (150 MHz, DMSO-d_6): δ 17.3, 21.2, 22.8, 23.5, 24.2, 24.3, 24.5, 25.2, 26.5 (3 carbon atoms), 28.1, 28.2, 28.3, 29.1, 34.8, 36.3, 38.6, 39.7, 40.1, 40.5, 46.8, 50.1, 50.4, 51.6, 54.2, 59.1, 59.2, 71.4, 84.2, 114.8 (2 carbon atoms), 116.2 (TFA), 118.2 (TFA), 127.6, 130.0 (2 carbon atoms), 153.8 (2 carbon atoms), 155.7, 156.8, 158.5 (q, *J* 31 Hz) (TFA), 168.3, 169.1, 169.8, 170.5, 171.3, 173.8. HRMS (ESI): *m/z* $[M+2H]^{2+}$ calcd. for $[C_{45}H_{75}N_{13}O_9]^{2+}$ 470.7900, found 470.7912. RP-HPLC (220 nm): > 99% (t_R = 10.3 min, *k* = 12.2). $C_{45}H_{73}N_{13}O_9 \cdot C_6H_3F_9O_6$ (940.16 + 342.07).

Arg-(N^{ω}-5-hexynylaminocarbonyl)Arg-Pro-Tyr-2-*tert*-butyl-Gly-Leu tris(hydrotrifluoroacetate) (3.08). The peptide was synthesized according to the general procedure (resin: 102.2 mg, 0.081 mmol). The product was purified by preparative RP-HPLC (column: Kinetex-XB C18; gradient: 0-35 min: A2/B 92:8-47:53, t_R = 23 min). Lyophilization of the eluate afforded **3.08** as white fluffy solid (38.7 mg, 37%). ^{1}H-NMR (600 MHz, DMSO-d_6): δ 0.80-0.94 (m, 15H), 1.41-1.74 (m, 15H), 1.74-1.89 (m, 3H), 1.95-2.03 (m, 1H), 2.14-2.19 (dt, 2H, *J* 6.8, 2.7 Hz), 2.64-2.72 (m, 1H), 2.76 (t, 1H, *J* 2.2 Hz), 2.85-2.92 (m, 1H), 3.05-3.15 (m, 4H), 3.19-3.28 (m, 2H), 3.52-3.64 (m, 2H), 3.78-3.86 (m, 1H), 4.17-4.24 (m, 1H), 4.28 (d, 1H, *J* 9.5 Hz), 4.28-4.39 (m, 1H), 4.43-4.57 (m, 2H), 6.59-6.62 (m, 2H), 6.62-7.20 (br s, 2H, interfering with the next listed signal), 6.97-7.00 (m, 2H), 7.20-7.51 (br s, 2H), 7.51-7.57 (br s, 1H), 7.63 (d, 1H, *J* 9.2 Hz), 7.76 (t, 1H, *J* 6.0 Hz), 7.94 (d, 1H, *J* 7.3 Hz), 8.02-8.31 (br s, 4H), 8.33-8.57 (br s, 2H), 8.68 (d, 1H, *J* 7.9 Hz), 8.95-9.12 (br s, 1H), 9.20 (s, 1H), 10.03-10.70 (br s, 1H), 12.21-12.80 (br s, 1H). ^{13}C-NMR (150 MHz, DMSO-d_6): δ 17.3, 21.2, 22.8, 24.08, 24.14, 24.3, 25.2, 26.5 (3 carbon atoms), 28.1, 28.2, 28.4, 29.1, 34.7, 36.3, 38.6, 39.7, 40.1, 40.6, 46.8, 50.1, 50.3, 51.7, 54.2, 59.1, 59.2, 71.4, 84.2, 114.8 (2 carbon atoms), 114.8, 116.1 (TFA), 118.1 (TFA), 127.6, 130.0 (2 carbon atoms), 153.8 (2 carbon atoms), 155.7, 156.8, 158.7 (q, *J* 31 Hz) (TFA), 168.3, 169.1, 169.8, 170.5, 171.2, 173.8. HRMS (ESI): *m/z* [*M*+H]$^+$ calcd. for $[C_{45}H_{74}N_{13}O_9]^+$ 940.5727, found 940.5724. RP-HPLC (220 nm): > 99% (t_R = 10.4 min, *k* = 12.7). $C_{45}H_{73}N_{13}O_9 \cdot C_6H_3F_9O_6$ (940.16 + 342.07).

N^{α}-(N^{α}-Methylarginyl)-N^{ω}-(5-hexynylaminocarbonyl)Arg-Pro-Tyr-2-*tert*-butyl-Gly-Leu tris(hydrotrifluoroacetate) (3.09). The peptide was synthesized according to the general procedure (resin: 76 mg, 0.060 mmol). The product was purified by preparative RP-HPLC (column: Kinetex-XB C18; gradient: 0-35 min: A2/B 92:8-47:53, t_R = 24 min). Lyophilization of the eluate afforded **3.09** as white fluffy solid (44 mg, 57%). ^{1}H-NMR (600 MHz, DMSO-d_6): δ 0.80-0.94 (m, 15H), 1.41-1.77 (m, 15H), 1.77-1.88 (m, 3H), 1.95-2.04 (m, 1H), 2.13-2.21 (m, 2H), 2.47 (s, 3H), 2.64-2.72 (m, 1H), 2.76 (t, 1H, *J* 2.7 Hz), 2.83-2.92 (m, 1H), 3.05-3.16 (m, 4H), 3.19-3.29 (m, 2H), 3.52-3.65 (m, 2H), 3.71-3.82 (m, 1H), 4.18-4.25 (m, 1H), 4.26-4.31 (m, 1H), 4.33-4.40 (m, 1H), 4.43-4.51 (m, 1H), 4.51-4.61 (m, 1H), 6.58-6.63 (m, 2H), 6.85-7.24 (br s, 2H, interfering with the next listed signal), 6.96-7.01 (m, 2H), 7.24-7.49 (br s, 2H), 7.53 (s, 1H), 7.63 (d, 1H, *J* 9.5 Hz), 7.82 (t, 1H, *J* 5.8 Hz), 7.94 (d, 1H, *J* 7.3 Hz), 8.19 (d, 1H, *J* 7.4 Hz), 8.37-8.65 (br s, 2H), 8.66-9.18 (m, 4H), 9.21 (s, 1H), 10.13-10.63 (br s, 1H), 12.09-12.80 (br s, 1H). ^{13}C-NMR (150 MHz, DMSO-d_6): δ 17.7, 21.6, 23.1, 24.1, 24.3, 24.6, 24.7, 25.5, 26.8 (3 carbon atoms), 27.2, 28.1, 28.4, 29.4, 31.4, 35.0, 36.5, 38.9, 39.7, 40.0, 40.3, 40.8, 47.3, 50.5, 50.9, 54.5, 59.6, 60.1, 71.6, 84.7, 115.1 (2 carbon atoms), 116.4 (TFA), 118.3 (TFA), 127.9, 130.4 (2 carbon atoms), 153.8, 153.9, 155.9, 156.8, 159.2 (q, *J* 32 Hz) (TFA), 167.3, 169.5, 170.2, 170.9, 171.7, 174.1. HRMS (ESI): *m/z* [*M*+H]$^+$ calcd. for $[C_{46}H_{76}N_{13}O_9]^+$ 954.5883, found 954.5884. RP-HPLC (220 nm): > 99% (t_R = 11.0 min, *k* = 11.2). $C_{46}H_{75}N_{13}O_9 \cdot C_6H_3F_9O_6$ (954.19 + 342.07).

{N^{ω}-[*N*-(4-{1-[6-Deoxy-6-fluoro-β-D-glucopyranosyl]-1*H*-1,2,3-triazol-4-yl}butyl)aminocarbonyl]}Arg-Arg-Pro-Tyr-2-*tert*-butyl-Gly-Leu tris(hydrotrifluoroacetate) (3.11). To a solution of **3.07** (3.94 mg, 2.96 µmol) and 6-deoxy-6-fluoro-ß-D-glucosyl azide (**3.10**) (2.45 mg, 11.8 µmol) in EtOH/PBS (1:9 v/v) (0.5 mL) were added a 0.2 M solution of copper(II)sulfate pentahydrate (17.8 µL, 3.55 µmol) in EtOH/PBS (1:9 v/v) and a 0.6 M solution of sodium ascorbate (17.8 µL, 10.7 µmol) in EtOH/PBS (1:9 v/v). The mixture was stirred at rt for 30 min (complete consumption of

3.07 was verified by analytical HPLC). The product was purified by preparative RP-HPLC (column: Kinetex Biphenyl; gradient: 0-30 min: A1/B 93:7-76:24, t_R = 21 min). Lyophilization of the eluate afforded **3.11** as white fluffy solid (1.53 mg, 45%). ^{1}H-NMR (600 MHz, DMSO-d_6): δ 0.79-0.96 (m, 15H), 1.46-1.65 (m, 12H), 1.65-1.76 (m, 3H), 1.76-1.91 (m, 3H), 1.94-2.07 (m, 1H), 2.63-2.71 (m, 2H), 2.84-2.92 (m, 1H), 2.82-2.93 (m, 1H), 3.05-3.16 (m, 4H), 3.23-3.28 (m, 3H), 3.40-3.47 (m, 2H), 3.50-3.66 (m, 2H), 3.67-3.78 (m, 2H), 3.78-3.86 (m, 1H), 4.17-4.25 (m, 1H), 4.28 (d, 1H, *J* 9.8 Hz), 4.31-4.39 (m, 1H), 4.42-4.66 (m, 4H), 5.35-5.51 (m, 3H), 5.57 (d, 1H, *J* 9.0 Hz), 6.56-6.63 (m, 2H), 6.63-7.08 (br s, 2H, interfering with the next listed signal), 6.97-7.01 (m, 2H), 7.08-7.48 (br s, 2H), 7.52 (s, 1H), 7.54-7.59 (m, 1H), 7.59-7.64 (d, 1H, *J* 9.4 Hz), 7.98 (d, 1H, *J* 8.1 Hz), 8.03 (s, 1H), 8-05-8.19 (br s, 3H), 8.22 (d, 1H, *J* 7.5 Hz), 8.26-8.56 (br s, 2H), 8.66 (d, 1H, *J* 7.5 Hz), 8.91-9.13 (br s, 1H), 9.18 (s, 1H), 9.79-10.05 (br s, 1H), 12.14-12.71 (br s, 1H). HRMS (ESI): *m/z* [*M*+H]$^+$ calcd. for $[C_{51}H_{84}FN_{16}O_{13}]^+$ 1147.6382, found 1147.6375. RP-HPLC (220 nm): > 99% (t_R = 8.0 min, *k* = 9.5). $C_{51}H_{83}FN_{16}O_{13} \cdot C_6H_3F_9O_6$ (1147.32 + 342.07).

Arg-{*N*$^\omega$-[*N*-(4-{1-[6-deoxy-6-fluoro-β-D-glucopyranosyl]-1*H*-1,2,3-triazol-4-yl}butyl)aminocarbonyl]}Arg-Pro-Tyr-2-*tert*-butyl-Gly-Leu tris(hydrotrifluoroacetate) (3.12). Compound **3.12** was prepared from **3.08** (9.7 mg, 7.57 µmol) and **3.10** (6.27 mg, 30.3 µmol) using the procedure for the preparation of **3.11**. The product was purified by preparative RP-HPLC (column: Kinetex Biphenyl; gradient: 0-35 min: A1/B 90:10-62:38, t_R = 21 min). Lyophilization of the eluate afforded **3.12** as white fluffy solid (8.72 mg, 77%). ^{1}H-NMR (600 MHz, DMSO-d_6): δ 0.78-0.96 (m, 15H), 1.44-1.76 (m, 15H), 1.76-1.91 (m, 3H), 1.94-2.06 (m, 1H), 2.63-2.68 (m, 2H), 2.84-2.93 (m, 1H), 3.07-3.16 (m, 4H), 3.23-3.29 (m, 3H), 3.43-3.45 (m, 2H), 3.56-3.61 (m, 2H), 3.69-3.82 (m, 3H), 4.17-4.26 (m, 1H), 4.28 (d, 1H, *J* 9.8 Hz), 4.31-4.38 (m, 1H), 4.44-4.66 (m, 4H), 5.29-5.54 (m, 3H), 5.56 (d, 1H, *J* 9.0 Hz), 6.59-6.63 (m, 2H), 6.63-7.10 (br s, 2H, interfering with the next listed signal), 6.97-7.01 (m, 2H), 7.10-7.51 (br s, 2H), 7.51-7.61 (m, 2 H), 7.63 (d, 1H, *J* 9.4 Hz), 7.95 (d, 1H, *J* 8.1 Hz), 8.03 (s, 1H), 8.06-8.19 (br s, 3H), 8.21 (d, 1H, *J* 7.5 Hz), 8.29-8.62 (br s, 2H), 8.67 (d, 1H, *J* 7.5 Hz), 8.85-9.09 (br s, 1H), 9.17 (s, 1H), 9.73-9.97 (br s, 1H), 12.34-12.65 (br s, 1H). HRMS (ESI): *m/z* [*M*+H]$^+$ calcd. for $[C_{51}H_{84}FN_{16}O_{13}]^+$ 1147.6382, found 1147.6380. RP-HPLC (220 nm): > 99% (t_R = 8.0 min, *k* = 9.5). $C_{51}H_{83}FN_{16}O_{13} \cdot C_6H_3F_9O_6$ (1147.32 + 342.07).

***N*$^\alpha$-(*N*$^\alpha$-Methylarginyl)-{*N*$^\omega$-[*N*-(4-{1-[6-deoxy-6-fluoro-β-D-glucopyranosyl]-1*H*-1,2,3-triazol-4-yl}butyl)aminocarbonyl]}Arg-Pro-Tyr-2-*tert*-butyl-Gly-Leu tris(hydrotrifluoroacetate) (3.13).** To a solution of **3.09** (12.0 mg, 9.26 µmol) and 6-deoxy-6-fluoro-ß-D-glucosyl azide (**3.10**) (5.4 mg, 26.0 µmol) in EtOH/PBS (1:9 v/v) (0.5 mL) were added a 0.2 M solution of copper(II)sulfate pentahydrate (56.0 µL, 11.1 µmol) in EtOH/PBS (1:9 v/v) and a 0.6 M solution of sodium ascorbate (46.0 µL, 27.8 µmol) in EtOH/PBS (1:9 v/v). The mixture was stirred at rt for 30 min (complete consumption of **3.09** was detected by analytical HPLC) and acidified by the addition of 10% aq. TFA (2.7 µL). The product was purified by preparative RP-HPLC (column: Kinetex-XB C18; gradient: 0-35 min: A2/B 92:8-55:45, t_R = 22 min). Lyophilization of the eluate afforded **3.13** as white fluffy solid (9.5 mg, 68%). ^{1}H-NMR (600 MHz, DMSO-d_6): δ 0.77-0.98 (m, 15H), 1.42-1.76 (m, 15H), 1.78-1.90 (m, 3H), 1.95-2.04 (m, 1H), 2.43-2.47 (m, 3H), 2.63-2.70 (m, 2H), 2.82-2.94 (m, 1H), 3.04-3.17 (m, 4H), 3.21-3.29 (m, 3H), 3.41-3.46 (m, 1H), 3.51-3.65 (m, 2H), 3.65-3.86 (m, 3H), 4.16-4.25 (m, 1H), 4.25-4.32 (m, 1H), 4.32-4.39 (m, 1H), 4.42-4.65 (m, 4H), 5.36-5.44 (m, 2H), 5.46 (d, 1H, *J* 5.5 Hz), 5.56 (d, 1H, *J* 9.0 Hz), 6.57-

6.66 (m, 2H), 6.69-7.13 (br s, 2H, interfering with the next listed signal), 6.97-7.01 (m, 2H), 7.13-7.45 (br s, 2H), 7.47-7.54 (m, 1 H), 7.57-7.68 (m, 2H), 7.94 (d, 1H, *J* 7.0 Hz), 8.03 (s, 1H), 8.16-8.25 (m, 1H), 8.25-8.73 (m, 3H), 8.73-9.11 (m, 4H), 9.17 (s, 1H), 9.76-10.04 (m, 1H), 12.38-12.59 (br s, 1H). HRMS (ESI): *m/z* [*M*+H]$^+$ calcd. for $[C_{52}H_{86}N_{16}O_{13}]^+$ 1161.6539, found 1161.6534. RP-HPLC (220 nm): 98% (t_R = 8.4 min, *k* = 8.7). $C_{52}H_{85}FN_{16}O_{13} \cdot C_6H_3F_9O_6$ (1161.35 + 342.07).

***N*$^{\omega}$-[(4-Aminobutyl)aminocarbonyl]Arg-Arg-Pro-Tyr-2-*tert*-butyl-Gly-Leu tetrakis(hydrotrifluoroacetate) (3.14).** The peptide was synthesized according to the general procedure (resin: 200 mg, 0.158 mmol). Purification by preparative RP-HPLC (column: Kinetex-XB C18; gradient: 0-35 min: A2/B 92:8-57:43, t_R = 18 min) yielded **3.14** as white fluffy solid (108.1 mg, 49%) with a HPLC purity of 95% (220 nm). A fraction (ca. 13 mg) was purified again (gradient: 0-18 min: A2/B 92:8-75:25, 18-40 min: 75:25-38:62, t_R = 19 min) yielding **3.14** with a HPLC purity of 97% (220 nm). ^{1}H-NMR (600 MHz, DMSO-d_6): δ 0.78-0.96 (m, 15H), 1.44-1.64 (m, 12H), 1.66-1.77 (m, 3H), 1.77-1.90 (m, 3H), 1.90-2.04 (m, 1H), 2.68 (dd, 1H, *J* 8.1, 14.0 Hz), 2.79 (s, 2H), 2.85-2.96 (m, 1H), 3.01-3.18 (m, 4H), 3.26 (s, 2H), 3.51-3.64 (m, 2H), 3.84 (s, 1H), 4.14-4.25 (m, 1H), 4.28 (d, 1H, *J* 9.5 Hz), 4.31-4.40 (m, 1H), 4.40-4.58 (m, 2H), 6.56-6.67 (m, 2H), 6.96-7.00 (m, 2H), 7.00-7.26 (br s, 2H), 7.26-7.56 (br s, 2H), 7.56-7.68 (m, 2H), 7.70-7.89 (m, 4H), 7.95 (d, 1H, *J* 7.8 Hz), 8.10-8.36 (m, 4H), 8.36-8.64 (m, 2H), 8.68 (d, 1H, *J* 7.4 Hz), 9.09 (br s, 1H), 9.17-9.38 (m, 1H), 10.76 (br s, 1H), 12.51 (br s, 1H). ^{13}C-NMR (150 MHz, DMSO-d_6): δ 21.2, 22.8, 23.5, 24.1, 24.3, 24.4, 24.6, 26.0, 26.5 (3 carbon atoms), 28.2, 28.3, 29.1, 34.7, 36.3, 38.5, 38.6, 39.8, 40.1, 40.5, 46.8, 50.2, 50.4, 51.6, 54.2, 59.1, 59.2, 114.8 (2 carbon atoms), 116.1 (TFA), 118.0 (TFA), 127.6, 130.0 (2 carbon atoms), 153.9, 153.9, 155.8, 156.9, 158.8 (q, *J* 32 Hz) (TFA), 168.3, 169.2, 169.8, 170.6, 171.3, 173.8. HRMS (ESI): *m/z* [*M*+2H]$^{2+}$ calcd. for $[C_{43}H_{76}N_{14}O_9]^{2+}$ 466.2954, found 466.2962. RP-HPLC (220 nm): 97% (t_R = 5.7 min, *k* = 6.5). $C_{43}H_{74}N_{14}O_9 \cdot C_8H_4F_{12}O_8$ (931.14 + 456.09).

***N*$^{\alpha}$-Methyl-*N*$^{\omega}$-[(4-aminobutyl)aminocarbonyl]Arg-Arg-Pro-Tyr-2-*tert*-butyl-Gly-Leu tetrakis(hydrotrifluoroacetate) (3.16).** The N-terminally non-methylated precursor peptide of peptide **3.16** was synthesized according to the general procedure (resin: 280 mg, 0.2212 mmol). N-terminal methylation: after coupling and Fmoc-deprotection of the last amino acid (arginine building block **3.06a**), the resin was washed with CH_2Cl_2 (5 ×), a solution of 2-nitrobenzenesulfonylchloride (147 mg, 0.664 mmol) and collidine (147 µL, 1.11 mmol) in CH_2Cl_2 (4.5 mL) was added to the resin and the mixture was shaken at rt for 2 h. The resin was washed with DMF (5 ×), and a solution of MTBD (127 µL, 0.885 mmol) and **3.15** (240 mg, 1.11 mmol) in DMF (5 mL) was added. After shaking at rt for 30 min, the resin was washed with DMF (3 ×) followed by the addition of a solution of DBU (165 µL, 1.11 mmol) and 2-mercaptoethanol (154 µL, 2.21 mmol) in DMF (5 mL) and shaking at rt for 30 min. After washing with DMF (5 ×), the resin was washed with K_2CO_3-treated CH_2Cl_2 and the peptide was cleaved off the resin as described in the general procedure. Purification by preparative RP-HPLC (column: Kinetex-XB C18; gradient: 0-35 min: A2/B 86:14-67:33, t_R = 15 min) afforded **3.16** as white fluffy solid (139.5 mg, 45%). ^{1}H-NMR (600 MHz, DMSO-d_6): δ 0.76-0.96 (m, 15H), 1.41-1.88 (m, 18H), 1.91-2.05 (m, 1H), 2.44-2.49 (m, 3H), 2.63-2.72 (m, 1H), 2.75-2.83 (m, 2H), 2.85-2.93 (m, 1H), 3.04-3.16 (m, 4H), 3.22-3.30 (m, 2H), 3.53-3.62 (m, 2H), 3.78-3.83 (m, 1H), 4.19-4.24 (m, 1H), 4.28 (d, 1H, *J* 9.5 Hz), 4.33-4.41 (m, 1H), 4.43-4.58 (m, 2H), 6.56-6.64 (m, 2H), 6.78-

7.23 (br s, 2H, interfering with the next listed signal), 6.96-7.00 (m, 2H), 7.23-7.55 (br s, 2H), 7.55-7.69 (m, 2H), 7.69-8.03 (m, 5H), 8.22 (d, 1H, *J* 7.6 Hz), 8.31-8.71 (m, 2H), 8.71-9.46 (m, 5H), 10.54-10.86 (m, 1H), 12.49 (br s, 1H). ^{13}C-NMR (150 MHz, DMSO-*d*$_6$): δ 21.2, 22.8, 23.4, 24.2, 24.3, 24.4, 24.6, 26.0, 26.5 (3 carbon atoms), 26.9, 28.1, 29.1, 31.1, 34.8, 36.3, 38.5, 38.6, 39.8, 40.1, 40.4, 46.8, 50.2, 50.6, 54.2, 59.1, 59.2, 59.8, 114.8 (2 carbon atoms), 116.0 (TFA), 117.9 (TFA), 127.6, 130.0 (2 carbon atoms), 153.9 (2 carbon atoms), 155.8, 156.9, 158.7 (q, *J* 32 Hz) (TFA), 166.9, 169.0, 169.8, 170.5, 171.2, 173.8. HRMS (ESI): *m/z* [*M*+2H]$^{2+}$ calcd. for [$C_{44}H_{78}N_{14}O_9$]$^{2+}$ 473.3033, found 473.3038. RP-HPLC (220 nm): 98% (t_R = 5.8 min, *k* = 6.6). $C_{44}H_{76}N_{14}O_9$ · $C_8H_4F_{12}O_8$ (945.18 + 456.09).

4-Pentynoic acid succinimidyl ester (3.17)[26]**.** 4-Pentynoic acid (2 g, 20.4 mmol) and *N*-hydroxysuccinimide (2.35 g, 20.4 mmol) were suspended in anhydrous CH_2Cl_2 (200 mL) under argon atmosphere, the mixture was cooled in an ice bath, and DCC (4.21 g, 20.4 mmol) was added under stirring. After 1 h, the ice bath was removed and stirring was continued at rt overnight. The white solid was separated by filtration and washed with CH_2Cl_2. The filtrate and the washings were combined, the volatiles were removed under reduced pressure, and the residue was subjected to crystallization (CH_2Cl_2/diethyl ether) to afford **3.17** as a colorless needle-like crystalline solid (1.31 g, 33%). The mother liquor was subjected to column chromatography (n-Hex/EtOAc 3:1-1:1) to obtain the residual product **3.17** as white solid (1.76 g, 44%). TLC: (light petroleum/EtOAc 1:1 v/v): R_f = 0.5. ^{1}H-NMR (300 MHz, $CDCl_3$): δ 2.04 (t, 1H, *J* 2.7 Hz), 2.57-2.63 (m, 2H), 2.83 (s, 4H), 2.84-2.90 (m, 2H). ^{13}C-NMR (100 MHz, DMSO-*d*$_6$): δ 13.4, 25.4, 29.6, 72.2, 82.0, 167.6, 170.1. HRMS (ESI): *m/z* [*M*+H]$^+$ calcd. for [$C_9H_{10}NO_4$]$^+$ 196.0604, found 196.0605. $C_9H_9NO_4$ (195.17).

{*N*$^\omega$-[*N*-(4-Pent-4-ynoylaminobutyl)aminocarbonyl]}Arg-Arg-Pro-Tyr-2-*tert*-butyl-Gly-Leu tris(hydrotrifluoroacetate) (3.18). A solution of **3.17** (3.95 mg, 20.3 µmol) in anhydrous DMF was added to a stirred solution of compound **3.14** tetrakis(hydrotrifluoroacetate) (42.15 mg, 30.4 µmol) and DIPEA (41.4 µL, 0.243 mmol) in anhydrous DMF/NMP (75:25 v/v) (250 µL) and stirring was continued at rt for 30 min. The mixture was acidified by addition of 10% aq. TFA (240 µL) and the product was purified by preparative RP-HPLC (column: Kinetex-XB C18; gradient: 0-35 min: A2/B 92:8-55:45, t_R = 23 min). Lyophilization of the eluate afforded **3.18** as white fluffy solid (16.2 mg, 59%). ^{1}H-NMR (600 MHz, DMSO-*d*$_6$): δ 0.80-0.93 (m, 15H), 1.35-1.46 (m, 4H), 1.46-1.64 (m, 8H), 1.64-1.76 (m, 3H), 1.76-1.90 (m, 3H), 1.94-2.04 (m, 1H), 2.22-2.28 (m, 2H), 2.32-2.37 (dt, 2H, *J* 7.2, 2.8 Hz), 2.64-2.71 (m, 1H), 2.74 (t, 1H, *J* 2.8 Hz), 2.85-2.92 (m, 1H), 3.01-3.16 (m, 6H), 3.22-3.28 (br s, 2H), 3.48-3.67 (m, 2H), 3.77-3.86 (m, 1H), 4.18-4.24 (m, 1H), 4.28 (d, 1H, *J* 9.5 Hz), 4.31-4.39 (m, 1H), 4.42-4.54 (m, 2H), 6.57-6.65 (m, 2H), 6.65-7.11 (br s, 2H, interfering with the next listed signal), 6.97-7.01 (m, 2H), 7.11-7.46 (br s, 2H), 7.50 (s, 1H), 7.55-7.67 (m, 2H), 7.88 (t, 1H, *J* 5.6 Hz), 7.98 (d, 1H, *J* 8.0 Hz), 8.04-8.28 (m, 4H), 8.29-8.56 (m, 2H), 8.59-8.73 (d, 1H, *J* 7.4 Hz), 8.99-9.12 (br s, 1H), 9.12-9.23 (m, 1H), 9.89-10.15 (br s, 1H), 12.35-12.61 (br s, 1H). HRMS (ESI): *m/z* [*M*+2H]$^{2+}$ calcd. for [$C_{48}H_{80}N_{14}O_{10}$]$^{2+}$ 506.3085, found 506.3097. RP-HPLC (220 nm): 96% (t_R = 8.5 min, *k* = 10.2). $C_{48}H_{78}N_{14}O_{10}$ · $C_6H_3F_9O_6$ (1011.24 + 342.07).

N^{α}-Methyl-{N^{ω}-[*N*-(4-pent-4-ynoylaminobutyl)aminocarbonyl]}Arg-Arg-Pro-Tyr-2-*tert*-butyl-Gly-Leu tris(hydrotrifluoroacetate) (3.19). A solution of **3.17** (1.96 mg, 10.1 µmol) in anhydrous DMF was added to a stirred solution of compound **3.16** tetrakis(hydrotrifluoroacetate) (11.7 mg, 8.38 µmol) and DIPEA (11.6 µL, 67.1 µmol) in anhydrous DMF/NMP (75:25 v/v) (68.9 µL) and stirring was continued at rt for 75 min. The mixture was acidified by addition of 10% aq. TFA (67.1 µL) and the product was purified by preparative RP-HPLC (column: Kinetex-XB C18; gradient: 0-35 min: A2/B 92:8-57:43, t_R = 21 min). Lyophilization of the eluate afforded **3.19** as white fluffy solid (10.3 mg, 90%). ^{1}H-NMR (600 MHz, DMSO-d_6): δ 0.81-0.93 (m, 15H), 1.32-1.89 (m, 19H), 1.96- 2.04 (m, 1H), 2.22-2.26 (m, 2H), 2.33-2.36 (m, 2H), 2.46-2.48 (m, 3H), 2.63-2.72 (m, 1H), 2.84-2.93 (m, 1H), 3.02-3.12 (m, 6H), 3.24-3.27 (m, 2H), 3.55-3.63 (m, 2H), 3.76-3.86 (m, 1H), 4.17-4.25 (m, 1H), 4.26-4.30 (m, 1H), 4.32-4.41 (m, 1H), 4.42-4.60 (m, 2H), 6.55-6.65 (m, 2H), 6.65-7.17 (br s, 2H, interfering with the next listed signal), 6.97-7.01 (m, 2H), 7.17-8.04 (m, 6H), 8.04-8.69 (m, 3H), 8.69-9.33 (m, 5H), 9.79-10.07 (m, 1H), 12.20-12.81 (br s, 1H). 1 exchangeable proton (NH, OH) of the presumably 3-fold protonated molecule could not be identified. HRMS (ESI): *m/z* $[M+2H]^{2+}$ calcd. for $[C_{49}H_{82}N_{14}O_{10}]^{2+}$ 513.3164, found 513.3174. RP-HPLC (220 nm): 99% (t_R = 8.8 min, k = 10.6). $C_{49}H_{80}N_{14}O_{10} \cdot C_6H_3F_9O_6$ (1025.27 + 342.07).

(N^{ω}-{*N*-[4-(3-{1-[6-deoxy-6-fluoro-β-D-glucopyranosyl]-1*H*-1,2,3-triazol-4-yl}propanoyl)aminobutyl]aminocarbonyl})Arg-Arg-Pro-Tyr-2-*tert*-butyl-Gly-Leu tris(hydrotrifluoroacetate) (3.20). Compound **3.20** was prepared from **3.18** (3.6 mg, 2.6 µmol) and **3.10** (2.2 mg, 10.6 µmol) using the procedure for the preparation of **3.11**. The product was purified by preparative RP-HPLC (column: Kinetex Biphenyl; gradient: 0-35 min: A1/B 90:10-62:38, t_R = 20 min). Lyophilization of the eluate afforded **3.20** as white fluffy solid (0.81 mg, 25%). HRMS (ESI): *m/z* $[M+H]^+$ calcd. for $[C_{54}H_{89}FN_{17}O_{14}]^+$ 1218.6753, found 1218.6737. RP-HPLC (220 nm): > 99% (t_R = 7.6 min, k = 9.0). $C_{54}H_{88}FN_{17}O_{14} \cdot C_6H_3F_9O_6$ (1218.40 + 342.07).

N^{α}-Methyl-(N^{ω}-{*N*-[4-(3-{1-[6-deoxy-6-fluoro-β-D-glucopyranosyl]-1*H*-1,2,3-triazol-4-yl}propanoyl)aminobutyl]aminocarbonyl})Arg-Arg-Pro-Tyr-2-*tert*-butyl-Gly-Leu tris(hydrotrifluoroacetate) (3.21). A solution of **3.10** (1.4 mg, 6.75 µmol) in EtOH/PBS (1:9 v/v) (114 µL) and a solution of **3.19** (3.6 mg, 2.6 µmol) in NMP (108 µL) were combined. A 1 M solution of copper(II)sulfate pentahydrate (3.1 µL, 3.12 µmol) in PBS and a 1 M solution of sodium ascorbate (7.8 µL, 7.79 µmol) in PBS were added and the mixture was stirred at rt for 30 min. After acidification by addition of 10% aq. TFA (1 µL) the product was purified by preparative RP-HPLC (column: Gemini-NX C18; gradient: 0-35 min: A2/B 81:19-62:38, t_R = 11 min). Lyophilization of the eluate afforded **3.21** as white fluffy solid (3.2 mg, 79%). ^{1}H-NMR (600 MHz, DMSO-d_6): δ 0.80-0.96 (m, 15H), 1.34-1.44 (m, 4H), 1.44-1.90 (m, 14H), 1.93-2.06 (m, 1H), 2.40-2.49 (m, 5H), 2.63-2.71 (m, 1H), 2.80-2.93 (m, 3H), 2.97-3.18 (m, 6H), 3.20-3.28 (m, 3H), 3.40-3.44 (m, 1H), 3.51-3.65 (m, 2H), 3.67-3.85 (m, 3H), 4.17-4.24 (m, 1H), 4.28 (d, 1H, *J* 9.4 Hz), 4.33-4.40 (m, 1H), 4.43-4.65 (m, 4H), 5.38-5.48 (m, 2H), 5.57 (d, 1H, *J* 9.3 Hz), 6.58-6.63 (m, 2H), 6.63-7.16 (br s, 2H, interfering with the next listed signal), 6.97-7.01 (m, 2H), 7.16-7.78 (m, 4H), 7.78-8.11 (m, 3H), 8.12-8.59 (m, 3H), 8.61-9.36 (m, 4H), 9.88 (br s, 1H), 12.49 (br s, 1H). 3 exchangeable protons (NH, OH) of the 3-fold protonated molecule could not be identified. HRMS (ESI): *m/z* $[M+H]^+$ calcd. for $[C_{55}H_{91}FN_{17}O_{14}]^+$ 1232.6910, found 1232.6919. RP-HPLC (220 nm): 98% (t_R = 7.6 min, k = 9.0). $C_{55}H_{90}FN_{17}O_{14} \cdot C_6H_3F_9O_6$ (1232.43 + 342.07).

3.5.3 Radioligand competition binding assay

Radioligand competition binding experiments with [^{3}H]UR-MK300 at hNTS$_1$R-expressing intact human HT-29 colon carcinoma cells (grown in antibiotic-free RPMI medium supplemented with 7.5% FCS) were performed at 23 ± 1 °C as described previously[16]. The latest determination of the K_d value of [^{3}H]UR-MK300 in this assay yielded a K_d of 0.55 ± 0.03 nM (mean value ± SEM from two independent determinations performed in triplicate)[13]. Unspecific binding was subtracted from total binding to obtain specific binding. Data analysis was performed by plotting % specifically bound radioligand (100% = specifically bound radioligand in the absence of competitor) over log(concentration of competitor) followed by a four-parameter logistic fit (SigmaPlot 12.5, Systat Software). Resulting pIC_{50} values were converted to IC_{50} values and K_i values were calculated from the IC_{50} values according to the Cheng-Prusoff equation[33] using a K_d value of 0.55 nM. The K_i values from individual experiments were transformed to pK_i values, followed by the calculation of mean pK_i values ± SEM.

3.5.4 Investigation of the stability of 3.11-3.14, 3.16 and 3.18-3.21 in human plasma

The metabolic stabilities of **3.11**-**3.14**, **3.16** and **3.18**-**3.21** (*cf*. Table 3.2) were investigated in human blood plasma/PBS (136.9 mM NaCl, 2.68 mM KCl, 5.62 mM Na_2HPO_4, 1.09 mM NaH_2PO_4 and 1.47 mM KH_2PO_4) pH 7.4 (1:2, v/v) according to a described procedure[13] with the following modifications: 5 mM stock solutions in EtOH/0.04% aq TFA (30:70 v/v) (**3.11**-**3.13**), MeCN/0.025% aq TFA (30:70 v/v) (**3.14**), MeCN/0.04% aq TFA (30:70 v/v) (**3.16**, **3.19** and **3.21**) or EtOH/H_2O (40:60 v/v) (**3.18**, **3.20**) were used for the addition of the peptides to plasma/PBS (1:2 v/v). As the RP-HPLC purity of 1-Methyl-D-Trp (internal standard, IS) was < 95% (data not shown), the compound was purified by preparative HPLC to give a purity of > 99%. The concentration of the peptides in plasma/PBS (1:2 v/v) was 80 and 4 µM (recovery determination) or 100 µM (stability tests). The obtained recoveries and the recovery ratios (peptide/internal standard) are summarized in Table A3.1 (Appendix). Data analysis was based on UV detection at 220 nm. Additionally, the stability of compound **3.21** was investigated in mouse plasma/PBS (1:2 v/v) using the same procedure as described above for human plasma. Mouse plasma was obtained by the collection of blood from anesthetized mice via cardiac puncture using a syringe that was rinsed with sodium heparin (25000 I.E., Ratiopharm, Ulm, Germany). The heparinized blood was transferred into a 2-mL reaction vessel, followed by centrifugation (1,200 × g, 4 °C, 10 min). The supernatants were pooled, centrifuged again (1,200 × g, 4 °C, 10 min), the plasma was aliquoted and stored at −80 °C. The concentration of **3.21** in plasma/PBS (1:2 v/v) was 80 and 4 µM (recovery determination) or 100 µM (stability tests). The obtained recoveries and the recovery ratios (**3.21**/IS) are summarized in Table A3.2 (Appendix). Data analysis was based on UV detection at 220 nm.

3.5.5 Radiosynthesis of [^{18}F]3.21

The ^{18}F-labeled glycosyl azide 6-deoxy-6-[^{18}F]fluoroglucosyl azide ([^{18}F]**3.10**) was prepared and used for the following CuAAC as described previously with slight modifications[21]. In brief, [^{18}F]fluoride was eluted from a Sep-Pak® Light (46 mg) Accell™ Plus QMA carbonate cartridge with a solution of Kryptofix® 2.2.2 (10 mg), potassium carbonate (0.1 M, 17.5 µL), KH_2PO_4 (0.1 M, 17.5 µL) in water (165 µL) and acetonitrile (800 µL). After azeotropic

drying, the tosyl-precursor 2,3,4-tri-O-acetyl-6-O-tosylglucosyl azide (9 mg, 19 µmol) in anhydrous acetonitrile (450 µL) was added and the mixture was stirred at 85 °C for 5 min. The product 2,3,4-tri-O-acetyl-6-deoxy-6-[^{18}F]fluoroglucosyl azide was isolated by semi-preparative HPLC (column: Kromasil C8, 125 × 8 mm, gradient: 0-30 min: A1/0.1% TFA in MeCN 70:30-30:70, t_R = 9.6 min) followed by SPE (Sep-Pak® light C18 cartridge, Waters). Starting from 1000 MBq [^{18}F]fluoride, this procedure yielded 400-450 MBq of 2,3,4-tri-O-acetyl-6-deoxy-6-[^{18}F]fluoroglucosyl azide (40-45 % activity yield (AY)) after a total synthesis time of about 30 min. For subsequent CuAAC, deacetylation was achieved by treatment with NaOH (60 mM, 270 µL) for 5 min at 60 °C to afford [^{18}F]**3.10**, and a mixture of $Cu(OAc)_2$ (4 mM, 10 µL), THPTA (20 mM, 10 µL), sodium ascorbate (100 mM, 10 µL) and alkyne **3.19** (10 mM, 5 µL) in sodium phosphate buffer (0.5 M, pH 8.0, 270 µL) was added. After stirring for 10 min at 60 °C the radiochemical yield of [^{18}F]**3.21** was 92% as determined by radio-HPLC (column: Chromolith RP-18, 100 × 4.6 mm, gradient: 0-5 min: A1/0.1% TFA in MeCN 90:10-50:50, t_R = 2.97 min). The mixture was diluted with aqueous TFA (0.1%, 400 µL) and the product was isolated by semipreparative HPLC (column: Kromasil C8, 125 × 8 mm; gradient: 0-20 min: A1/0.1% TFA in MeCN 85:15-50:50, t_R = 7.2 min; see Figure A3.4, Appendix). The product fraction was diluted with water (15 mL) and passed through an RP-18 cartridge (SepPak® light C18, Waters). The product was eluted with ethanol (1 mL). For all further experiments, the ethanol was evaporated in vacuo and the tracer was formulated with saline (0.9%). Starting from [^{18}F]fluoride (600-1000 MBq), [^{18}F]**3.21** was obtained in an AY of 20-23% (referred to [^{18}F]fluoride) in a total synthesis time of 65-70 min in molar activities of 75-130 GBq/µmol (n = 5).

3.5.6 In vitro characterization of [^{18}F]3.21 by determination of $logD_{7.4}$, stability in human serum and plasma, and binding to plasma proteins

All experiments were performed as described before[34]. In brief, the $logD_{7.4}$ value was determined via an octanol/water partition assay and provided as mean value ± SD from three independent experiments, each performed in triplicates. The stability of [^{18}F]**3.21** was determined by analytical radio-HPLC from human serum and human plasma samples (see Figure A3.5, Appendix). The percentage of binding of [^{18}F]**3.21** to human plasma proteins was determined by spin-column chromatography using MicroSpin™ G-50 columns (Cytiva, Amersham) and averaged in triplicate experiments.

3.5.7 Tumor model

All mouse experiments were approved by the local animal protection authorities (Government of Central Franconia, Germany, no. 55.2-2532-2-279), were carried out in compliance with the ARRIVE guidelines and performed in accordance with the relevant institutional guidelines and EU regulations. Mice were maintained in groups in an IVC recovery unit (25 ± 1 °C, Tecniplast S.p.A, Italy) with autoclaved bedding, food, and water on a daily 12 h light/dark cycle. Female nude mice (8-10 weeks old, Crl:NMRI-Foxn1nu, Charles River) were used for animal studies and were kept under pathogen-free conditions at the Franz-Penzoldt-Zentrum (Friedrich-Alexander University Erlangen-Nürnberg). A cell suspension of HT-29 cells (2×10^6) in PBS (100 µL) was injected in the upper back of

each mouse. After 2 weeks the tumors were between 5-8 mm in diameter and the mice were used for biodistribution or PET studies.

3.5.8 Biodistribution in HT-29 tumor-bearing nude mice

The tumor-bearing mice were anesthetized with O_2/isoflurane (3-4% isoflurane, 0.8 L/min O_2). Subsequently, the body weight and tumor size were determined, and the mice were laid on a heating pad (37 °C). About 1-3 MBq [^{18}F]**3.21** (in 100 µL NaCl (0.9%) were injected via the tail vein. After 30, 60 or 90 min the mice (n = 4 for each time point) were euthanized by cervical dislocation under deep isoflurane anesthesia and the following organs/tissues of the mice were removed, weighed, and radioactivity counted in the γ-counter (Wallac Wizard, PerkinElmer): blood, lung, liver, heart, spleen, kidney, HT-29 tumor, brain, intestine, pancreas, duodenum, muscle, and femur. The results were presented as the percentage of injected dose per gram organ (%ID/g), and tumor-to-organ ratios were calculated thereof. All measurements were corrected for decay.

3.5.9 Small-animal PET imaging

The HT-29 tumor-bearing mice (n = 4) were anesthetized using O_2/isoflurane (3-4% isoflurane, 0.8 L/min O_2) and laid on a heating pad (37 °C). Venous access was laid into the tail vein of the animals, and the cannula was fixed by an instant adhesive on the tail and the mice were transferred to the PET scanner. A dynamic PET scan was started from 0 to 60 min after injection of [^{18}F]**3.21** (2.5-2.9 MBq, 100 µL). Blocking experiments were performed on the following day with the same mice. For this purpose, the mice were injected with radiotracer together with **2.07** (100 nmol per mouse) and also scanned from 0-60 min after injection. After iterative maximum a posteriori image reconstruction of the decay and attenuation-corrected images, regions of interest (ROIs) were drawn over the tumors using the software PMOD (PMOD Technologies LLC, Switzerland). The radioactivity concentration within the regions was obtained from the mean value within the multiple ROIs and then converted to percentage of injected dose per gram organ (%ID/g).

3.5.10 Stability in mouse blood

Two NMRI mice were anesthetized with isoflurane and injected with [^{18}F]**3.21** (7-8 MBq) into the tail vein. One mouse was sacrificed by cervical dislocation after 10 min, the other mouse after 20 min, and approximately 100 µL blood were collected from the abdomen and transferred into Li-heparinized Microvettes® (100 LH, Sarstedt) and the Microvette® was centrifuged (2,000 × g, 5 min). The supernatant was transferred in a reaction vial and the same volume of aqueous TFA (10%) was added. The vial was centrifuged (20,000 × g, 5 min) and a sample of the resulting supernatant (100 µL) was analyzed by radio-HPLC (column: Chromolith RP-18e, 100 × 4.6 mm, gradient: 0-5 min: A1/0.1% TFA in MeCN 90:10-50:50).

3.6 References

1. Maoret, J.J.; Pospai, D.; Rouyer-Fessard, C.; Couvineau, A.; Laboisse, C.; Voisin, T.; Laburthe, M. Neurotensin receptor and its mRNA are expressed in many human colon cancer cell lines but not in normal colonic epithelium: Binding studies and RT-PCR experiments. *Biochem Biophys Res Commun* **1994**, *203*, 465-471, doi:10.1006/bbrc.1994.2205.

2. Reubi, J.C.; Waser, B.; Friess, H.; Büchler, M.; Laissue, J. Neurotensin receptors: A new marker for human ductal pancreatic adenocarcinoma. *Gut* **1998**, *42*, 546-550, doi:10.1136/gut.42.4.546.

3. Souazé, F.; Dupouy, S.; Viardot-Foucault, V.; Bruyneel, E.; Attoub, S.; Gespach, C.; Gompel, A.; Forgez, P. Expression of neurotensin and NT1 receptor in human breast cancer: A potential role in tumor progression. *Cancer Res* **2006**, *66*, 6243-6249, doi:10.1158/0008-5472.CAN-06-0450.

4. Dupouy, S.; Mourra, N.; Doan, V.K.; Gompel, A.; Alifano, M.; Forgez, P. The potential use of the neurotensin high affinity receptor 1 as a biomarker for cancer progression and as a component of personalized medicine in selective cancers. *Biochimie* **2011**, *93*, 1369-1378, doi:10.1016/j.biochi.2011.04.024.

5. Wu, Z.; Martinez-Fong, D.; Trédaniel, J.; Forgez, P. Neurotensin and its high affinity receptor 1 as a potential pharmacological target in cancer therapy. *Front Endocrinol (Lausanne)* **2012**, *3*, 184, doi:10.3389/fendo.2012.00184.

6. Körner, M.; Waser, B.; Strobel, O.; Büchler, M.; Reubi, J.C. Neurotensin receptors in pancreatic ductal carcinomas. *EJNMMI Res* **2015**, *5*, 17, doi:10.1186/s13550-015-0094-2.

7. Binder, E.B.; Kinkead, B.; Owens, M.J.; Nemeroff, C.B. Neurotensin and dopamine interactions. *Pharmacol Rev* **2001**, *53*, 453-486.

8. Ferraro, L.; Beggiato, S.; Borroto-Escuela, D.O.; Ravani, L.; O'Connor, W.T.; Tomasini, M.C.; Borelli, A.C.; Agnati, L.F.; Antonelli, T.; Tanganelli, S.; et al. Neurotensin NTS1-dopamine D2 receptor-receptor interactions in putative receptor heteromers: Relevance for Parkinson's disease and schizophrenia. *Curr Protein Pept Sci* **2014**, *15*, 681-690, doi:10.2174/1389203715666140901105253.

9. Rostène, W.H.; Alexander, M.J. Neurotensin and neuroendocrine regulation. *Front Neuroendocrinol* **1997**, *18*, 115-173, doi:10.1006/frne.1996.0146.

10. Carraway, R.; Leeman, S.E. The isolation of a new hypotensive peptide, neurotensin, from bovine hypothalami. *J Biol Chem* **1973**, *248*, 6854-6861.

11. Maschauer, S.; Prante, O. Radiopharmaceuticals for imaging and endoradiotherapy of neurotensin receptor-positive tumors. *J Labelled Comp Radiopharm* **2018**, *61*, 309-325, doi:10.1002/jlcr.3581.

12. Bruehlmeier, M.; García-Garayoa, E.; Blanc, A.; Holzer, B.; Gergely, S.; Tourwé, D.; Schubiger, P.A.; Bläuenstein, P. Stabilization of neurotensin analogues: Effect on peptide catabolism, biodistribution and tumor binding. *Nucl Med Biol* **2002**, *29*, 321-327, doi:10.1016/s0969-8051(01)00304-3.

13. Schindler, L.; Bernhardt, G.; Keller, M. Modifications at Arg and Ile give neurotensin(8-13) derivatives with high stability and retained NTS_1 receptor affinity. *ACS Med Chem Lett* **2019**, *10*, 960-965, doi:10.1021/acsmedchemlett.9b00122.

14. Maschauer, S.; Einsiedel, J.; Hübner, H.; Gmeiner, P.; Prante, O. ^{18}F- and ^{68}Ga-labeled neurotensin peptides for PET imaging of neurotensin receptor 1. *J Med Chem* **2016**, *59*, 6480-6492, doi:10.1021/acs.jmedchem.6b00675.

15. Maschauer, S.; Einsiedel, J.; Haubner, R.; Hocke, C.; Ocker, M.; Hübner, H.; Kuwert, T.; Gmeiner, P.; Prante, O. Labeling and glycosylation of peptides using click chemistry: A general approach to ^{18}F-glycopeptides as effective imaging probes for positron emission tomography. *Angew Chem Int Ed Engl* **2010**, *49*, 976-979, doi:10.1002/anie.200904137.

16. Keller, M.; Kuhn, K.K.; Einsiedel, J.; Hübner, H.; Biselli, S.; Mollereau, C.; Wifling, D.; Svobodová, J.; Bernhardt, G.; Cabrele, C.; et al. Mimicking of arginine by functionalized N^{ω}-carbamoylated arginine as a new broadly applicable approach to labeled bioactive peptides: High affinity angiotensin, neuropeptide Y, neuropeptide FF, and neurotensin receptor ligands as examples. *J Med Chem* **2016**, *59*, 1925-1945, doi:10.1021/acs.jmedchem.5b01495.

17. Spinnler, K.; von Krüchten, L.; Konieczny, A.; Schindler, L.; Bernhardt, G.; Keller, M. An alkyne-functionalized arginine for solid-phase synthesis enabling "bioorthogonal" peptide conjugation. *ACS Med Chem Lett* **2020**, *11*, 334-339, doi:10.1021/acsmedchemlett.9b00388.

18. Maschauer, S.; Einsiedel, J.; Hocke, C.; Hübner, H.; Kuwert, T.; Gmeiner, P.; Prante, O. Synthesis of a ^{68}Ga-labeled peptoid-peptide hybrid for imaging of neurotensin receptor expression in vivo. *ACS Med Chem Lett* **2010**, *1*, 224-228, doi:10.1021/ml1000728.

19. Alshoukr, F.; Rosant, C.; Maes, V.; Abdelhak, J.; Raguin, O.; Burg, S.; Sarda, L.; Barbet, J.; Tourwé, D.; Pelaprat, D.; et al. Novel neurotensin analogues for radioisotope targeting to neurotensin receptor-positive tumors. *Bioconjug Chem* **2009**, *20*, 1602-1610, doi:10.1021/bc900151z.

20. Keller, M.; Mahuroof, S.A.; Hong Yee, V.; Carpenter, J.; Schindler, L.; Littmann, T.; Pegoli, A.; Hübner, H.; Bernhardt, G.; Gmeiner, P.; et al. Fluorescence labeling of neurotensin(8-13) via arginine residues gives molecular tools with high receptor affinity. *ACS Med Chem Lett* **2020**, *11*, 16-22, doi:10.1021/acsmedchemlett.9b00462.

21. Maschauer, S.; Haubner, R.; Kuwert, T.; Prante, O. ^{18}F-Glyco-RGD peptides for PET imaging of integrin expression: Efficient radiosynthesis by click chemistry and modulation of biodistribution by glycosylation. *Mol Pharm* **2014**, *11*, 505-515, doi:10.1021/mp4004817.

22. Potemkin, R.; Strauch, B.; Kuwert, T.; Prante, O.; Maschauer, S. Development of ^{18}F-fluoroglycosylated PSMA-ligands with improved renal clearance behavior. *Mol Pharm* **2020**, *17*, 933-943, doi:10.1021/acs.molpharmaceut.9b01179.

23. Moradi, S.V.; Hussein, W.M.; Varamini, P.; Simerska, P.; Toth, I. Glycosylation, an effective synthetic strategy to improve the bioavailability of therapeutic peptides. *Chem Sci* **2016**, *7*, 2492-2500, doi:10.1039/c5sc04392a.

24. Apostol, C.R.; Hay, M.; Polt, R. Glycopeptide drugs: A pharmacological dimension between "Small Molecules" and "Biologics". *Peptides* **2020**, *131*, 170369, doi:10.1016/j.peptides.2020.170369.

25. Miller, S.C.; Scanlan, T.S. Site-selective N-methylation of peptides on solid support. *J Am Chem Soc* **1997**, *119*, 2301-2302, doi:10.1021/ja9635443.

26. Eaton, B.; Gold, L. Parallel SELEX allowing for asymmetrical reactions in combinatorial chemistry. U.S. Patent, US5858660A, 1999.

27. Toms, J.; Kogler, J.; Maschauer, S.; Daniel, C.; Schmidkonz, C.; Kuwert, T.; Prante, O. Targeting fibroblast activation protein: Radiosynthesis and preclinical evaluation of an ^{18}F-labeled FAP inhibitor. *J Nucl Med* **2020**, *61*, 1806-1813, doi:10.2967/jnumed.120.242958.

28. Delanghe, S.; Delanghe, J.R.; Speeckaert, R.; Van Biesen, W.; Speeckaert, M.M. Mechanisms and consequences of carbamoylation. *Nat Rev Nephrol* **2017**, *13*, 580-593, doi:10.1038/nrneph.2017.103.

29. Yadav, S.P.S.; Sandoval, R.M.; Zhao, J.; Huang, Y.; Wang, E.; Kumar, S.; Campos-Bilderback, S.B.; Rhodes, G.; Mechref, Y.; Molitoris, B.A.; et al. Mechanism of how carbamylation reduces albumin binding to FcRn contributing to increased vascular clearance. *Am J Physiol Renal Physiol* **2021**, *320*, F114-F129, doi:10.1152/ajprenal.00428.2020.

30. Wang, M.; Zhang, H.; Wang, H.; Feng, H.; Deng, H.; Wu, Z.; Lu, H.; Li, Z. Development of [^{18}F]AlF-NOTA-NT as PET agents of neurotensin receptor-1 positive pancreatic cancer. *Mol Pharm* **2018**, *15*, 3093-3100, doi:10.1021/acs.molpharmaceut.8b00192.

31. Landau, B.R.; Spring-Robinson, C.L.; Muzic, R.F., Jr.; Rachdaoui, N.; Rubin, D.; Berridge, M.S.; Schumann, W.C.; Chandramouli, V.; Kern, T.S.; Ismail-Beigi, F. 6-Fluoro-6-deoxy-D-glucose as a tracer of glucose transport. *Am J Physiol Endocrinol Metab* **2007**, *293*, E237-245, doi:10.1152/ajpendo.00022.2007.

32. Shinde, S.S.; Maschauer, S.; Prante, O. Sweetening pharmaceutical radiochemistry by ^{18}F-fluoroglycosylation: Recent progress and future prospects. *Pharmaceuticals (Basel)* **2021**, *14*, 1175, doi:10.3390/ph14111175.

33. Cheng, Y.; Prusoff, W.H. Relationship between the inhibition constant (K_I) and the concentration of inhibitor which causes 50 per cent inhibition (I_{50}) of an enzymatic reaction. *Biochem Pharmacol* **1973**, *22*, 3099-3108, doi:10.1016/0006-2952(73)90196-2.

34. Maschauer, S.; Ott, J.J.; Bernhardt, G.; Kuwert, T.; Keller, M.; Prante, O. ^{18}F-labelled triazolyl-linked argininamides targeting the neuropeptide Y Y_1R for PET imaging of mammary carcinoma. *Sci Rep* **2019**, *9*, 12990, doi:10.1038/s41598-019-49399-0.

3.7 Appendix

3.7.1 General experimental conditions

If not otherwise stated, solvents and buffer components, purchased from commercial suppliers, were of analytical grade. Gradient grade MeOH for HPLC was obtained from Merck (Darmstadt, Germany) and gradient grade acetonitrile for HPLC was from Sigma-Aldrich (Taufkirchen, Germany). Diethyl ether was from Fisher Chemicals (Loughborough, United Kingdom), EtOAc was from VWR Chemicals (Ismaning, Germany), and *N*,*N*-Diisopropylethylamine (DIPEA, 99%) was from ABCR (Karlsruhe, Germany). Anhydrous *N*,*N*-Dimethylformamide (DMF) (99.8%), n-hexane, 1,1,1,3,3,3-hexafluoro-2-propanol (HFIP), 7-methyl-1,5,7-triazabicyclo[4.4.0]dec-5-en (MTBD), methyl-4-nitrobenzenesulfonate (**3.15**), 2-mercaptoethanol, *N*-hydroxysuccinimide, *N*,*N*′-dicyclohexylcarbodiimide (DCC), sodium L-ascorbate and 1-methyl-D-Trp were purchased from Sigma-Aldrich. DMF (for peptide synthesis, packed under nitrogen, code D/3848/PB17), 1-methyl-2-pyrrolidone (NMP) (for peptide synthesis, nitrogen flushed), anhydrous NMP (99.5%), CH_2Cl_2 and 1-hydroxy-1*H*-benzotriazole (HOBt) hydrate were obtained from Acros Organics/Fisher Scientific (Nidderau, Germany). Trifluoroacetic acid and absolute EtOH were purchased from Honeywell (Seelze, Germany). 4-Pentynoic acid, collidine, 2-nitrobenzenesulfonylchloride and 1,8-diazabicyclo[5.4.0]undec-7-ene (DBU) were from Alfa Aesar/ThermoFisher (Heysham, Great Britain). Piperidine and *N*,*N*,*N*′,*N*′-tetramethyl-*O*-(1*H*-benzotriazole-1-yl)-uronium hexafluorophosphate (HBTU) were from Iris Biotech (Marktredwitz, Germany). Deuterated solvents were obtained from Deutero (Kastellaun, Germany). Bovine serum albumin (BSA) was purchased from Serva (Heidelberg, Germany). Ammonium acetate (98%) and copper(II)sulfate pentahydrate were from Merck. H-Leu-2-ClTrt resin (loading: 0.79 mmol/g), Fmoc-N-Me-Arg(Pbf)-OH, Fmoc-Pro-OH, Fmoc-Tle-OH (Fmoc-α-*tert*-butylglycine)) were purchased from Merck Biosciences (Schwalbach am Taunus, Germany). Fmoc-Arg(Pbf)-OH and Fmoc-Tyr(*t*Bu)-OH were obtained from Iris Biotech. Peptide **1** (tris(hydrotrifluoroacetate)) was purchased from SynPeptide (Shanghai, China). Succinimidyl pentynoate (**3.17**)[1] and 6-deoxy-6-fluoro-ß-D-glucosyl azide (**3.10**)[2] were prepared according to described procedures. Millipore water was used throughout for the preparation of buffers, stock solutions and HPLC eluents. 1.5- and 2-mL polypropylene reaction vessels with screw cap (in the following referred to as "reaction vessel with screw cap") from Süd-Laborbedarf (Gauting, Germany) were used for the preparation and storage of stock solutions, and for small-scale reactions. 1.5- or 2-mL polypropylene reaction vessels (in the following referred to as "reaction vessel") from Sarstedt (Nümbrecht, Germany) were used for the preparation of diluted solutions, and for the investigation of stabilities in plasma. For the evaporation of solvents in 1.5- or 2-mL reaction vessels, a Savant Speed-Vac Plus SC110A vacuum concentrator (Thermo Fischer Scientific, Waltham, MA) was used. NMR spectra were recorded on a Bruker Avance 600 instrument (^{1}H: 600 MHz, T = 300 K, ^{13}C: 151 MHz, T = 300 K), a Bruker Avance 400 instrument (^{1}H: 400 MHz, T = 300 K, ^{13}C: 101 MHz, T = 300 K) or a Bruker Avance 300 instrument (^{1}H: 300 MHz, T = 300 K, ^{13}C: 75 MHz, T = 300 K) (Bruker, Karlsruhe, Germany). The spectra were calibrated based on the solvent residual peaks (^{1}H-NMR: $CDCl_3$: δ = 7.26 ppm, DMSO-d_6: δ = 2.50 ppm; ^{13}C-NMR: DMSO-d_6: δ = 39.50 ppm). ^{1}H-NMR data are reported as follows: chemical shift δ in ppm (multiplicity (s = singlet, d = doublet, t = triplet, q = quartet, m = multiplet, br s = broad

singlet), integral, coupling constant *J* in Hz). Thin layer chromatography was performed on Merck silica gel 60 F254 TLC aluminum plates. High resolution mass spectra (HRMS) were acquired with an Agilent 6540 UHD Accurate-Mass Q-TOF LC/MS system coupled to an Agilent 1290 HPLC system (Agilent Technologies, Santa Clara, CA), using an ESI source. Analyses were performed using the following LC method: column: Luna Omega C18, 1.6 µm, 50 × 2.1 mm (Phenomenex, Aschaffenburg, Germany), column temperature: 40 °C, flow: 0.6 mL/min, solvent/linear gradient: 0-4 min: 0.1% aq HCOOH/0.1% HCOOH in MeCN 95:5-2:98, 4-5 min: 2:98. Preparative HPLC was performed with a system from Knauer (Berlin, Germany) consisting of two K-1800 pumps and a K-2001 detector. A Kinetex-XB C18, 5 µm, 250 mm × 21 mm (Phenomenex), a Kinetex Biphenyl, 5 µm, 250 mm × 21 mm (Phenomenex) or a Gemini-NX C18, 5 µm, 250 mm × 21 mm (Phenomenex) served as RP-columns at a flow rate of 20 mL/min. Mixtures of 0.1% aq TFA (A1) and acetonitrile (B), or 0.2% aq TFA (A2) and B were used as mobile phase. A detection wavelength of 220 nm was used throughout. Collected fractions were lyophilized using an Alpha 2-4 LD apparatus (Martin Christ, Osterode am Harz, Germany) or a Scanvac CoolSafe 100-9 freeze-dryer (Labogene, Allerød, Denmark) both equipped with a vacuubrand RZ 6 rotary vane vacuum pump. Analytical HPLC analysis of compounds **3.07**-**3.09**, **3.11**-**3.14**, **3.16** and **3.18**-**3.21** was performed with a system from Agilent Technologies consisting of a 1290 Infinity binary pump equipped with a degasser, a 1290 Infinity Autosampler, a 1290 Infinity Thermostated Column Compartment, a 1260 Infinity Diode Array Detector and a 1260 Infinity Fluorescence Detector. A Kinetex-XB C18, 2.5 µm, 100 × 3 mm (Phenomenex) served as stationary phase at a flow rate of 0.6 mL/min. The oven temperature was set to 25 °C. Mixtures of 0.04% aq TFA (A3) and B were used as mobile phase. The following linear gradient was applied: 0-12 min: A3/B 90:10-70:30, 12-16 min: 70:30-5:95, 16-20 min: 5:95. The injection volume was 20 µL. UV detection was performed at 220 nm and fluorescence detection at 275/305 nm. Retention (capacity) factors *k* were calculated from the retention times t_R according to $k = (t_R - t_0)/t_0$ (t_0 = dead time). Synthesized peptides were characterized by ^{1}H- and ^{13}C-NMR spectroscopy, HRMS, and RP-HPLC analysis. Additionally, ^{1}H-COSY NMR spectra were acquired of peptides **3.07**-**3.09**, **3.14**, **3.16**, **3.19** and **3.21**. The purity of all final compounds, determined by RP-HPLC (220 nm), was ≥ 96%.

Annotation concerning the ^{1}H-NMR spectra (solvent: DMSO-d_6): in order to allow an integration of the signals interfering with the broad water signal at ca 3.5 ppm, ^{1}H-NMR spectra were additionally recorded in DMSO-d_6/D_2O (10:1 or 4:1 v/v) (spectra and data not shown).

Radio-HPLC was performed on an Agilent 1100 system (Agilent Technologies) with a quaternary pump and variable wavelength detector and radio-HPLC detector HERM LB 500 (Berthold Technologies, Germany). No-carrier-added [^{18}F]fluoride was produced through the ^{18}O(p,n)^{18}F reaction on a PETtrace 800 cyclotron (General Electric, Uppsala, Sweden) using $H_2[^{18}O]O$ as the target at the Universitätsklinikum Würzburg (Klinik und Poliklinik für Nuklearmedizin, Experimentelle Nuklearmedizin, Radiopharmazie/PET-Zentrum, Prof. Samuel Samnick) and transported by road to Erlangen.

3.7.2 Figures A3.1-A3.5 and Tables A3.1-A3.3

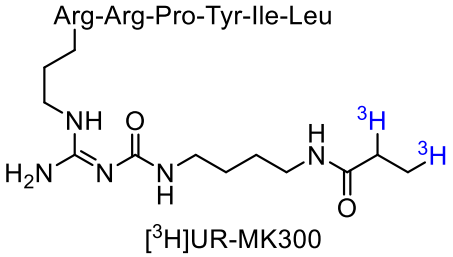

Figure A3.1. Structure of the tritium-labeled NT(8-13)-derived radioligand [^{3}H]UR-MK300 used for NTS$_1$R competition binding studies (reported K_d = 0.51 nM)[3].

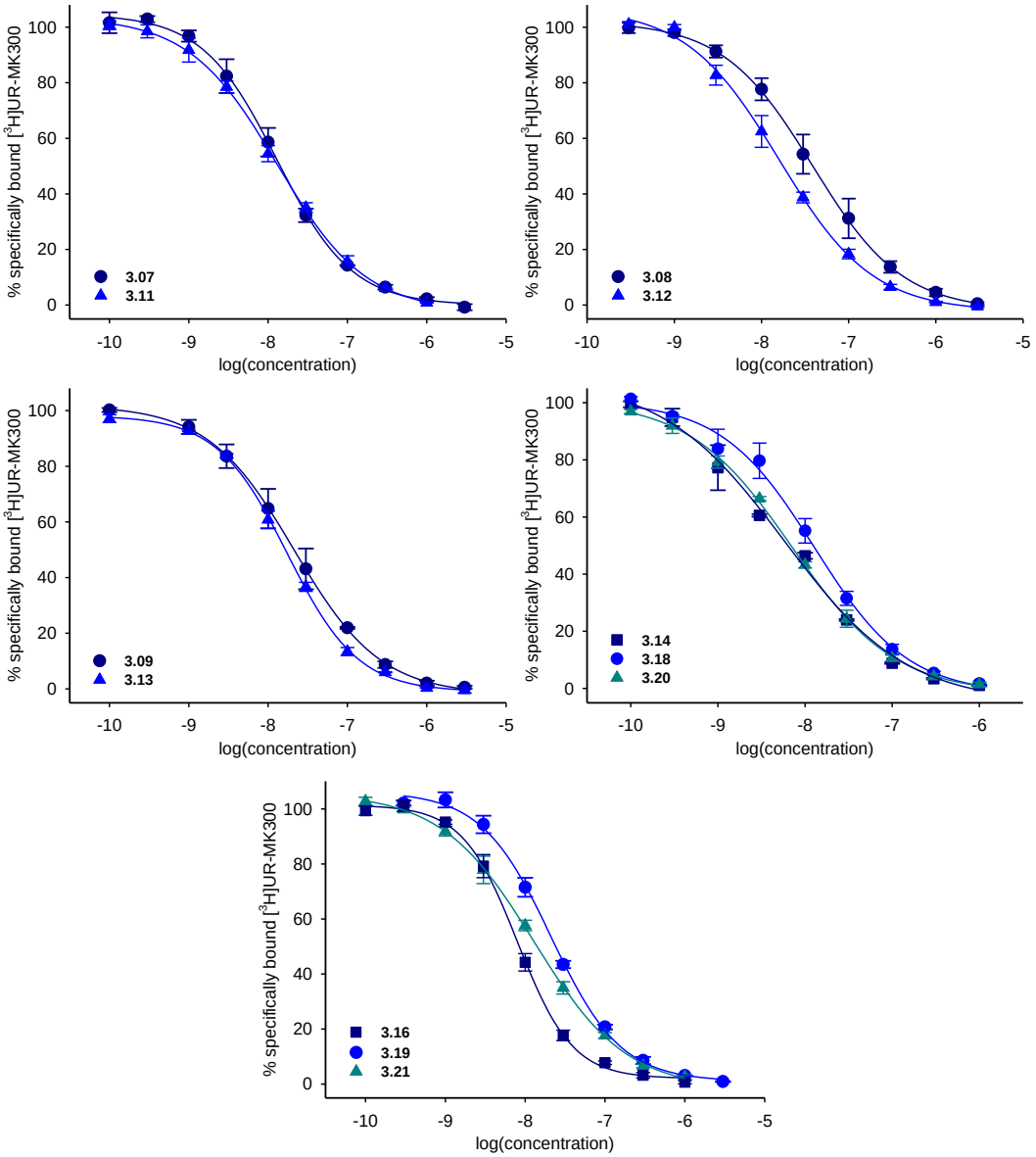

Figure A3.2. Radioligand displacement curves from competition binding experiments with [^{3}H]UR-MK300 (K_d = 0.55 nM, c = 1 nM) and **3.07**-**3.09**, **3.11**-**3.14**, **3.16** or **3.18**-**3.21** at intact hNTS$_1$R-expressing HT-29 cells. Amino-functionalized precursor peptides are represented by squares, alkyne-functionalized peptides are represented by circles, and compounds conjugated to the sugar moiety are represented by triangles. Data represent mean values ± SEM from at least two independent experiments (performed in triplicate).

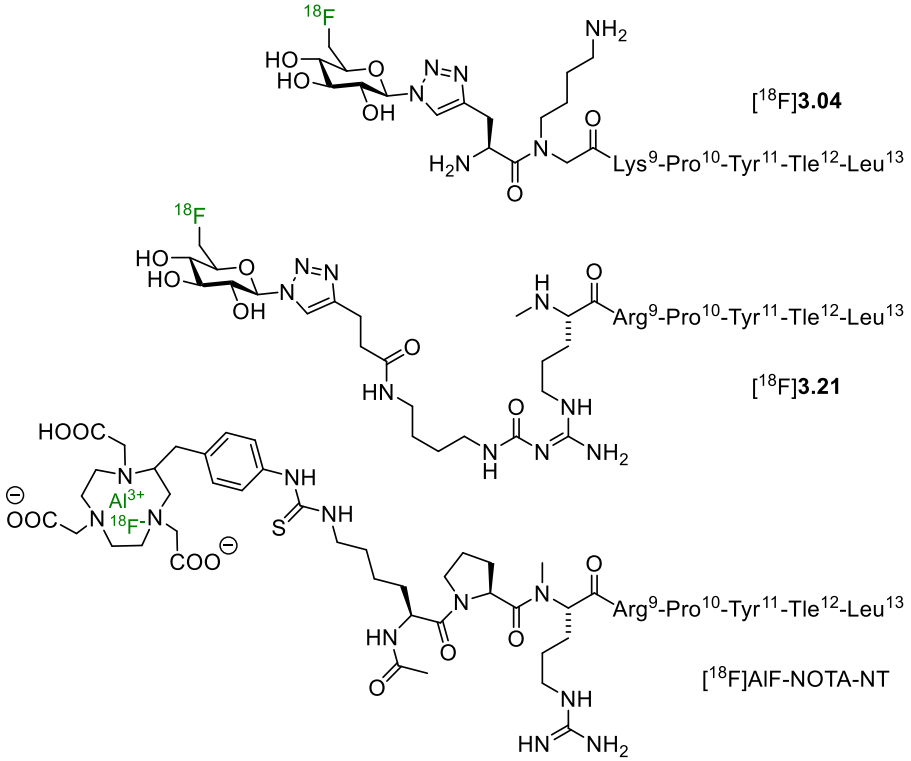

Figure A3.3. Structures of the NT(8-13)-derived NTS_1R PET ligands [^{18}F]**3.04**[4] and [^{18}F]**3.21** (this work), both conjugated to an ^{18}F-labeled 6-deoxy-6-fluoroglucosyl moiety, and the NT(6-13)-derived [^{18}F]AlF-NOTA-NT[5], containing $^{18}F^-$, non-covalently bound to Al^{3+} in the NOTA chelator.

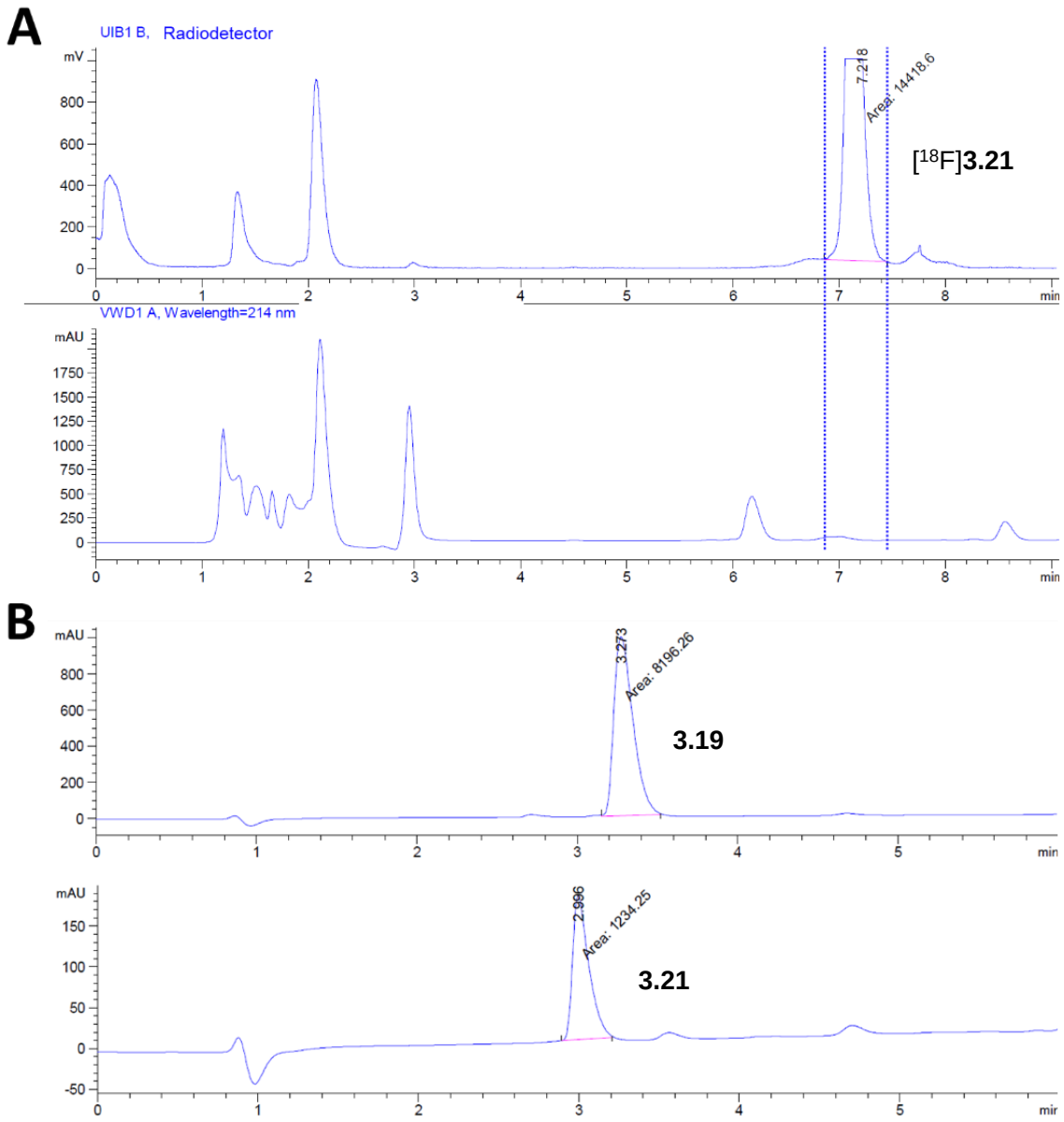

Figure A3.4. (A) Semipreparative HPLC run for isolation of [^{18}F]**3.21** (column: Kromasil C8, 125 × 8 mm; gradient: 0-20 min: A1/0.1% TFA in MeCN 85:15-50:50, t_R ([^{18}F]**3.21**) = 7.2 min; note: t_R (**3.19**) > 9 min, not recorded). (B) HPLC analysis of glycopeptide **3.21** compared to the alkyne precursor **3.19** revealed that **3.19** is more lipophilic than **3.21** (column: Chromolith RP-18, 100 × 4.6 mm, flow: 4 mL/min, gradient: 0-5 min: A1/0.1% TFA in MeCN 90:10-50:50, t_R (**3.21**) = 3.0 min, t_R (**3.19**) = 3.3 min; detection at 214 nm).

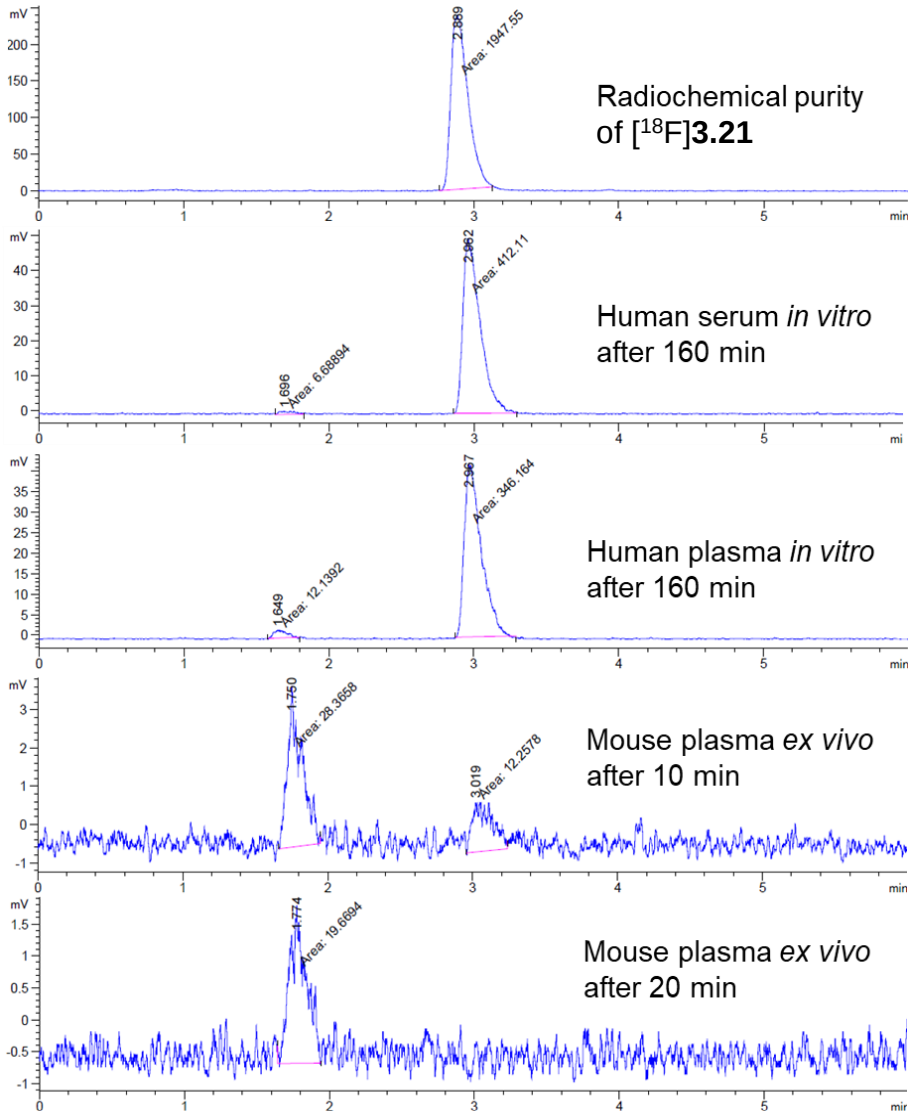

Figure A3.5. Radiochemical purity and stability *in vitro* and *ex vivo* (after i.v. injection) of [^{18}F]**3.21**. Column: Chromolith RP-18, 100 × 4.6 mm, flow: 4 mL/min, gradient: 0-5 min: A1/0.1% TFA in MeCN 90:10-50:50.

Table A3.1. Recoveries of peptides **3.11**-**3.14, 3.16** and **3.18**-**3.21** from human plasma/PBS (1:2 v/v) and ratios of peptide-recovery over recovery of IS.

Compd.	Peptide concentration 80 μM			Peptide concentration 4 μM		
	recovery peptide (%)[a]	recovery IS (%)[a]	ratio[b]	recovery peptide (%)[a]	recovery IS (%)[a]	ratio[b]
3.11	94	107	0.88	94	99	0.95
	91	99	0.92	89	100	0.89
	97	109	0.89	94	102	0.92
	89	97	0.92	91	99	0.92
	92	101	0.91	104	108	0.96
			(0.90 ± 0.01)			(0.93 ± 0.01)
3.12	91	106	0.85	92	96	0.96
	93	107	0.87	116	105	1.11
	94	110	0.85	103	99	1.03
	92	107	0.86	110	100	1.10
			(0.86 ± 0.01)			(1.05 ± 0.03)
3.13	86	104	0.82	103	101	1.03
	88	103	0.85	104	106	0.98
	92	104	0.89	104	98	1.06
	89	99	0.90	93	89	1.05
			(0.86 ± 0.02)			(1.03 ± 0.02)
3.14	85	104	0.82	88	105	0.84
	84	106	0.79	96	110	0.87
	84	103	0.82	94	109	0.87
	88	107	0.82	94	106	0.89
				88	100	0.88
			(0.81 ± 0.01)			(0.87 ± 0.01)
3.16	91	104	0.87	91	97	0.93
	88	104	0.85	91	99	0.92
	88	105	0.84	98	106	0.93
	94	110	0.85	101	109	0.93
			(0.85 ± 0.01)			(0.93 ± 0.01)
3.18	95	104	0.91	102	103	0.99
	111	120	0.93	119	122	0.97
	99	107	0.92	104	98	1.06
	98	110	0.89	112	112	1.00
	109	120	0.91	98	103	0.95
			(0.91 ± 0.01)			(0.99 ± 0.02)
3.19	93	101	0.92	106	94	1.12
	93	100	0.93	100	94	1.07
	96	101	0.95	97	88	1.10
	101	106	0.96	105	100	1.05
			(0.94 ± 0.01)			(1.09 ± 0.02)
3.20	86	97	0.88	109	100	1.09
	94	103	0.91	109	103	1.06
	90	99	0.91	110	108	1.02
	89	96	0.92	113	109	1.03
				115	107	1.07
			(0.91 ± 0.01)			(1.05 ± 0.01)

Table A3.1 continued

3.21	96	104	0.92	102	103	0.99
	99	106	0.93	112	107	1.05
	103	111	0.92	110	109	1.01
	104	112	0.93	119	115	1.03
				108	109	0.99
			(0.93 ± 0.01)			(1.01 ± 0.01)

[a]Recoveries of the peptides and of IS from human plasma/PBS (1:2 v/v) using a peptide concentration of 80 µM or 4 µM and an IS concentration of 10 µM (four or five independent experiments). [b]Ratios of peptide recovery over recovery of the IS calculated for individual experiments, as well as mean recovery ratios ± SEM (given in parenthesis). Note: When the remaining intact peptide concentration in plasma was > 20 µM, recovery ratios based on the 80 µM peptide concentrations were used to calculate peptide recoveries of the plasma stability samples. When the remaining intact peptide concentration was < 20 µM, recovery ratios based on the 4 µM peptide concentrations were used to calculate peptide recoveries of the plasma stability samples.

Table A3.2. Recoveries of potential PET ligand **3.21** from mouse plasma/PBS (1:2 v/v) and ratios of peptide-recovery over recovery of IS.

Compd.	Peptide concentration 80 µM			Peptide concentration 4 µM		
	recovery peptide (%)[a]	recovery IS (%)[a]	ratio[b]	recovery peptide (%)[a]	recovery IS (%)[a]	ratio[b]
3.21	95	103	0.92	105	105	1.00
	92	102	0.90	101	104	0.98
	96	105	0.91	107	105	1.02
	93	100	0.93	107	104	1.03
				108	108	0.99
			(0.92 ± 0.01)			(1.00 ± 0.01)

[a]Recoveries of **3.21** and IS from mouse plasma/PBS (1:2 v/v) using a peptide concentration of 80 µM or 4 µM and an IS concentration of 10 µM (four or five independent experiments). [b]Ratios of peptide recovery over recovery of the IS calculated for individual experiments, as well as mean recovery ratios ± SEM (given in parenthesis). Note: As the remaining intact peptide concentration in plasma was > 20 µM, recovery ratios based on the 80 µM peptide concentrations were used to calculate peptide recoveries of the plasma stability samples.

Table A3.3. Biodistribution data (%ID/g) of [^{18}F]**3.21** in HT-29 tumor-bearing nude mice at 30, 60 and 90 min p.i. and tumor-to-tissue ratios calculated thereof from selected organs.[a]

	30 min	60 min	90 min
blood	1.7 ± 1.1	0.4 ± 0.4	0.1 ± 0.05
lung	1.5 ± 0.2	0.3 ± 0.2	0.3 ± 0.2
liver	5.1 ± 0.5	4.1 ± 0.3	3.7 ± 0.6
kidneys	16.0 ± 3.3	14.8 ± 3.0	11.9 ± 1.4
heart	0.6 ± 0.1	0.2 ± 0.1	0.07 ± 0.04
spleen	1.3 ± 0.3	1.0 ± 0.4	0.7 ± 0.1
brain	0.1 ± 0.05	0.04 ± 0.02	0.04 ± 0.05
muscle	2.6 ± 5.2	0.4 ± 0.5	0.08 ± 0.04
femur	2.2 ± 3.9	0.7 ± 1.1	0.2 ± 0.02
HT-29 tumor	4.8 ± 1.0	2.1 ± 0.6	2.6 ± 0.3
intestine	2.5 ± 1.5	1.8 ± 2.0	0.5 ± 0.5
pancreas	0.6 ± 0.4	0.7 ± 1.1	0.2 ± 0.2
duodenum	1.1 ± 0.3	1.4 ± 1.8	0.5 ± 0.3
tumor/blood	2.8	5.3	30.0
tumor/kidneys	0.3	0.1	0.2
tumor/muscle	7.6	6.0	32.6

[a]Values are given as the mean ± SD (n = 4).

3.7.3 RP-HPLC analyses of compounds 3.07-3.09, 3.11-3.14, 3.16 and 3.18-3.21

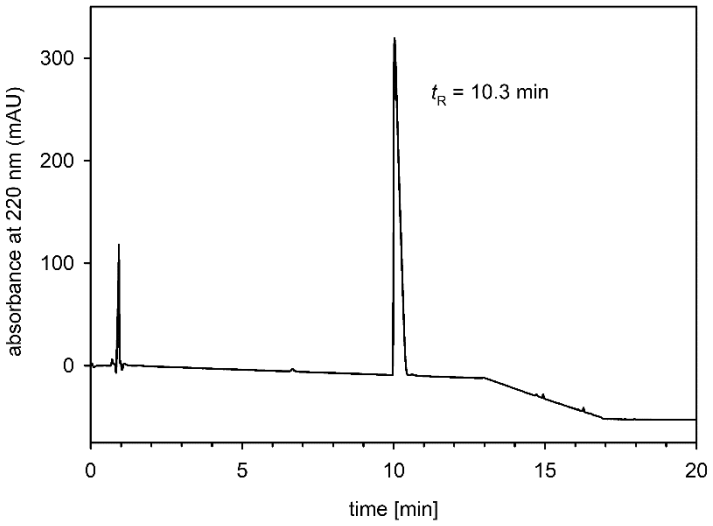

RP-HPLC analysis (purity control) of compound **3.07**

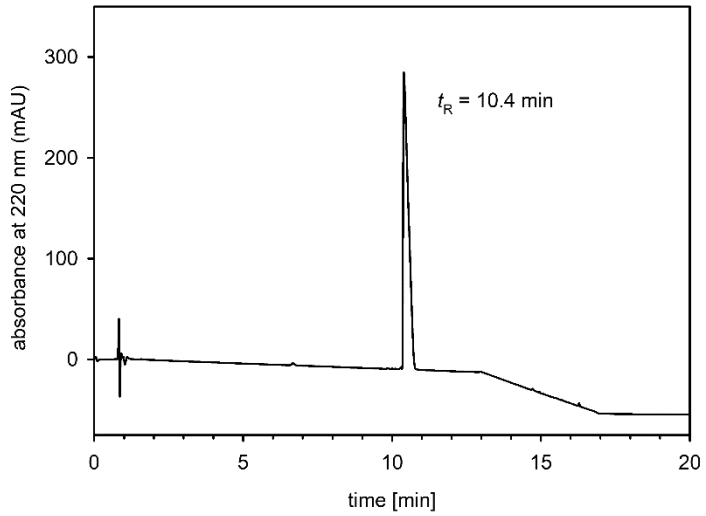

RP-HPLC analysis (purity control) of compound **3.08**

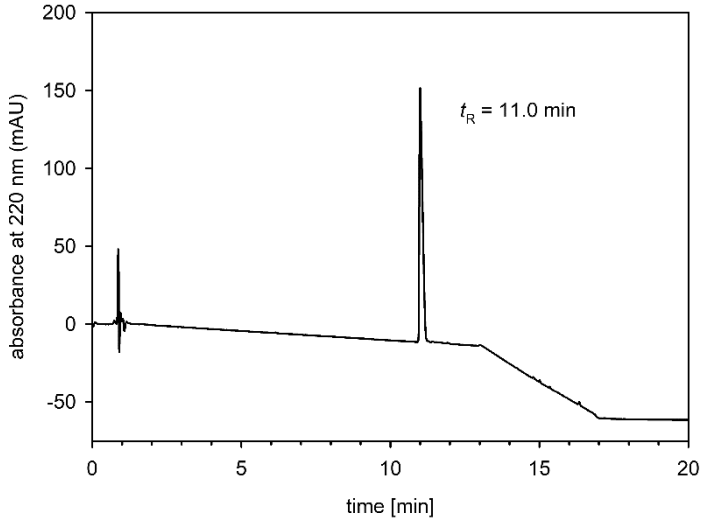

RP-HPLC analysis (purity control) of compound **3.09**

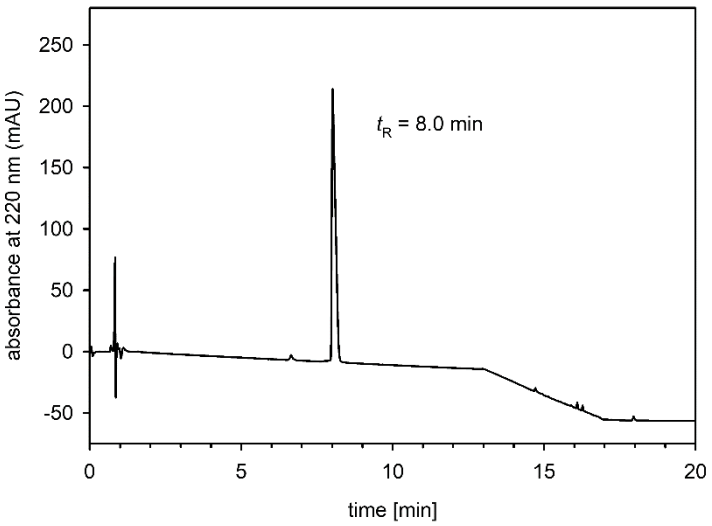

RP-HPLC analysis (purity control) of compound **3.11**

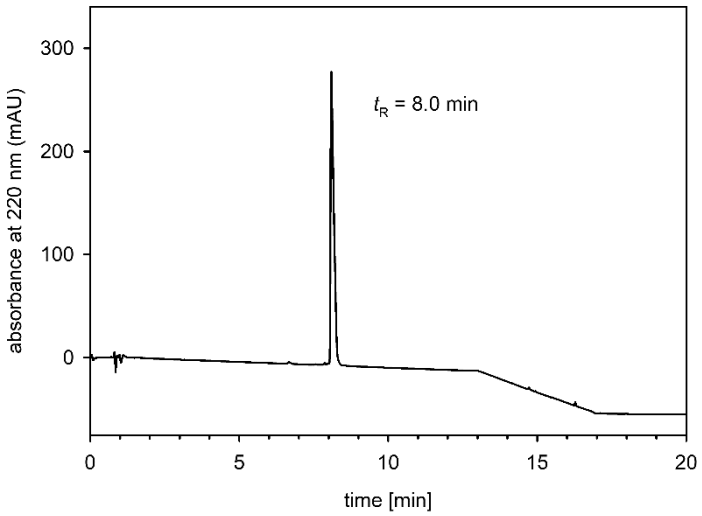

RP-HPLC analysis (purity control) of compound **3.12**

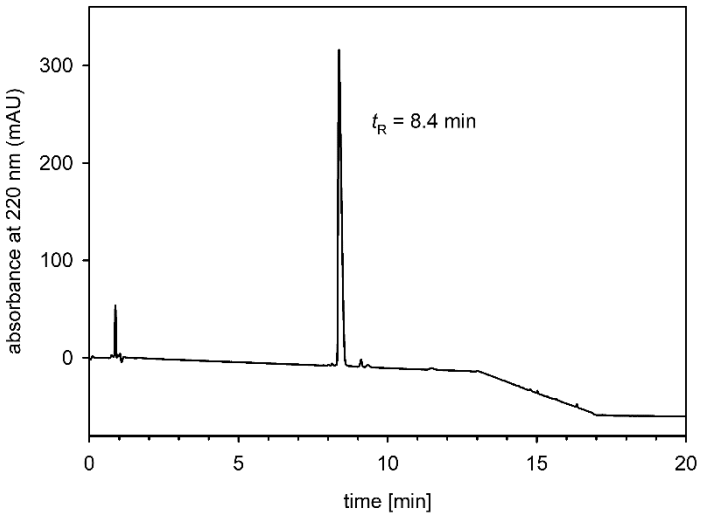

RP-HPLC analysis (purity control) of compound **3.13**

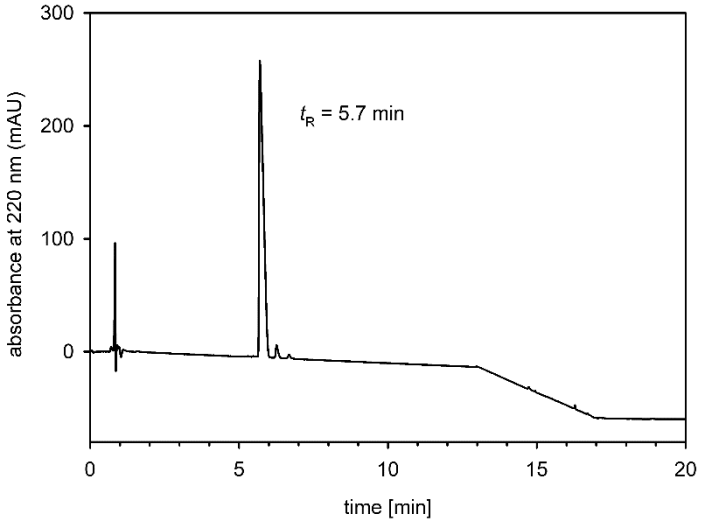

RP-HPLC analysis (purity control) of compound **3.14**

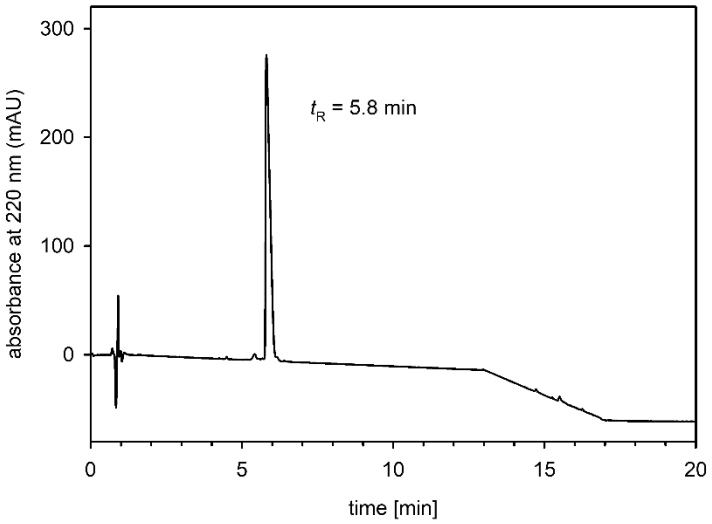

RP-HPLC analysis (purity control) of compound **3.16**

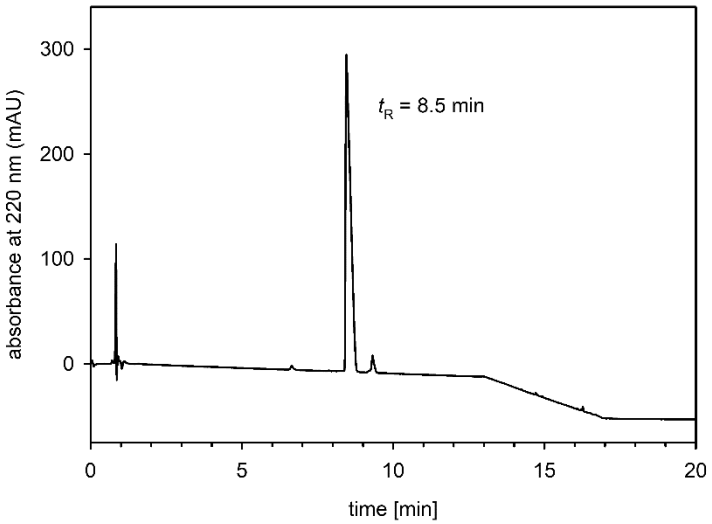

RP-HPLC analysis (purity control) of compound **3.18**

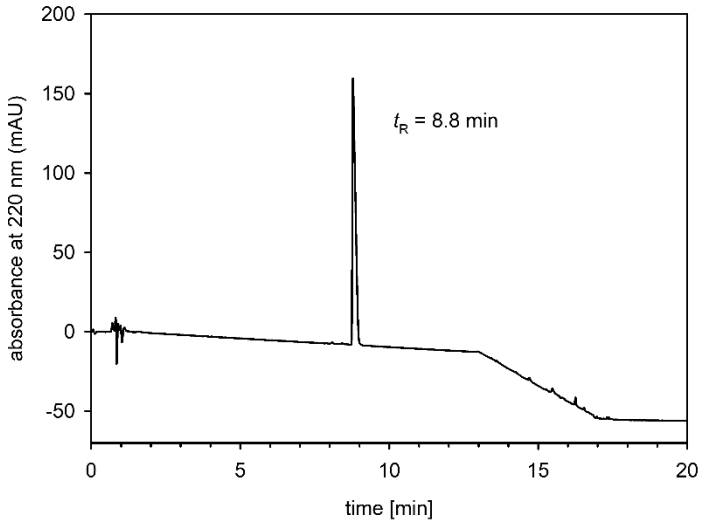

RP-HPLC analysis (purity control) of compound **3.19**

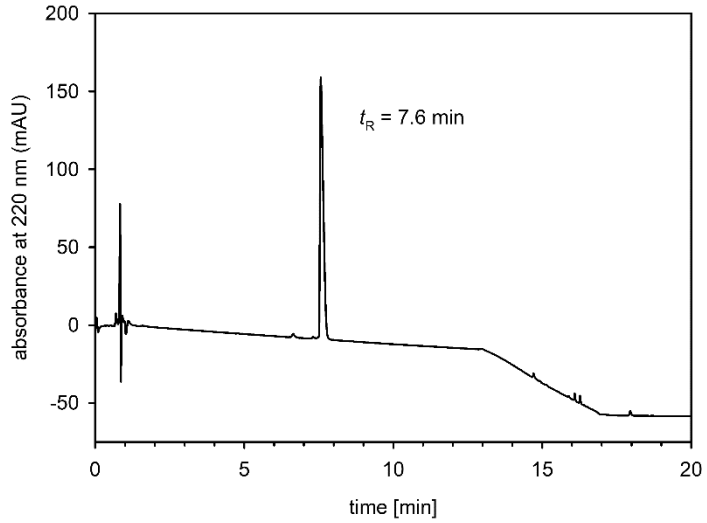

RP-HPLC analysis (purity control) of compound **3.20**

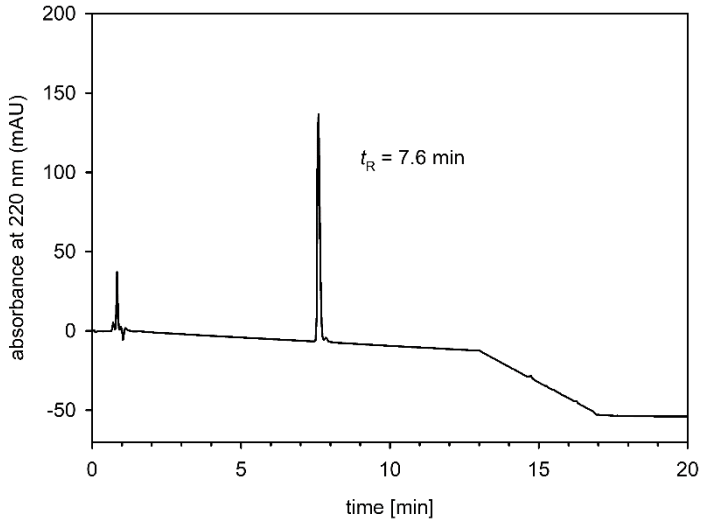

RP-HPLC analysis (purity control) of compound **3.21**

3.7.4 ^{1}H-NMR spectra of compounds 3.07-3.09, 3.11-3.14, 3.16, 3.18, 3.19 and 3.21, and ^{13}C-NMR spectra of compounds 3.07-3.09, 3.14, 3.16 and 3.17

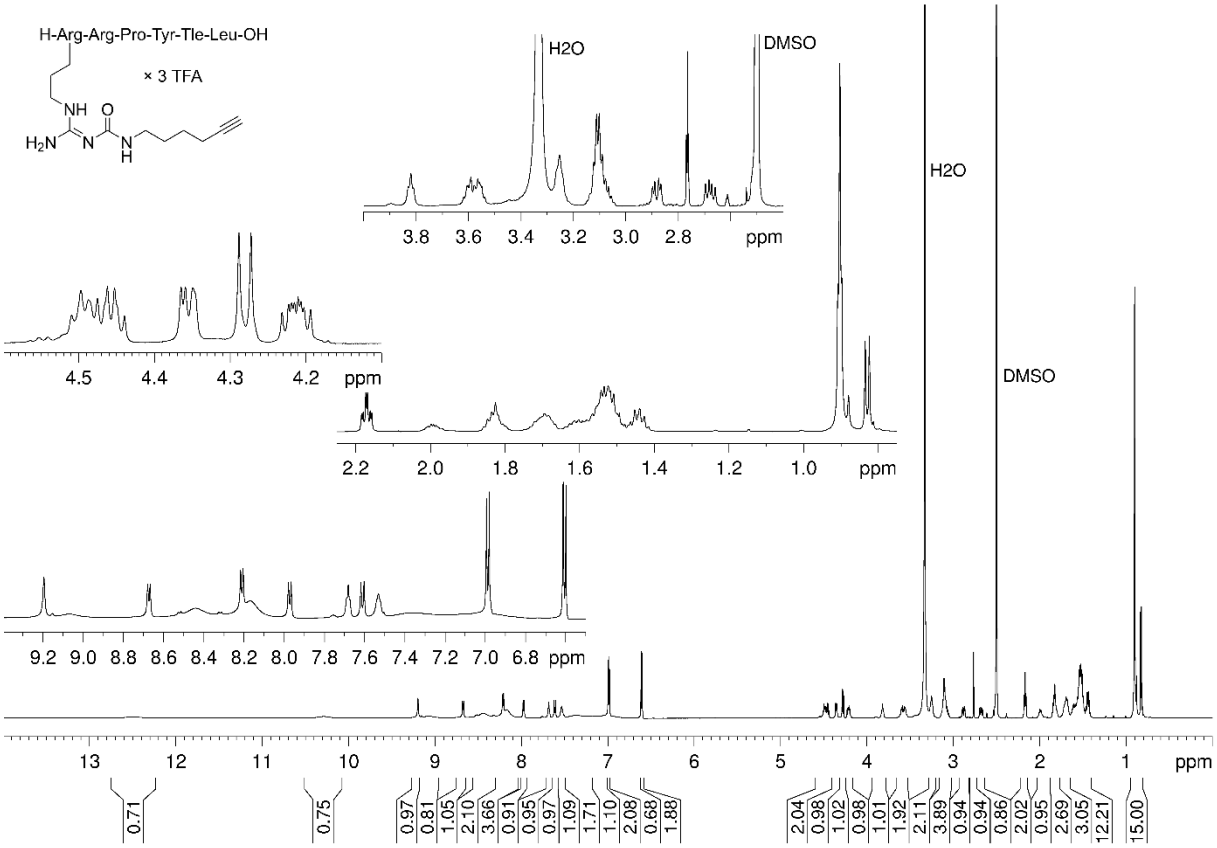

^{1}H-NMR spectrum (600 MHz, DMSO-d_6) of compound **3.07**

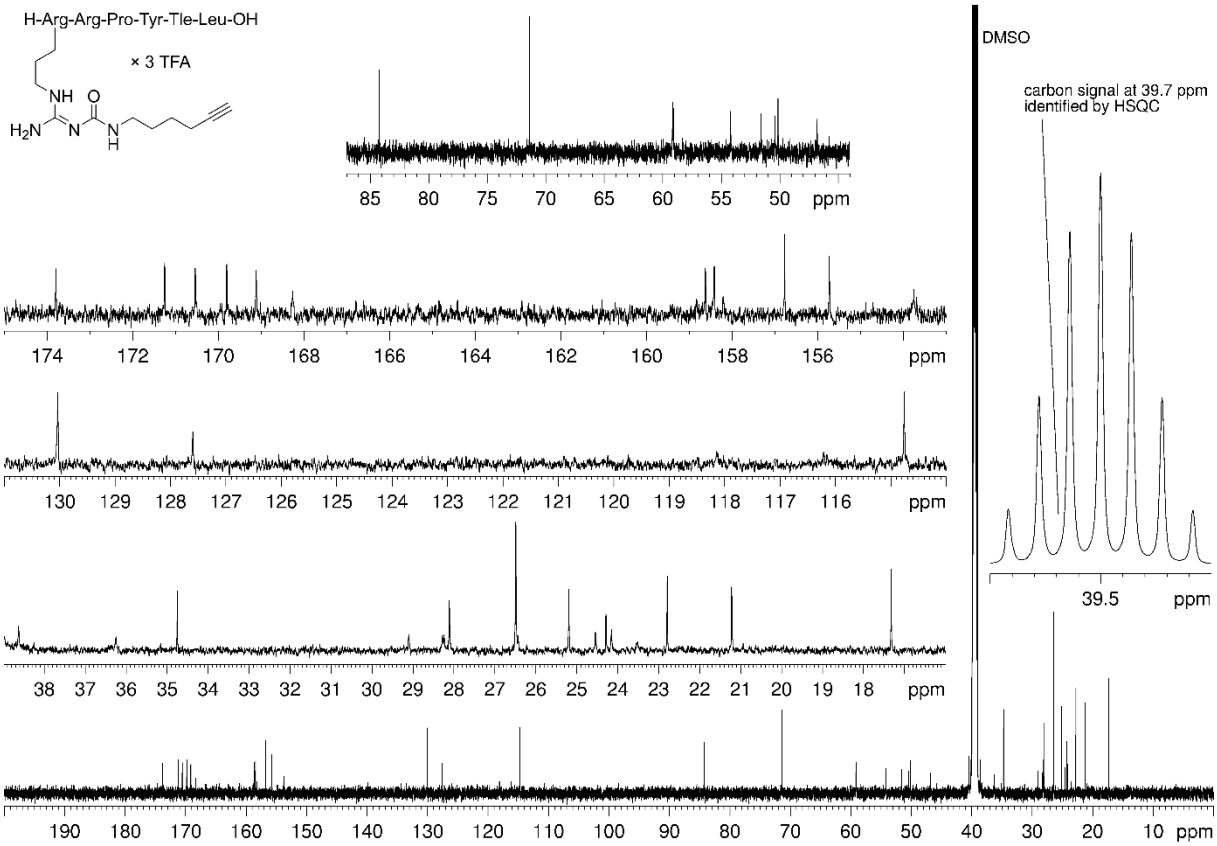

^{13}C-NMR spectrum (150 MHz, DMSO-d_6) of compound **3.07**

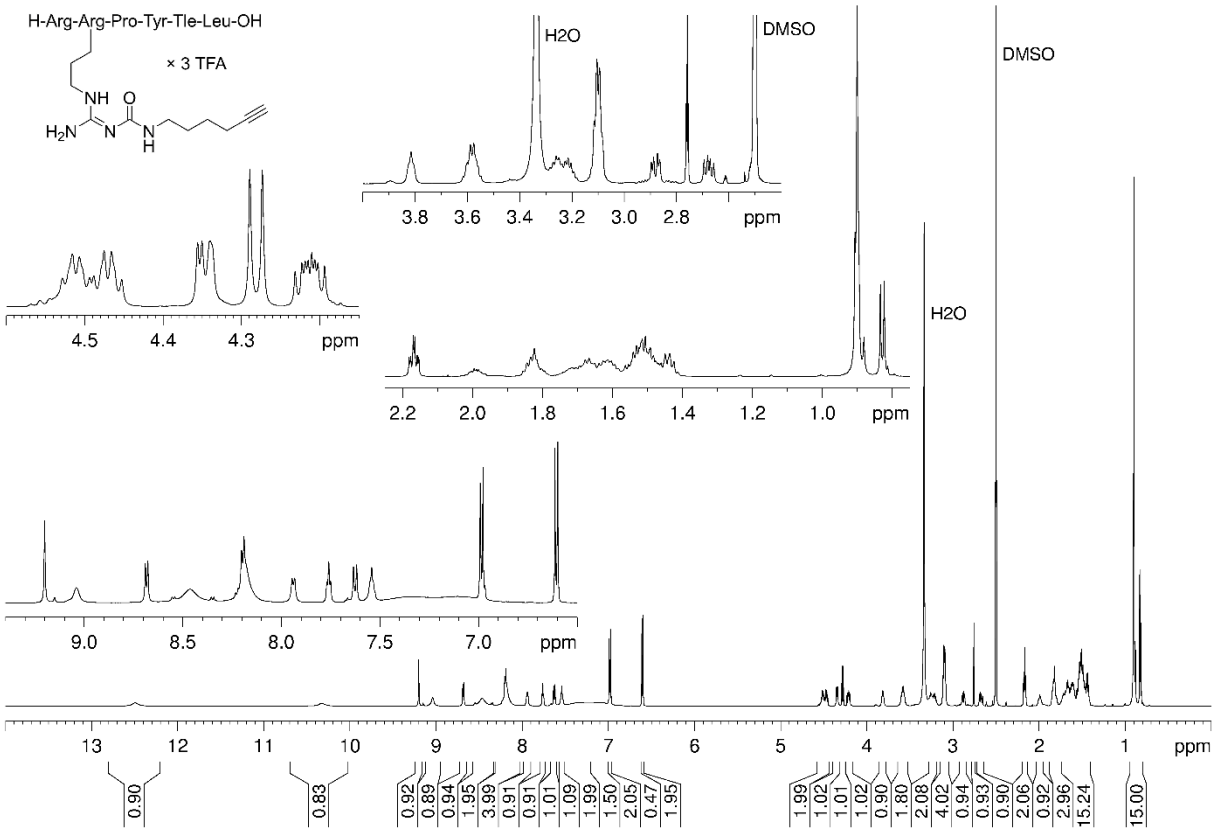

^{1}H-NMR spectrum (600 MHz, DMSO-d_6) of compound **3.08**

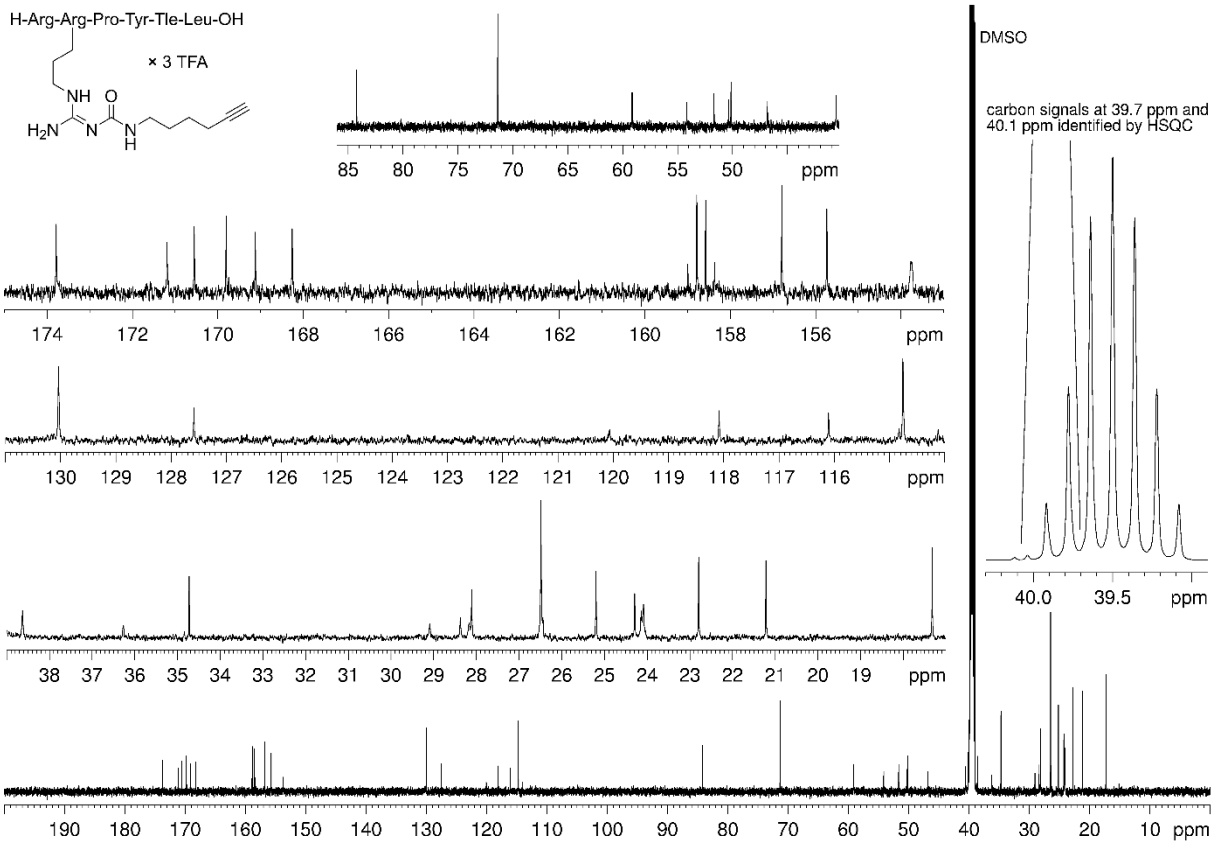

^{13}C-NMR spectrum (150 MHz, DMSO-d_6) of compound **3.08**

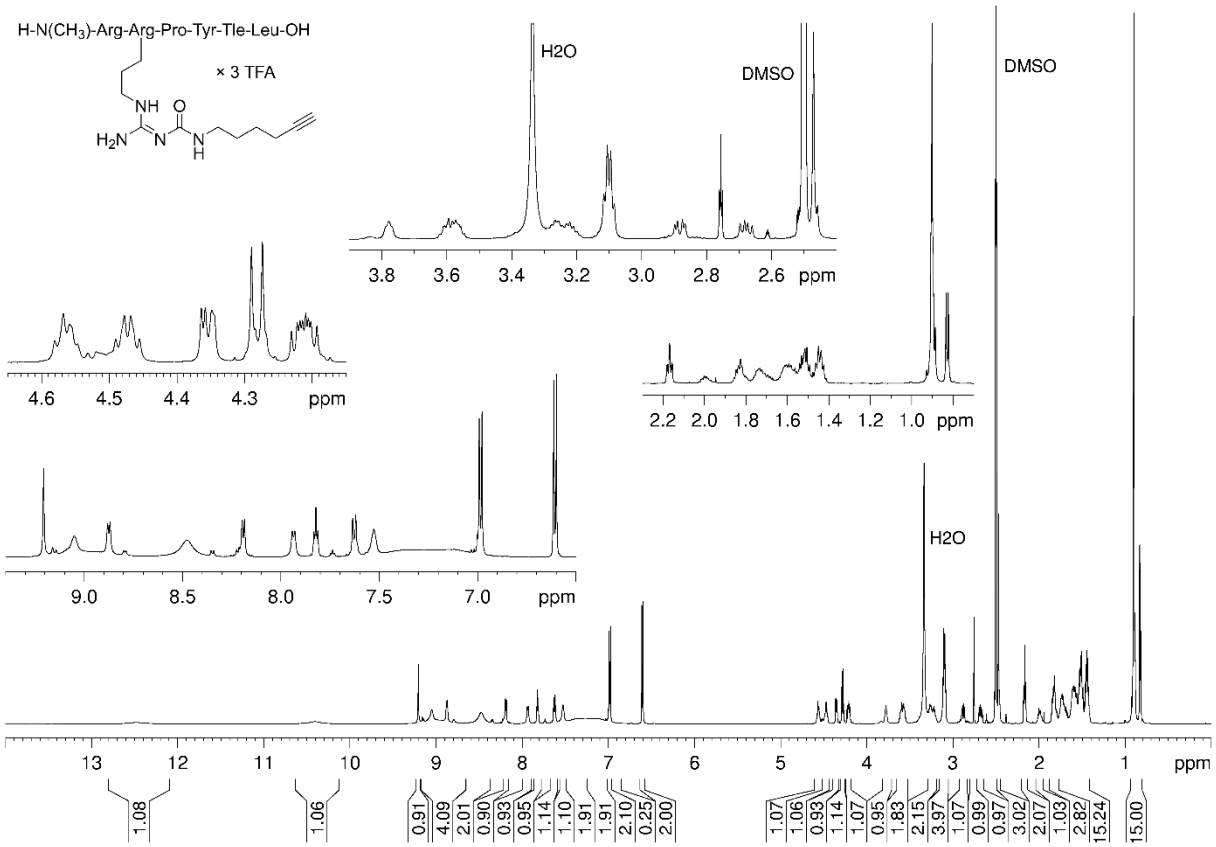

^{1}H-NMR spectrum (600 MHz, DMSO-d_6) of compound **3.09**

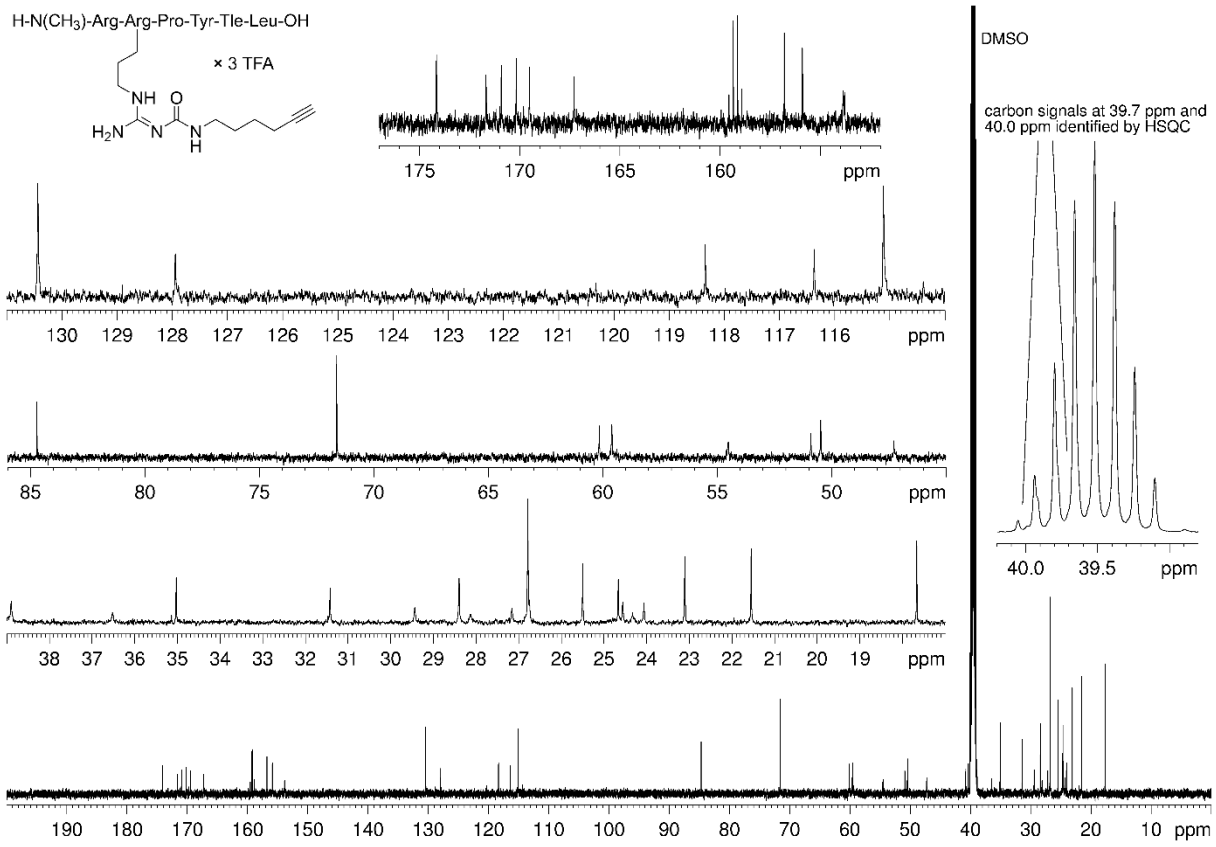

^{13}C-NMR spectrum (150 MHz, DMSO-d_6) of compound **3.09**

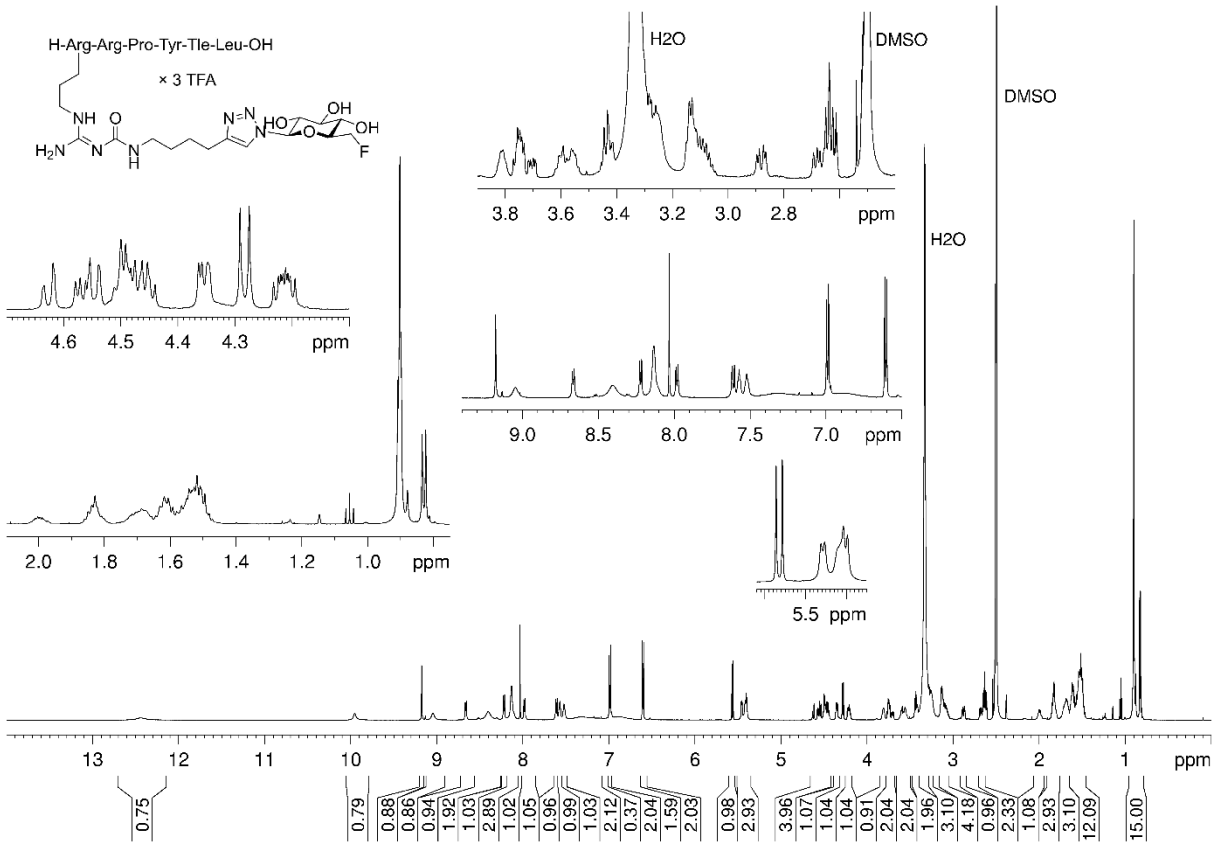

^{1}H-NMR spectrum (600 MHz, DMSO-d_6) of compound **3.11**

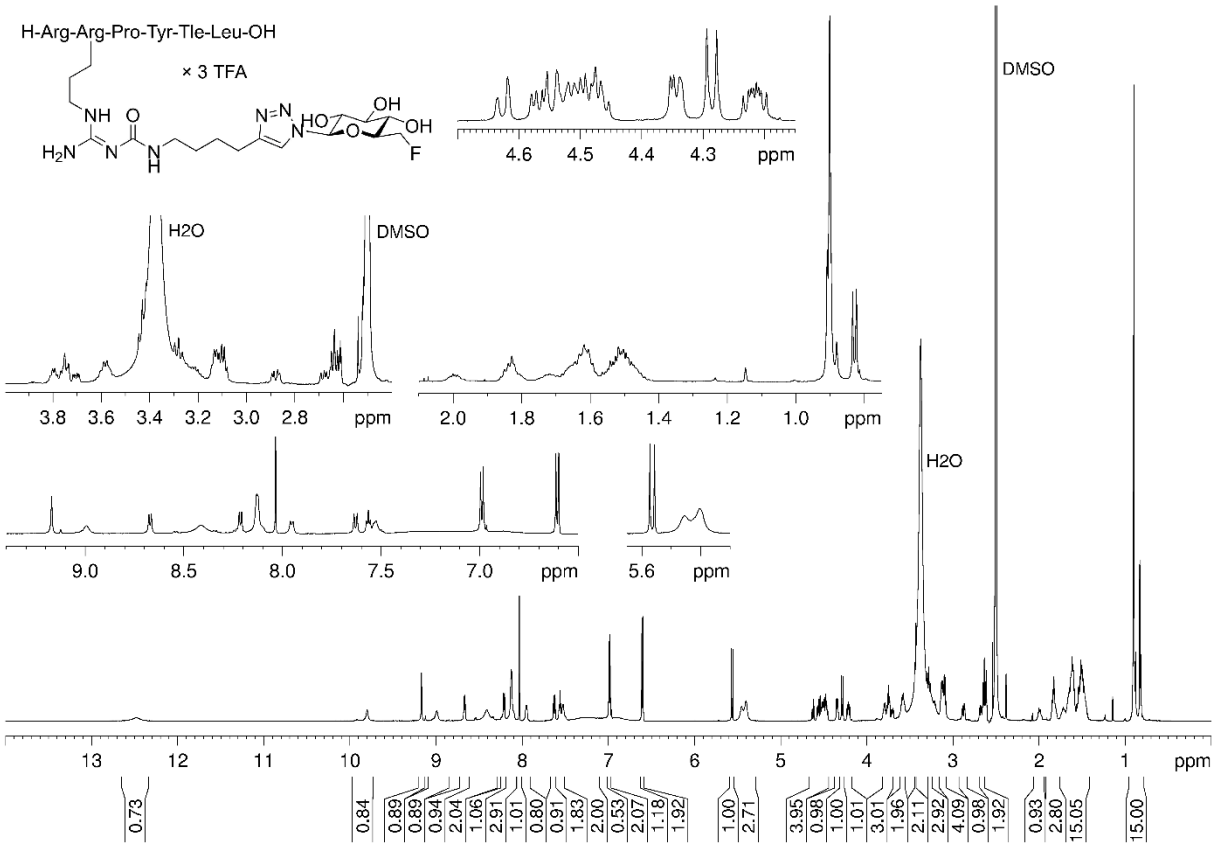

^{1}H-NMR spectrum (600 MHz, DMSO-d_6) of compound **3.12**

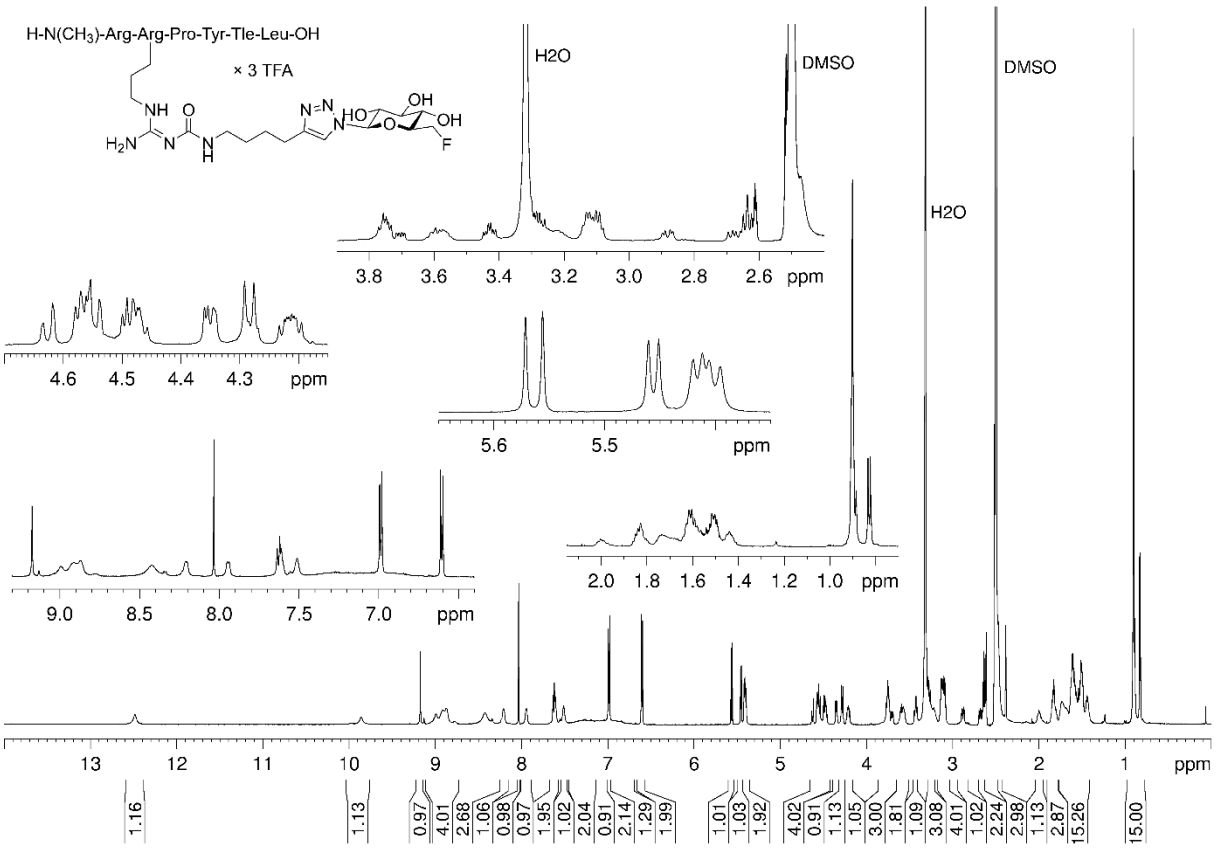

^{1}H-NMR spectrum (600 MHz, DMSO-d_6) of compound **3.13**

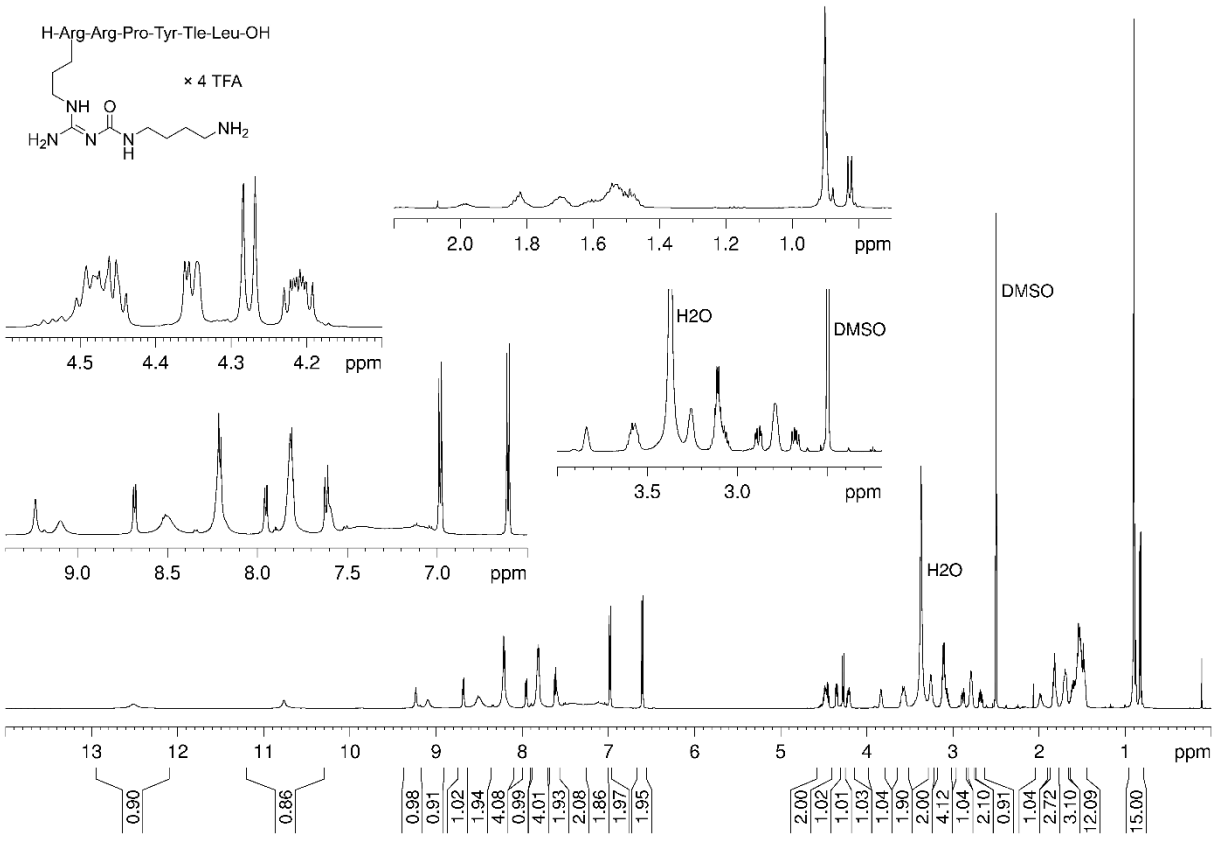

^{1}H-NMR spectrum (600 MHz, DMSO-d_6) of compound **3.14**

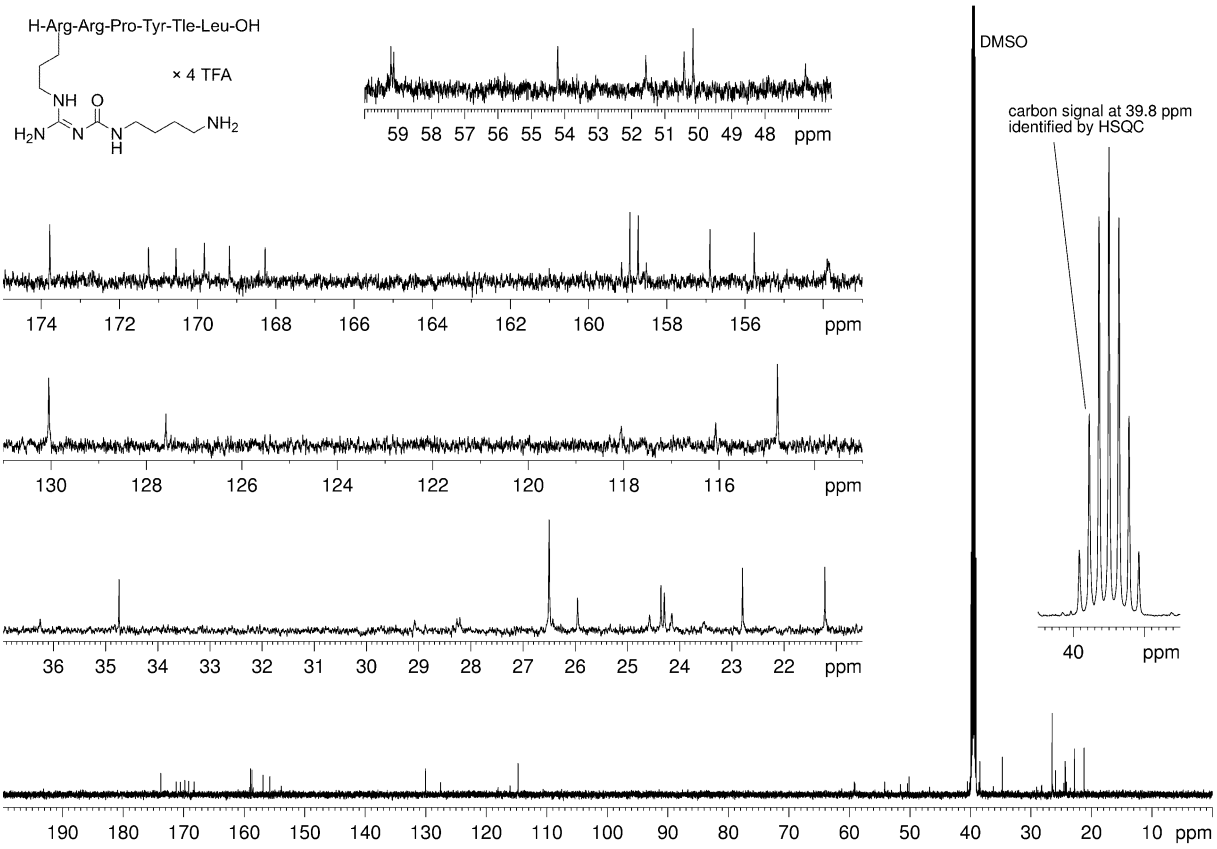

^{13}C-NMR spectrum (150 MHz, DMSO-d_6) of compound **3.14**

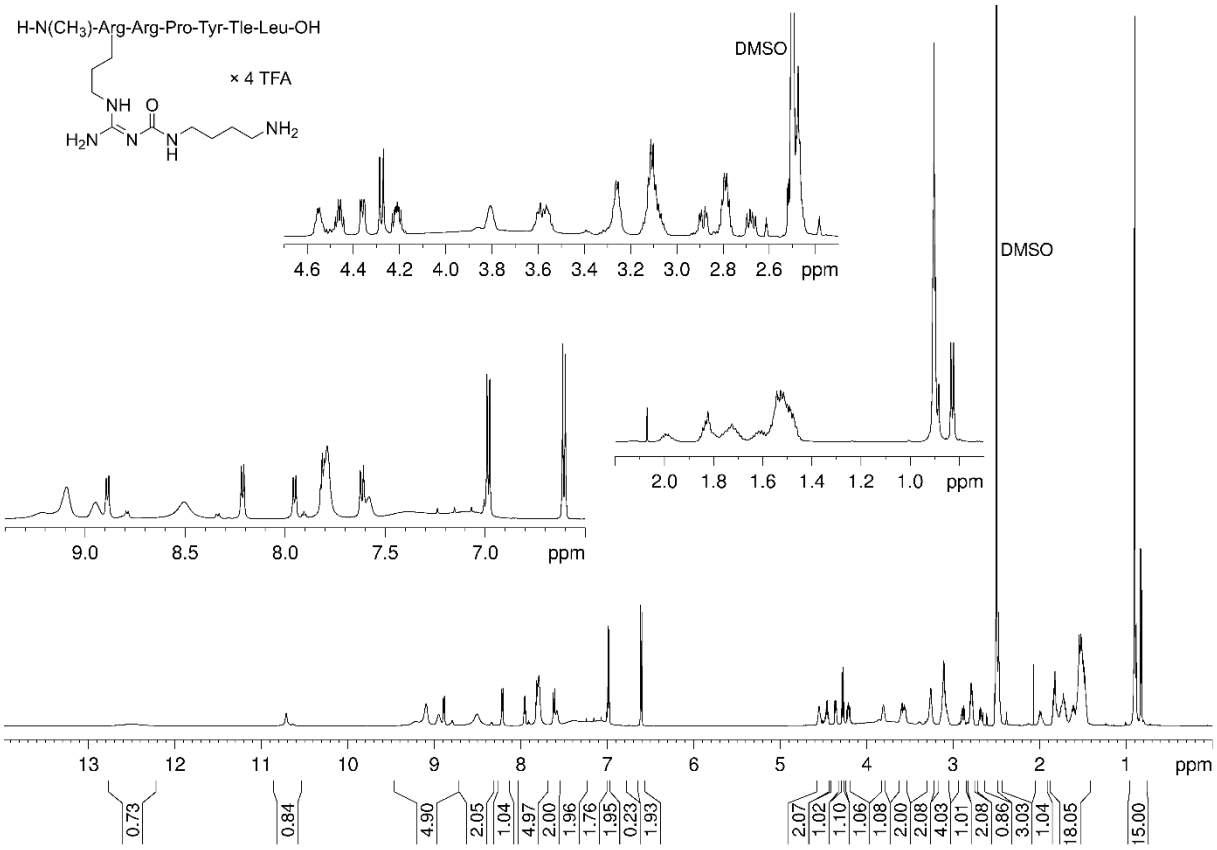

^{1}H-NMR spectrum (600 MHz, DMSO-d_6) of compound **3.16**

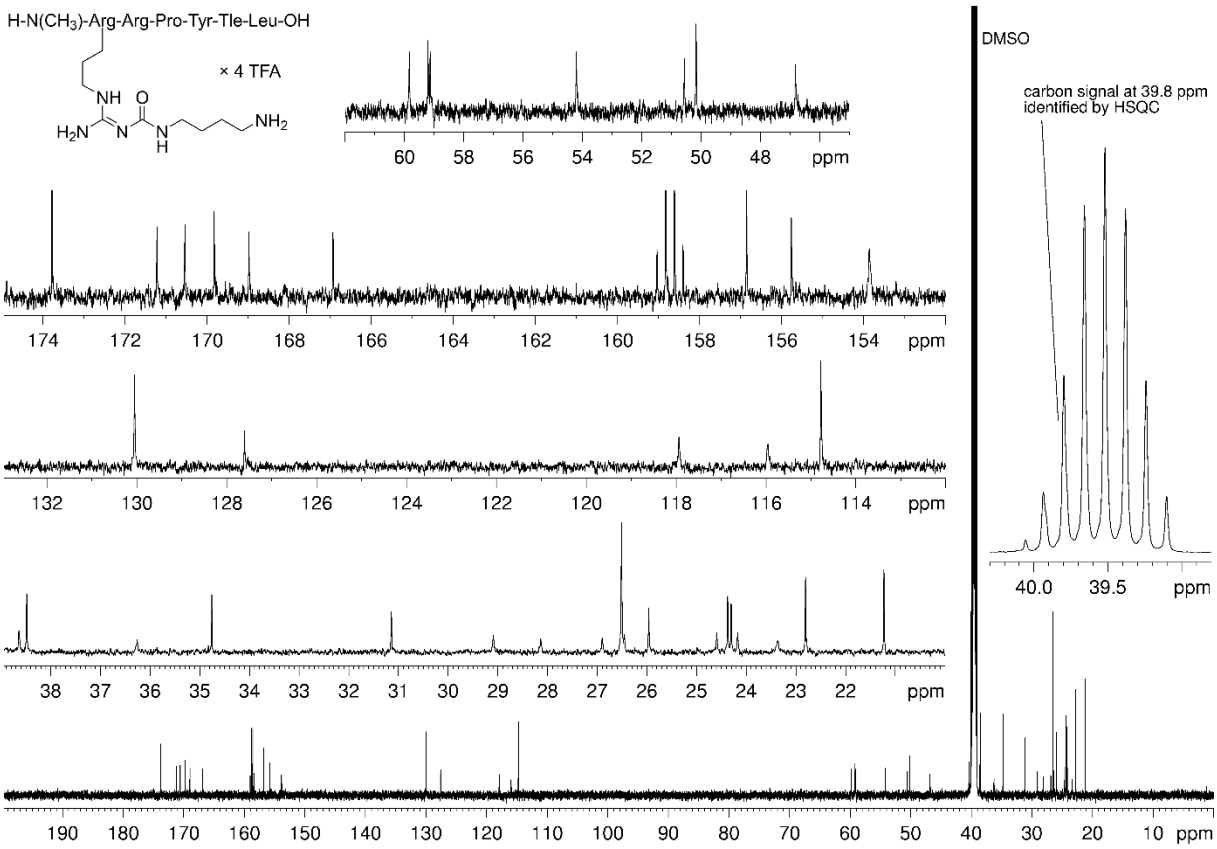

^{13}C-NMR spectrum (150 MHz, DMSO-d_6) of compound **3.16**

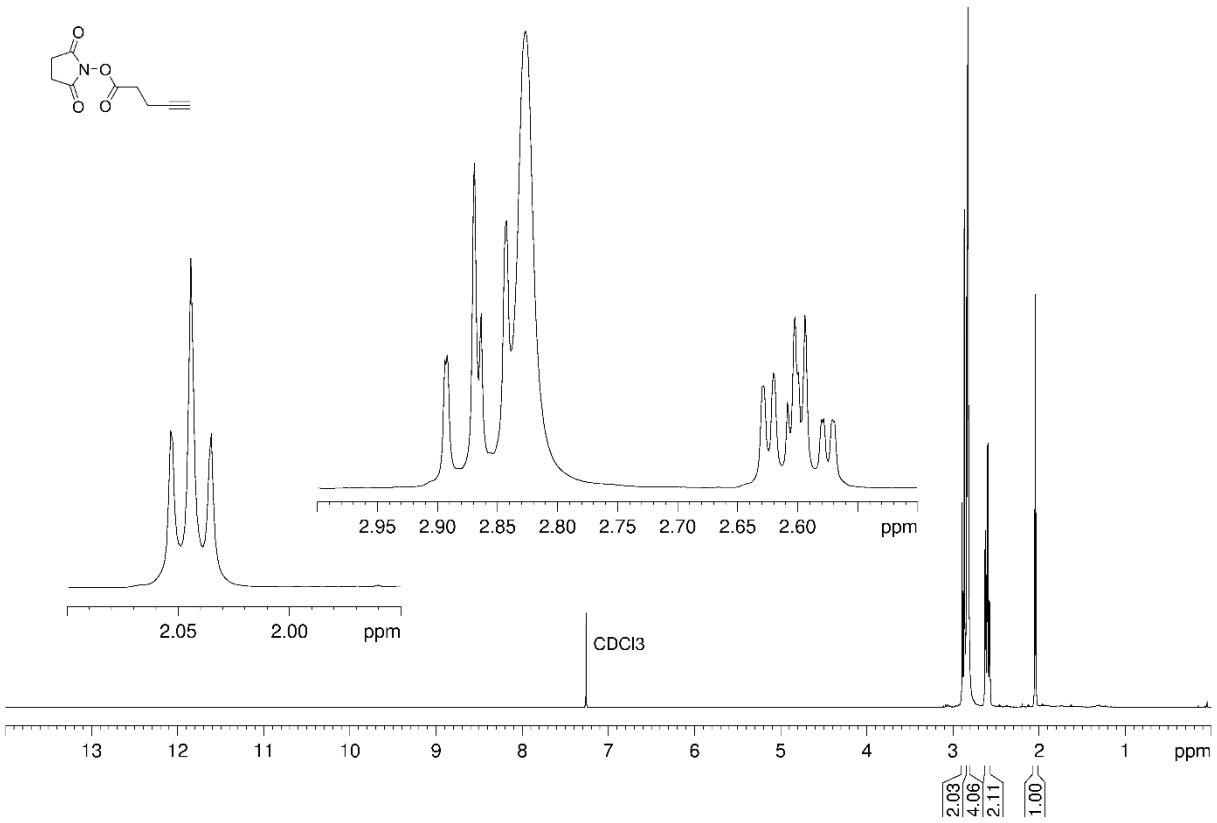

^{1}H-NMR spectrum (300 MHz, $CDCl_3$) of compound **3.17**

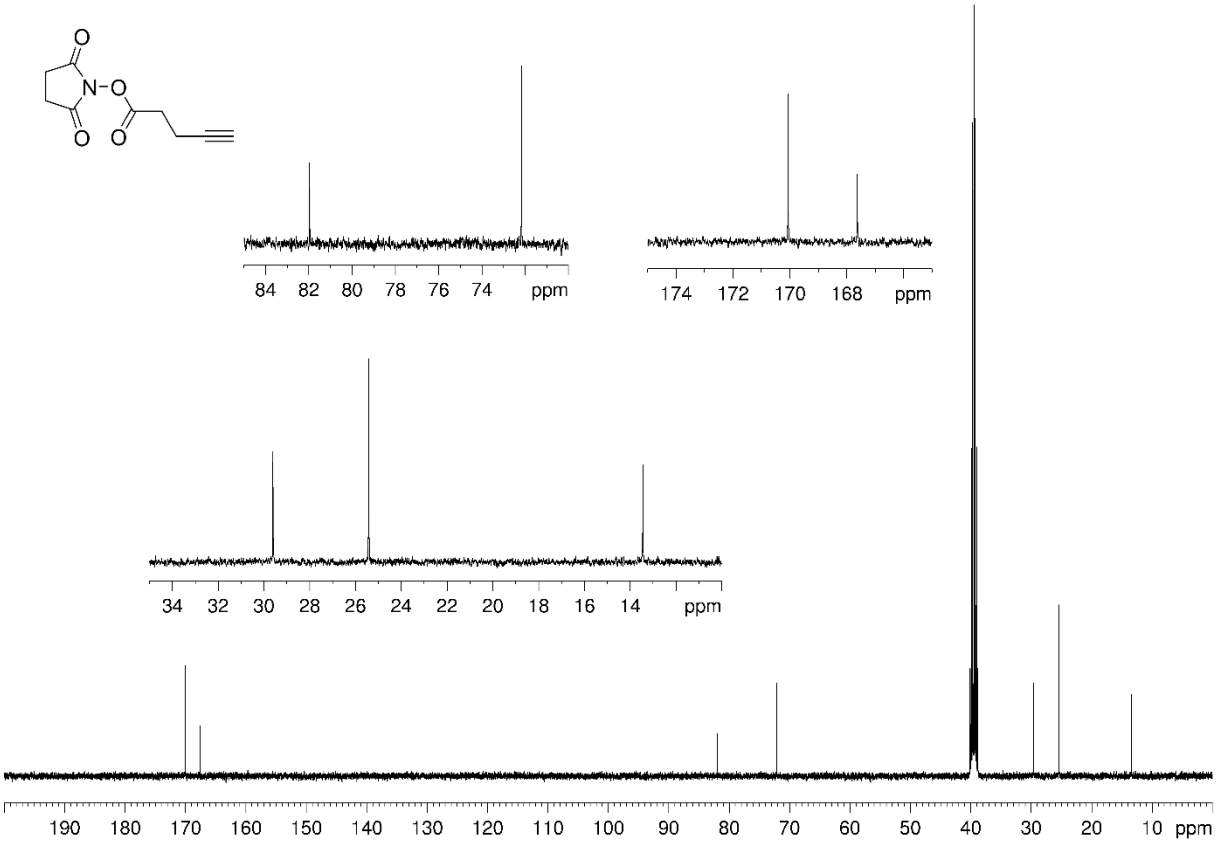

^{13}C-NMR spectrum (100 MHz, DMSO-d_6) of compound **3.17**

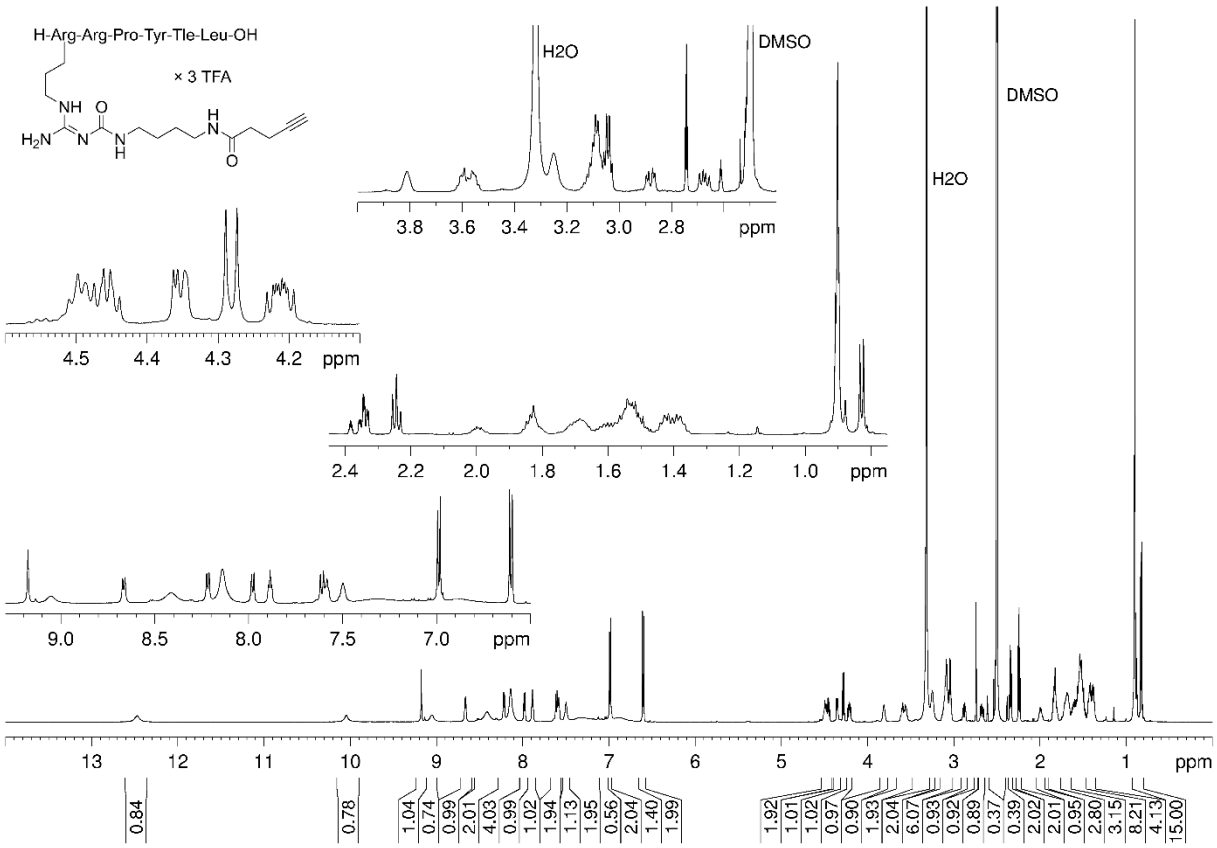

^{1}H-NMR spectrum (600 MHz, DMSO-d_6) of compound **3.18**

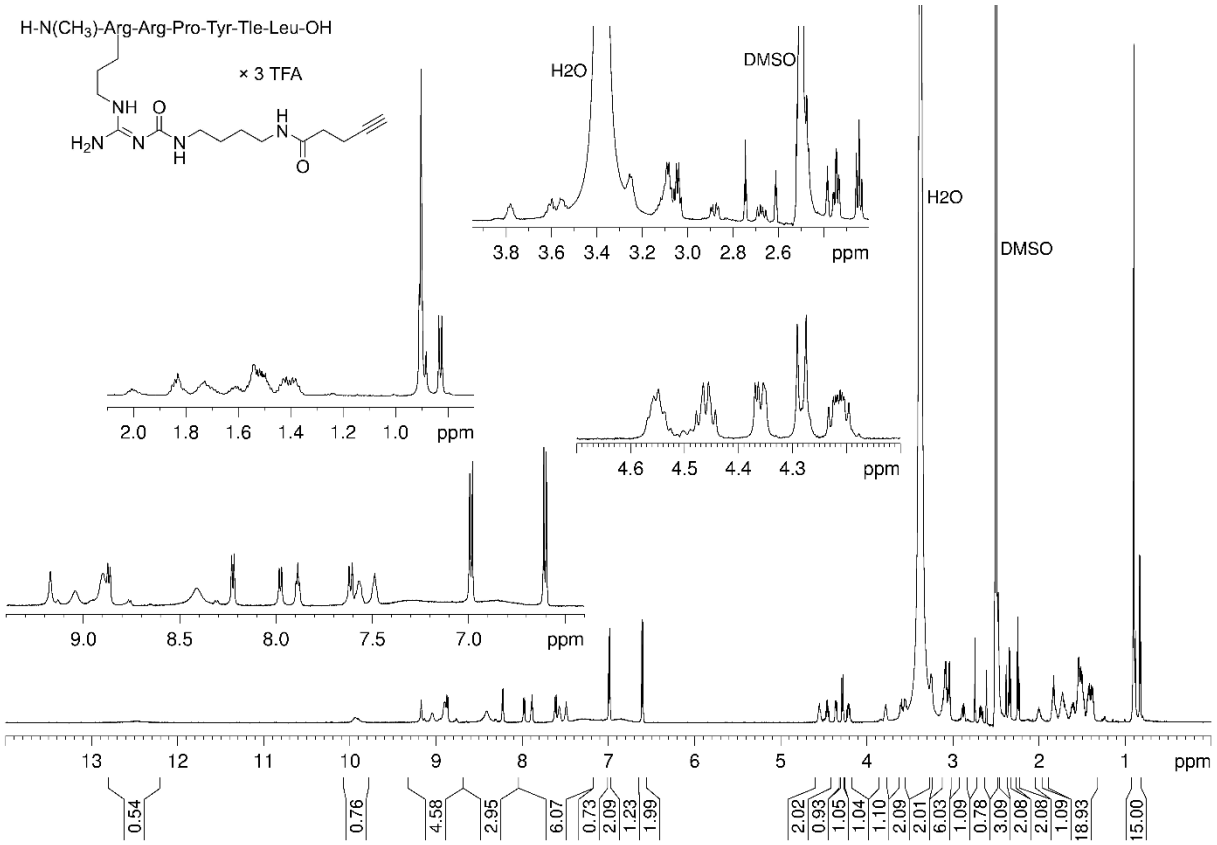

^{1}H-NMR spectrum (600 MHz, DMSO-d_6) of compound **3.19**

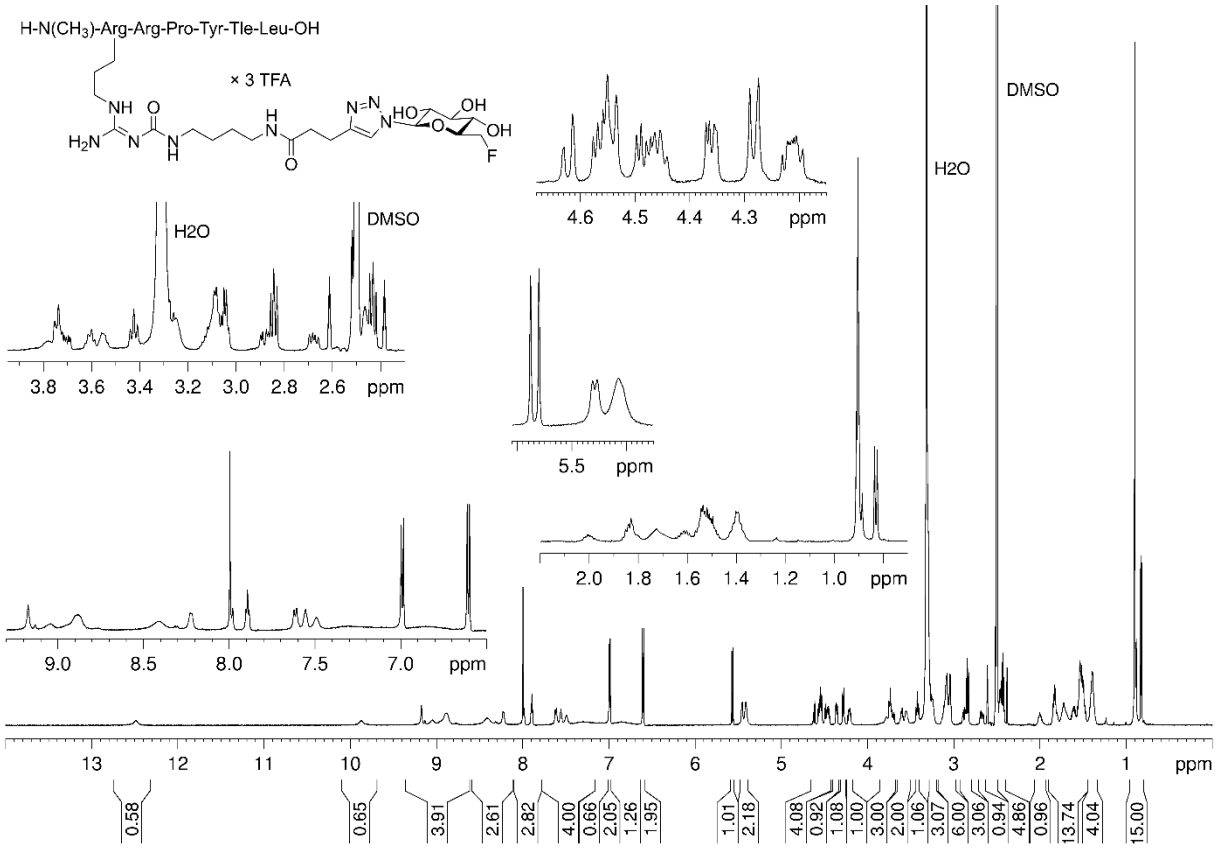

^{1}H-NMR spectrum (600 MHz, DMSO-d_6) of compound **3.21**

3.7.5 References

1. Eaton, B.; Gold, L. Parallel SELEX allowing for asymmetrical reactions in combinatorial chemistry. U.S. Patent, US5858660A, 1999.

2. Maschauer, S.; Haubner, R.; Kuwert, T.; Prante, O. ^{18}F-Glyco-RGD peptides for PET imaging of integrin expression: Efficient radiosynthesis by click chemistry and modulation of biodistribution by glycosylation. *Mol Pharm* **2014**, *11*, 505-515, doi:10.1021/mp4004817.

3. Keller, M.; Kuhn, K.K.; Einsiedel, J.; Hübner, H.; Biselli, S.; Mollereau, C.; Wifling, D.; Svobodová, J.; Bernhardt, G.; Cabrele, C.; et al. Mimicking of arginine by functionalized N^{ω}-carbamoylated arginine as a new broadly applicable approach to labeled bioactive peptides: High affinity angiotensin, neuropeptide Y, neuropeptide FF, and neurotensin receptor ligands as examples. *J Med Chem* **2016**, *59*, 1925-1945, doi:10.1021/acs.jmedchem.5b01495.

4. Maschauer, S.; Einsiedel, J.; Hübner, H.; Gmeiner, P.; Prante, O. ^{18}F- and ^{68}Ga-labeled neurotensin peptides for PET imaging of neurotensin receptor 1. *J Med Chem* **2016**, *59*, 6480-6492, doi:10.1021/acs.jmedchem.6b00675.

5. Wang, M.; Zhang, H.; Wang, H.; Feng, H.; Deng, H.; Wu, Z.; Lu, H.; Li, Z. Development of [^{18}F]AlF-NOTA-NT as PET agents of neurotensin receptor-1 positive pancreatic cancer. *Mol Pharm* **2018**, *15*, 3093-3100, doi:10.1021/acs.molpharmaceut.8b00192.

Chapter 4

Development of a neurotensin-derived ^{68}Ga-labeled PET ligand with high in vivo stability for imaging of NTS_1R-expressing tumors

Prior to the submission of this thesis, the content of this chapter was published in collaboration with partners:

Schindler, L.; Moosbauer, J.; Schmidt, D.; Spruss, T.; Grätz, L.; Lüdeke, S.; Hofheinz, F.; Meister, S.; Echtenacher, B.; Bernhardt, G.; Pietzsch, J.; Hellwig, D.; Keller, M. Development of a neurotensin-derived ^{68}Ga-labeled PET ligand with high in vivo stability for imaging of NTS_1 receptor-expressing tumors. *Cancers (Basel)* **2022**, *14*, 4922, doi:10.3390/cancers14194922.

The following experimental work and data processing was performed by co-authors:

Moosbauer, J.:	Syntheses of ^{68}Ga-labeled compounds
Schmidt, D.:	Establishment of PET scan protocols; performance of PET scans
Spruss, D.:	Animal anesthetization and removal of organs for biodistribution experiments
Grätz, L.:	Preparation of HEK293T-hNTS_2R cells
Lüdeke, S.:	Determination of the absolute configuration of diMe-Tyr in compounds **4.48** and **4.49** by CD spectroscopy
Keller, M.:	Performance of the internalization assay
Schmidt, D.; Hofheinz, F.; Meister, S.; Hellwig, D.:	Data analysis of the PET scans

Note: The compounds assigned with **2.01**, **2.02** and **2.07** in Chapter 2, as well as the compounds assigned with **3.06a** and **3.16** in Chapter 3 are also part of Chapter 4. To avoid an assignment of several numbers to the same compound, the numbers **2.01**, **2.02**, **2.07**, **3.06a** and **3.16** are also used in this chapter, which had been, as mentioned before, published as a scientific article prior to submission of this thesis. Instead of reorganizing the compound numbers, the numbers designating the same compounds as **2.01**, **2.02**, **2.07**, **3.06a** and **3.16** in the published article, were omitted in Chapter 4 resulting in gaps in compound numbering, i.e., **4.01**, **4.02**, **4.03**, **4.06** and **4.10** are missing.

4.1 Introduction

Neurotensin (NT), a linear 13 amino acid peptide, acts as a hormone in the gastrointestinal tract, regulating, inter alia, motility and mucosal regeneration[1], and as a neurotransmitter and neuromodulator in the central nervous system, where it is involved, inter alia, in the regulation of body temperature, food intake, blood pressure, nociception, memory, and hormone secretion[2-7]. The effects of neurotensin are mainly mediated by the neurotensin receptors 1 and 2 (NTS_1R, NTS_2R), members of the family of G-protein coupled receptors. The NTS_1R has emerged as an interesting target for tumor visualization and therapy due to its overexpression in a variety of tumors such as breast cancer, colorectal carcinoma, and (the prognostically poor) pancreatic adenocarcinoma[8-10]. The carboxyterminal hexapeptide of NT (NT(8-13), **2.01**, Figure 4.1A) was identified as the biologically active fragment, exhibiting the potency of full-length NT[11-13]. Therefore, peptide **2.01** has previously served as a lead structure for the development of imaging agents addressing the NTS_1R[14-20].

^{68}Ga- and ^{18}F-labeled ligands of cell-surface receptors that are (over-)expressed in malignant tumors are considered useful tools for in vivo cancer imaging by positron emission tomography (PET)[21-28]. ^{18}F-labeled PET tracers are advantageous with respect to half-life (about 110 min) and achievable resolution, but require a cyclotron for radionuclide synthesis and usually two or more radiosynthetic reaction steps[29,30]. In contrast, the advantage of ^{68}Ga-labeled PET tracers lies in their fast one-step radiosynthesis (incorporation of ^{68}Ga in a chelator moiety) and convenient radionuclide accessibility (^{68}Ge/^{68}Ga-generator); however, these tracers result in lower resolution images and the short half-life (68 min) does not allow a transfer between clinics. The development of PET ligands with favorable properties (e.g., high receptor affinity, high in vivo stability and appropriate pharmacokinetics) is challenging. The development of peptidic PET tracers, often acting as receptor agonists, can be convenient with respect to high target affinity and attachment of the label[31-33], but high proteolytic stability in vivo might not be easily achieved[33,34]. With respect to NTS_1R PET ligands, two main strategies have been pursued[26], i.e., investigations of peptidic agonists and of non-peptidic antagonists[35-37]. To date, reported ^{18}F- and ^{68}Ga-labeled NTS_1R antagonists exhibit higher receptor affinities and higher in vivo stabilities compared to peptidic NTS_1R PET ligands explored with regard to in vivo tumor imaging. However, the pharmacokinetic profile of the antagonists is not well-suited for PET imaging based on short-lived radionuclides[38]. Unlike antagonists, agonist binding induces receptor internalization; thus, peptidic PET ligands potentially allow for a higher tracer uptake in the tumor.

A

cpd.	sequence	K_i or IC_{50} (NTS_1R)
2.01	Arg-Arg-Pro-Tyr-Ile-Leu	0.33 nM[a]
2.02	Arg-Arg-Pro-Tyr-Tle-Leu	1.17 nM[a]
2.07	Me-Arg-Arg-Pro-Tyr-Tle-Leu	0.88 nM[a]
4.04	Ac-Lys(DOTA/Ga^{3+})-Pro-Me-Arg-Arg-Pro-Tyr-Tle-Leu	14 nM[b]
4.05	Lys(DOTA/Ga^{3+})-NLys-Lys-Pro-Tyr-Tle-Leu	19 nM[c]

Tle = *tert*-butylglycine = *tert*leucine

B

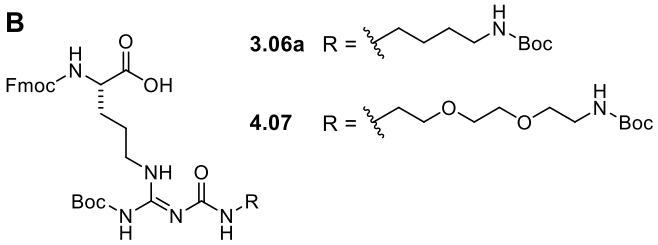

Figure 4.1. (A) Amino acid sequences and NTS_1R affinities of NT(8-13) (**2.01**), NT(8-13) derivatives **2.02** and **2.07**, and NT(8-13)-derived potential PET ligands **4.04** and **4.05**. (B) Structures of the reported arginine building blocks **3.06a** and **4.07** (Keller et al.[39]) which were applied in SPPS for the preparation of amino-functionalized precursor peptides. [a]K_i value, Schindler et al.[40] [b]IC_{50} value, Alshoukr et al.[41] [c]K_i value, Maschauer et al.[42]

Peptide **2.01** exhibits a plasma half-life of only a few minutes[40,43]; thus, NT(8-13) analogs require stabilizing structural modifications when intended to be used as tracers for NTS_1R-targeted tumor imaging. A previously reported approach based on the replacement of amide bonds in the core structure of **2.01** by triazoles revealed that high affinity of the respective ^{177}Lu-labeled analogs could not be combined with high in vitro serum stability[44]. The recent exploration of the introduction of trimethylsilylalanine instead of Ile^{12} or Leu^{13} for the preparation of ^{68}Ga-labeled derivatives of **2.01** resulted in only moderate in vitro plasma stabilities as well[38]. The replacement of Ile^{12} in analogs derived from **2.01** by Tle^{12} (α-*tert*-butyl-Gly) represents one of the most frequently applied modifications to prevent C-terminal degradation[14-19,41,42,45-54], but is insufficient to prevent proteolytic degradation when applied, e.g., to **2.01** as the only structural alteration (**2.02**, Figure 4.1A) due to persisting N-terminal degradation[40]. However, additional N-methylation of either Arg^8 or Arg^9 in **2.01** resulted in excellent in vitro plasma stabilities (e.g., compound **2.07**, Figure 4.1A)[40].

Among reported ^{68}Ga-labeled neurotensin-derived NTS_1R PET ligands, peptides [^{68}Ga]**4.04** and [^{68}Ga]**4.05** (Figure 4.1A), and the 1,4,7-triazacyclononane-1,4,7-triacetic acid (NOTA)-conjugated analog of **4.05** represent the most promising candidates in terms of NTS_1R affinity and achieved tumor-to-muscle activity ratios. Both peptides contain Tle in position 12, but differ with respect to the modification of the N-terminal segment. Whereas **4.04** is N^{α}-methylated at Arg^8 and represents an octapeptide, the hexapeptide **4.05** harbors a peptoid-like moiety at the N-terminus ($NLys^8$). For both peptides in vivo stability data were not reported. However, for the ^{111}In-labeled analog of **4.04**, 22% remaining intact tracer in blood plasma 15 min p.i. in mice has been reported[41], and for [^{68}Ga]**4.05** a high in vitro stability in human serum (93% remaining intact tracer after 1 h) has been described[42]. Notably, in **4.04** and **4.05**, the 1,4,7,10-tetraazacyclododecane-1,4,7,10-tetraacetic acid (DOTA) chelator is attached to the α- or ε-amino group of Lys,

which represents a common strategy for the conjugation of NT(8-13) analogs with chelating agents[16,19,52,54-57]. A recently introduced alternative strategy is the labeling of peptides via the side chain of Arg, based on amino-functionalized N^{ω}-carbamoylated arginines derived from building blocks **3.06a** and **4.07** (Figure 4.1B)[39,58,59]. Lately, the incorporation of **3.06a** in the stabilized NT(8-13) core structure (**2.07**) and the subsequent attachment of a fluoroglycosyl moiety to the carbamoylated arginine side chain afforded an ^{18}F-labeled NTS_1R PET ligand showing high receptor affinity (K_i of the "cold" ligand = 4.3 nM) and high tumor uptake in vivo[60].

In the present study, we aimed at the development of a peptidic NTS_1R PET ligand matching up with reported receptor antagonists in terms of NTS_1R affinity and in vivo stability. For this purpose, N^{ω}-carbamoylated arginines derived from **3.06a** or **4.07** were incorporated into **2.07** or slightly modified analogs of **2.07**, optimized with respect to plasma stability, followed by the attachment of a DOTA chelator to the modified arginine side chain and insertion of stable ("cold") Ga^{3+} or radioactive $^{68}Ga^{3+}$. The potential NTS_1R PET ligands ("cold" compounds) were characterized with respect to NTS_1R and NTS_2R affinity and plasma stability. For selected peptides, the ^{68}Ga-labeled analogs were prepared and studied in vivo in tumor-bearing mice.

4.2 Results and discussion

4.2.1 Chemistry

Standard Fmoc strategy solid-phase peptide synthesis (SPPS) was used for the preparation of the NT(8-13)-derived peptides **3.16**[60], **4.08**, **4.09**, **4.11** and **4.12**, containing an amino-functionalized arginine (position 8 or 9) derived from the reported Fmoc- and Boc-protected N^{ω}-carbamoylated arginine building blocks **3.06a**[39] or **4.07**[39] (structures shown in Figure 4.1B) (Scheme 4.1). Peptides **3.16**, **4.08**, **4.09**, **4.11** and **4.12** were N^{α}-methylated in position 8 (**3.16**, **4.08**, **4.09** and **4.12**) or 9 (**4.11**), and α-*tert*-butyl-Gly (Tle) was incorporated in position 12 in peptides **3.16**, **4.08**, **4.11** and **4.12** instead of Ile^{12}. Details on the coupling conditions are provided in Table A4.1 (Appendix).

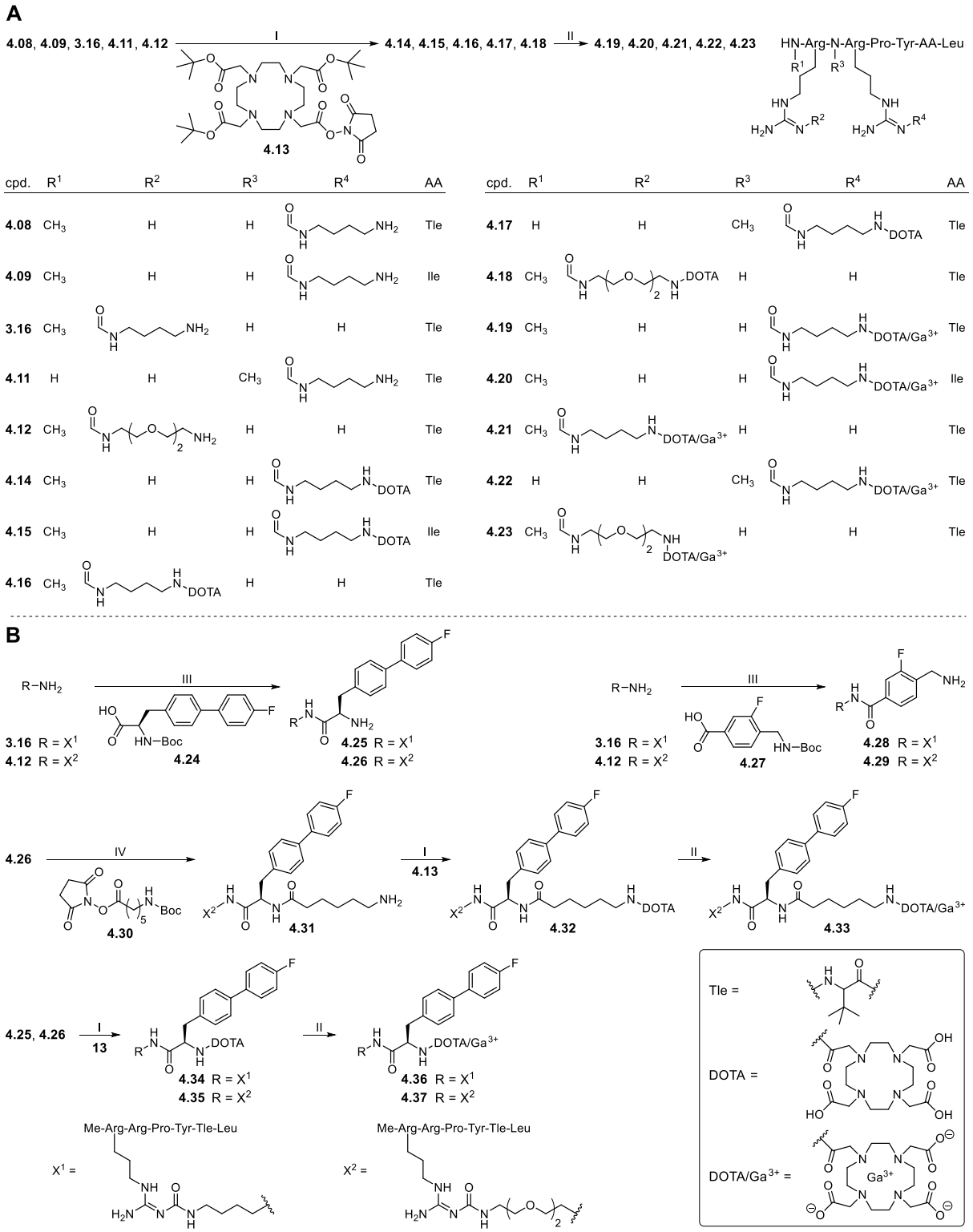

Scheme 4.1. (A) Synthesis of the potential NTS$_1$R PET ligands **4.19**-**4.23** from the amino-functionalized precursor peptides **3.16**, **4.08**, **4.09**, **4.11** and **4.12**. (B) Synthesis of amino-functionalized NT(8-13) derivatives containing a fluorinated biphenyl or benzoyl moiety (**4.25**, **4.26**, **4.28**, **4.29** and **4.31**) and preparation of the potential NTS$_1$R PET ligands **4.33**, **4.36** and **4.37**. Reagents and conditions: (I) (1) DIPEA, DMF/NMP 75:25 or 80:20 v/v, rt, 30 min, (2) TFA/H_2O 80:20 v/v, 50 °C, overnight, 72% (**4.14**), 62% (**4.15**), 75% (**4.16**), 28% (**4.17**), 93% (**4.18**), 69% (**4.32**), 78% (**4.34**), 81% (**4.35**); (II) preheating of a solution of the peptide (4 mM) in HEPES buffer (0.2 M, pH 4.2) to 60 °C, 5 min, addition of $Ga(NO_3)_3 \times H_2O$ in 10 mM HCl, 100 °C, 10-30 min, 95% (**4.19**), > 99% (**4.20**), 92% (**4.21**), 99% (**4.22**), 92% (**4.23**), 99% (**4.33**), 96% (**4.36**), 95% (**4.37**); (III) (1) DIPEA,

HOBt, HBTU, DMF/NMP 80:20 v/v, rt, 60-75 min, (2) TFA/H_2O 95:5 v/v, rt, 3.5 h, 46% (**4.25**), 47% (**4.26**), 24% (**4.28**), 32% (**4.29**); (IV) (1) DIPEA, DMF/NMP 75:25 v/v, rt, 45 min, (2) TFA/H_2O 95:5 v/v, rt, 3.5 h, 66% (**4.31**).

A reported procedure for the on-resin N^{α}-methylation of peptides[61], which was recently used for N^{α}-methylation of the carbamoylated arginine in **3.16**[60], was also successfully applied for N^{α}-methylation of the carbamoylated arginines in **4.11** and **4.12**. Coupling of Fmoc amino acids to an N^{α}-methylated N-terminal amino acid using the standard coupling reagents HOBt, HBTU and DIPEA proved to be unfeasible; therefore, **4.11** was prepared by applying a combination of oxyma and DIC as activation reagents. Detailed information on the synthesis procedures and the applied coupling conditions are given in the Appendix.

Compounds **3.16**, **4.08**, **4.09**, **4.11** and **4.12** served as starting materials for the syntheses of the chelator-conjugated peptides **4.14**-**4.18** using the tris-*t*Bu-protected DOTA reagent **4.13** for coupling to the amino-functionality of the N^{ω}-carbamoylated arginine in **3.16**, **4.08**, **4.09**, **4.11** and **4.12**. Attempts to introduce the DOTA moiety using a non-protected DOTA succinimidyl ester caused severe separation problems due to nearly identical HPLC retention times of precursor peptide and product. However, the *t*Bu-protected intermediates could easily be separated from the remaining starting material, followed by deprotection with acid overnight and purification, yielding **4.14**-**4.18** with HPLC purities of > 99%.

The "cold" PET ligands **4.19**-**4.23** were prepared by incubation of **4.14**-**4.18** with natural $^{69}Ga^{3+}$ in a HEPES buffer pH 4.2 at 100 °C (Scheme 4.1). Complete conversion of the starting material was achieved after only 10 min. Under these conditions, the peptides proved to be stable. It should be noted that the potential PET ligands **4.19**-**4.23** could not be separated from the remaining respective precursor peptide (C18 RP-HPLC) when using acetonitrile and 0.04% aqueous TFA as eluent. However, baseline separation was achieved using MeOH and 0.05% formic acid as mobile phase.

For the purpose of the preparation of less polar PET ligands, peptides **3.16** and **4.12**, containing a tetramethylene and a dioxaoctamethylene linker, respectively, in the amino-functionalized N^{ω}-carbamoylated arginine, were conjugated to the fluorinated biphenyl-Ala spacer **4.24**, yielding **4.25** and **4.26** (after subsequent Boc-deprotection), or to the fluorinated aminomethyl-benzoyl spacer **4.27**, affording **4.28** and **4.29** (after subsequent Boc-deprotection), using HOBt, HBTU and DIPEA as coupling reagents. The side chain of the carbamoylated arginine in **4.26** was further elongated by treatment with succinimidyl ester **4.30**, yielding a terminal aminohexanoyl moiety in the arginine side chain after subsequent Boc-deprotection (**4.31**).

Compounds **4.31**, **4.25** and **4.26** were treated with **4.13** as described above, giving the DOTA-conjugated compounds **4.32**, **4.34** and **4.35** after removal of protecting groups (note: **4.28** and **4.29** were not further processed by coupling to DOTA as they proved to be more polar (shorter RP-HPLC retention times) than **4.25**, **4.31** and **4.26**). Finally, **4.32**, **4.34** and **4.35** were converted into the potential PET ligands **4.33**, **4.36** and **4.37** by insertion of Ga^{3+}. Unlike the synthesis of **4.19**-**4.23**, complete conversion of the starting material was only achieved after incubation at 100 °C for 30 min (as verified by analytical HPLC).

Aiming at a PET ligand with high in vivo stability, a series of N-terminally methylated NT(8-13) derivatives was synthesized by SPPS containing various commercially available

unnatural amino acids in position 12 (**4.38**-**4.45**), 13 (**4.46** and **4.47**), or 11 (**4.48** and **4.49**) (Figure 4.2). Whereas the unnatural amino acids incorporated in peptides **4.38**-**4.47** represent enantiomerically pure derivatives of Ile and Leu, the incorporation of racemic ß,ß-dimethyl-tyrosine (ß,ß-diMe-Tyr) in position 11 yielded the epimers **4.48** and **4.49** (see Figure 4.2). In the case of **4.46** and **4.47**, a 2-ClTrt-Cl resin had to be used instead of a H-Leu-2-ClTrt resin. For the coupling of the carboxy-terminal amino acid, the 2-ClTrt-Cl resin was treated with the respective Fmoc amino acid and DIPEA in CH_2Cl_2 overnight. After quenching of unreacted starting material with MeOH, the loading of the resin with ß-cyclopropyl-Ala (**4.46**) or α-methyl-Leu (**4.47**) was estimated to amount to 50% compared to the original loading of the resin with chloride. After side chain deprotection and cleavage from the resin, the overall yields of **4.38**-**4.49** amounted to 15-74%.

Me-AA^1-Arg-Pro-AA^2-AA^3-AA^4

cpd.	AA^1	AA^2	AA^3	AA^4
4.38	Arg	Tyr	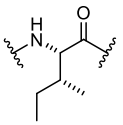	Leu
4.39	Arg	Tyr	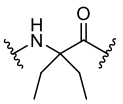	Leu
4.40	Arg	Tyr	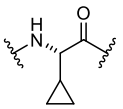	Leu
4.41	Arg	Tyr	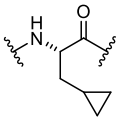	Leu
4.42	Arg	Tyr	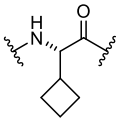	Leu
4.43	Arg	Tyr	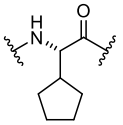	Leu
4.44	Arg	Tyr	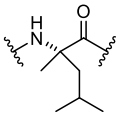	Leu

cpd.	AA^1	AA^2	AA^3	AA^4
4.45	Arg	Tyr	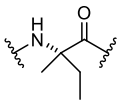	Leu
4.46	Arg	Tyr	Ile	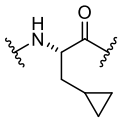
4.47	Arg	Tyr	Ile	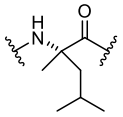
4.48 (*S*) **4.49** (*R*)	Arg	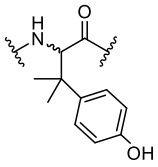	Ile	Leu
4.50 (*S*) **4.51** (*R*)	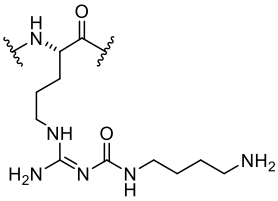	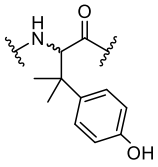	Ile	Leu
4.52 (*S*) **4.53** (*R*)	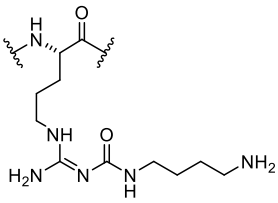	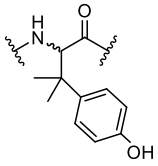	Tle	Leu

Figure 4.2. Structures of the C-terminally modified NT(8-13) derivatives **4.38**-**4.49** and the amino-functionalized precursor compounds **4.50**-**4.53**, representing derivatives of **4.48** and **4.49**.

Replacement of the N^{α}-methylated Arg^8 in **4.48** and **4.49** by an N^{α}-methylated, N^{ω}-carbamoylated arginine derived from **3.06a**, led to peptides **4.50** and **4.51**, and the additional replacement of Ile by Tle yielded **4.52** and **4.53** (Figure 4.2). Isolation of the epimers **4.50**/**4.51** and **4.52**/**4.53**, respectively, from one batch was necessary due to the usage of the same racemic ß,ß-diMe-Tyr building block as described for **4.48** and **4.49**.

The amino-functionalized peptides **4.50** and **4.52** were treated with **4.13** as described above for the synthesis of **3.16**, **4.08**, **4.09**, **4.11** and **4.12** (*cf.* Scheme 4.1) to give the DOTA-

conjugated compounds **4.54** and **4.55**, respectively, in high yields (76% and 79%) after subsequent Boc-deprotection (Scheme 4.2). Insertion of Ga^{3+} into the chelator moiety resulted in the PET ligand candidates **4.56** (UR-LS130) and **4.57** in high yields of 97% and 91%, respectively.

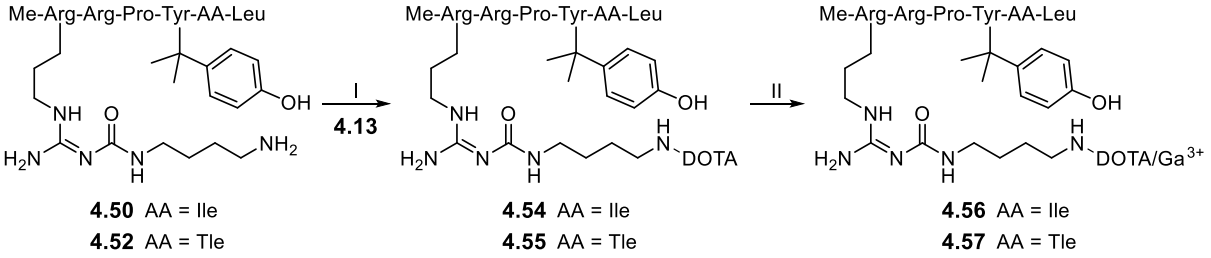

4.50 AA = Ile
4.52 AA = Tle

4.54 AA = Ile
4.55 AA = Tle

4.56 AA = Ile
4.57 AA = Tle

For structures of DOTA and DOTA/Ga^{3+} see **Scheme 4.1**.

Scheme 4.2. Synthesis of the potential NTS_1R PET ligands **4.56** and **4.57** containing a ß,ß-dimethylated tyrosine. Reagents and conditions: (I) (1) DIPEA, DMF/NMP 80:20 v/v, rt, 30 min, (2) TFA/H_2O 80:20 v/v, 50 °C, overnight, 76% (**4.54**), 79% (**4.55**); (II) preheating of a solution of the peptide (4 mM) in HEPES buffer (0.2 M, pH 4.2) to 60 °C, 5 min, addition of $Ga(NO_3)_3 \times H_2O$ in 10 mM HCl, 100 °C, 30 min, 97% (**4.56**), 91% (**4.57**).

4.2.2 Circular dichroism (CD) analysis

To determine the configuration at the α-carbon of the ß,ß-dimethylated tyrosine at position 11, we measured CD spectra of **4.48** and **4.49** and compared them to the CD spectrum of the peptide Me-Arg-Arg-Pro-Tyr-Ile-Leu[40], representing an all-L-configured reference compound with tyrosine instead of ß,ß-dimethylated tyrosine in position 11 as the only difference to **4.48** and **4.49** (Figure 4.3). To facilitate the assignment, we factorized the CD spectra into linearly independent spectral components by singular value decomposition (SVD), as described elsewhere[62]. As the three compounds differ in two properties, i.e., configuration at the α-carbon, ß,ß-dimethylation, or both, we expected three linear components, each contributing with a certain linear coefficient with either a positive or a negative sign. Indeed, performing the SVD on a set of nine spectra (three spectra each) resulted in three components being different from noise (*cf.* Figure 4.3B), whose reconstruction (under omission of linear components supposedly containing noise contribution only) resulted in nearly identical spectra as in Figure 4.3A (Figure 4.3C). Despite factorizing the SVD according to numerical variance and not to structural origin of spectral features, a rough assignment of the linear components was possible. Reconstruction of the spectra exclusively from spectral component 1 and the corresponding linear coefficients resulted in the spectra shown in Figure 4.3D. As this component represents the features with highest agreement between the three species, they are presumably associated with the backbone conformation of the peptides. In agreement with previous NMR and CD data on neurotensin in water[63], the maximum at 220 nm and the minimum at 190 nm indicate a lack of consecutive order in these peptides. After reconstruction of spectra with linear component 2, the resulting spectra for the reference compound and peptide **4.48** were nearly identical, whereas the spectrum reconstructed for **4.49** had the opposite sign. Therefore, component 2 is the one that indicates the configuration of the α-carbon, which allows assignment of the L-configuration to the ß,ß-dimethylated tyrosine in **4.48** and the D-configuration to the ß,ß-dimethylated tyrosine in **4.49**. Finally, component 3 accounts for all the remaining spectral differences between the three species such as contributions from presence or absence of ß,ß-dimethylation. The

configuration (*R* or *S*) of the ß,ß-dimethylated tyrosine in **4.50**-**4.53** was assigned based on the comparison of elution orders in RP-HPLC (**4.48**, **4.50** and **4.52** elute before **4.49**, **4.51** and **4.53**, respectively).

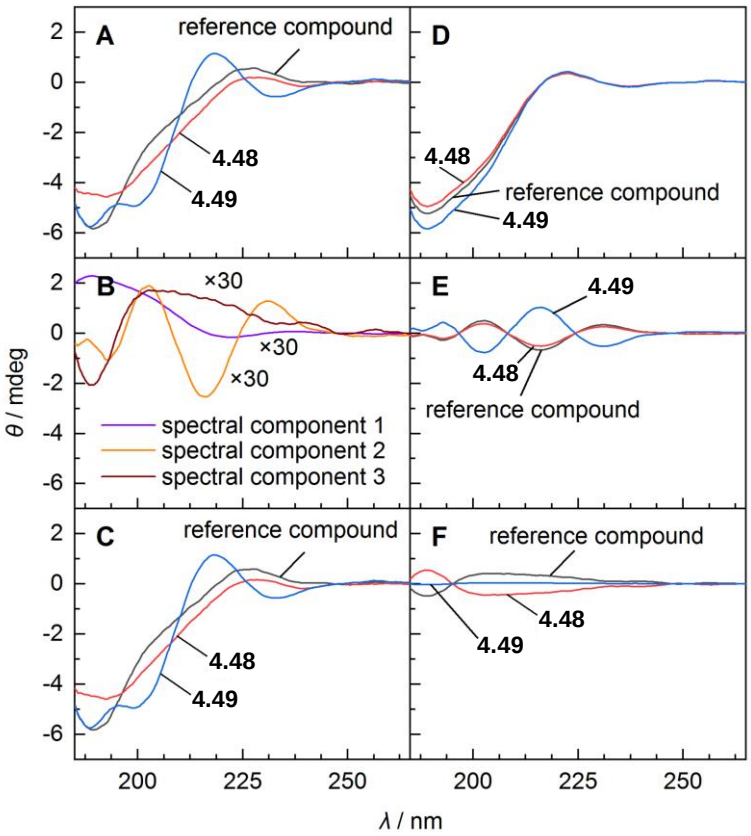

Figure 4.3. Circular dichroism (CD)-based identification of the absolute configuration of the dimethylated Tyr^{11} in **4.48** and **4.49** through spectral deconvolution and assignment of linearly independent spectral features to stereochemical and structural properties. (A) CD spectra of the two diastereomers **4.48** and **4.49** and an all-L-reference compound (Me-Arg-Arg-Pro-Tyr-Ile-Leu[40]). (B) Linearly independent components ("abstract spectra") from SVD, shared by the two diastereomers and the reference compound (rescaled by a factor of 30 for better comparison). (C) Reconstruction of full spectra from linear combination of the "abstract spectra" in panel B. (D) Contributions of component 1 to the full spectra in A or C correlating with CD contributions from the peptide backbone minus contributions from the fourth amino acid (tyrosine in the reference compound or ß,ß-dimethylated tyrosine in **4.48** and **4.49**). (E) Contributions of component 2 correlating with the configuration at the α-carbon of the fourth amino acid. Identical signs of the bands of this spectral component indicate the same configuration in **4.48** and the reference compound. (F) Contributions of component 3 accounting for spectral differences due to ß,ß-dimethylation that have not been considered in component 1 and component 2. As the SVD factorizes the experimental spectra with respect to highest spectral agreement, i.e., a 'compromise' spectrum formed from the spectra of the reference compound, **4.48** and **4.49**, absence of ß,ß-dimethylation in the reference compound is reflected by a negative contribution of component 3.

4.2.3 Peptide stability in human plasma

The stability of compounds **4.08**, **4.09**, **4.11**, **4.12**, **4.14**-**4.23**, **4.38**-**4.49** and **4.54**-**4.57** against proteolytic degradation was investigated in human plasma for up to 48 h as previously described[40]. For compounds **2.01**, **2.02**, **2.07**[40], **4.19**-**4.23**, **4.56** and **4.57**, the amount of remaining intact peptide after incubation in plasma at 37 °C is shown in Table 4.1 (for plasma stability data of compounds **3.16**, **4.08**, **4.09**, **4.11**, **4.12**, **4.14**-**4.18**, **4.38**-

4.49, **4.54** and **4.55** (Table A4.3) and recovery ratios of compounds **4.08**, **4.09**, **4.11**, **4.12**, **4.14**-**4.23** and **4.54**-**4.57** (Table A4.2) see Appendix).

Table 4.1. NTS_1R affinities of **2.01**, **2.02**, **2.07**, **4.19**-**4.23**, **4.33**, **4.36**, **4.37**, **4.56** and **4.57**, NTS_2R affinities of **2.01**, **2.07**, **4.19**-**4.22** and **4.56**, NTS_1R selectivities of **2.01**, **2.07**, **4.19**-**4.22** and **4.56**, and in vitro plasma stabilities of **2.01**, **2.02**, **2.07**, **4.19**-**4.23**, **4.56** and **4.57**, determined at 37 °C.

cpd.	pK_i ± SD/K_i [nM] NTS_1R[a]	pK_i ± SD/K_i [nM] NTS_2R[b]	NTS_1R Selectivity (Ratio $K_i(NTS_2R)$/ $K_i(NTS_1R)$)	% intact peptide in plasma after the given incubation time[c]				
				10 min	1 h	6 h	24 h	48 h
2.01	9.49/0.33[d]	8.61 ± 0.09/2.5	7.6	23[d]	< 1[d]	n.d.	< 1[d]	< 1[d]
2.02	8.93/1.2[d]	n.d.	-	11[d]	< 1[d]	n.d.	< 1[d]	< 1[d]
2.07	9.07/0.88[d]	8.01 ± 0.07/9.9	11	n.d.	> 99[d]	> 99[d]	98[d]	87[d]
4.19	7.80 ± 0.03/16	7.16 ± 0.18/73	4.6	n.d.	> 99	> 99	36 ± 1	4.2 ± 0.6
4.20	8.70 ± 0.10/2.0	7.70 ± 0.09/20	10	n.d.	> 99	77 ± 2	15 ± 1	4.6 ± 0.1
4.21	8.01 ± 0.08/9.9	7.25 ± 0.15/59	6.0	n.d.	> 99	> 99	26 ± 1	4.1 ± 0.1
4.22	7.70 ± 0.07/20	7.08 ± 0.16/88	4.4	n.d.	> 99	87 ± 2	30 ± 1	7.7 ± 1.0
4.23	8.13 ± 0.11/7.5	n.d.	-	n.d.	> 99	98 ± 6	46 ± 2	7.8 ± 0.6
4.33	8.61 ± 0.07/2.5	n.d.	-	n.d.	n.d.	n.d.	n.d.	n.d.
4.36	8.53 ± 0.02/3.0	n.d.	-	n.d.	n.d.	n.d.	n.d.	n.d.
4.37	8.38 ± 0.03/4.2	n.d.	-	n.d.	n.d.	n.d.	n.d.	n.d.
4.56	8.93 ± 0.17/1.2	8.35 ± 0.27/5.2	4.3	n.d.	> 99	> 99	77 ± 1	< 1
4.57	7.67 ± 0.04/21	n.d.	-	n.d.	> 99	> 99	68 ± 1	< 1

[a]Determined by radioligand competition binding with [^{3}H]UR-MK300 at HT-29 cells (K_d = 0.55 nM[40] or 0.41 nM, c = 1 nM); given are mean values ± SD (pK_i) and mean values (K_i) from two (**4.33**, **4.36** and **4.37**), three (**4.19**, **4.20**, **4.56** and **4.57**) or four (**4.21**-**4.23**) independent experiments, each performed in triplicate. [b]Determined by radioligand competition binding with [^{3}H]UR-MK300 at HEK293T-hNTS$_2$R cells (K_d = 6.9 nM or 4.0 nM, c = 10 nM); given are mean values ± SD (pK_i) and mean values (K_i) from two (**2.01**, **2.07** and **4.21**), three (**4.20**) or four (**4.19**, **4.22** and **4.56**) independent experiments, each performed in triplicate. [c]The initial concentration of the peptide in human plasma/PBS (1:2 v/v) was 100 µM. Data represent means ± SD from two or three independent experiments (SD not given when no decomposition was observed). [d]Schindler et al.[40].

The N^{α}-unmethylated peptides **2.01** and **2.02** were reported to undergo very rapid degradation in plasma[40,43]. Therefore, N-terminal methylation or methylation of Arg^9, both impairing NTS_1R binding only to a minor extent[40], was applied to the synthesized peptides throughout.

In the initial set of prepared peptides (**4.08**, **4.09**, **4.11**, **4.12** and **4.14**-**4.23**) low stability in plasma (≤ 15% intact peptide after 24 h) was found for compounds containing Ile in position 12 (**4.09**, **4.15** and **4.20**), confirming the importance of Tle^{12} for the stabilization of the C-terminus against proteolytic degradation. Compounds with Tle^{12}, devoid of a Ga^{3+}-occupied chelator (**3.16**, **4.08**, **4.11**, **4.12**, **4.14** and **4.16**-**4.18**), showed a high stability towards proteolytic degradation (≥ 93% intact peptide after 24 h). However, insertion of Ga^{3+} (**4.19** and **4.21**-**4.23**) led to a considerable decrease in stability (≤ 46% intact peptide after 24 h, Table 4.1). This observation can be explained by changes in compound

structure, hydrophilicity and charge distribution upon insertion of the gallium cation and rearrangement of the carboxylic arms of the chelators, thereby facilitating the recognition by proteases.

In the final set of compounds (**4.38**-**4.57**), high plasma stabilities (≥ 91% intact peptide after 24 h) were found for peptides **4.39**, **4.44**, **4.48** and **4.49**, as well as for the labeling precursors **4.54** and **4.55**, the latter even showing > 99% intact peptide after 48 h. Strikingly, peptides **4.48**, **4.49** and **4.54** do not comprise Tle but Ile in position 12. Therefore, the stabilizing effect must result from the diMe-Tyr in position 11. Insertion of Ga^{3+} in **4.54** and **4.55** (giving **4.56** and **4.57**) again provoked a substantial decrease in stability towards proteolytic degradation, nonetheless, the plasma half-lives of **4.56** and **4.57** were higher than those of the potential PET ligands **4.19**-**4.23** (*cf*. Table 4.1).

4.2.4 In vitro binding studies at the NTS$_1$R and NTS$_2$R, and NTS$_1$R agonistic activities

Except for compounds **4.28** and **4.29**, NTS$_1$R affinities were determined for all synthesized peptides (**4.08**, **4.09**, **4.11**, **4.12**, **4.14**-**4.23**, **4.25**, **4.26**, **4.32**-**4.50**, **4.52** and **4.54**-**4.57**) in a radiochemical competition binding assay using intact HT-29 colon carcinoma cells expressing the hNTS$_1$R[64], but not the NTS$_2$R[39]. The previously described radioligand [^{3}H]UR-MK300[39] (structure see Figure A4.1, Appendix) was used as radioligand. Selected compounds (**2.01**, **2.07**, **3.16**, **4.08**, **4.09**, **4.11**, **4.14**-**4.17**, **4.19**-**4.22**, **4.48**-**4.53** and **4.56**) were also investigated with respect to NTS$_2$R binding using the same radioligand and HEK293T cells stably expressing the hNTS$_2$R. The obtained K_i values are presented in Tables 4.1 and A4.3 (Appendix) and the resulting radioligand displacement curves are depicted in Figures A4.3, A4.4 and A4.5 (Appendix). The Ile-containing peptides **4.09**, **4.15**, **4.20**, **4.50**, **4.54** and **4.56** yielded lower K_i values (NTS$_1$R) than their respective Tle-containing analogs **4.08**, **4.14**, **4.19**, **4.52**, **4.55** and **4.57**, confirming the described affinity-decreasing effect of the Ile^{12}/Tle^{12} exchange in NT(8-13) analogs[14,40,50,52,54,65,66]. Ga^{3+}-containing DOTA-conjugated peptides consistently showed slightly higher NTS$_1$ and NTS$_2$ receptor affinities compared to the respective precursor compounds with an empty DOTA chelator (*cf*. Tables 4.1 and A4.3, Appendix). In terms of NTS$_1$R binding, the effect was most pronounced for the compound pairs **4.32/4.33** and **4.54/4.56** (4.8-fold and 4.9-fold increase in affinity upon insertion of Ga^{3+}). This phenomenon is in agreement with reported findings for DOTA- and (1,4,7-triazacyclononane-4,7-diyl)diacetic acid-1-glutaric acid (NODA-GA)-conjugated ^{68}Ga-labeled NTS$_1$R ligands[16,42], which were explained by changes in ligand structure as discussed above for the reduced plasma stabilities of the Ga^{3+}-containing peptides[16,42].

The difference with respect to the linker in the side chain of the N^{ω}-carbamoylated arginines of compounds **3.16** and **4.12** did not affect NTS$_1$R receptor affinity (K_i = 2.8 and 2.7 nM, respectively), but the change in the position of the N^{α}-methylated and N^{ω}-carbamoylated arginine (position 8 in **3.16**, position 9 in **4.11**) led to a slight decrease in NTS$_1$R affinity from K_i = 2.8 nM (**3.16**) to 13 nM (**4.11**). The latter finding is in agreement with reports on the higher importance of Arg^9 for NTS$_1$R binding compared to Arg^8 [41,67,68].

The initially prepared set of PET ligand candidates with Tle in position 12 (**4.19** and **4.21**-**4.23**) exhibited K_i values (NTS$_1$R) in the range of 7.5-20 nM. The second set of potential

PET ligands (**4.33**, **4.36** and **4.37**), containing a lipophilic fluorinated biphenyl moiety, showed higher NTS_1R affinities with K_i values of 2.5-4.2 nM. The position and the type of carbamoylated arginine played only a minor role in terms of NTS_1R binding for the potential PET ligands and their precursors. Within the final set of potential PET ligands (**4.56** and **4.57**), containing *S*-configured ß,ß-diMe-Tyr in position 11, the peptide with Ile in position 12 (**4.56**) displayed excellent NTS_1R binding (K_i = 1.2 nM), while its congener **4.57**, containing Tle in position 12, showed 18-fold lower NTS_1R affinity (K_i = 21 nM).

The series of NT(8-13) derivatives containing various unnatural amino acids in position 11, 12 or 13 (**4.38**-**4.49**) was prepared to develop a PET ligand with improved in vivo stability. As the side chains of Ile^{12} and Leu^{13} in **2.01** were hypothesized to contribute to receptor binding via hydrophobic interactions with aliphatic residues in the binding pocket of the NTS_1R[68,69], hydrophobic unnatural amino acids structurally related to Ile and Leu, were incorporated in position 12 or 13 (**4.38**-**4.47**, *cf*. Figure 4.2). The artificial amino acids were quite well tolerated with respect to NTS_1R binding, provided that they contained no additional alkyl substituent at the α-carbon (**4.38**, **4.40**-**4.43**, and **4.46**). The incorporation of amino acids with an additional alkyl group (methyl, ethyl) at the α-carbon resulted in a loss of NTS_1R binding (Table A4.3, Appendix). Strikingly, sub-nanomolar NTS_1R affinity (K_i = 0.14 nM) was achieved with compound **4.48**, containing *S*-configured ß,ß-diMe-Tyr^{11} instead of Tyr^{11}. As **4.48** showed also excellent in vitro plasma stability (see Table A4.3, Appendix), it served as a lead structure for the synthesis of the PET ligand candidates **4.56** and **4.57**. The epimer of **4.48** (peptide **4.49**), containing *R*-configured ß,ß-diMe-Tyr^{11}, displayed considerably lower NTS_1R binding compared to **4.48**. This was in agreement with the results of variations in position 11 of **2.01**, including the incorporation of D-configured tyrosine derivatives, revealing that D-configured tyrosine analogs caused a decrease in NTS_1R binding[40,66,70-72].

All compounds that were investigated at the NTS_2R showed lower K_i values at the NTS_1R than at the NTS_2R (difference most pronounced for peptide **4.15**: K_i values of 2.4 and 55 nM, respectively) revealing moderate NTS_1R selectivity (Table 4.1). However, it is unlikely that low or missing NTS_1R selectivity hampers the imaging of NTS_1R-expressing tumors in the periphery, as the NTS_2R is primarily expressed in the central nervous system[73-75].

In addition to the investigation of NTS_1R and NTS_2R binding, the agonistic activities of **4.21** and **4.56** at the G_q-coupled NTS_1R were determined in a Fura-2 Ca^{2+}-assay using HT-29 colon carcinoma cells. The potential PET ligands **4.21** and **4.56** proved to be full agonists with maximal responses comparable to that of **2.01** (see Figure A4.6, Appendix). As also found for **2.01**, the NTS_1R agonistic potencies of **4.21** and **4.56** were lower compared to their NTS_1R binding affinities (*cf*. Table 4.1 and Figure A4.6). A plausible explanation for this observation is in the non-equilibrium conditions in the case of the functional Ca^{2+}-assay precluding a complete association of the agonist to the receptor (signal is recorded within 3 min after agonist addition), which must be compensated by higher agonist concentrations.

4.2.5 Radiosynthesis and distribution coefficients

The potential PET tracers **4.21**, **4.33**, **4.37** and **4.56** all showed high NTS_1R affinity and high in vitro plasma stability. Thus, radiolabeling with $^{68}Ga^{3+}$ was performed to prepare

the respective PET tracers, i.e., [^{68}Ga]**4.21**, [^{68}Ga]**4.33**, [^{68}Ga]**4.37** and [^{68}Ga]**4.56**. This selection included two highly polar PET ligands ([^{68}Ga]**4.21**, [^{68}Ga]**4.56**) and two ligands bearing a lipophilic spacer ([^{68}Ga]**4.33**, [^{68}Ga]**4.37**), which can possibly result in different pharmacokinetic properties.

Radiosynthesis was performed by incubation of the precursor compounds **4.16**, **4.32**, **4.35** or **4.54** (7.5-15 nmol) in HEPES buffer pH 5.5 with [^{68}Ga]$GaCl_3$ at 125 °C for 6 or 16 min (for details see Experimental section). After the synthesis, the PET tracers were separated from the respective precursor using an analytical HPLC system in order to increase specific activity and to obtain a homogenous tracer preparation. The isolation from the precursors was feasible on a C18 reversed-phase material with mixtures of MeOH and 0.1% formic acid as mobile phase (comparable conditions as used for the purification of the "cold" PET ligands). For an exemplary chromatogram of the micro-preparative HPLC see Figure A4.7 (Appendix). Radiosynthesis and evaporation of the solvent was accomplished in approximately 90 min, and the separation of the PET tracer from the precursor including the second evaporation step took approximately another 50-60 min.

The hydrophilicity values of the PET ligands [^{68}Ga]**4.21**, [^{68}Ga]**4.33**, [^{68}Ga]**4.37** and [^{68}Ga]**4.56** were evaluated by the determination of the n-octanol/PBS distribution coefficients $logD_{7.4}$, which amounted to −3.87, −2.48, −2.59 and −3.06, respectively. Notably, compared to the most polar PET ligand ([^{68}Ga]**4.21**), the introduction of a lipophilic spacer ([^{68}Ga]**4.33**, [^{68}Ga]**4.37**) only led to an increase in $logD_{7.4}$ by less than 1.4 log units.

4.2.6 Biodistribution of PET ligands [^{68}Ga]4.21, [^{68}Ga]4.33, [^{68}Ga]4.37 and [^{68}Ga]4.56, and cellular uptake of [^{68}Ga]4.56

Biodistribution studies in HT-29 tumor-bearing nude mice were firstly performed with [^{68}Ga]**4.21** and resulted in a tumor-to-muscle ratio of 9.5 at 45 min after injection of the tracer (*cf*. Figure A4.8 and Table A4.4, Appendix). This result was comparable with the data reported for studies of the ^{68}Ga-labeled NTS$_1$R PET ligands [^{68}Ga]**4.04**[41] and [^{68}Ga]**4.05**[42] in the same xenograft mouse model (tumor-to-muscle ratios 60 min p.i.; approximately 14 and 8.8, respectively). As the fast renal elimination of [^{68}Ga]**4.21** potentially compromises its accumulation in the tumor, a second attempt with the less hydrophilic tracers [^{68}Ga]**4.33** and [^{68}Ga]**4.37**, potentially exhibiting longer systemic circulation, which could, in turn, result in an increased tumor uptake, was made. Although the introduction of the hydrophobic spacer in [^{68}Ga]**4.33** and [^{68}Ga]**4.37** had a marked impact on the predominant way of tracer elimination (shift from renal to nearly balanced renal and hepatobiliary excretion, *cf*. Figure 4.4A), tumor-to-muscle ratios 45 min p.i. (4.1 ([^{68}Ga]**4.33**) and 3.4 ([^{68}Ga]**4.37**)) were diminished even in comparison to [^{68}Ga]**4.21** (*cf*. Figure A4.8 and Table A4.4, Appendix). These results show that shifting the elimination pathway towards hepatobiliary excretion by decreasing the hydrophilicity of the tracer does not warrant an enhanced accumulation in the tumor, which might be explained by retained fast elimination despite an altered route of excretion. Irrespective of their different physicochemical properties, [^{68}Ga]**4.21**, [^{68}Ga]**4.33** or [^{68}Ga]**4.37** showed low in vivo stability, as concluded from HPLC analyses of urine samples revealing that intact [^{68}Ga]**4.21**, [^{68}Ga]**4.33** or [^{68}Ga]**4.37** accounted for less than 6% of the radioactivity in urine 45 min after tracer injection (Figure A4.9, Appendix). Notably, for these tracers, only one

main metabolite was found in the urine samples, being more polar than the respective intact tracer.

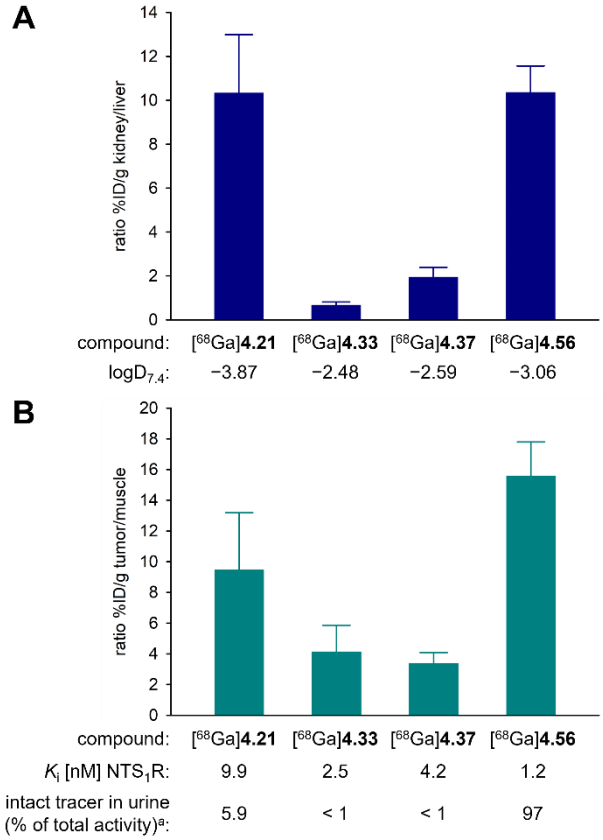

Figure 4.4. Ratio of the %ID/g values of (A) kidney and liver and of (B) tumor and muscle, obtained from biodistribution experiments with [^{68}Ga]**4.21**, [^{68}Ga]**4.33**, [^{68}Ga]**4.37** and [^{68}Ga]**4.56** in HT-29 tumor-bearing mice. Given are mean values ± SD from three ([^{68}Ga]**4.33**, [^{68}Ga]**4.37**) or four ([^{68}Ga]**4.21**, [^{68}Ga]**4.56**) independent experiments. [a]Given is the relative area (as percentage of the total peak area) of the peak corresponding to the intact PET ligand in the radiochromatogram of the HPLC analysis of the urine sample obtained 45 min after injection of the tracer.

Prompted by these findings, the focus was set on the development of NT(8-13)-derived PET tracers with higher proteolytic stability, as a low in vivo stability of the tracers could also be a major reason (other than fast elimination) for the low tracer accumulation in the tumor. The preparation and in vitro characterization of peptides **4.38**-**4.49** brought forth the potential PET tracer **4.56** exhibiting high NTS_1R affinity (K_i = 1.2 nM) and high in vitro plasma stability (Table 4.1). The biodistribution of [^{68}Ga]**4.56** in HT-29 tumor-bearing nude mice was investigated at 10, 25, and 45 min p.i. (Figure 4.5 and Table 4.2). Blocking experiments were performed for the time of highest tumor-uptake (45 min p.i.). At 10 min after injection of [^{68}Ga]**4.56**, the major fraction of activity was found in the kidneys (47 %ID/g), remaining at this level over time (47 %ID/g and 55 %ID/g after 25 min and 45 min, respectively). The activity in the liver was much lower (7.2, 5.7 and 5.2 %ID/g after 10, 25 and 45 min, respectively), indicating predominant renal excretion of [^{68}Ga]**4.56**, which was expected for this highly hydrophilic tracer (Table 4.2, Figure 4.4A). The activity in the blood dropped from 3.1 %ID/g (10 min p.i.) to 1.3 %ID/g (45 min p.i.), while it increased in the tumor from 3.6 %ID/g (10 min) over 7.3 %ID/g (25 min) to 8.4 %ID/g (45 min). Tumor-to-muscle ratios increased over time (3.3 at 10 min p.i. and 13 at 25 min p.i.), reaching a value of 16 after 45 min, which was considerably higher than

the tumor-to-muscle ratios of [^{68}Ga]**4.21**, [^{68}Ga]**4.33** and [^{68}Ga]**4.37** at 45 min p.i. (Table 4.2 and Table A4.4, Appendix). Co-injection of the non-labeled compound **4.48** with [^{68}Ga]**4.56** (blocking experiments) resulted in a tumor-to-muscle ratio of 1.8 (45 min p.i.), indicating that the uptake of [^{68}Ga]**4.56** in the tumor was NTS$_1$R-mediated. To evaluate the in vivo stability of [^{68}Ga]**4.56**, HPLC analyses of urine samples obtained 10 min and 45 min after tracer injection were performed, revealing that, in contrast to [^{68}Ga]**4.21**, [^{68}Ga]**4.33** and [^{68}Ga]**4.37**, intact [^{68}Ga]**4.56** accounted for more than 80% of the activity in urine (*cf.* Figure A4.11B and Figure A4.10, Appendix). The high in vivo stability of [^{68}Ga]**4.56**, which obviously contributes to an increased tracer accumulation in the tumor, was confirmed by HPLC analysis of an ex vivo blood plasma sample at 10 min p.i. showing that intact [^{68}Ga]**4.56** (identity confirmed by spiking of the plasma sample with **4.56**) accounted for more than 80% of the radioactivity in the processed sample (*cf.* Figure A4.11C-E, Appendix).

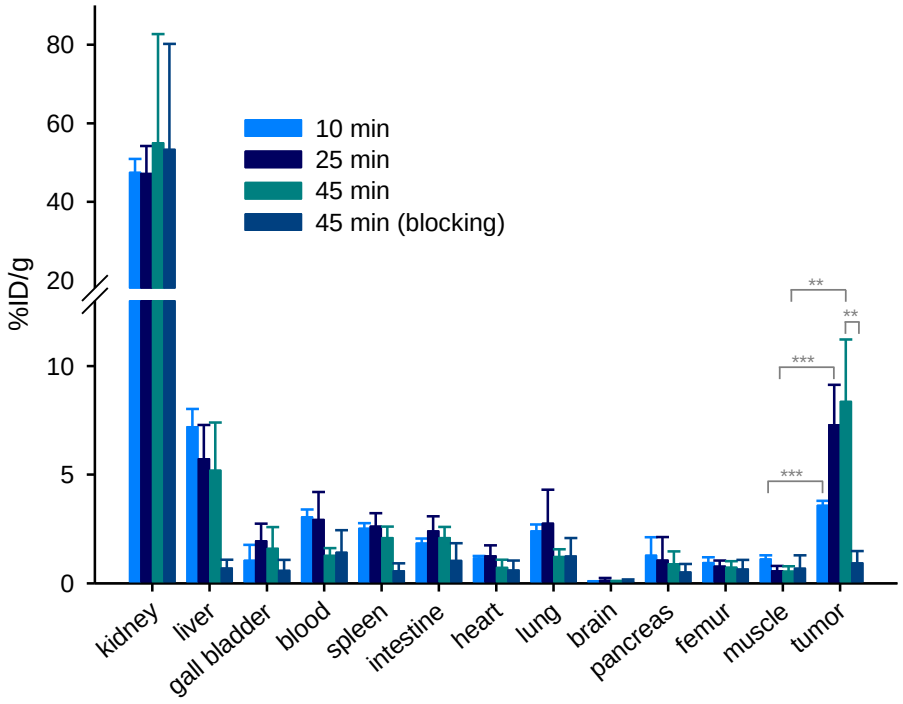

Figure 4.5. Biodistribution data (%ID/g tissue) of [^{68}Ga]**4.56** obtained from HT-29 tumor-bearing mice. Given are mean values ± SD (n = 4). Blocking data were obtained by co-injection of **4.48** (560-700 nmol/mouse). Statistical analysis of differences between tracer accumulation in the tumor of unblocked and blocked animals was performed by an unpaired two-tailed *t*-test ($p < 0.05$ was considered statistically significant). ** $p < 0.01$. *** $p < 0.001$.

Table 4.2. Ex vivo biodistribution data and tumor-to-muscle ratios of [^{68}Ga]**4.56** obtained from HT-29 tumor-bearing mice.[a]

tissue	uptake (%ID/g) at given times p.i.			
	10 min	25 min	45 min	45 min (blocking)
kidney	47 ± 3.4	47 ± 7.0	55 ± 28	53 ± 27
liver	7.2 ± 0.83	5.7 ± 1.6	5.2 ± 2.2	0.69 ± 0.39
gall bladder (bile)	1.1 ± 0.71	1.9 ± 0.79	1.6 ± 0.99	0.59 ± 0.49
blood	3.1 ± 0.34	2.9 ± 1.3	1.3 ± 0.33	1.4 ± 1.0
spleen	2.5 ± 0.25	2.6 ± 0.60	2.1 ± 0.52	0.56 ± 0.35
intestine	1.8 ± 0.22	2.4 ± 0.68	2.1 ± 0.49	1.0 ± 0.80
heart	1.2 ± 0.10	1.3 ± 0.49	0.72 ± 0.36	0.60 ± 0.44
lung	2.4 ± 0.30	2.8 ± 1.5	1.2 ± 0.34	1.3 ± 0.83
brain	0.079 ± 0.017	0.13 ± 0.11	0.061 ± 0.049	0.10 ± 0.074
pancreas	1.3 ± 0.83	1.1 ± 1.1	0.90 ± 0.57	0.51 ± 0.37
femur	0.95 ± 0.25	0.78 ± 0.27	0.73 ± 0.29	0.65 ± 0.43
muscle	1.1 ± 0.18	0.57 ± 0.23	0.55 ± 0.23	0.68 ± 0.61
tumor	3.6 ± 0.20	7.3 ± 1.8	8.4 ± 2.9	0.94 ± 0.55
tumor-to-muscle	3.3 ± 0.46	13 ± 3.0	16 ± 2.2	1.8 ± 0.78

[a]Given are mean values ± SD (n = 4). Blocking data were obtained by co-injection of **4.48** (560-700 nmol/mouse).

In reported studies, the ^{111}In-labeled analog of compound **4.04** was investigated in terms of in vivo stability 15 min after injection in mice, revealing 22% of remaining intact tracer in the plasma sample[41]. The ^{68}Ga-labeled analog of **4.05**, investigated in vitro in human serum, gave 93% intact tracer after 60 min of incubation[42]. In vivo studies in mice with a ^{68}Ga-labeled tracer structurally closely related to **4.05**, showing low NTS$_1$R affinity (K_i = 180 nM), resulted in 90% intact tracer in blood plasma 10 min after tracer administration[16]. Noteworthy, a recently reported ^{18}F-labeled fluoroglycosylated NTS$_1$R PET ligand derived from **3.16**, containing the same peptide core structure as [^{68}Ga]**4.21**, [^{68}Ga]**4.33** and [^{68}Ga]**4.37**, exhibited low in vivo stability in mice (30% of remaining intact tracer in plasma 10 min p.i., and no detectable tracer in plasma 20 min p.i.)[60]. Consequently, the high in vivo stability accomplished with [^{68}Ga]**4.56** in combination with retained high NTS$_1$R affinity, represents an important achievement in the field of peptidic NTS$_1$R PET ligands.

To estimate the internalization rate of NTS$_1$ receptors occupied by [^{68}Ga]**4.56**, HT-29 tumor cells were incubated with [^{68}Ga]**4.56** at 37 °C for up to 75 min followed by removal of extracellularly bound peptidic receptor ligand using the acid-strip method. This experiment showed that the fraction of internalized tracer was > 80% after only 5 min of incubation, reaching a plateau of approximately 95% after 55 min (Figure 4.6). This feature is considered favorable with respect to an accumulation of the tracer in the tumor in vivo, particularly when it comes to therapeutic applications using, e.g., alpha-emitting tracers such as ^{225}Ac-labeled radiopharmaceuticals.

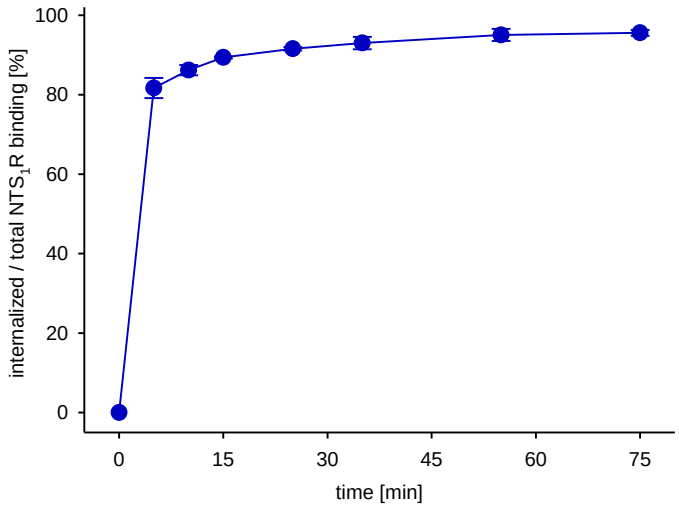

Figure 4.6. Fraction of specifically bound and internalized [^{68}Ga]**4.56** in HT-29 cells relative to the entire specific binding determined at 37 °C. Given are mean values ± SD of two independent experiments, each performed in triplicate.

4.2.7 PET/CT imaging with [^{68}Ga]4.56

Dynamic PET scans of HT-29 tumor-bearing nude mice injected with [^{68}Ga]**4.56** were performed for 45 min. Notably, a PET/CT scanner (Siemens Biograph mCT-S(40)) for clinical routine tumor diagnostics in patients was used for these studies. It was shown previously that this instrument is applicable for imaging of small animals with sufficiently large tumor implants[76,77]. Blocking experiments were carried out by co-injection of an excess of the NTS$_1$R ligand **4.48**. Time-activity-curves (TACs) for the tumor and muscle (from non-blocking and blocking experiments) as well as for the kidneys, generated from the SUVs acquired for the respective ROIs, are depicted in Figure 4.7A,B. These data confirmed the results from the biodistribution studies with [^{68}Ga]**4.56**: the tracer uptake in the tumor increased over time and the activity level in the kidneys reached a plateau after approximately 10 min. Thus, tumor-to-muscle ratios, determined from the SUVs (*cf.* inset table in Figure 4.7A), were comparable with the tumor-to-muscle ratios obtained from biodistribution studies. The blocking experiments confirmed the specific (NTS$_1$R-mediated) uptake of [^{68}Ga]**4.56** in the tumor (Figure 4.7A). Representative PET images of tumor-bearing mice injected with [^{68}Ga]**4.56** alone or with [^{68}Ga]**4.56** and an excess of **4.48** are shown in Figure 4.7C. Accumulation of the tracer in the tumor was clearly visible.

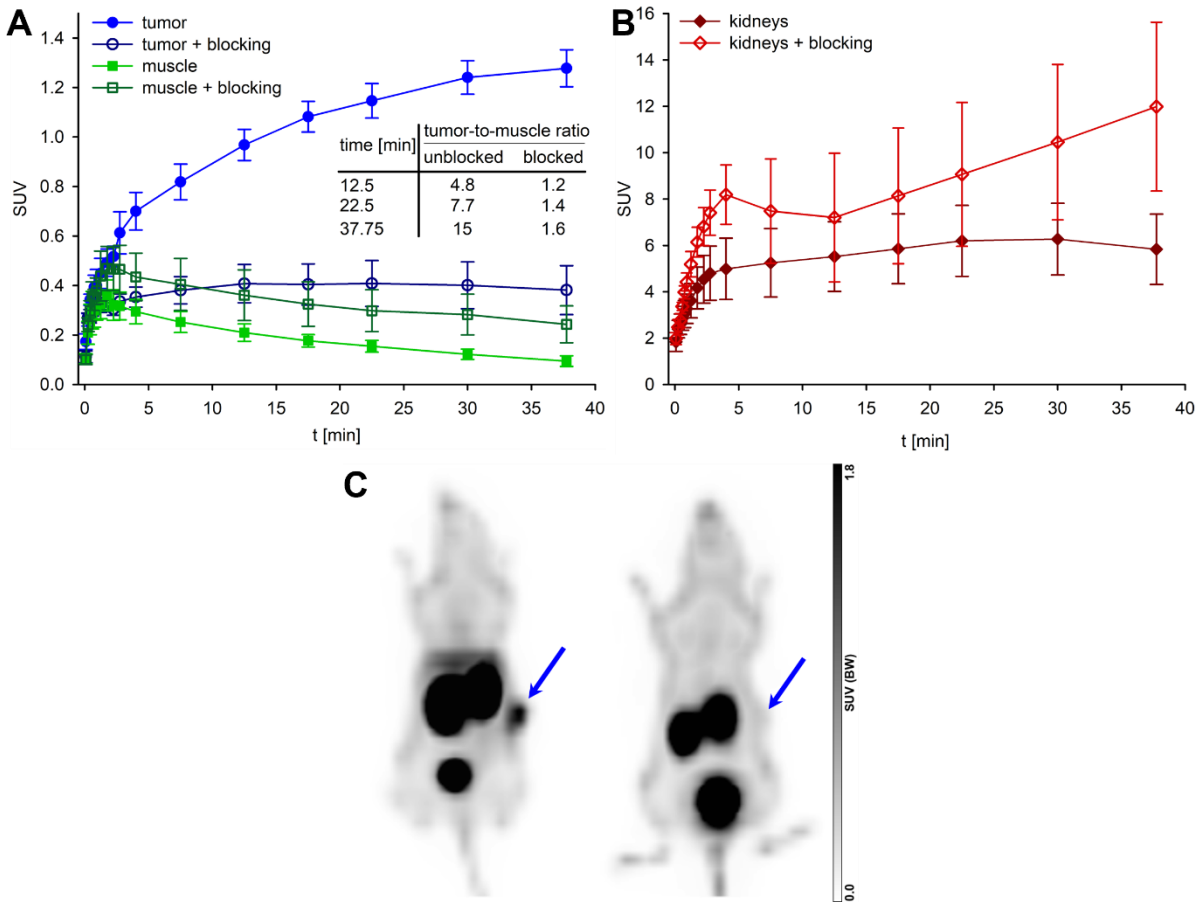

Figure 4.7. TACs and representative PET images from studies with [^{68}Ga]**4.56** in HT-29 tumor-bearing mice. (A) SUV_{mean} ± SD (n = 4) from 45 min-PET scans for the tumor (circles) and muscle (squares), and tumor-to-muscle ratios for selected times calculated based on the SUV values (inset table). Blocking data were obtained by co-injection of **4.48** (560-700 nmol/mouse). (B) SUV_{mean} ± SD (n = 4) for the kidneys (same PET scans as under A). (C) Maximum intensity projections of two representative PET images of HT-29 tumor-bearing mice after injection of [^{68}Ga]**4.56** (left) or co-injection of [^{68}Ga]**4.56** and **4.48** (right) (time frame: 10-45 min p.i.). The blue arrows indicate the tumors.

4.3 Conclusion

We herein describe the preparation, analysis and biological characterization of a series of peptidic PET tracer candidates, which led to the discovery of the DOTA(Ga^{3+})-conjugated NTS_1R ligand UR-LS130 (**4.56**) showing high stability in human plasma ($t_{1/2}$ > 24 h) and higher NTS_1R affinity (K_i = 1.2 nM) compared to previously reported NTS_1R PET ligands with high in vitro plasma stability. A novel feature of this Ga^{3+}-containing peptidic PET ligand is the attachment of the chelator via the side chain of an arginine. [^{68}Ga]**4.56** displayed high in vivo stability and a clear accumulation in NTS_1R-expressing HT-29 tumors. Notably, **4.56** contains no Tle, but Ile in position 12, like endogenous neurotensin. Instead, **4.56** contains a ß,ß-diMe-Tyr in position 11, leading to excellent stability in vitro and in vivo. To date, replacement of Ile^{12} by Tle^{12} is the state of the art to achieve proteolytic stabilization of the C-terminus of NT(8-13)-derived PET tracers. However, in the present study, we show that the Ile^{12}/Tle^{12} exchange can be insufficient to achieve high in vivo stability. Unlike the Ile^{12}/Tle^{12} exchange, which affects NTS_1R binding, the recently introduced alternative based on the exchange of Leu^{13} by trimethylsilylalanine proved to be beneficial with respect to NTS_1R binding, but turned out to be less favorable than the Tle^{12}-approach regarding proteolytic stability[38]. In contrast, the new diMe-Tyr^{11}-approach combines retained NTS_1R affinity and high tracer stability. Taking into consideration the reported impact of the metal ion chelator on a tracer's biodistribution profile and accumulation in the tumor[37,78], further improvement of the tracer [^{68}Ga]**4.56** could be undertaken by conjugation to a chelator different from DOTA. With [^{68}Ga]**4.56** we present the first peptidic NTS_1R PET ligand with high in vivo stability exhibiting comparable NTS_1R affinity as reported ^{177}Lu-labeled NTS_1R antagonists[79,80], which are favored over peptides for tumor endoradiotherapy due to higher in vivo stability[81]. Thus, the achievements of this work could promote the development of NT(8-13)-derived radiotherapeutics for cancer treatment, as an alternative to ^{177}Lu-labeled NTS_1R antagonists.

4.4 Experimental section

4.4.1 General experimental conditions

Solvents and buffer components, all purchased from commercial suppliers, were of analytical grade. Gradient grade MeOH for HPLC was obtained from Merck Chemicals (Darmstadt, Germany) and gradient grade MeCN for HPLC was from Sigma-Aldrich (Taufkirchen, Germany) or Merck. *N*,*N*-Diisopropylethylamine (DIPEA, 99%) and (*R*)-2-(Boc-amino)-3-(4'-fluoro-[1,1'-biphenyl]-4-yl)propanoic acid (**4.24**) were obtained from ABCR (Karlsruhe, Germany). HCOOH and K_2CO_3 were from Roth (Karlsruhe, Germany) and 1 M HCl was from VWR Chemicals (Fontenay-sous-Bois, France). Anhydrous *N*,*N*-dimethylformamide (DMF) (99.8%), 1,1,1,3,3,3-hexafluoro-2-propanol (HFIP), $Ga(NO_3)_3$ hydrate, 7-methyl-1,5,7-triazabicyclo [4.4.0]dec-5-ene (MTBD), methyl-4-nitrobenzenesulfonate, 2-mercaptoethanol, n-octanol and 1-methyl-D-Trp were purchased from Sigma-Aldrich. DMF (for peptide synthesis, packed under nitrogen, code D/3848/PB17), 1-methylpyrrolidin-2-one (NMP) (for peptide synthesis, nitrogen flushed), anhydrous NMP (99.5%), CH_2Cl_2 and 1-hydroxy-1*H*-benzotriazole (HOBt) hydrate were obtained from Acros Organics/Fisher Scientific (Nidderau, Germany). When used for the coupling of non-standard Fmoc-amino acids (SPPS), HOBt hydrate, containing up to 3% water, was dried using a lyophilizer. 4-[(Boc-amino)methyl]-3-fluoro-benzoic acid (> 95%) (**4.27**) was purchased from Activate Scientific (Prien am Chiemsee, Germany) and Boc-ε-aminocaproic acid succinimidyl ester (**4.30**) was purchased from Bachem (Bubendorf, Switzerland). DOTA-tris(*t*Bu)ester succinimidyl ester (**4.13**) was from CheMatech (Dijon, France). Trifluoroacetic acid (TFA) and absolute EtOH were obtained from Honeywell (Seelze, Germany). Collidine, 2-nitrobenzenesulfonylchloride and 1,8-diazabicyclo [5.4.0] undec-7-ene (DBU) were from Alfa Aesar/ThermoFisher (Heysham, UK). Piperidine and *N*,*N*,*N*',*N*'-tetramethyl-*O*-(1*H*-benzotriazole-1-yl)-uronium hexafluorophosphate (HBTU) were purchased from Iris Biotech (Marktredwitz, Germany). Deuterated solvents were obtained from Deutero (Kastellaun, Germany). Bovine serum albumin (BSA) was purchased from Serva (Heidelberg, Germany). Oxyma pure, *N,N'*-diisopropylcarbodiimide (DIC), H-Leu-2-ClTrt resin (loading: 0.79 mmol/g), Fmoc-N-Me-Arg(Pbf)-OH, Fmoc-Pro-OH, Fmoc-Ile-OH and Fmoc-Tle-OH (Fmoc-L-α-*tert*-butylglycine) were from Merck Biosciences (Schwalbach am Taunus, Germany). Cl-2-ClTrt resin (loading: 1.6 mmol/g), Fmoc-L-allo-Ile-OH, Fmoc-Deg-OH, Fmoc-L-cPrGly-OH and Fmoc-β,β-diMe-Tyr(*t*Bu)-OH (rac) were obtained from Iris Biotech. Fmoc-Arg(Pbf)-OH and Fmoc-Tyr(*t*Bu)-OH were from Iris Biotech or Carbolution (St. Ingbert, Germany). Fmoc-β-cyclopropyl-L-Ala-OH, Fmoc-β-cyclopentyl-L-Gly-OH, Fmoc-α-methyl-L-Leu-OH and (*S*)-Fmoc-α-ethyl-Ala-OH were from ABCR, and Fmoc-(*S*)-2-amino-2-cyclobutylacetic acid was from Merck Chemicals. Ultrapure 4-(2-hydroxyethyl)-1-piperazineethanesulfonic acid (HEPES) was from Gerbu (Heidelberg, Germany). Peptide **2.01** (tris(hydrotrifluoroacetate)) was purchased from SynPeptide (Shanghai, China). The syntheses of reference peptides **2.02**[40] and **2.07**[40], arginine building blocks **3.06a**[39] and **4.07**[39], NT(8-13) derivative **3.16**[60] and radioligand [^{3}H]UR-MK300[39] have been described elsewhere. Millipore water was used throughout for the preparation of buffers, stock solutions and HPLC eluents. 1.5- and 2-mL polypropylene reaction vessels with screw cap (in the following referred to as "reaction vessel with screw cap") from Süd-Laborbedarf (Gauting, Germany) were used for the preparation and storage of stock solutions, and for small-scale reactions. 1.5- or 2-mL

polypropylene reaction vessels (in the following referred to as "reaction vessel") from Sarstedt (Nümbrecht, Germany) were used for the preparation of serial dilutions, for the synthesis, determination of the distribution coefficient and biodistribution measurements of ^{68}Ga-labeled PET tracers and for the determination of stabilities in plasma. For the evaporation of solvents in 1.5- or 2-mL reaction vessels, a Savant Speed-Vac Plus SC110A vacuum concentrator (Thermo Fisher Scientific, Waltham, MA) was used. NMR spectra were recorded on a Bruker Avance 600 instrument (^{1}H: 600 MHz, ^{13}C: 151 MHz) (Bruker, Karlsruhe, Germany) at 300 K. The spectra were calibrated based on the solvent residual peaks (^{1}H-NMR: DMSO-d_6: δ = 2.50 ppm; ^{13}C-NMR: DMSO-d_6: δ = 39.52 ppm). ^{1}H-NMR data are reported as follows: chemical shift δ in ppm (multiplicity (s = singlet, d = doublet, m = multiplet, br s = broad singlet), integral, coupling constant J in Hz). High resolution mass spectra (HRMS) were acquired with an Agilent 6540 UHD Accurate-Mass Q-TOF LC/MS system coupled to an Agilent 1290 HPLC system (Agilent Technologies, Santa Clara, CA), using an ESI source. Analyses were performed using the following LC method: column: Luna Omega C18, 1.6 µm, 50 × 2.1 mm (Phenomenex, Aschaffenburg, Germany), column temperature: 40 °C, flow: 0.6 mL/min, solvent/linear gradient: 0-4 min: 0.1% aqueous HCOOH/0.1% HCOOH in MeCN 95:5-2:98, 4-5 min: 2:98. Preparative HPLC was performed with a system from Knauer (Berlin, Germany) consisting of two K-1800 pumps and a K-2001 detector (compounds **4.08**, **4.09**, **4.11**, **4.12**, **4.14**-**4.21**, **4.23**, **4.25**, **4.26**, **4.28**, **4.29**, **4.31**-**4.57**), or a Prep 150 LC System from Waters (Eschborn, Germany) consisting of a 2545 binary gradient module, a 2489 UV/visible detector, and a Waters Fraction Collector III (compound **4.22**). A Kinetex-XB C18, 5 µm, 250 mm × 21 mm (Phenomenex) or a Gemini-NX C18, 5 µm, 250 mm × 21 mm (Phenomenex) served as RP-columns at a flow rate of 20 mL/min. Mixtures of 0.2% aq TFA (A1) and acetonitrile (B1), or 0.1% aq TFA (A2) and B1 were used as mobile phase. A detection wavelength of 220 nm was used throughout. Collected fractions were lyophilized using an Alpha 2-4 LD apparatus (Martin Christ, Osterode am Harz, Germany) or a Scanvac CoolSafe 100-9 freeze-dryer (Labogene, Allerød, Denmark) both equipped with a Vacuubrand RZ 6 rotary vane vacuum pump. Analytical HPLC analysis of compounds **4.08**, **4.09**, **4.11**, **4.12**, **4.14**-**4.23**, **4.25**, **4.26**, **4.28**, **4.29** and **4.31**-**4.57** was performed with a system from Agilent Technologies consisting of a 1290 Infinity binary pump equipped with a degasser, a 1290 Infinity Autosampler, a 1290 Infinity Thermostated Column Compartment, a 1260 Infinity Diode Array Detector and a 1260 Infinity Fluorescence Detector. A Kinetex-XB C18, 2.6 µm, 100 × 3 mm (Phenomenex) served as stationary phase at a flow rate of 0.5 mL/min or 0.6 mL/min. The oven temperature was set to 25 °C. UV detection was performed at 220 nm and fluorescence detection at 275/305 nm. The injection volume was 20 µL. Mixtures of 0.04% aq TFA (A3), 0.05% aq HCOOH (A4) or 0.1% aq HCOOH (A5) and B1 or MeOH (B2) were used as mobile phase. The following linear gradients were applied for purity controls: compounds **4.08**, **4.09**, **4.11**, **4.12**, **4.14**-**4.18**, **4.25**, **4.26**, **4.28**, **4.29**, **4.31**-**4.35** and **4.38**-**4.57** (flow rate 0.6 mL/min): 0-12 min: A3/B1 90:10-70:30, 12-16 min: 70:30-5:95, 16-20 min: 5:95; compounds **4.19**-**4.23**, **4.36** and **4.37** (flow rate 0.5 mL/min): 0-12 min: A4/B2 95:5-70:30, 12-16 min: 70:30-5:95, 16-20 min: 5:95. The following linear gradient was used for the analysis of plasma stability samples: 0-12 min: A3/B1 90:10-73:27, 12-16 min: 73:27-5:95, 16-20 min: 5:95. Retention (capacity) factors k were calculated from the retention times t_R according to $k = (t_R - t_0)/t_0$ (t_0 = dead time). Peptides were characterized by ^{1}H- and ^{1}H-COSY NMR spectroscopy, HRMS, and RP-HPLC analysis. Additionally, ^{13}C-NMR spectra were acquired of **4.50** and **4.51**.

Annotation concerning the ^{1}H-NMR spectra (solvent: DMSO-d_6): in order to allow an integration of the signals interfering with the broad water signal at ca. 3.5 ppm, spectra were additionally recorded in DMSO-d_6/D_2O (4:1 v/v (**4.08**, **4.09**, **4.11**, **4.14**-**4.17**, **4.19**-**4.22**) or 5:1 v/v (**4.12**, **4.18**, **4.23**, **4.25**, **4.26**, **4.28**, **4.29**, **4.32**-**4.57**)) (data not shown).

Additional analytical data of compounds (HPLC analyses, ^{1}H- and ^{13}C-NMR spectra) are provided in the Appendix.

4.4.2 Cell culture and preparation of HEK293T cells stably expressing the human NTS_2R

All cells were cultured in 75 or 175 cm^2 flasks (Sarstedt, Nümbrecht, Germany) in a humidified atmosphere (95% air, 5% CO_2) at 37 °C. HT-29 colon carcinoma cells (DSMZ-no. ACC 299) were maintained in antibiotic-free RPMI medium (Sigma-Aldrich) supplemented with 7.5% fetal bovine serum (FBS) (Sigma-Aldrich). HEK293T cells stably expressing the human NTS_2R (HEK293T-hNTS_2R cells) were essentially generated following a previously described procedure[82]. In brief, HEK293T cells (kind gift from Prof. Dr. Wulf Schneider, Institute for Medical Microbiology and Hygiene, University of Regensburg, Germany) were seeded on a 6-well plate (Sarstedt, Nümbrecht, Germany) in Dulbecco's modified Eagle's medium (Sigma-Aldrich) supplemented with 10% FBS, L-glutamine (2 mM) (Sigma-Aldrich) and Penicillin-Streptomycin (100 IU/mL and 0.1 mg/mL, respectively) (Sigma-Aldrich) at a density of 6×10^5 cells/well. On the next day, cells were transfected with 2 µg of cDNA encoding the hNTS_2R (cDNA Resource Center, Rolla, MO, USA, catalog no. NTSR200000) using X-tremeGENE™ HP (Roche Diagnostics, Mannheim, Germany) as transfection reagent according to the manufacturer's protocol. After two days of transfection, cells were detached with trypsin-ethylenediamine-tetraacetic acid (EDTA, Biochrom, Berlin, Germany) and transferred to a 15-cm dish (Sarstedt, Nümbrecht, Germany). After the cells had attached to the dish, G418 (Biochrom, Berlin, Germany) was added at a final concentration of 1 mg/mL. Selection was achieved by exchanging the medium every two to three days for two weeks. Subsequently, a clone with high NTS_2R-expression, which was assessed radiochemically after addition of 10 nM of [^{3}H]UR-MK300, was isolated. Cultivation was then continued with a reduced G418 concentration in the culture medium of 600 µg/mL.

4.4.3 Radiochemical binding assays

4.4.3.1 NTS_1R binding

Radioligand competition binding experiments with [^{3}H]UR-MK300 (specific activity: 47.0 Ci/mmol[39] or 65.0 Ci/mmol; for structure see Figure A4.1, Appendix) at hNTS_1R-expressing intact human HT-29 colon carcinoma cells were performed at 23 ± 1 °C as described previously[39]. Two different batches of the radioligand [^{3}H]UR-MK300 were used. The K_d values of [^{3}H]UR-MK300 amounted to 0.55 nM (mean value from two independent saturation binding experiments, each performed in triplicate)[40] and 0.41 ± 0.12 nM (mean value ± SD from two independent saturation binding experiments, each performed in triplicate, data not shown). Specific binding data (obtained by subtracting unspecific binding from total binding) were normalized (100% = specifically bound radioligand in the absence of competitor) and plotted over log(concentration of competitor) followed by a four-parameter logistic fit (SigmaPlot 12.5, Systat Software, San José, CA,

USA) (note: in the case of **4.40**, the lower curve plateau of the sigmoidal fit was constrained to > 0). Resulting pIC_{50} values were converted to IC_{50} values and K_i values were calculated from the IC_{50} values according to the Cheng-Prusoff equation[83] using a K_d value of 0.55 nM (**4.08**, **4.09**, **4.11**, **4.14**-**4.17** and **4.19**-**4.22**) or 0.41 nM (**4.12**, **4.18**, **4.23**, **4.25**, **4.26**, **4.32**-**4.50**, **4.52** and **4.54**-**4.57**). The K_i values from individual experiments were transformed to pK_i values, followed by the calculation of mean pK_i values ± SD.

4.4.3.2 NTS_2R binding

NTS_2R saturation and competition binding experiments were performed at intact HEK293T-hNTS_2R cells at 23 ± 1 °C using [^{3}H]UR-MK300[39] as radioligand (two different batches were used; specific activities: 47.0 Ci/mmol[39] and 65.0 Ci/mmol). Two days prior to the experiment, white 96-well plates with clear bottoms (Costar, catalog no. 3610) were treated with poly-D-lysine hydrobromide (Sigma-Aldrich) for 10 min. The wells were washed with H_2O and the plates were dried on air at rt overnight. Alternatively, plates were treated with a sterile solution of 5% (w/v) gelatin (Sigma-Aldrich) in H_2O (50 µL) at rt for 1.5-2 h. The gelatin solution was removed, followed by the addition of a solution of 2.5% (v/v) of glutaraldehyde (Sigma-Aldrich) in H_2O (50 µL) at rt for 10 min. After removal of the glutaraldehyde solution, the wells were washed twelve times with H_2O and two times with culture medium (150-300 µL). One day before the experiment, cells were seeded in the treated plates at a density of 9×10^4 cells/well. On the day of the experiment, the culture medium was carefully removed using a multi-channel pipette (Transferpette S-12, Brand, Wertheim, Germany) and the cells were washed once with Dulbecco's phosphate-buffered saline (D-PBS) containing Ca^{2+} and Mg^{2+} (1.8 mM $CaCl_2$, 2.68 mM KCl, 1.47 mM KH_2PO_4, 3.98 mM $MgSO_4$, 136.9 mM NaCl and 8.06 mM Na_2HPO_4) (200 µL, rt) followed by the careful pre-filling of the wells with 180 µL (total binding) or 160 µL (unspecific and competition binding) of D-PBS, supplemented with 1% BSA and 100 µg/mL bacitracin (Serva, Heidelberg, Germany) (in the following referred to as binding buffer). To determine total binding, 20 µL of a solution of the radioligand in binding buffer (10-fold concentrated compared to the final concentration) were added. For the determination of unspecific binding, 20 µL of a solution of **2.01** in binding buffer (10-fold concentrated, used in 500-fold excess compared to the radioligand) and 20 µL of a 10-fold concentrated solution of the radioligand in binding buffer were added. To determine the displacing effect of a compound of interest, 20 µL of a solution of the respective compound in binding buffer (10-fold concentrated) and 20 µL of a 10-fold concentrated solution of the radioligand in binding buffer were added. During the incubation period of 2 h at 23 °C, the plates were gently shaken. After incubation, the liquid was carefully removed using a multi-channel pipette and the cells were carefully washed twice with ice-cold D-PBS (200 µL). 25 µL of lysis solution (8 M urea, 3 M acetic acid, and 1% Triton-X-100 in H_2O) were added to each well and the plates were shaken at rt for 25 min, followed by the addition of liquid scintillator (Ultima Gold, PerkinElmer, Waltham, MA, USA) (200 µL). The plates were sealed with a transparent sealing tape (permanent seal for microplates, PerkinElmer, product no. 1450-461) and turned upside down several times to achieve complete mixing. Prior to the measurement of the radioactivity with a MicroBeta2 plate counter (PerkinElmer), the plates were kept in the dark for at least 1 h. All experiments were performed in triplicate. The K_d values of [^{3}H]UR-MK300, determined for the different batches of radioligand by saturation binding experiments, amounted to 6.9 ± 1.8 nM (mean value ± SD from six independent determinations, each performed in triplicate) and 4.0 ±

1.5 nM (mean value ± SD from three independent determinations, each performed in triplicate) (for representative saturation binding curves see Figure A4.2, Appendix). Data from competition binding experiments were analyzed as described for NTS_1R binding using a K_d value of 6.9 nM (**2.01**, **4.08**, **4.09**, **4.14**, **4.15**, and **4.19**) or 4.0 nM (**2.07**, **3.16**, **4.09**, **4.11**, **4.15**-**4.17**, **4.19**-**4.22**, **4.48**-**4.53** and **4.56**). Note: in the cases of **4.49**-**4.53** and **4.56**, the lower curve plateau of the sigmoidal fit was constrained to > 0.

4.4.4 Fura-2 Ca^{2+}-assay

The fura-2 calcium assay on intact $hNTS_1R$-expressing HT-29 cells was performed as previously described for human erythroleukemia cells[84] using a Perkin-Elmer LS50 B spectrofluorimeter (PerkinElmer, Rodgau, Germany). At a confluency of 80-95%, cells were trypsinized, detached from the culture flask and the assay was performed as described in the protocol. Net Ca^{2+}-responses (basal cytosolic Ca^{2+}-concentration subtracted from the measured Ca^{2+}-concentration), induced by **2.01**, **4.21** and **4.56**, were normalized (100% = effect elicited by 300 nM NT(8-13)) and plotted over log(concentration of agonist) followed by a four-parameter logistic fit (SigmaPlot 12.5, Systat Software).

4.4.5 Investigation of the stability of 4.08, 4.09, 4.11, 4.12, 4.14-4.23, 4.38-4.49 and 4.54-4.57 in human plasma

The proteolytic stabilities of **4.08**, **4.09**, **4.11**, **4.12**, **4.14**-**4.23**, **4.38**-**4.49** and **4.54**-**4.57** were investigated in human blood plasma/PBS (136.9 mM NaCl, 2.68 mM KCl, 5.62 mM Na_2HPO_4, 1.09 mM NaH_2PO_4 and 1.47 mM KH_2PO_4) pH 7.4 (1:2, v/v) according to a described procedure[40] with the following modifications: 5 mM stock solutions in MeCN/0.04% aq TFA (30:70 v/v) were used throughout for the addition of the peptides to plasma/PBS (1:2 v/v). As the RP-HPLC purity of 1-methyl-D-Trp, used as internal standard (IS) was < 95% (data not shown), the compound was purified by preparative HPLC to give a purity of > 99%. The concentration of the peptides in plasma/PBS (1:2 v/v) was 80 and 4 µM (recovery determination) or 100 µM (stability tests). Data analysis was based on UV detection at 220 nm (**4.08**, **4.09**, **4.11**, **4.12**, **4.14**-**4.18**, **4.21**-**4.23**, **4.38**-**4.49** and **4.54**-**4.57**) or fluorescence detection at 275/305 nm (**4.19** and **4.20**). Reference samples, representing 100% recovery, were prepared in duplicate (**4.08**, **4.09**, **4.11**, **4.14**-**4.16** and **4.19**-**4.21**) or quadruplicate (**4.12**, **4.17**, **4.18**, **4.22**, **4.23**, **4.38**-**4.49** and **4.54**-**4.57**). Recovery ratios were obtained by dividing the recovery of the peptide by the recovery of IS for each individual sample (n = 3-5). The obtained recoveries and the recovery ratios are summarized in Table A4.2 (Appendix). Note: in the case of compounds **4.38**-**4.49**, which were prepared for testing the effects of various unnatural amino acids on peptide stability, no recovery ratios were determined. Instead, the recovery ratios determined for the previously reported, structurally closely related peptide Me-Arg-Arg-Pro-Tyr-Ile-Leu[40] were used for calculating the amount of remaining intact peptide in plasma.

4.4.6 Circular dichroism (CD) analysis

CD spectra of 100 µM aqueous solutions of **4.48** and **4.49** and a reference compound with the amino acid sequence Me-Arg-Arg-Pro-Tyr-Ile-Leu[40] were recorded in a 1 cm path length cuvette at 20 °C with a Jasco J-810 spectropolarimeter (Jasco, Tokyo, Japan) equipped with a PTC-423S Peltier temperature controller (Jasco). Instrumental parameters: spectral range, 180-300 nm; bandwidth, 1 nm; scanning speed, 500 nm/min.

Each spectrum represents the average of three spectra, each recorded with 20 accumulations, after solvent subtraction. An "economy-size" singular-value decomposition (SVD) on a set of nine spectra (matrix A consisting of three spectra for each of **4.48**, **4.49** and the reference compound) was calculated in MATLAB (MathWorks, Natick, MA) as $A = U \cdot S \cdot V^T$. Here, U is a matrix whose columns contain the linearly independent spectral components, S is a diagonal matrix containing the singular values, and V^T is the transpose of matrix V, which contains the linear coefficients associated with the spectral components in U.

4.4.7 Synthesis, in vitro and in vivo characterization of PET tracers [^{68}Ga]4.21, [^{68}Ga]4.33, [^{68}Ga]4.37 and [^{68}Ga]4.56

4.4.7.1 PET tracer synthesis

The preparation of the ^{68}Ga-labeled PET ligands [^{68}Ga]**4.21**, [^{68}Ga]**4.33**, [^{68}Ga]**4.37** and [^{68}Ga]**4.56** was performed on a Scintomics GRP® synthesizer module (Scintomics GmbH, Fürstenfeldbruck, Germany) with the Scintomics Control Center software, the Reagent and Hardware Kit SC-01 and SC-01-H (ABX, Radeberg, Germany) and a Isomed 2010 activimeter (MED Nuklear-Medizintechnik, Dresden, Germany) for activity measurements. [^{68}Ga]$GaCl_3$ was eluted from a ^{68}Ge/^{68}Ga-generator GalliaPharm (Eckert&Ziegler, Berlin, Germany) with 0.1 M HCl (Eckert&Ziegler) (approximately 9 mL). A 0.12-0.15 mM solution of the precursor compound (**4.16**, **4.32**, **4.35** or **4.54**) in ultrapure H_2O (Merck) (100 µL) was added to a HEPES buffer (ABX Kit; 1.5 M, pH 5.5) (3 mL), combined with the gallium eluate and the mixture was incubated for 6 min ([^{68}Ga]**4.21**, [^{68}Ga]**4.33**, [^{68}Ga]**4.56**) or 16 min ([^{68}Ga]**4.37**) at 125 °C, cooled down to approximately 120 °C and loaded on a C18 cartridge (Sep-Pak C18 Plus Short Cartridge, 55-105 µm, Waters, Milford, MA, USA). After a washing step with H_2O (ca. 8 mL), the product was eluted from the cartridge with EtOH (effective volume ca. 1 mL) and the eluate was transferred into a 2-mL reaction vessel. The solvent was evaporated in a Savant Speed-Vac SVC100H vacuum concentrator (Savant Instruments, Farmingdale, NY, USA) equipped with pre-heated (100 °C) rotor inserts (aluminum blocks with bores for 1.5- and 2-mL reaction vessels) for approximately 50 min (note: a complete evaporation to dryness was avoided; the residual volume was approximately 10-30 µL), followed by uptake in 0.1% aq HCOOH (80-100 µL). The solution was subjected to preparative work-up using an HPLC system composed of a P4000 pump (Thermo Separation Products), a Degassex DG-4400 degasser (Phenomenex), a 2487 UV/visible detector (Waters) and a Rheodyne manual injector equipped with a 200-µL loop (note: the pump was directly controlled via the front panel and the UV/Vis-detector was remote-controlled using Waters Millennium Software). For the detection of γ-radiation, a B20/G-10 RADEye (Thermo Scientific, Erlangen, Germany) was placed close to the outlet tubing of the UV/Vis-detector (note: the vessel used for waste collection was shielded from the RADEye by 2 cm of lead). The stationary phase, a Luna C18(2), 3 µm, 150 × 4.6 mm (Phenomenex), was placed in a box of lead (wall thickness: 2 cm). The flow rate was 0.5 mL/min. Mixtures of A5 and B2 were used as mobile phase. The following linear gradients were applied: [^{68}Ga]**4.21**: 0-16 min: A5/B2 85:15-65:35, 16-17 min: 65:35-5:95, 17-22 min: 5:95; [^{68}Ga]**4.33** and [^{68}Ga]**4.37**: 0-16 min: A5/B2 65:35-45:55, 16-17 min: 45:55-5:95, 17-22 min: 5:95; [^{68}Ga]**4.56**: 0-16 min: A5/B2 80:20-60:40, 16-17 min: 60:40-5:95, 17-22 min: 5:95. UV detection was performed at 220 nm and 275 nm (note: the chosen conditions enabled a

separation of excessive labeling precursor from the Ga^{3+}-labeled species. For an exemplary chromatogram of a co-injection of **4.32** and **4.33** (50 µM each, injection volume 75 µL), and a chromatogram of the separation of [^{68}Ga]**4.33** from remaining **4.32** after radiosynthesis see Figure A4.7, Appendix). The eluate, containing the PET ligand, was collected in a 2 mL reaction vessel immediately followed by removal of the solvent in a vacuum concentrator equipped with pre-heated (100 °C) aluminum blocks (35-40 min). However, a complete evaporation of the solvent was avoided. The aqueous residue (20-40 µL) was taken up in PBS (ABX Kit) (80-500 µL) yielding a solution referred to as "tracer stock" in the following (final activity 0.157-1.69 GBq/mL). Quality controls of the PET ligands were performed by HPLC analysis using a system from Agilent Technologies (Waldbronn, Germany) consisting of a 1100 Series quaternary pump equipped with a 1260 Infinity degasser, a 1100 Series Autosampler, a 1100 Series Thermostated Column Compartment, a 1100 Series Diode Array Detector, and a GABI Star radiometric detector (Raytest Isotopenmessgeräte GmbH, Straubenhardt, Germany). A Luna C18(2), 3 µm, 100 × 4.6 mm (Phenomenex) served as stationary phase. The flow rate was 0.95 mL/min and the temperature of the column compartment was set to 25 °C. The following linear gradients were applied: [^{68}Ga]**4.21**: 0-9 min: A3/B1 95:5-72:28, 9-12 min: 72:28-5:95, 12-16 min: 5:95; [^{68}Ga]**4.33** and [^{68}Ga]**4.37**: 0-9 min: A3/B1 95:5-55:45, 9-12 min: 55:45-5:95, 12-16 min: 5:95; [^{68}Ga]**4.56**: 0-9 min: A3/B1 95:5-65:35, 9-12 min: 65:35-5:95, 12-16 min: 5:95. UV detection was performed at 220 nm. Dilutions of the tracer stocks (5-25 µL, 0.17-1.39 MBq) were injected into the HPLC system. PET tracer-specific details about the syntheses including radiochemical yields and purities are provided in Table 4.3.

Table 4.3. PET ligand specific parameters for the radiosynthesis of [^{68}Ga]**4.21**, [^{68}Ga]**4.33**, [^{68}Ga]**4.37** and [^{68}Ga]**4.56**.

PET ligand	labeling precursor	amount of precursor	total product activity[a]	decay-corrected RCY (%)[b]	HPLC analysis:[b] purity, t_R, k
[^{68}Ga]**4.21**	**4.16**	10-20 µg, 7.5-15.0 nmol	78.71-111.4 MBq	67-77	97-99%, 8.1-8.2 min, 4.8-4.9
[^{68}Ga]**4.33**	**4.32**	20 µg, 11.5 nmol	93.51 MBq	75	95%, 8.1 min, 4.8
[^{68}Ga]**4.37**	**4.35**	20 µg, 12.2 nmol	69.05 MBq	77	99%, 7.8 min, 4.6
[^{68}Ga]**4.56**	**4.54**	20 µg, 14.7 nmol	95.80-168.6 MBq	67-80	92-99%, 7.3-7.4 min, 4.2-4.3

[a]Activity after separation of the PET tracer from the precursor by HPLC, removal of the solvent and uptake in PBS; given is the range over the performed syntheses. [b]Given is the range over the performed syntheses. RCY = radiochemical yield.

4.4.7.2 Determination of the distribution coefficient log$D_{7.4}$ of PET ligands [^{68}Ga]4.21, [^{68}Ga]4.33, [^{68}Ga]4.37 and [^{68}Ga]4.56

The distribution coefficients log$D_{7.4}$ of the radiotracers [^{68}Ga]**4.21**, [^{68}Ga]**4.33**, [^{68}Ga]**4.37** and [^{68}Ga]**4.56** were determined by adding a solution of the tracer in PBS (100 µL, ca. 0.20-0.34 MBq) to a mixture of n-octanol (500 µL) and PBS (pH 7.4) (400 µL) in a 2-mL HPLC vial (Agilent, article number 5182-0714) with a screw cap equipped with a septum (Agilent, article number 5182-0717). After vortexing the mixture for 2 min, two 100 µL aliquots of the upper phase (n-octanol) were taken. To obtain a sample of the lower phase

(PBS), the HPLC vial was held upside down and approximately 100-150 µL of the aqueous phase were removed using a syringe equipped with a canula and collected in a reaction vessel. Two 10 µL aliquots of the aqueous phase were subjected to measurement. The activity of the aliquots was measured with a Canberra Genie 2000 system (Canberra, Rüsselsheim, Germany) using the Gamma Acquisition & Analysis Software Genie 2000 3.4.1. Experiments were performed in triplicate. The decay-corrected counts per minute (cpm) values were averaged (n = 3) and transformed to a distribution coefficient $logD_{7.4}$ according to $logD_{7.4} = log(A_{octanol}/A_{aqueous})$, where $A_{octanol}$ is the mean of the decay-corrected cpm values obtained for samples of the n-octanol phase, and $A_{aqueous}$ is the mean of the decay-corrected cpm values obtained for samples of the aqueous phase.

4.4.7.3 Mouse xenograft model

8-12 weeks old female NMRI nude (nu/nu) mice (body weight 22-32 g) (Charles River, Sulzfeld, Germany) were kept under specified pathogen free (SPF) conditions at 23 °C, 55% relative humidity and a 12 h light/dark cycle in the central animal facility of the University of Regensburg using type III cages from Tecniplast (Hohenpeißenberg, Germany). The animals took food (Ssniff, Soest, Germany) and autoclaved tap water ad libitum. For tumor cell implantation, the culture medium of HT-29 cells was removed, the cells were detached from the culture flask by incubation for 2 min in trypsin-EDTA and the suspension was centrifuged (164 × g, rt, 5 min). The supernatant was removed, and the cell pellet was washed twice with sterile PBS or serum-free medium (5-6 mL). The cells were resuspended in sterile PBS to a final density of 1×10^7 cells/mL. Mice were injected subcutaneously into the right flank with the HT-29 cell suspension (100 µL). After 2-4 weeks, when the tumors had reached a size of 50-500 mm^3, animals were used for biodistribution and PET/computed tomography (CT) imaging studies (note: for PET/CT studies, the tumor size was at least 200 mm^3).

4.4.7.4 Animal anesthetization

Mice were anesthetized by i.p. injection (100 µL per 10 g body weight) using a mixture that was prepared by addition of ketamin (Medistar Arzneimittelvertrieb, Ascheberg, Germany, 10 wt%, 800 µL) and xylazine (Serumwerk, Bernburg (Saale), Germany, 2 wt%, 200 µL) to PBS (9 mL).

4.4.7.5 Biodistribution studies

Aliquots of the tracer stock were diluted in PBS to give a volume of 200 µL. 80-100 µL (0.9-5.9 MBq) of this solution were injected into anesthetized HT-29 tumor-bearing nude mice via the tail vein. Animals were kept on a heating plate (set to 40 °C) or a pre-heated (ca. 45 °C) gel cushion and were killed by cardiac puncture 10 min, 25 min or 45 min p.i. immediately followed by taking blood, urine and tissue (i.e., tumor, kidney, liver, gall bladder, spleen, small intestine, heart, lung, brain, pancreas, femur and muscle) samples. Radioactivity measurement of the samples was performed with the Canberra Genie 2000 system described for the determination of the distribution coefficient $logD_{7.4}$. Decay-corrected measured activities (cpm) were converted into activities (MBq) on the basis of an activity measurement with a ^{68}Ge-calibration standard source (Eckert&Ziegler, Berlin, Germany). Sample activities were converted to percentage of injected dose per gram tissue (%ID/g). Blocking experiments were performed by co-injection of the tracer with NTS_1R ligand **4.48** (ca. 700 nmol per mouse). Mice were killed 45 min p.i. and analyzed as

described above. The animals used for the 45-min biodistribution experiments were the same as used for the PET/CT imaging studies.

4.4.7.6 HPLC analysis of urine from mice injected with [^{68}Ga]4.21, [^{68}Ga]4.33, [^{68}Ga]4.37 or [^{68}Ga]4.56

The analysis was performed with the urine obtained from biodistribution and PET imaging studies, respectively (t = 10 or 45 min). The urine was diluted with H_2O (1:2-1:100 depending on the activity in the urine) and 10-80 µL of this solution were subjected to analysis by analytical HPLC using the same HPLC system and conditions as described for the quality controls of the PET ligands. To confirm the identity of [^{68}Ga]**4.56** in the 45-min urine samples, an additional analysis was performed, using the aforementioned injection solution spiked with 100 µM **4.56**. Representative chromatograms of the HPLC analysis of the urine samples are shown in Figures A4.9-A4.11 (Appendix).

4.4.7.7 HPLC analysis of blood plasma from mice injected with [^{68}Ga]4.56

This analysis was performed with the blood obtained from biodistribution studies with [^{68}Ga]**4.56** (t = 10 min). Blood (ca. 200 µL) was taken from the heart using a syringe that was rinsed with sodium heparin (25000 I.E., Ratiopharm, Ulm, Germany). The heparinized blood was transferred into a 1.5-mL reaction vessel immediately followed by centrifugation (1,200 × g, 4 °C, 5 min) using a Biofuge fresco centrifuge (Heraeus, Hanau, Germany). The supernatant (ca. 100 µL) was treated with the same volume of 10% aq TFA (precipitation of proteins) and the mixture was centrifuged (16,100 × g, 4 °C, 10 min). The supernatant (70-100 µL) was subjected to analysis by analytical HPLC using the same HPLC system and conditions as described for the quality control of the PET ligand. To confirm the identity of [^{68}Ga]**4.56** in the plasma samples, an additional analysis was performed, using the aforementioned injection solution spiked with 100 µM **4.56**. Representative chromatograms of the HPLC analysis of the plasma samples are shown in Figure A4.11C-E (Appendix).

4.4.7.8 Determination of the internalization of [^{68}Ga]4.56 in HT-29 tumor cells

HT-29 cells were seeded in 24-well TC plates (Sarstedt, catalog no. 83.3922) one day prior to the experiment at a density of 4.5×10^5 cells/well. Shortly before the experiment, the culture medium was removed and the cells were washed once with PBS (500 µL, rt) followed by pre-filling of the wells with 250 µL of binding buffer (see procedure for NTS_2R binding studies). For the determination of unspecific binding, the binding buffer was supplemented with **2.01** (2 µM). 50 µL aliquots of the [^{68}Ga]**4.56** stock in PBS (1.5-2.8 MBq) were added to the wells, and the cells were incubated at 37 °C for 5, 10, 15, 25, 35, 55, or 75 min under gentle shaking. After completed incubation, the plates were immediately placed on ice, the liquid was removed by suction and the cells were washed twice with ice-cold PBS (500 µL). The cells were washed twice with ice-cold acid strip buffer (50 mM glycine and 125 mM NaCl in H_2O, pH 3.0) (300 µL) for 5 min each, and the washings were combined in 5-mL polypropylene tubes. The cells were then lysed by the addition of lysis solution (see procedure for NTS_2R binding studies) (250 µL) and shaken at 37 °C for 15 min. The lysates were transferred into 5-mL polypropylene tubes, the wells were washed with lysis solution (250 µL) and the washings were combined with the lysates. The activities were measured with the Canberra Genie 2000 system as described for the determination of the distribution coefficient $logD_{7.4}$. The decay-corrected cpm values of

unspecific binding were subtracted from the decay-corrected cpm values of total binding to obtain specific binding data for both surface-bound [^{68}Ga]**4.56** (acid strip) and internalized [^{68}Ga]**4.56** (cell lysate). The amount of internalized specific binding was normalized based on total specific binding, and the mean values from two independent experiments (each performed in triplicate) were plotted against the incubation time.

4.4.7.9 PET/CT imaging with [^{68}Ga]4.56

PET/computed tomography (CT) imaging was performed using an EARL-certified clinical PET/CT scanner (Biograph mCT-S(40) with TrueV and Flow-4R technology, Siemens Healthcare, Erlangen, Germany) exhibiting, at 1 cm off-center, a spatial resolution for ^{18}F of 4.1 mm in transversal and 4.7 mm in axial direction according to the NEMA NU2-2007 standard[85]. This PET/CT scanner is capable of obtaining PET images in small animal experiments with reported recovery coefficients from NEMA NU 4 phantom measurements of 0.21, 0.59, and 1.16 in rods with a diameter of 2, 3, and 4 mm, respectively[76]. After positioning the animal, topograms were acquired (70 kVp, 60 mA, slice 0.6 mm, manually terminated craniocaudal movement) with tube position at bottom and lateral for anteroposterior and lateral view, respectively. A CT scan (70 kVp, 140 mA) was performed without dose reduction (CARE Dose 4D and CARE kV off) with the minimal slice scanning thickness of 0.6 mm (40 × 0.6 mm) with a pitch of 0.35 and a rotation time of 0.5 s resulting in a typical acquisition time of about 27 s. For attenuation correction of the PET data acquisition, axial CT images were reconstructed with the full field of view (FoV) of 780 mm by the FAST reconstruction algorithm using the "B30f medium smooth" kernel with an increment of 0.6 mm, typically resulting in 369 images. For visual analysis, axial CT images were reconstructed with a reduced FoV of 100 mm by the SAFIRE reconstruction algorithm (strength = 3) by the "I49f medium" kernel with an increment of 0.3 mm, typically resulting in 737 images. For PET data acquisition, the animal bed was positioned in the center of the PET detector. Simultaneously with the injection of the tracer, a dynamic PET scan (list mode for 45 min in a single bed position) was started.

4.4.7.10 Tracer administration

Aliquots of the tracer stock of [^{68}Ga]**4.56** were diluted in PBS to give a volume of 200 µL. 80-100 µL of this solution (3.2-5.9 MBq per mouse) were injected into the tail vein of anesthetized HT-29 tumor-bearing nude mice placed in the scanner. During the PET scan, mice were kept on a pre-warmed (approximately 45 °C) gel pad. Immediately after the PET scan, mice were killed followed by taking blood, urine, tumor tissue and organ tissues. Blocking experiments were carried out by co-injection of the tracer with **4.48** (ca. 700 nmol per mouse).

4.4.7.11 Imaging analysis

For dynamic analysis of the PET images, list mode data were replayed according to the following frame scheme: 6 × 10 s, 4 × 30 s, 1 × 2 min, 4 × 5 min, 2 × 10 min. All PET scans were corrected for normalization, detector dead time, attenuation, scatter, decay, random coincidences and prompt gamma coincidences. Attenuation corrected PET images (512 × 512 pixels, pixel size 0.40 mm, slice thickness 2.03 mm) were reconstructed by iterative reconstruction (8 iterations, 24 subsets, point spread function modelling) with a Gaussian post reconstruction filter with 1.0 mm full width at half maximum (FWHM). Additionally, static frames from 5 min to 10 min and for the entire acquisition of 45 min were

reconstructed (512 × 512 pixels, pixel size 0.40 mm, slice thickness 0.6 mm) from the list mode data. By means of static recording over the complete acquisition period, possible movements of the mouse could be excluded. For determination of the tracer uptake in tumors and kidneys corresponding regions of interest (ROIs) were generated using a fixed threshold of 45% of the maximum tracer accumulation for tumors and 40% of the maximum tracer accumulation for kidneys. The resulting delineations were inspected visually and corrected manually if necessary. Manual correction was performed for all tumors in mice used for blocking experiments which exhibited only low diffuse tracer accumulation. For determination of the tracer uptake in the muscles, a ROI was delineated manually in the left femoral muscles observing a volume of approximately 0.05 mL. The ROIs were transferred to all time frames of the respective dynamic study. Time-activity-curves (TACs) were generated by computing the mean standardized uptake value normalized to body weight (SUV_{mean}) in each frame. ROI definition and ROI analyses were performed using the ROVER software, version 3.0.64 (ABX GmbH, Radeberg, Germany).

4.5 References

1. Bugni, J.M.; Pothoulakis, C. Neurotensin. In *Handbook of biologically active peptides (section XIII: gastrointestinal peptides)*, 2nd ed.; Kastin, A.J., Ed.; Academic press: 2013; pp. 1265-1270.
2. St-Gelais, F.; Jomphe, C.; Trudeau, L.E. The role of neurotensin in central nervous system pathophysiology: What is the evidence? *J Psychiatr Neurosci* **2006**, *31*, 229-245.
3. Mazella, J.; Vincent, J.P. Functional roles of the NTS2 and NTS3 receptors. *Peptides* **2006**, *27*, 2469-2475, doi:10.1016/j.peptides.2006.04.026.
4. Boules, M.; Li, Z.; Smith, K.; Fredrickson, P.; Richelson, E. Diverse roles of neurotensin agonists in the central nervous system. *Front Endocrinol (Lausanne)* **2013**, *4*, 36, doi:10.3389/fendo.2013.00036.
5. Xiao, Z.Y.; Cilz, N.I.; Kurada, L.; Hu, B.Q.; Yang, C.X.; Wada, E.; Combs, C.K.; Porter, J.E.; Lesage, F.; Lei, S.B. Activation of neurotensin receptor 1 facilitates neuronal excitability and spatial learning and memory in the entorhinal cortex: Beneficial actions in an Alzheimer's disease model. *J Neurosci* **2014**, *34*, 7027-7042, doi:10.1523/Jneurosci.0408-14.2014.
6. Schroeder, L.E.; Leinninger, G.M. Role of central neurotensin in regulating feeding: Implications for the development and treatment of body weight disorders. *Bba-Mol Basis Dis* **2018**, *1864*, 900-916, doi:10.1016/j.bbadis.2017.12.036.
7. Sarret, P.; Cavelier, F. Neurotensin and its receptors. In *Reference Module in Neuroscience and Biobehavioral Psychology*; Elsevier: Amsterdam, the Netherlands, 2017.
8. Maoret, J.J.; Pospai, D.; Rouyer-Fessard, C.; Couvineau, A.; Laboisse, C.; Voisin, T.; Laburthe, M. Neurotensin receptor and its mRNA are expressed in many human colon cancer cell lines but not in normal colonic epithelium: Binding studies and RT-PCR experiments. *Biochem Biophys Res Commun* **1994**, *203*, 465-471, doi:10.1006/bbrc.1994.2205.
9. Reubi, J.C.; Waser, B.; Friess, H.; Büchler, M.; Laissue, J. Neurotensin receptors: A new marker for human ductal pancreatic adenocarcinoma. *Gut* **1998**, *42*, 546-550, doi:10.1136/gut.42.4.546.
10. Souazé, F.; Dupouy, S.; Viardot-Foucault, V.; Bruyneel, E.; Attoub, S.; Gespach, C.; Gompel, A.; Forgez, P. Expression of neurotensin and NT1 receptor in human breast cancer: A potential role in tumor progression. *Cancer Res* **2006**, *66*, 6243-6249, doi:10.1158/0008-5472.CAN-06-0450.
11. Carraway, R.; Leeman, S.E. The amino acid sequence of a hypothalamic peptide, neurotensin. *J Biol Chem* **1975**, *250*, 1907-1911.
12. Tyler, B.M.; Douglas, C.L.; Fauq, A.; Pang, Y.P.; Stewart, J.A.; Cusack, B.; McCormick, D.J.; Richelson, E. In vitro binding and CNS effects of novel neurotensin agonists that cross the blood-brain barrier. *Neuropharmacology* **1999**, *38*, 1027-1034, doi:10.1016/s0028-3908(99)00011-8.

13. Vincent, J.P.; Mazella, J.; Kitabgi, P. Neurotensin and neurotensin receptors. *Trends Pharmacol Sci* **1999**, *20*, 302-309, doi:10.1016/s0165-6147(99)01357-7.

14. Bergmann, R.; Scheunemann, M.; Heichert, C.; Mäding, P.; Wittrisch, H.; Kretzschmar, M.; Rodig, H.; Tourwé, D.; Iterbeke, K.; Chavatte, K.; et al. Biodistribution and catabolism of ^{18}F-labeled neurotensin(8-13) analogs. *Nucl Med Biol* **2002**, *29*, 61-72, doi:10.1016/s0969-8051(01)00284-0.

15. García-Garayoa, E.; Bläuenstein, P.; Blanc, A.; Maes, V.; Tourwé, D.; Schubiger, P.A. A stable neurotensin-based radiopharmaceutical for targeted imaging and therapy of neurotensin receptor-positive tumours. *Eur J Nucl Med Mol Imaging* **2009**, *36*, 37-47, doi:10.1007/s00259-008-0894-y.

16. Maschauer, S.; Einsiedel, J.; Hocke, C.; Hübner, H.; Kuwert, T.; Gmeiner, P.; Prante, O. Synthesis of a ^{68}Ga-labeled peptoid-peptide hybrid for imaging of neurotensin receptor expression in vivo. *ACS Med Chem Lett* **2010**, *1*, 224-228, doi:10.1021/ml1000728.

17. Maschauer, S.; Einsiedel, J.; Haubner, R.; Hocke, C.; Ocker, M.; Hübner, H.; Kuwert, T.; Gmeiner, P.; Prante, O. Labeling and glycosylation of peptides using click chemistry: A general approach to ^{18}F-glycopeptides as effective imaging probes for positron emission tomography. *Angew Chem Int Ed Engl* **2010**, *49*, 976-979, doi:10.1002/anie.200904137.

18. Maschauer, S.; Ruckdeschel, T.; Tripal, P.; Haubner, R.; Einsiedel, J.; Hübner, H.; Gmeiner, P.; Kuwert, T.; Prante, O. *In vivo* monitoring of the antiangiogenic effect of neurotensin receptor-mediated radiotherapy by small-animal positron emission tomography: A pilot study. *Pharmaceuticals (Basel)* **2014**, *7*, 464-481, doi:10.3390/ph7040464.

19. Jia, Y.; Shi, W.; Zhou, Z.; Wagh, N.K.; Fan, W.; Brusnahan, S.K.; Garrison, J.C. Evaluation of DOTA-chelated neurotensin analogs with spacer-enhanced biological performance for neurotensin-receptor-1-positive tumor targeting. *Nucl Med Biol* **2015**, *42*, 816-823, doi:10.1016/j.nucmedbio.2015.07.010.

20. Deng, H.; Wang, H.; Zhang, H.; Wang, M.; Giglio, B.; Ma, X.; Jiang, G.; Yuan, H.; Wu, Z.; Li, Z. Imaging neurotensin receptor in prostate cancer with ^{64}Cu-labeled neurotensin analogs. *Mol Imaging* **2017**, *16*, 1-11, doi:10.1177/1536012117711369.

21. Mankoff, D.A.; Link, J.M.; Linden, H.M.; Sundararajan, L.; Krohn, K.A. Tumor receptor imaging. *J Nucl Med* **2008**, *49 Suppl 2*, 149S-163S, doi:10.2967/jnumed.107.045963.

22. Correia, J.D.; Paulo, A.; Raposinho, P.D.; Santos, I. Radiometallated peptides for molecular imaging and targeted therapy. *Dalton Trans* **2011**, *40*, 6144-6167, doi:10.1039/c0dt01599g.

23. Fani, M.; Maecke, H.R. Radiopharmaceutical development of radiolabelled peptides. *Eur J Nucl Med Mol Imaging* **2012**, *39 Suppl 1*, 11-30, doi:10.1007/s00259-011-2001-z.

24. Morgat, C.; Mishra, A.K.; Varshney, R.; Allard, M.; Fernandez, P.; Hindié, E. Targeting neuropeptide receptors for cancer imaging and therapy: Perspectives

with bombesin, neurotensin, and neuropeptide-Y receptors. *J Nucl Med* **2014**, *55*, 1650-1657, doi:10.2967/jnumed.114.142000.

25. Hofman, M.S.; Lau, W.F.; Hicks, R.J. Somatostatin receptor imaging with ^{68}Ga DOTATATE PET/CT: Clinical utility, normal patterns, pearls, and pitfalls in interpretation. *Radiographics* **2015**, *35*, 500-516, doi:10.1148/rg.352140164.

26. Maschauer, S.; Prante, O. Radiopharmaceuticals for imaging and endoradiotherapy of neurotensin receptor-positive tumors. *J Labelled Comp Radiopharm* **2018**, *61*, 309-325, doi:10.1002/jlcr.3581.

27. Desai, H.; Borges-Neto, S.; Wong, T.Z. Molecular imaging and therapy for neuroendocrine tumors. *Curr Treat Options Oncol* **2019**, *20*, 78, doi:10.1007/s11864-019-0678-6.

28. Damuka, N.; Solingapuram Sai, K.K. Method to development of PET radiopharmaceutical for cancer imaging. In *Cancer Biomarkers*, 1st ed.; Deep, G., Ed.; Humana: New York, NY, 2022; Volume 2413, pp. 13-22.

29. Richter, S.; Wuest, F. ^{18}F-Labeled peptides: The future is bright. *Molecules* **2014**, *19*, 20536-20556, doi:10.3390/molecules191220536.

30. Kumar, K.; Ghosh, A. ^{18}F-AlF Labeled peptide and protein conjugates as positron emission tomography imaging pharmaceuticals. *Bioconjug Chem* **2018**, *29*, 953-975, doi:10.1021/acs.bioconjchem.7b00817.

31. Schottelius, M.; Wester, H.J. Molecular imaging targeting peptide receptors. *Methods* **2009**, *48*, 161-177, doi:10.1016/j.ymeth.2009.03.012.

32. Lee, S.; Xie, J.; Chen, X. Peptide-based probes for targeted molecular imaging. *Biochemistry* **2010**, *49*, 1364-1376, doi:10.1021/bi901135x.

33. Fani, M.; Maecke, H.R.; Okarvi, S.M. Radiolabeled peptides: Valuable tools for the detection and treatment of cancer. *Theranostics* **2012**, *2*, 481-501, doi:10.7150/thno.4024.

34. Werle, M.; Bernkop-Schnürch, A. Strategies to improve plasma half life time of peptide and protein drugs. *Amino Acids* **2006**, *30*, 351-367, doi:10.1007/s00726-005-0289-3.

35. Lang, C.; Maschauer, S.; Hübner, H.; Gmeiner, P.; Prante, O. Synthesis and evaluation of a ^{18}F-labeled diarylpyrazole glycoconjugate for the imaging of NTS1-positive tumors. *J Med Chem* **2013**, *56*, 9361-9365, doi:10.1021/jm401491e.

36. Schulz, J.; Rohracker, M.; Stiebler, M.; Goldschmidt, J.; Grosser, O.S.; Osterkamp, F.; Pethe, A.; Reineke, U.; Smerling, C.; Amthauer, H. Comparative evaluation of the biodistribution profiles of a series of nonpeptidic neurotensin receptor-1 antagonists reveals a promising candidate for theranostic applications. *J Nucl Med* **2016**, *57*, 1120-1123, doi:10.2967/jnumed.115.170530.

37. Renard, E.; Moreau, M.; Bellaye, P.S.; Guillemin, M.; Collin, B.; Prignon, A.; Denat, F.; Goncalves, V. Positron emission tomography imaging of neurotensin receptor-positive tumors with ^{68}Ga-labeled antagonists: The chelate makes the difference again. *J Med Chem* **2021**, *64*, 8564-8578, doi:10.1021/acs.jmedchem.1c00523.

38. Fanelli, R.; Chastel, A.; Previti, S.; Hindié, E.; Vimont, D.; Zanotti-Fregonara, P.; Fernandez, P.; Garrigue, P.; Lamare, F.; Schollhammer, R.; et al. Silicon-containing neurotensin analogues as radiopharmaceuticals for NTS_1-positive tumors imaging. *Bioconjugate Chem* **2020**, *31*, 2339-2349, doi:10.1021/acs.bioconjchem.0c00419.

39. Keller, M.; Kuhn, K.K.; Einsiedel, J.; Hübner, H.; Biselli, S.; Mollereau, C.; Wifling, D.; Svobodová, J.; Bernhardt, G.; Cabrele, C.; et al. Mimicking of arginine by functionalized N^{ω}-carbamoylated arginine as a new broadly applicable approach to labeled bioactive peptides: High affinity angiotensin, neuropeptide Y, neuropeptide FF, and neurotensin receptor ligands as examples. *J Med Chem* **2016**, *59*, 1925-1945, doi:10.1021/acs.jmedchem.5b01495.

40. Schindler, L.; Bernhardt, G.; Keller, M. Modifications at Arg and Ile give neurotensin(8-13) derivatives with high stability and retained NTS_1 receptor affinity. *ACS Med Chem Lett* **2019**, *10*, 960-965, doi:10.1021/acsmedchemlett.9b00122.

41. Alshoukr, F.; Prignon, A.; Brans, L.; Jallane, A.; Mendes, S.; Talbot, J.N.; Tourwé, D.; Barbet, J.; Gruaz-Guyon, A. Novel DOTA-neurotensin analogues for ^{111}In scintigraphy and ^{68}Ga PET imaging of neurotensin receptor-positive tumors. *Bioconjug Chem* **2011**, *22*, 1374-1385, doi:10.1021/bc200078p.

42. Maschauer, S.; Einsiedel, J.; Hübner, H.; Gmeiner, P.; Prante, O. ^{18}F- and ^{68}Ga-labeled neurotensin peptides for PET imaging of neurotensin receptor 1. *J Med Chem* **2016**, *59*, 6480-6492, doi:10.1021/acs.jmedchem.6b00675.

43. García-Garayoa, E.; Allemann-Tannahill, L.; Bläuenstein, P.; Willmann, M.; Carrel-Rémy, N.; Tourwé, D.; Iterbeke, K.; Conrath, P.; Schubiger, P.A. *In vitro* and *in vivo* evaluation of new radiolabeled neurotensin(8-13) analogues with high affinity for NT1 receptors. *Nucl Med Biol* **2001**, *28*, 75-84, doi:10.1016/s0969-8051(00)00190-6.

44. Mascarin, A.; Valverde, I.E.; Vomstein, S.; Mindt, T.L. 1,2,3-Triazole stabilized neurotensin-based radiopeptidomimetics for improved tumor targeting. *Bioconjugate Chem* **2015**, *26*, 2143-2152, doi:10.1021/acs.bioconjchem.5b00444.

45. Tyler-McMahon, B.M.; Stewart, J.A.; Farinas, F.; McCormick, D.J.; Richelson, E. Highly potent neurotensin analog that causes hypothermia and antinociception. *Eur J Pharmacol* **2000**, *390*, 107-111, doi:10.1016/s0014-2999(99)00877-8.

46. Bruehlmeier, M.; García-Garayoa, E.; Blanc, A.; Holzer, B.; Gergely, S.; Tourwé, D.; Schubiger, P.A.; Bläuenstein, P. Stabilization of neurotensin analogues: Effect on peptide catabolism, biodistribution and tumor binding. *Nucl Med Biol* **2002**, *29*, 321-327, doi:10.1016/s0969-8051(01)00304-3.

47. García-Garayoa, E.; Bläuenstein, P.; Bruehlmeier, M.; Blanc, A.; Iterbeke, K.; Conrath, P.; Tourwé, D.; Schubiger, P.A. Preclinical evaluation of a new, stabilized neurotensin(8-13) pseudopeptide radiolabeled with ^{99m}Tc. *J Nucl Med* **2002**, *43*, 374-383.

48. Bläuenstein, P.; García-Garayoa, E.; Rüegg, D.; Blanc, A.; Tourwé, D.; Beck-Sickinger, A.; Schubiger, P.A. Improving the tumor uptake of ^{99m}Tc-labeled

neuropeptides using stabilized peptide analogues. *Cancer Biother Radiopharm* **2004**, *19*, 181-188, doi:10.1089/108497804323071959.

49. Maes, V.; García-Garayoa, E.; Bläuenstein, P.; Tourwé, D. Novel ^{99m}Tc-labeled neurotensin analogues with optimized biodistribution properties. *J Med Chem* **2006**, *49*, 1833-1836, doi:10.1021/jm051172f.

50. Nock, B.A.; Nikolopoulou, A.; Reubi, J.C.; Maes, V.; Conrath, P.; Tourwé, D.; Maina, T. Toward stable N_4-modified neurotensins for NTS1-receptor-targeted tumor imaging with ^{99m}Tc. *J Med Chem* **2006**, *49*, 4767-4776, doi:10.1021/jm060415g.

51. Maina, T.; Nikolopoulou, A.; Stathopoulou, E.; Galanis, A.S.; Cordopatis, P.; Nock, B.A. [^{99m}Tc]Demotensin 5 and 6 in the NTS1-R-targeted imaging of tumours: Synthesis and preclinical results. *Eur J Nucl Med Mol Imaging* **2007**, *34*, 1804-1814, doi:10.1007/s00259-007-0489-z.

52. Alshoukr, F.; Rosant, C.; Maes, V.; Abdelhak, J.; Raguin, O.; Burg, S.; Sarda, L.; Barbet, J.; Tourwé, D.; Pelaprat, D.; et al. Novel neurotensin analogues for radioisotope targeting to neurotensin receptor-positive tumors. *Bioconjug Chem* **2009**, *20*, 1602-1610, doi:10.1021/bc900151z.

53. Boules, M.; Liang, Y.; Briody, S.; Miura, T.; Fauq, I.; Oliveros, A.; Wilson, M.; Khaniyev, S.; Williams, K.; Li, Z.; et al. NT79: A novel neurotensin analog with selective behavioral effects. *Brain Res* **2010**, *1308*, 35-46, doi:10.1016/j.brainres.2009.10.050.

54. Mascarin, A.; Valverde, I.E.; Mindt, T.L. Structure-activity relationship studies of amino acid substitutions in radiolabeled neurotensin conjugates. *ChemMedChem* **2016**, *11*, 102-107, doi:10.1002/cmdc.201500468.

55. Chavatte, K.; Terriere, D.; Jeannin, L.; Iterbeke, K.; Briejer, M.; Schuurkes, J.; Mertens, J.J.R.; Bruyneel, E.; Tourwé, D.; Leysen, J.E.; et al. Labelling and evaluation of new stabilised neurotensin (8-13) analogues for single photon emission tomography (SPET). *J Labelled Comp Radiopharm* **1999**, *42*, 423-435, doi:10.1002/(Sici)1099-1344(199905)42:5<423::Aid-Jlcr201>3.0.Co;2-S.

56. De León-Rodriguez, L.M.; Kovacs, Z.; Dieckmann, G.R.; Sherry, A.D. Solid-phase synthesis of DOTA-peptides. *Chem Eur J* **2004**, *10*, 1149-1155, doi:10.1002/chem.200305389.

57. Guérin, B.; Ait-Mohand, S.; Tremblay, M.C.; Dumulon-Perreault, V.; Fournier, P.; Bénard, F. Total solid-phase synthesis of NOTA-functionalized peptides for PET imaging. *Org Lett* **2010**, *12*, 280-283, doi:10.1021/ol902601x.

58. Kuhn, K.K.; Ertl, T.; Dukorn, S.; Keller, M.; Bernhardt, G.; Reiser, O.; Buschauer, A. High affinity agonists of the neuropeptide Y (NPY) Y_4 receptor derived from the C-terminal pentapeptide of human pancreatic polypeptide (hPP): Synthesis, stereochemical discrimination, and radiolabeling. *J Med Chem* **2016**, *59*, 6045-6058, doi:10.1021/acs.jmedchem.6b00309.

59. Keller, M.; Mahuroof, S.A.; Hong Yee, V.; Carpenter, J.; Schindler, L.; Littmann, T.; Pegoli, A.; Hübner, H.; Bernhardt, G.; Gmeiner, P.; et al. Fluorescence labeling of neurotensin(8-13) via arginine residues gives molecular tools with high receptor

affinity. *ACS Med Chem Lett* **2020**, *11*, 16-22, doi:10.1021/acsmedchemlett.9b00462.

60. Schindler, L.; Wohlfahrt, K.; Gluhacevic von Krüchten, L.; Prante, O.; Keller, M.; Maschauer, S. Neurotensin analogs by fluoroglycosylation at N^{ω}-carbamoylated arginines for PET imaging of NTS1-positive tumors. *Sci Rep* **2022**, *12*, 15028, doi:10.1038/s41598-022-19296-0.

61. Miller, S.C.; Scanlan, T.S. Site-selective N-methylation of peptides on solid support. *J Am Chem Soc* **1997**, *119*, 2301-2302, doi:10.1021/ja9635443.

62. Müller, C.; Gleixner, J.; Tahk, M.J.; Kopanchuk, S.; Laasfeld, T.; Weinhart, M.; Schollmeyer, D.; Betschart, M.U.; Lüdeke, S.; Koch, P.; et al. Structure-based design of high-affinity fluorescent probes for the neuropeptide Y Y_1 receptor. *J Med Chem* **2022**, *65*, 4832-4853, doi:10.1021/acs.jmedchem.1c02033.

63. Khatun, U.L.; Goswami, S.K.; Mukhopadhyay, C. Modulation of the neurotensin solution structure in the presence of ganglioside GM1 bicelle. *Biophys Chem* **2012**, *168-169*, 48-59, doi:10.1016/j.bpc.2012.06.003.

64. Vita, N.; Laurent, P.; Lefort, S.; Chalon, P.; Dumont, X.; Kaghad, M.; Gully, D.; Le Fur, G.; Ferrara, P.; Caput, D. Cloning and expression of a complementary DNA encoding a high affinity human neurotensin receptor. *FEBS Lett* **1993**, *317*, 139-142, doi:10.1016/0014-5793(93)81509-x.

65. Kokko, K.P.; Hadden, M.K.; Orwig, K.S.; Mazella, J.; Dix, T.A. In vitro analysis of stable, receptor-selective neurotensin[8-13] analogues. *J Med Chem* **2003**, *46*, 4141-4148, doi:10.1021/jm0300633.

66. Richelson, E.; McCormick, D.J.; Pang, Y.P.; Phillips, K.S. Peptide analogs that are potent and selective for human neurotensin receptor subtype 2. US2009/0062212A1, March 5 2009.

67. Cusack, B.; McCormick, D.J.; Pang, Y.P.; Souder, T.; Garcia, R.; Fauq, A.; Richelson, E. Pharmacological and biochemical profiles of unique neurotensin 8-13 analogs exhibiting species selectivity, stereoselectivity, and superagonism. *J Biol Chem* **1995**, *270*, 18359-18366, doi:10.1074/jbc.270.31.18359.

68. Barroso, S.; Richard, F.; Nicolas-Ethève, D.; Reversat, J.L.; Bernassau, J.M.; Kitabgi, P.; Labbé-Jullié, C. Identification of residues involved in neurotensin binding and modeling of the agonist binding site in neurotensin receptor 1. *J Biol Chem* **2000**, *275*, 328-336, doi:10.1074/jbc.275.1.328.

69. Pang, Y.P.; Cusack, B.; Groshan, K.; Richelson, E. Proposed ligand binding site of the transmembrane receptor for neurotensin(8-13). *J Biol Chem* **1996**, *271*, 15060-15068, doi:10.1074/jbc.271.25.15060.

70. Härterich, S.; Koschatzky, S.; Einsiedel, J.; Gmeiner, P. Novel insights into GPCR-peptide interactions: Mutations in extracellular loop 1, ligand backbone methylations and molecular modeling of neurotensin receptor 1. *Bioorg Med Chem* **2008**, *16*, 9359-9368, doi:10.1016/j.bmc.2008.08.051.

71. Einsiedel, J.; Held, C.; Hervet, M.; Plomer, M.; Tschammer, N.; Hübner, H.; Gmeiner, P. Discovery of highly potent and neurotensin receptor 2 selective neurotensin mimetics. *J Med Chem* **2011**, *54*, 2915-2923, doi:10.1021/jm200006c.

72. Eiselt, E.; Gonzalez, S.; Martin, C.; Chartier, M.; Betti, C.; Longpré, J.M.; Cavelier, F.; Tourwé, D.; Gendron, L.; Ballet, S.; et al. Neurotensin analogues containing cyclic surrogates of tyrosine at position 11 improve NTS2 selectivity leading to analgesia without hypotension and hypothermia. *ACS Chem Neurosci* **2019**, *10*, 4535-4544, doi:10.1021/acschemneuro.9b00390.

73. Chalon, P.; Vita, N.; Kaghad, M.; Guillemot, M.; Bonnin, J.; Delpech, B.; Le Fur, G.; Ferrara, P.; Caput, D. Molecular cloning of a levocabastine-sensitive neurotensin binding site. *FEBS Lett* **1996**, *386*, 91-94, doi:10.1016/0014-5793(96)00397-3.

74. Mazella, J.; Botto, J.M.; Guillemare, E.; Coppola, T.; Sarret, P.; Vincent, J.P. Structure, functional expression, and cerebral localization of the levocabastine-sensitive neurotensin/neuromedin N receptor from mouse brain. *J Neurosci* **1996**, *16*, 5613-5620.

75. Vita, N.; Oury-Donat, F.; Chalon, P.; Guillemot, M.; Kaghad, M.; Bachy, A.; Thurneyssen, O.; Garcia, S.; Poinot-Chazel, C.; Casellas, P.; et al. Neurotensin is an antagonist of the human neurotensin NT_2 receptor expressed in Chinese hamster ovary cells. *Eur J Pharmacol* **1998**, *360*, 265-272, doi:10.1016/s0014-2999(98)00678-5.

76. DiFilippo, F.P.; Patel, S.; Asosingh, K.; Erzurum, S.C. Small-animal imaging using clinical positron emission tomography/computed tomography and super-resolution. *Mol Imaging* **2012**, *11*, 210-219.

77. Kayed, H.; Meyer, P.; He, Y.; Kraenzlin, B.; Fink, C.; Gretz, N.; Schoenberg, S.O.; Sadick, M. Evaluation of the metabolic response to cyclopamine therapy in pancreatic cancer xenografts using a clinical PET-CT system. *Transl Oncol* **2012**, *5*, 335-343, doi:10.1593/tlo.12166.

78. Fani, M.; Del Pozzo, L.; Abiraj, K.; Mansi, R.; Tamma, M.L.; Cescato, R.; Waser, B.; Weber, W.A.; Reubi, J.C.; Maecke, H.R. PET of somatostatin receptor-positive tumors using ^{64}Cu- and ^{68}Ga-somatostatin antagonists: The chelate makes the difference. *J Nucl Med* **2011**, *52*, 1110-1118, doi:10.2967/jnumed.111.087999.

79. Schulz, J.; Rohracker, M.; Stiebler, M.; Goldschmidt, J.; Stöber, F.; Noriega, M.; Pethe, A.; Lukas, M.; Osterkamp, F.; Reineke, U.; et al. Proof of therapeutic efficacy of a ^{177}Lu-labeled neurotensin receptor 1 antagonist in a colon carcinoma xenograft model. *J Nucl Med* **2017**, *58*, 936-941, doi:10.2967/jnumed.116.185140.

80. Osterkamp, F.; Smerling, C.; Reineke, U.; Haase, C.; Ungewiss, J. Neurotensin receptor ligands. US10961199B2, March 30 2021.

81. Baum, R.P.; Singh, A.; Schuchardt, C.; Kulkarni, H.R.; Klette, I.; Wiessalla, S.; Osterkamp, F.; Reineke, U.; Smerling, C. ^{177}Lu-3BP-227 for neurotensin receptor 1-targeted therapy of metastatic pancreatic adenocarcinoma - first clinical results. *J Nucl Med* **2018**, *59*, 809-814, doi:10.2967/jnumed.117.193847.

82. Grätz, L.; Laasfeld, T.; Allikalt, A.; Gruber, C.G.; Pegoli, A.; Tahk, M.J.; Tsernant, M.L.; Keller, M.; Rinken, A. BRET- and fluorescence anisotropy-based assays for real-time monitoring of ligand binding to M_2 muscarinic acetylcholine receptors. *Biochim Biophys Acta Mol Cell Res* **2021**, *1868*, 118930, doi:10.1016/j.bbamcr.2020.118930.

83. Cheng, Y.; Prusoff, W.H. Relationship between the inhibition constant (K_I) and the concentration of inhibitor which causes 50 per cent inhibition (I_{50}) of an enzymatic reaction. *Biochem Pharmacol* **1973**, *22*, 3099-3108, doi:10.1016/0006-2952(73)90196-2.

84. Müller, M.; Knieps, S.; Gessele, K.; Dove, S.; Bernhardt, G.; Buschauer, A. Synthesis and neuropeptide Y Y1 receptor antagonistic activity of *N*,*N*-disubstituted omega-guanidino- and omega-aminoalkanoic acid amides. *Arch Pharm (Weinheim)* **1997**, *330*, 333-342, doi:10.1002/ardp.19973301104.

85. Jakoby, B.W.; Bercier, Y.; Conti, M.; Casey, M.E.; Bendriem, B.; Townsend, D.W. Physical and clinical performance of the mCT time-of-flight PET/CT scanner. *Phys Med Biol* **2011**, *56*, 2375-2389, doi:10.1088/0031-9155/56/8/004.

4.6 Appendix

4.6.1 Figures A4.1-A4.11 and Tables A4.1-A4.4

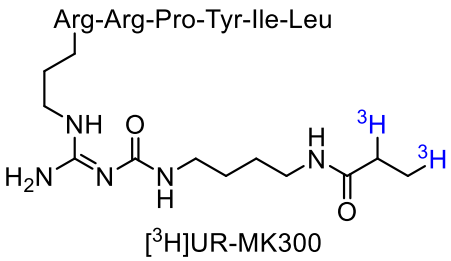

Figure A4.1. Structure of the tritium-labeled NT(8-13)-derived radioligand [^{3}H]UR-MK300 used for NTS$_1$R and NTS$_2$R binding studies[1].

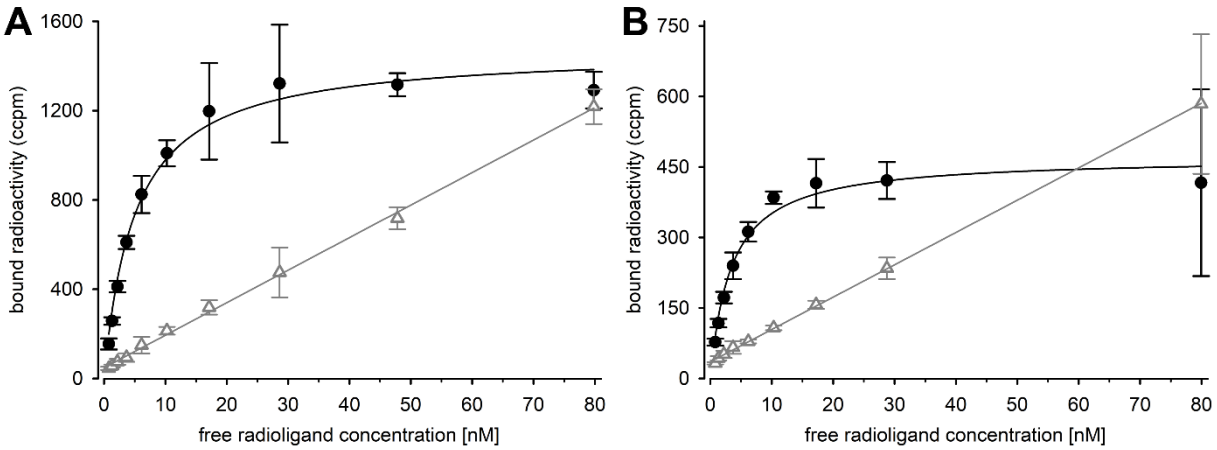

Figure A4.2. Representative saturation isotherms and unspecific binding curves from experiments with two batches of [^{3}H]UR-MK300 at HEK293T-hNTS$_2$R cells, giving K_d values of (A) 6.9 ± 1.8 nM (mean value ± SD from six independent determinations, each performed in triplicate) and (B) 4.0 ± 1.5 nM (mean value ± SD from three independent determinations, each performed in triplicate).

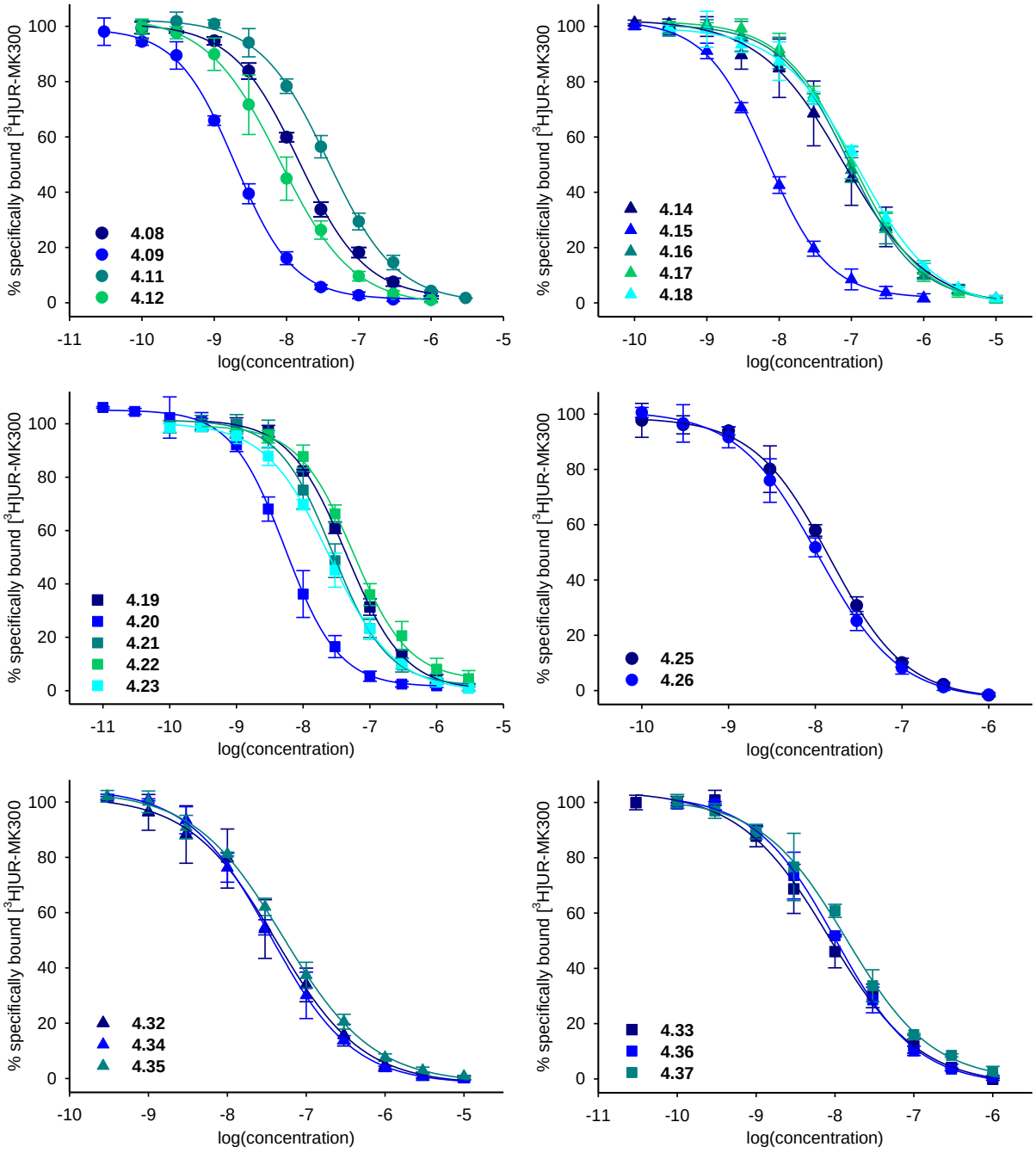

Figure A4.3. Radioligand displacement curves from competition binding experiments with [^{3}H]UR-MK300 (K_d = 0.55 nM or 0.41 nM, c = 1 nM) and **4.08**, **4.09**, **4.11**, **4.12**, **4.14**-**4.23**, **4.25**, **4.26** and **4.32**-**4.37** at intact hNTS$_1$R-expressing HT-29 cells. Amino-functionalized precursor peptides are represented by circles, DOTA-conjugated peptides are represented by triangles, and Ga^{3+}-containing compounds are represented by squares. Data represent mean values ± SD from at least two independent experiments (performed in triplicate).

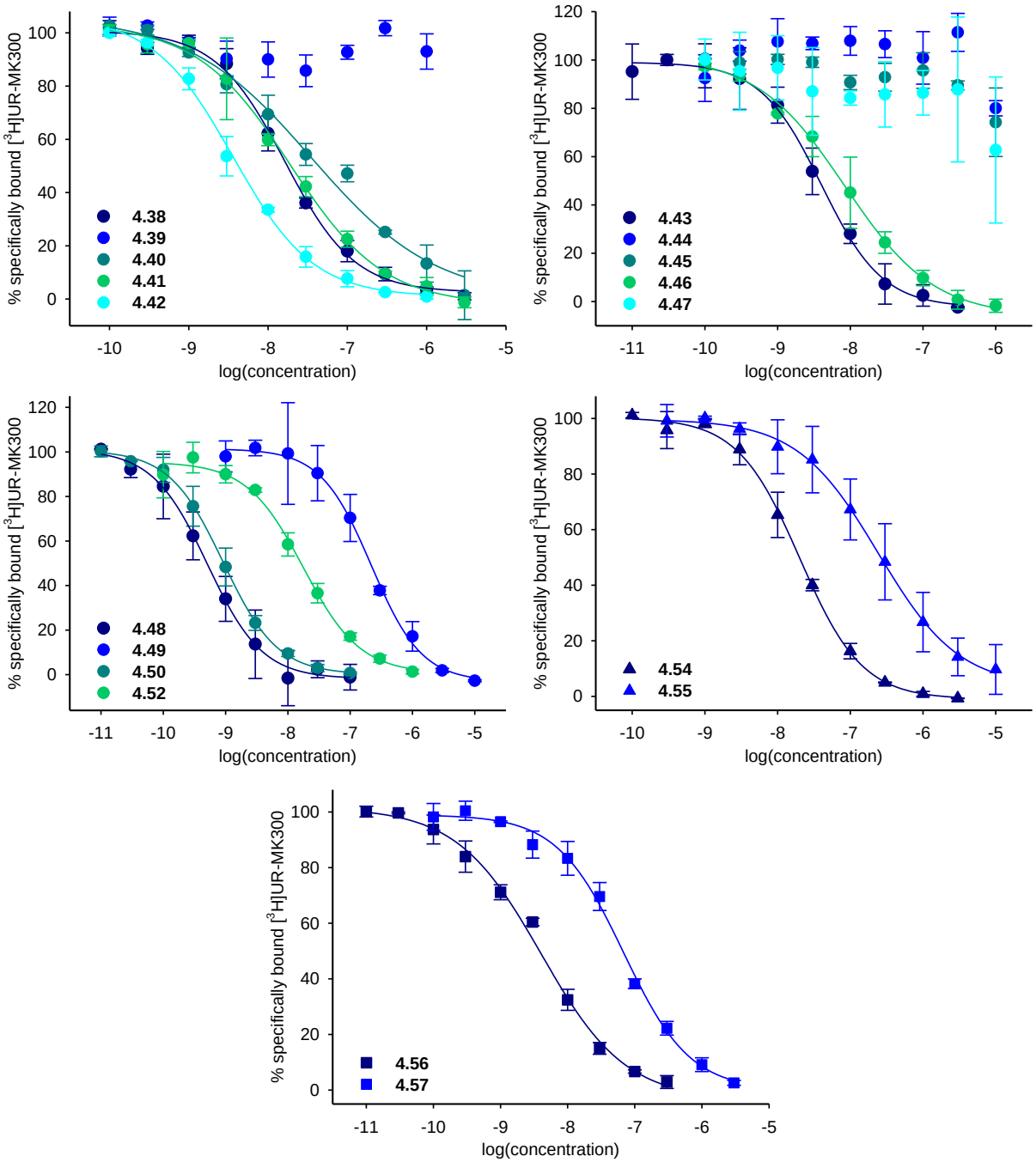

Figure A4.4. Radioligand displacement curves from competition binding experiments with [^{3}H]UR-MK300 (K_d = 0.41 nM, c = 1 nM) and **4.38**-**4.50**, **4.52** and **4.54**-**4.57** at intact hNTS$_1$R-expressing HT-29 cells. Amino-functionalized precursor peptides are represented by circles, DOTA-conjugated peptides are represented by triangles, and Ga^{3+}-containing compounds are represented by squares. Data represent mean values ± SD from at least two independent experiments (performed in triplicate).

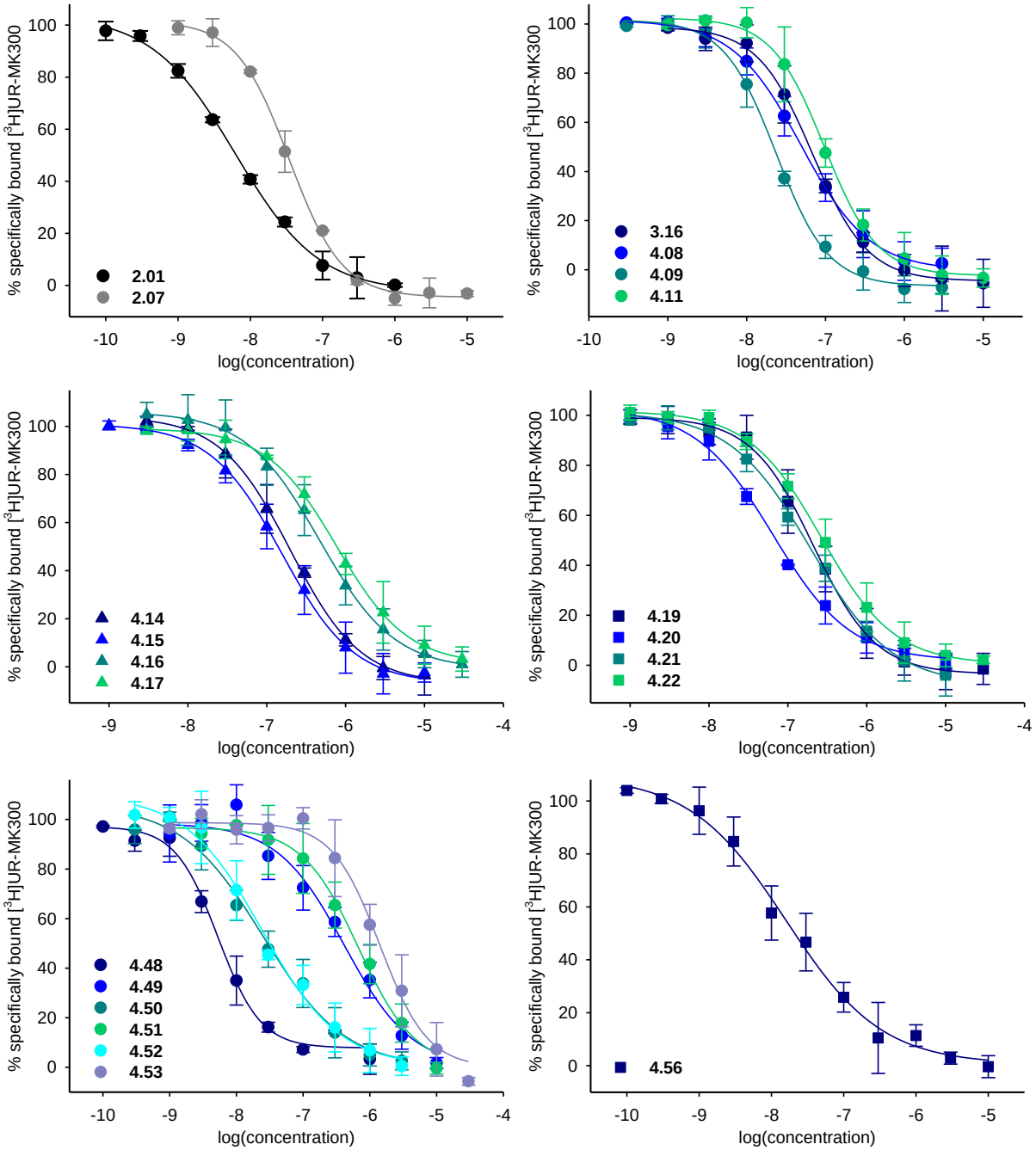

Figure A4.5. Radioligand displacement curves from competition binding experiments with [^{3}H]UR-MK300 (K_d = 6.9 nM or 4.0 nM, c = 10 nM) and **2.01**, **2.07**, **3.16**, **4.08**, **4.09**, **4.11**, **4.14**-**4.17**, **4.19**-**4.22**, **4.48**-**4.53** or **4.56** at intact HEK293T-hNTS$_2$R cells. Reference compounds and amino-functionalized precursor peptides are represented by circles, DOTA-conjugated peptides are represented by triangles, and Ga^{3+}-containing compounds are represented by squares. Data represent mean values ± SD from at least two independent experiments (performed in triplicate).

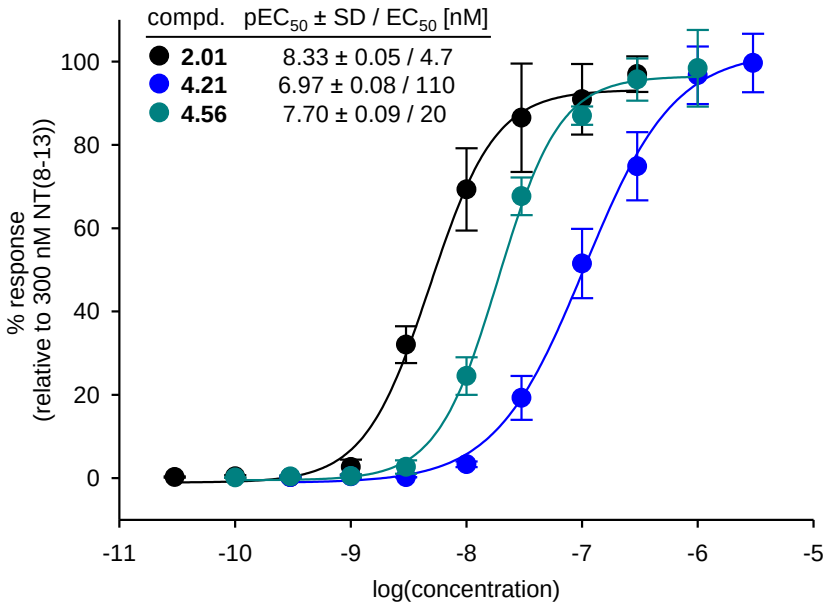

Figure A4.6. Concentration response curves and agonistic potencies (pEC_{50}, EC_{50}) of **2.01**, **4.21** and **4.56** from fura-2 Ca^{2+}-assays using intact hNTS$_1$R-expressing HT-29 cells. Data represent mean values ± SD from three or four independent experiments (performed in singlet).

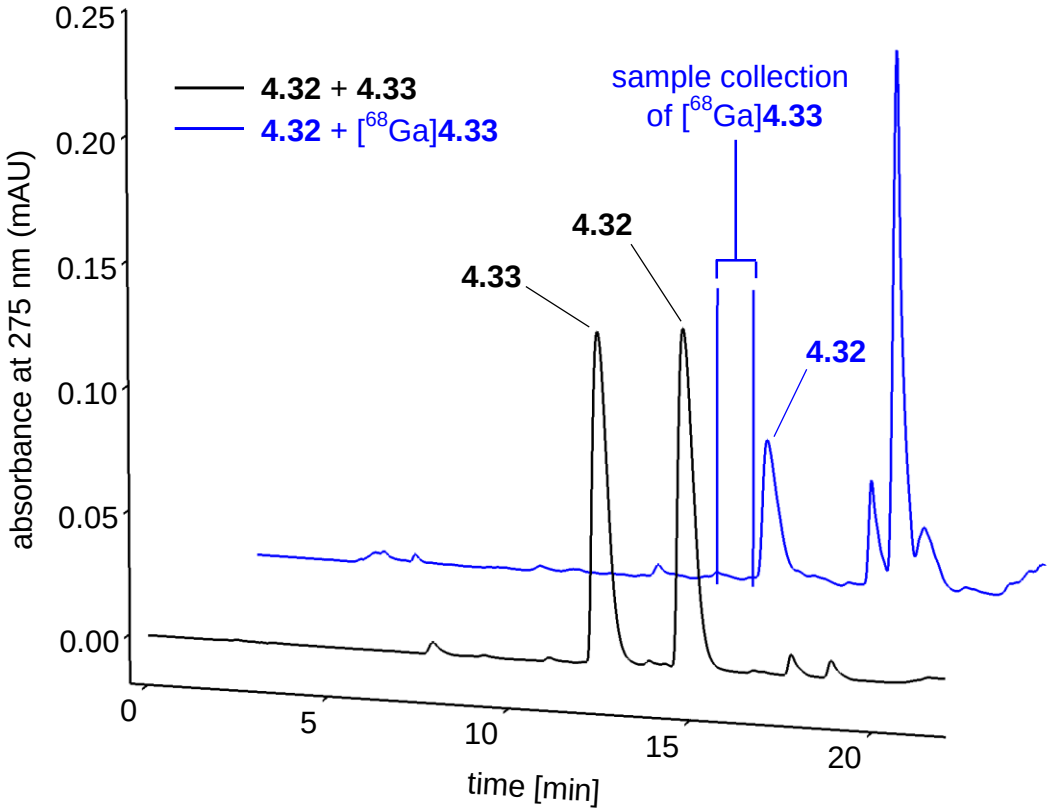

Figure A4.7. Chromatogram of the RP-HPLC analysis of a mixture of the labeling precursor **4.32** and the "cold" PET ligand **4.33** (50 µM each, injection volume 75 µL) (black line), and chromatogram of the preparative HPLC run for the separation of the PET tracer [^{68}Ga]**4.33** from **4.32** after radiosynthesis (blue line). The vertical blue lines give the beginning and the end of tracer collection.

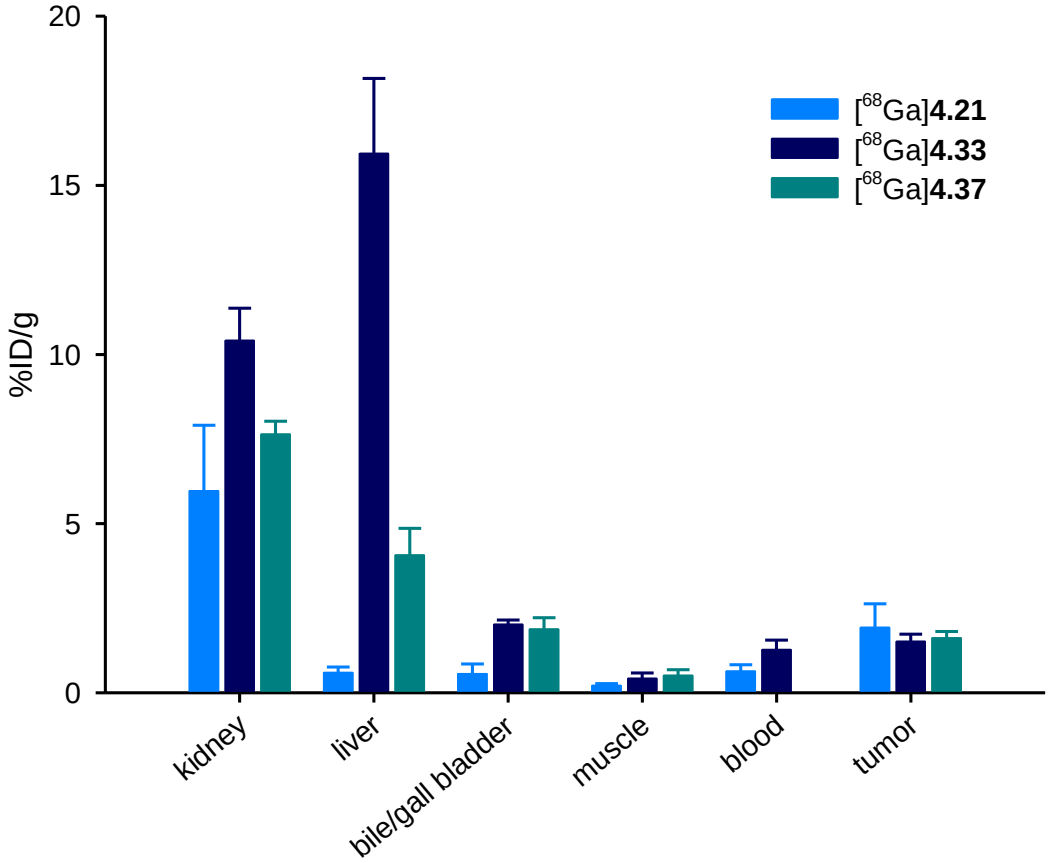

Figure A4.8. Biodistribution data (%ID/g tissue) of [^{68}Ga]**4.21**, [^{68}Ga]**4.33** and [^{68}Ga]**4.37** from HT-29 tumor-bearing mice. Given are mean values ± SD (n = 3 ([^{68}Ga]**4.33**, [^{68}Ga]**4.37**) or n = 4 ([^{68}Ga]**4.21**)) gained at 45 min p.i.

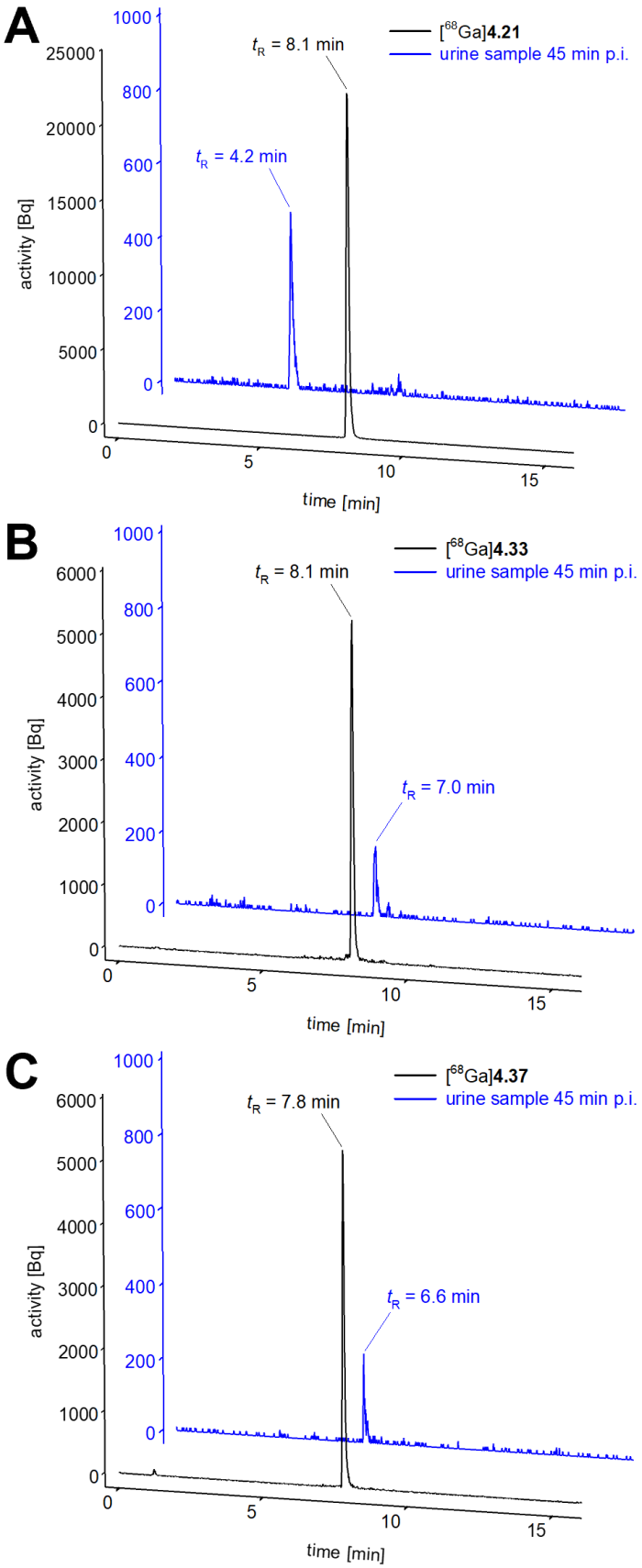

Figure A4.9. Representative chromatograms of the RP-HPLC quality controls of the PET tracers [^{68}Ga]**4.21** (A), [^{68}Ga]**4.33** (B) and [^{68}Ga]**4.37** (C) after radiosynthesis (black lines) and of the RP-HPLC analyses of urine samples obtained from mice 45 min after injection of the respective PET tracers.

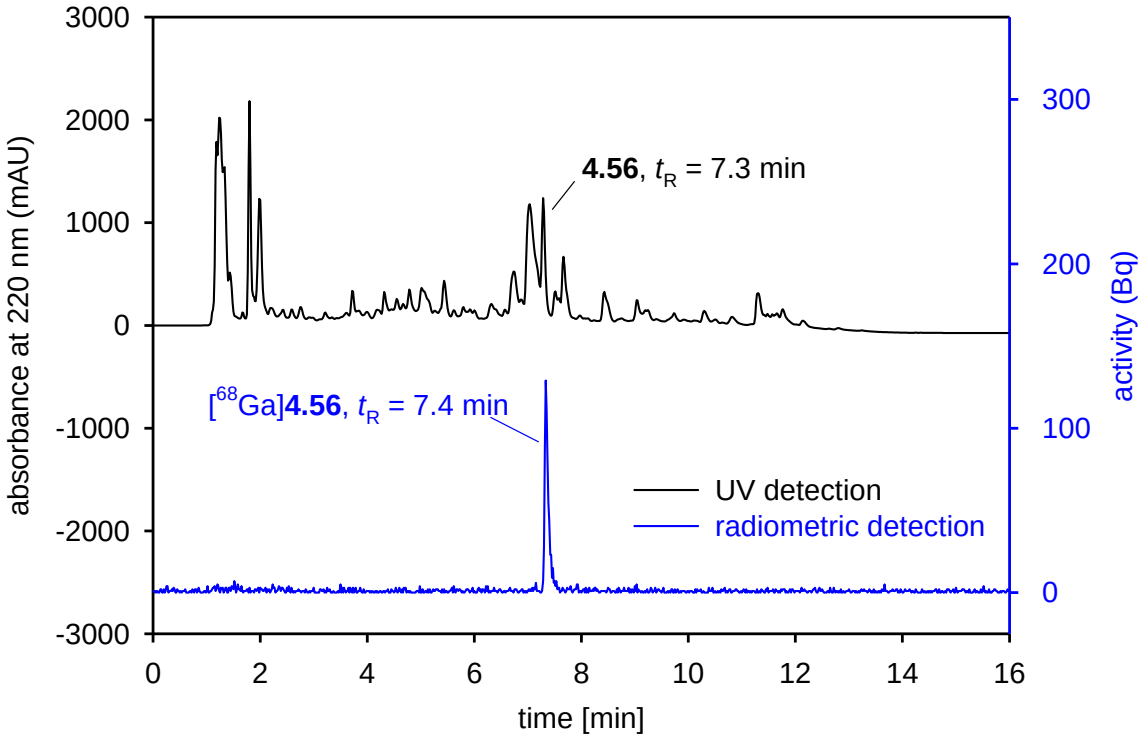

Figure A4.10. RP-HPLC analysis of an ex vivo urine sample from a mouse 45 min after injection of [^{68}Ga]**4.56**, spiked with **4.56** (100 µM). The blue line shows radiodetection and the black line shows UV detection at 220 nm.

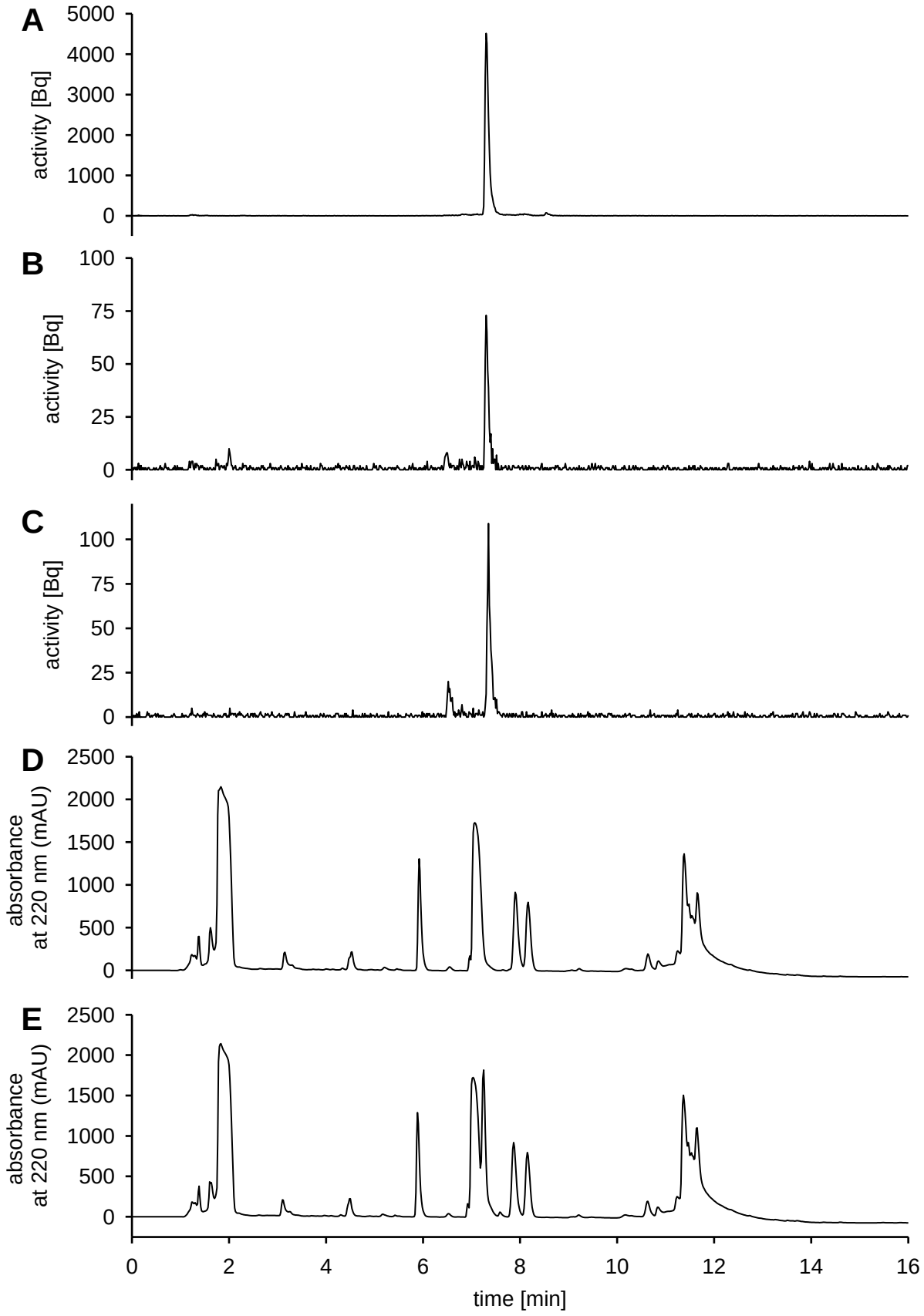

Figure A4.11. Chromatograms of the RP-HPLC analyses of different samples of [^{68}Ga]**4.56** using radio- or UV-detection. (A) quality control after radiosynthesis; (B) ex vivo urine sample obtained from a mouse 10 min after injection of [^{68}Ga]**4.56**; (C) ex vivo plasma sample (10 min p.i.) from the same mouse as under B; (D) UV-detection of the analysis from C; (E) plasma sample from C and D spiked with **4.56** (100 µM).

Table A4.1. Equivalents and conditions applied for SPPS.

Fmoc-aa	equiv. Fmoc-aa	equiv. HBTU/HOBt/DIPEA	coupling conditions[a]
Fmoc-Arg(Pbf)-OH	5	4.9/5/10	„double“, 35 °C
Fmoc-Pro-OH	5	4.9/5/10	„double“, 35 °C
Fmoc-Tyr(*t*Bu)-OH	5	4.9/5/10	„double“, 35 °C
Fmoc-Ile-OH	5	4.9/5/10	„double“, 35 °C
Fmoc-Tle-OH (for **4.08**, **4.52** and **4.53**)	4	3.95/4/8	„double“, 35 °C
Fmoc-Tle-OH (for **4.11**)	5		„double“, 35 °C
Fmoc-Tle-OH (for **4.12**)	4.4	4.35/4.4/8.8	„double“, 35 °C
Fmoc-N-Me-Arg(Pbf)-OH[b]	3.5	3.45/3.5/7	„double“, 35 °C
Fmoc-L-allo-Ile-OH[b]	5	4.9/5/10	„double“, 35 °C
Fmoc-Deg-OH[b]	5	4.9/5/10	„double“, 35 °C
Fmoc-L-cPrGly-OH[b]	5	4.9/5/10	„double“, 35 °C
Fmoc-ß-cyclopropyl-L-Ala-OH[b]	5	4.9/5/10	„double“, 35 °C
Fmoc-(*S*)-2-amino-2-cyclobutylacetic acid[b]	5	4.9/5/10	„double“, 35 °C
Fmoc-ß-cyclopentyl-L-Gly-OH[b]	5	4.9/5/10	„double“, 35 °C
(*S*)-Fmoc-α-ethyl-Ala-OH[b]	5	4.9/5/10	„double“, 35 °C
Fmoc-α-methyl-L-Leu-OH[b]	3	2.95/3/6	„double“, 35 °C
Fmoc-ß,ß-diMe-Tyr(*t*Bu)-OH (rac)[b]	3	2.95/3/6	„double“, 35 °C
3.06a (for **4.08** and **4.09**)[b]	3	3/3/6	“single”, 14 h, 35 °C
3.06a (for **4.11**)[b]	3		“single”, 14 h, 35 °C
3.06a (for **4.50**-**4.53**)[b]	3	3/3/6	„double“, 35 °C
4.07[b]	2.6	2.6/2.6/5.2	“single”, 14 h, 35 °C

[a]In the case of “double coupling”, the length of one coupling step varied between 45 min and overnight. [b]Anhydrous DMF and NMP was used for the coupling reactions.

Table A4.2. Recoveries of peptides **4.08**, **4.09**, **4.11**, **4.12**, **4.14**-**4.23** and **4.54**-**4.57** from human plasma/PBS (1:2 v/v) and ratios of peptide-recovery over recovery of IS.

Compd.	Peptide concentration 80 µM			Peptide concentration 4 µM		
	recovery peptide (%)[a]	recovery IS (%)[a]	ratio[b]	recovery peptide (%)[a]	recovery IS (%)[a]	ratio[b]
4.08	82	98	0.84	103	98	1.05
	84	102	0.83	103	102	1.00
	82	96	0.86	100	100	1.01
				106	102	1.04
			(0.84 ± 0.02)			(1.03 ± 0.02)
4.09	90	103	0.87	92	101	0.90
	85	99	0.86	92	109	0.85
	86	98	0.88	88	100	0.88
	83	97	0.86	96	113	0.85
	85	96	0.89			
			(0.87 ± 0.01)			(0.87 ± 0.03)
4.11	90	104	0.87	98	96	1.02
	89	105	0.84	101	103	0.98
	90	106	0.85	101	99	1.02
	91	106	0.86	98	99	1.00
	88	99	0.89	96	96	1.00
			(0.86 ± 0.02)			(1.00 ± 0.02)
4.12	90	95	0.95	109	101	1.07
	99	110	0.90	111	100	1.12
	95	104	0.92	107	97	1.10
	90	97	0.93	109	100	1.10
	89	98	0.91			
			(0.92 ± 0.02)			(1.09 ± 0.02)
4.14	93	101	0.92	96	103	0.93
	79	84	0.94	90	99	0.91
	82	89	0.92	90	98	0.92
				94	105	0.90
			(0.93 ± 0.01)			(0.91 ± 0.01)
4.15	89	96	0.93	73	94	0.77
	90	104	0.87	80	103	0.78
	84	98	0.86	79	105	0.76
	84	99	0.84			
	86	95	0.91			
			(0.88 ± 0.04)			(0.77 ± 0.01)
4.16	93	96	0.97	99	103	0.97
	102	107	0.95	108	110	0.99
	106	109	0.97	99	100	0.98
	99	103	0.96	107	113	0.95
				102	109	0.94
			(0.96 ± 0.01)			(0.97 ± 0.02)

Table A4.2 continued

4.17	84	88	0.96	123	88	1.40
	86	87	0.99	129	88	1.46
	85	88	0.96	121	82	1.48
	86	86	1.01	130	90	1.44
	85	89	0.96	124	84	1.47
			(0.97 ± 0.02)			(1.45 ± 0.03)
4.18	108	118	0.92	104	99	1.05
	104	110	0.94	105	103	1.02
	99	107	0.93	114	108	1.06
	105	112	0.95	103	100	1.03
	105	110	0.95			
			(0.94 ± 0.01)			(1.04 ± 0.02)
4.19	91	112	0.81	112	111	1.01
	88	110	0.80	110	102	1.07
	86	108	0.80	112	102	1.10
	86	105	0.82	112	109	1.03
			(0.81 ± 0.01)			(1.05 ± 0.04)
4.20	103	123	0.84	102	103	0.99
	111	134	0.82	98	102	0.96
	99	114	0.87	102	100	1.02
	90	107	0.85	108	108	1.00
	102	119	0.86			
			(0.85 ± 0.02)			(0.99 ± 0.03)
4.21	98	108	0.91	115	99	1.16
	92	104	0.89	120	105	1.14
	97	108	0.90	118	105	1.13
	91	100	0.91	120	101	1.19
	89	102	0.88	112	101	1.11
			(0.90 ± 0.02)			(1.15 ± 0.03)
4.22	80	89	0.89	96	83	1.16
	81	91	0.89	90	86	1.06
	76	86	0.88	100	89	1.13
	77	84	0.91	100	90	1.11
			(0.89 ± 0.01)			(1.11 ± 0.04)
4.23	88	100	0.87	112	111	1.01
	96	105	0.91	98	96	1.02
	97	109	0.89	107	105	1.02
	104	119	0.88	106	103	1.03
	98	109	0.90			
			(0.89 ± 0.02)			(1.02 ± 0.01)
4.54	90	97	0.94	96	96	1.00
	90	96	0.94	100	99	1.01
	94	97	0.98	106	99	1.07
	89	93	0.95	107	109	0.98
	91	99	0.92	103	95	1.09
			(0.94 ± 0.02)			(1.03 ± 0.05)

Table A4.2 continued

4.55	91	96	0.95	97	96	1.01
	102	105	0.97	99	101	0.99
	88	91	0.96	102	106	0.96
	89	94	0.95	94	94	0.99
				103	100	1.02
			(0.96 ± 0.01)			(0.99 ± 0.02)
4.56	94	103	0.92	99	100	0.99
	84	94	0.89	100	93	1.07
	91	101	0.91	101	97	1.04
	87	96	0.91	109	107	1.01
	90	99	0.91	105	107	0.98
			(0.91 ± 0.01)			(1.02 ± 0.04)
4.57	85	97	0.88	104	105	0.99
	83	91	0.91	96	95	1.01
	90	98	0.92	100	102	0.98
	88	92	0.96	94	95	0.99
	100	106	0.94	91	90	1.01
			(0.92 ± 0.03)			(1.00 ± 0.02)

[a]Recoveries of the peptides and of IS from human plasma/PBS (1:2 v/v) using a peptide concentration of 80 µM or 4 µM and an IS concentration of 10 µM (three, four or five independent experiments). [b]Ratios of peptide recovery over recovery of the IS calculated for individual experiments, as well as mean recovery ratios ± SD (given in parenthesis). Note: When the remaining intact peptide concentration in plasma was > 20 µM, recovery ratios based on the 80 µM peptide concentrations were used to calculate peptide recoveries of the plasma stability samples. When the remaining intact peptide concentration was < 20 µM, recovery ratios based on the 4 µM peptide concentrations were used to calculate peptide recoveries of the plasma stability samples.

Table A4.3. NTS$_1$R affinities of **3.16**, **4.08**, **4.09**, **4.11**, **4.12**, **4.14**-**4.18**, **4.25**, **4.26**, **4.32**, **4.34**, **4.35**, **4.38**-**4.50**, **4.52**, **4.54** and **4.55**, NTS$_2$R affinities of **3.16**, **4.08**, **4.09**, **4.11**, **4.14**-**4.17** and **4.48**-**4.53**, NTS$_1$R selectivities of **3.16**, **4.08**, **4.09**, **4.11**, **4.14**-**4.17**, **4.48**-**4.50** and **4.52**, and in vitro plasma stabilities of **3.16**, **4.08**, **4.09**, **4.11**, **4.12**, **4.14**-**4.18**, **4.38**-**4.49**, **4.54** and **4.55**, determined at 37 °C.

cpd.	pK_i ± SD/ K_i [nM] NTS$_1$R[a]	pK_i ± SD/ K_i [nM] NTS$_2$R[b]	NTS$_1$R selectivity (ratio K_i(NTS$_2$R)/ K_i(NTS$_1$R))	% intact peptide in plasma after the given incubation time[c]			
				1 h	6 h	24 h	48 h
3.16	8.55/2.8[d]	7.72 ± 0.09/19	6.8	> 99[d]	> 99[d]	> 99[d]	> 99[d]
4.08	8.28 ± 0.05/5.3	7.68 ± 0.11/22	4.2	> 99	> 99	> 99	> 99
4.09	9.16 ± 0.02/0.69	8.10 ± 0.19/8.3	12	99 ± 2	57 ± 2	3.0 ± 0.1	1.4 ± 0.3
4.11	7.88 ± 0.04/13	7.57 ± 0.10/27	2.1	> 99	> 99	> 99	> 99
4.12	8.61 ± 0.23/2.7	n.d.	-	97 ± 3	97 ± 3	94 ± 3	91 ± 3
4.14	7.66 ± 0.39/28	7.11 ± 0.07/79	2.8	> 99	> 99	> 99	> 99
4.15	8.62 ± 0.005/2.4	7.27 ± 0.10/55	23	78 ± 1	8.3 ± 0.4	< 1	< 1
4.16	7.48 ± 0.02/33	6.86 ± 0.25/150	4.5	> 99	> 99	93 ± 3	84 ± 2
4.17	7.45 ± 0.09/36	6.65 ± 0.10/230	6.4	97 ± 1	99 ± 1	98 ± 1	97 ± 1
4.18	7.45 ± 0.07/36	n.d.	-	> 99	99 ± 1	94 ± 1	86 ± 1

Table A4.3 continued

4.25	8.37 ± 0.08/4.3	n.d.	-	n.d.	n.d.	n.d.	n.d.
4.26	8.52 ± 0.11/3.1	n.d.	-	n.d.	n.d.	n.d.	n.d.
4.32	7.97 ± 0.19/12	n.d.	-	n.d.	n.d.	n.d.	n.d.
4.34	7.99 ± 0.06/10	n.d.	-	n.d.	n.d.	n.d.	n.d.
4.35	7.87 ± 0.12/14	n.d.	-	n.d.	n.d.	n.d.	n.d.
4.38	8.33 ± 0.06/4.8	n.d.	-	92 ± 1	87 ± 1	70 ± 1	52 ± 1
4.39	< 6/> 1000	n.d.	-	93 ± 1	94 ± 1	93 ± 1	93 ± 1
4.40	8.05 ± 0.21/9.6	n.d.	-	88 ± 1	58 ± 1	< 1	< 1
4.41	8.31 ± 0.12/5.0	n.d.	-	92 ± 1	74 ± 1	15 ± 1	< 1
4.42	8.98 ± 0.05/1.1	n.d.	-	91 ± 1	79 ± 1	32 ± 1	< 1
4.43	8.92 ± 0.09/1.2	n.d.	-	99 ± 1	95 ± 1	78 ± 1	58 ± 1
4.44	< 6/> 1000	n.d.	-	94 ± 1	91 ± 4	91 ± 1	87 ± 1
4.45	< 6/> 1000	n.d.	-	93 ± 1	92 ± 1	86 ± 1	77 ± 1
4.46	8.63 ± 0.22/2.6	n.d.	-	25 ± 2	< 1	< 1	< 1
4.47	< 6/> 1000	n.d.	-	89 ± 1	88 ± 1	81 ± 1	73 ± 1
4.48	9.86 ± 0.17/0.14	8.82 ± 0.07/1.5	11	90 ± 4	97 ± 6	92 ± 1	92 ± 1
4.49	7.25 ± 0.06/56	6.95 ± 0.12/110	2.0	96 ± 2	96 ± 1	94 ± 5	95 ± 2
4.50	9.60 ± 0.12/0.26	8.23 ± 0.28/6.8	26	n.d.	n.d.	n.d.	n.d.
4.51	n.d.	6.76 ± 0.07/170	-	n.d.	n.d.	n.d.	n.d.
4.52	8.30 ± 0.21/5.4	8.22 ± 0.22/6.5	1.2	n.d.	n.d.	n.d.	n.d.
4.53	n.d.	6.40 ± 0.24/450	-	n.d.	n.d.	n.d.	n.d.
4.54	8.23 ± 0.08/5.9	n.d.	-	> 99	> 99	> 99	> 99
4.55	7.10 ± 0.20/85	n.d.	-	> 99	> 99	> 99	> 99

[a]Determined by radioligand competition binding with [^{3}H]UR-MK300 at HT-29 cells (K_d = 0.55 nM[2] or 0.41 nM, c = 1 nM); given are mean values ± SD (pK_i) and mean values (K_i) from two (**4.08**, **4.15**, **4.42**), three (**4.09**, **4.11**, **4.16**, **4.17**, **4.25**, **4.32**, **4.34**, **4.38**, **4.40**, **4.41**, **4.43**, **4.46**, **4.48**-**4.50**, **4.52**, **4.54**, **4.55**), four (**4.12**, **4.18**, **4.26**, **4.35**) or five (**4.14**) independent experiments, each performed in triplicate. [b]Determined by radioligand competition binding with [^{3}H]UR-MK300 at HEK293T-hNTS$_2$R cells (K_d = 6.9 nM or 4.0 nM, c = 10 nM); given are mean values ± SD (pK_i) and mean values (K_i) from two (**4.09**, **4.14**), three (**3.16**, **4.08**, **4.11**, **4.16**, **4.17**, **4.48**, **4.49**, **4.51**, **4.52**) or four (**4.15**, **4.50**, **4.53**) independent experiments, each performed in triplicate. [c]The initial concentration of the peptide in human plasma/PBS (1:2 v/v) was 100 µM. Data represent means ± SD from two or three independent experiments (SD not given when no decomposition was observed). [d]Schindler et al.[3] n.d. = not determined.

Table A4.4. *Ex vivo* biodistribution data and tumor-to-muscle ratios of [^{68}Ga]**4.21**, [^{68}Ga]**4.33** and [^{68}Ga]**4.37**.[a]

tissue	uptake (%ID/g) 45 min p.i.		
	[^{68}Ga]**4.21**	[^{68}Ga]**4.33**	[^{68}Ga]**4.37**
kidney	6.0 ± 1.9	10 ± 0.96	7.6 ± 0.39
liver	0.59 ± 0.17	16 ± 2.2	4.1 ± 0.79
gall bladder (bile)	0.55 ± 0.29	2.0 ± 0.14	1.9 ± 0.34
muscle	0.21 ± 0.062	0.41 ± 0.17	0.50 ± 0.18
blood	0.63 ± 0.20	1.3 ± 0.29	n.d.
tumor	1.9 ± 0.70	1.5 ± 0.22	1.6 ± 0.19
tumor-to-muscle	9.5 ± 3.7	4.1 ± 1.7	3.4 ± 0.71

[a]Given are mean values ± SD (n = 3 ([^{68}Ga]**4.33**, [^{68}Ga]**4.37**) or n = 4 ([^{68}Ga]**4.21**)). Organ uptake values were obtained at 45 min p.i. from HT-29 tumor-bearing mice.

4.6.2 General procedure for manual solid-phase peptide synthesis (SPPS)

The synthesis was performed according to a reported procedure[1] with minor modifications. The resin was allowed to swell in the solvent for 45 min before the beginning of the synthesis. For coupling conditions see Table A4.1.

4.6.3 General procedure for the conjugation of the DOTA chelator to peptides

The reaction was performed in a 2-mL reaction vessel with screw cap, equipped with a magnetic micro stirrer. DIPEA (27 equiv. (**4.14**-**4.17**), 15 equiv. (**4.34**, **4.35**), 13 equiv. (**4.18**, **4.32**) or 12 equiv. (**4.54**, **4.55**)) was added to a solution of the peptide (2.2 equiv. (**4.14**-**4.17**), 1.25 equiv. (**4.34**, **4.35**), 1.1 equiv. (**4.18**, **4.32**) or 1 equiv. (**4.54**, **4.55**)) in DMF/NMP (75:25 v/v) or DMF/NMP (80:20 v/v) (26-230 µL), followed by the addition of DOTA tris(*tert*-butyl) succinimidyl ester (**4.13**, 1 equiv.) dissolved in anhydrous DMF or DMF/NMP (80:20 v/v) (6-30 µL). After stirring at rt for 30 min, 10% aq TFA (corresponding to 18 equiv. TFA (**4.14**-**4.17**), 10 equiv. TFA (**4.34**, **4.35**), 9 equiv. TFA (**4.18**, **4.35**) or 8 equiv. TFA (**4.54**, **4.55**)) was added. The protected intermediate was isolated by preparative HPLC. After lyophilization of the eluate, TFA/H_2O (80:20 v/v) (0.5-3 mL) was added, and the mixture was stirred at 50 °C overnight. The crude product was taken up in H_2O (25-100 mL), and the solution was subjected to lyophilization. The DOTA-conjugated peptide was purified by preparative HPLC.

4.6.4 General procedure for the incorporation of Ga^{3+} into DOTA-conjugated peptides

The incorporation reaction was performed in a 2-mL reaction vessel with screw cap. A solution of the peptide (4 mM) in HEPES buffer (0.2 M, pH 4.2) was heated to 60 °C for 5 min, followed by the addition of a solution of $Ga(NO_3)_3 \times H_2O$ (3 equiv., 0.4 M) in aqueous HCl (10 mM). The mixture was shaken at 100 °C for 10 min (**4.19**-**4.23**) or 30 min (**4.33**, **4.36**, **4.37**, **4.56**, **4.57**) using a Thermocell mixing block from Bioer (Hangzhou, China), and the product was purified by preparative HPLC.

4.6.5 Synthesis protocols and analytical data of compounds 4.08, 4.09, 4.11, 4.12, 4.14-4.23, 4.25, 4.26, 4.28, 4.29 and 4.31-4.57

***N*$^{\alpha}$-(*N*$^{\alpha}$-Methylarginyl)-*N*$^{\omega}$-[(4-aminobutyl)aminocarbonyl]Arg-Pro-Tyr-α-*tert*-butyl-Gly-Leu tetrakis(hydrotrifluoroacetate) (4.08).** Peptide **4.08** was synthesized according to the general procedure for SPPS using a H-Leu-2-ClTrt resin (loading 0.79 mmol/g) (109 mg, 0.086 mmol). Purification by preparative RP-HPLC (column: Kinetex-XB C18, gradient: 0-35 min: A1/B1 92:8-57:43, t_R = 18 min) afforded **4.08** as white fluffy solid (68.7 mg, 57%). ^{1}H-NMR (600 MHz, DMSO-d_6): δ 0.80-0.95 (m, 15H), 1.39-1.63 (m, 12H), 1.63-1.90 (m, 6H), 1.92-2.06 (m, 1H), 2.46-2.48 (m, 3H), 2.64-2.72 (m, 1H), 2.76-2.81 (m, 2H), 2.85-2.92 (m, 1H), 3.05-3.12 (m, 4H), 3.22-3.27 (m, 2H), 3.55-3.59 (m, 2H), 3.75-3.80 (m, 1H), 4.17-4.24 (m, 1H), 4.27-4.31 (m, 1H), 4.31-4.39 (m, 1H), 4.44-4.59 (m, 2H), 6.55-6.64 (m, 2H), 6.64-7.15 (br s, 2H, interfering with the next listed signal), 6.97-7.01 (m, 2H), 7.15-7.53 (br s, 2H), 7.53-7.66 (m, 2H), 7.66-7.90 (m, 4H), 7.97 (d, 1H, *J* 7.4 Hz), 8.17-8.27 (m, 1H), 8.31-8.67 (m, 2H), 8.68-9.12 (m, 4H), 9.12-9.25 (m, 1H), 10.27-10.56 (m, 1H), 12.49 (br s, 1H). HRMS: *m*/*z* [*M*+2H]$^{2+}$ calcd. for [$C_{44}H_{78}N_{14}O_9$]$^{2+}$ 473.3033, found 473.3039. RP-HPLC (220 nm): > 99% (t_R = 5.8 min, *k* = 6.6). $C_{44}H_{76}N_{14}O_9$ · $C_8H_4F_{12}O_8$ (945.18 + 456.09).

***N*$^{\alpha}$-(*N*$^{\alpha}$-Methylarginyl)-*N*$^{\omega}$-[(4-aminobutyl)aminocarbonyl]Arg-Pro-Tyr-Ile-Leu tetrakis(hydrotrifluoroacetate) (4.09).** Peptide **4.09** was synthesized according to the general procedure for SPPS using a H-Leu-2-ClTrt resin (loading 0.79 mmol/g) (120 mg, 0.095 mmol). Purification by preparative RP-HPLC (column: Kinetex-XB C18, gradient: 0-35 min: A1/B1 92:8-57:43, t_R = 18 min) afforded **4.09** as white fluffy solid (58.8 mg, 44%). ^{1}H-NMR (600 MHz, DMSO-d_6): δ 0.76-0.87 (m, 9H), 0.87-0.92 (m, 3H), 0.99-1.10 (m, 1H), 1.40-1.64 (m, 13H), 1.64-1.89 (m, 7H), 1.94-2.05 (m, 1H), 2.45-2.48 (m, 3H), 2.64-2.72 (m, 1H), 2.76-2.82 (m, 2H), 2.83-2.89 (m, 1H), 3.07-3.13 (m, 4H), 3.22-3.28 (m, 2H), 3.58-3.62 (m, 2H), 3.76-3.80 (m, 1H), 4.17-4.26 (m, 2H), 4.28-4.39 (m, 1H), 4.39-4.50 (m, 1H), 4.50-4.61 (m, 1H), 6.53-6.65 (m, 2H), 6.65-7.13 (br s, 2H, interfering with the next listed signal), 6.98-7.00 (m, 2H), 7.13-7.48 (br s, 2H), 7.48-7.61 (m, 1H), 7.61-7.82 (m, 5H), 7.82-8.00 (m, 1H), 8.19 (d, 1H, *J* 7.7 Hz), 8.26-8.70 (m, 2H), 8.70-9.10 (m, 4H), 9.10-9.25 (m, 1H), 10.42 (s, 1H), 12.50 (br s, 1H). HRMS: *m*/*z* [*M*+2H]$^{2+}$ calcd. for [$C_{44}H_{78}N_{14}O_9$]$^{2+}$ 473.3033, found 473.3047. RP-HPLC (220 nm): > 99% (t_R = 6.0 min, *k* = 6.9). $C_{44}H_{76}N_{14}O_9$ · $C_8H_4F_{12}O_8$ (945.18 + 456.09).

***N*$^{\alpha}$-Arginyl-*N*$^{\alpha}$-methyl-*N*$^{\omega}$-[(4-aminobutyl)aminocarbonyl]Arg-Pro-Tyr-α-*tert*-butyl-Gly-Leu tetrakis(hydrotrifluoroacetate) (4.11).** Peptide **4.11** was synthesized according to the general procedure for SPPS using a H-Leu-2-ClTrt resin (loading 0.79 mmol/g) (60 mg, 0.047 mmol), with the following modification: Fmoc amino acids (Fmoc-Arg(Pbf)-OH, Fmoc-Pro-OH, Fmoc-Tle-OH, Fmoc-Tyr(tBu)-OH (used in 5-fold excess) and **3.06a** (used in 3-fold excess)) were pre-activated with oxyma/DIC (5/5 equiv. and 3/3 equiv., respectively) instead of HBTU/HOBt. After coupling of arginine building block **3.06a** and Fmoc-deprotection, the resin was washed with CH_2Cl_2 (5 ×), a solution of 2-nitrobenzenesulfonylchloride (31.5 mg, 0.142 mmol) and collidine (31.4 µL, 0.237 mmol) in CH_2Cl_2 (1.25 mL) was added and the mixture was shaken at rt for 2 h. The resin was washed with DMF (5 ×), and a solution of MTBD (27.2 µL, 0.190 mmol) and methyl-4-nitrobenzenesulfonate (51.5 mg, 0.237 mmol) in DMF (1.5 mL) was added. After shaking

at rt for 30 min, the resin was washed with DMF (3 ×) followed by the addition of a solution of DBU (35.4 µL, 0.237 mmol) and 2-mercaptoethanol (33.1 µL, 0.474 mmol) in DMF (1.25 mL) and shaking at rt for 30 min. The resin was washed with DMF (5 ×) followed by coupling of Fmoc-Arg(Pbf)-OH as described above. Fmoc-deprotection and cleavage from the resin was performed as described in the general procedure for SPPS. Purification by preparative RP-HPLC (column: Gemini NX-C18, gradient: 0-35 min: A1/B1 92:8-57:43, t_R = 16 min) afforded **4.11** as white fluffy solid (39.0 mg, 59%). ^{1}H-NMR (600 MHz, DMSO-d_6): δ 0.79-0.95 (m, 15H), 1.42-1.80 (m, 18H), 1.92-2.03 (m, 1H), 2.66-2.72 (m, 1H), 2.76-2.81 (m, 2H), 2.84-2.95 (m, 4H), 3.06-3.14 (m, 4H), 3.22-3.28 (m, 3H), 3.50-3.51 (m, 1H), 4.17-4.23 (m, 1H), 4.25-4.32 (m, 2H), 4.32-4.40 (m, 1H), 4.41-4.47 (m, 1H), 5.12-5.18 (m, 1H), 6.59-6.64 (m, 2H), 6.64-7.19 (br s, 2H, interfering with the next listed signal), 6.98-7.01 (m, 2H), 7.19-7.52 (br s, 2H), 7.52-7.64 (m, 2H), 7.64-7.82 (m, 4H), 7.99 (d, 1H, *J* 7.9 Hz), 8.05-8.30 (m, 4H), 8.35-8.61 (m, 2H), 8.88-9.10 (m, 1H), 9.10-9.25 (m, 1H), 10.21-10.55 (m, 1H), 12.47 (br s, 1H). HRMS: *m/z* [*M*+3H]$^{3+}$ calcd. for [$C_{44}H_{79}N_{14}O_9$]$^{3+}$ 315.8713, found 315.8722. RP-HPLC (220 nm): 99% (t_R = 5.7 min, *k* = 6.5). $C_{44}H_{76}N_{14}O_9$ · $C_8H_4F_{12}O_8$ (945.18 + 456.09).

***N*$^{\alpha}$-Methyl-*N*$^{\omega}$-[(8-amino-3,6-dioxaoctyl)aminocarbonyl]Arg-Arg-Pro-Tyr-*a*-*tert*-butyl-Gly-Leu tetrakis(hydrotrifluoroacetate) (4.12).** Peptide **4.12** was synthesized according to the general procedure for SPPS using a H-Leu-2-ClTrt resin (loading 0.79 mmol/g) (100 mg, 0.079 mmol), with the following modification: after coupling of arginine building block **4.07** and Fmoc-deprotection, the resin was washed with CH_2Cl_2 (5 ×), a solution of 2-nitrobenzenesulfonylchloride (52.5 mg, 0.237 mmol) and collidine (52.4 µL, 0.395 mmol) in CH_2Cl_2 (1.5 mL) was added and the mixture was shaken at rt for 2 h. The resin was washed with DMF (5 ×), and a solution of MTBD (45.4 µL, 0.316 mmol) and methyl-4-nitrobenzenesulfonate (85.8 mg, 0.395 mmol) in DMF (1.8 mL) was added. After shaking at rt for 30 min, the resin was washed with DMF (3 ×) followed by the addition of a solution of DBU (59.0 µL, 0.395 mmol) and 2-mercaptoethanol (55.1 µL, 0.790 mmol) in DMF (1.5 mL) and shaking at rt for 30 min. The resin was washed with DMF (5 ×) followed by cleavage from the resin as described in the general procedure for SPPS. Purification by preparative RP-HPLC (column: Gemini-NX C18, gradient: 0-30 min: A1/B1 92:8-60:40, t_R = 13 min) afforded **4.12** as white fluffy solid (63.1 mg, 55%). ^{1}H-NMR (600 MHz, DMSO-d_6): δ 0.79-0.95 (m, 15H), 1.43-1.88 (m, 14H), 1.94-2.04 (m, 1H), 2.44-2.48 (m, 3H), 2.64-2.71 (m, 1H), 2.85-2.93 (m, 1H), 2.93-3.02 (m, 2H), 3.05-3.15 (m, 2H), 3.24-3.28 (m, 4H), 3.45-3.48 (m, 2H), 3.50-3.64 (m, 8H), 3.72-3.88 (m, 1H), 4.17-4.26 (m, 1H), 4.26-4.31 (m, 1H), 4.31-4.39 (m, 1H), 4.42-4.61 (m, 2H), 6.55-6.62 (m, 2H), 6.62-7.12 (br s, 2H, interfering with the next listed signal), 6.97-7.01 (m, 2H), 7.12-7.44 (br s, 2H), 7.44-7.56 (m, 1H), 7.56-7.67 (m, 2H), 7.67-7.92 (m, 3H), 7.97 (d, 1H, *J* 7.7 Hz), 8.22 (d, 1H, *J* 7.5 Hz), 8.27-8.66 (m, 2H), 8.66-9.32 (m, 5H), 10.20-10.54 (m, 1H), 12.48 (br s, 1H). HRMS: *m/z* [*M*+3H]$^{3+}$ calcd. for [$C_{46}H_{83}N_{14}O_{11}$]$^{3+}$ 335.8783, found 335.8791. RP-HPLC (220 nm): 89% (t_R = 6.2 min, *k* = 7.2). $C_{46}H_{80}N_{14}O_{11}$ · $C_8H_4F_{12}O_8$ (1005.23 + 456.09).

***N*$^{\alpha}$-(*N*$^{\alpha}$-Methylarginyl)-*N*$^{\omega}$-{[4-(N-{2-[4,7,10-tris(carboxymethyl)-1,4,7,10-tetraazacyclododecan-1-yl]acetyl})aminobutyl]aminocarbonyl}Arg-Pro-Tyr-*α*-*tert*-butyl-Gly-Leu tetrakis(hydrotrifluoroacetate) (4.14).** Compound **4.14** was prepared from **4.08** (34.2 mg, 24.4 µmol) and **4.13** (9.0 mg, 11.0 µmol) according to the general procedure for DOTA-conjugation. Isolation of the protected intermediate: column: Kinetex-XB C18, gradient: 0-18 min: A1/B1 92:8-75:25, 18-40 min: 75:25-38:62, t_R = 28 min. Purification of the product by preparative RP-HPLC (column: Kinetex-XB C18, gradient: 0-35 min: A1/B1 92:8-57:43, t_R = 18 min) afforded **4.14** as white fluffy solid (14.1 mg, 72%). ^{1}H-NMR (600 MHz, DMSO-d_6): δ 0.81-0.85 (m, 3H), 0.87-0.95 (m, 12H), 1.40-1.64 (m, 12H), 1.64-1.89 (m, 6H), 1.95-2.06 (m, 1H), 2.46-2.48 (m, 3H), 2.65-2.71 (m, 1H), 2.85-2.90 (m, 1H), 3.00-3.27 (m, 25H), 3.53-3.84 (m, 10H), 4.18-4.24 (m, 1H), 4.27-4.31 (m, 1H), 4.31-4.39 (m, 1H), 4.45-4.61 (m, 2H), 6.56-6.64 (m, 2H), 6.64-7.09 (br s, 2H, interfering with the next listed signal), 6.97-7.00 (m, 2H), 7.09-7.56 (br s, 3H), 7.60-7.83 (m, 2H), 7.92-8.00 (m, 1H), 8.03-8.63 (m, 4H), 8.68-9.11 (m, 3H), 9.11-9.51 (m, 2H), 11.83-12.94 (m, 2H). 4 exchangeable protons (NH, OH) of the presumably 4-fold protonated molecule could not be identified. HRMS: *m/z* [*M*+2H]$^{2+}$ calcd. for [$C_{60}H_{104}N_{18}O_{16}$]$^{2+}$ 666.3933, found 666.3943. RP-HPLC (220 nm): > 99% (t_R = 6.1 min, *k* = 7.0). $C_{60}H_{102}N_{18}O_{16}$ · $C_8H_4F_{12}O_8$ (1331.59 + 456.09).

***N*$^{\alpha}$-(*N*$^{\alpha}$-Methylarginyl)-*N*$^{\omega}$-{[4-(N-{2-[4,7,10-tris(carboxymethyl)-1,4,7,10-tetraazacyclododecan-1-yl]acetyl})aminobutyl]aminocarbonyl}Arg-Pro-Tyr-Ile-Leu tetrakis(hydrotrifluoroacetate) (4.15).** Compound **4.15** was prepared from **4.09** (32.8 mg, 23.4 µmol) and **4.13** (8.6 mg, 10.5 µmol) according to the general procedure for DOTA-conjugation. Isolation of the protected intermediate: column: Kinetex-XB C18, gradient: 0-18 min: A1/B1 92:8-75:25, 18-40 min: 75:25-38:62, t_R = 28 min. Purification of the product by preparative RP-HPLC (column: Kinetex-XB C18, gradient: 0-35 min: A1/B1 92:8-57:43, t_R = 18 min) afforded **4.15** as white fluffy solid (11.7 mg, 62%). ^{1}H-NMR (600 MHz, DMSO-d_6): δ 0.76-0.87 (m, 9H), 0.87-0.93 (m, 3H), 0.98-1.10 (m, 1H), 1.36-1.65 (m, 13H), 1.65-1.90 (m, 7H), 1.93-2.07 (m, 1H), 2.46-2.48 (m, 3H), 2.64-2.72 (m, 1H), 2.84-2.89 (m, 1H), 2.95-3.28 (m, 25H), 3.53-3.86 (m, 10H), 4.17-4.25 (m, 2H), 4.28-4.37 (m, 1H), 4.39-4.50 (m, 1H), 4.50-4.62 (m, 1H), 6.55-6.69 (m, 2H), 6.69-7.13 (br s, 2H, interfering with the next listed signal), 6.97-7.00 (m, 2H), 7.13-7.67 (br s, 3H), 7.67-8.06 (m, 3H), 8.06-8.49 (m, 3H), 8.49-9.63 (m, 6H), 11.80-12.93 (m, 2H). 4 exchangeable protons (NH, OH) of the presumably 4-fold protonated molecule could not be identified. HRMS: *m/z* [*M*+2H]$^{2+}$ calcd. for [$C_{60}H_{104}N_{18}O_{16}$]$^{2+}$ 666.3933, found 666.3946. RP-HPLC (220 nm): > 99% (t_R = 6.3 min, *k* = 7.3). $C_{60}H_{102}N_{18}O_{16}$ · $C_8H_4F_{12}O_8$ (1331.59 + 456.09).

***N*$^{\alpha}$-Methyl-*N*$^{\omega}$-{[4-(N-{2-[4,7,10-tris(carboxymethyl)-1,4,7,10-tetraazacyclododecan-1-yl]acetyl})aminobutyl]aminocarbonyl}Arg-Arg-Pro-Tyr-*α*-*tert*-butyl-Gly-Leu tetrakis(hydrotrifluoroacetate) (4.16).** Compound **4.16** was prepared from **3.16** (34.2 mg, 24.4 µmol) and **4.13** (9.0 mg, 11.0 µmol) according to the general procedure for DOTA-conjugation. Isolation of the protected intermediate: column: Kinetex-XB C18, gradient: 0-18 min: A1/B1 92:8-75:25, 18-40 min: 75:25-38:62, t_R = 28 min. Purification of the product by preparative RP-HPLC (column: Kinetex-XB C18, gradient: 0-35 min: A1/B1 92:8-57:43, t_R = 19 min) afforded **4.16** as white fluffy solid (14.7 mg, 75%). ^{1}H-NMR (600 MHz, DMSO-d_6): δ 0.81-0.94 (m, 15H), 1.40-1.87 (m, 18H), 1.96-2.04 (m, 1H), 2.46-2.49 (m, 3H), 2.65-2.71 (m, 1H), 2.86-2.92 (m, 1H), 3.04-3.33 (m,

24H), 3.56-3.62 (m, 5H), 3.81-3.91 (m, 6H), 4.19-4.23 (m, 1H), 4.26-4.29 (m, 1H), 4.33-4.39 (m, 1H), 4.43-4.50 (m, 1H), 4.52-4.59 (m, 1H), 6.59-6.63 (m, 2H), 6.63-7.10 (br s, 2H, interfering with the next listed signal), 6.97-7.00 (m, 2H), 7.10-7.54 (br s, 3H), 7.54-7.72 (m, 2H), 7.97 (d, 1H, *J* 7.7 Hz), 8.07-8.74 (m, 4H), 8.74-9.38 (m, 5H), 11.21-13.33 (m, 2H). 4 exchangeable protons (NH, OH) of the presumably 4-fold protonated molecule could not be identified. HRMS: *m/z* [*M*+3H]$^{3+}$ calcd. for [$C_{60}H_{105}N_{18}O_{16}$]$^{3+}$ 444.5980, found 444.5989. RP-HPLC (220 nm): 99% (t_R = 6.0 min, k = 6.9). $C_{60}H_{102}N_{18}O_{16}$ · $C_8H_4F_{12}O_8$ (1331.59 + 456.09).

***N*$^{\alpha}$-Arginyl-*N*$^{\alpha}$-methyl-*N*$^{\omega}$-{[4-(N-{2-[4,7,10-tris(carboxymethyl)-1,4,7,10-tetraazacyclododecan-1-yl]acetyl})aminobutyl]aminocarbonyl}Arg-Pro-Tyr-α-*tert*-butyl-Gly-Leu tetrakis(hydrotrifluoroacetate) (4.17).** Compound **4.17** was prepared from **4.11** (18.7 mg, 13.3 µmol) and **4.13** (4.9 mg, 6.0 µmol) according to the general procedure for DOTA-conjugation. Isolation of the protected intermediate: column: Kinetex-XB C18, gradient: 0-18 min: A1/B1 92:8-75:25, 18-40 min: 75:25-38:62, t_R = 28 min). Purification of the product by preparative RP-HPLC (column: Kinetex-XB C18, gradient: 0-35 min: A1/B1 92:8-57:43, t_R = 19 min) afforded **4.17** as white fluffy solid (3.0 mg, 28%). ^{1}H-NMR (600 MHz, DMSO-d_6): δ 0.81-0.85 (m, 3H), 0.86-0.94 (m, 12H), 1.40-1.79 (m, 18H), 1.92-2.02 (m, 1H), 2.66-2.72 (m, 1H), 2.82-2.95 (m, 5H), 3.02-3.29 (m, 25H), 3.47-3.84 (m, 8H), 4.17-4.25 (m, 1H), 4.25-4.32 (m, 2H), 4.32-4.40 (m, 1H), 4.43-4.49 (m, 1H), 5.12-5.19 (m, 1H), 6.58-6.63 (m, 2H), 6.63-7.17 (br s, 2H, interfering with the next listed signal), 6.98-7.02 (m, 2H), 7.17-7.53 (br s, 2H), 7.53-7.59 (m, 1H), 7.64-7.79 (m, 1H), 7.79-8.53 (m, 7H), 9.02-9.50 (m, 2H), 12.37 (br s, 1H). 7 exchangeable protons (NH, OH) of the presumably 4-fold protonated molecule could not be identified. HRMS: *m/z* [*M*+3H]$^{3+}$ calcd. for [$C_{60}H_{105}N_{18}O_{16}$]$^{3+}$ 444.5980, found 444.5994. RP-HPLC (220 nm): > 99% (t_R = 6.2 min, k = 7.2). $C_{60}H_{102}N_{18}O_{16}$ · $C_8H_4F_{12}O_8$ (1331.59 + 456.09).

***N*$^{\alpha}$-Methyl-*N*$^{\omega}$-{[8-(N-{2-[4,7,10-tris(carboxymethyl)-1,4,7,10-tetraazacyclododecan-1-yl]acetyl})amino-3,6-dioxaoctyl]aminocarbonyl}Arg-Arg-Pro-Tyr-α-*tert*-butyl-Gly-Leu tetrakis(hydrotrifluoroacetate) (4.18).** Compound **4.18** was prepared from **4.12** (9.3 mg, 6.36 µmol) and **4.13** (4.67 mg, 5.73 µmol) according to the general procedure for DOTA-conjugation. Isolation of the protected intermediate: column: Gemini-NX C18, gradient: 0-6 min: A1/B1 85:15-79:21, 6-28 min: 79:21-40:60, t_R = 18 min. Purification of the product by preparative RP-HPLC (column: Gemini-NX C18, gradient: 0-35 min: A1/B1 97:3-60:40, t_R = 22 min) afforded **4.18** as white fluffy solid (9.8 mg, 93%). ^{1}H-NMR (600 MHz, DMSO-d_6): δ 0.78-1.02 (m, 15H), 1.47-1.87 (m, 14H), 1.97-2.03 (m, 1H), 2.47-2.48 (m, 3H), 2.66-2.70 (m, 1H), 2.87-2.90 (m, 1H), 3.09-3.29 (m, 24H), 3.51-3.59 (m, 10H), 3.60-3.80 (m, 9H), 4.19-4.24 (m, 1H), 4.26-4.31 (m, 1H), 4.32-4.39 (m, 1H), 4.42-4.50 (m, 1H), 4.50-4.59 (m, 1H), 6.58-6.62 (m, 2H), 6.62-7.09 (br s, 2H, interfering with the next listed signal), 6.97-7.00 (m, 2H), 7.09-7.46 (br s, 2H), 7.46-7.65 (m, 3H), 7.98 (d, 1H, *J* 8.0 Hz), 8.10-8.76 (m, 4H), 8.76-9.30 (m, 4H), 11.78-12.80 (m, 1H). 6 exchangeable protons (NH, OH) of the presumably 4-fold protonated molecule could not be identified. HRMS: *m/z* [*M*+2H]$^{2+}$ calcd. for [$C_{62}H_{108}N_{18}O_{18}$]$^{2+}$ 696.4039, found 696.4048. RP-HPLC (220 nm): 99% (t_R = 6.6 min, k = 7.7). $C_{62}H_{106}N_{18}O_{18}$ · $C_8H_4F_{12}O_8$ (1391.64 + 456.09).

***N*$^{\alpha}$-(*N*$^{\alpha}$-Methylarginyl)-*N*$^{\omega}$-{[4-(N-{2-[gallium(III)-4,7,10-tris(carboxymethyl)-1,4,7,10-tetraazacyclododecan-1-yl]acetyl})aminobutyl]aminocarbonyl}Arg-Pro-Tyr-*α-tert*-butyl-Gly-Leu tris(hydrotrifluoroacetate) (4.19).** Compound **4.19** was prepared from **4.14** (4.8 mg, 2.7 µmol) according to the general procedure for the insertion of Ga^{3+}. Purification by preparative RP-HPLC (column: Kinetex-XB C18, gradient: 0-35 min: A2/B1 92:8-57:43, t_R = 17 min) yielded **4.19** as white fluffy solid (4.5 mg, 95%). ^{1}H-NMR (600 MHz, DMSO-d_6): δ 0.80-0.94 (m, 15H), 1.36-1.89 (m, 18H), 1.96-2.05 (m, 1H), 2.47-2.48 (m, 3H), 2.64-2.71 (m, 1H), 2.85-2.92 (m, 1H), 3.08-3.12 (m, 4H), 3.25-3.30 (m, 9H), 3.48-3.50 (m, 6H), 3.57-3.81 (m, 16H), 4.18-4.24 (m, 1H), 4.25-4.31 (m, 1H), 4.32-4.38 (m, 1H), 4.44-4.51 (m, 1H), 4.53-4.60 (m, 1H), 6.59-6.62 (m, 2H), 6.62-7.15 (br s, 2H, interfering with the next listed signal), 6.98-7.01 (m, 2H), 7.15-7.47 (br s, 2H), 7.47-7.56 (m, 1H), 7.56-7.70 (m, 2H), 7.90-8.05 (m, 1H), 8.15-8.27 (m, 1H), 8.28-8.65 (m, 3H), 8.85-9.02 (m, 3H), 9.14-9.21 (m, 1H), 10.03-10.30 (m, 1H), 12.25-12.80 (m, 1H), 13.03-13.57 (m, 1H). HRMS: *m/z* [*M*+2H]$^{2+}$ calcd. for $[C_{60}H_{101}GaN_{18}O_{16}]^{2+}$ 699.3444, found 699.3455. RP-HPLC (220 nm): > 99% (t_R = 10.0 min, *k* = 12.2). $C_{60}H_{99}GaN_{18}O_{16}$ · $C_6H_3F_9O_6$ (1398.29 + 342.07).

***N*$^{\alpha}$-(*N*$^{\alpha}$-Methylarginyl)-*N*$^{\omega}$-{[4-(N-{2-[gallium(III)-4,7,10-tris(carboxymethyl)-1,4,7,10-tetraazacyclododecan-1-yl]acetyl})aminobutyl]aminocarbonyl}Arg-Pro-Tyr-Ile-Leu tris(hydrotrifluoroacetate) (4.20).** Compound **4.20** was prepared from **4.15** (4.9 mg, 2.8 µmol) according to the general procedure for the insertion of Ga^{3+}. Purification by preparative RP-HPLC (column: Kinetex-XB C18, gradient: 0-35 min: A2/B1 92:8-57:43, t_R = 17 min) yielded **4.20** as white fluffy solid (4.9 mg, > 99%). ^{1}H-NMR (600 MHz, DMSO-d_6): δ 0.77-0.93 (m, 12H), 0.99-1.09 (m, 1H), 1.37-1.87 (m, 20H), 1.92-2.06 (m, 1H), 2.46-2.48 (m, 3H), 2.64-2.71 (m, 1H), 2.82-2.89 (m, 1H), 3.03-3.22 (m, 10H), 3.26-3.30 (m, 8H), 3.60-3.82 (m, 17H), 4.17-4.26 (m, 2H), 4.32-4.37 (m, 1H), 4.40-4.48 (m, 1H), 4.52-4.60 (m, 1H), 6.56-6.63 (m, 2H), 6.63-7.13 (br s, 2H, interfering with the next listed signal), 6.97-7.01 (m, 2H), 7.13-7.47 (br s, 2H), 7.47-7.56 (m, 1H), 7.62-7.70 (m, 1H), 7.70-7.81 (m, 1H), 7.83-7.94 (m, 1H), 8.20 (d, 1H, *J* 7.6 Hz), 8.25-8.64 (m, 3H), 8.86-9.20 (m, 4H), 9.99-10.35 (m, 1H), 12.51 (br s, 1H), 13.29 (br s, 1H). HRMS: *m/z* [*M*+2H]$^{2+}$ calcd. for $[C_{60}H_{101}GaN_{18}O_{16}]^{2+}$ 699.3444, found 699.3456. RP-HPLC (220 nm): > 99% (t_R = 10.7 min, *k* = 13.1). $C_{60}H_{99}GaN_{18}O_{16}$ · $C_6H_3F_9O_6$ (1398.29 + 342.07).

***N*$^{\alpha}$-Methyl-*N*$^{\omega}$-{[4-(N-{2-[gallium(III)-4,7,10-tris(carboxymethyl)-1,4,7,10-tetraazacyclododecan-1-yl]acetyl})aminobutyl]aminocarbonyl}Arg-Arg-Pro-Tyr-*α-tert*-butyl-Gly-Leu tris(hydrotrifluoroacetate) (4.21).** Compound **4.21** was prepared from **4.16** (4.8 mg, 2.7 µmol) according to the general procedure for the insertion of Ga^{3+}. Purification by preparative RP-HPLC (column: Kinetex-XB C18, gradient: 0-35 min: A2/B1 92:8-57:43, t_R = 17 min) yielded **4.21** as white fluffy solid (4.3 mg, 92%). ^{1}H-NMR (600 MHz, DMSO-d_6): δ 0.78-0.97 (m, 15H), 1.37-1.86 (m, 18H), 1.95-2.04 (m, 1H), 2.44-2.48 (m, 3H), 2.64-2.71 (m, 1H), 2.85-2.92 (m, 1H), 3.01-3.18 (m, 9H), 3.22-3.34 (m, 13H), 3.64-3.83 (m, 13H), 4.19-4.25 (m, 1H), 4.26-4.30 (m, 1H), 4.33-4.38 (m, 1H), 4.42-4.50 (m, 1H), 4.50-4.59 (m, 1H), 6.58-6.63 (m, 2H), 6.63-7.12 (br s, 2H, interfering with the next listed signal), 6.97-7.00 (m, 2H), 7.12-7.48 (br s, 2H), 7.48-7.57 (m, 1H), 7.57-7.74 (m, 2H), 7.97 (d, 1H, *J* 7.7 Hz), 8.11-8.60 (m, 4H), 8.85-9.22 (m, 4H), 10.03-10.30 (m, 1H), 12.49 (br s, 1H), 13.30 (br s, 1H). HRMS: *m/z* [*M*+2H]$^{2+}$ calcd. for $[C_{60}H_{101}GaN_{18}O_{16}]^{2+}$ 699.3444,

found 699.3448. RP-HPLC (220 nm): > 99% (t_R = 9.5 min, k = 11.5). $C_{60}H_{99}GaN_{18}O_{16}$ · $C_6H_3F_9O_6$ (1398.29 + 342.07).

***N*$^{\alpha}$-Arginyl-*N*$^{\alpha}$-methyl-*N*$^{\omega}$-{[4-(N-{2-[gallium(III)-4,7,10-tris(carboxymethyl)-1,4,7,10-tetraazacyclododecan-1-yl]acetyl})aminobutyl]aminocarbonyl}Arg-Pro-Tyr-α-*tert*-butyl-Gly-Leu tris(hydrotrifluoroacetate) (4.22).** Compound **4.22** was prepared from **4.17** (1.7 mg, 0.97 µmol) according to the general procedure for the insertion of Ga^{3+}. Purification by preparative RP-HPLC (column: Kinetex-XB C18, gradient: 0-35 min: A2/B1 92:8-57:43, t_R = 16 min) yielded **4.22** as white fluffy solid (1.7 mg, 99%). ^{1}H-NMR (600 MHz, DMSO-d_6): δ 0.80-0.95 (m, 15H), 1.37-1.79 (m, 18H), 1.94-2.01 (m, 1H), 2.66-2.72 (m, 1H), 2.86-2.95 (m, 4H), 3.04-3.28 (m, 21H), 3.47-3.79 (m, 13H), 4.18-4.25 (m, 1H), 4.26-4.33 (m, 2H), 4.33-4.39 (m, 1H), 4.41-4.48 (m, 1H), 5.10-5.18 (m, 1H), 6.58-6.63 (m, 2H), 6.63-7.14 (br s, 2H, interfering with the next listed signal), 6.98-7.02 (m, 2H), 7.14-7.46 (br s, 2H), 7.46-7.60 (m, 2H), 7.60-7.76 (m, 1H), 7.97 (d, 1H, J 7.9 Hz), 8.04-8.61 (m, 6H), 8.78-9.04 (m, 1H), 9.17 (s, 1H), 9.85-10.07 (m, 1H), 12.15-12.86 (m, 1H), 12.91-13.48 (m, 1H). HRMS: m/z $[M+2H]^{2+}$ calcd. for $[C_{60}H_{101}GaN_{18}O_{16}]^{2+}$ 699.3444, found 699.3454. RP-HPLC (220 nm): 98% (t_R = 9.6 min, k = 11.6). $C_{60}H_{99}GaN_{18}O_{16}$ · $C_6H_3F_9O_6$ (1398.29 + 342.07).

***N*$^{\alpha}$-Methyl-*N*$^{\omega}$-{[8-(N-{2-[gallium(III)-4,7,10-tris(carboxymethyl)-1,4,7,10-tetraazacyclododecan-1-yl]acetyl})amino-3,6-dioxaoctyl]aminocarbonyl}Arg-Arg-Pro-Tyr-α-*tert*-butyl-Gly-Leu tris(hydrotrifluoroacetate) (4.23).** Compound **4.23** was prepared from **4.18** (3.0 mg, 1.62 µmol) according to the general procedure for the insertion of Ga^{3+}. Purification by preparative RP-HPLC (column: Gemini-NX C18, gradient: 0-35 min: A2/B1 97:3-60:40, t_R = 21 min) yielded **4.23** as white fluffy solid (2.7 mg, 92%). ^{1}H-NMR (600 MHz, DMSO-d_6): δ 0.77-0.97 (m, 15H), 1.42-1.90 (m, 14H), 1.94-2.04 (m, 1H), 2.45-2.49 (m, 3H), 2.64-2.73 (m, 1H), 2.85-2.92 (m, 1H), 3.07-3.31 (m, 20H), 3.40-3.83 (m, 23H), 4.16-4.25 (m, 1H), 4.25-4.31 (m, 1H), 4.33-4.40 (m, 1H), 4.42-4.59 (m, 2H), 6.56-6.63 (m, 2H), 6.63-7.12 (br s, 2H, interfering with the next listed signal), 6.97-7.00 (m, 2H), 7.12-7.49 (br s, 2H), 7.49-7.81 (m, 3H), 7.98 (d, 1H, J 7.7 Hz), 8.22 (d, 1H, J 7.6 Hz), 8.28-8.65 (m, 3H), 8.78-9.20 (m, 4H), 10.05-10.40 (m, 1H), 12.48 (br s, 1H), 13.28 (br s, 1H). HRMS: m/z $[M+3H]^{3+}$ calcd. for $[C_{62}H_{106}GaN_{18}O_{18}]^{3+}$ 486.5724, found 486.5733. RP-HPLC (220 nm): > 99% (t_R = 10.7 min, k = 13.1). $C_{62}H_{103}GaN_{18}O_{18}$ · $C_6H_3F_9O_6$ (1458.34 + 342.07).

***N*$^{\alpha}$-Methyl-*N*$^{\omega}$-({4-N-[4-(4-fluorophenyl)phenylalanyl]aminobutyl}aminocarbonyl)Arg-Arg-Pro-Tyr-α-*tert*-butyl-Gly-Leu tetrakis(hydrotrifluoroacetate) (4.25).** HBTU (4.0 mg, 10.4 µmol) and DIPEA (3.6 µL, 20.9 µmol) were added to a solution of HOBt (1.4 mg, 10.4 µmol) and **4.24** (5.4 mg, 14.9 µmol) in DMF/NMP (80:20 v/v) (15 µL) in a 2-mL reaction vessel. The mixture was vortexed, incubated for 5 min at rt and added to a solution of **3.16** (29.8 mg, 21.3 µmol) and DIPEA (14.8 µL, 85.2 µmol) in DMF/NMP (80:20 v/v) (18 µL) in a 2-mL reaction vessel with screw cap equipped with a magnetic micro stirrer. After stirring at rt for 60 min, 10% aq TFA (106.1 µL, 106 µmol) was added. The protected intermediate was isolated by preparative HPLC (column: Gemini-NX C18, gradient: 0-6 min: A1/B1 85:15-82:18, 6-15 min: 82:18-70:30, 15-25 min: 70:30-60:40, 25-30 min: 60:40-40:60, t_R = 26 min). After lyophilization of the eluate, TFA/H_2O (95:5 v/v) (2 mL) was added, and the mixture

was stirred at rt for 2.5 h. Additional TFA (1 mL) was added and stirring was continued for 1 h. The crude product was dissolved in H_2O (40 mL) and the solution was subjected to lyophilization. Purification of the product by preparative RP-HPLC (column: Gemini-NX C18, gradient: 0-5 min: A1/B1 85:15-70:30, 5-15 min: 70:30-50:50, t_R = 9 min) afforded **4.25** as white fluffy solid (7.9 mg, 46%). ^{1}H-NMR (600 MHz, DMSO-d_6): δ 0.79-0.95 (m, 15H), 1.27-1.38 (m, 4H), 1.43-1.88 (m, 14H), 1.93-2.03 (m, 1H), 2.38-2.49 (m, 3H), 2.64-2.72 (m, 1H), 2.85-2.93 (m, 1H), 2.95-3.17 (m, 8H), 3.18-3.25 (m, 2H), 3.43-3.88 (m, 3H), 3.88-3.98 (m, 1H), 4.16-4.31 (m, 2H), 4.31-4.40 (m, 1H), 4.40-4.58 (m, 2H), 6.57-6.62 (m, 2H), 6.62-7.10 (br s, 2H, interfering with the next listed signal), 6.97-7.00 (m, 2H), 7.10-7.57 (br s, 2H, interfering with the next two listed signals), 7.27-7.32 (m, 4H), 7.40-7.50 (m, 1H), 7.57-7.78 (m, 6H), 7.78-8.60 (m, 8H), 8.60-9.44 (m, 4H), 10.32 (br s, 1H), 12.49 (br s, 1H). 1 exchangeable proton (NH, OH) of the presumably 4-fold protonated molecule could not be identified. HRMS: *m/z* [*M*+2H]$^{2+}$ calcd. for $[C_{59}H_{90}FN_{15}O_{10}]^{2+}$ 593.8484, found 593.8491. RP-HPLC (220 nm): > 99% (t_R = 10.9 min, *k* = 13.3). $C_{59}H_{88}FN_{15}O_{10}$ · $C_8H_4F_{12}O_8$ (1186.45 + 456.09).

N^{α}-Methyl-N^{ω}-({8-N-[4-(4-fluorophenyl)-phenylalanyl]amino-3,6-dioxaoctyl}aminocarbonyl)Arg-Arg-Pro-Tyr-*a*-*tert*-butyl-Gly-Leu tetrakis(hydrotrifluoroacetate) (4.26). Compound **4.26** was prepared from **4.12** (29.2 mg, 20.0 µmol) and **4.24** (5.0 mg, 14.0 µmol) according to the procedure for the synthesis of **4.25**. Isolation of the protected intermediate: column: Gemini-NX C18, gradient: 0-6 min: A1/B1 85:15-82:18, 6-15 min: 82:18-70:30, 15-25 min: 70:30-60:40, 25-30 min: 60:40-40:60, t_R = 26 min. Purification of the product by preparative RP-HPLC (column: Gemini-NX C18, gradient: 0-5 min: A1/B1 85:15-70:30, 5-15 min: 70:30-50:50, t_R = 10 min) afforded **4.26** as white fluffy solid (7.76 mg, 47%). ^{1}H-NMR (600 MHz, DMSO-d_6): δ 0.80-0.95 (m, 15H), 1.38-1.90 (m, 14H), 1.94-2.05 (m, 1H), 2.40-2.48 (m, 3H), 2.64-2.71 (m, 1H), 2.86-2.92 (m, 1H), 2.97-3.02 (m, 1H), 3.04-3.26 (m, 8H), 3.34-3.44 (m, 5H), 3.45-3.49 (m, 4H), 3.52-3.64 (m, 2H), 3.64-3.92 (m, 1H), 3.95-4.03 (m, 1H), 4.18-4.30 (m, 2H), 4.32-4.39 (m, 1H), 4.43-4.59 (m, 2H), 6.57-6.63 (m, 2H), 6.63-7.11 (br s, 2H, interfering with the next listed signal), 6.97-7.00 (m, 2H), 7.11-7.57 (br s, 2H, interfering with the next two listed signals), 7.27-7.33 (m, 4H), 7.39-7.49 (m, 1H), 7.57-7.72 (m, 6H), 7.97 (d, 1H, *J* 7.7 Hz), 8.00-8.70 (m, 7H), 8.70-9.37 (m, 4H), 10.30 (br s, 1H), 12.49 (br s, 1H). 1 exchangeable proton (NH, OH) of the presumably 4-fold protonated molecule could not be identified. HRMS: *m/z* [*M*+H]$^+$ calcd. for $[C_{61}H_{93}FN_{15}O_{12}]^+$ 1246.7107, found 1246.7112. RP-HPLC (220 nm): 99% (t_R = 11.5 min, *k* = 14.1). $C_{61}H_{92}FN_{15}O_{12}$ · $C_8H_4F_{12}O_8$ (1246.50 + 456.09).

N^{α}-Methyl-N^{ω}-{[4-N-(4-aminomethyl-3-fluorobenzoyl)aminobutyl]aminocarbonyl}Arg-Arg-Pro-Tyr-*a*-*tert*-butyl-Gly-Leu tetrakis(hydrotrifluoroacetate) (4.28). Compound **4.28** was prepared from **3.16** (16.6 mg, 11.9 µmol) and **4.27** (2.2 mg, 8.30 µmol) according to the procedure for the synthesis of **4.25** (modification: stirring of the mixture for 75 min instead of 60 min). Isolation of the protected intermediate: column: Gemini-NX C18, gradient: 0-6 min: A1/B1 85:15-82:18, 6-16 min: 82:18-70:30, 16-30 min: 70:30-60:40, t_R = 23 min. Purification of the product by preparative RP-HPLC (column: Gemini-NX C18, gradient: 0-5 min: A1/B1 85:15-80:20, 5-15 min: 80:20-60:40, t_R = 11 min) afforded **4.28** as white fluffy solid (2.2 mg, 24%). ^{1}H-NMR (600 MHz, DMSO-d_6): δ 0.77-0.97 (m, 15H), 1.39-1.90 (m, 18H), 1.94-2.05

(m, 1H), 2.45-2.49 (m, 3H), 2.64-2.71 (m, 1H), 2.84-2.94 (m, 1H), 3.05-3.17 (m, 4H), 3.23-3.28 (m, 4H), 3.50-3.64 (m, 2H), 3.73-3.88 (m, 1H), 4.08-4.17 (m, 2H), 4.17-4.24 (m, 1H), 4.26-4.31 (m, 1H), 4.32-4.40 (m, 1H), 4.41-4.60 (m, 2H), 6.57-6.62 (m, 2H), 6.62-7.09 (br s, 2H, interfering with the next listed signal), 6.97-7.00 (m, 2H), 7.09-7.44 (br s, 2H), 7.44-7.67 (m, 4H), 7.67-7.76 (m, 2H), 7.98 (d, 1H, *J* 7.7 Hz), 8.05-8.59 (m, 6H), 8.59-8.66 (m, 1H), 8.73-9.25 (m, 4H), 9.86-10.16 (m, 1H), 12.44 (br s, 1H). 1 exchangeable proton (NH, OH) of the presumably 4-fold protonated molecule could not be identified. HRMS: *m/z* [*M*+2H]$^{2+}$ calcd. for [$C_{52}H_{84}FN_{15}O_{10}$]$^{2+}$ 548.8249, found 548.8262. RP-HPLC (220 nm): > 99% (t_R = 7.0 min, *k* = 8.2). $C_{52}H_{82}FN_{15}O_{10}$ · $C_8H_4F_{12}O_8$ (1096.32 + 456.09).

***N*$^{\alpha}$-Methyl-*N*$^{\omega}$-{[8-N-(4-aminomethyl-3-fluorobenzoyl)amino-3,6-dioxaoctyl]aminocarbonyl}Arg-Arg-Pro-Tyr-*a*-*tert*-butyl-Gly-Leu tetrakis(hydrotrifluoroacetate) (4.29).** Compound **4.29** was prepared from **4.12** (12.2 mg, 8.35 µmol) and **4.27** (1.6 mg, 5.84 µmol) according to the procedure for the synthesis of **4.25**. Isolation of the protected intermediate: column: Gemini-NX C18, gradient: 0-6 min: A1/B1 85:15-82:18, 6-15 min: 82:18-70:30, 15-25 min: 70:30-60:40, t_R = 22 min. Purification of the product by preparative RP-HPLC (column: Gemini-NX C18, gradient: 0-5 min: A1/B1 85:15-80:20, 5-15 min: 80:20-60:40, t_R = 11 min) afforded **4.29** as white fluffy solid (2.1 mg, 32%). ^{1}H-NMR (600 MHz, DMSO-d_6): δ 0.78-0.96 (m, 15H), 1.44-1.88 (m, 14H), 1.95-2.04 (m, 1H), 2.44-2.48 (m, 3H), 2.65-2.72 (m, 1H), 2.85-2.91 (m, 1H), 3.07-3.15 (m, 2H), 3.23-3.29 (m, 4H), 3.42-3.47 (m, 4H), 3.53-3.61 (m, 8H), 3.78-3.80 (m, 1H), 4.12-4.15 (m, 2H), 4.20-4.23 (m, 1H), 4.27-4.29 (m, 1H), 4.34-4.38 (m, 1H), 4.44-4.57 (m, 2H), 6.57-6.62 (m, 2H), 6.62-7.11 (br s, 2H, interfering with the next listed signal), 6.97-7.00 (m, 2H), 7.11-7.46 (br s, 2H), 7.46-7.54 (m, 1H), 7.54-7.77 (m, 5H), 7.97 (d, 1H, *J* 7.9 Hz), 8.11-8.65 (m, 6H), 8.65-8.72 (m, 1H), 8.72-9.31 (m, 5H), 10.05-10.33 (m, 1H), 12.49 (br s, 1H). HRMS: *m/z* [*M*+2H]$^{2+}$ calcd. for [$C_{54}H_{88}FN_{15}O_{12}$]$^{2+}$ 578.8355, found 578.8369. RP-HPLC (220 nm): 99% (t_R = 7.1 min, *k* = 8.3). $C_{54}H_{86}FN_{15}O_{12}$ · $C_8H_4F_{12}O_8$ (1156.37 + 456.09).

***N*$^{\alpha}$-Methyl-*N*$^{\omega}$-({8-N-[*N*$^{\alpha}$-(6-aminohexanoyl)-4-(4-fluorophenyl)-phenylalanyl]amino-3,6-dioxaoctyl}aminocarbonyl)Arg-Arg-Pro-Tyr-*a*-*tert*-butyl-Gly-Leu tetrakis(hydrotrifluoroacetate) (4.31).** The reaction was performed in a 2-mL reaction vessel with screw cap, equipped with a magnetic micro stirrer. DIPEA (2.5 µL, 14.3 µmol) and a solution of *N*-Boc-6-aminohexanoic acid succinimidyl ester (**4.30**) (1.06 mg, 3.22 µmol) in anhydrous DMF/NMP (75:25 v/v) (4 µL) were added to a solution of **4.26** (6.09 mg, 3.58 µmol) in anhydrous DMF/NMP (75:25 v/v) (41 µL). The mixture was stirred at rt for 45 min followed by the addition of 10% aq TFA (14.3 µL, 14.3 µmol). The protected intermediate was isolated by preparative HPLC (column: Gemini-NX C18, gradient: 0-5 min: A1/B1 85:15-70:30, 5-15 min: 70:30-50:50, 15-25 min: 50:50-30:70, t_R = 14 min) and the eluate was subjected to lyophilization. TFA/H_2O (95:5 v/v) (2 mL) was added, and the mixture was stirred at rt for 3 h. Additional TFA (1 mL) was added and stirring was continued for 30 min. The crude product was dissolved in H_2O (40 mL) and the mixture was subjected to lyophilization. Purification of the product by preparative RP-HPLC (column: Gemini-NX C18, gradient: 0-5 min: A1/B1 85:15-70:30, 5-15 min: 70:30-50:50, t_R = 10 min) gave **4.31** as white fluffy solid (3.84 mg, 66%). HRMS: *m/z* [*M*+2H]$^{2+}$ calcd. for [$C_{67}H_{105}FN_{16}O_{13}$]$^{2+}$ 680.4010, found 680.4019. RP-HPLC (220 nm): > 99% (t_R = 12.2 min, *k* = 15.1). $C_{67}H_{103}FN_{16}O_{13}$ · $C_8H_4F_{12}O_8$ (1359.66 + 456.09).

***N*$^{\alpha}$-Methyl-*N*$^{\omega}$-({8-N-[*N*$^{\alpha}$-(6-N-{2-[4,7,10-tris(carboxymethyl)-1,4,7,10-tetraazacyclododecan-1-yl]acetyl}-aminohexanoyl)-4-(4-fluorophenyl)-phenylalanyl]amino-3,6-dioxaoctyl}aminocarbonyl)Arg-Arg-Pro-Tyr-*α-tert*-butyl-Gly-Leu tetrakis(hydrotrifluoroacetate) (4.32).** Compound **4.32** was prepared from **4.31** (3.84 mg, 2.11 µmol) and **4.13** (1.55 mg, 1.90 µmol) according to the general procedure for DOTA-conjugation (modification: stirring of the mixture for 45 min instead of 30 min). Isolation of the protected intermediate: column: Gemini-NX C18, gradient: 0-5 min: A1/B1 85:15-70:30, 5-15 min: 70:30-50:50, t_R = 14 min. Purification of the product by preparative RP-HPLC (column: Gemini-NX C18, gradient: 0-5 min: A1/B1 85:15-70:30, 5-15 min: 70:30-50:50, t_R = 10 min) afforded **4.32** as white fluffy solid (2.9 mg, 69%). ^{1}H-NMR (600 MHz, DMSO-d_6): δ 0.80-0.94 (m, 15H), 1.07-1.18 (m, 2H), 1.28-1.43 (m, 4H), 1.45-1.89 (m, 14H), 1.95-2.10 (m, 3H), 2.44-2.47 (m, 3H), 2.64-2.71 (m, 1H), 2.72-3.26 (m, 29H), 3.40-3.73 (m, 18H), 3.76-3.83 (m, 1H), 4.17-4.25 (m, 1H), 4.25-4.30 (m, 1H), 4.32-4.39 (m, 1H), 4.42-4.60 (m, 3H), 6.58-6.62 (m, 2H), 6.62-7.12 (br s, 2H, interfering with the next listed signal), 6.97-7.00 (m, 2H), 7.12-7.45 (br s, 2H, interfering with the next listed signal), 7.25-7.32 (m, 4H), 7.45-7.52 (m, 1H), 7.52-7.56 (m, 2H), 7.56-7.72 (m, 4H), 7.81-8.30 (m, 5H), 8.30-9.44 (m, 6H), 10.22-10.69 (m, 1H), 11.12-12.83 (m, 2H). 4 exchangeable protons (NH, OH) of the presumably 4-fold protonated molecule could not be identified. HRMS: *m/z* [*M*+2H]$^{2+}$ calcd. for [$C_{83}H_{131}FN_{20}O_{20}$]$^{2+}$ 873.4911, found 873.4920. RP-HPLC (220 nm): 99% (t_R = 12.5 min, *k* = 15.4). $C_{83}H_{129}FN_{20}O_{20}$ · $C_8H_4F_{12}O_8$ (1746.06 + 456.09).

***N*$^{\alpha}$-Methyl-*N*$^{\omega}$-({8-N-[*N*$^{\alpha}$-(6-N-{2-[gallium(III)-4,7,10-tris(carboxymethyl)-1,4,7,10-tetraazacyclododecan-1-yl]acetyl}-aminohexanoyl)-4-(4-fluorophenyl)-phenylalanyl]amino-3,6-dioxaoctyl}aminocarbonyl)Arg-Arg-Pro-Tyr-*α-tert*-butyl-Gly-Leu tris(hydrotrifluoroacetate) (4.33).** Compound **4.33** was prepared from **4.32** (1.81 mg, 0.82 µmol) according to the general procedure for the insertion of Ga^{3+}. Purification by preparative RP-HPLC (column: Gemini-NX C18, gradient: 0-5 min: A1/B1 85:15-75:25, 5-10 min: 75:25-67:33, 10-20 min: 67:33-55:45, t_R = 14 min) yielded **4.33** as white fluffy solid (1.76 mg, 99%). ^{1}H-NMR (600 MHz, DMSO-d_6): δ 0.81-0.94 (m, 15H), 1.07-1.16 (m, 2H), 1.27-1.41 (m, 4H), 1.47-1.64 (m, 8H), 1.64-1.87 (m, 6H), 1.95-2.07 (m, 3H), 2.44-2.47 (m, 3H), 2.64-2.71 (m, 1H), 2.74-2.81 (m, 1H), 2.85-2.91 (m, 1H), 2.91-3.02 (m, 3H), 3.07-3.10 (m, 1H), 3.10-3.29 (m, 18H), 3.34-3.37 (m, 4H), 3.37-3.49 (m, 7H), 3.49-3.51 (m, 3H), 3.58-3.76 (m, 10H), 4.17-4.25 (m, 1H), 4.25-4.31 (m, 1H), 4.33-4.38 (m, 1H), 4.43-4.60 (m, 3H), 6.57-6.62 (m, 2H), 6.62-7.10 (br s, 2H, interfering with the next listed signal), 6.97-7.01 (m, 2H), 7.10-7.45 (br s, 2H, interfering with the next listed signal), 7.25-7.32 (m, 4H), 7.45-7.52 (m, 1H), 7.52-7.72 (m, 6H), 7.86-8.12 (m, 3H), 8.12-8.61 (m, 4H), 8.78-9.21 (m, 4H), 9.85-10.20 (m, 1H), 12.48 (br s, 1H), 13.27 (br s, 1H). HRMS: *m/z* [*M*+2H]$^{2+}$ calcd. for [$C_{83}H_{128}FGaN_{20}O_{20}$]$^{2+}$ 906.4421, found 906.4431. RP-HPLC (220 nm): 99% (t_R = 12.5 min, *k* = 15.4). $C_{83}H_{126}FGaN_{20}O_{20}$ · $C_6H_3F_9O_6$ (1812.76 + 342.07).

***N*$^{\alpha}$-Methyl-*N*$^{\omega}$-{[4-N-(*N*$^{\alpha}$-{2-[4,7,10-tris(carboxymethyl)-1,4,7,10-tetraazacyclododecan-1-yl]acetyl}-4-{4-fluorophenyl}phenylalanyl)aminobutyl]aminocarbonyl}Arg-Arg-Pro-Tyr-*α-tert*-butyl-Gly-Leu tetrakis(hydrotrifluoroacetate) (4.34).** Compound **4.34** was prepared from **4.25** (7.9 mg, 4.81 µmol) and **4.13** (3.14 mg, 3.85 µmol) according to the general procedure for DOTA-conjugation. Isolation of the protected intermediate: column: Gemini-NX C18, gradient: 0-5 min: A1/B1 85:15-70:30, 5-15 min: 70:30-50:50, t_R = 13 min.

Purification of the product by preparative RP-HPLC (column: Gemini-NX C18, gradient: 0-5 min: A1/B1 85:15-70:30, 5-15 min: 70:30-50:50, t_R = 9 min) afforded **4.34** as white fluffy solid (6.1 mg, 78%). ^{1}H-NMR (600 MHz, DMSO-d_6): δ 0.81-0.94 (m, 15H), 1.33-1.44 (m, 4H), 1.46-1.87 (m, 14H), 1.95-2.05 (m, 1H), 2.46-2.49 (m, 3H), 2.65-2.70 (m, 1H), 2.77-3.26 (m, 28H), 3.55-3.67 (m, 5H), 3.67-3.93 (m, 5H), 4.19-4.24 (m, 1H), 4.26-4.30 (m, 1H), 4.33-4.39 (m, 1H), 4.42-4.60 (m, 3H), 6.58-6.62 (m, 2H), 6.62-7.12 (br s, 2H, interfering with the next listed signal), 6.97-7.00 (m, 2H), 7.12-7.54 (br s, 2H, interfering with the next listed signal), 7.26-7.33 (m, 4H), 7.54-7.57 (m, 2H), 7.57-7.71 (m, 4H), 7.71-8.53 (m, 6H), 8.53-9.32 (m, 6H), 11.49 (br s, 1H), 12.47 (br s, 1H). 4 exchangeable protons (NH, OH) of the presumably 4-fold protonated molecule could not be identified. HRMS: *m/z* [*M*+2H]$^{2+}$ calcd. for [$C_{75}H_{116}FN_{19}O_{17}$]$^{2+}$ 786.9385, found 786.9394. RP-HPLC (220 nm): > 99% (t_R = 11.2 min, *k* = 13.7). $C_{75}H_{114}FN_{19}O_{17}$ · $C_8H_4F_{12}O_8$ (1572.85 + 456.09).

***N*$^{\alpha}$-Methyl-*N*$^{\omega}$-{[8-N-(*N*$^{\alpha}$-{2-[4,7,10-tris(carboxymethyl)-1,4,7,10-tetraazacyclododecan-1-yl]acetyl}-4-{4-fluorophenyl}-phenylalanyl)amino-3,6-dioxaoctyl]aminocarbonyl}Arg-Arg-Pro-Tyr-α-*tert*-butyl-Gly-Leu tetrakis(hydrotrifluoroacetate) (4.35).** Compound **4.35** was prepared from **4.26** (6.6 mg, 3.86 µmol) and **4.13** (2.52 mg, 3.09 µmol) according to the general procedure for DOTA-conjugation. Isolation of the protected intermediate: column: Gemini-NX C18, gradient: 0-5 min: A1/B1 85:15-70:30, 5-15 min: 70:30-50:50, t_R = 13 min. Purification of the product by preparative RP-HPLC (column: Gemini-NX C18, gradient: 0-5 min: A1/B1 85:15-70:30, 5-15 min: 70:30-50:50, t_R = 10 min) afforded **4.35** as white fluffy solid (5.2 mg, 81%). ^{1}H-NMR (600 MHz, DMSO-d_6): δ 0.80-0.95 (m, 15H), 1.47-1.87 (m, 14H), 1.95-2.03 (m, 1H), 2.46-2.48 (m, 3H), 2.64-2.70 (m, 1H), 2.75-2.79 (m, 1H), 2.84-2.91 (m, 3H), 3.23-3.41 (m, 24H), 3.49-3.61 (m, 16H), 3.77-3.87 (m, 2H), 4.18-4.24 (m, 1H), 4.27-4.29 (m, 1H), 4.32-4.40 (m, 1H), 4.43-4.50 (m, 1H), 4.50-4.58 (m, 1H), 4.60-4.71 (m, 1H), 6.56-6.62 (m, 2H), 6.62-7.09 (br s, 2H, interfering with the next listed signal), 6.97-7.00 (m, 2H), 7.09-7.43 (br s, 2H, interfering with the next listed signal), 7.26-7.34 (m, 4H), 7.43-7.52 (m, 1H), 7.52-7.64 (m, 4H), 7.64-7.69 (m, 2H), 7.87-8.02 (m, 1H), 8.07-8.83 (m, 5H), 8.83-9.29 (m, 4H), 10.19-11.03 (m, 1H), 11.99-12.87 (m, 1H). 5 exchangeable protons (NH, OH) of the presumably 4-fold protonated molecule could not be identified. HRMS: *m/z* [*M*+2H]$^{2+}$ calcd. for [$C_{77}H_{120}FN_{19}O_{19}$]$^{2+}$ 816.9490, found 816.9497. RP-HPLC (220 nm): 97% (t_R = 12.1 min, *k* = 14.9). $C_{77}H_{118}FN_{19}O_{19}$ · $C_8H_4F_{12}O_8$ (1632.90 + 456.09).

***N*$^{\alpha}$-Methyl-*N*$^{\omega}$-{[4-N-(*N*$^{\alpha}$-{2-[gallium(III)-4,7,10-tris(carboxymethyl)-1,4,7,10-tetraazacyclododecan-1-yl]acetyl}-4-(4-fluorophenyl)phenylalanyl)aminobutyl]aminocarbonyl}Arg-Arg-Pro-Tyr-α-*tert*-butyl-Gly-Leu tris(hydrotrifluoroacetate) (4.36).** Compound **4.36** was prepared from **4.34** (3.49 mg, 1.72 µmol) according to the general procedure for the insertion of Ga^{3+}. Purification by preparative RP-HPLC (column: Gemini-NX C18, gradient: 0-5 min: A1/B1 85:15-75:25, 5-10 min: 75:25-67:33, 10-20 min: 67:33-55:45, t_R = 12 min) yielded **4.36** as white fluffy solid (3.26 mg, 96%). ^{1}H-NMR (600 MHz, DMSO-d_6): δ 0.79-0.95 (m, 15H), 1.31-1.43 (m, 4H), 1.44-1.89 (m, 14H), 1.95-2.04 (m, 1H), 2.43-2.48 (m, 3H), 2.64-2.85 (m, 3H), 2.85-3.29 (m, 22H), 3.35-3.90 (m, 14H), 4.17-4.25 (m, 1H), 4.25-4.31 (m, 1H), 4.31-4.41 (m, 1H), 4.41-4.59 (m, 3H), 6.57-6.63 (m, 2H), 6.63-7.12 (br s, 2H, interfering with the next listed signal), 6.97-7.00 (m, 2H), 7.12-7.45 (br s, 2H, interfering with the next listed signal), 7.26-7.33 (m, 4H), 7.45-7.53 (m, 1H), 7.53-7.76 (m, 6H), 7.97 (d, 1H, *J* 7.8 Hz), 8.03-8.16

(m, 1H), 8.22 (d, 1H, *J* 7.3 Hz), 8.28-8.65 (m, 2H), 8.68-9.26 (m, 5H), 9.75-10.27 (m, 1H), 12.47 (br s, 1H), 13.27 (br s, 1H). HRMS: *m/z* [*M*+3H]$^{3+}$ calcd. for [$C_{75}H_{114}FGaN_{19}O_{17}$]$^{3+}$ 546.9288, found 546.9299. RP-HPLC (220 nm): > 99% (t_R = 14.4 min, *k* = 17.9). $C_{75}H_{111}FGaN_{19}O_{17}$ · $C_6H_3F_9O_6$ (1639.55 + 342.07).

***N*$^{\alpha}$-Methyl-*N*$^{\omega}$-{[8-N-(*N*$^{\alpha}$-{2-[gallium(III)-4,7,10-tris(carboxymethyl)-1,4,7,10-tetraazacyclododecan-1-yl]acetyl}-4-{4-fluorophenyl}-phenylalanyl)amino-3,6-dioxaoctyl]aminocarbonyl}Arg-Arg-Pro-Tyr-*a*-*tert*-butyl-Gly-Leu tris(hydrotrifluoroacetate) (4.37).** Compound **4.37** was prepared from **4.35** (3.33 mg, 1.59 µmol) according to the general procedure for the insertion of Ga^{3+}. Purification by preparative RP-HPLC (column: Gemini-NX C18, gradient: 0-5 min: A1/B1 85:15-75:25, 5-10 min: 75:25-67:33, 10-20 min: 67:33-55:45, t_R = 12 min) yielded **4.37** as white fluffy solid (3.09 mg, 95%). ^{1}H-NMR (600 MHz, DMSO-d_6): δ 0.80-0.94 (m, 15H), 1.47-1.87 (m, 14H), 1.95-2.05 (m, 1H), 2.44-2.47 (m, 3H), 2.64-2.71 (m, 1H), 2.71-2.96 (m, 4H), 3.01-3.28 (m, 19H), 3.33-3.46 (m, 9H), 3.46-3.68 (m, 12H), 3.68-3.83 (m, 2H), 4.17-4.25 (m, 1H), 4.26-4.30 (m, 1H), 4.32-4.40 (m, 1H), 4.42-4.61 (m, 3H), 6.54-6.62 (m, 2H), 6.62-7.11 (br s, 2H, interfering with the next listed signal), 6.97-7.00 (m, 2H), 7.11-7.42 (br s, 2H, interfering with the next listed signal), 7.26-7.33 (m, 4H), 7.42-7.52 (m, 1H), 7.52-7.85 (m, 6H), 7.88-8.68 (m, 5H), 8.68-9.29 (m, 5H), 10.00-10.36 (m, 1H), 12.49 (br s, 1H), 13.28 (br s, 1H). HRMS: *m/z* [*M*+2H]$^{2+}$ calcd. for [$C_{77}H_{117}FGaN_{19}O_{19}$]$^{2+}$ 849.9001, found 849.9012. RP-HPLC (220 nm): > 99% (t_R = 14.5 min, *k* = 18.1). $C_{77}H_{115}FGaN_{19}O_{19}$ · $C_6H_3F_9O_6$ (1699.60 + 342.07).

***N*$^{\alpha}$-Methyl-Arg-Arg-Pro-Tyr-2-((1*R*)-1-methylpropyl)-Gly-Leu tris(hydrotrifluoroacetate) (4.38).** Peptide **4.38** was synthesized according to the general procedure for SPPS using a H-Leu-2-ClTrt resin (loading 0.79 mmol/g) (40 mg, 0.0316 mmol). Purification by preparative RP-HPLC (column: Gemini-NX C18, gradient: 0-5 min: A1/B1 95:5-90:10, 5-10 min: 90:10-80:20, 10-30 min: 80:20-60:40, t_R = 18 min) afforded **4.38** as white fluffy solid (13.8 mg, 37%). ^{1}H-NMR (600 MHz, DMSO-d_6): δ 0.74-0.80 (m, 3H), 0.82-0.87 (m, 6H), 0.88-0.92 (m, 3H), 1.00-1.09 (m, 1H), 1.32-1.40 (m, 1H), 1.40-1.59 (m, 7H), 1.59-1.89 (m, 8H), 1.95-2.04 (m, 1H), 2.42-2.48 (m, 3H), 2.65-2.75 (m, 1H), 2.85-2.92 (m, 1H), 3.04-3.16 (m, 4H), 3.53-3.64 (m, 2H), 3.74-3.83 (m, 1H), 4.18-4.26 (m, 1H), 4.32-4.39 (m, 2H), 4.41-4.60 (m, 2H), 6.59-6.63 (m, 2H), 6.63-7.18 (br s, 4H, interfering with the next listed signal), 6.99-7.01 (m, 2H), 7.19-7.60 (br s, 4H), 7.60-7.76 (m, 3H), 7.93 (d, 1H, *J* 7.9 Hz), 8.13 (d, 1H, *J* 7.7 Hz), 8.73-9.06 (m, 3H), 9.11-9.23 (m, 1H), 12.47 (br s, 1H). HRMS: *m/z* [*M*+2H]$^{2+}$ calcd. for [$C_{39}H_{68}N_{12}O_8$]$^{2+}$ 416.2636, found 416.2645. RP-HPLC (220 nm): 99% (t_R = 6.7 min, *k* = 7.8). $C_{39}H_{66}N_{12}O_8$ · $C_6H_3F_9O_6$ (831.03 + 342.07).

***N*$^{\alpha}$-Methyl-Arg-Arg-Pro-Tyr-*a*,*a*-diethyl-Gly-Leu tris(hydrotrifluoroacetate) (4.39).** Peptide **4.39** was synthesized according to the general procedure for SPPS using a H-Leu-2-ClTrt resin (loading 0.79 mmol/g) (40 mg, 0.0316 mmol). Purification by preparative RP-HPLC (column: Gemini-NX C18, gradient: 0-5 min: A1/B1 95:5-90:10, 5-10 min: 90:10-80:20, 10-30 min: 80:20-55:45, t_R = 18 min) afforded **4.39** as white fluffy solid (9.1 mg, 25%). ^{1}H-NMR (600 MHz, DMSO-d_6): δ 0.31-0.49 (m, 3H), 0.57-0.70 (m, 3H), 0.79-0.82 (m, 3H), 0.87-0.90 (m, 3H), 1.40-1.87 (m, 15H), 1.87-2.01 (m, 1H), 2.01-2.14 (m, 1H), 2.25-2.38 (m, 2H), 2.43-2.48 (m, 3H), 2.65-2.75 (m, 1H), 2.88-2.94 (m, 1H), 3.04-3.18 (m, 4H), 3.51-3.64 (m, 2H), 3.72-3.88 (m, 1H), 4.12-4.22 (m, 1H), 4.23-4.41 (m, 2H), 4.46-4.62

(m, 1H), 6.61-6.70 (m, 2H), 6.70-7.14 (br s, 4H, interfering with the next listed signal), 7.03-7.06 (m, 2H), 7.14-7.54 (br s, 4H, interfering with the next listed signal), 7.37-7.40 (m, 1H), 7.54-7.76 (m, 2H), 8.16 (d, 1H, *J* 7.9 Hz), 8.46 (d, 1H, *J* 7.4 Hz), 8.68-9.12 (m, 3H), 9.15-9.25 (m, 1H), 12.57 (br s, 1H). HRMS: *m/z* $[M+2H]^{2+}$ calcd. for $[C_{39}H_{68}N_{12}O_8]^{2+}$ 416.2636, found 416.2644. RP-HPLC (220 nm): 99% (t_R = 7.4 min, k = 8.7). $C_{39}H_{66}N_{12}O_8 \cdot C_6H_3F_9O_6$ (831.03 + 342.07).

***N*$^{\alpha}$-Methyl-Arg-Arg-Pro-Tyr-α-cyclopropyl-Gly-Leu tris(hydrotrifluoroacetate) (4.40).** Peptide **4.40** was synthesized according to the general procedure for SPPS using a H-Leu-2-ClTrt resin (loading 0.79 mmol/g) (40 mg, 0.0316 mmol). Purification by preparative RP-HPLC (column: Gemini-NX C18, gradient: 0-5 min: A1/B1 95:5-90:10, 5-10 min: 90:10-80:20, 10-30 min: 80:20-55:45, t_R = 15 min) afforded **4.40** as white fluffy solid (25.3 mg, 69%). ^{1}H-NMR (600 MHz, DMSO-d_6): δ 0.29-0.35 (m, 1H), 0.35-0.42 (m, 2H), 0.42-0.48 (m, 1H), 0.83-0.87 (m, 3H), 0.87-0.92 (m, 3H), 0.99-1.05 (m, 1H), 1.42-1.87 (m, 14H), 1.96-2.06 (m, 1H), 2.42-2.48 (m, 3H), 2.65-2.73 (m, 1H), 2.84-2.91 (m, 1H), 3.06-3.15 (m, 4H), 3.54-3.63 (m, 2H), 3.76-3.86 (m, 1H), 3.91-3.98 (m, 1H), 4.21-4.30 (m, 1H), 4.30-4.37 (m, 1H), 4.37-4.44 (m, 1H), 4.46-4.58 (m, 1H), 6.55-6.65 (m, 2H), 6.65-7.13 (br s, 4H, interfering with the next listed signal), 6.99-7.02 (m, 2H), 7.13-7.56 (br s, 4H), 7.56-7.72 (m, 2H), 7.79-8.01 (m, 2H), 8.08-8.19 (m, 1H), 8.73-9.04 (m, 3H), 9.18 (s, 1H), 12.54 (br s, 1H). HRMS: *m/z* $[M+2H]^{2+}$ calcd. for $[C_{38}H_{64}N_{12}O_8]^{2+}$ 408.2480, found 408.2487. RP-HPLC (220 nm): 97% (t_R = 5.2 min, k = 5.8). $C_{38}H_{62}N_{12}O_8 \cdot C_6H_3F_9O_6$ (814.99 + 342.07).

***N*$^{\alpha}$-Methyl-Arg-Arg-Pro-Tyr-β-cyclopropyl-Ala-Leu tris(hydrotrifluoroacetate) (4.41).** Peptide **4.41** was synthesized according to the general procedure for SPPS using a H-Leu-2-ClTrt resin (loading 0.79 mmol/g) (40 mg, 0.0316 mmol). Purification by preparative RP-HPLC (column: Gemini-NX C18, gradient: 0-5 min: A1/B1 95:5-90:10, 5-10 min: 90:10-78:22, 10-30 min: 78:22-50:50, t_R = 16 min) afforded **4.41** as white fluffy solid (17.5 mg, 47%). ^{1}H-NMR (600 MHz, DMSO-d_6): δ 0.02-0.15 (m, 2H), 0.27-0.44 (m, 2H), 0.62-0.77 (m, 1H), 0.82-0.93 (m, 6H), 1.36-1.89 (m, 16H), 1.95-2.05 (m, 1H), 2.40-2.48 (m, 3H), 2.66-2.75 (m, 1H), 2.86-2.92 (m, 1H), 3.05-3.14 (m, 4H), 3.54-3.55 (m, 1H), 3.60-3.62 (m, 1H), 3.75-3.80 (m, 1H), 4.21-4.29 (m, 1H), 4.29-4.44 (m, 3H), 4.49-4.60 (m, 1H), 6.57-6.62 (m, 2H), 6.62-7.12 (br s, 4H, interfering with the next listed signal), 7.00-7.02 (m, 2H), 7.12-7.57 (br s, 4H), 7.57-7.73 (m, 2H), 7.77-7.96 (m, 2H), 8.11-8.21 (m, 1H), 8.74-9.03 (m, 3H), 9.09-9.27 (m, 1H), 12.55 (br s, 1H). HRMS: *m/z* $[M+3H]^{3+}$ calcd. for $[C_{39}H_{67}N_{12}O_8]^{3+}$ 277.1729, found 277.1739. RP-HPLC (220 nm): 98% (t_R = 5.9 min, k = 6.8). $C_{39}H_{64}N_{12}O_8 \cdot C_6H_3F_9O_6$ (829.02 + 342.07).

***N*$^{\alpha}$-Methyl-Arg-Arg-Pro-Tyr-α-cyclobutyl-Gly-Leu tris(hydrotrifluoroacetate) (4.42).** Peptide **4.42** was synthesized according to the general procedure for SPPS using a H-Leu-2-ClTrt resin (loading 0.79 mmol/g) (40 mg, 0.0316 mmol). Purification by preparative RP-HPLC (column: Gemini-NX C18, gradient: 0-5 min: A1/B1 95:5-90:10, 5-10 min: 90:10-78:22, 10-30 min: 78:22-50:50, t_R = 15 min) afforded **4.42** as white fluffy solid (27.6 mg, 74%). ^{1}H-NMR (600 MHz, DMSO-d_6): δ 0.81-0.93 (m, 6H), 1.37-1.95 (m, 20H), 1.95-2.06 (m, 1H), 2.44-2.48 (m, 3H), 2.52-2.54 (m, 1H), 2.66-2.74 (m, 1H), 2.84-2.91 (m, 1H), 3.05-3.14 (m, 4H), 3.54-3.62 (m, 2H), 3.76-3.86 (m, 1H), 4.17-4.26 (m, 1H), 4.27-4.38 (m, 2H), 4.38-4.45 (m, 1H), 4.48-4.59 (m, 1H), 6.57-6.63 (m, 2H), 6.63-7.15 (br s, 4H, interfering with the next listed signal), 6.99-7.01 (m, 2H), 7.15-7.58 (br s, 4H), 7.58-7.71

(m, 2H), 7.76-7.83 (m, 1H), 7.86-7.95 (m, 1H), 8.11-8.22 (m, 1H), 8.71-9.07 (m, 3H), 9.09-9.24 (m, 1H), 12.51 (br s, 1H). HRMS: *m/z* [*M*+3H]$^{3+}$ calcd. for [$C_{39}H_{67}N_{12}O_8$]$^{3+}$ 277.1729, found 277.1738. RP-HPLC (220 nm): 99% (t_R = 6.0 min, k = 6.9). $C_{39}H_{64}N_{12}O_8$ · $C_6H_3F_9O_6$ (829.02 + 342.07).

***N*$^{\alpha}$-Methyl-Arg-Arg-Pro-Tyr-α-cyclopentyl-Gly-Leu tris(hydrotrifluoroacetate) (4.43).** Peptide **4.43** was synthesized according to the general procedure for SPPS using a H-Leu-2-ClTrt resin (loading 0.79 mmol/g) (40 mg, 0.0316 mmol). Purification by preparative RP-HPLC (column: Gemini-NX C18, gradient: 0-5 min: A1/B1 95:5-90:10, 5-10 min: 90:10-80:20, 10-30 min: 80:20-55:45, t_R = 17 min) afforded **4.43** as white fluffy solid (26.8 mg, 71%). ^{1}H-NMR (600 MHz, DMSO-d_6): δ 0.81-0.93 (m, 6H), 1.20-1.27 (m, 1H), 1.31-1.39 (m, 1H), 1.39-1.89 (m, 20H), 1.95-2.06 (m, 1H), 2.08-2.15 (m, 1H), 2.44-2.48 (m, 3H), 2.64-2.71 (m, 1H), 2.83-2.91 (m, 1H), 3.05-3.14 (m, 4H), 3.54-3.63 (m, 2H), 3.75-3.86 (m, 1H), 4.16-4.29 (m, 2H), 4.29-4.60 (m, 3H), 6.57-6.62 (m, 2H), 6.62-7.13 (br s, 4H, interfering with the next listed signal), 6.98-7.01 (m, 2H), 7.13-7.56 (br s, 4H), 7.56-7.71 (m, 2H), 7.79-7.93 (m, 2H), 8.16-8.26 (m, 1H), 8.72-9.03 (m, 3H), 9.09-9.26 (m, 1H), 12.49 (br s, 1H). HRMS: *m/z* [*M*+3H]$^{3+}$ calcd. for [$C_{40}H_{69}N_{12}O_8$]$^{3+}$ 281.8448, found 281.8457. RP-HPLC (220 nm): 99% (t_R = 6.8 min, k = 7.9). $C_{40}H_{66}N_{12}O_8$ · $C_6H_3F_9O_6$ (843.04 + 342.07).

***N*$^{\alpha}$-Methyl-Arg-Arg-Pro-Tyr-α-methyl-Leu-Leu tris(hydrotrifluoroacetate) (4.44).** Peptide **4.44** was synthesized according to the general procedure for SPPS using a H-Leu-2-ClTrt resin (loading 0.79 mmol/g) (40 mg, 0.0316 mmol). Purification by preparative RP-HPLC (column: Gemini-NX C18, gradient: 0-5 min: A1/B1 95:5-90:10, 5-10 min: 90:10-75:25, 10-30 min: 75:25-45:55, t_R = 16 min) afforded **4.44** as white fluffy solid (26.3 mg, 70%). ^{1}H-NMR (600 MHz, DMSO-d_6): δ 0.70-0.89 (m, 12H), 1.27-1.38 (m, 3H), 1.38-1.91 (m, 16H), 1.98-2.08 (m, 1H), 2.18-2.28 (m, 1H), 2.45-2.48 (m, 3H), 2.62-2.70 (m, 1H), 2.86-2.95 (m, 1H), 3.05-3.15 (m, 4H), 3.53-3.63 (m, 2H), 3.74-3.85 (m, 1H), 4.13-4.24 (m, 1H), 4.27-4.39 (m, 2H), 4.44-4.59 (m, 1H), 6.61-6.66 (m, 2H), 6.66-7.13 (br s, 4H, interfering with the next listed signal), 7.01-7.05 (m, 2H), 7.13-7.53 (br s, 4H), 7.53-7.72 (m, 3H), 8.04-8.12 (m, 1H), 8.31-8.37 (m, 1H), 8.74-9.03 (m, 3H), 9.14-9.23 (m, 1H), 12.55 (br s, 1H). HRMS: *m/z* [*M*+3H]$^{3+}$ calcd. for [$C_{40}H_{71}N_{12}O_8$]$^{3+}$ 282.5167, found 282.5175. RP-HPLC (220 nm): 99% (t_R = 8.3 min, k = 9.9). $C_{40}H_{68}N_{12}O_8$ · $C_6H_3F_9O_6$ (845.06 + 342.07).

***N*$^{\alpha}$-Methyl-Arg-Arg-Pro-Tyr-α-ethyl-D-Ala-Leu tris(hydrotrifluoroacetate) (4.45).** Peptide **4.45** was synthesized according to the general procedure for SPPS using a H-Leu-2-ClTrt resin (loading 0.79 mmol/g) (40 mg, 0.0316 mmol). Purification by preparative RP-HPLC (column: Gemini-NX C18, gradient: 0-5 min: A1/B1 95:5-90:10, 5-10 min: 90:10-80:20, 10-30 min: 80:20-60:40, t_R = 17 min) afforded **4.45** as white fluffy solid (26.3 mg, 72%). ^{1}H-NMR (600 MHz, DMSO-d_6): δ 0.58-0.72 (m, 3H), 0.80-0.91 (m, 6H), 1.35 (s, 3H), 1.40-1.89 (m, 15H), 1.98-2.07 (m, 1H), 2.12-2.21 (m, 1H), 2.45-2.48 (m, 3H), 2.65-2.75 (m, 1H), 2.88-2.95 (m, 1H), 3.05-3.18 (m, 4H), 3.49-3.68 (m, 2H), 3.70-3.87 (m, 1H), 4.19-4.39 (m, 3H), 4.48-4.59 (m, 1H), 6.61-6.67 (m, 2H), 6.67-7.13 (br s, 4H, interfering with the next listed signal), 7.01-7.05 (m, 2H), 7.13-7.51 (br s, 4H), 7.51-7.74 (m, 3H), 7.82-7.97 (m, 1H), 8.12-8.22 (m, 1H), 8.73-9.05 (m, 3H), 9.14-9.25 (m, 1H), 12.51 (br s, 1H). HRMS: *m/z* [*M*+3H]$^{3+}$ calcd. for [$C_{38}H_{67}N_{12}O_8$]$^{3+}$ 273.1729, found 273.1738. RP-HPLC (220 nm): 98% (t_R = 6.4 min, k = 7.4). $C_{38}H_{64}N_{12}O_8$ · $C_6H_3F_9O_6$ (817.01 + 342.07).

***N*$^{\alpha}$-Methyl-Arg-Arg-Pro-Tyr-Ile-β-cyclopropyl-Ala tris(hydrotrifluoroacetate) (4.46).** Peptide **4.46** was synthesized on a 2-ClTrt-Cl resin (loading 1.6 mmol/g) (40 mg, 0.064 mmol, 1 equiv.). The resin was treated with a solution of Fmoc-ß-cyclopropyl-Ala-OH (45.0 mg, 0.128 mmol, 2 equiv.) and DIPEA (111.5 µL, 0.64 mmol, 10 equiv.) in CH_2Cl_2 (0.5 mL) at 35 °C for 15 h. MeOH (65 µL) and CH_2Cl_2 (100 µL) were added and shaking was continued at rt for 15 min. The liquid was removed by filtration and the resin was washed with CH_2Cl_2 (3 ×), MeOH (3 ×) and DMF/NMP (80:20 v/v) (4 ×). Fmoc-deprotection of ß-cyclopropyl-Ala and further SPPS was performed according to the general procedure for SPPS (note: the amounts of Fmoc-amino acids and coupling reagents were calculated based on the assumption that the loading of the resin with ß-cyclopropyl-Ala was 50% compared to the original loading, i.e., 0.8 mmol/g). Purification by preparative RP-HPLC (column: Gemini-NX C18, gradient: 0-5 min: A1/B1 95:5-90:10, 5-10 min: 90:10-80:20, 10-30 min: 80:20-55:45, t_R = 15 min) afforded **4.46** as white fluffy solid (27.4 mg, 37%). ^{1}H-NMR (600 MHz, DMSO-d_6): δ 0.01-0.17 (m, 2H), 0.32-0.44 (m, 2H), 0.71-0.89 (m, 7H), 1.00-1.10 (m, 1H), 1.37-1.90 (m, 15H), 1.94-2.06 (m, 1H), 2.43-2.48 (m, 3H), 2.63-2.73 (m, 1H), 2.83-2.91 (m, 1H), 3.04-3.14 (m, 4H), 3.54-3.63 (m, 2H), 3.75-4.86 (m, 1H), 4.18-4.27 (m, 2H), 4.27-4.39 (m, 1H), 4.39-4.59 (m, 2H), 6.57-6.64 (m, 2H), 6.64-7.13 (br s, 4H, interfering with the next listed signal), 6.99-7.01 (m, 2H), 7.13-7.56 (br s, 4H), 7.56-7.79 (m, 3H), 7.93 (d, 1H, *J* 8.0 Hz), 8.18-8.34 (m, 1H), 8.70-9.23 (m, 4H), 12.52 (br s, 1H). HRMS: *m/z* [*M*+3H]$^{3+}$ calcd. for $[C_{39}H_{67}N_{12}O_8]^{3+}$ 277.1729, found 277.1741. RP-HPLC (220 nm): 99% (t_R = 5.3 min, *k* = 6.0). $C_{39}H_{64}N_{12}O_8 \cdot C_6H_3F_9O_6$ (829.02 + 342.07).

***N*$^{\alpha}$-Methyl-Arg-Arg-Pro-Tyr-Ile-α-methyl-Leu tris(hydrotrifluoroacetate) (4.47).** Peptide **4.47** was synthesized on a 2-ClTrt-Cl resin (loading 1.6 mmol/g) (40 mg, 0.064 mmol, 1 equiv.). The resin was treated with a solution of Fmoc-α-methyl-Leu-OH (47.0 mg, 0.128 mmol, 2 equiv.) and DIPEA (111.5 µL, 0.64 mmol, 10 equiv.) in CH_2Cl_2 (0.5 mL) at 35 °C for 15 h. MeOH (65 µL) was added and shaking was continued at rt for 15 min. The liquid was removed by filtration and the resin was washed with CH_2Cl_2 (3 ×), MeOH (3 ×) and DMF/NMP (80:20 v/v) (4 ×). Fmoc-deprotection of α-methyl-Leu and further SPPS was performed according to the general procedure for SPPS (note: the amounts of Fmoc-amino acids and coupling reagents were calculated based on the assumption that the loading of the resin with α-methyl-Leu was 50% compared to the original loading, i.e., 0.8 mmol/g). Purification by preparative RP-HPLC (column: Gemini-NX C18, gradient: 0-5 min: A1/B1 95:5-90:10, 5-10 min: 90:10-75:25, 10-30 min: 75:25-45:55, t_R = 16 min) afforded **4.47** as white fluffy solid (11.7 mg, 15%). ^{1}H-NMR (600 MHz, DMSO-d_6): δ 0.77-0.87 (m, 12H), 1.00-1.09 (m, 1H), 1.35-1.87 (m, 19H), 1.96-2.05 (m, 1H), 2.45-2.48 (m, 3H), 2.63-2.74 (m, 1H), 2.83-2.92 (m, 1H), 3.06-3.16 (m, 4H), 3.52-3.64 (m, 2H), 3.74-3.88 (m, 1H), 4.16-4.22 (m, 1H), 4.28-4.38 (m, 1H), 4.39-4.59 (m, 2H), 6.59-6.64 (m, 2H), 6.64-7.14 (br s, 4H, interfering with the next listed signal), 7.00-7.03 (m, 2H), 7.14-7.57 (br s, 4H), 7.57-7.71 (m, 2H), 7.74-7.86 (m, 2H), 7.91 (d, 1H, *J* 8.0 Hz), 8.73-9.06 (m, 3H), 9.08-9.24 (m, 1H), 12.51 (br s, 1H). HRMS: *m/z* [*M*+3H]$^{3+}$ calcd. for $[C_{40}H_{71}N_{12}O_8]^{3+}$ 282.5167, found 282.5175. RP-HPLC (220 nm): > 99% (t_R = 8.1 min, *k* = 9.7). $C_{40}H_{68}N_{12}O_8 \cdot C_6H_3F_9O_6$ (845.06 + 342.07).

***N*$^{\alpha}$-Methyl-Arg-Arg-Pro-β,β-dimethyl-Tyr-Ile-Leu tris(hydrotrifluoroacetate) (4.48) and *N*$^{\alpha}$-methyl-Arg-Arg-Pro-β,β-dimethyl-D-Tyr-Ile-Leu tris(hydrotrifluoroacetate) (4.49).** Peptides **4.48** and **4.49** were synthesized according to the general procedure for SPPS using a H-Leu-2-ClTrt resin (loading 0.79 mmol/g) (40 mg, 0.0316 mmol). Purification by preparative RP-HPLC (column: Gemini-NX C18, gradient: 0-5 min: A1/B1 95:5-90:10, 5-10 min: 90:10-73:27, 10-30 min: 73:27-63:37, **4.48**: t_R = 14 min, **4.49**: t_R = 15 min) afforded the epimers **4.48** and **4.49** as white fluffy solids (**4.48**: 16.7 mg, 44%, **4.49**: 11.8 mg, 31%). **4.48**: ^{1}H-NMR (600 MHz, DMSO-d_6): δ 0.74-0.86 (m, 9H), 0.88-0.92 (m, 3H), 0.96-1.05 (m, 1H), 1.20-1.31 (m, 6H), 1.37-1.60 (m, 8H), 1.60-1.93 (m, 9H), 2.46-2.49 (m, 3H), 3.06-3.15 (m, 4H), 3.49-3.52 (m, 1H), 3.56-3.61 (m, 1H), 3.76-3.90 (m, 1H), 4.03-4.17 (m, 1H), 4.17-4.27 (m, 1H), 4.37-4.44 (m, 1H), 4.52-4.60 (m, 1H), 4.61-4.68 (m, 1H), 6.59-6.65 (m, 2H), 6.65-7.17 (br s, 4H, interfering with the next listed signal), 7.11-7.14 (m, 2H), 7.17-7.60 (br s, 4H, interfering with the next listed signal), 7.32-7.34 (m, 1H), 7.60-7.72 (m, 3H), 8.08-8.16 (m, 1H), 8.79-9.06 (m, 3H), 9.08-9.21 (m, 1H), 12.48 (br s, 1H). HRMS: *m/z* [*M*+3H]$^{3+}$ calcd. for [$C_{41}H_{73}N_{12}O_8$]$^{3+}$ 287.1886, found 287.1896. RP-HPLC (220 nm): 97% (t_R = 7.3 min, k = 8.6). $C_{41}H_{70}N_{12}O_8$ · $C_6H_3F_9O_6$ (859.09 + 342.07). **4.49**: ^{1}H-NMR (600 MHz, DMSO-d_6): δ 0.72-0.81 (m, 6H), 0.82-0.86 (m, 3H), 0.87-0.97 (m, 4H), 1.20-1.25 (m, 3H), 1.25-1.35 (m, 5H), 1.40-1.60 (m, 8H), 1.60-1.83 (m, 7H), 2.46-2.48 (m, 3H), 3.04-3.14 (m, 4H), 3.45-3.48 (m, 1H), 3.53-3.57 (m, 1H), 3.73-3.81 (m, 1H), 4.08-4.19 (m, 2H), 4.36-4.43 (m, 1H), 4.46-4.55 (m, 1H), 4.86-4.92 (m, 1H), 6.58-6.65 (m, 2H), 6.65-7.11 (br s, 4H), 7.11-7.57 (br s, 4H, interfering with the next listed signal), 7.15-7.17 (m, 2H), 7.57-7.77 (m, 4H), 8.21 (d, 1H, *J* 7.1 Hz), 8.75-9.06 (m, 3H), 9.09-9.17 (m, 1H), 12.45 (br s, 1H). HRMS: *m/z* [*M*+3H]$^{3+}$ calcd. for [$C_{41}H_{73}N_{12}O_8$]$^{3+}$ 287.1886, found 287.1894. RP-HPLC (220 nm): 99% (t_R = 9.3 min, k = 11.2). $C_{41}H_{70}N_{12}O_8$ · $C_6H_3F_9O_6$ (859.09 + 342.07).

***N*$^{\alpha}$-Methyl-*N*$^{\omega}$-[(4-aminobutyl)aminocarbonyl]Arg-Arg-Pro-β,β-dimethyl-Tyr-Ile-Leu tetrakis(hydrotrifluoroacetate) (4.50) and *N*$^{\alpha}$-methyl-*N*$^{\omega}$-[(4-aminobutyl)aminocarbonyl]Arg-Arg-Pro-β,β-dimethyl-D-Tyr-Ile-Leu tetrakis(hydrotrifluoroacetate) (4.51).** Peptides **4.50** and **4.51** were synthesized according to the general procedure for SPPS using a H-Leu-2-ClTrt resin (loading 0.79 mmol/g) (40 mg, 0.0316 mmol), with the following modification: after coupling of arginine building block **3.06a** and Fmoc-deprotection, the resin was washed with CH_2Cl_2 (5 ×), a solution of 2-nitrobenzenesulfonylchloride (21.0 mg, 0.095 mmol) and collidine (20.9 µL, 0.158 mmol) in CH_2Cl_2 (0.75 mL) was added and the mixture was shaken at rt for 2 h. The resin was washed with DMF (5 ×), and a solution of MTBD (18.2 µL, 0.126 mmol) and methyl-4-nitrobenzenesulfonate (34.3 mg, 0.158 mmol) in DMF (0.9 mL) was added. After shaking at rt for 30 min, the resin was washed with DMF (3 ×) followed by the addition of a solution of DBU (23.6 µL, 0.158 mmol) and 2-mercaptoethanol (22.0 µL, 0.316 mmol) in DMF (0.75 mL) and shaking at rt for 30 min. The resin was washed with DMF (5 ×) followed by cleavage from the resin as described in the general procedure for SPPS. Purification by preparative RP-HPLC (column: Gemini-NX C18, gradient: 0-5 min: A1/B1 85:15-80:20, 5-8 min: 80:20-73:27, 8-35 min: 73:27-70:30, **4.50**: t_R = 11 min, **4.51**: t_R = 12 min) afforded the epimers **4.50** and **4.51** as white fluffy solids (**4.50**: 11.5 mg, 25%, **4.51**: 7.9 mg, 17%). **4.50**: ^{1}H-NMR (600 MHz, DMSO-d_6): δ 0.73-0.96 (m, 12H), 0.96-1.06 (m, 1H), 1.15-1.33 (m, 6H), 1.33-1.96 (m, 21H), 2.46-2.49 (m, 3H), 2.75-2.82 (m, 2H), 3.04-3.20 (m, 4H), 3.20-3.32 (m, 2H), 3.44-3.63 (m, 2H), 3.80-3.93 (m, 1H),

4.08-4.18 (m, 1H), 4.20-4.27 (m, 1H), 4.38-4.44 (m, 1H), 4.51-4.69 (m, 2H), 6.58-6.65 (m, 2H), 6.79-7.27 (br s, 2H, interfering with the next listed signal), 7.11-7.14 (m, 2H), 7.27-7.30 (m, 1H), 7.30-7.72 (br s, 2H, interfering with the next listed signal), 7.55-7.68 (m, 2H), 7.72-7.91 (m, 4H), 8.06-8.16 (m, 1H), 8.31-8.73 (m, 2H), 8.80-9.39 (m, 5H), 10.61-10.87 (m, 1H), 12.50 (br s, 1H). ^{13}C-NMR (151 MHz, DMSO-*d*$_6$): δ 10.9, 15.1, 21.1, 23.0, 23.4, 24.2, 24.2, 24.2, 24.4, 24.5, 24.5, 26.0, 26.9, 27.0, 28.1, 28.6, 31.1, 36.7, 38.5, 38.6, 39.8, 40.1, 40.2, 40.4, 46.9, 50.0, 50.5, 56.6, 59.3, 59.8, 59.8, 114.3 (2 carbon atoms), 116.0 (TFA), 117.9 (TFA), 119.9, 127.4 (2 carbon atoms), 136.2, 153.9, 155.3, 156.9, 158.8 (q, *J* 32 Hz) (TFA), 167.0, 169.4, 169.4, 170.6, 170.7, 173.9. HRMS: *m/z* [*M*+H]$^+$ calcd. for [$C_{46}H_{81}N_{14}O_9$]$^+$ 973.6305, found 973.6309. RP-HPLC (220 nm): 97% (t_R = 7.1 min, *k* = 8.3). $C_{46}H_{80}N_{14}O_9$ · $C_8H_4F_{12}O_8$ (973.24 + 456.09). **4.51**: ^{1}H-NMR (600 MHz, DMSO-*d*$_6$): δ 0.71-0.96 (m, 13H), 1.18-1.37 (m, 8H), 1.42-1.86 (m, 19H), 2.44-2.49 (m, 3H), 2.75-2.84 (m, 2H), 3.02-3.18 (m, 4H), 3.20-3.29 (m, 2H), 3.43-3.50 (m, 1H), 3.50-3.59 (m, 1H), 3.76-3.84 (m, 1H), 4.08-4.19 (m, 2H), 4.35-4.43 (m, 1H), 4.47-4.56 (m, 1H), 4.84-4.90 (m, 1H), 6.60-6.64 (m, 2H), 6.64-7.24 (br s, 2H, interfering with the next listed signal), 7.14-7.17 (m, 2H), 7.24-7.55 (br s, 2H), 7.55-7.73 (m, 3H), 7.73-7.90 (m, 4H), 8.12-8.24 (m, 1H), 8.31-8.71 (m, 2H), 8.79-9.01 (m, 2H), 9.01-9.34 (m, 3H), 10.66-10.88 (m, 1H), 12.48 (br s, 1H). ^{13}C-NMR (151 MHz, DMSO-*d*$_6$): δ 11.1, 15.3, 21.5, 22.7, 23.4, 23.9, 24.0, 24.2, 24.3, 24.4, 24.5, 26.0, 26.3, 26.9, 28.1, 29.3, 31.1, 37.0, 38.5, 38.6, 39.7, 40.1, 40.4, 41.0, 46.7, 50.6, 50.6, 56.5, 59.2, 59.5, 59.8, 114.4 (2 carbon atoms), 116.0 (TFA), 117.9 (TFA), 119.9, 127.3 (2 carbon atoms), 136.8, 153.9, 155.4, 156.9, 158.8 (q, *J* 32 Hz) (TFA), 166.9, 168.9, 169.4, 170.2, 171.2, 173.9. HRMS: *m/z* [*M*+H]$^+$ calcd. for [$C_{46}H_{81}N_{14}O_9$]$^+$ 973.6305, found 973.6307. RP-HPLC (220 nm): 95% (t_R = 8.5 min, *k* = 10.2). $C_{46}H_{80}N_{14}O_9$ · $C_8H_4F_{12}O_8$ (973.24 + 456.09).

***N*$^\alpha$-Methyl-*N*$^\omega$-[(4-aminobutyl)aminocarbonyl]Arg-Arg-Pro-β,β-dimethyl-Tyr-α-*tert*-butyl-Gly-Leu tetrakis(hydrotrifluoroacetate) (4.52) and *N*$^\alpha$-methyl-*N*$^\omega$-[(4-aminobutyl)aminocarbonyl]Arg-Arg-Pro-β,β-dimethyl-D-Tyr-α-*tert*-butyl-Gly-Leu tetrakis(hydrotrifluoroacetate) (4.53).** Peptides **4.52** and **4.53** were synthesized according to the general procedure for SPPS using a H-Leu-2-ClTrt resin (loading 0.79 mmol/g) (25 mg, 0.01975 mmol), with the following modification: after coupling of arginine building block **3.06a** and Fmoc-deprotection, the resin was washed with CH_2Cl_2 (5 ×), a solution of 2-nitrobenzenesulfonylchloride (13.1 mg, 0.059 mmol) and collidine (13.1 µL, 0.099 mmol) in CH_2Cl_2 (0.5 mL) was added and the mixture was shaken at rt for 2 h. The resin was washed with DMF (5 ×), and a solution of MTBD (11.3 µL, 0.079 mmol) and methyl-4-nitrobenzenesulfonate (21.4 mg, 0.099 mmol) in DMF (0.6 mL) was added. After shaking at rt for 30 min, the resin was washed with DMF (3 ×) followed by the addition of a solution of DBU (14.7 µL, 0.099 mmol) and 2-mercaptoethanol (13.8 µL, 0.198 mmol) in DMF (0.5 mL) and shaking at rt for 30 min. The resin was washed with DMF (5 ×) followed by cleavage from the resin as described in the general procedure for SPPS. Purification by preparative RP-HPLC (column: Gemini-NX C18, gradient: 0-5 min: A1/B1 85:15-80:20, 5-8 min: 80:20-73:27, 8-35 min: 73:27-70:30, **4.52**: t_R = 11 min, **4.53**: t_R = 12 min) afforded the epimers **4.52** and **4.53** as white fluffy solids (**4.52**: 5.2 mg, 19%, **4.53**: 5.0 mg, 18%). **4.52**: ^{1}H-NMR (600 MHz, DMSO-*d*$_6$): δ 0.79-0.94 (m, 15H), 1.19-1.32 (m, 6H), 1.44-1.84 (m, 18H), 1.86-1.95 (m, 1H), 2.47-2.49 (m, 3H), 2.76-2.81 (m, 2H), 3.07-3.14 (m, 4H), 3.24-3.28 (m, 2H), 3.50-3.52 (m, 1H), 3.56-3.60 (m, 1H), 3.78-3.85 (m, 1H), 4.18-4.29 (m, 2H), 4.40-4.45 (m, 1H), 4.53-4.61 (m, 1H), 4.68-4.74 (m, 1H), 6.57-6.65 (m, 2H), 6.70-7.09 (br s, 2H), 7.09-7.15 (m, 2H), 7.15-7.51 (br s, 2H, interfering with the next

listed signal), 7.37-7.45 (m, 2H), 7.53-7.78 (m, 5H), 8.12-8.18 (m, 1H), 8.31-8.64 (m, 2H), 8.78-9.22 (m, 5H), 10.16-10.53 (m, 1H), 12.46 (br s, 1H). HRMS: *m/z* [*M*+H]$^+$ calcd. for [$C_{46}H_{81}N_{14}O_9$]$^+$ 973.6305, found 973.6303. RP-HPLC (220 nm): 98% (t_R = 7.1 min, k = 8.3). $C_{46}H_{80}N_{14}O_9$ · $C_8H_4F_{12}O_8$ (973.24 + 456.09). **4.53**: ^{1}H-NMR (600 MHz, DMSO-d_6): δ 0.78-0.91 (m, 15H), 1.19-1.32 (m, 7H), 1.42-1.80 (m, 18H), 2.42-2.48 (m, 3H), 2.77-2.83 (m, 2H), 3.06-3.15 (m, 4H), 3.22-3.26 (m, 2H), 3.48-3.54 (m, 2H), 3.75-3.83 (m, 1H), 4.09-4.23 (m, 2H), 4.37-4.42 (m, 1H), 4.47-4.56 (m, 1H), 4.87-4.94 (m, 1H), 6.60-6.65 (m, 2H), 6.65-7.13 (br s, 2H), 7.13-7.19 (m, 2H), 7.19-7.53 (br s, 2H, interfering with the next listed signal), 7.44-7.49 (m, 1H), 7.53-7.87 (m, 6H), 8.16-8.26 (m, 1H), 8.33-8.65 (m, 2H), 8.70-9.21 (m, 5H), 10.29-10.63 (m, 1H), 12.44 (br s, 1H). HRMS: *m/z* [*M*+H]$^+$ calcd. for [$C_{46}H_{81}N_{14}O_9$]$^+$ 973.6305, found 973.6307. RP-HPLC (220 nm): 93% (t_R = 8.5 min, k = 10.2). $C_{46}H_{80}N_{14}O_9$ · $C_8H_4F_{12}O_8$ (973.24 + 456.09).

***N*^{α}-Methyl-*N*^{ω}-{[4-(N-{2-[4,7,10-tris(carboxymethyl)-1,4,7,10-tetraazacyclododecan-1-yl]acetyl})aminobutyl]aminocarbonyl}Arg-Arg-Pro-β,β-dimethyl-Tyr-Ile-Leu tetrakis(hydrotrifluoroacetate) (4.54).** Compound **4.54** was prepared from **4.50** (9.7 mg, 6.79 µmol) and **4.13** (5.54 mg, 6.79 µmol) according to the general procedure for DOTA-conjugation (modification: stirring of the mixture for 45 min instead for 30 min). Isolation of the protected intermediate: column: Gemini-NX C18, gradient: 0-5 min: A1/B1 90:10-80:20, 5-10 min: 80:20-72:28, 10-20 min: 72:28-60:40, t_R = 19 min. Purification of the product by preparative RP-HPLC (column: Gemini-NX C18, gradient: 0-5 min: A1/B1 90:10-80:20, 5-10 min: 80:20-72:28, 10-20 min: 72:28-60:40, t_R = 11 min) afforded **4.54** as white fluffy solid (9.4 mg, 76%). ^{1}H-NMR (600 MHz, DMSO-d_6): δ 0.73-0.95 (m, 12H), 0.96-1.04 (m, 1H), 1.19-1.30 (m, 6H), 1.36-1.94 (m, 21H), 2.47-2.49 (m, 3H), 3.06-3.25 (m, 17H), 3.56-3.96 (m, 18H), 4.10-4.13 (m, 1H), 4.21-4.25 (m, 1H), 4.39-4.44 (m, 1H), 4.53-4.59 (m, 1H), 4.61-4.67 (m, 1H), 6.59-6.64 (m, 2H), 6.64-7.17 (br s, 2H, interfering with the next listed signal), 7.10-7.14 (m, 2H), 7.17-7.57 (br s, 2H, interfering with the next listed signal), 7.30-7.34 (m, 1H), 7.57-7.71 (m, 2H), 8.07-8.16 (m, 1H), 8.22-8.56 (m, 2H), 8.77-9.46 (m, 5H), 11.28-13.36 (m, 2H). 6 exchangeable protons (NH, OH) of the presumably 4-fold protonated molecule could not be identified. HRMS: *m/z* [*M*+3H]$^{3+}$ calcd. for [$C_{62}H_{109}N_{18}O_{16}$]$^{3+}$ 453.9417, found 453.9425. RP-HPLC (220 nm): 98% (t_R = 7.0 min, k = 8.2). $C_{62}H_{106}N_{18}O_{16}$ · $C_8H_4F_{12}O_8$ (1359.64 + 456.09).

***N*^{α}-Methyl-*N*^{ω}-{[4-(N-{2-[4,7,10-tris(carboxymethyl)-1,4,7,10-tetraazacyclododecan-1-yl]acetyl})aminobutyl]aminocarbonyl}Arg-Arg-Pro-β,β-dimethyl-Tyr-*α*-*tert*-butyl-Gly-Leu tetrakis(hydrotrifluoroacetate) (4.55).** Compound **4.55** was prepared from **4.52** (7.5 mg, 5.25 µmol) and **4.13** (4.28 mg, 5.25 µmol) according to the general procedure for DOTA-conjugation (modification: stirring of the mixture for 45 min instead for 30 min). Isolation of the protected intermediate: column: Gemini-NX C18, gradient: 0-5 min: A1/B1 90:10-80:20, 5-10 min: 80:20-72:28, 10-20 min: 72:28-60:40, t_R = 19 min. Purification of the product by preparative RP-HPLC (column: Gemini-NX C18, gradient: 0-5 min: A1/B1 90:10-80:20, 5-10 min: 80:20-72:28, 10-20 min: 72:28-60:40, t_R = 11 min) afforded **4.55** as white fluffy solid (7.5 mg, 79%). ^{1}H-NMR (600 MHz, DMSO-d_6): δ 0.80-0.93 (m, 15H), 1.21-1.29 (m, 6H), 1.39-1.85 (m, 18H), 1.86-1.96 (m, 1H), 2.47-2.49 (m, 3H), 2.94-3.22 (m, 17H), 3.47-3.59 (m, 5H), 3.59-3.92 (m, 13H), 4.20-4.26 (m, 2H), 4.40-4.46 (m, 1H), 4.53-4.59 (m, 1H), 4.68-4.74 (m, 1H), 6.56-6.65 (m, 2H), 6.65-7.12 (br s, 2H), 7.12-7.15 (m, 2H), 7.15-7.60 (br s, 2H, interfering with the next listed

signal), 7.37-7.45 (m, 2H), 7.60-7.70 (m, 1H), 8.12-8.19 (m, 1H), 8.25-8.58 (m, 2H), 8.78-9.49 (m, 5H), 11.65-13.27 (m, 2H). 6 exchangeable protons (NH, OH) of the presumably 4-fold protonated molecule could not be identified. HRMS: *m/z* [*M*+3H]$^{3+}$ calcd. for [$C_{62}H_{109}N_{18}O_{16}$]$^{3+}$ 453.9417, found 453.9428. RP-HPLC (220 nm): 98% (t_R = 7.0 min, k = 8.2). $C_{62}H_{106}N_{18}O_{16}$ · $C_8H_4F_{12}O_8$ (1359.64 + 456.09).

***N*$^{\alpha}$-Methyl-*N*$^{\omega}$-{[4-(N-{2-[gallium(III)-4,7,10-tris(carboxymethyl)-1,4,7,10-tetraazacyclododecan-1-yl]acetyl})aminobutyl]aminocarbonyl}Arg-Arg-Pro-β,β-dimethyl-Tyr-Ile-Leu tris(hydrotrifluoroacetate) (4.56).** Compound **4.56** was prepared from **4.54** (3.5 mg, 1.93 µmol) according to the general procedure for the insertion of Ga^{3+}. Purification by preparative RP-HPLC (column: Gemini-NX C18, gradient: 0-5 min: A1/B1 90:10-80:20, 5-10 min: 80:20-72:28, 10-20 min: 72:28-60:40, t_R = 12 min) yielded **4.56** as white fluffy solid (3.3 mg, 97%). ^{1}H-NMR (600 MHz, DMSO-d_6): δ 0.73-0.86 (m, 9H), 0.88-0.93 (m, 3H), 0.96-1.03 (m, 1H), 1.21-1.30 (m, 6H), 1.36-1.85 (m, 20H), 1.85-1.95 (m, 1H), 2.47-2.48 (m, 3H), 3.05-3.30 (m, 20H), 3.47-3.48 (m, 3H), 3.63-3.82 (m, 12H), 4.10-4.14 (m, 1H), 4.21-4.26 (m, 1H), 4.38-4.45 (m, 1H), 4.54-4.66 (m, 2H), 6.58-6.66 (m, 2H), 6.66-7.10 (br s, 2H), 7.10-7.15 (m, 2H), 7.15-7.48 (br s, 2H, interfering with the next listed signal), 7.31-7.35 (m, 1H), 7.48-7.56 (m, 1H), 7.56-7.67 (m, 2H), 8.07-8.16 (m, 1H), 8.30-8.63 (m, 3H), 8.89-9.15 (m, 4H), 9.97-10.25 (m, 1H), 12.48 (br s, 1H), 13.29 (br s, 1H). HRMS: *m/z* [*M*+2H]$^{2+}$ calcd. for [$C_{62}H_{105}GaN_{18}O_{16}$]$^{2+}$ 713.3600, found 713.3605. RP-HPLC (220 nm): 98% (t_R = 7.4 min, k = 8.7). $C_{62}H_{103}GaN_{18}O_{16}$ · $C_6H_3F_9O_6$ (1426.34 + 342.07).

***N*$^{\alpha}$-Methyl-*N*$^{\omega}$-{[4-(N-{2-[gallium(III)-4,7,10-tris(carboxymethyl)-1,4,7,10-tetraazacyclododecan-1-yl]acetyl})aminobutyl]aminocarbonyl}Arg-Arg-Pro-β,β-dimethyl-Tyr-*α-tert*-butyl-Gly-Leu tris(hydrotrifluoroacetate) (4.57).** Compound **4.57** was prepared from **4.55** (1.8 mg, 0.991 µmol) according to the general procedure for the insertion of Ga^{3+}. Purification by preparative RP-HPLC (column: Gemini-NX C18, gradient: 0-5 min: A1/B1 90:10-80:20, 5-10 min: 80:20-72:28, 10-20 min: 72:28-60:40, t_R = 12 min) yielded **4.57** as white fluffy solid (1.6 mg, 91%). ^{1}H-NMR (600 MHz, DMSO-d_6): δ 0.77-0.98 (m, 15H), 1.19-1.29 (m, 6H), 1.37-1.83 (m, 18H), 1.87-1.95 (m, 1H), 2.46-2.48 (m, 3H), 3.02-3.17 (m, 9H), 3.25-3.32 (m, 11H), 3.63-3.70 (m, 7H), 3.70-3.85 (m, 8H), 4.20-4.27 (m, 2H), 4.40-4.46 (m, 1H), 4.53-4.60 (m, 1H), 4.67-4.74 (m, 1H), 6.58-6.63 (m, 2H), 6.63-7.10 (br s, 2H), 7.10-7.60 (br s, 2H, interfering with the next three listed signals), 7.12-7.15 (m, 2H), 7.37-7.45 (m, 2H), 7.49-7.54 (m, 1H), 7.60-7.65 (m, 1H), 8.15 (d, 1H, *J* 7.8 Hz), 8.25-8.61 (m, 3H), 8.86-9.17 (m, 4H), 10.03-10.28 (m, 1H), 12.46 (br s, 1H), 13.30 (br s, 1H). HRMS: *m/z* [*M*+2H]$^{2+}$ calcd. for [$C_{62}H_{105}GaN_{18}O_{16}$]$^{2+}$ 713.3600, found 713.3606. RP-HPLC (220 nm): 98% (t_R = 7.5 min, k = 8.9). $C_{62}H_{103}GaN_{18}O_{16}$ · $C_6H_3F_9O_6$ (1426.34 + 342.07).

4.6.6 RP-HPLC chromatograms of compounds 4.08, 4.09, 4.11, 4.12, 4.14-4.23, 4.25, 4.26, 4.28, 4.29 and 4.31-4.57

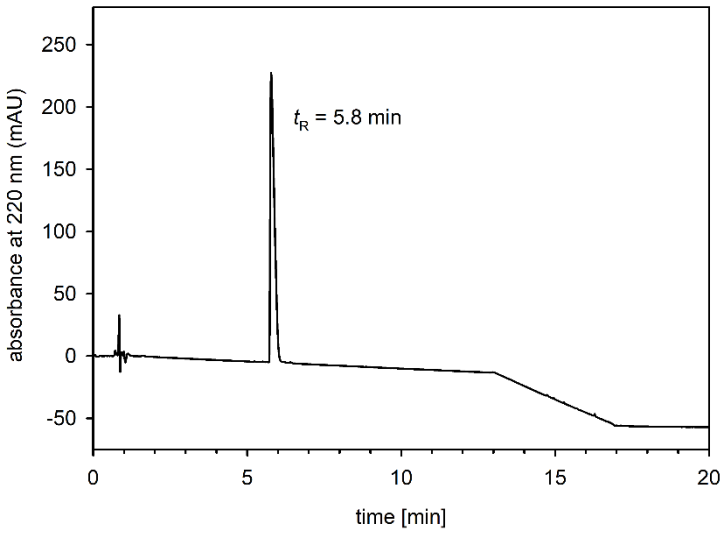

RP-HPLC analysis (purity control) of compound **4.08**

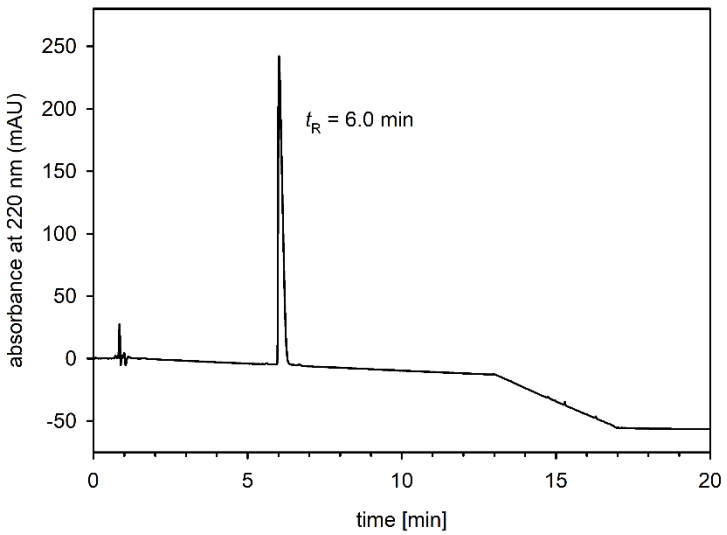

RP-HPLC analysis (purity control) of compound **4.09**

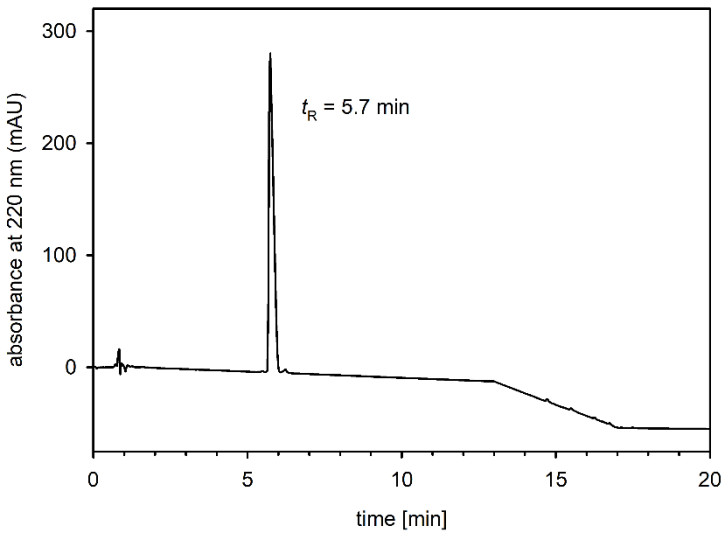

RP-HPLC analysis (purity control) of compound **4.11**

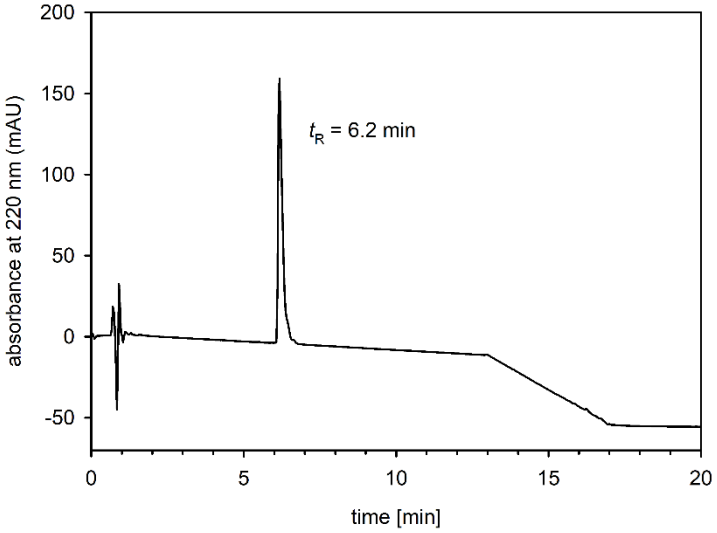

RP-HPLC analysis (purity control) of compound **4.12**

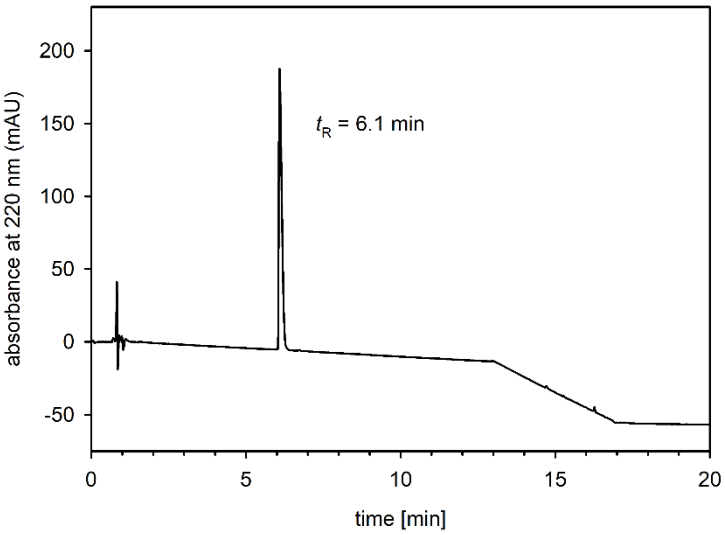

RP-HPLC analysis (purity control) of compound **4.14**

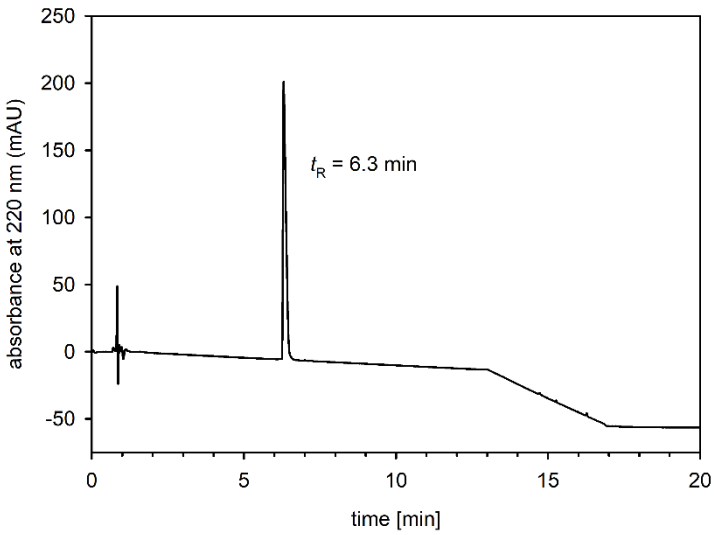

RP-HPLC analysis (purity control) of compound **4.15**

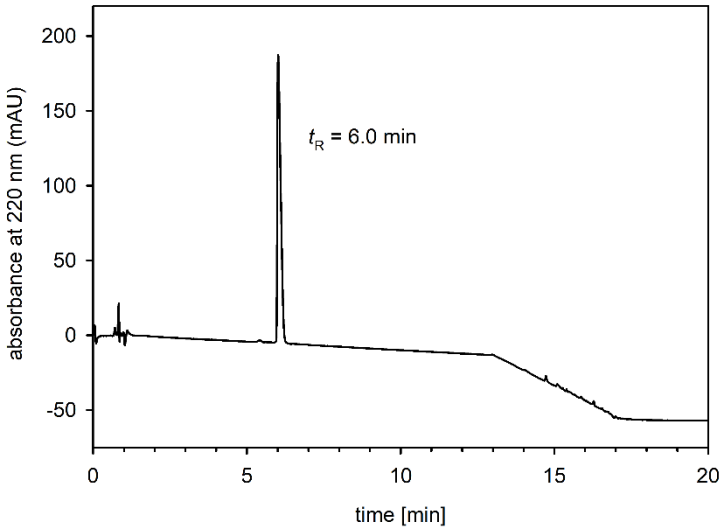

RP-HPLC analysis (purity control) of compound **4.16**

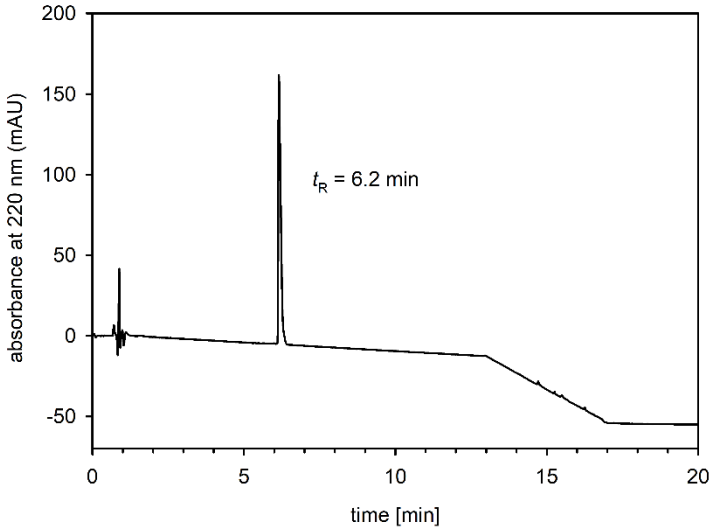

RP-HPLC analysis (purity control) of compound **4.17**

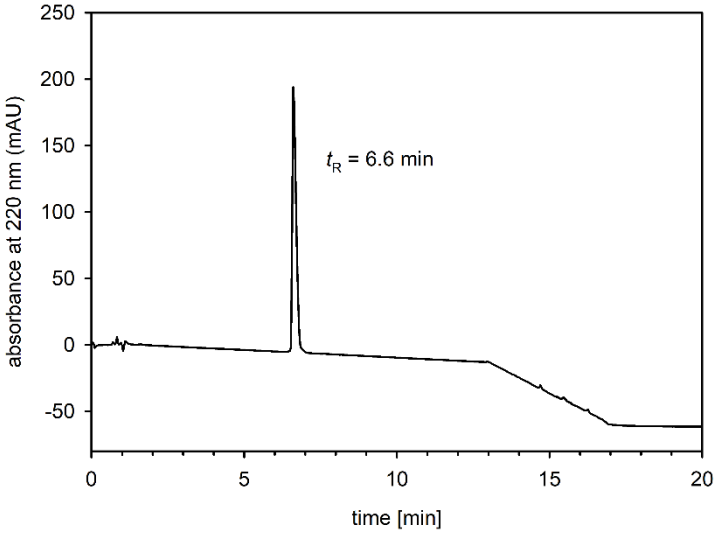

RP-HPLC analysis (purity control) of compound **4.18**

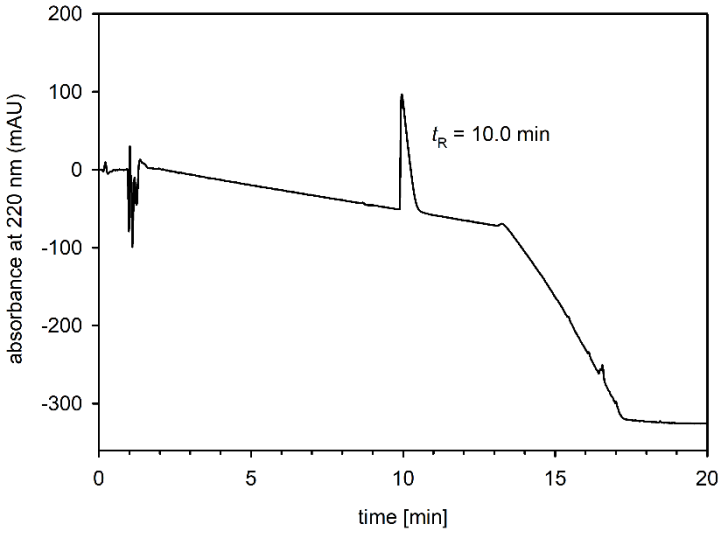

RP-HPLC analysis (purity control) of compound **4.19**

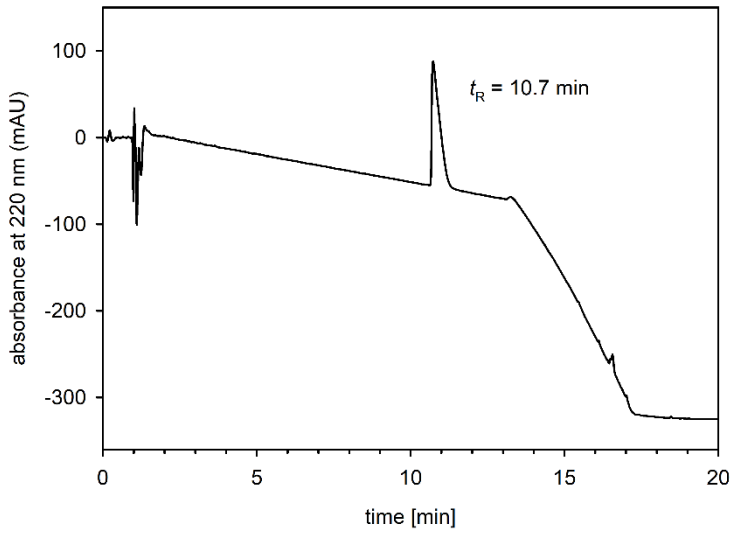

RP-HPLC analysis (purity control) of compound **4.20**

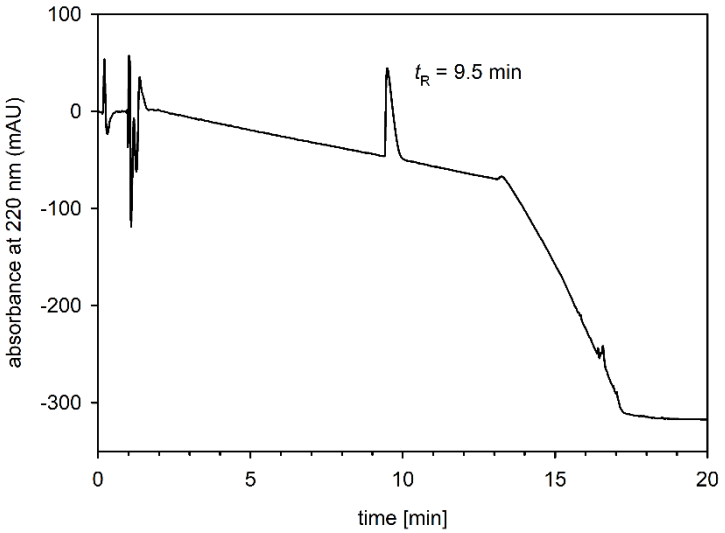

RP-HPLC analysis (purity control) of compound **4.21**

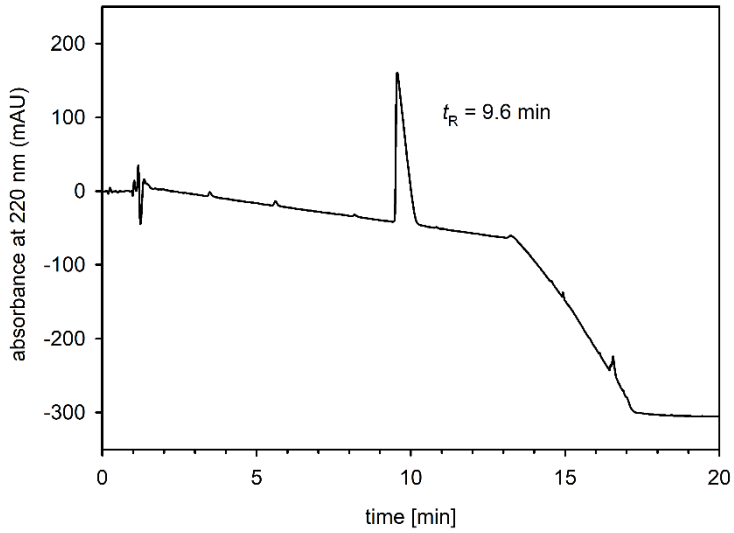

RP-HPLC analysis (purity control) of compound **4.22**

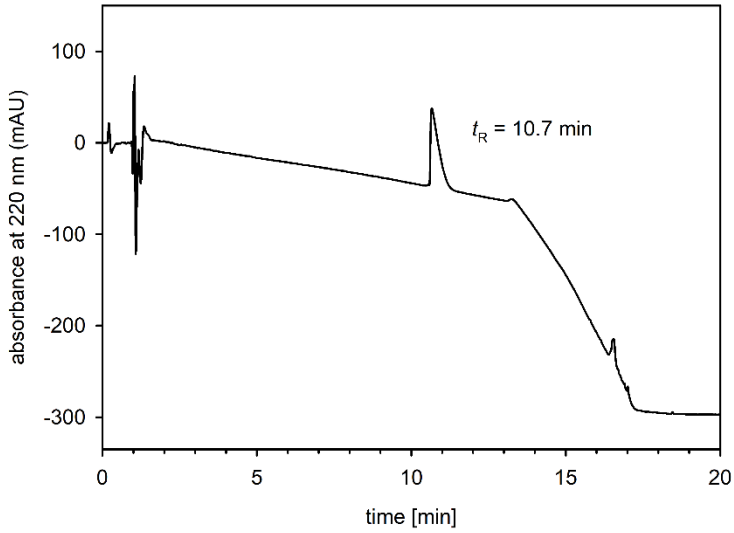

RP-HPLC analysis (purity control) of compound **4.23**

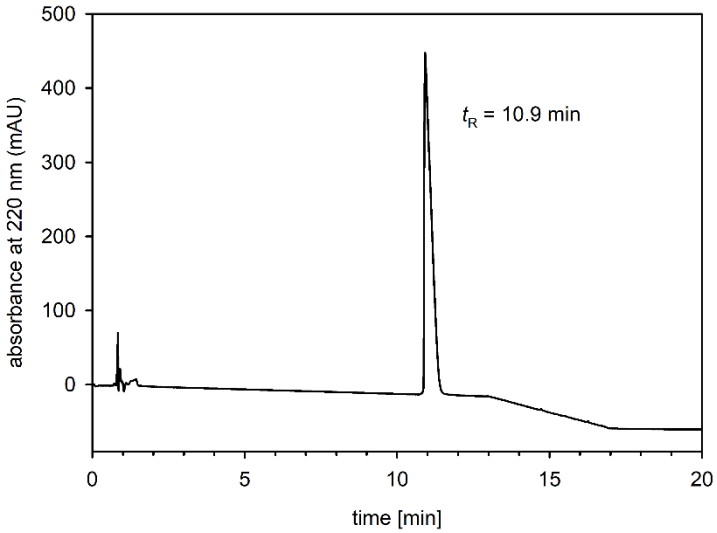

RP-HPLC analysis (purity control) of compound **4.25**

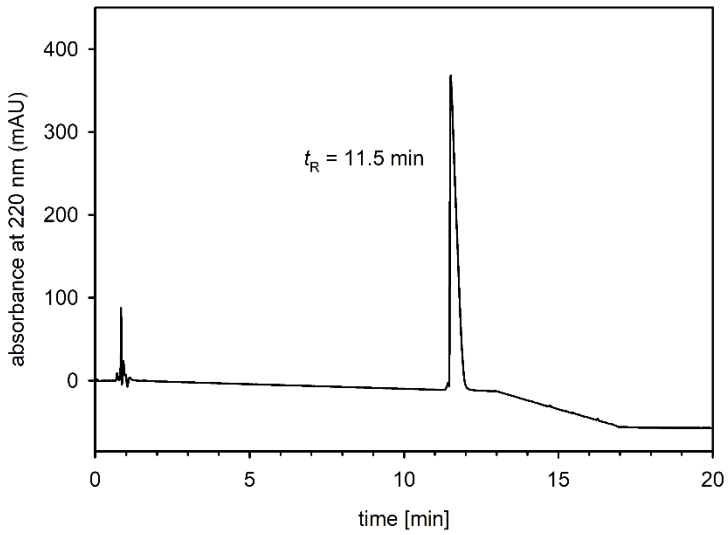

RP-HPLC analysis (purity control) of compound **4.26**

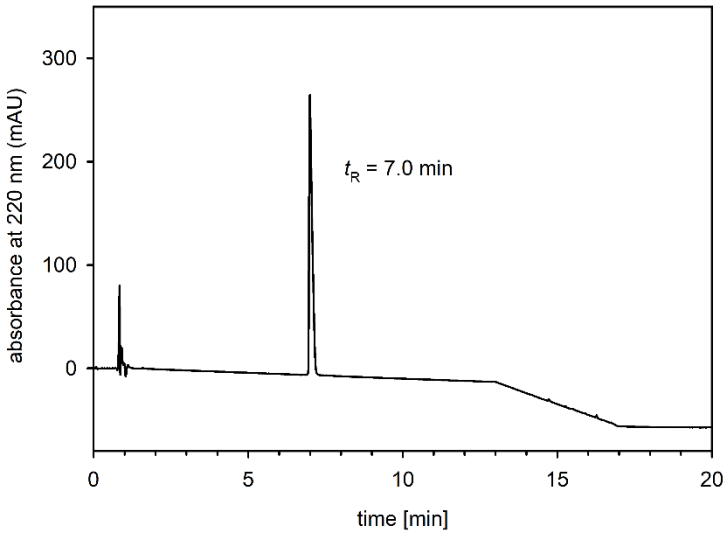

RP-HPLC analysis (purity control) of compound **4.28**

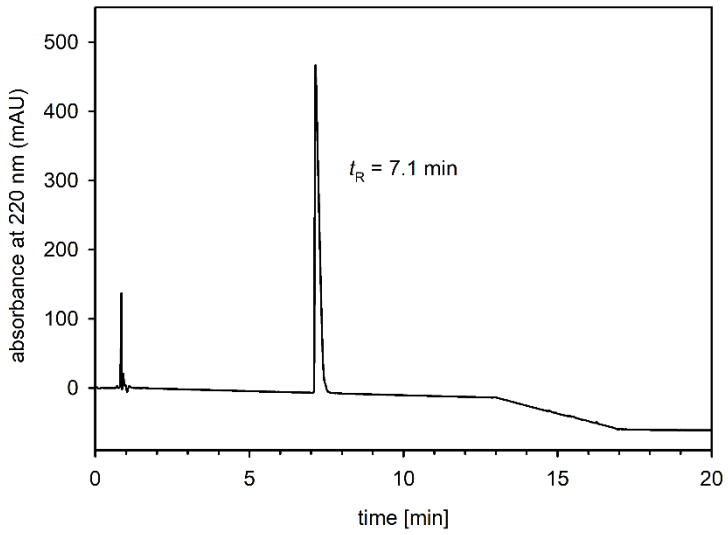

RP-HPLC analysis (purity control) of compound **4.29**

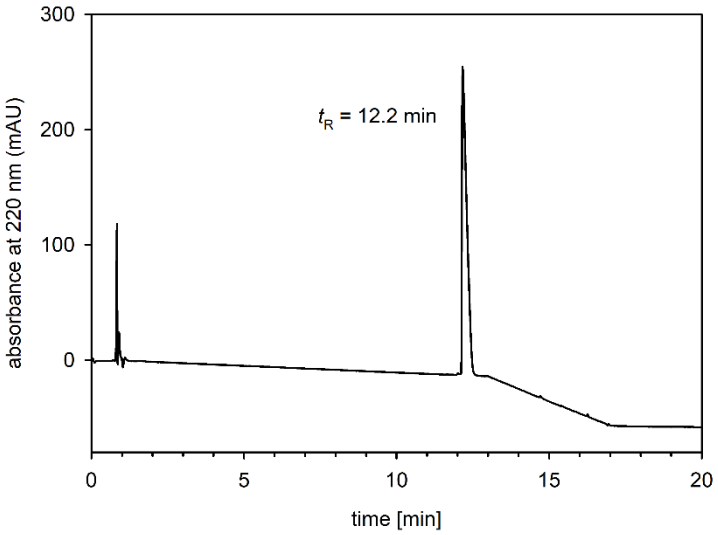

RP-HPLC analysis (purity control) of compound **4.31**

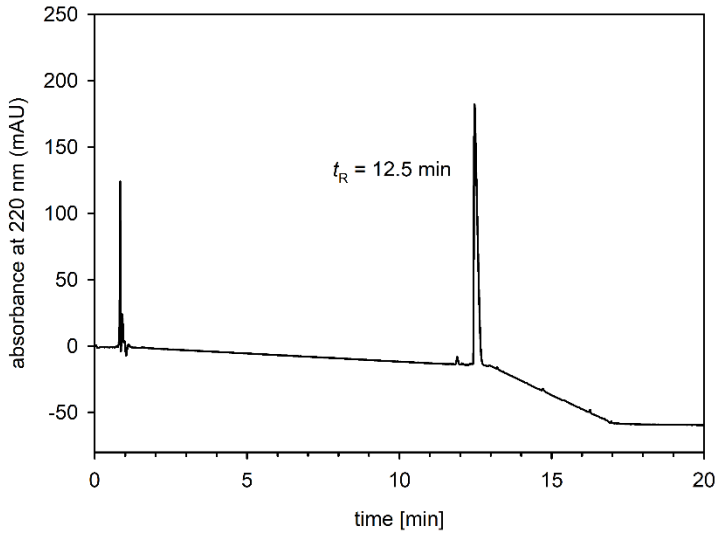

RP-HPLC analysis (purity control) of compound **4.32**

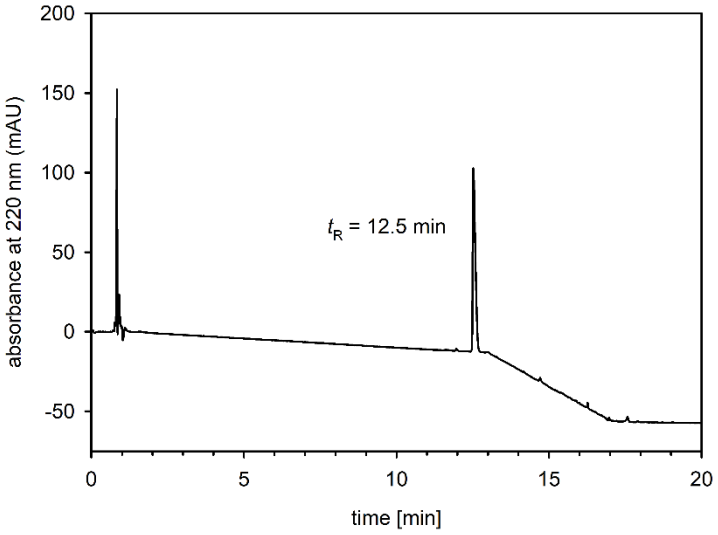

RP-HPLC analysis (purity control) of compound **4.33**

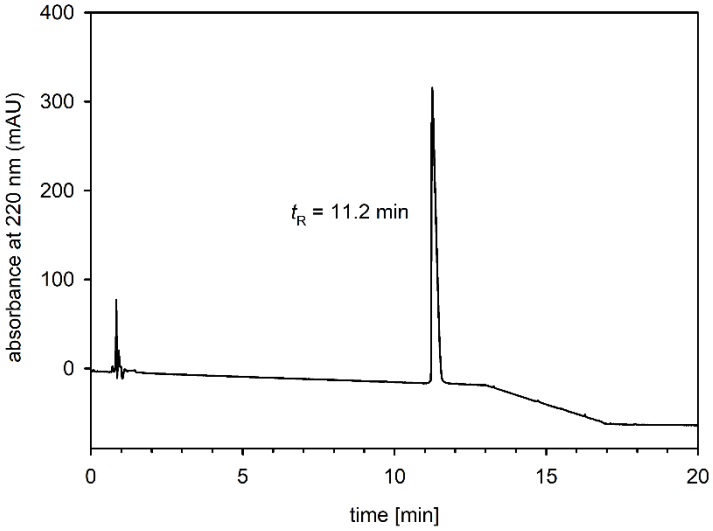

RP-HPLC analysis (purity control) of compound **4.34**

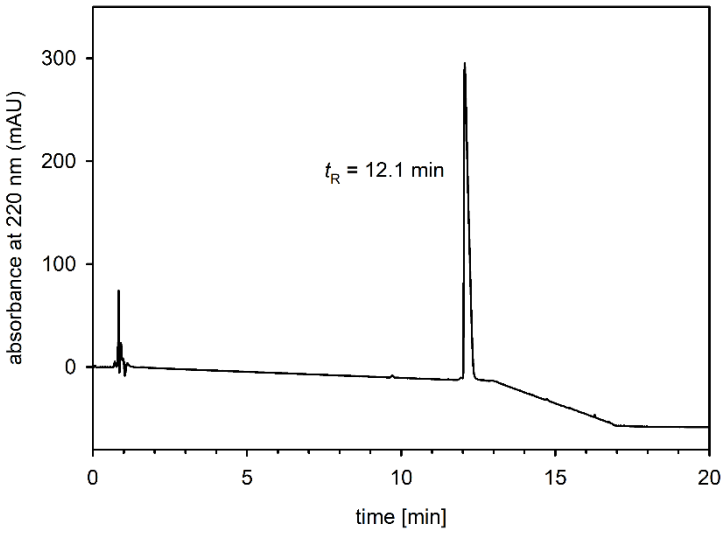

RP-HPLC analysis (purity control) of compound **4.35**

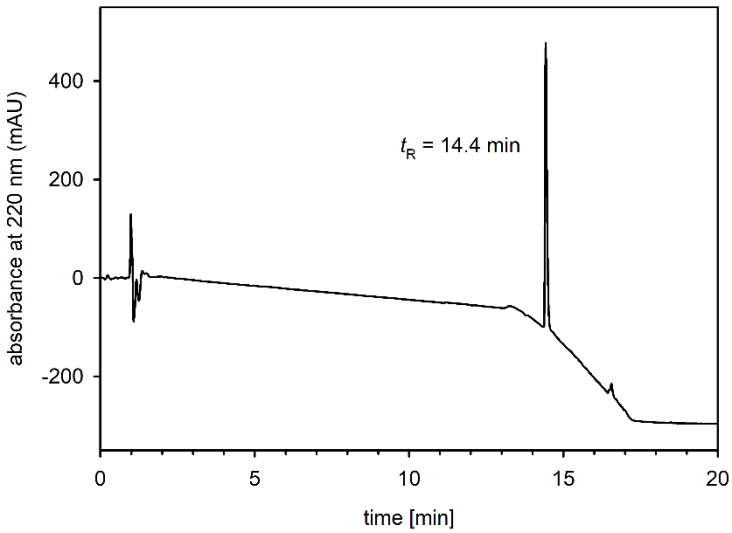

RP-HPLC analysis (purity control) of compound **4.36**

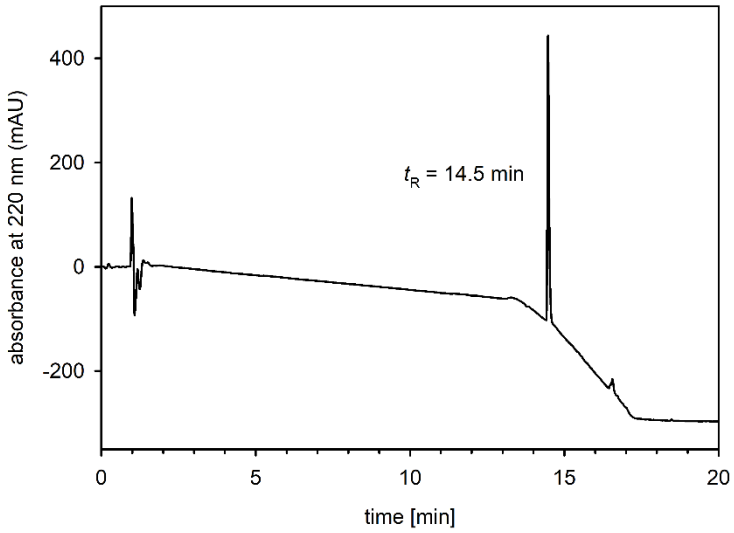

RP-HPLC analysis (purity control) of compound **4.37**

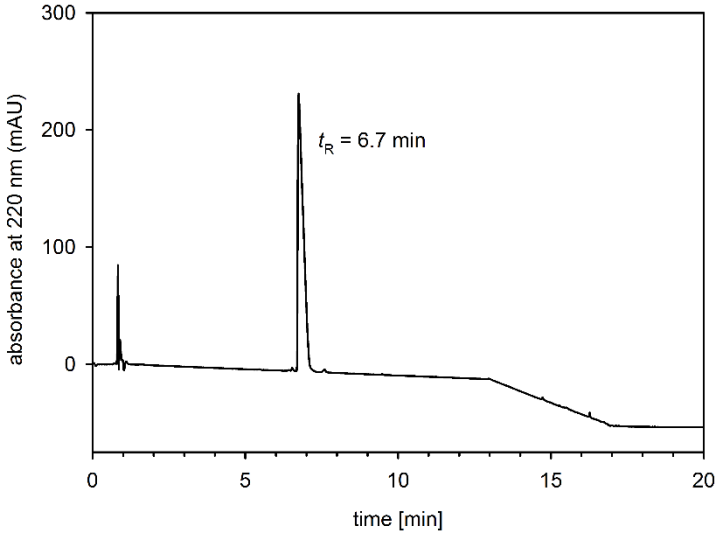

RP-HPLC analysis (purity control) of compound **4.38**

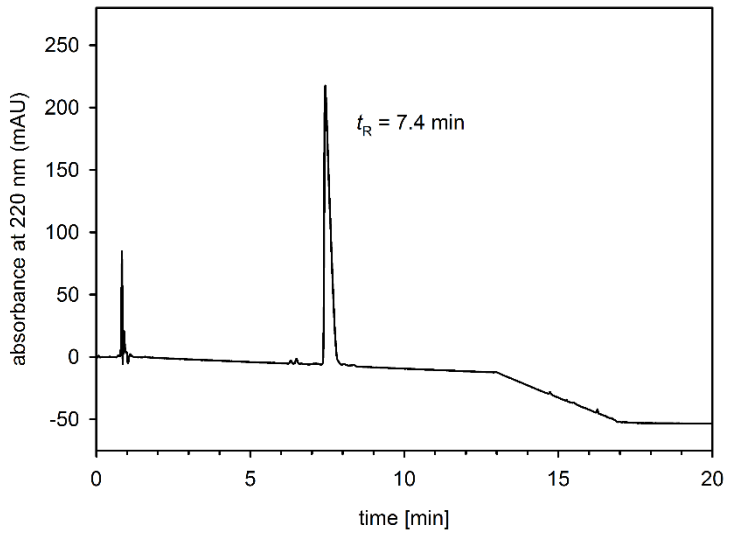

RP-HPLC analysis (purity control) of compound **4.39**

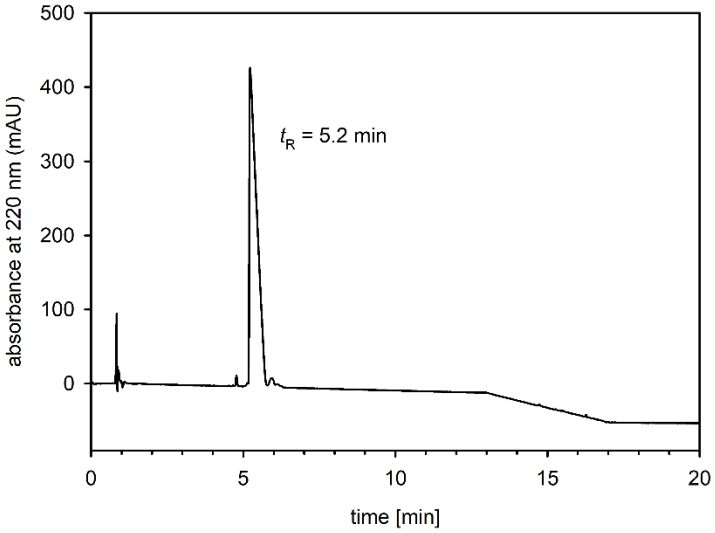

RP-HPLC analysis (purity control) of compound **4.40**

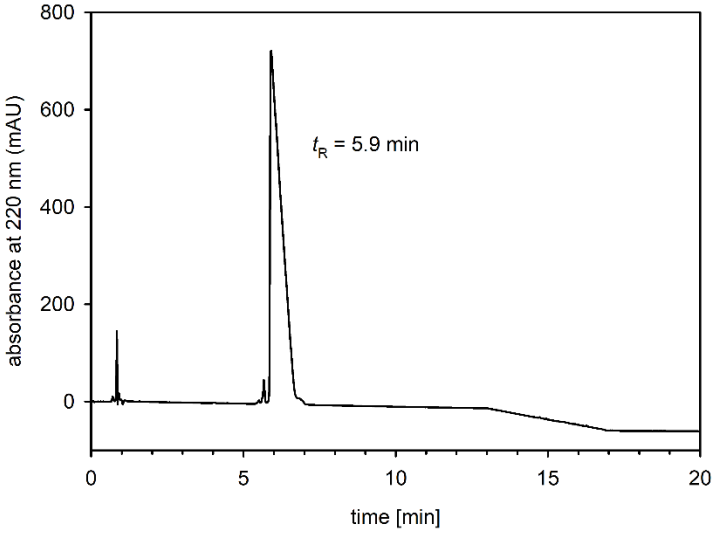

RP-HPLC analysis (purity control) of compound **4.41**

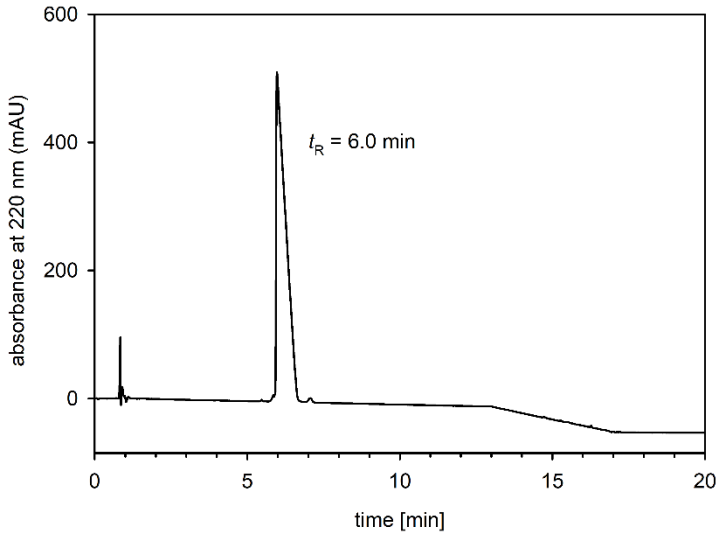

RP-HPLC analysis (purity control) of compound **4.42**

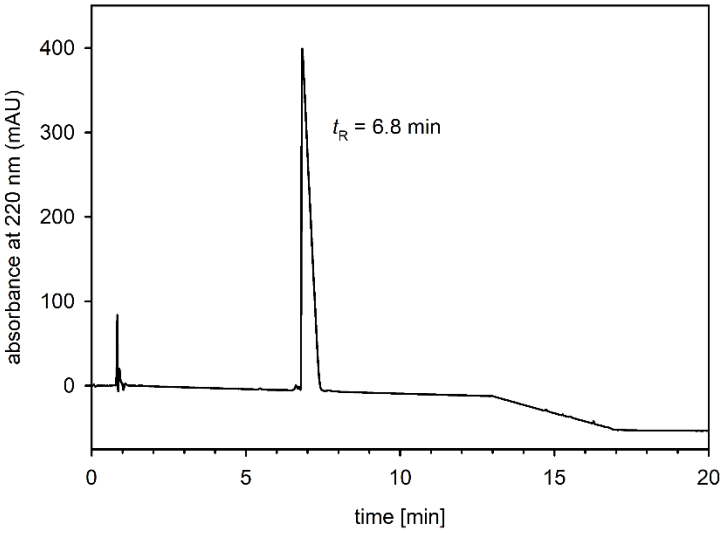

RP-HPLC analysis (purity control) of compound **4.43**

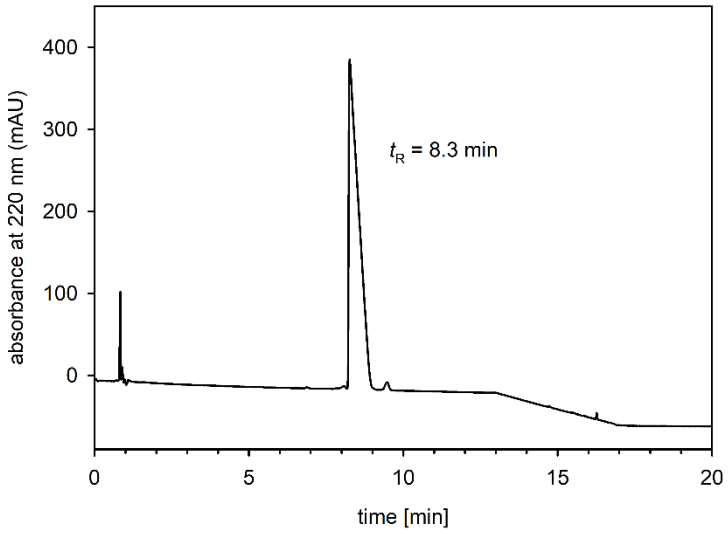

RP-HPLC analysis (purity control) of compound **4.44**

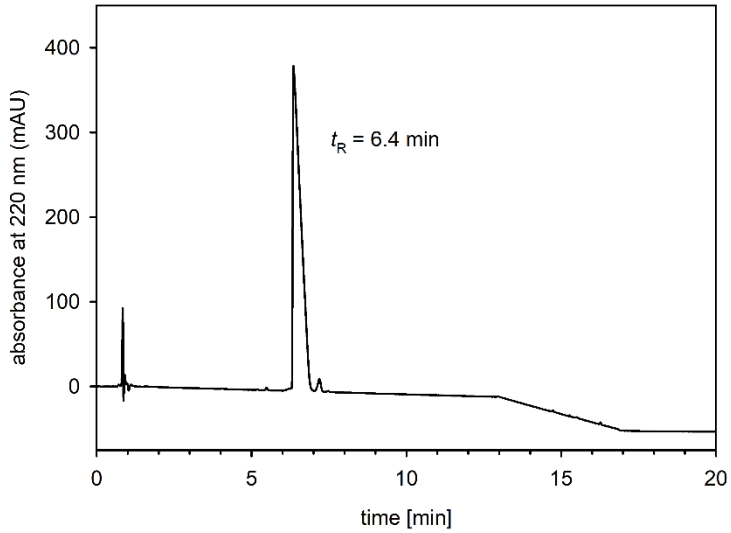

RP-HPLC analysis (purity control) of compound **4.45**

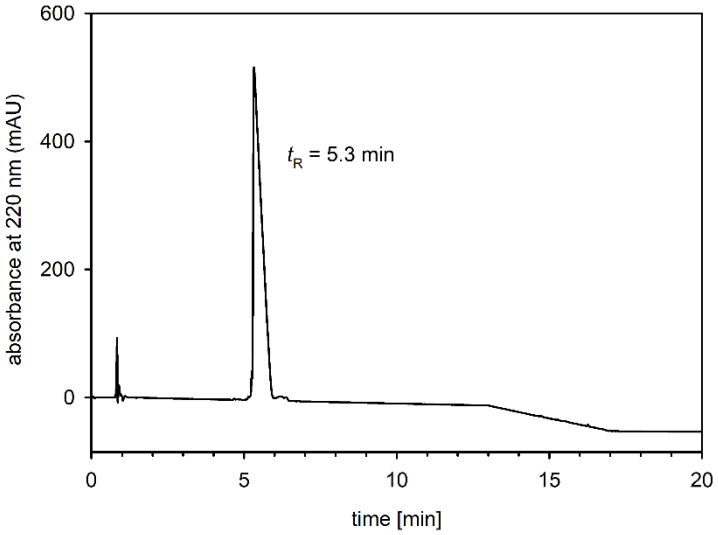

RP-HPLC analysis (purity control) of compound **4.46**

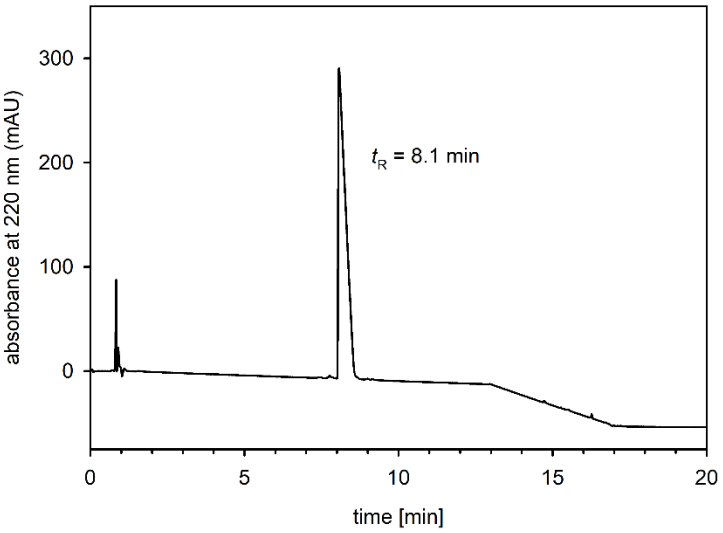

RP-HPLC analysis (purity control) of compound **4.47**

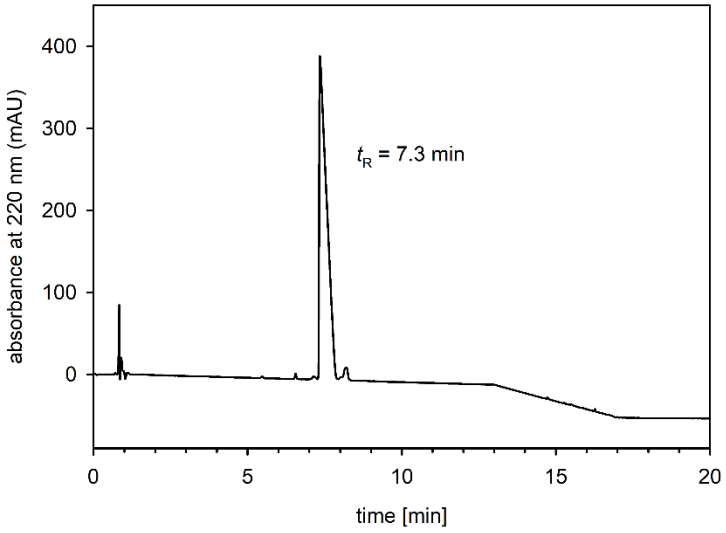

RP-HPLC analysis (purity control) of compound **4.48**

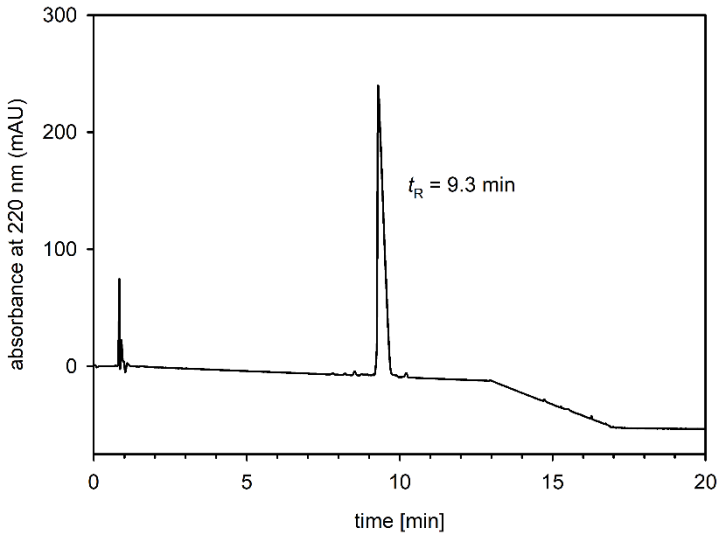

RP-HPLC analysis (purity control) of compound **4.49**

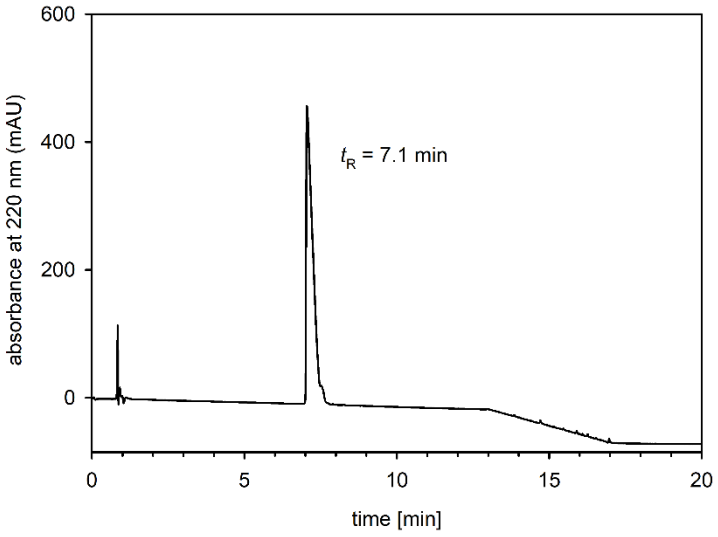

RP-HPLC analysis (purity control) of compound **4.50**

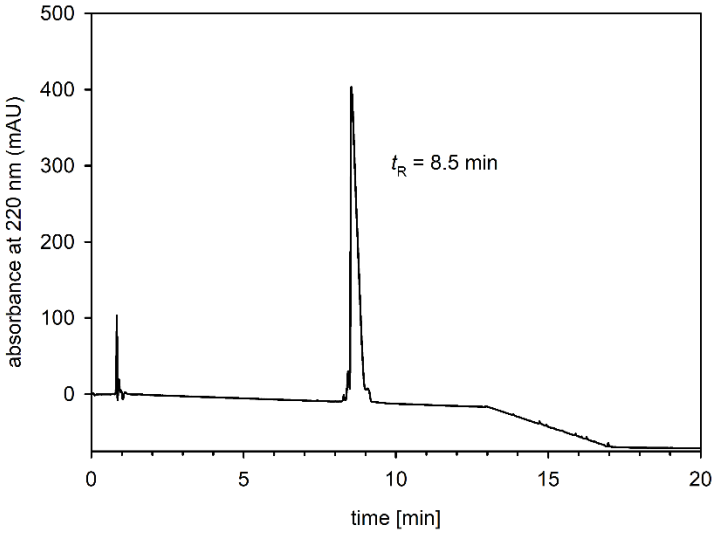

RP-HPLC analysis (purity control) of compound **4.51**

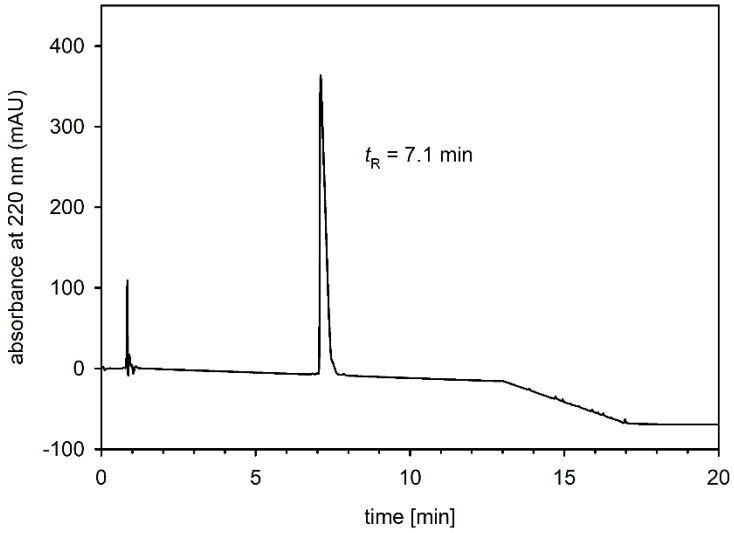

RP-HPLC analysis (purity control) of compound **4.52**

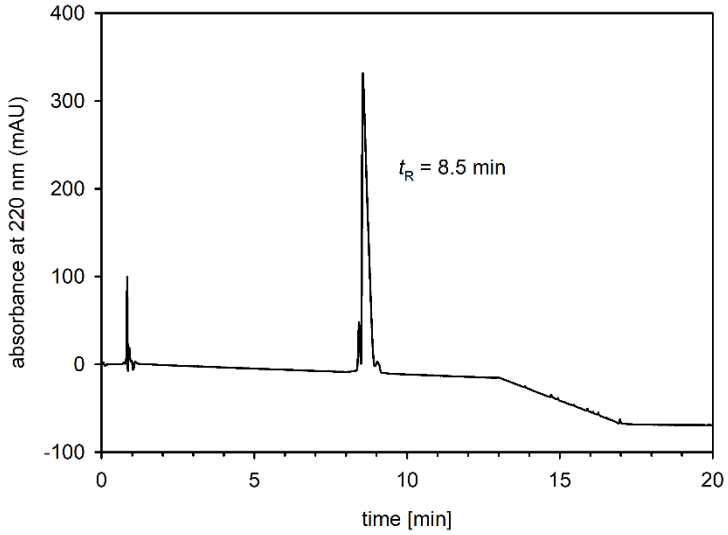

RP-HPLC analysis (purity control) of compound **4.53**

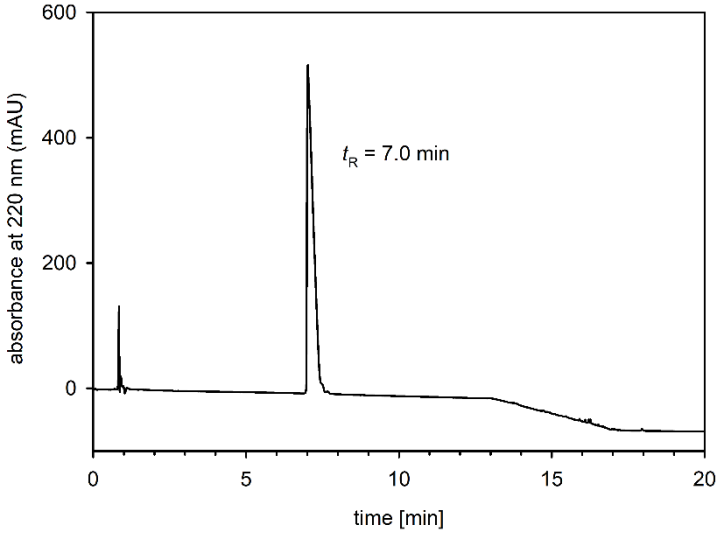

RP-HPLC analysis (purity control) of compound **4.54**

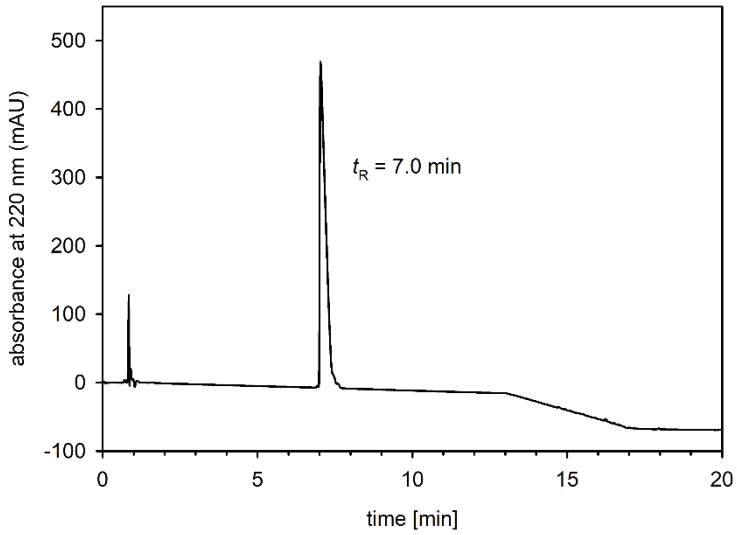

RP-HPLC analysis (purity control) of compound **4.55**

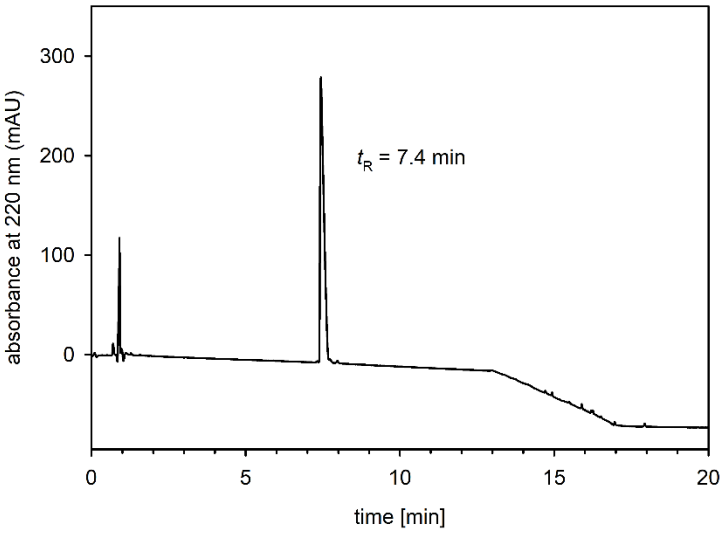

RP-HPLC analysis (purity control) of compound **4.56**

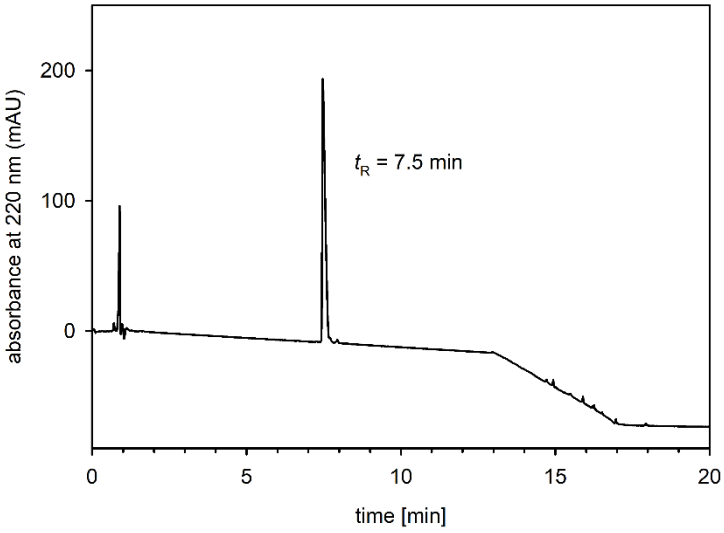

RP-HPLC analysis (purity control) of compound **4.57**

4.6.7 ^{1}H-NMR spectra of compounds 4.08, 4.09, 4.11, 4.12, 4.14-4.23, 4.25, 4.26, 4.28, 4.29 and 4.32-4.57, and ^{13}C-NMR spectra of compounds 4.50 and 4.51

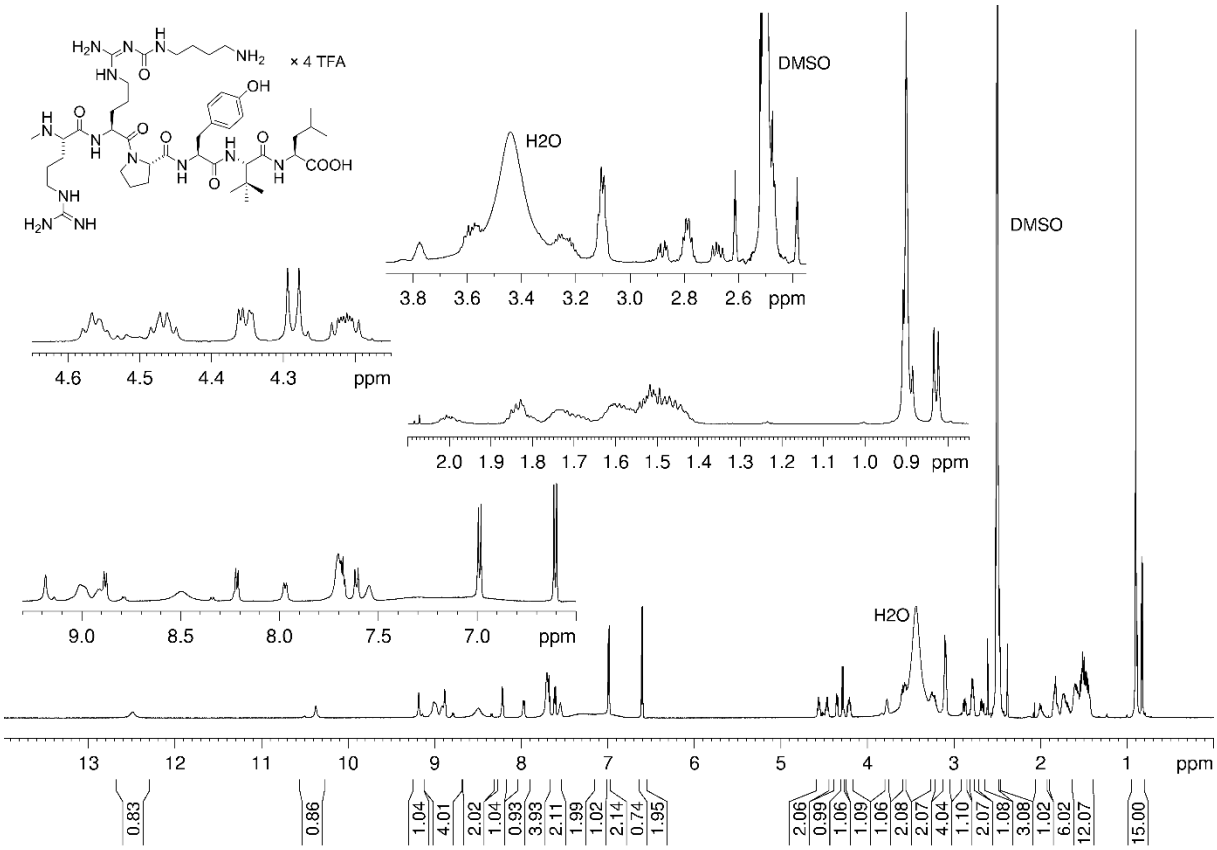

^{1}H-NMR spectrum (600 MHz, DMSO-d_6) of compound **4.08**

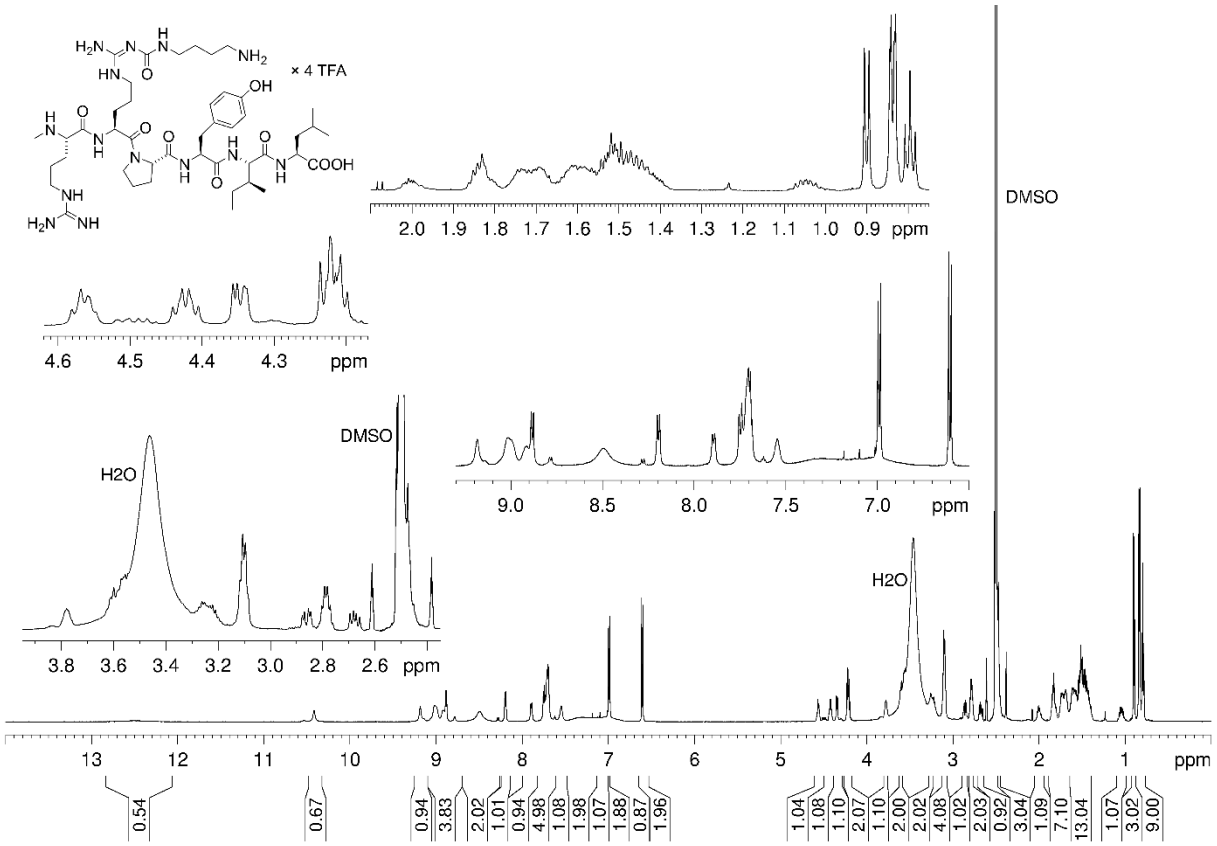

^{1}H-NMR spectrum (600 MHz, DMSO-d_6) of compound **4.09**

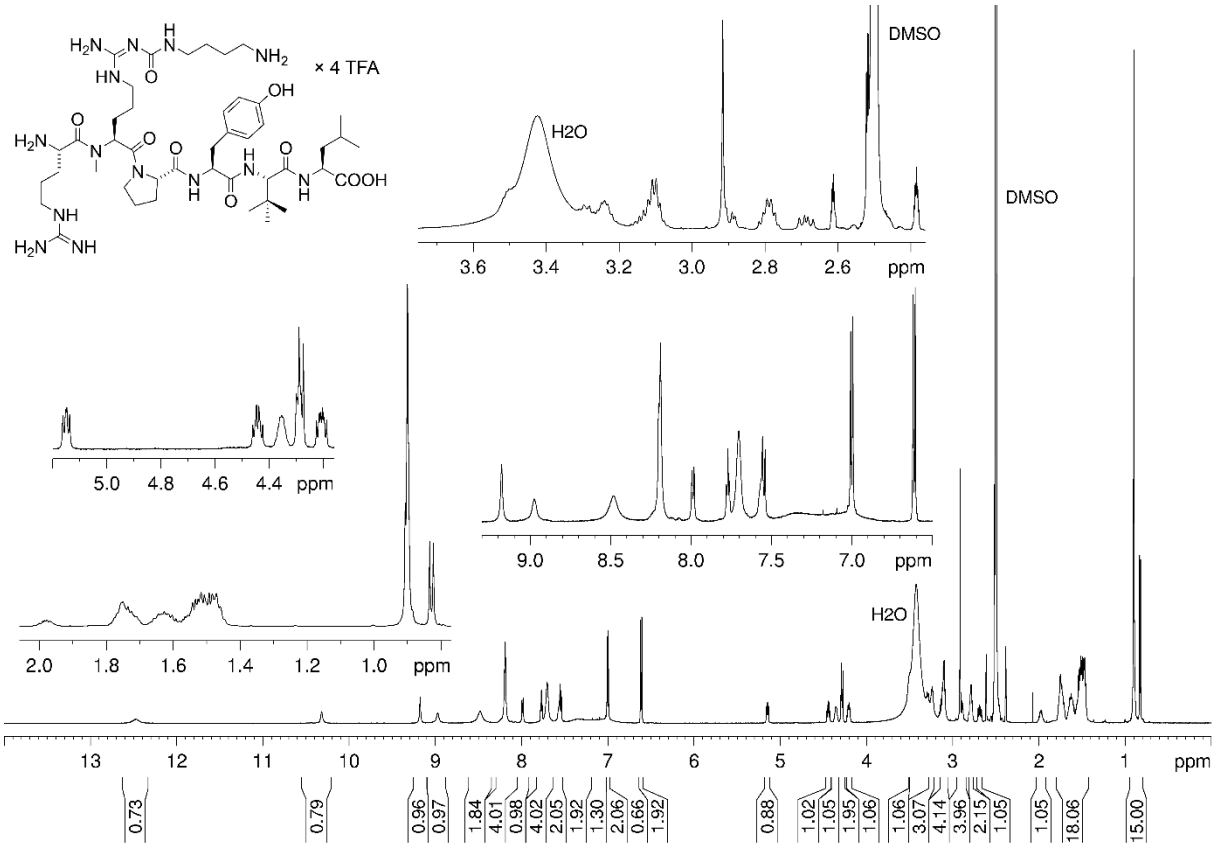

^{1}H-NMR spectrum (600 MHz, DMSO-d_6) of compound **4.11**

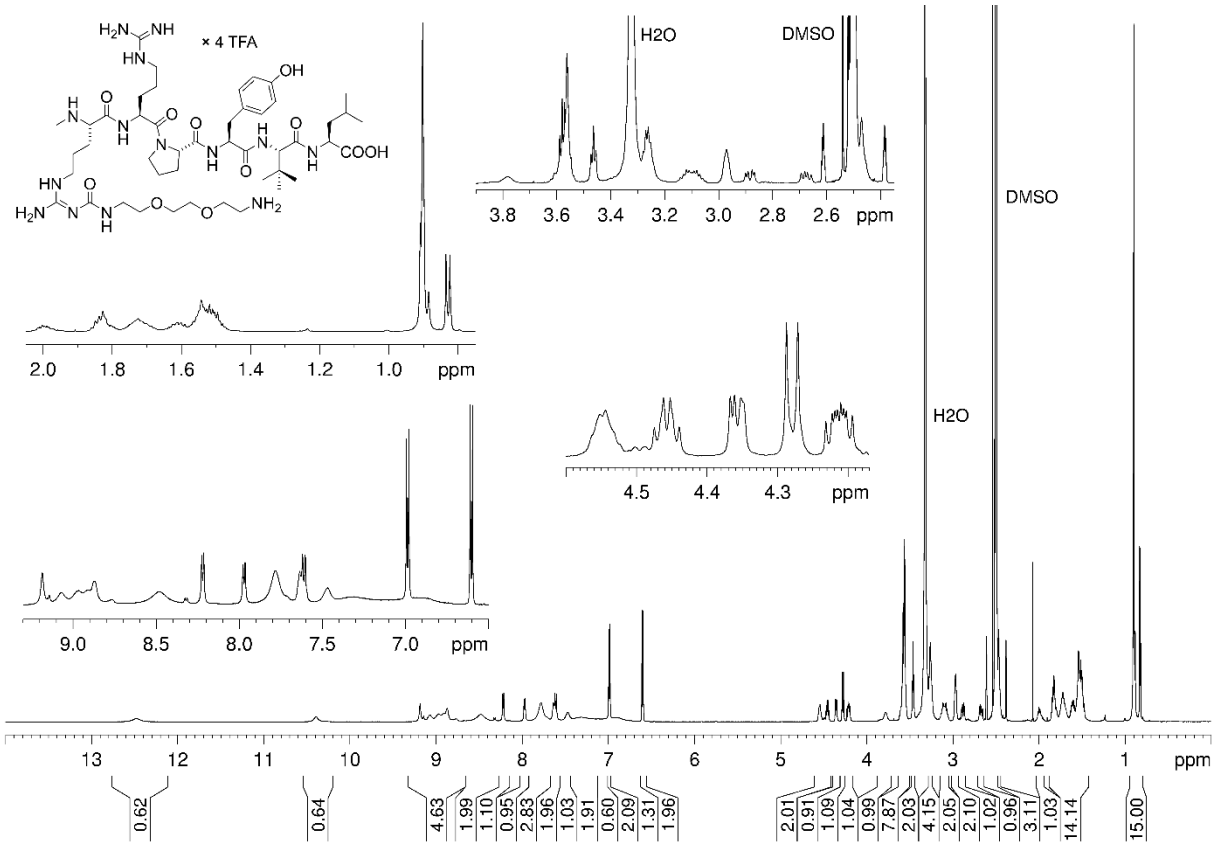

^{1}H-NMR spectrum (600 MHz, DMSO-d_6) of compound **4.12**

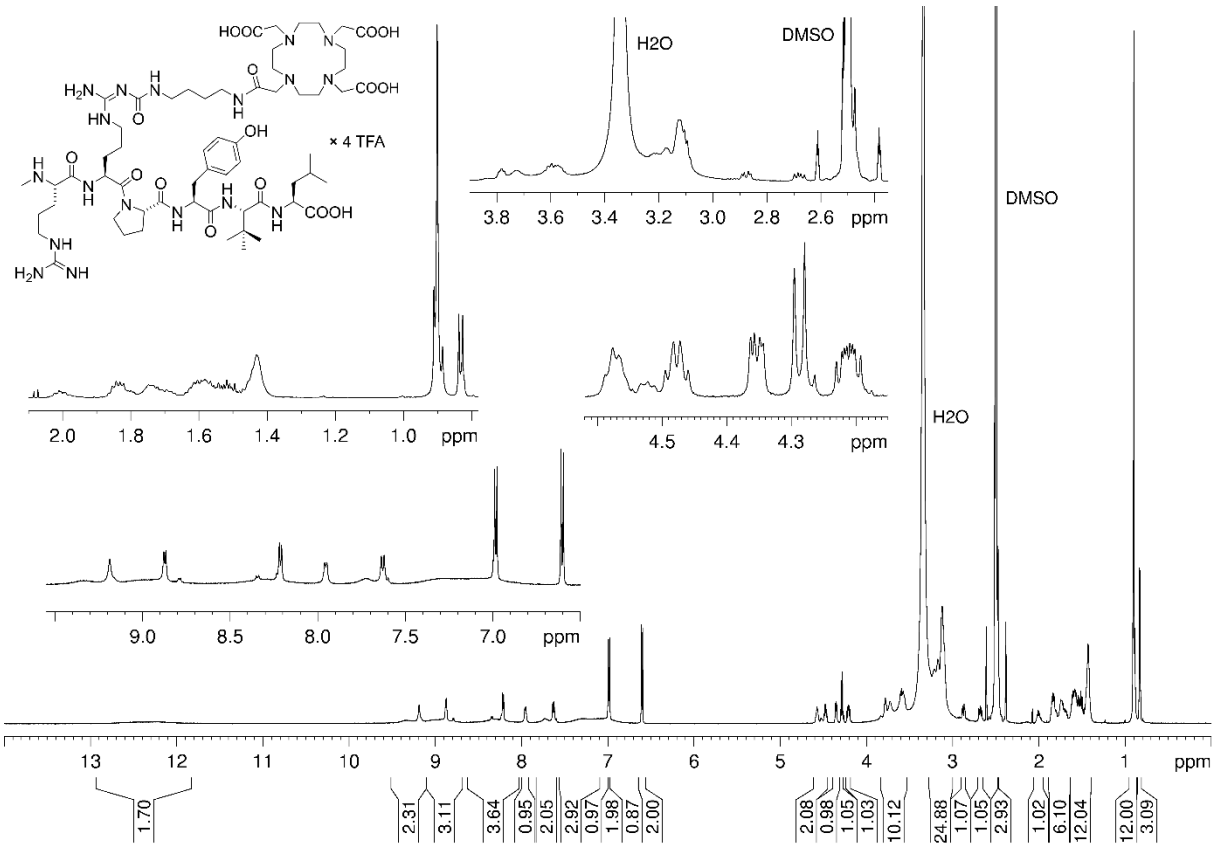

^{1}H-NMR spectrum (600 MHz, DMSO-d_6) of compound **4.14**

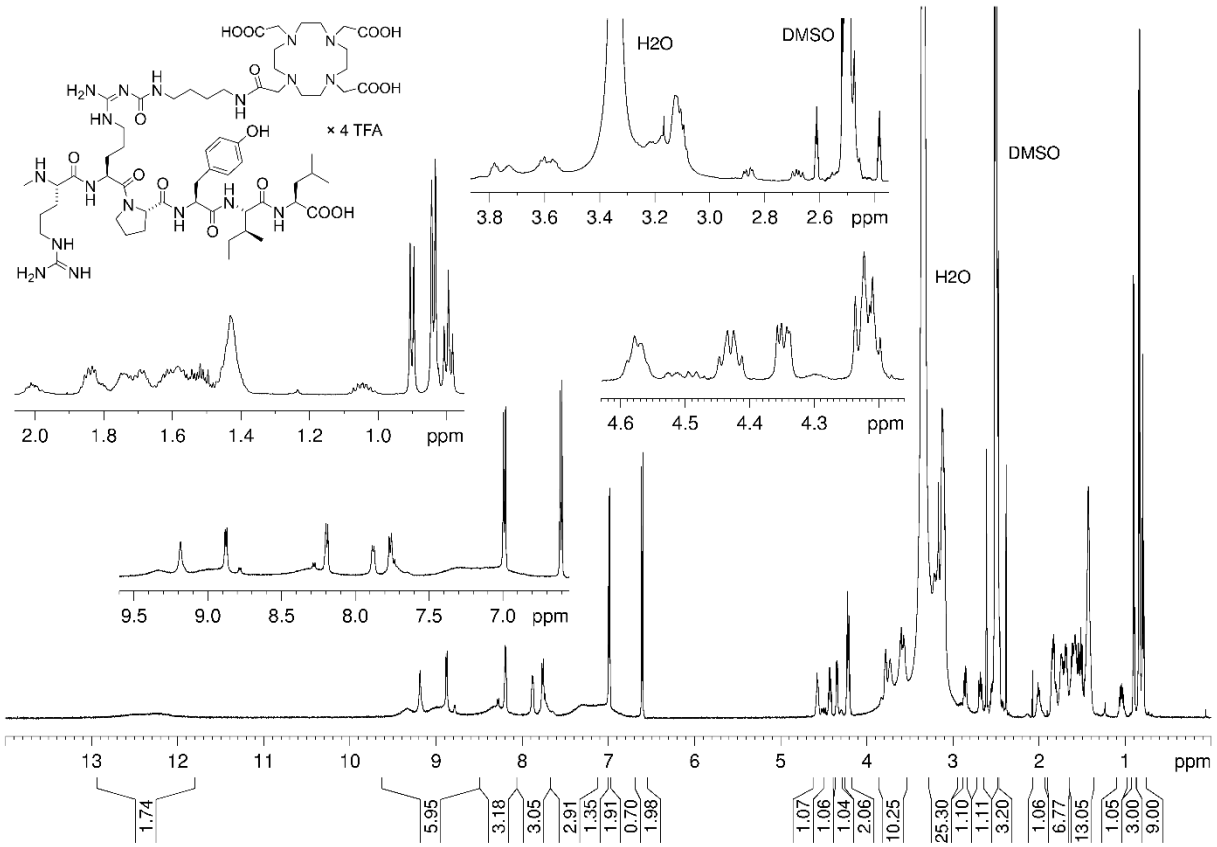

^{1}H-NMR spectrum (600 MHz, DMSO-d_6) of compound **4.15**

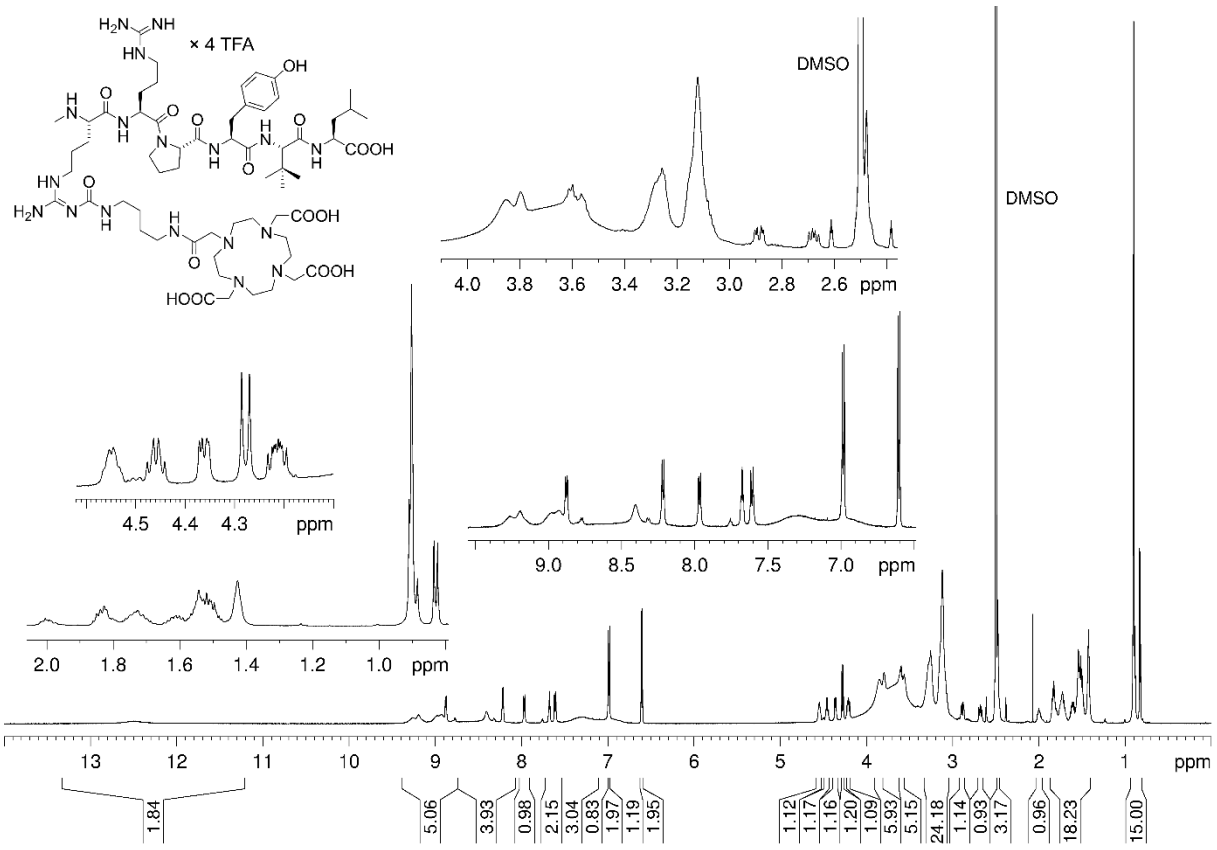

^{1}H-NMR spectrum (600 MHz, DMSO-d_6) of compound **4.16**

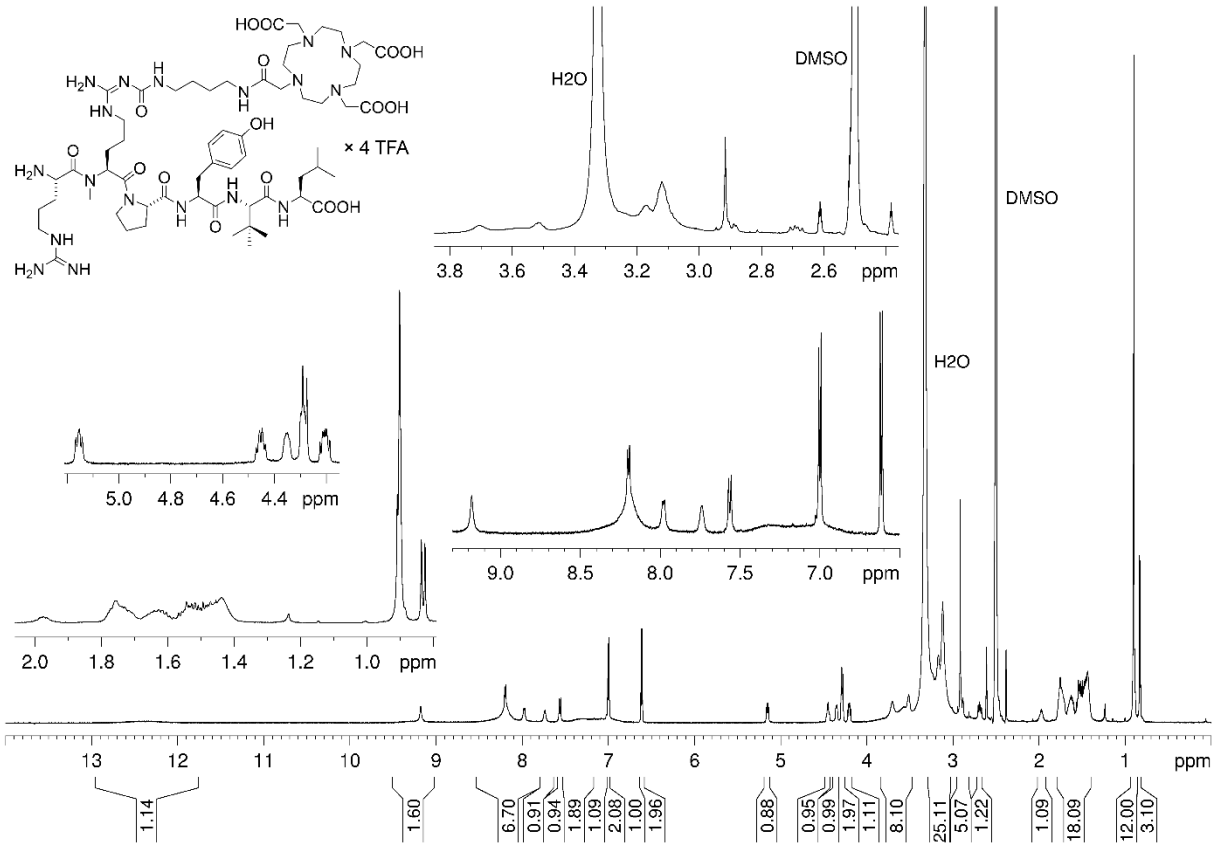

^{1}H-NMR spectrum (600 MHz, DMSO-d_6) of compound **4.17**

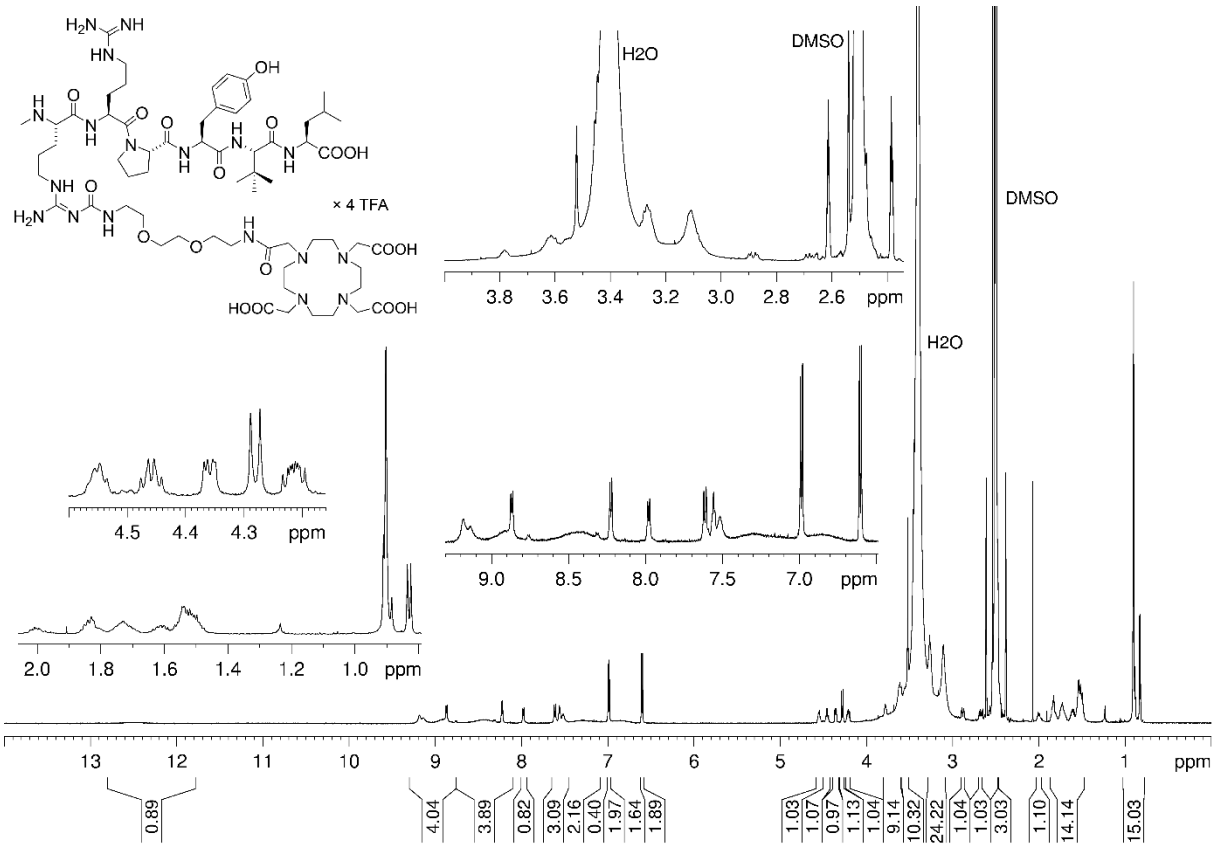

^{1}H-NMR spectrum (600 MHz, DMSO-d_6) of compound **4.18**

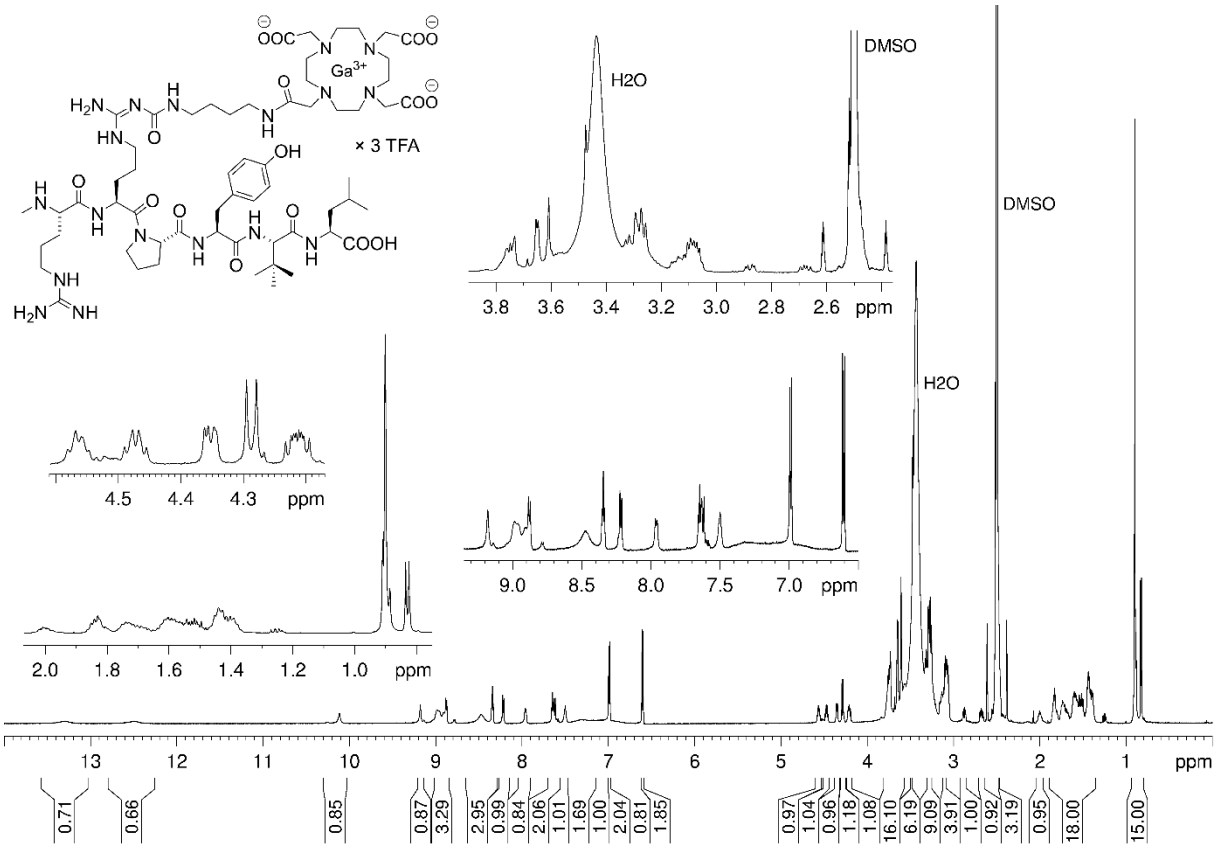

^{1}H-NMR spectrum (600 MHz, DMSO-d_6) of compound **4.19**

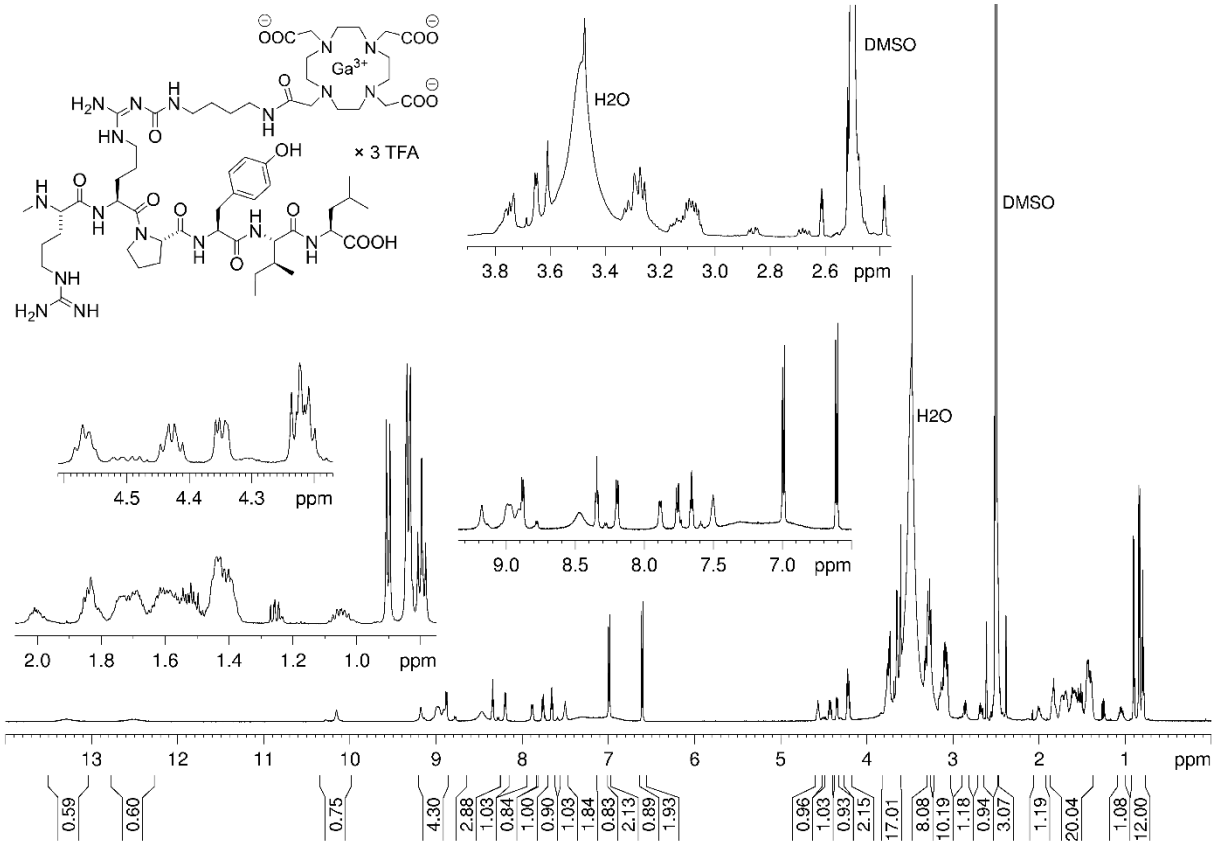

^{1}H-NMR spectrum (600 MHz, DMSO-d_6) of compound **4.20**

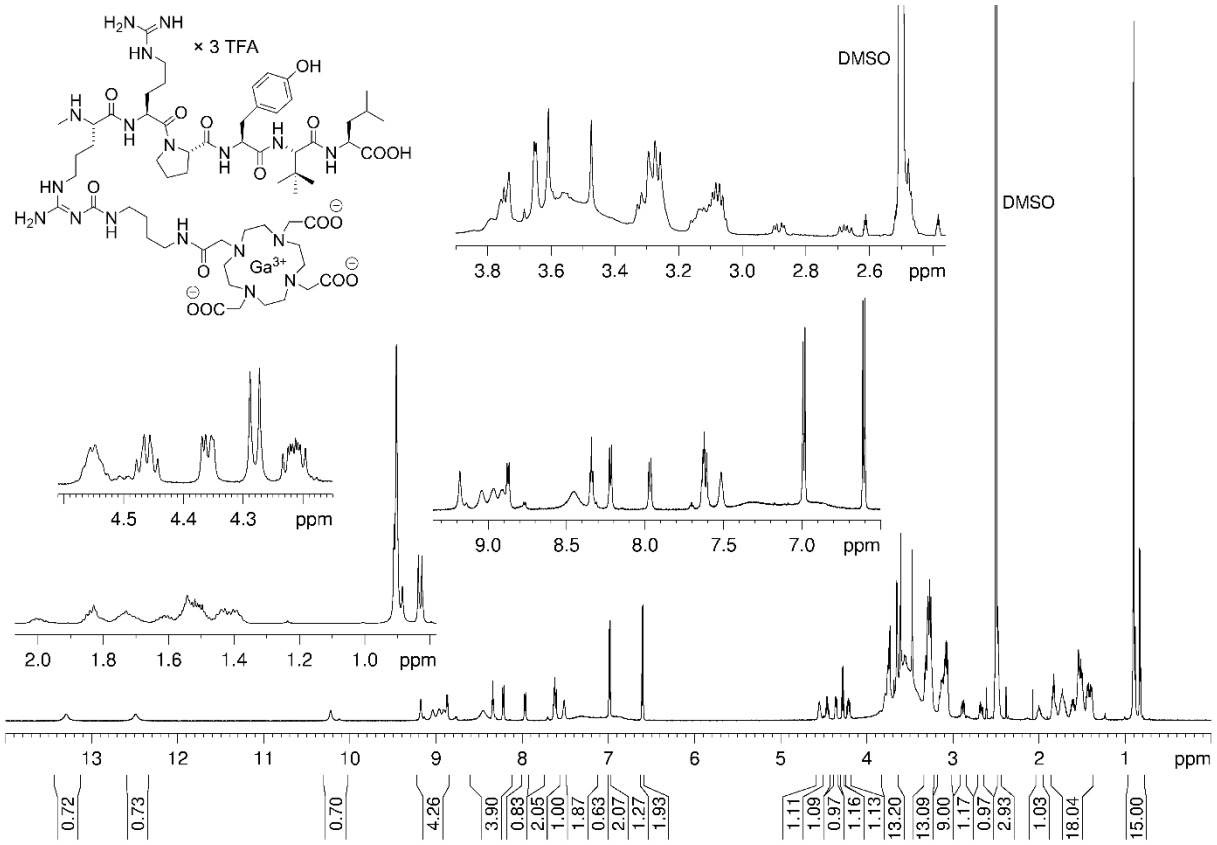

^{1}H-NMR spectrum (600 MHz, DMSO-d_6) of compound **4.21**

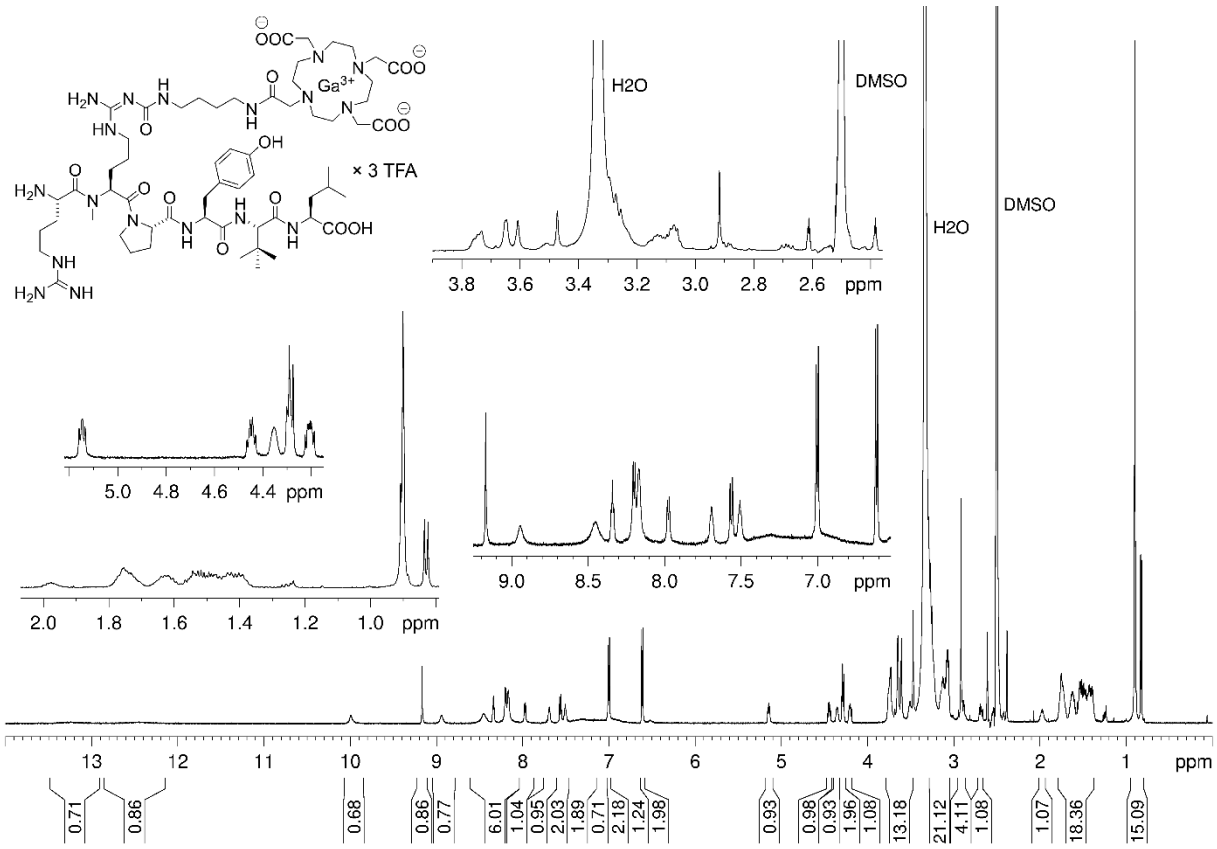

^{1}H-NMR spectrum (600 MHz, DMSO-d_6) of compound **4.22**

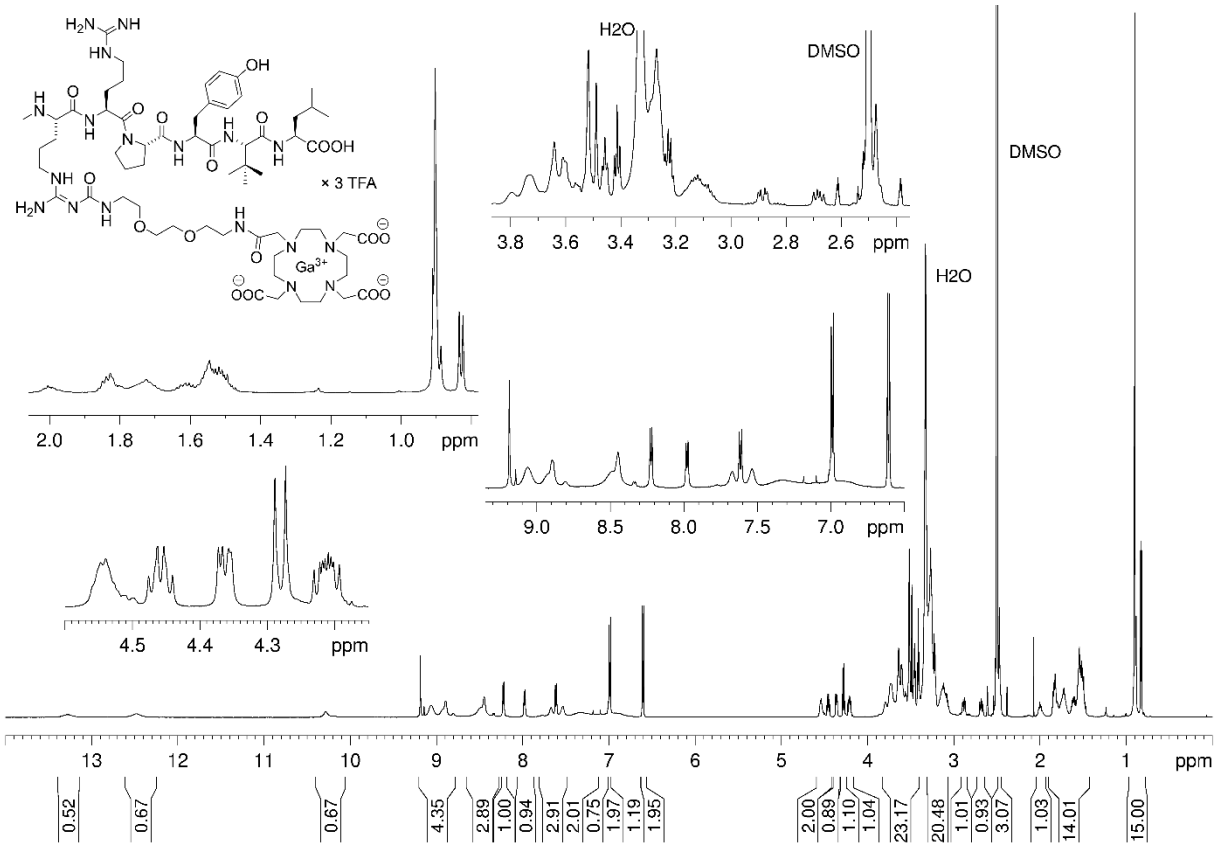

^{1}H-NMR spectrum (600 MHz, DMSO-d_6) of compound **4.23**

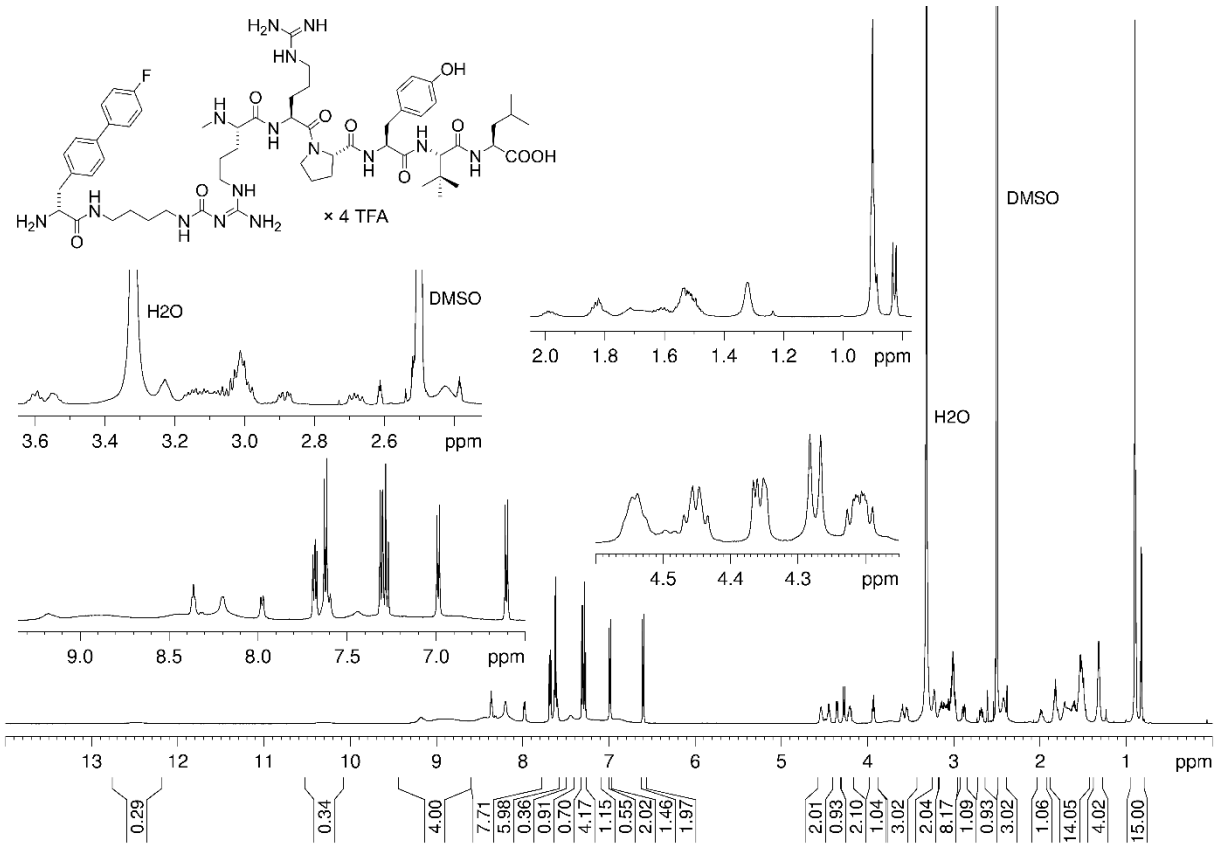

^{1}H-NMR spectrum (600 MHz, DMSO-d_6) of compound **4.25**

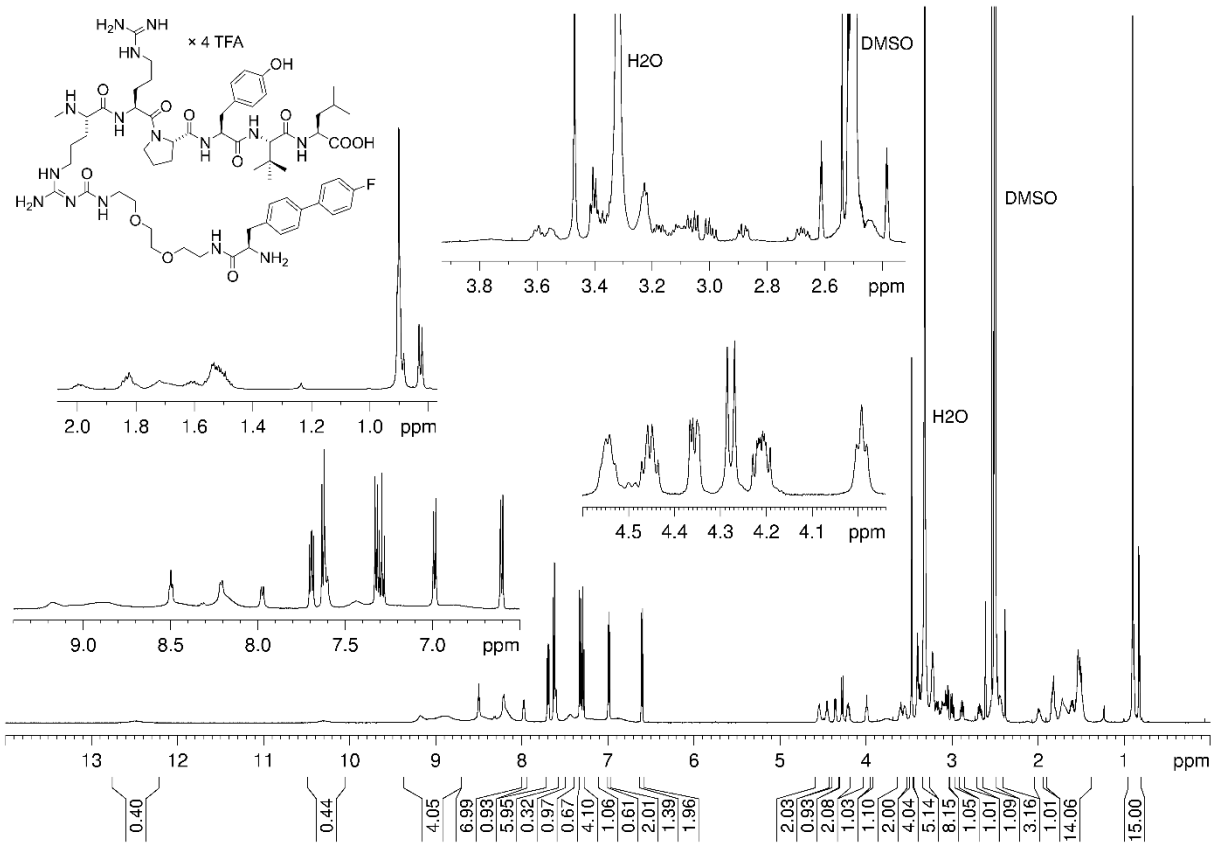

^{1}H-NMR spectrum (600 MHz, DMSO-d_6) of compound **4.26**

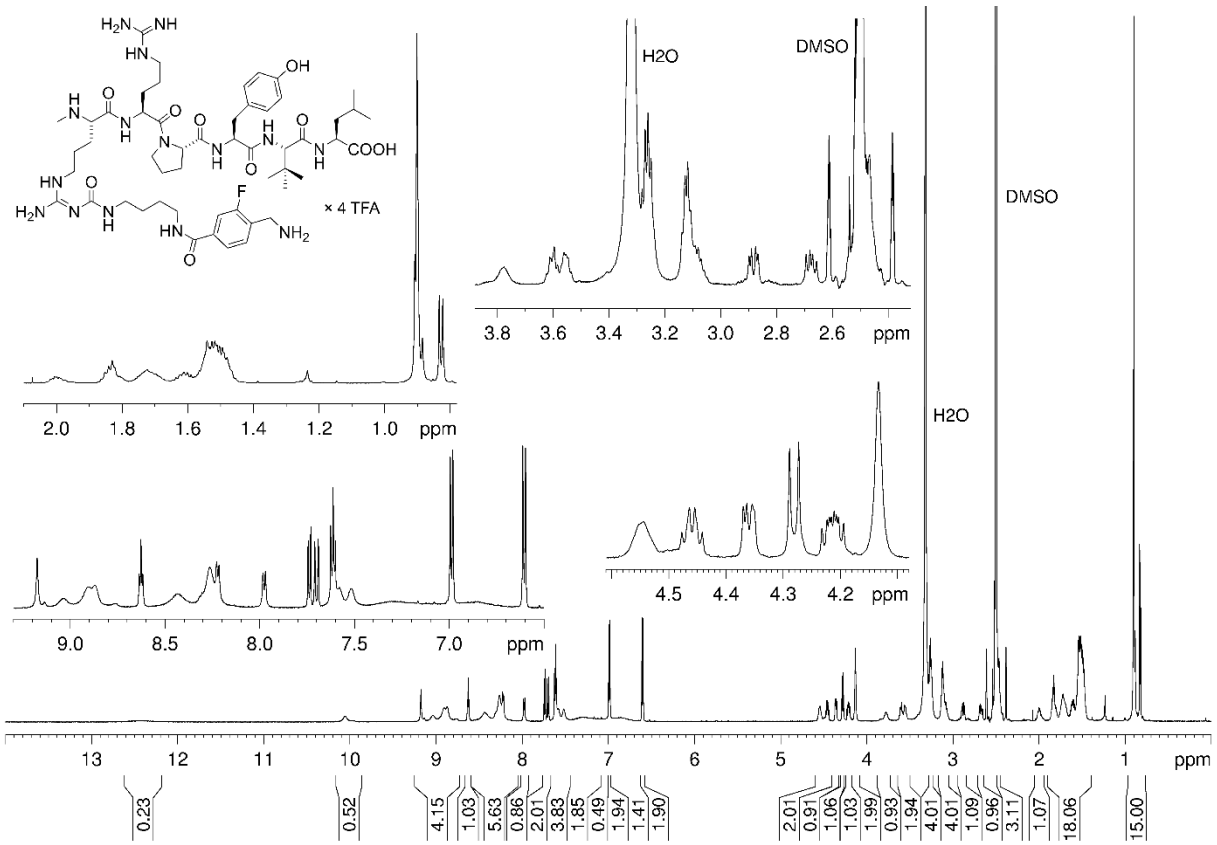

^{1}H-NMR spectrum (600 MHz, DMSO-d_6) of compound **4.28**

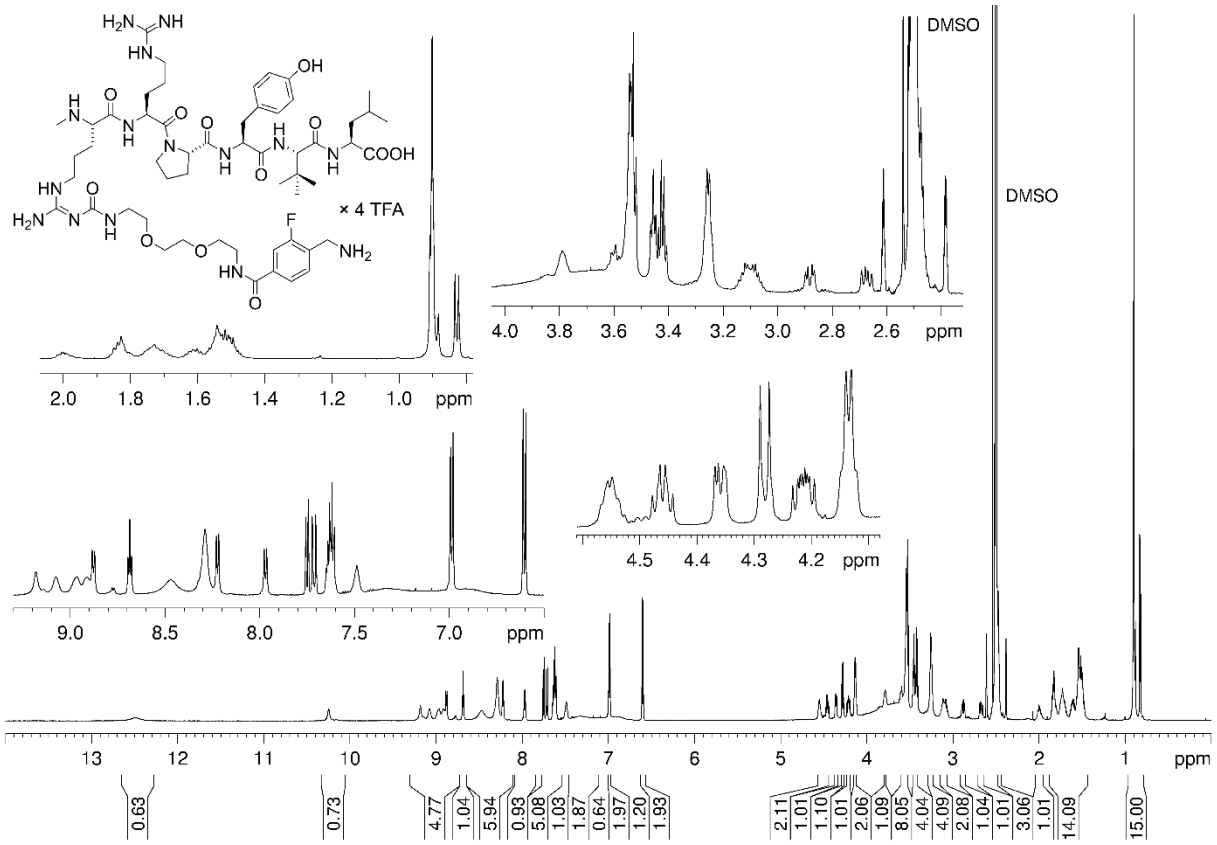

^{1}H-NMR spectrum (600 MHz, DMSO-d_6) of compound **4.29**

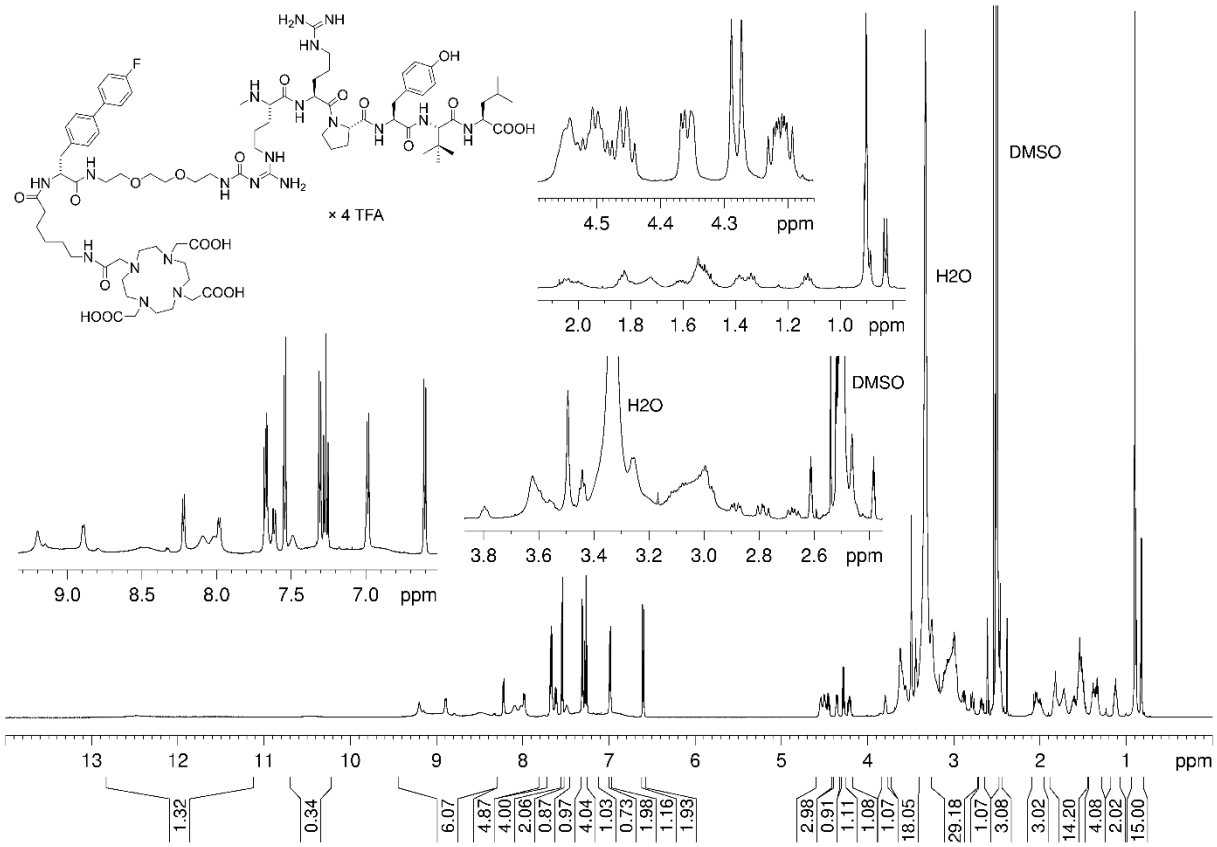

^{1}H-NMR spectrum (600 MHz, DMSO-d_6) of compound **4.32**

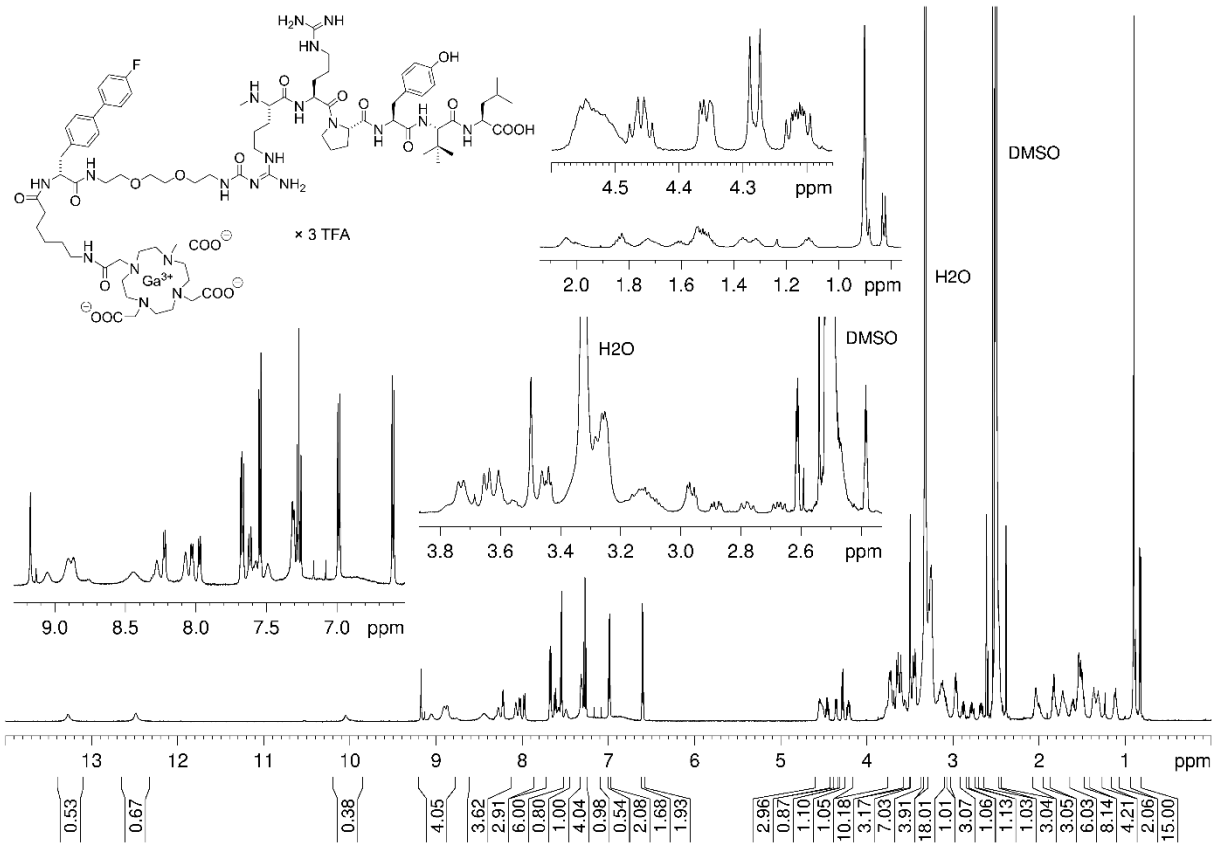

^{1}H-NMR spectrum (600 MHz, DMSO-d_6) of compound **4.33**

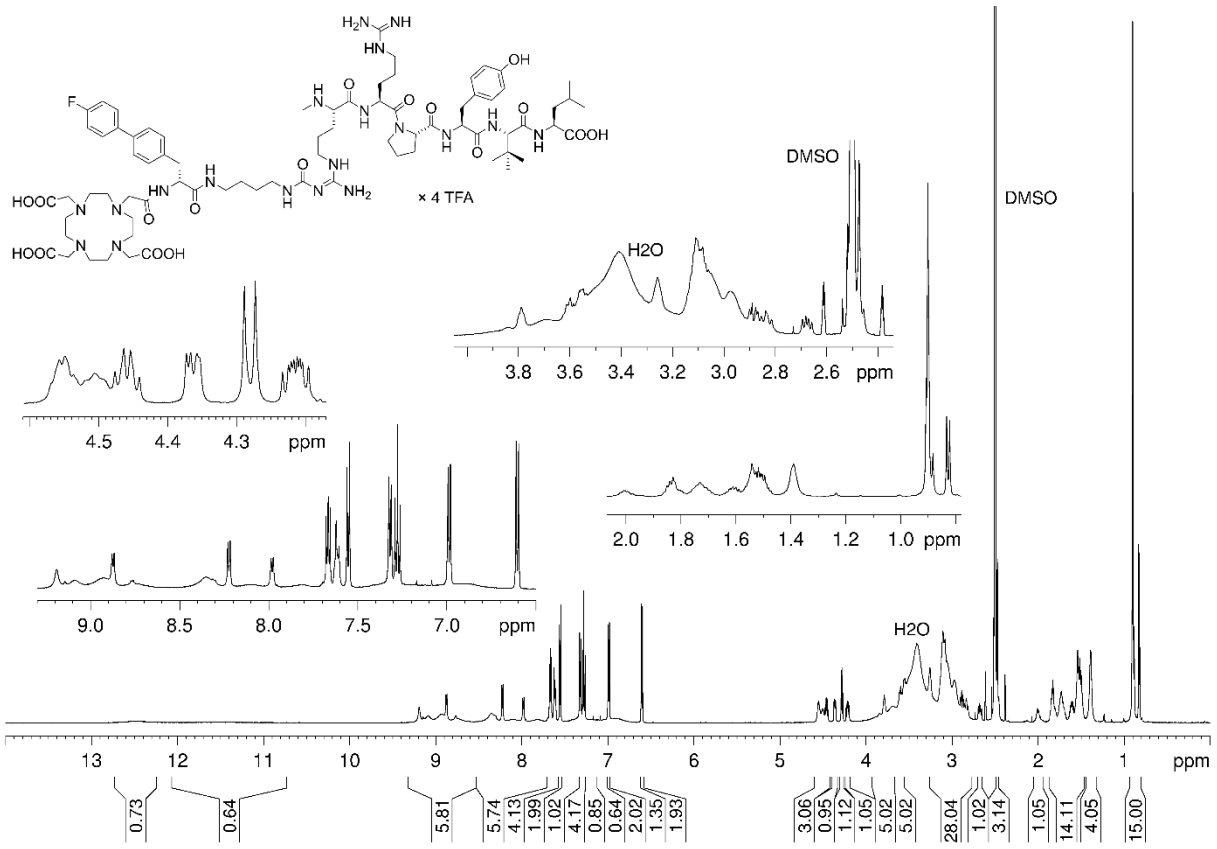

^{1}H-NMR spectrum (600 MHz, DMSO-d_6) of compound **4.34**

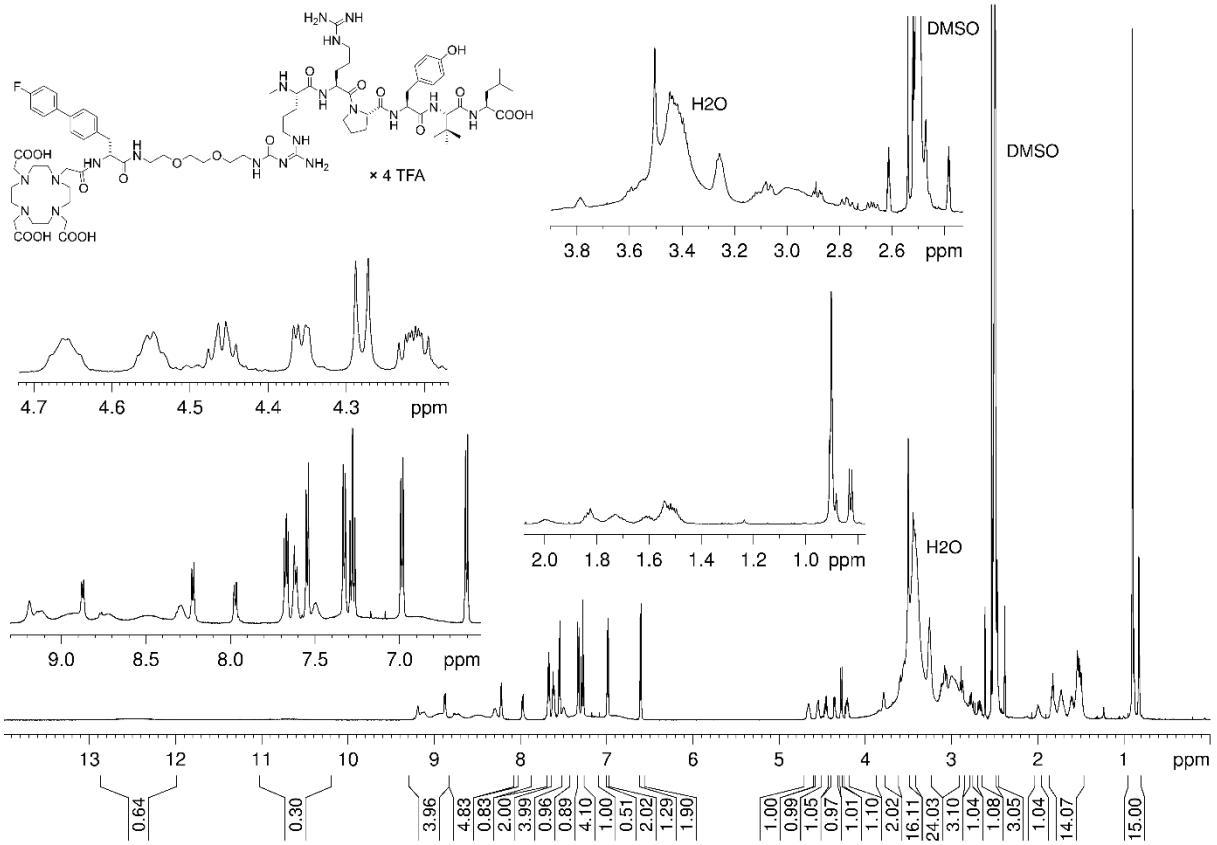

^{1}H-NMR spectrum (600 MHz, DMSO-d_6) of compound **4.35**

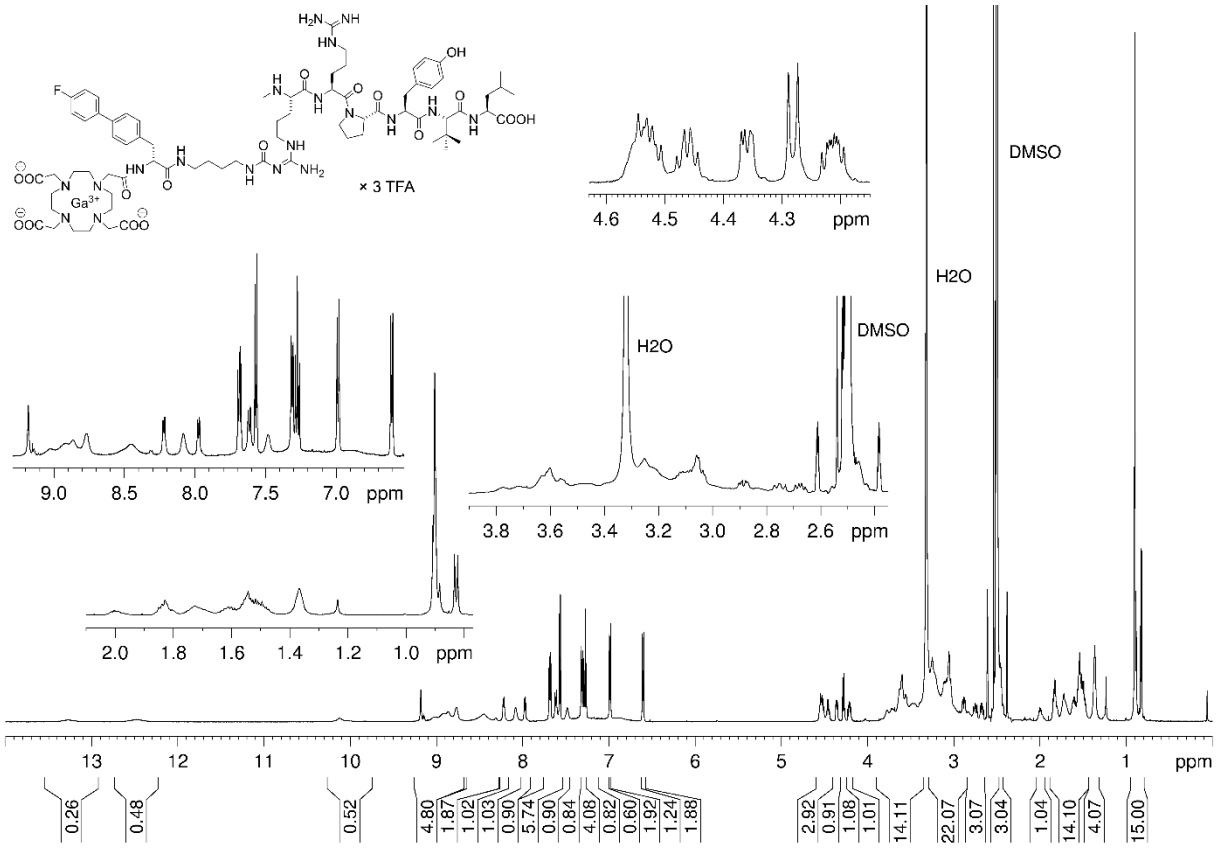

^{1}H-NMR spectrum (600 MHz, DMSO-d_6) of compound **4.36**

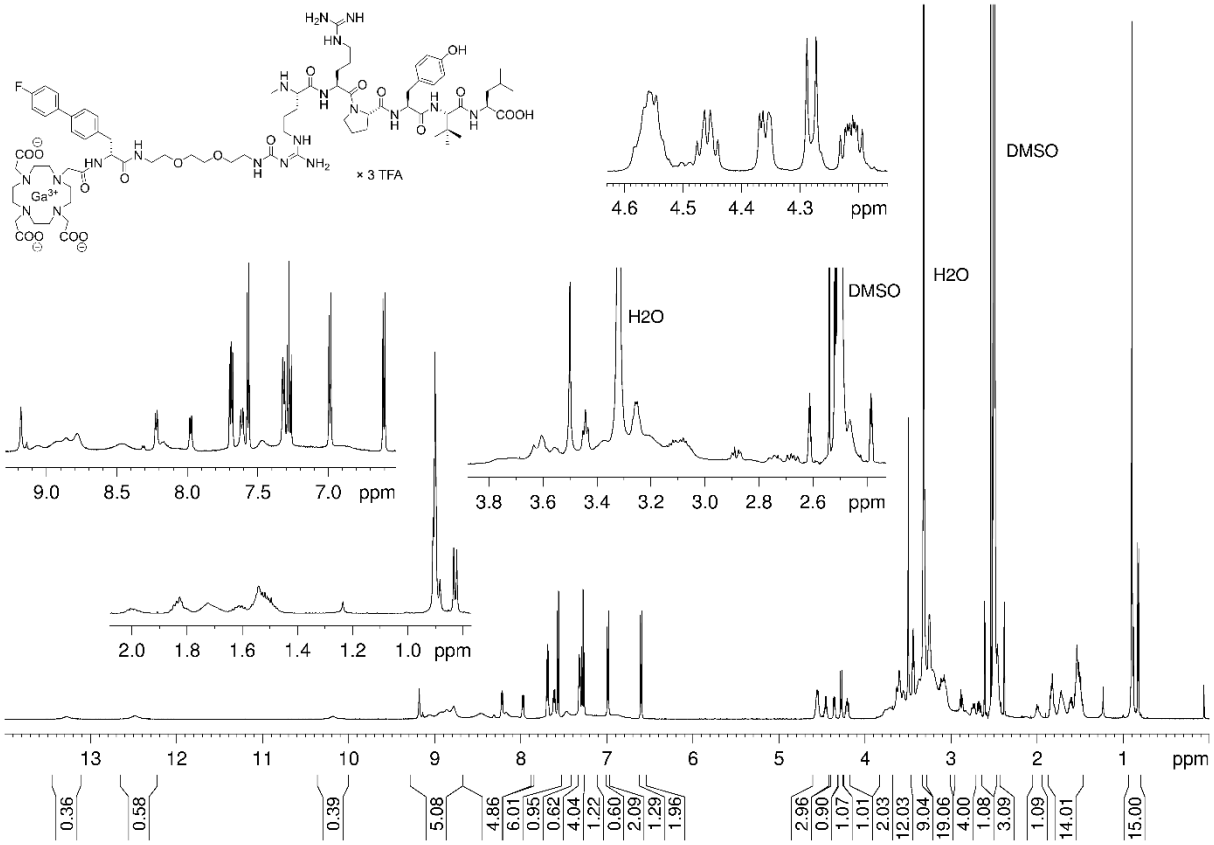

^{1}H-NMR spectrum (600 MHz, DMSO-d_6) of compound **4.37**

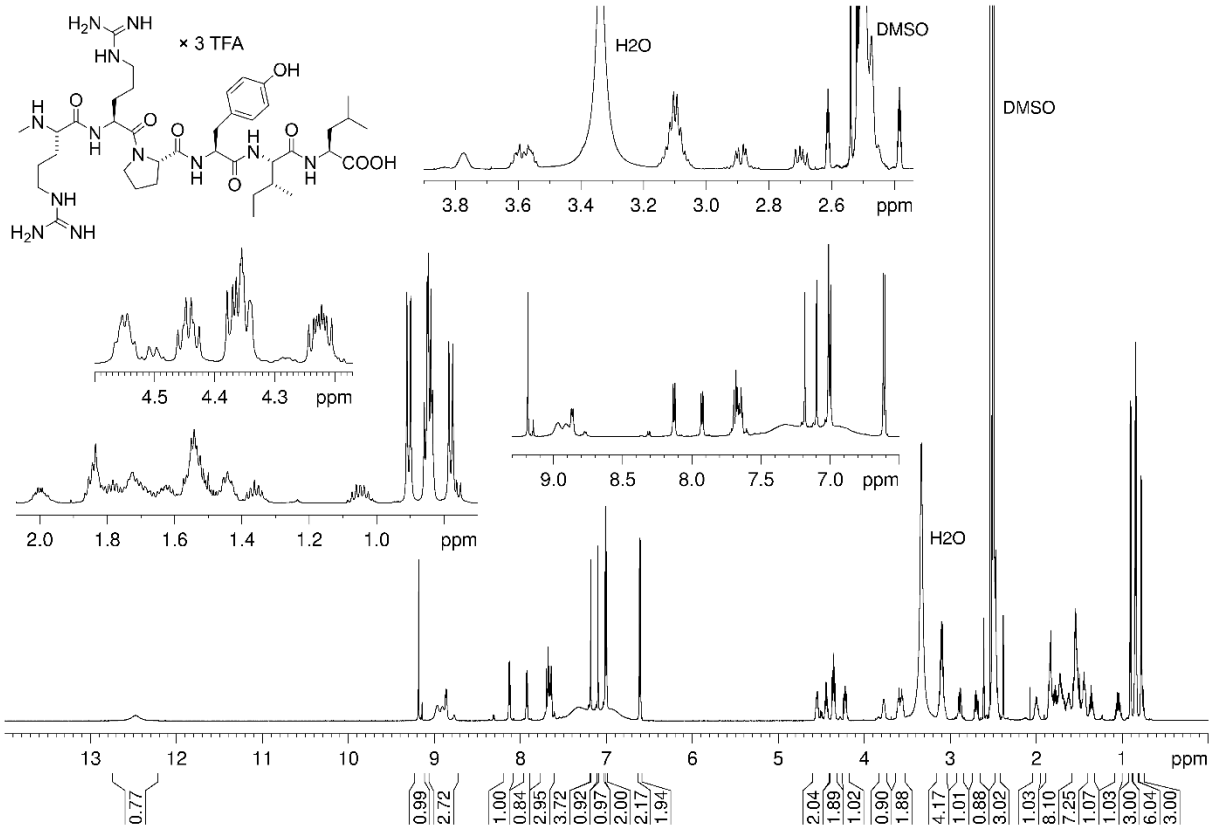

^{1}H-NMR spectrum (600 MHz, DMSO-d_6) of compound **4.38**

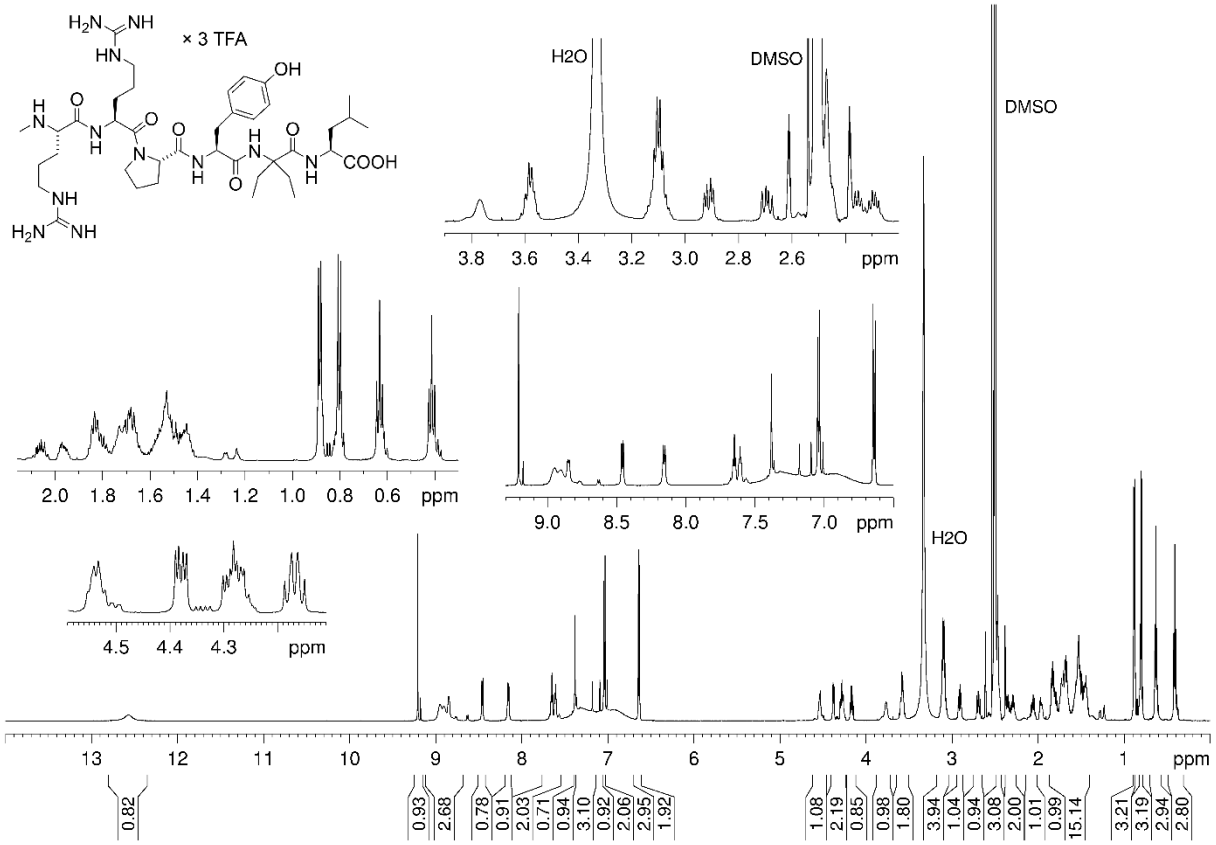

^{1}H-NMR spectrum (600 MHz, DMSO-d_6) of compound **4.39**

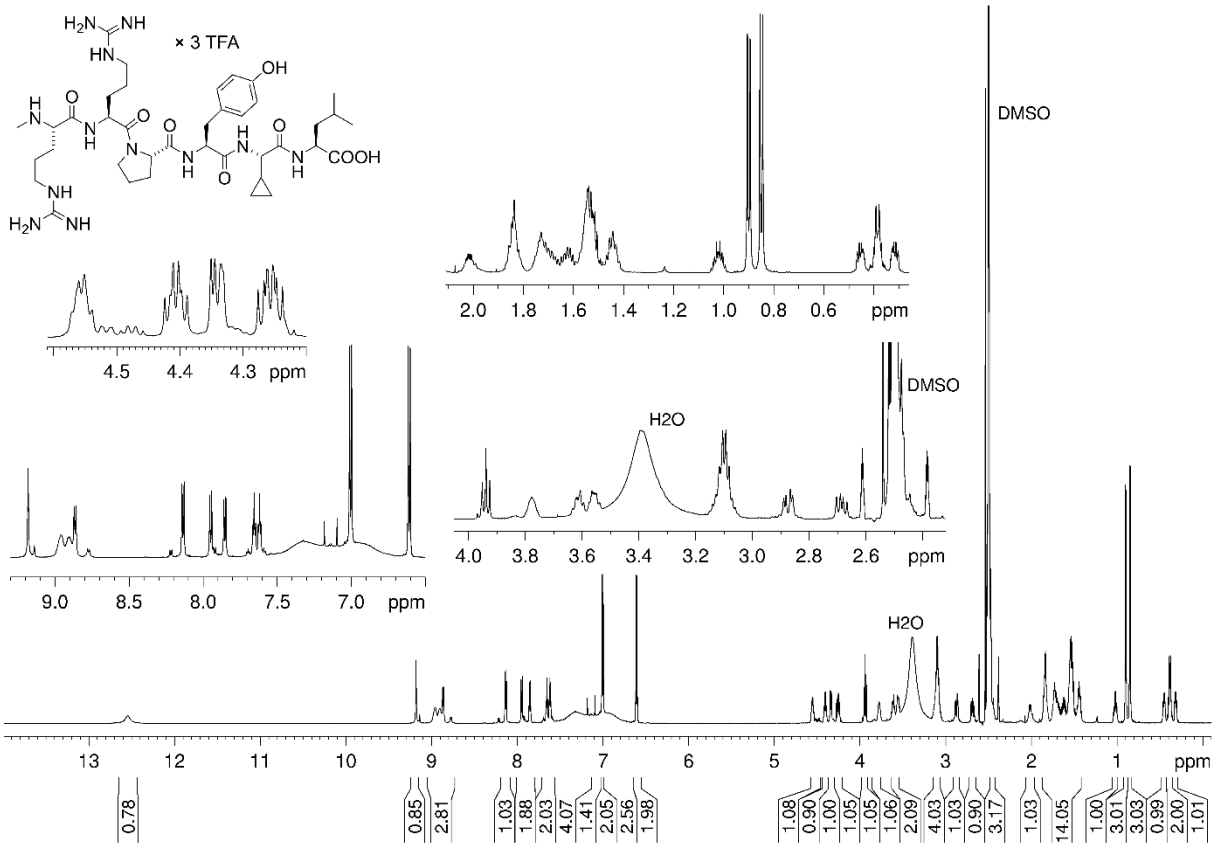

^{1}H-NMR spectrum (600 MHz, DMSO-d_6) of compound **4.40**

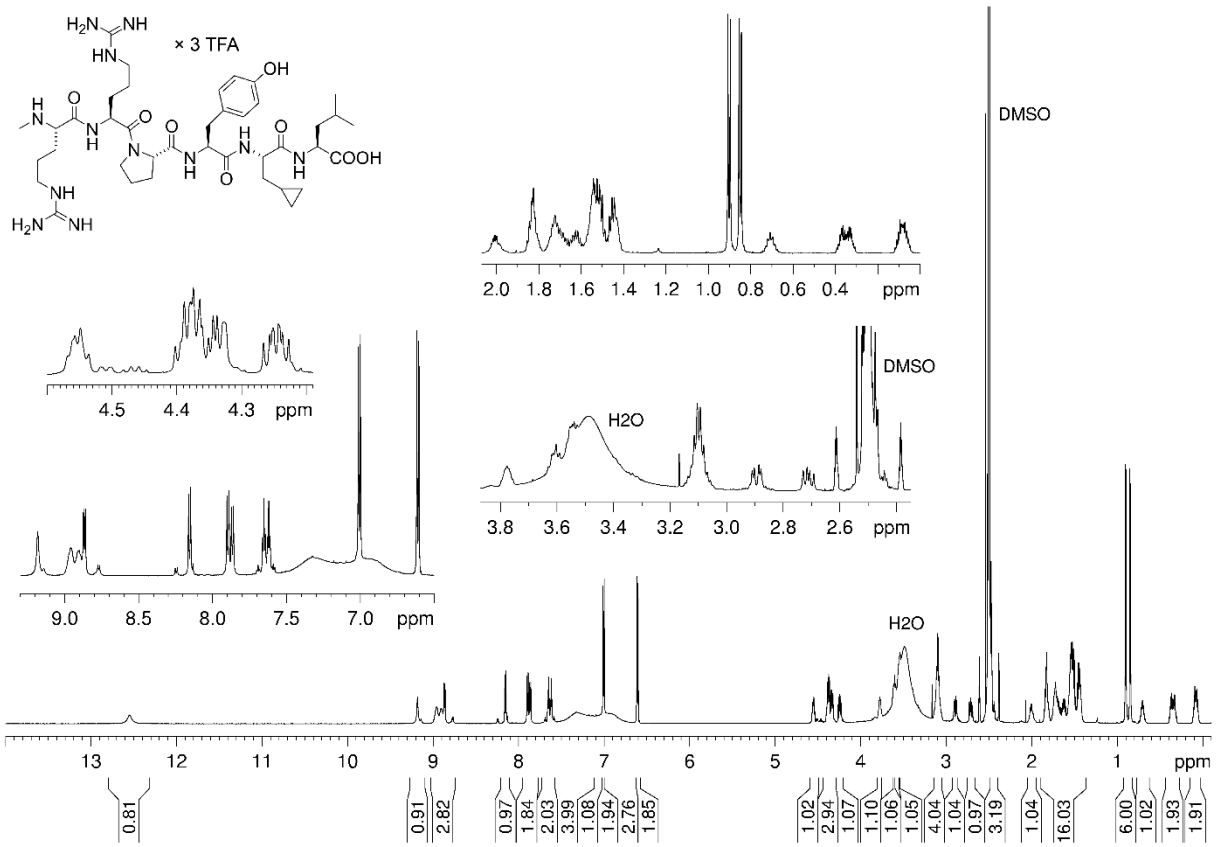

^{1}H-NMR spectrum (600 MHz, DMSO-d_6) of compound **4.41**

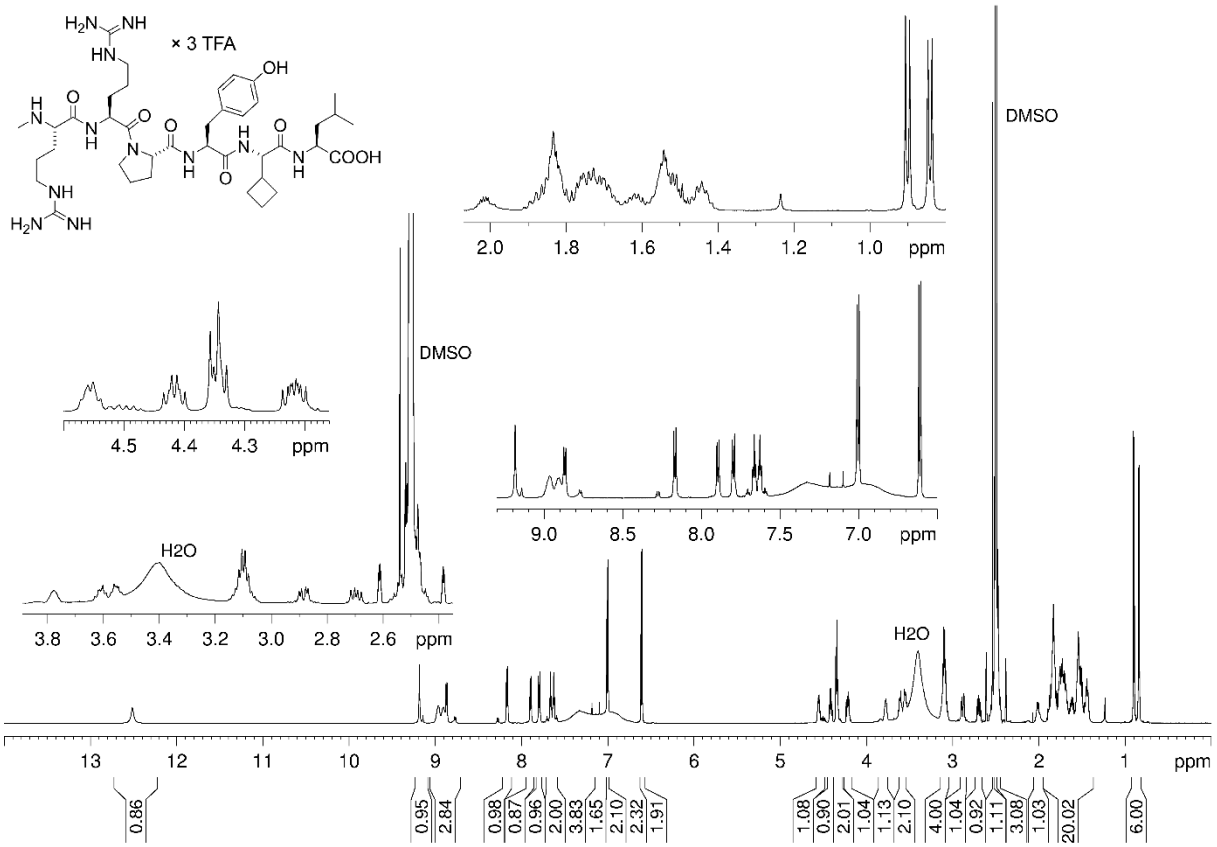

^{1}H-NMR spectrum (600 MHz, DMSO-d_6) of compound **4.42**

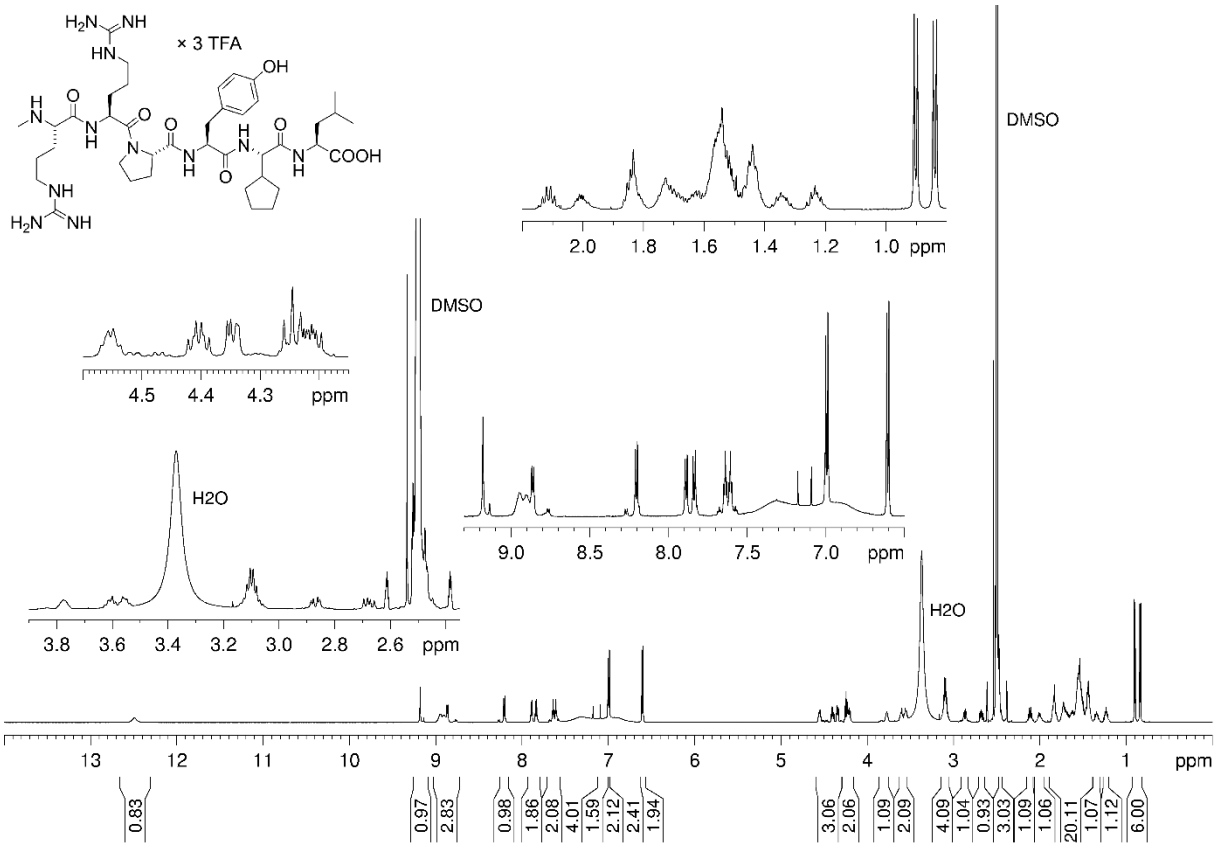

^{1}H-NMR spectrum (600 MHz, DMSO-d_6) of compound **4.43**

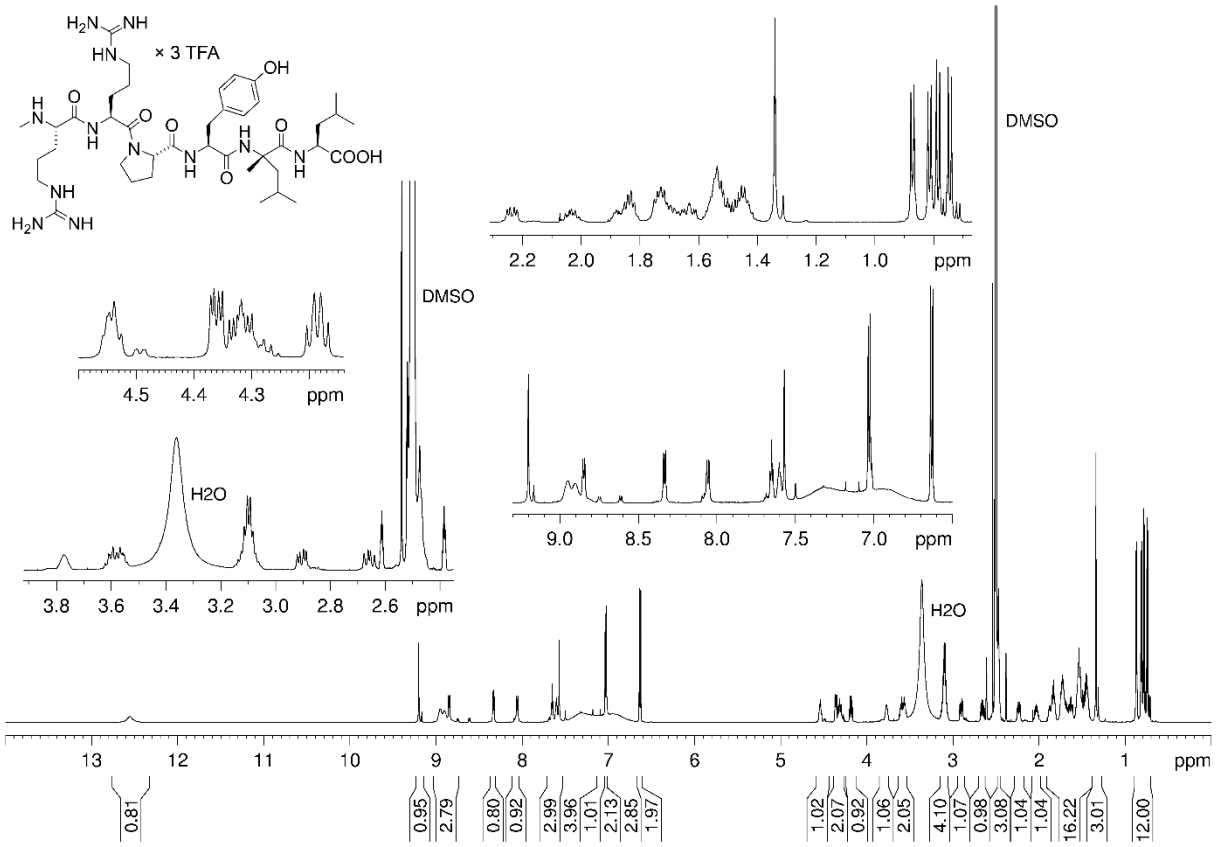

^{1}H-NMR spectrum (600 MHz, DMSO-d_6) of compound **4.44**

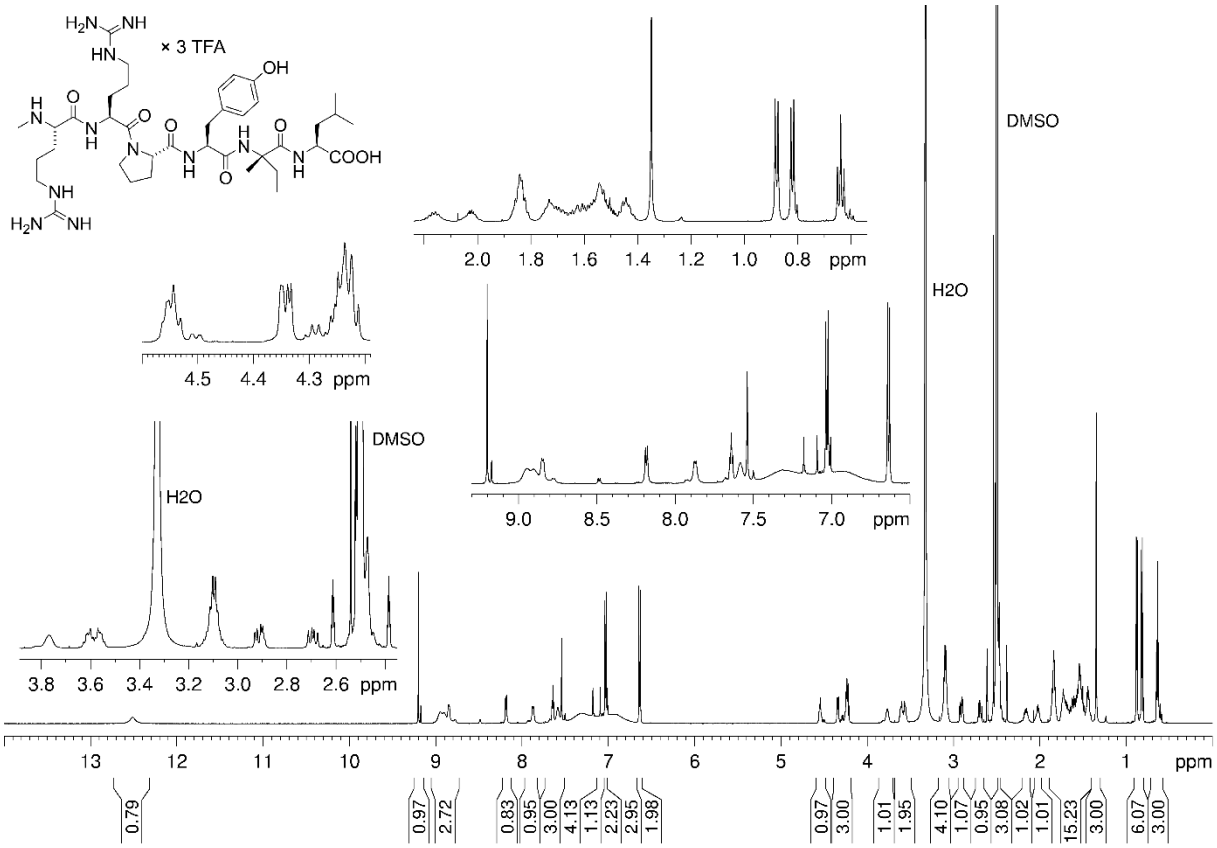

^{1}H-NMR spectrum (600 MHz, DMSO-d_6) of compound **4.45**

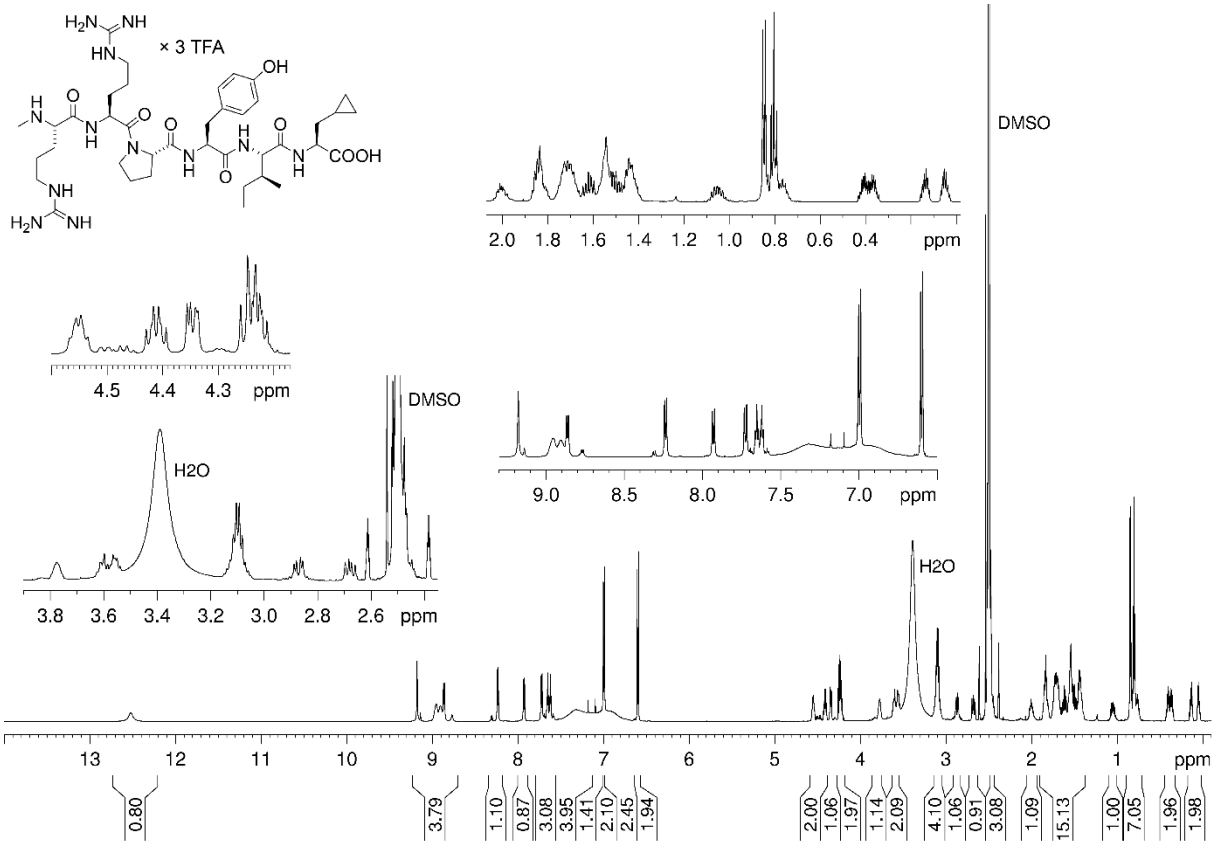

^{1}H-NMR spectrum (600 MHz, DMSO-d_6) of compound **4.46**

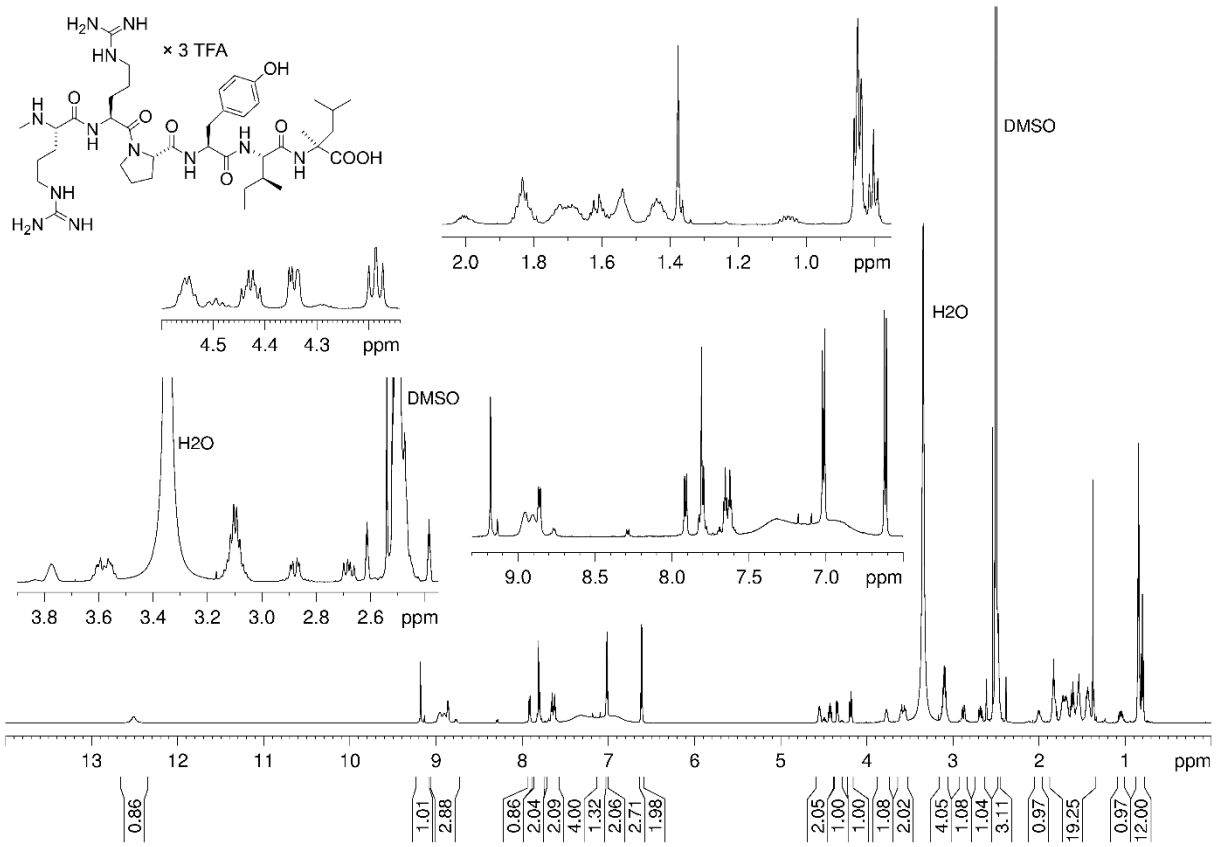

^{1}H-NMR spectrum (600 MHz, DMSO-d_6) of compound **4.47**

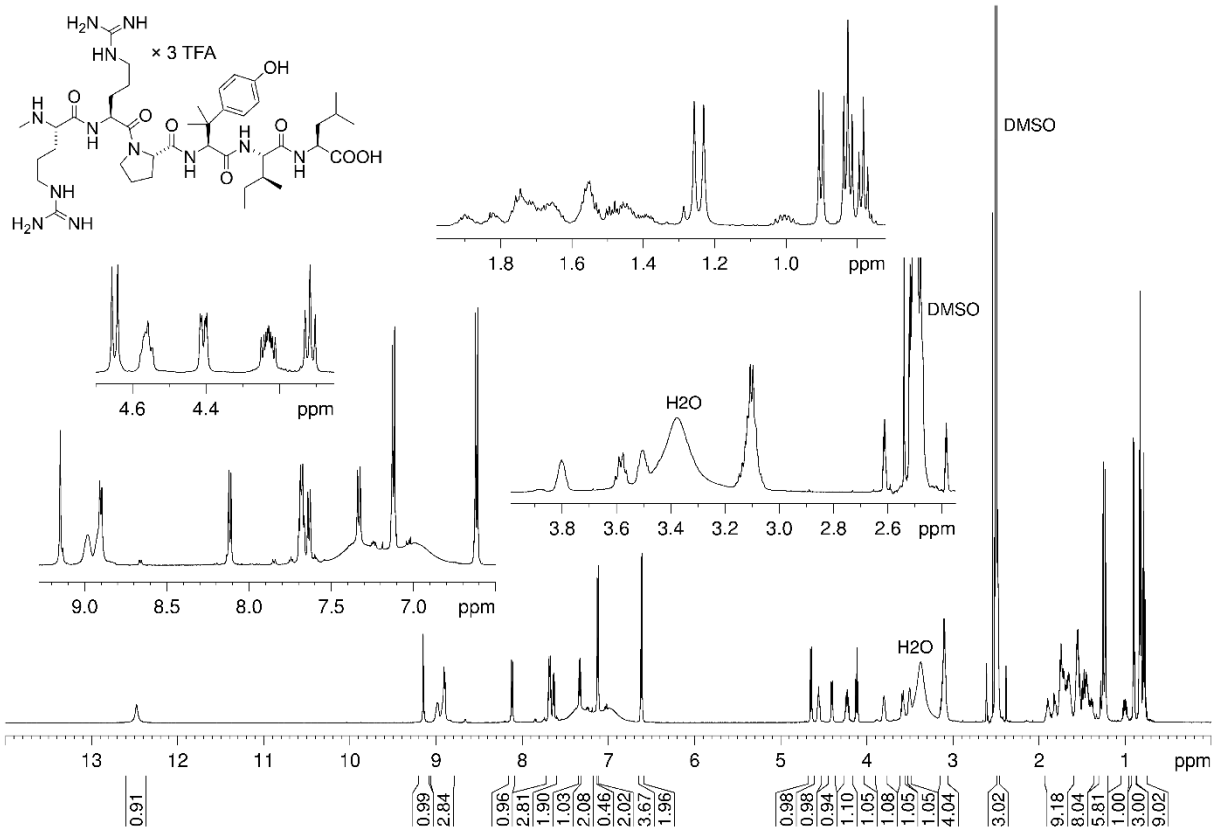

^{1}H-NMR spectrum (600 MHz, DMSO-d_6) of compound **4.48**

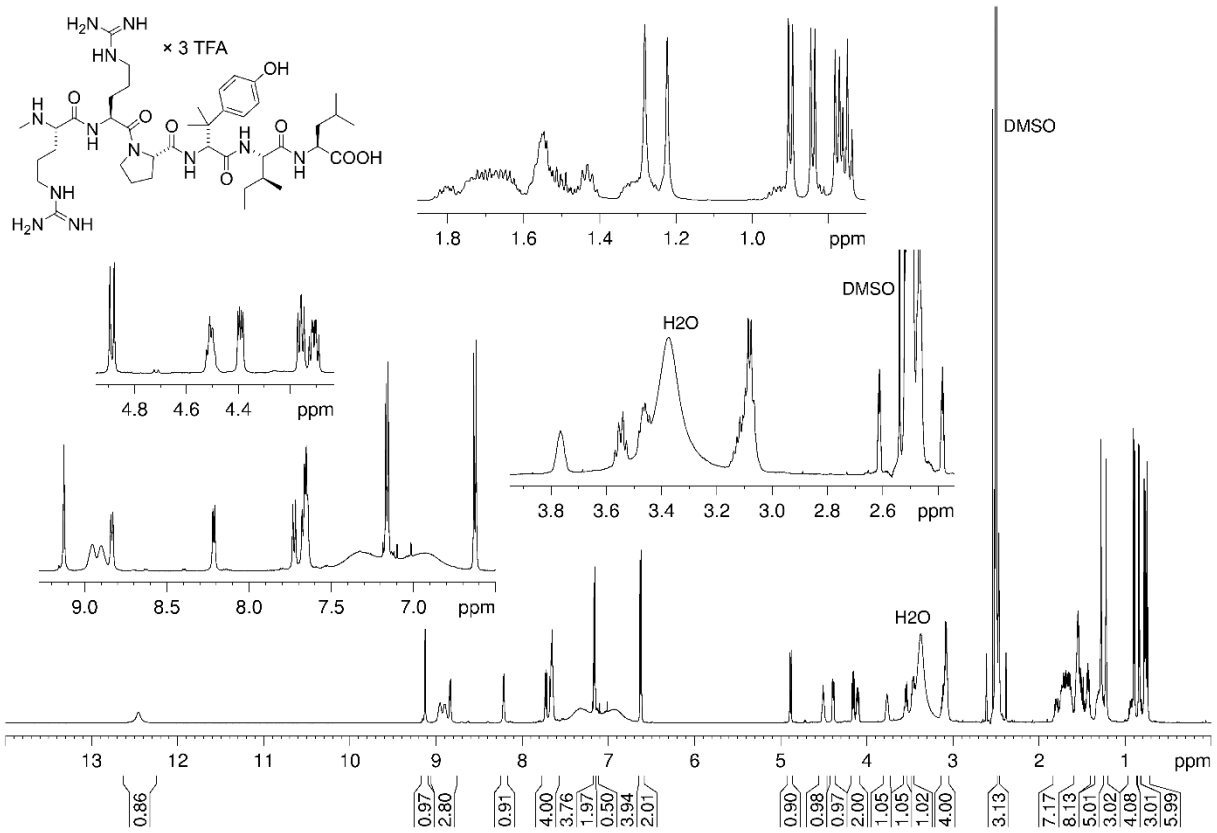

^{1}H-NMR spectrum (600 MHz, DMSO-d_6) of compound **4.49**

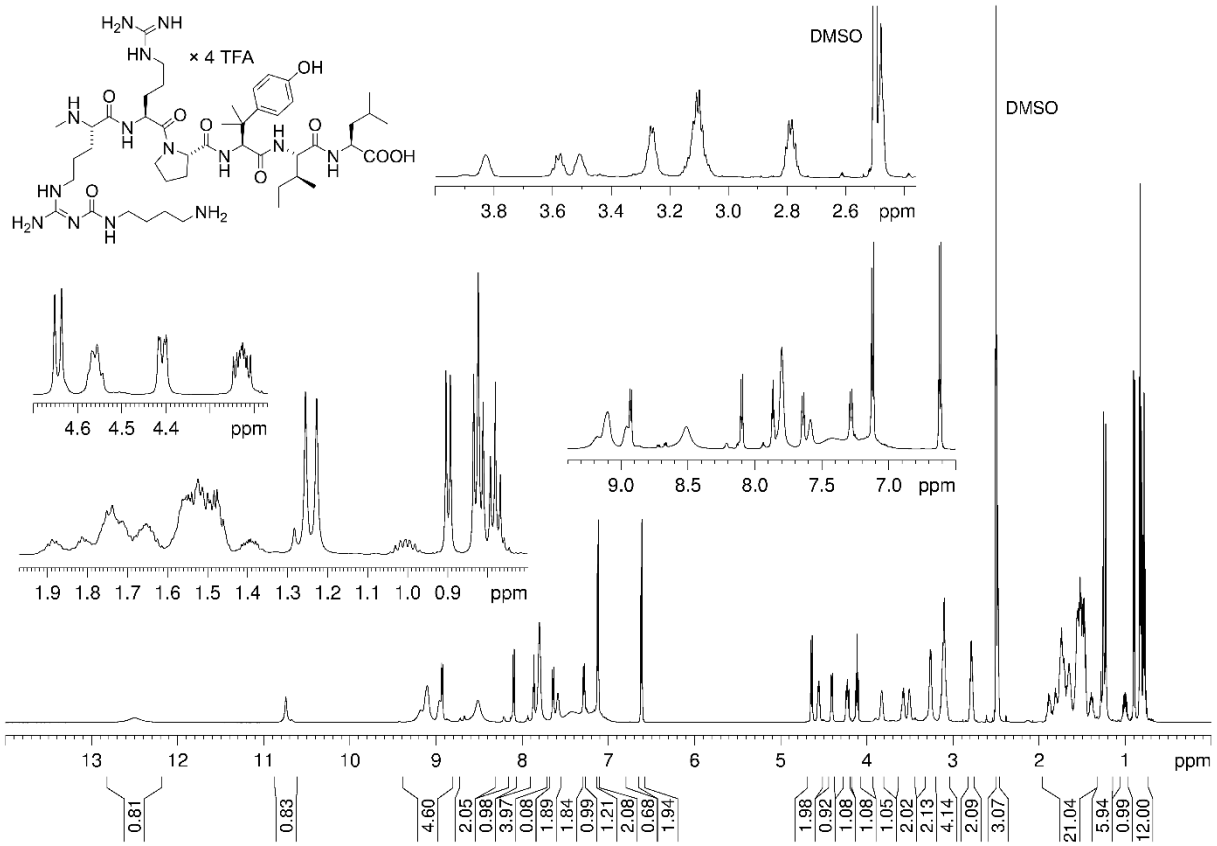

^{1}H-NMR spectrum (600 MHz, DMSO-d_6) of compound **4.50**

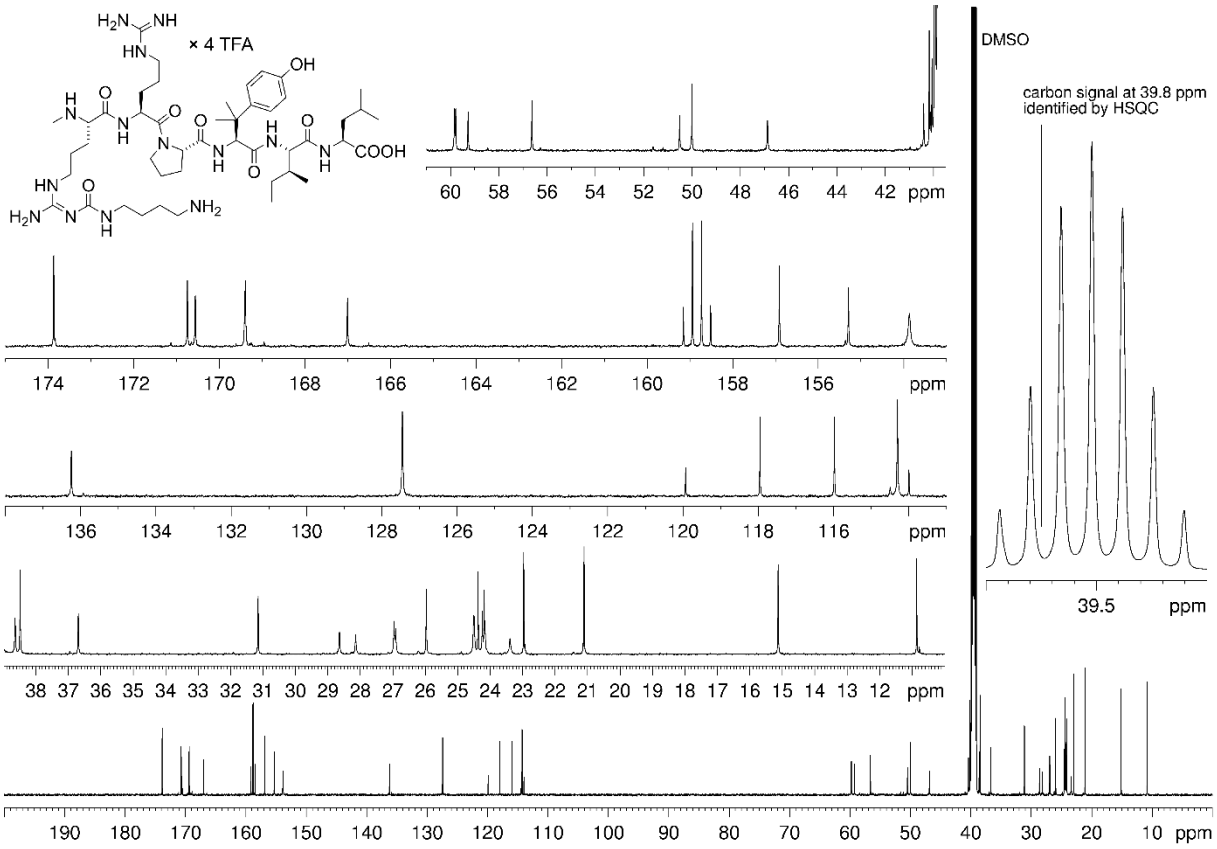

^{13}C-NMR spectrum (151 MHz, DMSO-d_6) of compound **4.50**

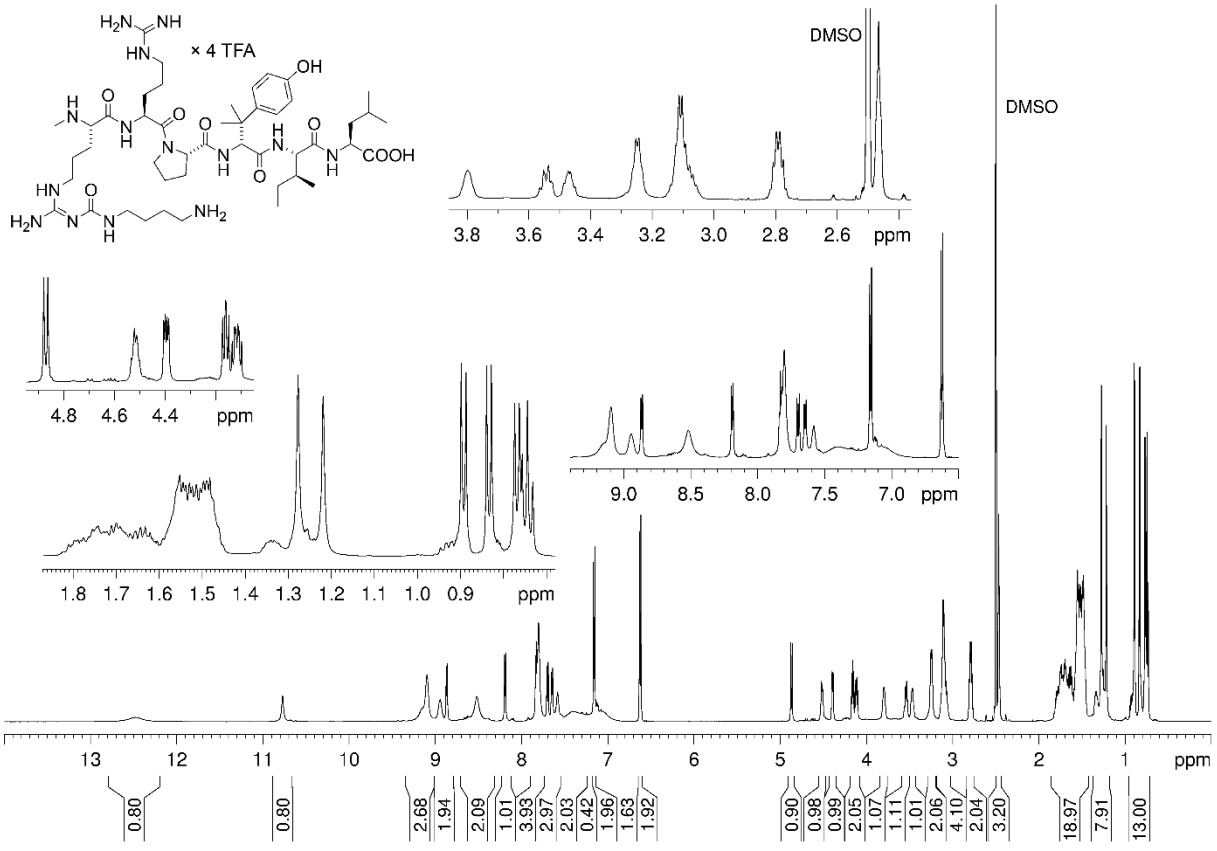

^{1}H-NMR spectrum (600 MHz, DMSO-d_6) of compound **4.51**

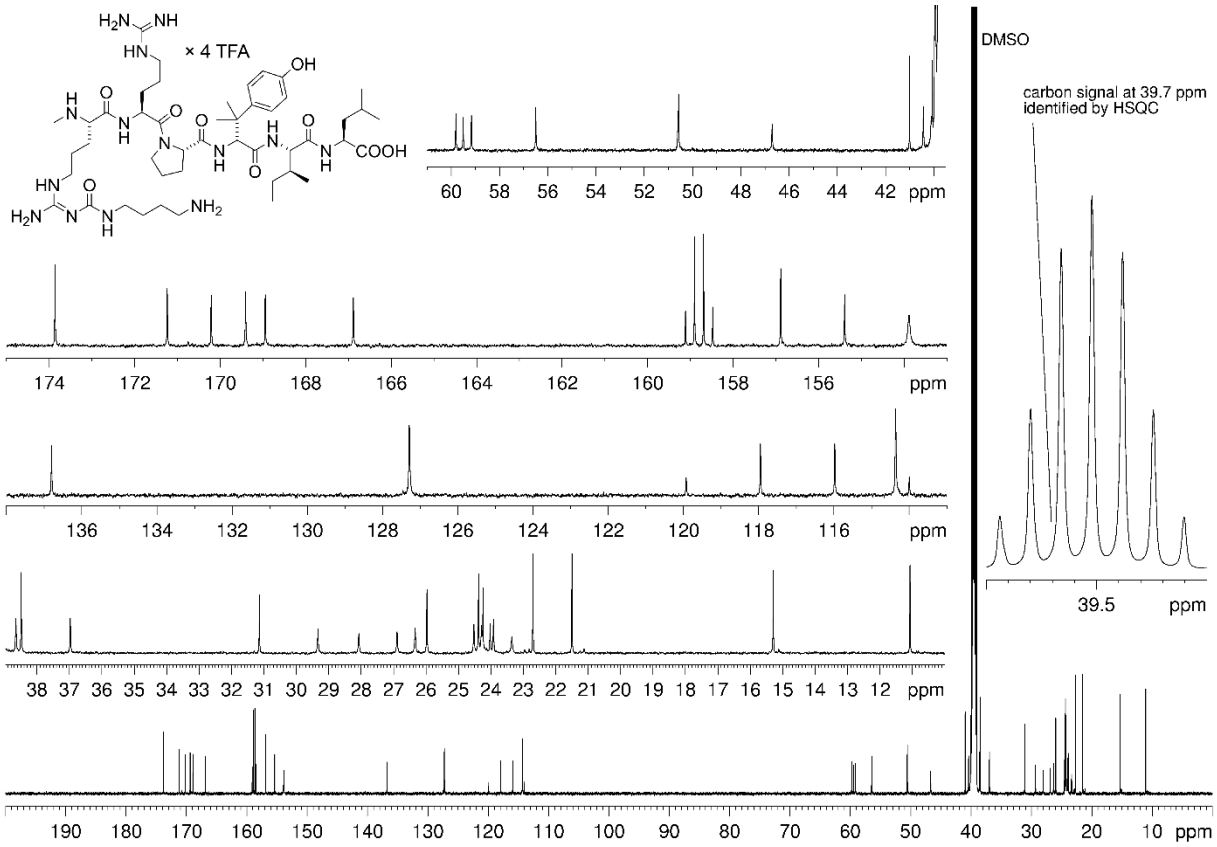

^{13}C-NMR spectrum (151 MHz, DMSO-d_6) of compound **4.51**

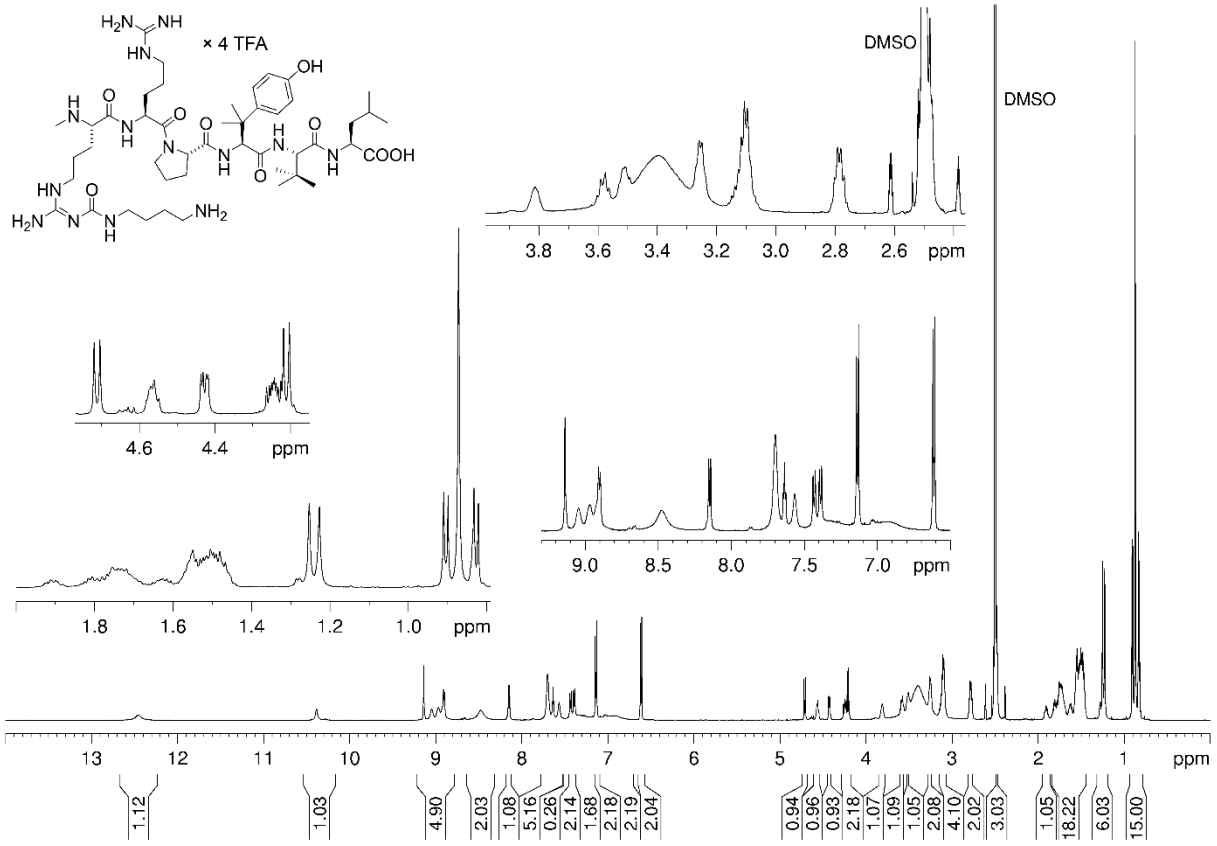

^{1}H-NMR spectrum (600 MHz, DMSO-d_6) of compound **4.52**

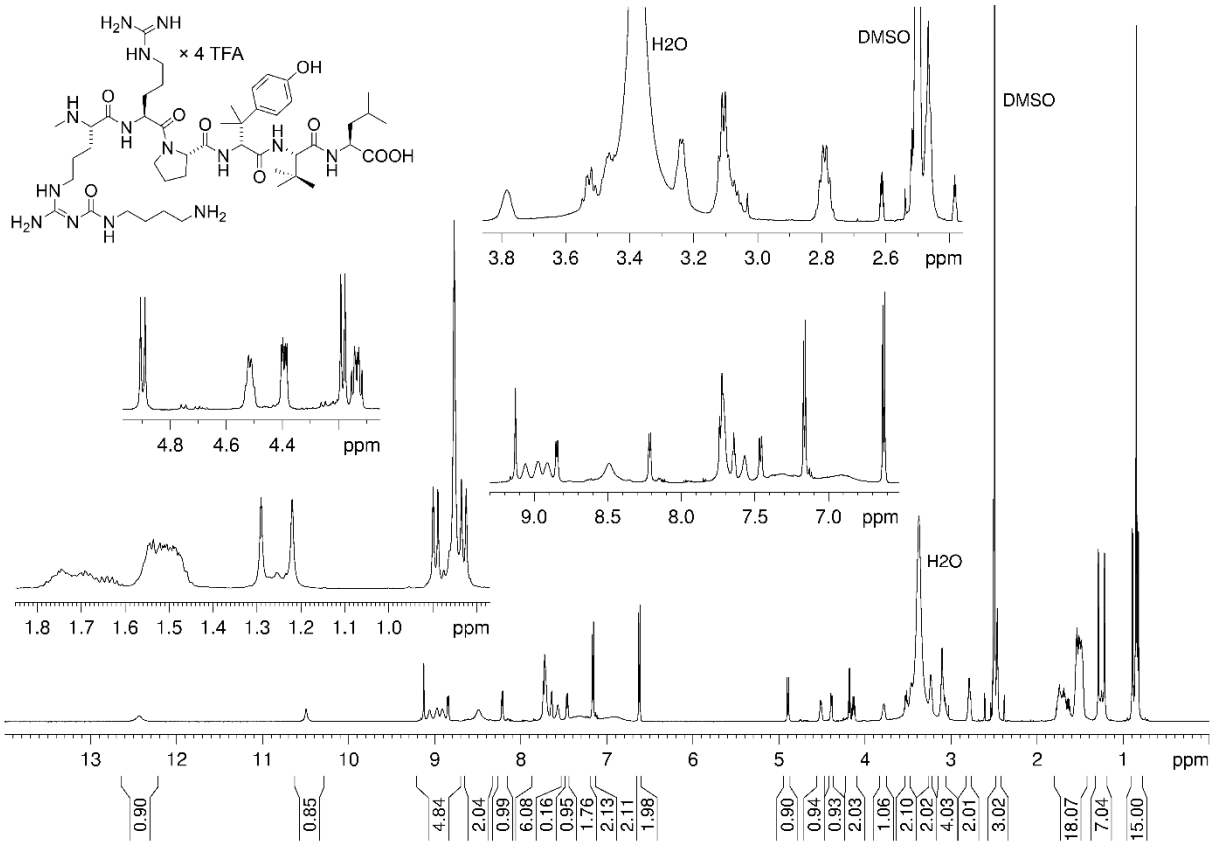

^{1}H-NMR spectrum (600 MHz, DMSO-d_6) of compound **4.53**

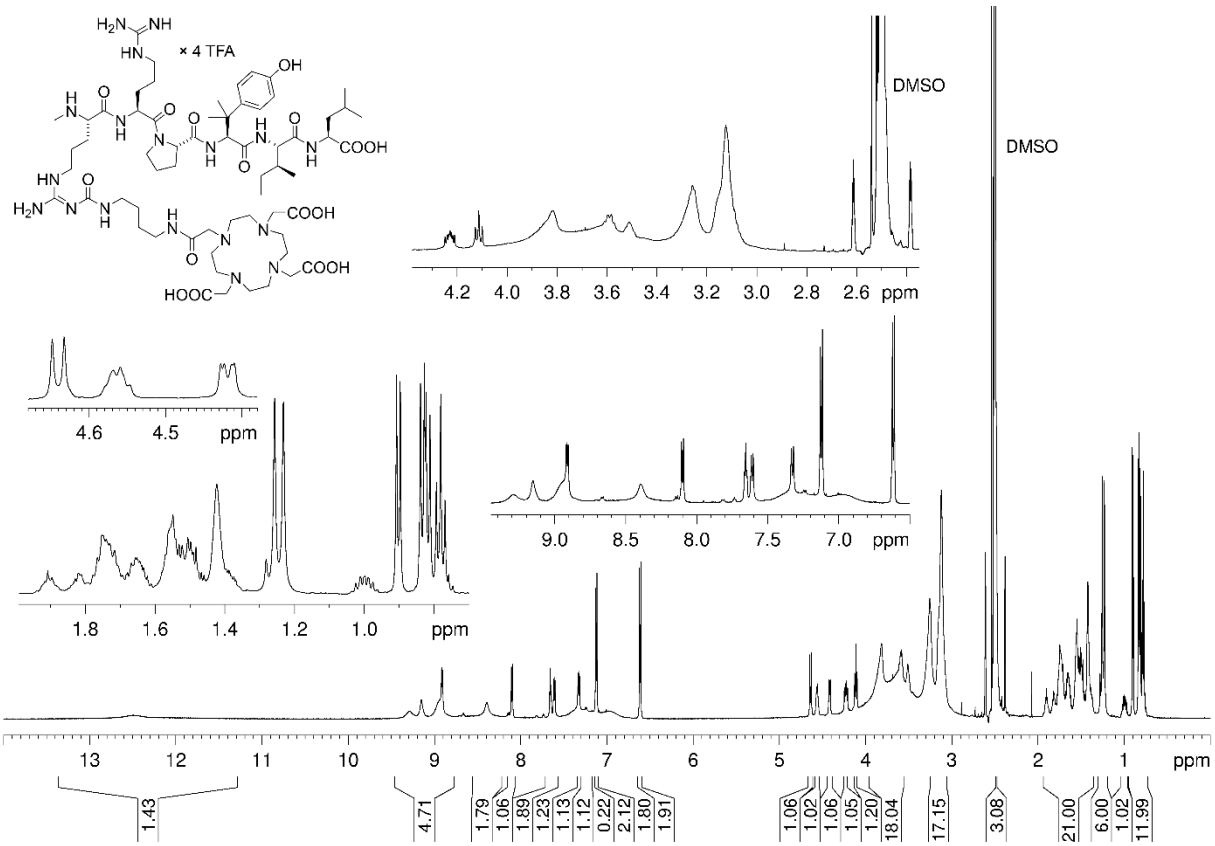

^{1}H-NMR spectrum (600 MHz, DMSO-d_6) of compound **4.54**

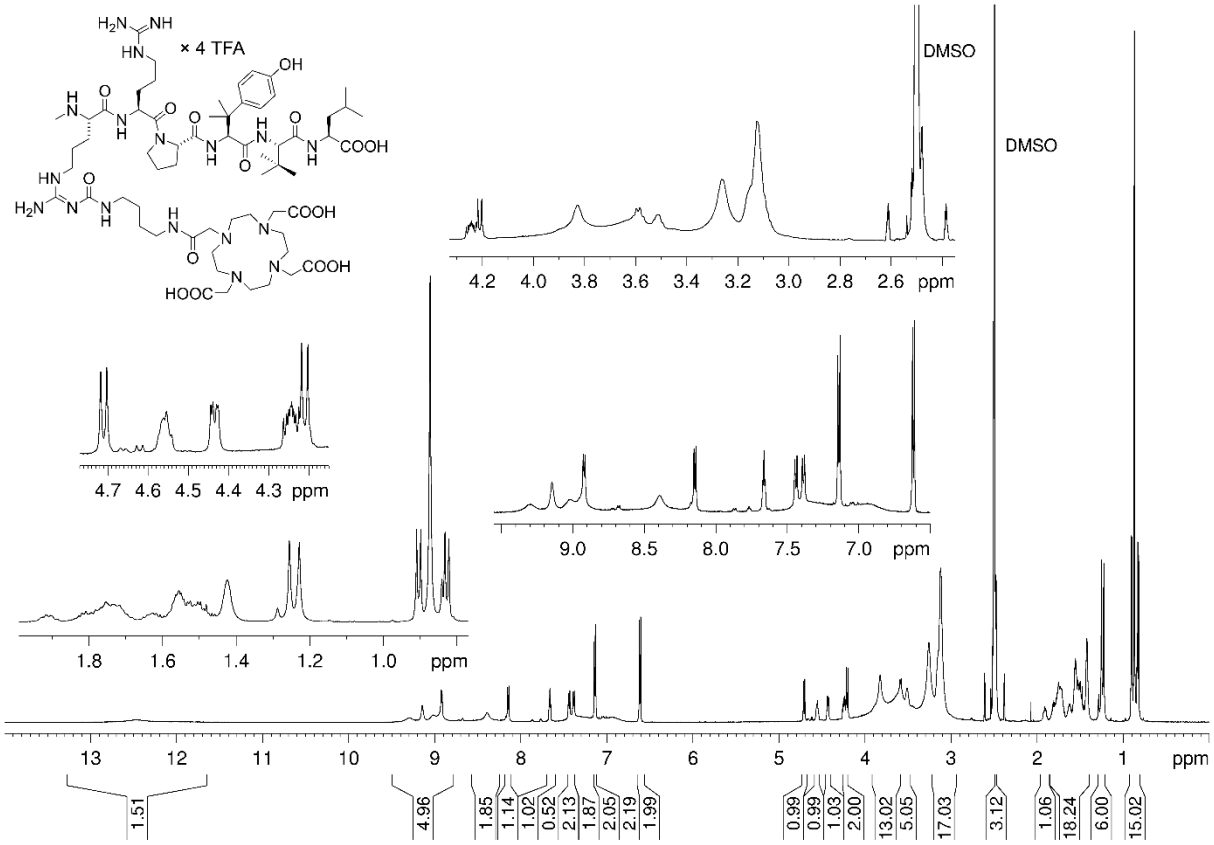

^{1}H-NMR spectrum (600 MHz, DMSO-d_6) of compound **4.55**

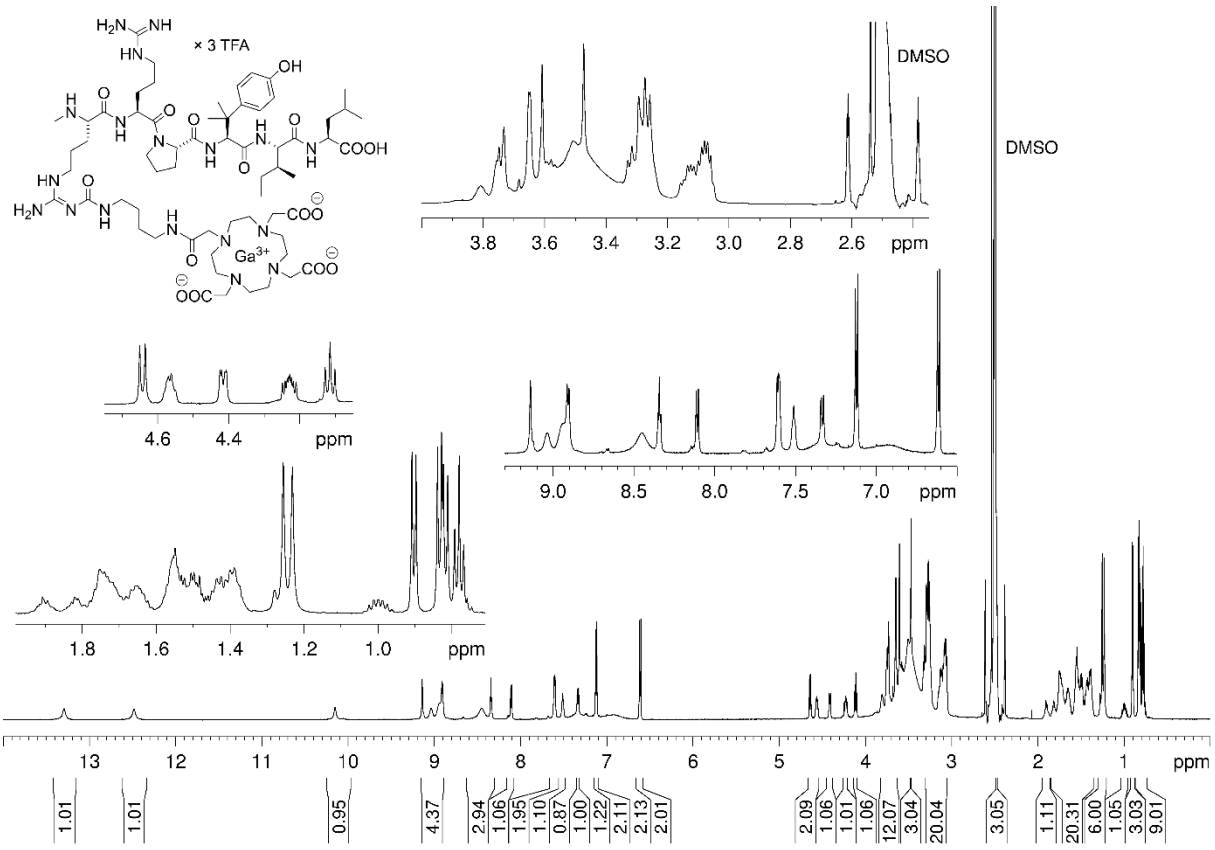

^{1}H-NMR spectrum (600 MHz, DMSO-d_6) of compound **4.56**

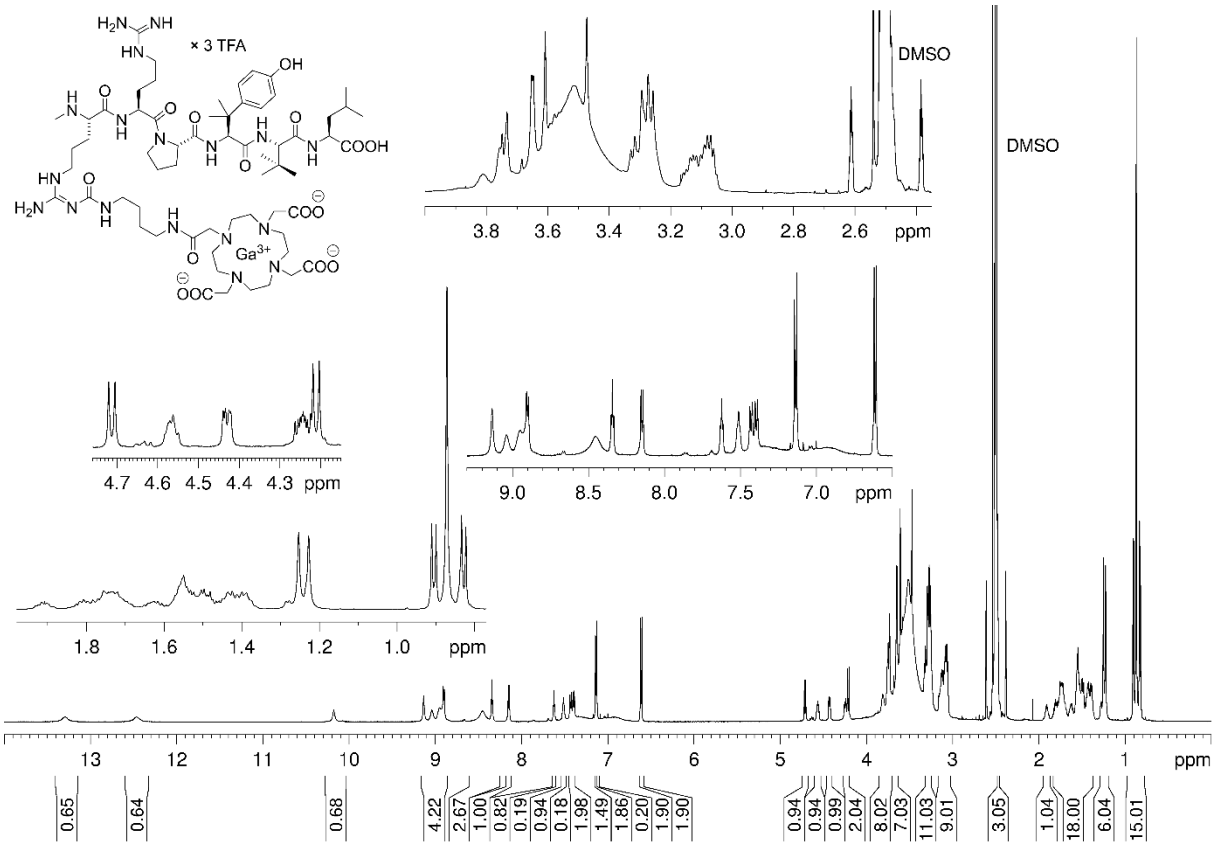

^{1}H-NMR spectrum (600 MHz, DMSO-d_6) of compound **4.57**

4.6.8 References

1. Keller, M.; Kuhn, K.K.; Einsiedel, J.; Hübner, H.; Biselli, S.; Mollereau, C.; Wifling, D.; Svobodová, J.; Bernhardt, G.; Cabrele, C.; et al. Mimicking of arginine by functionalized N^{ω}-carbamoylated arginine as a new broadly applicable approach to labeled bioactive peptides: High affinity angiotensin, neuropeptide Y, neuropeptide FF, and neurotensin receptor ligands as examples. *J Med Chem* **2016**, *59*, 1925-1945, doi:10.1021/acs.jmedchem.5b01495.

2. Schindler, L.; Bernhardt, G.; Keller, M. Modifications at Arg and Ile give neurotensin(8-13) derivatives with high stability and retained NTS_1 receptor affinity. *ACS Med Chem Lett* **2019**, *10*, 960-965, doi:10.1021/acsmedchemlett.9b00122.

3. Schindler, L.; Wohlfahrt, K.; Gluhacevic von Krüchten, L.; Prante, O.; Keller, M.; Maschauer, S. Neurotensin analogs by fluoroglycosylation at N^{ω}-carbamoylated arginines for PET imaging of NTS1-positive tumors. *Sci Rep* **2022**, *12*, 15028, doi:10.1038/s41598-022-19296-0.

Chapter 5

Fluoroglycosylated derivatives of the cyclic pentapeptide FC131: synthesis and characterization of potential CXCR4 PET ligands

Notes:

The preparation of reference peptide **5.02** was performed within the scope of the Master thesis of Katrin Spinnler (Institute of Pharmacy, University of Regensburg, 2016).

The preparation of building block **5.05** was performed within the scope of the Master thesis of Lara von Krüchten (Institute of Pharmacy, University of Regensburg, 2017).

The preparation of HEK293T cells stably co-expressing NlucN-mGsi and CXCR4-NlucC fusion proteins and the functional characterization of the described ligands **5.01** and **5.02** was performed within the scope of the Doctoral thesis of Carina Höring (Institute of Pharmacy, University of Regensburg, 2022).

5.1 Introduction

The human CXCR4 receptor is a 352 amino acid peptide belonging to the family of rhodopsin-like G-protein coupled receptors (GPCRs)[1-3] and it is expressed in most hematopoietic stem or progenitor cell types[4-6]. The endogenous ligand of the CXCR4 is the stromal cell-derived factor SDF-1α (**5.01**, see Figure 5.1A)[4,7-9], also referred to as CXCL12, a peptide of 89 amino acids expressed in a variety of tissues, e.g., bone marrow, liver, lungs and some regions of the central nervous system[6,9,10]. **5.01** is a member of the CXC-type chemokine family[11] and can thus activate and direct leukocytes along a chemotactic gradient[12,13]. The interaction of **5.01** with the CXCR4 was reported to be involved in the homing of stem cells to particular sites during embryonal development[14], hematopoiesis[15-17] and organogenesis[6,10,18]. Additionally, overexpression of the CXCR4 was described for a number of tumors, e.g., prostate cancer[19,20], breast cancer[10,21] and leukemia[10,22,23]. This overexpression is furthermore assumed to play a significant role in site-specific metastasis[21,22,24-26] and activation of tumor cell survival[9,27,28] via interaction with its chemotactic ligand **5.01**. Besides this, the CXCR4 serves as a cofactor for the fusion of the human immunodeficiency virus (HIV) and its entry into human T-cells[29], which is why receptor antagonists are considered promising agents for HIV treatment[7,8,30-32]. Recently, the interest in such compounds was further promoted by several reports on the presumable involvement of the CXCR4 in the severity of the coronavirus disease 2019 (COVID-19) infection progress[33-37].

The involvement of the CXCL12-CXCR4 axis in the above-mentioned malignancies triggered the search for suitable receptor antagonists considered useful tools for their treatment. Derived from the promising cyclopeptidic receptor ligand T140[31], the high affinity CXCR4 antagonist FC131 (cyclo[D-Tyr^1-Arg^2-Arg^3-Nal^4-Gly^5], **5.02**, see Figure 5.1B) was described in 2003[38]. The exchange of Arg^2 by an N^{α}-methylated, N^{δ}-acylated D-ornithine gave the core structure of the 1,4,7,10-tetraazacyclododecane-1,4,7,10-tetraacetic acid (DOTA)-conjugated ligand Pentixafor (**5.03**, also referred to as CPCR4-2; for structure see Figure 5.1B)[39]. Ga-Pentixafor (**5.04**, Figure 5.1B) is the cold analog of a CXCR4 positron emission tomography (PET) ligand with equal receptor affinity (IC_{50} = 5 nM[39]) as compared to that of **5.02** (IC_{50} = 4 nM[38]).

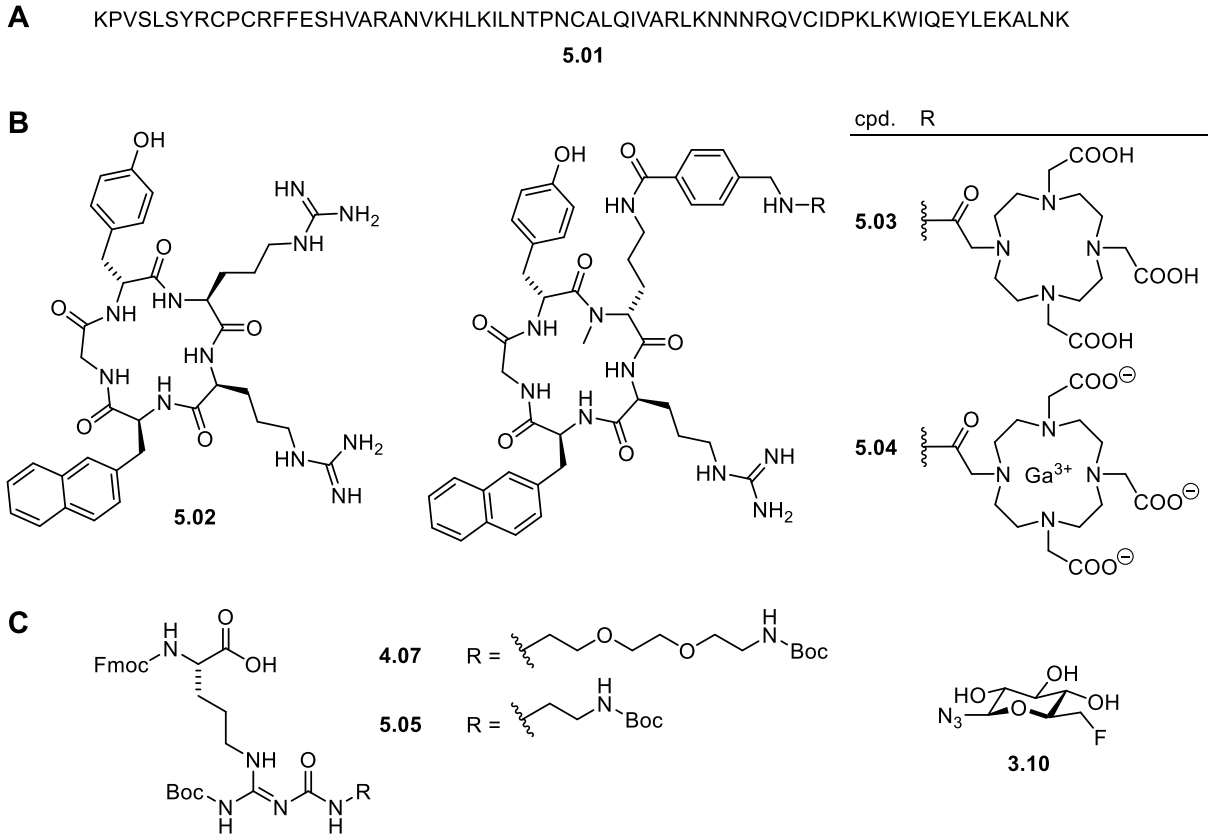

Figure 5.1. (A) Amino acid sequence of the endogenous CXCR4 ligand SDF-1α (**5.01**). (B) Structures of the described CXCR4 antagonist FC131 (**5.02**)[38] and the PET ligand precursor Pentixafor (**5.03**) for the ^{68}Ga-labeled CXCR4 imaging probe [^{68}Ga]Ga-Pentixafor ("cold" analog: **5.04**)[39]. (C) Structures of the *N*ω-carbamoylated arginine building blocks **4.07**[40] and **5.05**, and the fluorinated azido sugar **3.10**[41] used for the preparation of CXCR4 ligands derived from **5.02**.

The ^{68}Ga-labeled CXCR4 PET tracer [^{68}Ga]**5.04** was investigated in vivo in tumor-bearing mice, resulting in specific tracer accumulation in the tumor entities with high tumor-to-organ ratios[39,42]. The usefulness of this PET tracer for cancer diagnosis was confirmed in clinical trials involving patients suffering from multiple myeloma[43-46], different types of lymphoma[46-49] or leukemia[50,51].

Prompted by the encouraging performance of [^{68}Ga]**5.04** in the clinical stage we aimed at the development of ^{18}F-labeled CXCR4 ligands based on the parent compound **5.02**. The preparation of PET tracers by labeling with ^{18}F is advantageous over the use of ^{68}Ga with respect to the lower energy of positrons emitted by ^{18}F and the consequently higher spatial resolution for PET as well as with regard to its convenient half-life of 110 min[52]. Cyclopeptides derived from **5.02** and **5.03** have already been labeled with ^{18}F by conjugation to radiofluorinated moieties[53,54] or by chelation of [^{18}F]AlF^{2+} [55]. However, the respective tracers revealed only poor performance in vivo in terms of high accumulation in elimination organs and moderate specific binding, and have thus not reportedly been subject of subsequent (pre-)clinical investigations[52,56].

A newly introduced labeling strategy for arginine-containing peptides allows the attachment of a chelator or radiolabel via the side chain of Arg[40]. This approach, which is based on the bioisosteric replacement of a certain arginine by a synthetic *N*ω-carbamoylated arginine[40], has recently successfully been applied to a cyclic pentapeptide, yielding an alkyne-functionalized derivative of **5.02** (compound **25** in Spinnler et al.[57]). In

the present study, the same concept was used to prepare amino-functionalized analogs of **5.02** by incorporation of N^{ω}-carbamoylated arginines derived from building blocks **4.07** and **5.05** (for structures see Figure 5.1C) in position 2 or 3 of **5.02**. The amino-functionalized analogs of **5.02** were converted to alkyne-functionalized cyclic peptides followed by conjugation to a described fluoroglycosyl azide[41] (**3.10**, Figure 5.1C) to obtain potential CXCR4 PET ligands.

5.2 Results and discussion

5.2.1 Synthesis of the reference compounds 5.03, 5.04, the linear precursors 5.11-5.14 and the cyclic peptides 5.15-5.26

The reported CXCR4 ligand **5.03**[39] and its Ga^{3+}-labeled analog **5.04**[39] were prepared to be used as reference compounds for investigations at the CXCR4. The side chain-protected linear pentapeptide **5.06** was synthesized via standard Fmoc solid-phase peptide synthesis (SPPS) using oxyma and DIC as activation reagents for amino acid coupling (Scheme 5.1). After coupling and Fmoc-deprotection of the side chain-Boc-protected D-Orn in position 2, the ornithine was N^{α}-methylated on-resin using a reported procedure[58], which was recently also successfully applied for the N^{α}-methylation of N^{ω}-carbamoylated arginines[59,60]. Following completion of the pentapeptide sequence and cleavage from the solid support, cyclization of **5.06** was performed using HOBt, PyBOP and DIPEA as activation reagents. Side chain-deprotection with 95% aqueous trifluoroacetic acid for 4 h yielded cyclic peptide **5.07** (note: after 4 h, the compound still carried the Pbf-protecting group at the side chain of Arg^3, which was not considered unfavorable for the subsequent step; thus, the Pbf-protected peptide was used for the following reaction). HOBt, HBTU and DIPEA served as activation reagents for the coupling of benzoic acid building block **5.08** to **5.07** (Scheme 5.1), giving the fully deprotected peptide **5.09** after treatment with TFA. In order to conjugate the amino-functionality of the aminomethyl-benzoic acid linker to the DOTA chelator, **5.09** was initially treated with the *t*Bu-protected DOTA reagent **4.13** (see Chapter 4), which has recently proven to enable a simpler separation of the DOTA-conjugated product from the starting material by preparative HPLC[60]. However, subsequent acidic *t*Bu-deprotection of the chelator overnight led to the complete re-opening of the macrocycle by hydrolysis of an amide bond (as confirmed by mass spectrometry, data not shown). Consequently, DOTA-conjugation was performed using the non-protected DOTA succinimidyl ester **5.10**, giving cyclic peptide **5.03**. The separation of **5.03** from non-converted starting material (**5.09**) turned out to be unfeasible using acetonitrile and aqueous TFA as HPLC eluents (C18 RP-HPLC) due to nearly identical HPLC retention times of **5.03** and **5.09**. Isolation and purification of the product **5.03** was finally achieved using a mixture of 0.1% aqueous formic acid and acetonitrile containing 0.1% formic acid as HPLC eluents. The potential PET ligand **5.04** was quantitatively obtained by incubation of **5.03** with $^{69}Ga^{3+}$ in HEPES buffer pH 4.2 at 100 °C for 10 min (Scheme 5.1) as verified by analytical HPLC (data not shown) and mass spectrometry.

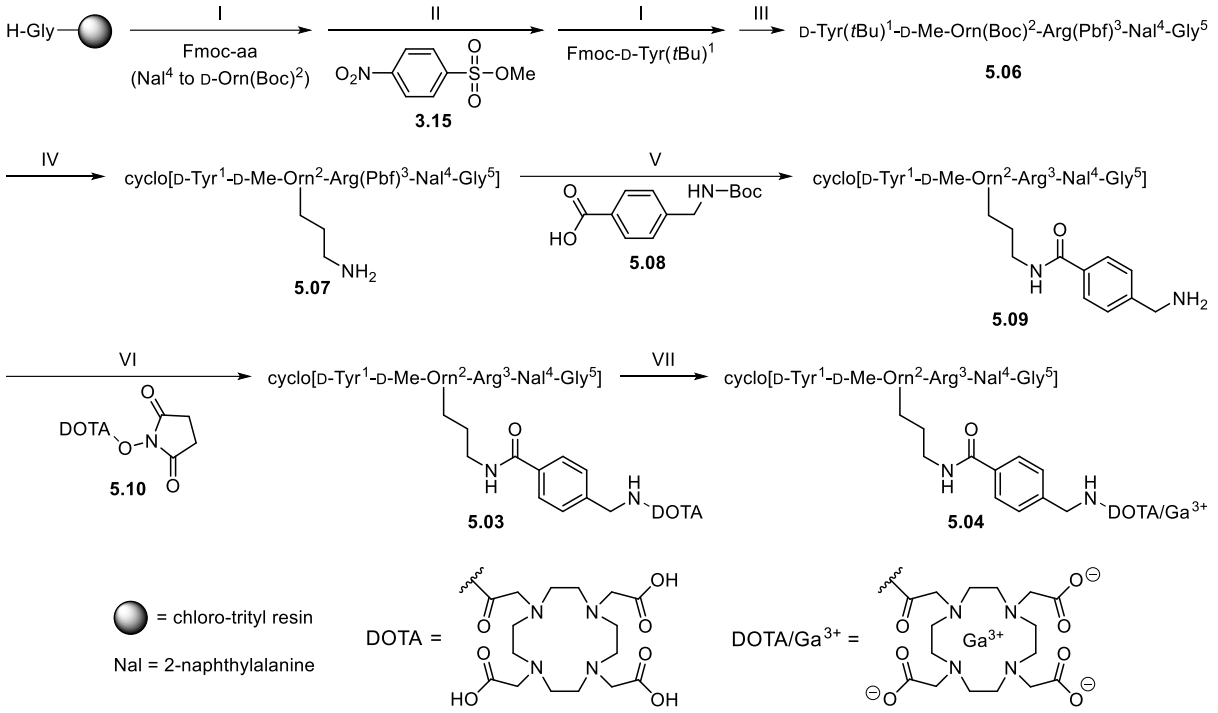

Scheme 5.1. Synthesis of the CXCR4 antagonist **5.03** (Pentixafor) and its Ga^{3+}-containing analog **5.04**. Reagents and conditions: (I) Fmoc-strategy SPPS using oxyma and DIC, solvent: DMF/NMP (80:20 v/v), 35 °C, 2 × 60 min or 2 × 90 min, Fmoc-deprotection: 20% piperidine in DMF/NMP (80:20 v/v), rt, 2 × 10 min; (II) (1) collidine, 2-nitrobenzenesulfonylchloride, CH_2Cl_2, rt, 2 h, (2) MTBD, DMF, rt, 30 min, (3) DBU, 2-mercaptoethanol, DMF, rt, 30 min; (III) HFIP/CH_2Cl_2 (1:3 v/v), rt, 2 × 20 min; (IV) (1) HOBt, DIPEA, PyBOP, anhydrous DMF, rt, 5 h, (2) TFA/H_2O (95:5 v/v), rt, 4 h, 30%; (V) (1) HOBt, HBTU, DIPEA, anhydrous DMF/NMP (80:20 v/v), rt, 40 min, (2) TFA/H_2O (95:5 v/v), rt, 4 h, 59%; (VI) DIPEA, DMF/NMP (75:25 v/v), rt, 30 min, 58%; (VII) preheating of a solution of the peptide (4 mM) in HEPES buffer (0.2 M, pH 4.2) to 60 °C, 5 min, addition of $Ga(NO_3)_3 \times H_2O$ in 10 mM HCl, 100 °C, 10 min, 99%.

Aiming at CXCR4 PET ligands derived from the described receptor antagonist **5.02**[38], Fmoc SPPS was applied for the preparation of the linear, side chain-protected peptides **5.11**-**5.14** using the *N*ω-carbamoylated arginine building blocks **4.07**[40] or **5.05** (for structures see Figure 5.1C) for amino acid coupling in position 2 (**5.11**, **5.12**) or 3 (**5.13**, **5.14**) (*cf*. Scheme 5.2). By using a H-Gly-2-ClTrt resin, glycine was placed at the C-terminus of the side chain-protected linear pentapeptides to prevent epimerization during peptide cyclization, which was performed using HOBt and PyBOP as coupling reagents in the presence of DIPEA. Side chain-deprotection with 95% aqueous TFA for 3 h gave the cyclic compounds **5.15**-**5.18** (Scheme 5.2) in good yields (46-59%).

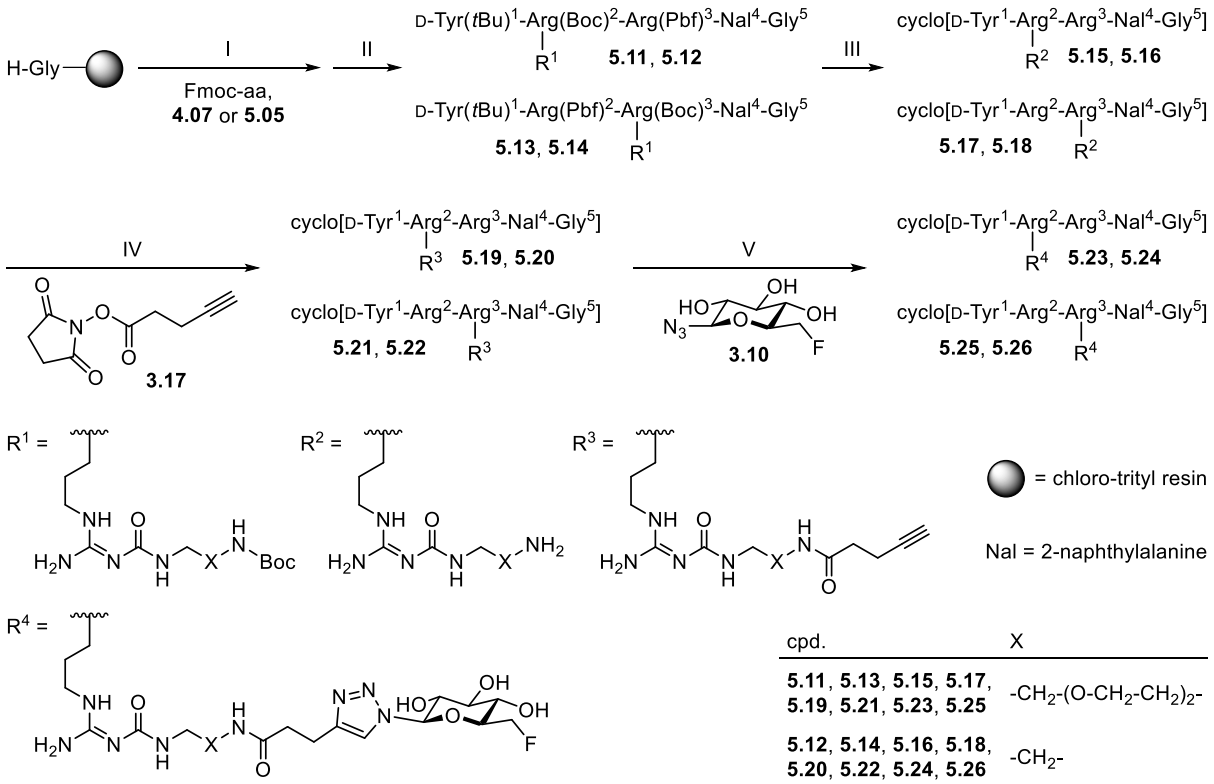

Scheme 5.2. Synthesis of the potential CXCR4 PET ligands **5.23**-**5.26**. Reagents and conditions: (I) Fmoc strategy SPPS using HBTU/HOBt and DIPEA, solvent: DMF/NMP (80:20 v/v), 35 °C, 2 × 1 h, 2 × 2 h or 1 × 17 h, Fmoc-deprotection: 20% piperidine in DMF/NMP (80:20 v/v), rt, 2 × 5-10 min; (II) HFIP/CH_2Cl_2 (1:4 v/v), rt, 2 × 20 min; (III) (1) HOBt, DIPEA, PyBOP, anhydrous DMF, rt, 5 h, (2) TFA/H_2O (95:5 v/v), rt, 3 h, 46% (**5.15**), 48% (**5.16**), 59% (**5.17**), 55% (**5.18**); (IV) DIPEA, anhydrous DMF/NMP (75:25 v/v), rt, 3 h 30 min, 68% (**5.19**), 71% (**5.20**), 68% (**5.21**), 73% (**5.22**); (V) $CuSO_4$, sodium ascorbate, PBS, NMP and EtOH/PBS (1:9 v/v), rt, 30 min or 60 min, 33% (**5.23**), 58% (**5.24**), 63% (**5.25**), 38% (**5.26**).

As the unnatural arginine residues introduced by the incorporation of **4.07** and **5.05** contain a terminal amino group in the side chain, peptides **5.15**-**5.18** were alkyne-functionalized by treatment with succinimidyl ester **3.17**[61] in the presence of DIPEA, giving compounds **5.19**-**5.22** in good yields of 68-73% (Scheme 5.2). The potential PET ligands **5.23**-**5.26** were prepared from **5.19**-**5.22** and **3.10**[41] via copper(I)-catalyzed azide-alkyne cycloaddition (CuAAC). In a first attempt to synthesize compound **5.23**, the use of EtOH/PBS (1:9 v/v) as solvent turned out to be unsuitable due to poor solubility of the starting material (peptide **5.19**) in this mixture. Therefore, the successful preparation of the 'click' reaction products **5.23**-**5.26** was performed using NMP/PBS of approximately 1:1 as solvent (Scheme 5.2).

5.2.2 Peptide stability in human plasma

To assess the stability of the cyclic, sugar-conjugated peptides **5.23**-**5.26** against proteolytic degradation a previously described procedure was used[62]. The compounds were incubated in human plasma for up to 48 h. The determined amounts of remaining intact peptide in plasma are summarized in Table 5.1 (for recovery ratios of **5.23**-**5.26** see Table 5.3).

Table 5.1. In vitro plasma stabilities of **5.23**-**5.26** determined at 37 °C.

cpd.	% intact peptide in plasma after the given incubation time[a]			
	1 h	6 h	24 h	48 h
5.23	> 99	> 99	> 99	> 99
5.24	> 99	> 99	> 99	> 99
5.25	> 99	> 99	> 99	99 ± 2
5.26	> 99	> 99	66 ± 1	49 ± 1

[a]The initial concentration of the peptide in human plasma/PBS (1:2 v/v) was 100 μM. Data represent means ± SEM from two or three independent experiments (SEM not given when no decomposition was observed).

Except for compound **5.26**, the peptides showed no proteolytic degradation during 48 h of incubation, being in agreement with known concepts: the incorporation of D-amino acids in the peptide sequence or peptide cyclization are two of the most commonly used strategies to improve the metabolic stability of peptides, taking advantage of rigidifying the conformation and hence impeding the accessibility for endo- and exopeptidases[63-65]. Noteworthy, also the conjugation to a sugar moiety was reported to render peptides less prone towards enzymatic degradation[66-70].

5.2.3 Mini-G protein recruitment assay

Assessment of the receptor affinities of compounds **5.15**-**5.26** via radioligand competition binding assays was not feasible in-house due to the lack of a suitable, e.g., ^{3}H-labeled CXCR4 radioligand and of an established binding assay system for the CXCR4. However, a recently described functional CXCR4 assay (split-NanoLuc complementation assay based on mini-G protein recruitment[71]) allowed an estimation of the binding affinities of receptor antagonists by inhibiting the agonist-induced mini-G protein recruitment. The assay principle is based on cells co-expressing a minimalized G protein (mini-G, mG) fused to the N-terminal fragment of the engineered luciferase NanoLuc (NLucN-mG) and a GPCR of interest fused to the C-terminal fragment of the NanoLuc (GPCR-NLucC)[71]. Upon agonist-induced activation of the GPCR, recruitment of the mini-G protein to the receptor leads to the reassembly of a functional NanoLuc. Subsequent enzymatic conversion of the luciferase substrate furimazine generates luminescence signals in an agonist concentration-dependent manner, which allows the determination of EC_{50} values (agonists) or IC_{50} values (antagonists). Conversion of the IC_{50} values into pK_b values via the Cheng-Prusoff equation[72] provides a measure for the CXCR4 affinities of the studied antagonists.

The potency of the standard agonist **5.01** and the antagonistic activity of the antagonist **5.02** were determined elsewhere[71], but raw data were re-processed for consistency reasons (Figure 5.2, Table 5.2). The resulting pEC_{50} value of 8.20 (**5.01**, *cf*. Figure 5.2A) and pIC_{50} value of 6.49 (corresponding to a pK_b value of 7.27, **5.02**, *cf*. Table 5.2) were in good agreement with data from the literature (pEC_{50} = 8.27[73], pIC_{50} = 6.4[74]). For comparison of peptides **5.15**-**5.22** and the fluoroglycosylated compounds **5.23**-**5.26** with the reported DOTA-conjugated reference compounds **5.03** and **5.04**, and for a comparison with literature data, **5.03** and **5.04** were also investigated with respect to CXCR4 antagonistic activities (*cf*. Figure 5.2B and Table 5.2). For **5.03** and **5.04**, only IC_{50} values are reported (150 nM and 5 nM, respectively)[39], which were obtained from radioligand CXCR4 competition binding assays using, according to what is provided in the respective article,

a non-characterized radioligand (no K_d value given)[39,75-77]. Thus, a direct comparison of the literature data with the results of the present functional assays is limited. However, the CXCR4 affinity measures of **5.03** and **5.04** obtained from the mini-G protein recruitment assay (K_b = 270 nM and 12 nM, respectively, Table 5.2) were in good agreement with the reported IC_{50} values of **5.03** and **5.04**, confirming the markedly higher CXCR4 affinity of the Ga^{3+}-containing peptide **5.04** over the Ga^{3+}-free compound **5.03**.

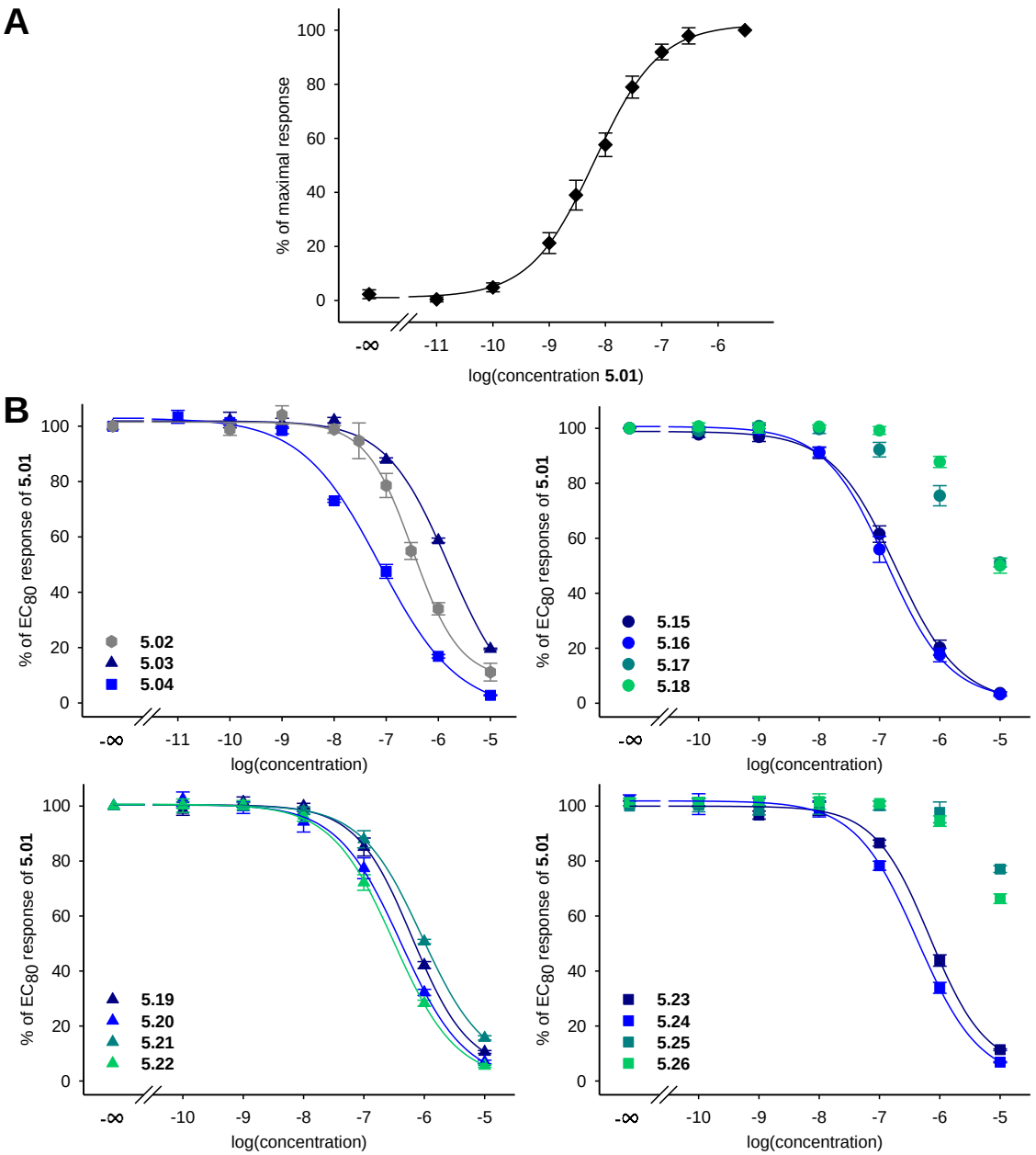

Figure 5.2. (A) Concentration response curve of the CXCR4 agonist **5.01** obtained from a mini-G protein recruitment assay performed with HEK293T cells stably co-expressing NlucN-mGsi and CXCR4-NLucC proteins[71]. Presented are mean values ± SEM from three independent experiments (performed in triplicate). pEC_{50} value of **5.01**: 8.20 ± 0.10 (mean ± SEM from three independent experiments). (B) Inhibiting effects of the antagonists **5.02-5.04** and **5.15-5.26** on the mini-G protein recruitment induced by **5.01** (c = 33 nM; same assay as under A performed in antagonist mode). Data represent mean values ± SEM from three independent experiments (performed in triplicate).

Table 5.2. CXCR4 antagonistic activities of **5.02**-**5.04** and **5.15**-**5.26** determined in a CXCR4 mini-G protein recruitment assay using **5.01** (c = 33 nM) as agonist.[a]

cpd.	pK_b ± SEM / K_b [nM]	cpd.	pK_b ± SEM / K_b [nM]	cpd.	pK_b ± SEM / K_b [nM]	cpd.	pK_b ± SEM / K_b [nM]
5.02	7.27 ± 0.04 / 55	**5.15**	7.51 ± 0.07 / 32	**5.19**	6.98 ± 0.02 / 105	**5.23**	6.93 ± 0.04 / 117
5.03	6.57 ± 0.03 / 270	**5.16**	7.65 ± 0.09 / 23	**5.20**	7.19 ± 0.03 / 65	**5.24**	7.15 ± 0.02 / 70
5.04	7.94 ± 0.10 / 12	**5.17**	< 6 / > 1000	**5.21**	6.82 ± 0.02 / 153	**5.25**	< 6 / > 1000
		5.18	< 6 / > 1000	**5.22**	7.29 ± 0.03 / 52	**5.26**	< 6 / > 1000

[a]Given are mean values ± SEM (pK_b) and mean values (K_b) from three independent experiments, each performed in triplicate.

Concentration response curves, obtained from functional studies with the cyclic antagonists **5.15**-**5.26** at the CXCR4, are depicted in Figure 5.2B, and the corresponding pK_b values are summarized in Table 5.2. Whereas full inhibition curves were obtained for **5.15**, **5.16** and **5.19-5.24**, the data obtained for **5.17**, **5.18**, **5.25** and **5.26**, all containing an N^{ω}-carbamoylated arginine in position 3, could not be fitted due to low CXCR4 affinities (pK_b < 6). Interestingly, within the series of alkyne-functionalized peptides (**5.19-5.22**), the position of the N^{ω}-carbamoyl substituent (Arg^2 vs. Arg^3) had no effect on the CXCR4 antagonistic activities (pK_b of **5.19** and **5.21**: 6.98 vs. 6.82, pK_b of **5.20** and **5.22**: 7.19 vs. 7.29). This means that in position 3 the alkyne-functionalized N^{ω}-carbamoylated arginine is tolerated (**5.21**, **5.22**), whereas the amino-functionalized arginine (**5.17**, **5.18**) and the glycosylated arginine (**5.25**, **5.26**) are not tolerated. A plausible explanation for this observation can possibly be found by the aid of computational chemistry (docking studies, simulations; not performed in this work). The strong impairment of CXCR4 binding caused by a modification of Arg^3 is in agreement with reports on the stronger contribution of Arg^3 in **5.02** to CXCR4 binding compared to Arg^2 [54,78].

The type of the linker in the N^{ω}-carbamoyl substituent (dioxaoctamethylene vs. dimethylene) had almost no effect on the CXCR4 affinity (Table 5.2). The most pronounced difference was observed for the alkyne-functionalized peptides **5.21** and **5.22** (pK_b: 6.82 vs. 7.29). Notably, the potential CXCR4 PET ligand **5.23** showed only twofold lower CXCR4 affinity than the parent peptide **5.02**, and the potential PET ligand **5.24** displayed nearly equal CXCR4 affinity compared **5.02** (Table 5.2). This demonstrates that the pursued approach (replacement of arginine by a functionalized N^{ω}-carbamoylated arginine) was successful with regard to the Arg^2 position.

Out of the four "sets" of cyclic peptides, exchange of Arg in position 2 in the scaffold of **5.02** by an N^{ω}-carbamoylated arginine containing a dimethylene linker, as in compounds **5.16**, **5.20** and **5.24**, yielded the ligand candidates with the highest antagonistic activities at the CXCR4 (pK_b = 7.65, 7.19 and 7.15, respectively; *cf*. Table 5.2). Notably, the functional activity of cyclopeptide **5.24**, representing the "cold" analog of a ^{18}F-PET ligand, is only marginally lower compared to **5.04**, the "cold" form of a ^{68}Ga-PET tracer (pK_b = 7.94, see Table 5.2). However, aiming at CXCR4 ligands with higher affinity and potency, additional structural modifications as well as the setup of a robust binding assay system for further evaluation and characterization of the ligands will be necessary.

5.3 Conclusion

The development of antagonistic CXCR4 ligands is of particular interest not only concerning the treatment of HIV[7,8,30-32] and COVID-19[36,37], but also with respect to molecular imaging and therapy of various types of cancer[45,48-50,79-84]. However, no ^{18}F-labeled CXCR4 PET ligand, useful for cancer diagnosis, has reached the clinic so far. Here we describe the synthesis and in vitro evaluation of the "cold" analogs of CXCR4 PET ligands derived from the cyclic peptidic CXCR4 antagonist FC131[38]. The conjugation to a fluorinated sugar[41] via the side chain of an N^{ω}-carbamoylated arginine, introduced in position 2, afforded a stable ($t_{1/2}$ in human plasma > 24 h) potential CXCR4 PET ligand (**5.24**) being only slightly less potent than the described CXCR4 PET ligand [^{68}Ga]Pentixafor (pK_b = 7.15 vs. 7.94). Therefore, in future studies compound **5.24** could serve as a starting point for the development of ^{18}F-labeled CXCR4 PET ligands useful for in vivo tumor imaging.

5.4 Experimental section

5.4.1 General experimental conditions

Solvents and buffer components, purchased from commercial suppliers, were of analytical grade. Gradient grade MeOH for HPLC was obtained from Merck Chemicals (Darmstadt, Germany) and gradient grade MeCN for HPLC was from Sigma-Aldrich (Taufkirchen, Germany) or Merck. *N*,*N*-Diisopropylethylamine (DIPEA, 99%) was obtained from ABCR (Karlsruhe, Germany). HCOOH and K_2CO_3 were from Roth (Karlsruhe, Germany), and EtOAc and 1 M HCl were from VWR Chemicals (Ismaning, Germany). Anhydrous *N*,*N*-dimethylformamide (DMF) (99.8%), 1,1,1,3,3,3-hexafluoro-2-propanol (HFIP), $Ga(NO_3)_3$ hydrate, 7-methyl-1,5,7-triazabicyclo[4.4.0]dec-5-ene (MTBD), methyl-4-nitrobenzenesulfonate (**3.15**), 2-mercaptoethanol, sodium ascorbate and 1-methyl-D-Trp were purchased from Sigma-Aldrich. DMF (for peptide synthesis, packed under nitrogen, code D/3848/PB17), 1-methylpyrrolidin-2-one (NMP) (for peptide synthesis, nitrogen flushed), anhydrous NMP (99.5%), CH_2Cl_2 and 1-hydroxy-1*H*-benzotriazole (HOBt) hydrate were obtained from Acros Organics/Fisher Scientific (Nidderau, Germany). When used for the coupling of non-standard Fmoc-amino acids (SPPS), HOBt hydrate, containing up to 3% water, was dried using a lyophilizer. DOTA succinimidyl ester (**5.10**) was from CheMatech (Dijon, France). Trifluoroacetic acid (TFA) and absolute EtOH were obtained from Honeywell (Seelze, Germany). Collidine, 2-nitrobenzenesulfonylchloride, 1,8-diazabicyclo[5.4.0]undec-7-ene (DBU) and 4-(Boc-aminomethyl)benzoic acid (**5.08**) were from Alfa Aesar/ThermoFisher (Heysham, UK). Piperidine, *N*,*N*,*N*′,*N*′-tetramethyl-*O*-(1*H*-benzotriazole-1-yl)-uronium hexafluorophosphate (HBTU) and benzotriazole-1-yl-oxy-tris-pyrrolidino-phosphonium hexafluorophosphate (PyBOP) were purchased from Iris Biotech (Marktredwitz, Germany). Deuterated solvents were obtained from Deutero (Kastellaun, Germany). Bovine serum albumin (BSA) and bacitracin were purchased from Serva (Heidelberg, Germany). Oxyma pure, *N,N*'-diisopropylcarbodiimide (DIC), H-Gly-2-ClTrt resin (loading: 0.54 mmol/g) and Fmoc-Arg(Pbf)-OH were from Merck Biosciences (Schwalbach am Taunus, Germany). Fmoc-D-Tyr(*t*Bu)-OH, Fmoc-2-Nal-OH and Fmoc-D-Orn(Boc)-OH were obtained from Iris Biotech. Copper(II)sulfate pentahydrate was from Merck Chemicals. Ultrapure 4-(2-hydroxyethyl)-1-piperazineethanesulfonic acid (HEPES) was from Gerbu (Heidelberg, Germany). Peptide **5.01** (tris(hydrotrifluoroacetate)) (SDF-1α) was purchased from PeproTech (Hamburg, Germany). The syntheses of arginine building block **4.07**[40] and succinimidyl pentynoate **3.17**[59,61] were described elsewhere. Reference peptide **5.02**[38] and compounds **5.11** and **5.15** were prepared within the scope of the Master thesis of Katrin Spinnler (Institute of Pharmacy, University of Regensburg, 2016); **5.11** and **5.15** were re-synthesized. The synthesis of arginine building block **5.05** was performed in analogy to building block **3.06a**[40] and will be described elsewhere. 6-Deoxy-6-fluoro-β-D-glycosyl azide (**3.10**)[41] was a kind gift from Prof. Dr. Olaf Prante, Department of Nuclear Medicine, Molecular Imaging and Radiochemistry, Friedrich-Alexander-Universität Erlangen-Nürnberg (FAU), Germany. Millipore water was used throughout for the preparation of buffers, stock solutions and HPLC eluents. 1.5- and 2-mL polypropylene reaction vessels with screw cap (in the following referred to as "reaction vessel with screw cap") from Süd-Laborbedarf (Gauting, Germany) were used for the preparation and storage of stock solutions, and for small-scale reactions. 1.5- or 2-mL polypropylene reaction vessels (in the following referred to as "reaction vessel") from

Sarstedt (Nümbrecht, Germany) were used for the preparation of serial dilutions, and for the determination of stabilities in plasma. For the evaporation of solvents in 1.5- or 2-mL reaction vessels, a Savant Speed-Vac Plus SC110A vacuum concentrator (Thermo Fisher Scientific, Waltham, MA) was used. NMR spectra were recorded on a Bruker Avance 600 instrument (^{1}H: 600 MHz, ^{13}C: 151 MHz) (Bruker, Karlsruhe, Germany) at 300 K. The spectra were calibrated based on the solvent residual peaks (^{1}H-NMR: DMSO-d_6: δ = 2.50 ppm; ^{13}C-NMR: DMSO-d_6: δ = 39.52 ppm). ^{1}H-NMR data are reported as follows: chemical shift δ in ppm (multiplicity (s = singlet, d = doublet, m = multiplet, br s = broad singlet), integral, coupling constant J in Hz). High resolution mass spectra (HRMS) were acquired with an Agilent 6540 UHD Accurate-Mass Q-TOF LC/MS system coupled to an Agilent 1290 HPLC system (Agilent Technologies, Santa Clara, CA), using an ESI source. Analyses were performed using the following LC method: column: Luna Omega C18, 1.6 µm, 50 × 2.1 mm (Phenomenex, Aschaffenburg, Germany), column temperature: 40 °C, flow: 0.6 mL/min, solvent/linear gradient: 0-4 min: 0.1% aqueous HCOOH/0.1% HCOOH in MeCN 95:5-2:98, 4-5 min: 2:98. Preparative HPLC was performed with a system from Knauer (Berlin, Germany) consisting of two K-1800 pumps and a K-2001 detector (compounds **5.03**, **5.04**, **5.07**, the protected precursor of **5.09**, **5.09**, **5.15**-**5.22**, **5.25** and **5.26**), or a Prep 150 LC System from Waters (Eschborn, Germany) consisting of a 2545 binary gradient module, a 2489 UV/visible detector, and a Waters Fraction Collector III (compounds **5.23** and **5.24**). A Kinetex-XB C18, 5 µm, 250 mm × 21 mm (Phenomenex) or a Gemini-NX C18, 5 µm, 250 mm × 21 mm (Phenomenex) served as RP-columns at a flow rate of 20 mL/min. Mixtures of 0.02% aq TFA (A1) and MeCN (B1), 0.2% aq TFA (A2) and B1, or 0.1% aq HCOOH (A3) and 0.1% HCOOH in MeCN (B2) were used as mobile phase. A detection wavelength of 220 nm was used throughout. Collected fractions were lyophilized using an Alpha 2-4 LD apparatus (Martin Christ, Osterode am Harz, Germany) or a Scanvac CoolSafe 100-9 freeze-dryer (Labogene, Allerød, Denmark) both equipped with a vacuubrand RZ 6 rotary vane vacuum pump. Analytical HPLC analysis of compounds **5.03**, **5.04** and **5.15**-**5.26** was performed with a system from Agilent Technologies consisting of a 1290 Infinity binary pump equipped with a degasser, a 1290 Infinity Autosampler, a 1290 Infinity Thermostated Column Compartment, a 1260 Infinity Diode Array Detector and a 1260 Infinity Fluorescence Detector. A Kinetex-XB C18, 2.6 µm, 100 × 3 mm (Phenomenex) served as stationary phase at a flow rate of 0.6 mL/min. The oven temperature was set to 25 °C. UV detection was performed at 220 nm and fluorescence detection at 275/305 nm. The injection volume was 20 µL. Mixtures of 0.04% aq TFA (A4) or A3 and B1 or B2 were used as mobile phase. The following linear gradients were applied for purity controls: compounds **5.03** and **5.04**: 0-12 min: A3/B2 85:15-75:25, 12-16 min: 75:25-5:95, 16-20 min: 5:95; compounds **5.15**-**5.26**: 0-12 min: A4/B1 90:10-70:30, 12-16 min: 70:30-5:95, 16-20 min: 5:95. The following linear gradient was used for the analysis of plasma stability samples: 0-12 min: A4/B1 90:10-73:27, 12-16 min: 73:27-5:95, 16-20 min: 5:95. Retention (capacity) factors k were calculated from the retention times t_R according to $k = (t_R - t_0)/t_0$ (t_0 = dead time). All peptides were characterized by HRMS and RP-HPLC analysis, and peptides **5.03**, **5.04** and **5.15**-**5.22** were characterized by ^{1}H-NMR spectroscopy. Additionally, ^{1}H-COSY-, ^{13}C-, HSQC- and HMBC-NMR spectra were acquired of **5.15**-**5.18**.

Annotation concerning the ^{1}H-NMR spectra (solvent: DMSO-d_6): in order to allow an integration of the signals interfering with the broad water signal at ca 3.5 ppm, ^{1}H-NMR

spectra were additionally recorded in DMSO-d_6/D_2O (9:1 v/v (**5.15**-**5.22**) or 5:1 v/v (**5.03**, **5.04**)) (spectra and data not shown).

Additional analytical data of compounds (HPLC analyses, ^1H- and ^{13}C-NMR spectra) are provided in the Appendix.

5.4.2 General procedure for SPPS

Peptides were synthesized by manual SPPS according to a reported procedure[40] with the following modifications: The resin was allowed to swell in the solvent for 45 min prior to the beginning of the synthesis. Fmoc-Arg(Pbf)-OH and Fmoc-D-Tyr(*t*Bu)-OH were used in 5-fold excess, Fmoc-Nal-OH was used in 4-fold excess, and the arginine building blocks **4.07** and **5.05** were used in 3-fold excess. Amino acid coupling was performed with HBTU/HOBt/DIPEA (Fmoc-Arg(Pbf)-OH, Fmoc-D-Tyr(*t*Bu)-OH: 4.95/5/10 equiv., Fmoc-Nal-OH: 3.95/4/8 equiv., **4.07**, **5.05**: 3/3/6 equiv.). For the coupling of the arginine building blocks **4.07** and **5.05**, anhydrous solvents (DMF, NMP) were used. Except for the arginine derivatives **4.07** and **5.05**, "double coupling" was performed (2 × 60 min or 2 × 90 min at 35 °C). For **4.07** and **5.05**, "single coupling" was performed with a longer reaction time (17 h at 35 °C). Peptides were cleaved from the resin with CH_2Cl_2/HFIP (4:1 v/v) at rt for 2 × 20 min.

5.4.3 General procedure for the cyclization of peptides

The reaction was performed in a round-bottom flask equipped with a magnetic micro-stirrer. The crude linear peptide (1 equiv.) was dissolved in anhydrous DMF to give a 1 mM solution. HOBt (2.5 equiv.), DIPEA (5 equiv.) and PyBOP (1.63 equiv.) were added under stirring and the reaction mixture was stirred at rt for 5 h. Water/brine (10:1 v/v) (190-390 mL) was added and the side chain-protected cyclic product was extracted with EtOAc (3 × 100-200 mL). The volatiles of the combined organic phases were removed under reduced pressure and the intermediate was purified by preparative HPLC. After lyophilization of the eluate, TFA/H_2O (95:5 v/v) (5.5 mL) was added and the mixture was stirred at rt for 3 h. H_2O (180 mL) was added and the mixture was subjected to lyophilization. The deprotected cyclic peptide was purified by preparative HPLC.

5.4.4 General procedure for the alkynylation of cyclic peptides

A solution of **3.17** (1.3 equiv., 0.04 mg/µL) in anhydrous DMF was added to a stirred solution of the peptide (1 equiv.) and DIPEA (6 equiv.) in anhydrous DMF/NMP (75:25 v/v) (66-69 µL) and stirring was continued at rt for 3.5 h. 10% aq TFA (corresponding to 6 equiv. TFA) was added and the product was purified by preparative RP-HPLC.

5.4.5 General procedure for copper(I)-catalyzed 'click' reaction

A solution of fluoroglycosyl azide **3.10** (2.6 equiv.) in EtOH/PBS (136.9 mM NaCl, 2.68 mM KCl, 5.62 mM Na_2HPO_4, 1.09 mM NaH_2PO_4 and 1.47 mM KH_2PO_4) (1:9 v/v) (62-116 µL) was added to a solution of the alkynylated peptide (1 equiv.) in NMP (59-110 µL). A solution of copper(II)sulfate pentahydrate (1.2 equiv., 1 M) in PBS and a solution of sodium ascorbate (3 equiv., 1 M) in PBS were added and the mixture was stirred at rt for 30 min. 10% aq TFA (1 µL) was added and the product was purified by preparative RP-HPLC.

5.4.6 Synthesis protocols and analytical data of compounds 5.03, 5.04 and 5.15-5.26

cyclo[D-Tyr-N^{α}-methyl-N^{δ}-({4-[(N-{2-[4,7,10-tris(carboxymethyl)-1,4,7,10-tetraazacyclododecan-1-yl]acetyl})aminomethyl]phenyl}carbonyl)-D-Orn-Arg-β-(naphtha-2-yl)Ala-Gly] bis(hydroformate) (5.03)[39]. The side chain-protected linear precursor peptide D-Tyr(*t*Bu)-D-Me-Orn(Boc)-Arg(Pbf)-Nal-Gly (**5.06**) was synthesized according to the general procedure for SPPS using a H-Gly-2-ClTrt resin (loading 0.54 mmol/g) (150 mg, 0.081 mmol), with the following modification: all amino acids were used in 5-fold excess and were pre-activated with oxyma/DIC (5/5 equiv.) instead of HBTU/HOBt. After coupling and Fmoc-deprotection of the D-Orn(Boc) building block, the resin was washed with CH_2Cl_2 (5 ×), a solution of 2-nitrobenzenesulfonylchloride (53.9 mg, 0.243 mmol) and collidine (53.7 µL, 0.405 mmol) in CH_2Cl_2 (1.5 mL) was added and the mixture was shaken at rt for 2 h. The resin was washed with DMF (5 ×), and a solution of MTBD (46.5 µL, 0.324 mmol) and methyl-4-nitrobenzenesulfonate **3.15** (88.0 mg, 0.405 mmol) in DMF (1.8 mL) was added. After shaking at rt for 30 min, the resin was washed with DMF (3 ×) followed by the addition of a solution of DBU (60.4 µL, 0.405 mmol) and 2-mercaptoethanol (56.5 µL, 0.810 mmol) in DMF (1.5 mL) and shaking at rt for 30 min. The resin was washed with DMF (5 ×) followed by coupling of Fmoc-D-Tyr(*t*Bu)-OH as described above. Cleavage from the resin was performed with CH_2Cl_2/HFIP (3:1 v/v) at rt for 2 × 20 min. Yield of crude **5.06**: 29.0 mg, 32%, RP-HPLC (220 nm) ca. 76%.

Crude **5.06** (29.0 mg, 25.7 µmol) was cyclized according to the general procedure with the following modifications: after cyclization, brine (246 mL) was added and the product was extracted with EtOAc (4 × 33 mL). The organic phases were combined and the volatiles were removed by evaporation. The residue was dissolved in TFA/H_2O (95:5 v/v) (4 mL) and the mixture was stirred at rt for 4 h. The solution was transferred into water (30 mL) and the mixture was subjected to lyophilization. Purification by preparative HPLC (column: Gemini-NX C18, gradient: 0-10 min: A2/B1 97:3-60:40, 10-30 min: 60:40-45:55, t_R = 18 min) afforded **5.07** as white fluffy solid (8.3 mg, 30%), an intermediate still carrying the Pbf-protecting group at Arg^3.

DIPEA (47.3 µL, 271.7 µmol) was added to a solution of HOBt (18.4 mg, 135.8 µmol), building block **5.08** (34.1 mg, 135.8 µmol) and HBTU (50.5 mg, 133.1 µmol) in anhydrous DMF/NMP (80:20 v/v) (300 µL). The mixture was pre-incubated for 3 min, followed by the addition of peptide **5.07** (29.0 mg, 27.2 µmol) and stirring at rt for 40 min. 10% aq TFA (272 µL) was added, and the Pbf- and Boc-protected intermediate was purified by preparative HPLC (column: Gemini-NX C18, gradient: 0-8 min: A2/B1 75:25-47:53, 8-26 min: 47:53-38:62, t_R = 19 min). The intermediate was dissolved in TFA/H_2O (95:5 v/v) (6 mL) and the mixture was stirred at rt for 4 h. The solution was transferred into water (30 mL) and the mixture was subjected to lyophilization. Purification by preparative HPLC (column: Gemini-NX C18, gradient: 0-35 min: A2/B1 90:10-55:45, t_R = 20 min) afforded the deprotected intermediate **5.09** as white fluffy solid (17.0 mg, 59%). DIPEA (10.8 µL, 62.1 µmol) was added to a solution of **5.09** (11.0 mg, 10.4 µmol) in DMF/NMP (75:25 v/v) (73 µL) and the mixture was combined with a solution of DOTA reagent **5.10** (7.88 mg, 10.4 µmol) in anhydrous DMF (26 µL). After shaking at rt for 30 min, 10% aq TFA (41.4 µL) was added. Purification by preparative HPLC (column: Gemini-NX C18, gradient: 0-5 min: A3/B2 90:10-85:15, 5-15 min: 85:15-75:25, 15-25 min: 75:25-60:40, t_R =

14 min) afforded **5.03** as white fluffy solid (7.9 mg, 58%). ^{1}H-NMR (600 MHz, DMSO-d_6, at least two rotamers, resulting in signal splitting, were evident): δ 0.88-0.98 (m, 0.5H), 1.07-1.36 (m, 3.5H), 1.41-1.70 (m, 3H), 1.84-1.98 (m, 1H), 2.62-2.67 (m, 1H), 2.67-2.75 (m, 4H), 2.75-2.97 (m, 8H), 2.97-3.17 (m, 12H), 3.17-3.27 (m, 7H), 3.43-3.50 (m, 3H), 3.65-3.76 (m, 1H), 3.77-3.99 (m, 2H), 4.15-4.48 (m, 3.5H), 4.65-4.76 (m, 1H), 4.88-4.97 (m, 0.5H), 6.36-7.30 (br s, 2H, interfering with the next two listed signals), 6.59-6.74 (m, 2H), 6.92-7.04 (m, 2H), 7.30-7.59 (m, 7H), 7.59-8.14 (m, 8H), 8.17-8.82 (m, 5H), 8.82-8.94 (m, 1H), 8.94-11.26 (m, 4H). HRMS: *m/z* $[M+2H]^{2+}$ calcd. for $[C_{60}H_{82}N_{14}O_{14}]^{2+}$ 611.3062, found 611.3072. RP-HPLC (220 nm): 99% (t_R = 5.2 min, k = 5.8). $C_{60}H_{80}N_{14}O_{14} \cdot C_2H_4O_4$ (1221.38 + 92.05).

cyclo[D-Tyr-N^{α}-methyl-N^{δ}-({4-[(N-{2-[gallium(III)-4,7,10-tris(carboxymethyl)-1,4,7,10-tetraazacyclododecan-1-yl]acetyl})aminomethyl]phenyl}carbonyl)-D-Orn-Arg-β-(naphtha-2-yl)Ala-Gly] hydrotrifluoroacetate (5.04)[39]. The incorporation reaction was performed in a 2-mL reaction vessel with screw cap. A solution of **5.03** (1.80 mg, 1.37 µmol, 4 mM) in HEPES buffer (0.2 M, pH 4.2) was heated to 60 °C for 5 min, followed by the addition of a solution of $Ga(NO_3)_3 \times H_2O$ (1.13 mg, 4.11 µmol, 0.4 M) in aqueous HCl (10 mM). The mixture was shaken at 100 °C for 10 min using a Thermocell mixing block from Bioer (Hangzhou, China). Purification by preparative RP-HPLC (column: Gemini-NX C18, gradient: 0-22 min: A2/B1 84:16-60:40, t_R = 12 min) yielded **5.04** as white fluffy solid (1.9 mg, 99%). ^{1}H-NMR (600 MHz, DMSO-d_6, at least two rotamers, resulting in signal splitting, were evident): δ 1.05-1.14 (m, 0.5H), 1.18-1.34 (m, 2.5H), 1.36-1.68 (m, 4H), 1.91-2.04 (m, 1H), 2.61-2.65 (m, 1.5H), 2.68-2.73 (m, 0.5H), 2.83-2.91 (m, 3H), 2.98-3.12 (m, 3H), 3.19-3.35 (m, 16H), 3.60-3.78 (m, 12H), 3.80-3.89 (m, 1H), 3.89-4.02 (m, 1H), 4.29-4.43 (m, 3.5H), 4.61-4.73 (m, 1H), 4.78-4.90 (m, 0.5H), 6.60-6.67 (m, 2H), 6.67-7.05 (br s, 1.5H, interfering with the next two listed signals), 6.90-6.93 (m, 1H), 6.93-6.99 (m, 1H), 7.05-7.43 (br s, 1.5H, interfering with the next three listed signals), 7.13-7.16 (m, 0.5H), 7.19-7.22 (m, 0.5H), 7.32-7.40 (m, 3.5H), 7.43-7.52 (m, 3H), 7.61-7.68 (m, 1H), 7.72-7.99 (m, 5H), 8.10-8.19 (m, 1H), 8.21-8.31 (m, 0.5H), 8.40-8.52 (m, 1H), 8.61-8.84 (m, 1H), 8.86-8.97 (m, 1H), 9.10-9.32 (m, 1H), 13.04-13.51 (m, 1H). HRMS: *m/z* $[M+2H]^{2+}$ calcd. for $[C_{60}H_{79}GaN_{14}O_{14}]^{2+}$ 644.2573, found 644.2582. RP-HPLC (220 nm): > 99% (t_R = 5.4 min, k = 6.1). $C_{60}H_{77}GaN_{14}O_{14} \cdot C_2HF_3O_2$ (1288.08 + 114.02).

cyclo[D-Tyr-N^{ω}-[*N*-(8-amino-3-6-dioxaoctyl)aminocarbonyl]Arg-Arg-β-(naphtha-2-yl)Ala-Gly] tris(hydrotrifluoroacetate) (5.15). The side chain-protected linear precursor peptide D-Tyr(*t*Bu)-N^{ω}-[*N*-(8-*tert*-butoxycarbonylamino-3-6-dioxaoctyl)aminocarbonyl]-$N^{\omega'}$-*tert*-butoxycarbonyl-Arg-Arg(Pbf)-ß-(naphtha-2-yl)Ala-Gly (**5.11**) was synthesized according to the general procedure for SPPS using a H-Gly-2-ClTrt resin (loading 0.54 mmol/g) (175 mg, 0.095 mmol; yield of crude **5.11**: 91.2 mg, 67%, RP-HPLC (220 nm) ca. 86%). Crude **5.11** (44.6 mg, 31.2 µmol) was cyclized according to the general procedure. Isolation of the protected intermediate by preparative HPLC: column: Kinetex XB-C18, gradient: 0-30 min: A1/B1 62:38-9:91, t_R = 18 min. Purification of the product by preparative HPLC (column: Kinetex XB-C18, gradient: 0-35 min: A2/B1 92:8-62:38, t_R = 22 min) afforded **5.15** as white fluffy solid (17.9 mg, 46%). ^{1}H-NMR (600 MHz, DMSO-d_6): δ 1.23-1.48 (m, 5H), 1.49-1.59 (m, 1H), 1.59-1.73 (m, 2H), 2.70-2.82 (m, 2H), 2.92-3.07 (m, 4H), 3.09-3.23 (m, 4H), 3.26-3.30 (m, 2H), 3.44-3.51 (m, 2H), 3.51-3.64 (m, 7H), 3.69-3.78 (m, 1H), 3.88-3.97 (m, 1H), 4.02-4.17 (m, 1H), 4.17-4.30 (m, 1H), 4.30-4.42 (m, 1H), 6.57-6.69 (m, 2H), 6.69-7.21 (br s, 2H, interfering with the next listed signal),

6.92-6.95 (m, 2H), 7.21-7.63 (br s, 2H, interfering with the next two listed signals), 7.35-7.38 (m, 1H), 7.43-7.51 (m, 3H), 7.63-8.04 (m, 10H), 8.04-8.12 (m, 1H), 8.24-8.69 (m, 4H), 8.87-9.39 (m, 2H), 10.51 (br s, 1H). ^{13}C-NMR (151 MHz, DMSO-*d*$_6$): δ 24.5, 25.1, 27.7, 28.9, 36.1 (2 carbon atoms), 38.6, 39.1, 40.2, 40.3, 42.8, 54.0, 54.1, 55.3, 55.8, 66.7, 68.8, 69.4, 69.6, 115.0 (2 carbon atoms), 116.1 (TFA), 118.1 (TFA), 120.1, 125.5, 126.1, 127.2, 127.3, 127.3, 127.5, 127.7, 127.7, 130.0 (2 carbon atoms), 131.8, 133.0, 135.5, 153.7, 155.9, 156.8, 158.7 (q, *J* 31 Hz) (TFA), 169.4, 170.7, 170.7, 171.1, 171.2. HRMS: *m/z* [*M*+2H]$^{2+}$ calcd. for [$C_{43}H_{63}N_{13}O_9$]$^{2+}$ 452.7430, found 452.7436. RP-HPLC (220 nm): 99% (t_R = 7.4 min, *k* = 8.7). $C_{43}H_{61}N_{13}O_9$ · $C_6H_3F_9O_6$ (904.04 + 342.07).

cyclo[D-Tyr-*N*$^{\omega}$-[(2-aminoethyl)aminocarbonyl]Arg-Arg-β-(naphtha-2-yl)Ala-Gly] tris(hydrotrifluoroacetate) (5.16). The side chain-protected linear precursor peptide D-Tyr(*t*Bu)-*N*$^{\omega}$-[(2-*tert*-butoxycarbonylaminoethyl)aminocarbonyl]-*N*$^{\omega}$'-*tert*-butoxycarbonyl-Arg-Arg(Pbf)-ß-(naphtha-2-yl)Ala-Gly (**5.12**) was synthesized according to the general procedure for SPPS using a H-Gly-2-ClTrt resin (loading 0.54 mmol/g) (175 mg, 0.095 mmol; yield of crude **5.12**: 85.4 mg, 67%, RP-HPLC (220 nm) ca. 84%). Crude **5.12** (40.6 mg, 30.3 µmol) was cyclized according to the general procedure. Isolation of the protected intermediate by preparative HPLC: column: Kinetex XB-C18, gradient: 0-30 min: A1/B1 62:38-9:91, t_R = 19 min. Purification of the product by preparative HPLC (column: Kinetex XB-C18, gradient: 0-35 min: A2/B1 92:8-62:38, t_R = 22 min) afforded **5.16** as white fluffy solid (16.9 mg, 48%). ^{1}H-NMR (600 MHz, DMSO-*d*$_6$): δ 1.23-1.47 (m, 5H), 1.49-1.59 (m, 1H), 1.59-1.73 (m, 2H), 2.68-2.84 (m, 2H), 2.89-2.96 (m, 2H), 2.99-3.06 (m, 2H), 3.10-3.22 (m, 4H), 3.33-3.37 (m, 2H), 3.55-3.57 (m, 1H), 3.71-3.76 (m, 1H), 3.89-3.97 (m, 1H), 4.06-4.16 (m, 1H), 4.21-4.28 (m, 1H), 4.31-4.39 (m, 1H), 6.54-6.72 (m, 2H), 6.72-7.19 (br s, 2H, interfering with the next listed signal), 6.92-6.95 (m, 2H), 7.19-7.56 (br s, 2H, interfering with the next two listed signals), 7.35-7.38 (m, 1H), 7.44-7.49 (m, 2H), 7.56-7.76 (m, 3H), 7.76-8.01 (m, 8H), 8.02-8.12 (m, 1H), 8.20-8.81 (m, 4H), 8.90-9.37 (m, 2H), 10.79 (br s, 1H). ^{13}C-NMR (151 MHz, DMSO-*d*$_6$): δ 24.5, 25.1, 27.7, 28.9, 36.1 (2 carbon atoms), 37.2, 38.5, 40.2, 40.3, 42.8, 54.0 (2 carbon atoms), 55.3, 55.8, 115.0 (2 carbon atoms), 116.0 (TFA), 118.0 (TFA), 125.5, 126.1, 127.2, 127.3, 127.3, 127.5, 127.7, 127.7, 130.0 (2 carbon atoms), 131.8, 133.0, 135.6, 153.8, 154.4, 155.9, 156.8, 158.9 (q, *J* 32 Hz) (TFA), 169.4, 170.7, 170.8, 171.1, 171.1. HRMS: *m/z* [*M*+2H]$^{2+}$ calcd. for [$C_{39}H_{55}N_{13}O_7$]$^{2+}$ 408.7168, found 408.7176. RP-HPLC (220 nm): 99% (t_R = 7.0 min, *k* = 8.2). $C_{39}H_{53}N_{13}O_7$ · $C_6H_3F_9O_6$ (815.94 + 342.07).

cyclo[D-Tyr-Arg-*N*$^{\omega}$-[*N*-(8-amino-3-6-dioxaoctyl)aminocarbonyl]Arg-β-(naphtha-2-yl)Ala-Gly] tris(hydrotrifluoroacetate) (5.17). The side chain-protected linear precursor peptide D-Tyr(*t*Bu)-Arg(Pbf)-*N*$^{\omega}$-[*N*-(8-*tert*-butoxycarbonylamino-3-6-dioxaoctyl)aminocarbonyl]-*N*$^{\omega}$'-*tert*-butoxycarbonyl-Arg-ß-naphtha-2-yl)Ala-Gly (**5.13**) was synthesized according to the general procedure for SPPS using a H-Gly-2-ClTrt resin (loading 0.54 mmol/g) (175 mg, 0.095 mmol; yield of crude **5.13**: 95.3 mg, 70%, RP-HPLC (220 nm) ca. 91%). Crude **5.13** (45.2 mg, 31.6 µmol) was cyclized according to the general procedure. Isolation of the protected intermediate by preparative HPLC: column: Kinetex XB-C18, gradient: 0-30 min: A1/B1 62:38-9:91, t_R = 18 min. Purification of the product by preparative HPLC (column: Kinetex XB-C18, gradient: 0-35 min: A2/B1 92:8-62:38, t_R = 21 min) afforded **5.17** as white fluffy solid (23.4 mg, 59%). ^{1}H-NMR (600 MHz, DMSO-*d*$_6$): δ 1.21-1.38 (m, 4H), 1.39-1.48 (m, 1H), 1.48-1.59 (m, 1H), 1.59-1.75 (m, 2H), 2.69-2.83 (m,

2H), 2.94-3.05 (m, 4H), 3.10-3.21 (m, 4H), 3.26-3.30 (m, 2H), 3.47-3.49 (m, 2H), 3.53-3.59 (m, 7H), 3.71-3.80 (m, 1H), 3.86-3.95 (m, 1H), 4.07-4.15 (m, 1H), 4.21-4.29 (m, 1H), 4.32-4.40 (m, 1H), 6.57-6.69 (m, 2H), 6.69-7.16 (br s, 2H, interfering with the next listed signal), 6.91-6.94 (m, 2H), 7.16-7.61 (br s, 2H, interfering with the next two listed signals), 7.35-7.38 (m, 1H), 7.42-7.53 (m, 3H), 7.61-7.69 (m, 2H), 7.72-8.00 (m, 8H), 8.04-8.13 (m, 1H), 8.23-8.73 (m, 4H), 8.89-9.38 (m, 2H), 10.57 (br s, 1H). ^{13}C-NMR (151 MHz, DMSO-*d*$_6$): δ 24.6, 25.0, 27.7, 28.9, 36.1, 36.1, 38.6, 39.0, 40.1, 40.4, 42.9, 54.0, 54.2, 55.2, 55.6, 66.7, 68.8, 69.4, 69.6, 115.0 (2 carbon atoms), 116.1 (TFA), 118.1 (TFA), 125.4, 126.0, 127.2, 127.3, 127.3, 127.4, 127.7 (2 carbon atoms), 130.0 (2 carbon atoms), 131.8, 133.0, 135.6, 153.6, 153.9, 155.9, 156.8, 158.7 (q, *J* 32 Hz) (TFA), 169.3, 170.6, 170.7, 171.1, 171.2. HRMS: *m/z* [*M*+2H]$^{2+}$ calcd. for [$C_{43}H_{63}N_{13}O_9$]$^{2+}$ 452.7430, found 452.7436. RP-HPLC (220 nm): 99% (t_R = 7.0 min, *k* = 8.2). $C_{43}H_{61}N_{13}O_9$ · $C_6H_3F_9O_6$ (904.04 + 342.07).

cyclo[D-Tyr-Arg-*N*$^{\omega}$-[(2-aminoethyl)aminocarbonyl]Arg-β-(naphtha-2-yl)Ala-Gly] tris(hydrotrifluoroacetate) (5.18). The side chain-protected linear precursor peptide D-Tyr(*t*Bu)-Arg(Pbf)-*N*$^{\omega}$-[(2-*tert*-butoxycarbonylaminoethyl)aminocarbonyl]-*N*$^{\omega'}$-*tert*-butoxycarbonyl-Arg-ß-(naphtha-2-yl)Ala-Gly (**5.14**) was synthesized according to the general procedure for SPPS using a H-Gly-2-ClTrt resin (loading 0.54 mmol/g) (175 mg, 0.095 mmol; yield of crude **5.14**: 97.3 mg, 77%, RP-HPLC (220 nm) ca. 86%). Crude **5.14** (51.4 mg, 38.3 µmol) was cyclized according to the general procedure. Isolation of the protected intermediate by preparative HPLC: column: Kinetex XB-C18, gradient: 0-30 min: A1/B1 62:38-9:91, t_R = 19 min. Purification of the product by preparative HPLC (column: Kinetex XB-C18, gradient: 0-35 min: A2/B1 92:8-62:38, t_R = 21 min) afforded **5.18** as white fluffy solid (24.3 mg, 55%). ^{1}H-NMR (600 MHz, DMSO-*d*$_6$): δ 1.26-1.47 (m, 5H), 1.49-1.59 (m, 1H), 1.59-1.78 (m, 2H), 2.67-2.84 (m, 2H), 2.88-2.97 (m, 2H), 2.98-3.05 (m, 2H), 3.09-3.21 (m, 4H), 3.34-3.38 (m, 2H), 3.54-3.56 (m, 1H), 3.72-3.76 (m, 1H), 3.88-3.93 (m, 1H), 4.08-4.15 (m, 1H), 4.19-4.30 (m, 1H), 4.30-4.41 (m, 1H), 6.58-6.70 (m, 2H), 6.70-7.17 (br s, 2H, interfering with the next listed signal), 6.91-6.94 (m, 2H), 7.17-7.53 (br s, 2H, interfering with the next two listed signals), 7.35-7.38 (m, 1H), 7.43-7.48 (m, 2H), 7.53-7.71 (m, 3H), 7.71-8.03 (m, 8H), 8.03-8.15 (m, 1H), 8.20-8.82 (m, 4H), 8.90-9.44 (m, 2H), 10.83 (br s, 1H). ^{13}C-NMR (151 MHz, DMSO-*d*$_6$): δ 24.6, 25.0, 27.7, 28.9, 36.2 (2 carbon atoms), 37.1, 38.4, 40.1, 40.4, 42.9, 54.1, 54.1, 55.2, 55.7, 115.0 (2 carbon atoms), 116.0 (TFA), 118.0 (TFA), 125.5, 126.0, 127.2, 127.3 (2 carbon atoms), 127.4, 127.7, 127.7, 130.0 (2 carbon atoms), 131.8, 133.0, 135.5, 153.7, 154.3, 155.9, 156.8, 158.8 (q, *J* 32 Hz) (TFA), 169.3, 170.6, 170.7, 171.1, 171.2. HRMS: *m/z* [*M*+2H]$^{2+}$ calcd. for [$C_{39}H_{55}N_{13}O_7$]$^{2+}$ 408.7168, found 408.7175. RP-HPLC (220 nm): 98% (t_R = 6.5 min, *k* = 7.6). $C_{39}H_{53}N_{13}O_7$ · $C_6H_3F_9O_6$ (815.94 + 342.07).

cyclo[D-Tyr-*N*$^{\omega}$-[*N*-(8-pent-4-ynoylamino-3-6-dioxaoctyl)aminocarbonyl]Arg-Arg-β-(naphtha-2-yl)Ala-Gly] bis(hydrotrifluoroacetate) (5.19). Compound **5.19** was prepared from **5.15** (10.1 mg, 8.1 µmol) and **3.17** (2.1 mg, 10.5 µmol) according to the general procedure for alkynylation. Purification by preparative RP-HPLC (column: Kinetex-XB C18, gradient: 0-35 min: A2/B1 92:8-55:45, t_R = 24 min) yielded **5.19** as white fluffy solid (6.7 mg, 68%). ^{1}H-NMR (600 MHz, DMSO-*d*$_6$): δ 1.23-1.46 (m, 5H), 1.49-1.59 (m, 1H), 1.59-1.73 (m, 2H), 2.24-2.30 (m, 2H), 2.32-2.36 (m, 2H), 2.72-2.81 (m, 3H), 3.00-3.05 (m, 2H), 3.11-3.17 (m, 3H), 3.19-3.22 (m, 3H), 3.26-3.28 (m, 2H), 3.40-3.40 (m, 2H), 3.47-3.48 (m, 2H), 3.51-3.54 (m, 5H), 3.73-3.77 (m, 1H), 3.90-3.96 (m, 1H), 4.07-4.13 (m,

1H), 4.21-4.28 (m, 1H), 4.28-4.38 (m, 1H), 6.62-6.65 (m, 2H), 6.65-7.08 (br s, 2H, interfering with the next listed signal), 6.92-6.95 (m, 2H), 7.08-7.64 (br s, 2H, interfering with the next two listed signals), 7.35-7.38 (m, 1H), 7.45-7.55 (m, 4H), 7.67 (s, 1H), 7.77-7.91 (m, 4H), 7.92-8.01 (m, 2H), 8.03-8.11 (m, 1H), 8.25-8.32 (m, 1H), 8.37-8.45 (m, 2H), 8.91 (br s, 1H), 9.15 (s, 1H), 9.76 (br s, 1H). 1 exchangeable proton (NH) of the presumably 2-fold protonated molecule could not be identified. HRMS: *m/z* $[M+2H]^{2+}$ calcd. for $[C_{48}H_{67}N_{13}O_{10}]^{2+}$ 492.7561, found 492.7571. RP-HPLC (220 nm): 99% (t_R = 10.1 min, k = 12.3). $C_{48}H_{65}N_{13}O_{10} \cdot C_4H_2F_6O_4$ (984.13 + 228.05).

cyclo[D-Tyr-*N*ω-[(2-pent-4-ynoylaminoethyl)aminocarbonyl]Arg-Arg-β-(naphtha-2-yl)Ala-Gly] bis(hydrotrifluoroacetate) (5.20). Compound **5.20** was prepared from **5.16** (9.4 mg, 8.1 µmol) and **3.17** (2.1 mg, 10.5 µmol) according to the general procedure for alkynylation. Purification by preparative RP-HPLC (column: Kinetex-XB C18, gradient: 0-35 min: A2/B1 92:8-55:45, t_R = 23 min) yielded **5.20** as white fluffy solid (6.5 mg, 71%). ^{1}H-NMR (600 MHz, DMSO-d_6): δ 1.25-1.45 (m, 5H), 1.50-1.58 (m, 1H), 1.59-1.73 (m, 2H), 2.26-2.29 (m, 2H), 2.32-2.37 (m, 2H), 2.70-2.81 (m, 3H), 3.01-3.05 (m, 2H), 3.12-3.21 (m, 8H), 3.54-3.56 (m, 1H), 3.73-3.77 (m, 1H), 3.91-3.95 (m, 1H), 4.05-4.14 (m, 1H), 4.19-4.28 (m, 1H), 4.30-4.38 (m, 1H), 6.61-6.66 (m, 2H), 6.66-7.08 (br s, 2H, interfering with the next listed signal), 6.92-6.95 (m, 2H), 7.08-7.80 (br s, 2H, interfering with the next three listed signals), 7.34-7.38 (m, 1H), 7.44-7.52 (m, 4H), 7.65-7.68 (m, 1H), 7.80-7.91 (m, 4H), 7.94-8.10 (m, 3H), 8.23-8.54 (m, 4H), 8.87 (br s, 1H), 9.16 (s, 1H), 9.81 (br s, 1H). HRMS: *m/z* $[M+2H]^{2+}$ calcd. for $[C_{44}H_{59}N_{13}O_8]^{2+}$ 448.7299, found 448.7307. RP-HPLC (220 nm): 99% (t_R = 9.5 min, k = 11.5). $C_{44}H_{57}N_{13}O_8 \cdot C_4H_2F_6O_4$ (896.02 + 228.05).

cyclo[D-Tyr-Arg-*N*ω-[*N*-(8-pent-4-ynoylamino-3-6-dioxaoctyl)aminocarbonyl]Arg-β-(naphtha-2-yl)Ala-Gly] bis(hydrotrifluoroacetate) (5.21). Compound **5.21** was prepared from **5.17** (10.0 mg, 8.0 µmol) and **3.17** (2.0 mg, 10.4 µmol) according to the general procedure for alkynylation. Purification by preparative RP-HPLC (column: Kinetex-XB C18, gradient: 0-35 min: A2/B1 92:8-55:45, t_R = 24 min) yielded **5.21** as white fluffy solid (6.6 mg, 68%). ^{1}H-NMR (600 MHz, DMSO-d_6): δ 1.24-1.34 (m, 4H), 1.38-1.44 (m, 1H), 1.50-1.57 (m, 1H), 1.62-1.70 (m, 2H), 2.25-2.28 (m, 2H), 2.32-2.36 (m, 2H), 2.71-2.81 (m, 3H), 2.98-3.05 (m, 2H), 3.11-3.21 (m, 6H), 3.26-3.29 (m, 2H), 3.38-3.40 (m, 2H), 3.47-3.56 (m, 7H), 3.73-3.79 (m, 1H), 3.88-3.95 (m, 1H), 4.06-4.14 (m, 1H), 4.20-4.27 (m, 1H), 4.31-4.39 (m, 1H), 6.63-6.65 (m, 2H), 6.65-7.04 (br s, 2H, interfering with the next listed signal), 6.92-6.95 (m, 2H), 7.04-7.51 (br s, 2H, interfering with the next two listed signals), 7.36-7.38 (m, 1H), 7.41-7.47 (m, 3H), 7.51-7.57 (m, 1H), 7.66 (s, 1H), 7.79-7.85 (m, 4H), 7.93-7.98 (m, 2H), 8.05-8.09 (m, 1H), 8.22-8.50 (m, 4H), 8.92 (br s, 1H), 9.17 (s, 1H), 9.75 (br s, 1H). HRMS: *m/z* $[M+2H]^{2+}$ calcd. for $[C_{48}H_{67}N_{13}O_{10}]^{2+}$ 492.7561, found 492.7569. RP-HPLC (220 nm): 99% (t_R = 10.3 min, k = 12.6). $C_{48}H_{65}N_{13}O_{10} \cdot C_4H_2F_6O_4$ (984.13 + 228.05).

cyclo[D-Tyr-Arg-*N*ω-[(2-pent-4-ynoylaminoethyl)aminocarbonyl]Arg-β-(naphtha-2-yl)Ala-Gly] bis(hydrotrifluoroacetate) (5.22). Compound **5.22** was prepared from **5.18** (9.7 mg, 8.4 µmol) and **3.17** (2.1 mg, 10.9 µmol) according to the general procedure for alkynylation. Purification by preparative RP-HPLC (column: Kinetex-XB C18, gradient: 0-35 min: A2/B1 92:8-55:45, t_R = 23 min) yielded **5.22** as white fluffy solid (6.9 mg, 73%). ^{1}H-NMR (600 MHz, DMSO-d_6): δ 1.25-1.43 (m, 5H), 1.50-1.57 (m, 1H), 1.59-1.71 (m, 2H), 2.25-2.29 (m, 2H), 2.34-2.37 (m, 2H), 2.71-2.81 (m, 3H), 2.99-3.04 (m, 2H), 3.11-3.19 (m,

8H), 3.53-3.56 (m, 1H), 3.74-3.79 (m, 1H), 3.90-3.94 (m, 1H), 4.06-4.16 (m, 1H), 4.20-4.27 (m, 1H), 4.32-4.39 (m, 1H), 6.63-6.66 (m, 2H), 6.66-7.06 (br s, 2H, interfering with the next listed signal), 6.92-6.95 (m, 2H), 7.06-7.78 (br s, 2H, interfering with the next three listed signals), 7.35-7.41 (m, 1H), 7.41-7.54 (m, 4H), 7.65-7.68 (m, 1H), 7.78-7.87 (m, 4H), 7.94-8.03 (m, 2H), 8.06-8.11 (m, 1H), 8.19-8.48 (m, 4H), 8.88 (br s, 1H), 9.17 (s, 1H), 9.85 (br s, 1H). HRMS: *m/z* $[M+2H]^{2+}$ calcd. for $[C_{44}H_{59}N_{13}O_8]^{2+}$ 448.7299, found 448.7307. RP-HPLC (220 nm): 99% (t_R = 9.6 min, k = 11.6). $C_{44}H_{57}N_{13}O_8 \cdot C_4H_2F_6O_4$ (896.02 + 228.05).

cyclo[D-Tyr-*N*ω-{*N*-[8-(3-{1-[1,6-bisdeoxy-6-fluoro-β-D-glucopyranos-1-yl]-1*H*-1,2,3-triazol-4yl}propanoyl)amino-3-6-dioxaoctyl]aminocarbonyl}Arg-Arg-β-(naphtha-2-yl)Ala-Gly] bis(hydrotrifluoroacetate) (5.23). Compound **5.23** was prepared from **5.19** (2.3 mg, 1.91 µmol) and **3.10** (1.0 mg, 4.96 µmol) according to the general procedure for 'click' reactions (modification: shaking of the mixture for 60 min instead of 30 min). Purification by preparative RP-HPLC (column: Gemini-NX C18, gradient: 0-35 min: A2/B1 81:19-62:38, t_R = 15 min) yielded **5.23** as white fluffy solid (0.9 mg, 33%). HRMS: *m/z* $[M+2H]^{2+}$ calcd. for $[C_{54}H_{77}FN_{16}O_{14}]^{2+}$ 596.2889, found 596.2900. RP-HPLC (220 nm): > 99% (t_R = 9.1 min, k = 11.0). $C_{54}H_{75}FN_{16}O_{14} \cdot C_4H_2F_6O_4$ (1191.29 + 228.05).

cyclo[D-Tyr-*N*ω-{[2-(3-{1-[1,6-bisdeoxy-6-fluoro-β-D-glucopyranos-1-yl]-1*H*-1,2,3-triazol-4yl}propanoyl)aminoethyl]aminocarbonyl}Arg-Arg-β-(naphtha-2-yl)Ala-Gly] bis(hydrotrifluoroacetate) (5.24). Compound **5.24** was prepared from **5.20** (3.2 mg, 2.80 µmol) and **3.10** (1.5 mg, 7.29 µmol) according to the general procedure for 'click' reactions. Purification by preparative RP-HPLC (column: Gemini-NX C18, gradient: 0-35 min: A2/B1 81:19-62:38, t_R = 13 min) yielded **5.24** as white fluffy solid (2.2 mg, 58%). HRMS: *m/z* $[M+2H]^{2+}$ calcd. for $[C_{50}H_{69}FN_{16}O_{12}]^{2+}$ 552.2627, found 552.2639. RP-HPLC (220 nm): > 99% (t_R = 8.7 min, k = 10.4). $C_{50}H_{67}FN_{16}O_{12} \cdot C_4H_2F_6O_4$ (1103.18 + 228.05).

cyclo[D-Tyr-Arg-*N*ω-{*N*-[8-(3-{1-[1,6-bisdeoxy-6-fluoro-β-D-glucopyranos-1-yl]-1*H*-1,2,3-triazol-4yl}propanoyl)amino-3-6-dioxaoctyl]aminocarbonyl}Arg-β-(naphtha-2-yl)Ala-Gly] bis(hydrotrifluoroacetate) (5.25). Compound **5.25** was prepared from **5.21** (3.2 mg, 2.61 µmol) and **3.10** (1.4 mg, 6.78 µmol) according to the general procedure for 'click' reactions. Purification by preparative RP-HPLC (column: Gemini-NX C18, gradient: 0-35 min: A2/B1 81:19-62:38, t_R = 14 min) yielded **5.25** as white fluffy solid (2.4 mg, 63%). HRMS: *m/z* $[M+2H]^{2+}$ calcd. for $[C_{54}H_{77}FN_{16}O_{14}]^{2+}$ 596.2889, found 596.2899. RP-HPLC (220 nm): 99% (t_R = 9.1 min, k = 11.0). $C_{54}H_{75}FN_{16}O_{14} \cdot C_4H_2F_6O_4$ (1191.29 + 228.05).

cyclo[D-Tyr-Arg-*N*ω-{[2-(3-{1-[1,6-bisdeoxy-6-fluoro-β-D-glucopyranos-1-yl]-1*H*-1,2,3-triazol-4yl}propanoyl)aminoethyl]aminocarbonyl}Arg-β-(naphtha-2-yl)Ala-Gly] bis(hydrotrifluoroacetate) (5.26). Compound **5.26** was prepared from **5.22** (1.5 mg, 1.29 µmol) and **3.10** (0.70 mg, 3.36 µmol) according to the general procedure for 'click' reactions. Purification by preparative RP-HPLC (column: Gemini-NX C18, gradient: 0-35 min: A2/B1 81:19-62:38, t_R = 13 min) yielded **5.26** as white fluffy solid (0.7 mg, 38%). HRMS: *m/z* $[M+2H]^{2+}$ calcd. for $[C_{50}H_{69}FN_{16}O_{12}]^{2+}$ 552.2627, found 552.2634. RP-HPLC (220 nm): 99% (t_R = 8.5 min, k = 10.2). $C_{50}H_{67}FN_{16}O_{12} \cdot C_4H_2F_6O_4$ (1103.18 + 228.05).

5.4.7 Investigation of the stability of 5.23-5.26 in human plasma

The stabilities of **5.23**-**5.26** against proteolytic degradation were investigated in human blood plasma/PBS pH 7.4 (1:2, v/v) in analogy to a described procedure[62] with the following modifications: 5 mM stock solutions in MeCN/0.04% aq TFA (30:70 v/v) were used throughout for the addition of the peptides to plasma/PBS (1:2 v/v). As the RP-HPLC purity of 1-methyl-D-Trp, used as internal standard (IS) was < 95% (data not shown), the compound was purified by preparative HPLC to give a purity of > 99%. The concentration of the peptides in plasma/PBS (1:2 v/v) was 80 µM and 4 µM (recovery determination) or 100 µM (stability tests). Data analysis was based on UV detection at 220 nm. Reference samples, representing 100% recovery, were prepared in duplicate (**5.23**, **5.24**) or quadruplicate (**5.25**, **5.26**). Recovery ratios were obtained by dividing the recovery of the peptide by the recovery of IS for each individual sample (n = 4-5). The obtained recoveries and the recovery ratios are summarized in Table 5.3.

Table 5.3. Recoveries of peptides **5.23**-**5.26** from human plasma/PBS (1:2 v/v) and ratios of peptide-recovery over recovery of IS.

Compd.	Peptide concentration 80 µM			Peptide concentration 4 µM		
	recovery peptide (%)[a]	recovery IS (%)[a]	ratio[b]	recovery peptide (%)[a]	recovery IS (%)[a]	ratio[b]
5.23	92	101	0.91	110	106	1.04
	91	100	0.92	110	109	1.01
	94	103	0.92	106	100	1.06
	94	101	0.93	109	106	1.03
	96	102	0.94	106	104	1.01
			(0.92 ± 0.01)			(1.03 ± 0.01)
5.24	98	104	0.94	104	101	1.04
	99	108	0.91	104	102	1.02
	100	104	0.96	103	102	1.01
	101	106	0.95	108	103	1.05
	95	102	0.93			
			(0.94 ± 0.01)			(1.03 ± 0.01)
5.25	82	94	0.88	106	100	1.07
	76	87	0.88	104	98	1.06
	77	88	0.87	98	97	1.01
	84	94	0.89	105	98	1.07
				105	103	1.02
			(0.88 ± 0.01)			(1.05 ± 0.01)
5.26	82	98	0.84	100	102	0.98
	87	102	0.85	96	101	0.96
	86	98	0.87	94	95	0.99
	86	97	0.88	97	103	0.94
	88	100	0.88			
			(0.87 ± 0.01)			(0.97 ± 0.01)

[a]Recoveries of the peptides and of IS from human plasma/PBS (1:2 v/v) using a peptide concentration of 80 µM or 4 µM and an IS concentration of 10 µM (four or five independent experiments). [b]Ratios of peptide recovery over recovery of IS calculated for individual experiments, as well as mean recovery ratios ± SEM (given in parenthesis). Note: As the remaining intact peptide concentration in plasma was throughout > 20 µM, recovery ratios based on the 80 µM peptide concentrations were used to calculate peptide recoveries of the plasma stability samples. Recovery ratios based on the 4 µM peptide concentrations were intended to be used for the calculation of peptide recoveries of plasma stability samples with < 20 µM remaining intact peptide (not applied).

5.4.8 CXCR4 mini-G protein recruitment assay

The CXCR4 antagonistic activities of the cyclic peptides **5.15**-**5.26** and the reference compounds **5.03** and **5.04** were assessed in a mini-G protein recruitment assay (performed in antagonist mode) according to a described procedure[71] (note: functional characterization of the described ligands **5.01** and **5.02** was performed elsewhere[71]; due to reasons of consistency raw data for **5.01** and **5.02** were re-analyzed in the present study as described below) using HEK293T cells stably co-expressing NlucN-mGsi and CXCR4-NlucC fusion proteins[71]. In brief, cells were seeded on a white 96-well plate with white bottom (Brand, Wertheim, Germany) in Leibovitz' L-15 medium (Fisher Scientific, Nidderau, Germany) supplemented with 10 mM HEPES (Serva, Heidelberg, Germany), 5% fetal calf serum (FCS; Merck Biochrom, Darmstadt, Germany) and Penicillin-Streptomycin (100 IU/mL and 0.1 mg/mL, respectively) (Sigma-Aldrich, Taufkirchen, Germany) at a density of 1×10^5 cells/well (70 µL medium per well) one day before the experiment. L-15 medium with 10 mM HEPES, 5% FCS, 0.1% BSA and 100 µg/mL bacitracin served as assay buffer and was also used for the preparation of 10-fold concentrated serial dilutions of the test compounds. On the day of the experiment, the substrate furimazine (Promega, Mannheim, Germany; 10 µL, diluted in assay buffer, final dilution = 1:1000) and the antagonist dilutions (10 µL) were added to the cells for preincubation for 15 min, during which the basal luminescence was recorded using an EnSpire plate reader (Perkin Elmer, Rodgau, Germany). The luminescence signal, as a result of split-NanoLuc complementation, was measured for 45 min after the addition of CXCR4 agonist **5.01** (10 µL of a 10-fold concentrated solution in assay buffer) to the cells (final concentration = 33 nM, which corresponds approximately to EC_{80}). Maximal response (100%) values were determined in the absence of antagonist, and L-15 controls (0%) were performed in the absence of both agonist and antagonist. Fluctuations in cell density and substrate concentrations were compensated by dividing the raw relative luminescence units (RLU) for each well after addition of the agonist by the RLU of the same well at the end of the 15 min-basal recording (inter-well correction). Baseline drifts were corrected by dividing the RLU of sample wells by the mean RLU of the L-15 controls. Maximum luminescence values of each sample concentration (determined in triplicate) were normalized by dividing them by the mean maximum luminescence value of the 100% controls. Data analysis was performed by plotting the averaged normalized luminescence intensities over log(concentration of the antagonist) followed by a four-parameter logistic fit (SigmaPlot 12.5, Systat Software). For calculation of the functional parameters of the agonist **5.01**, the maximum intensity values of each agonist sample concentration (performed in triplicate; raw data taken from the Doctoral Thesis of Carina Höring[71]) were normalized by dividing them by the mean maximum intensity value elicited by 3000 nM **5.01**. Data analysis was performed as described for the antagonists. pIC_{50} values of antagonists were converted to IC_{50} values and K_b values were calculated from the IC_{50} values according to the Cheng-Prusoff equation[72] using an EC_{50} value of **5.01** of 6.62 nM. K_b values from individual experiments were transformed to pK_b values, followed by the calculation of mean pK_b values ± SEM.

5.5 References

1. Loetscher, M.; Geiser, T.; O'Reilly, T.; Zwahlen, R.; Baggiolini, M.; Moser, B. Cloning of a human seven-transmembrane domain receptor, LESTR, that is highly expressed in leukocytes. *J Biol Chem* **1994**, *269*, 232-237.

2. Zlotnik, A.; Yoshie, O. Chemokines: A new classification system and their role in immunity. *Immunity* **2000**, *12*, 121-127, doi:10.1016/s1074-7613(00)80165-x.

3. Vassilatis, D.K.; Hohmann, J.G.; Zeng, H.; Li, F.; Ranchalis, J.E.; Mortrud, M.T.; Brown, A.; Rodriguez, S.S.; Weller, J.R.; Wright, A.C.; et al. The G protein-coupled receptor repertoires of human and mouse. *Proc Natl Acad Sci U S A* **2003**, *100*, 4903-4908, doi:10.1073/pnas.0230374100.

4. Murphy, P.M.; Baggiolini, M.; Charo, I.F.; Hebert, C.A.; Horuk, R.; Matsushima, K.; Miller, L.H.; Oppenheim, J.J.; Power, C.A. International union of pharmacology. XXII. Nomenclature for chemokine receptors. *Pharmacol Rev* **2000**, *52*, 145-176.

5. Horuk, R. Chemokine receptors. *Cytokine Growth Factor Rev* **2001**, *12*, 313-335, doi:10.1016/s1359-6101(01)00014-4.

6. Kucia, M.; Jankowski, K.; Reca, R.; Wysoczynski, M.; Bandura, L.; Allendorf, D.J.; Zhang, J.; Ratajczak, J.; Ratajczak, M.Z. CXCR4-SDF-1 signalling, locomotion, chemotaxis and adhesion. *J Mol Histol* **2004**, *35*, 233-245, doi:10.1023/b:hijo.0000032355.66152.b8.

7. Bleul, C.C.; Farzan, M.; Choe, H.; Parolin, C.; Clark-Lewis, I.; Sodroski, J.; Springer, T.A. The lymphocyte chemoattractant SDF-1 is a ligand for LESTR/fusin and blocks HIV-1 entry. *Nature* **1996**, *382*, 829-833, doi:10.1038/382829a0.

8. Oberlin, E.; Amara, A.; Bachelerie, F.; Bessia, C.; Virelizier, J.L.; Arenzana-Seisdedos, F.; Schwartz, O.; Heard, J.M.; Clark-Lewis, I.; Legler, D.F.; et al. The CXC chemokine SDF-1 is the ligand for LESTR/fusin and prevents infection by T-cell-line-adapted HIV-1. *Nature* **1996**, *382*, 833-835, doi:10.1038/382833a0.

9. Balkwill, F. Cancer and the chemokine network. *Nat Rev Cancer* **2004**, *4*, 540-550, doi:10.1038/nrc1388.

10. Teixidó, J.; Martínez-Moreno, M.; Díaz-Martínez, M.; Sevilla-Movilla, S. The good and bad faces of the CXCR4 chemokine receptor. *Int J Biochem Cell Biol* **2018**, *95*, 121-131, doi:10.1016/j.biocel.2017.12.018.

11. Shirozu, M.; Nakano, T.; Inazawa, J.; Tashiro, K.; Tada, H.; Shinohara, T.; Honjo, T. Structure and chromosomal localization of the human stromal cell-derived factor 1 (SDF1) gene. *Genomics* **1995**, *28*, 495-500, doi:10.1006/geno.1995.1180.

12. Baggiolini, M.; Dewald, B.; Moser, B. Interleukin-8 and related chemotactic cytokines--CXC and CC chemokines. *Adv Immunol* **1994**, *55*, 97-179.

13. Springer, T.A. Traffic signals on endothelium for lymphocyte recirculation and leukocyte emigration. *Annu Rev Physiol* **1995**, *57*, 827-872, doi:10.1146/annurev.ph.57.030195.004143.

14. Zlotnik, A.; Yoshie, O. The chemokine superfamily revisited. *Immunity* **2012**, *36*, 705-716, doi:10.1016/j.immuni.2012.05.008.

15. Nagasawa, T.; Hirota, S.; Tachibana, K.; Takakura, N.; Nishikawa, S.; Kitamura, Y.; Yoshida, N.; Kikutani, H.; Kishimoto, T. Defects of B-cell lymphopoiesis and bone-marrow myelopoiesis in mice lacking the CXC chemokine PBSF/SDF-1. *Nature* **1996**, *382*, 635-638, doi:10.1038/382635a0.

16. Nagasawa, T.; Tachibana, K.; Kishimoto, T. A novel CXC chemokine PBSF/SDF-1 and its receptor CXCR4: Their functions in development, hematopoiesis and HIV infection. *Semin Immunol* **1998**, *10*, 179-185, doi:10.1006/smim.1998.0128.

17. Zou, Y.R.; Kottmann, A.H.; Kuroda, M.; Taniuchi, I.; Littman, D.R. Function of the chemokine receptor CXCR4 in haematopoiesis and in cerebellar development. *Nature* **1998**, *393*, 595-599, doi:10.1038/31269.

18. Ma, Q.; Jones, D.; Borghesani, P.R.; Segal, R.A.; Nagasawa, T.; Kishimoto, T.; Bronson, R.T.; Springer, T.A. Impaired B-lymphopoiesis, myelopoiesis, and derailed cerebellar neuron migration in CXCR4- and SDF-1-deficient mice. *Proc Natl Acad Sci U S A* **1998**, *95*, 9448-9453, doi:10.1073/pnas.95.16.9448.

19. Taichman, R.S.; Cooper, C.; Keller, E.T.; Pienta, K.J.; Taichman, N.S.; McCauley, L.K. Use of the stromal cell-derived factor-1/CXCR4 pathway in prostate cancer metastasis to bone. *Cancer Res* **2002**, *62*, 1832-1837.

20. Sun, Y.X.; Wang, J.; Shelburne, C.E.; Lopatin, D.E.; Chinnaiyan, A.M.; Rubin, M.A.; Pienta, K.J.; Taichman, R.S. Expression of CXCR4 and CXCL12 (SDF-1) in human prostate cancers (PCa) in vivo. *J Cell Biochem* **2003**, *89*, 462-473, doi:10.1002/jcb.10522.

21. Müller, A.; Homey, B.; Soto, H.; Ge, N.; Catron, D.; Buchanan, M.E.; McClanahan, T.; Murphy, E.; Yuan, W.; Wagner, S.N.; et al. Involvement of chemokine receptors in breast cancer metastasis. *Nature* **2001**, *410*, 50-56, doi:10.1038/35065016.

22. Kucia, M.; Reca, R.; Miekus, K.; Wanzeck, J.; Wojakowski, W.; Janowska-Wieczorek, A.; Ratajczak, J.; Ratajczak, M.Z. Trafficking of normal stem cells and metastasis of cancer stem cells involve similar mechanisms: Pivotal role of the SDF-1-CXCR4 axis. *Stem Cells* **2005**, *23*, 879-894, doi:10.1634/stemcells.2004-0342.

23. Furusato, B.; Mohamed, A.; Uhlén, M.; Rhim, J.S. CXCR4 and cancer. *Pathol Int* **2010**, *60*, 497-505, doi:10.1111/j.1440-1827.2010.02548.x.

24. Tanaka, T.; Bai, Z.; Srinoulprasert, Y.; Yang, B.G.; Hayasaka, H.; Miyasaka, M. Chemokines in tumor progression and metastasis. *Cancer Sci* **2005**, *96*, 317-322, doi:10.1111/j.1349-7006.2005.00059.x.

25. Zlotnik, A. Involvement of chemokine receptors in organ-specific metastasis. *Contrib Microbiol* **2006**, *13*, 191-199, doi:10.1159/000092973.

26. Balkwill, F. The significance of cancer cell expression of the chemokine receptor CXCR4. *Semin Cancer Biol* **2004**, *14*, 171-179, doi:10.1016/j.semcancer.2003.10.003.

27. Zhou, Y.; Larsen, P.H.; Hao, C.; Yong, V.W. CXCR4 is a major chemokine receptor on glioma cells and mediates their survival. *J Biol Chem* **2002**, *277*, 49481-49487, doi:10.1074/jbc.M206222200.

28. Broxmeyer, H.E.; Cooper, S.; Kohli, L.; Hangoc, G.; Lee, Y.; Mantel, C.; Clapp, D.W.; Kim, C.H. Transgenic expression of stromal cell-derived factor-1/CXC chemokine ligand 12 enhances myeloid progenitor cell survival/antiapoptosis in vitro in response to growth factor withdrawal and enhances myelopoiesis in vivo. *J Immunol* **2003**, *170*, 421-429, doi:10.4049/jimmunol.170.1.421.

29. Feng, Y.; Broder, C.C.; Kennedy, P.E.; Berger, E.A. HIV-1 entry cofactor: Functional cDNA cloning of a seven-transmembrane, G protein-coupled receptor. *Science* **1996**, *272*, 872-877, doi:10.1126/science.272.5263.872.

30. Murakami, T.; Nakajima, T.; Koyanagi, Y.; Tachibana, K.; Fujii, N.; Tamamura, H.; Yoshida, N.; Waki, M.; Matsumoto, A.; Yoshie, O.; et al. A small molecule CXCR4 inhibitor that blocks T cell line-tropic HIV-1 infection. *J Exp Med* **1997**, *186*, 1389-1393, doi:10.1084/jem.186.8.1389.

31. Tamamura, H.; Xu, Y.; Hattori, T.; Zhang, X.; Arakaki, R.; Kanbara, K.; Omagari, A.; Otaka, A.; Ibuka, T.; Yamamoto, N.; et al. A low-molecular-weight inhibitor against the chemokine receptor CXCR4: A strong anti-HIV peptide T140. *Biochem Biophys Res Commun* **1998**, *253*, 877-882, doi:10.1006/bbrc.1998.9871.

32. Tsutsumi, H.; Tanaka, T.; Ohashi, N.; Masuno, H.; Tamamura, H.; Hiramatsu, K.; Araki, T.; Ueda, S.; Oishi, S.; Fujii, N. Therapeutic potential of the chemokine receptor CXCR4 antagonists as multifunctional agents. *Biopolymers* **2007**, *88*, 279-289, doi:10.1002/bip.20653.

33. Silvin, A.; Chapuis, N.; Dunsmore, G.; Goubet, A.G.; Dubuisson, A.; Derosa, L.; Almire, C.; Hénon, C.; Kosmider, O.; Droin, N.; et al. Elevated calprotectin and abnormal myeloid cell subsets discriminate severe from mild COVID-19. *Cell* **2020**, *182*, 1401-1418, doi:10.1016/j.cell.2020.08.002.

34. Khalil, B.A.; Elemam, N.M.; Maghazachi, A.A. Chemokines and chemokine receptors during COVID-19 infection. *Comput Struct Biotechnol J* **2021**, *19*, 976-988, doi:10.1016/j.csbj.2021.01.034.

35. Mamazhakypov, A.; Viswanathan, G.; Lawrie, A.; Schermuly, R.T.; Rajagopal, S. The role of chemokines and chemokine receptors in pulmonary arterial hypertension. *Br J Pharmacol* **2021**, *178*, 72-89, doi:10.1111/bph.14826.

36. Neidleman, J.; Luo, X.; George, A.F.; McGregor, M.; Yang, J.; Yun, C.; Murray, V.; Gill, G.; Greene, W.C.; Vasquez, J.; et al. Distinctive features of SARS-CoV-2-specific T cells predict recovery from severe COVID-19. *Cell reports* **2021**, *36*, 109414, doi:10.1101/2021.01.22.21250054.

37. Daoud, S.; Taha, M. Ligand-based modeling of CXC chemokine receptor 4 and identification of inhibitors of novel chemotypes as potential leads towards new anti-COVID-19 treatments. *Med Chem* **2022**, *18*, 871-883, doi:10.2174/1573406418666220118153541.

38. Fujii, N.; Oishi, S.; Hiramatsu, K.; Araki, T.; Ueda, S.; Tamamura, H.; Otaka, A.; Kusano, S.; Terakubo, S.; Nakashima, H.; et al. Molecular-size reduction of a potent CXCR4-chemokine antagonist using orthogonal combination of conformation- and sequence-based libraries. *Angew Chem Int Ed Engl* **2003**, *42*, 3251-3253, doi:10.1002/anie.200351024.

39. Demmer, O.; Gourni, E.; Schumacher, U.; Kessler, H.; Wester, H.J. PET imaging of CXCR4 receptors in cancer by a new optimized ligand. *ChemMedChem* **2011**, *6*, 1789-1791, doi:10.1002/cmdc.201100320.

40. Keller, M.; Kuhn, K.K.; Einsiedel, J.; Hübner, H.; Biselli, S.; Mollereau, C.; Wifling, D.; Svobodová, J.; Bernhardt, G.; Cabrele, C.; et al. Mimicking of arginine by functionalized N^{ω}-carbamoylated arginine as a new broadly applicable approach to labeled bioactive peptides: High affinity angiotensin, neuropeptide Y, neuropeptide FF, and neurotensin receptor ligands as examples. *J Med Chem* **2016**, *59*, 1925-1945, doi:10.1021/acs.jmedchem.5b01495.

41. Maschauer, S.; Haubner, R.; Kuwert, T.; Prante, O. ^{18}F-Glyco-RGD peptides for PET imaging of integrin expression: Efficient radiosynthesis by click chemistry and modulation of biodistribution by glycosylation. *Mol Pharm* **2014**, *11*, 505-515, doi:10.1021/mp4004817.

42. Gourni, E.; Demmer, O.; Schottelius, M.; D'Alessandria, C.; Schulz, S.; Dijkgraaf, I.; Schumacher, U.; Schwaiger, M.; Kessler, H.; Wester, H.J. PET of CXCR4 expression by a ^{68}Ga-labeled highly specific targeted contrast agent. *J Nucl Med* **2011**, *52*, 1803-1810, doi:10.2967/jnumed.111.098798.

43. Philipp-Abbrederis, K.; Herrmann, K.; Knop, S.; Schottelius, M.; Eiber, M.; Lückerath, K.; Pietschmann, E.; Habringer, S.; Gerngross, C.; Franke, K.; et al. *In vivo* molecular imaging of chemokine receptor CXCR4 expression in patients with advanced multiple myeloma. *EMBO Mol Med* **2015**, *7*, 477-487, doi:10.15252/emmm.201404698.

44. Lapa, C.; Lückerath, K.; Rudelius, M.; Schmid, J.S.; Schoene, A.; Schirbel, A.; Samnick, S.; Pelzer, T.; Buck, A.K.; Kropf, S.; et al. [^{68}Ga]Pentixafor-PET/CT for imaging of chemokine receptor 4 expression in small cell lung cancer--initial experience. *Oncotarget* **2016**, *7*, 9288-9295, doi:10.18632/oncotarget.7063.

45. Lapa, C.; Schreder, M.; Schirbel, A.; Samnick, S.; Kortüm, K.M.; Herrmann, K.; Kropf, S.; Einsele, H.; Buck, A.K.; Wester, H.J.; et al. [^{68}Ga]Pentixafor-PET/CT for imaging of chemokine receptor CXCR4 expression in multiple myeloma - Comparison to [^{18}F]FDG and laboratory values. *Theranostics* **2017**, *7*, 205-212, doi:10.7150/thno.16576.

46. Buck, A.K.; Haug, A.; Dreher, N.; Lambertini, A.; Higuchi, T.; Lapa, C.; Weich, A.; Pomper, M.G.; Wester, H.J.; Zehnder, A.; et al. Imaging of C-X-C motif chemokine receptor 4 expression in 690 patients with solid or hematologic neoplasms using ^{68}Ga-pentixaFor PET. *J Nucl Med* **2022**, *63*, 1687-1692, doi:10.2967/jnumed.121.263693.

47. Wester, H.J.; Keller, U.; Schottelius, M.; Beer, A.; Philipp-Abbrederis, K.; Hoffmann, F.; Simeček, J.; Gerngross, C.; Lassmann, M.; Herrmann, K.; et al.

Disclosing the CXCR4 expression in lymphoproliferative diseases by targeted molecular imaging. *Theranostics* **2015**, *5*, 618-630, doi:10.7150/thno.11251.

48. Herhaus, P.; Lipkova, J.; Lammer, F.; Yakushev, I.; Vag, T.; Slotta-Huspenina, J.; Habringer, S.; Lapa, C.; Pukrop, T.; Hellwig, D.; et al. CXCR4-targeted PET imaging of central nervous system B-cell lymphoma. *J Nucl Med* **2020**, *61*, 1765-1771, doi:10.2967/jnumed.120.241703.

49. Mayerhoefer, M.E.; Raderer, M.; Lamm, W.; Pichler, V.; Pfaff, S.; Weber, M.; Kiesewetter, B.; Hacker, M.; Kazianka, L.; Staber, P.B.; et al. CXCR4 PET imaging of mantle cell lymphoma using [^{68}Ga]Pentixafor: Comparison with [^{18}F]FDG-PET. *Theranostics* **2021**, *11*, 567-578, doi:10.7150/thno.48620.

50. Walenkamp, A.M.E.; Lapa, C.; Herrmann, K.; Wester, H.J. CXCR4 ligands: The next big hit? *J Nucl Med* **2017**, *58*, 77S-82S, doi:10.2967/jnumed.116.186874.

51. Habringer, S.; Lapa, C.; Herhaus, P.; Schottelius, M.; Istvanffy, R.; Steiger, K.; Slotta-Huspenina, J.; Schirbel, A.; Hänscheid, H.; Kircher, S.; et al. Dual targeting of acute leukemia and supporting niche by CXCR4-directed theranostics. *Theranostics* **2018**, *8*, 369-383, doi:10.7150/thno.21397.

52. George, G.P.C.; Pisaneschi, F.; Nguyen, Q.D.; Aboagye, E.O. Positron emission tomographic imaging of CXCR4 in cancer: Challenges and promises. *Mol Imaging* **2015**, *14*, 1-19, doi:10.2310/7290.2014.00041.

53. Åberg, O.; Pisaneschi, F.; Smith, G.; Nguyen, Q.D.; Stevens, E.; Aboagye, E.O. ^{18}F-labelling of a cyclic pentapeptide inhibitor of the chemokine receptor CXCR4. *J Fluorine Chem* **2012**, *135*, 200-206, doi:10.1016/j.jfluchem.2011.11.003.

54. George, G.P.C.; Pisaneschi, F.; Stevens, E.; Nguyen, Q.D.; Åberg, O.; Spivey, A.C.; Aboagye, E.O. Scavenging strategy for specific activity improvement: Application to a new CXCR4-specific cyclopentapeptide positron emission tomography tracer. *J Labelled Compd Rad* **2013**, *56*, 679-685, doi:10.1002/jlcr.3095.

55. Poschenrieder, A.; Osl, T.; Schottelius, M.; Hoffmann, F.; Wirtz, M.; Schwaiger, M.; Wester, H.J. First ^{18}F-labeled pentixafor-based imaging agent for PET imaging of CXCR4 expression in vivo. *Tomography* **2016**, *2*, 85-93, doi:10.18383/j.tom.2016.00130.

56. Alluri, S.R.; Higashi, Y.; Kil, K.E. PET imaging radiotracers of chemokine receptors. *Molecules* **2021**, *26*, 5174, doi:10.3390/molecules26175174.

57. Spinnler, K.; von Krüchten, L.; Konieczny, A.; Schindler, L.; Bernhardt, G.; Keller, M. An alkyne-functionalized arginine for solid-phase synthesis enabling "bioorthogonal" peptide conjugation. *ACS Med Chem Lett* **2020**, *11*, 334-339, doi:10.1021/acsmedchemlett.9b00388.

58. Miller, S.C.; Scanlan, T.S. Site-selective N-methylation of peptides on solid support. *J Am Chem Soc* **1997**, *119*, 2301-2302, doi:10.1021/ja9635443.

59. Schindler, L.; Wohlfahrt, K.; Gluhacevic von Krüchten, L.; Prante, O.; Keller, M.; Maschauer, S. Neurotensin analogs by fluoroglycosylation at N^{ω}-carbamoylated arginines for PET imaging of NTS1-positive tumors. *Sci Rep* **2022**, *12*, 15028, doi:10.1038/s41598-022-19296-0.

60. Schindler, L.; Moosbauer, J.; Schmidt, D.; Spruss, T.; Grätz, L.; Lüdeke, S.; Hofheinz, F.; Meister, S.; Echtenacher, B.; Bernhardt, G.; et al. Development of a neurotensin-derived ^{68}Ga-labeled PET ligand with high in vivo stability for imaging of NTS_1 receptor-expressing tumors. *Cancers (Basel)* **2022**, *14*, 4922, doi:10.3390/cancers14194922.

61. Eaton, B.; Gold, L. Parallel SELEX allowing for asymmetrical reactions in combinatorial chemistry. U.S. Patent, US5858660A, 1999.

62. Schindler, L.; Bernhardt, G.; Keller, M. Modifications at Arg and Ile give neurotensin(8-13) derivatives with high stability and retained NTS_1 receptor affinity. *ACS Med Chem Lett* **2019**, *10*, 960-965, doi:10.1021/acsmedchemlett.9b00122.

63. Adessi, C.; Soto, C. Converting a peptide into a drug: Strategies to improve stability and bioavailability. *Curr Med Chem* **2002**, *9*, 963-978, doi:10.2174/0929867024606731.

64. Marsault, E.; Peterson, M.L. Macrocycles are great cycles: Applications, opportunities, and challenges of synthetic macrocycles in drug discovery. *J Med Chem* **2011**, *54*, 1961-2004, doi:10.1021/jm1012374.

65. Räder, A.F.B.; Reichart, F.; Weinmüller, M.; Kessler, H. Improving oral bioavailability of cyclic peptides by *N*-methylation. *Bioorg Med Chem* **2018**, *26*, 2766-2773, doi:10.1016/j.bmc.2017.08.031.

66. Fisher, J.F.; Harrison, A.W.; Bundy, G.L.; Wilkinson, K.F.; Rush, B.D.; Ruwart, M.J. Peptide to glycopeptide: Glycosylated oligopeptide renin inhibitors with attenuated in vivo clearance properties. *J Med Chem* **1991**, *34*, 3140-3143, doi:10.1021/jm00114a026.

67. Albert, R.; Marbach, P.; Bauer, W.; Briner, U.; Fricker, G.; Bruns, C.; Pless, J. SDZ CO 611: A highly potent glycated analog of somatostatin with improved oral activity. *Life Sci* **1993**, *53*, 517-525, doi:10.1016/0024-3205(93)90703-6.

68. Marastoni, M.; Spisani, S.; Tomatis, R. Synthesis and biological activity of D-glucopyranosyl peptide T derivatives. *Arzneimittelforschung* **1994**, *44*, 984-987.

69. Kihlberg, J.; Ahman, J.; Walse, B.; Drakenberg, T.; Nilsson, A.; Soderbergahlm, C.; Bengtsson, B.; Olsson, H. Glycosylated peptide hormones: Pharmacological properties and conformational studies of analogues of [1-desamino,8-D-arginine]vasopressin. *J Med Chem* **1995**, *38*, 161-169, doi:10.1021/jm00001a021.

70. Haubner, R.; Kuhnast, B.; Mang, C.; Weber, W.A.; Kessler, H.; Wester, H.J.; Schwaiger, M. [^{18}F]Galacto-RGD: Synthesis, radiolabeling, metabolic stability, and radiation dose estimates. *Bioconjug Chem* **2004**, *15*, 61-69, doi:10.1021/bc034170n.

71. Höring, C. Split-luciferase complementation and molecular dynamics studies for the mini-G protein-based functional characterization of GPCRs. Doctoral thesis, Regensburg, **2022**.

72. Cheng, Y.; Prusoff, W.H. Relationship between the inhibition constant (K_I) and the concentration of inhibitor which causes 50 per cent inhibition (I_{50}) of an enzymatic

reaction. *Biochem Pharmacol* **1973**, *22*, 3099-3108, doi:10.1016/0006-2952(73)90196-2.

73. Spiller, S.; Wippold, T.; Bellmann-Sickert, K.; Franz, S.; Saalbach, A.; Anderegg, U.; Beck-Sickinger, A.G. Protease-triggered release of stabilized CXCL12 from coated scaffolds in an ex vivo wound model. *Pharmaceutics* **2021**, *13*, doi:10.3390/pharmaceutics13101597.

74. Thiele, S.; Mungalpara, J.; Steen, A.; Rosenkilde, M.M.; Våbenø, J. Determination of the binding mode for the cyclopentapeptide CXCR4 antagonist FC131 using a dual approach of ligand modifications and receptor mutagenesis. *Br J Pharmacol* **2014**, *171*, 5313-5329, doi:10.1111/bph.12842.

75. Poschenrieder, A.; Schottelius, M.; Schwaiger, M.; Wester, H.J. Preclinical evaluation of [^{68}Ga]NOTA-pentixafor for PET imaging of CXCR4 expression in vivo - A comparison to [^{68}Ga]pentixafor. *EJNMMI Res* **2016**, *6*, 70-74, doi:10.1186/s13550-016-0227-2.

76. Schottelius, M.; Osl, T.; Poschenrieder, A.; Hoffmann, F.; Beykan, S.; Hänscheid, H.; Schirbel, A.; Buck, A.K.; Kropf, S.; Schwaiger, M.; et al. [^{177}Lu]pentixather: Comprehensive preclinical characterization of a first CXCR4-directed endoradiotherapeutic agent. *Theranostics* **2017**, *7*, 2350-2362, doi:10.7150/thno.19119.

77. Osl, T.; Schmidt, A.; Schwaiger, M.; Schottelius, M.; Wester, H.J. A new class of PentixaFor- and PentixaTher-based theranostic agents with enhanced CXCR4-targeting efficiency. *Theranostics* **2020**, *10*, 8264-8280, doi:10.7150/thno.45537.

78. Ueda, S.; Oishi, S.; Wang, Z.X.; Araki, T.; Tamamura, H.; Cluzeau, J.; Ohno, H.; Kusano, S.; Nakashima, H.; Trent, J.O.; et al. Structure-activity relationships of cyclic peptide-based chemokine receptor CXCR4 antagonists: Disclosing the importance of side-chain and backbone functionalities. *J Med Chem* **2007**, *50*, 192-198, doi:10.1021/jm0607350.

79. Herrmann, K.; Schottelius, M.; Lapa, C.; Osl, T.; Poschenrieder, A.; Hänscheid, H.; Lückerath, K.; Schreder, M.; Bluemel, C.; Knott, M.; et al. First-in-human experience of CXCR4-directed endoradiotherapy with ^{177}Lu- and ^{90}Y-labeled pentixather in advanced-stage multiple myeloma with extensive intra- and extramedullary disease. *J Nucl Med* **2016**, *57*, 248-251, doi:10.2967/jnumed.115.167361.

80. Lapa, C.; Herrmann, K.; Schirbel, A.; Hänscheid, H.; Lückerath, K.; Schottelius, M.; Kircher, M.; Werner, R.A.; Schreder, M.; Samnick, S.; et al. CXCR4-directed endoradiotherapy induces high response rates in extramedullary relapsed multiple myeloma. *Theranostics* **2017**, *7*, 1589-1597, doi:10.7150/thno.19050.

81. Kircher, M.; Herhaus, P.; Schottelius, M.; Buck, A.K.; Werner, R.A.; Wester, H.J.; Keller, U.; Lapa, C. CXCR4-directed theranostics in oncology and inflammation. *Ann Nucl Med* **2018**, *32*, 503-511, doi:10.1007/s12149-018-1290-8.

82. Lapa, C.; Hänscheid, H.; Kircher, M.; Schirbel, A.; Wunderlich, G.; Werner, R.A.; Samnick, S.; Kotzerke, J.; Einsele, H.; Buck, A.K.; et al. Feasibility of CXCR4-

directed radioligand therapy in advanced diffuse large B-cell lymphoma. *J Nucl Med* **2019**, *60*, 60-64, doi:10.2967/jnumed.118.210997.

83. Maurer, S.; Herhaus, P.; Lippenmeyer, R.; Hänscheid, H.; Kircher, M.; Schirbel, A.; Maurer, H.C.; Buck, A.K.; Wester, H.J.; Einsele, H.; et al. Side effects of CXC-chemokine receptor 4-directed endoradiotherapy with pentixather before hematopoietic stem cell transplantation. *J Nucl Med* **2019**, *60*, 1399-1405, doi:10.2967/jnumed.118.223420.

84. Linde, P.; Baues, C.; Wegen, S.; Trommer, M.; Quaas, A.; Rosenbrock, J.; Celik, E.; Marnitz, S.; Bruns, C.J.; Fischer, T.; et al. Pentixafor PET/CT for imaging of chemokine receptor 4 expression in esophageal cancer - a first clinical approach. *Cancer Imaging* **2021**, *21*, 22, doi:10.1186/s40644-021-00391-w.

5.6 Appendix

5.6.1 RP-HPLC chromatograms of compounds 5.03, 5.04 and 5.15-5.26

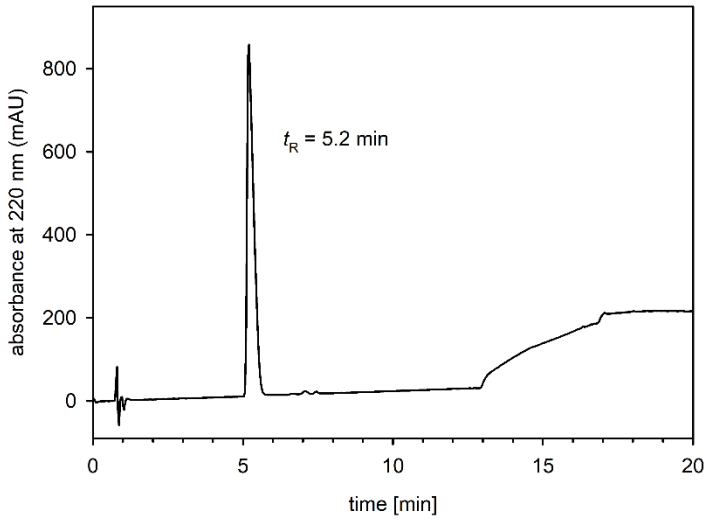

RP-HPLC analysis (purity control) of compound **5.03**

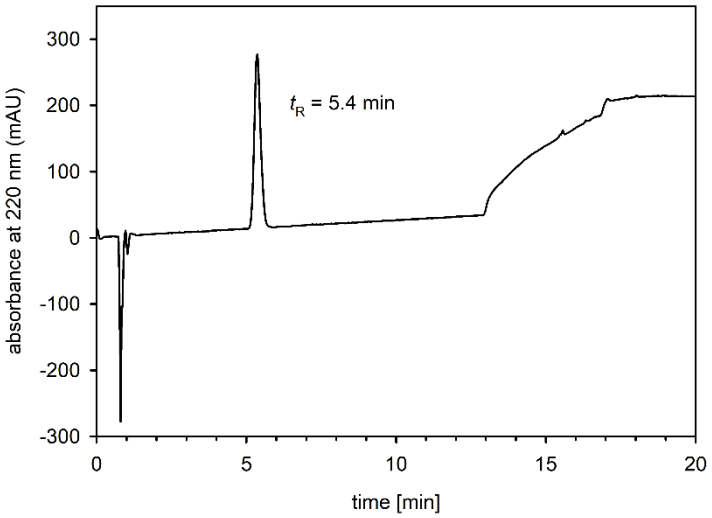

RP-HPLC analysis (purity control) of compound **5.04**

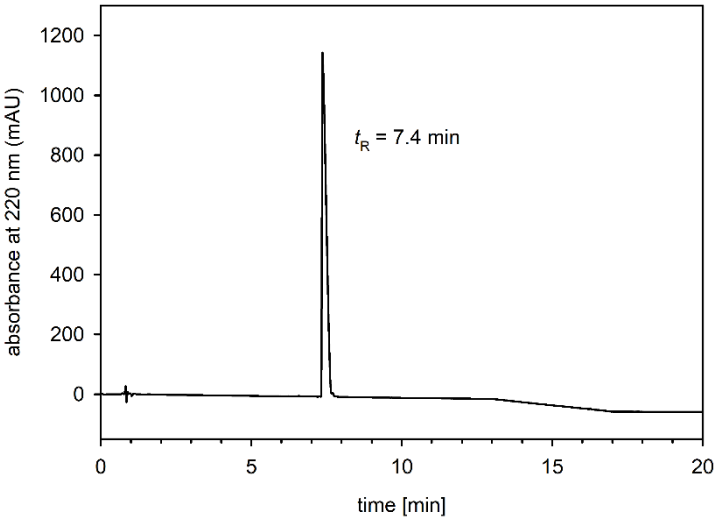

RP-HPLC analysis (purity control) of compound **5.15**

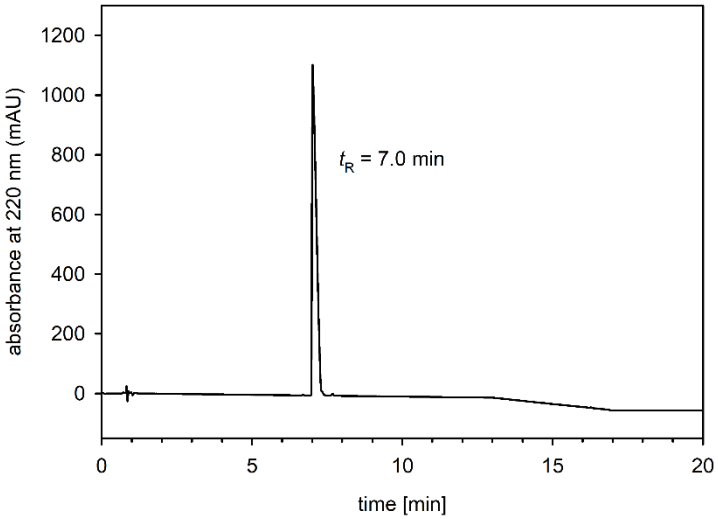

RP-HPLC analysis (purity control) of compound **5.16**

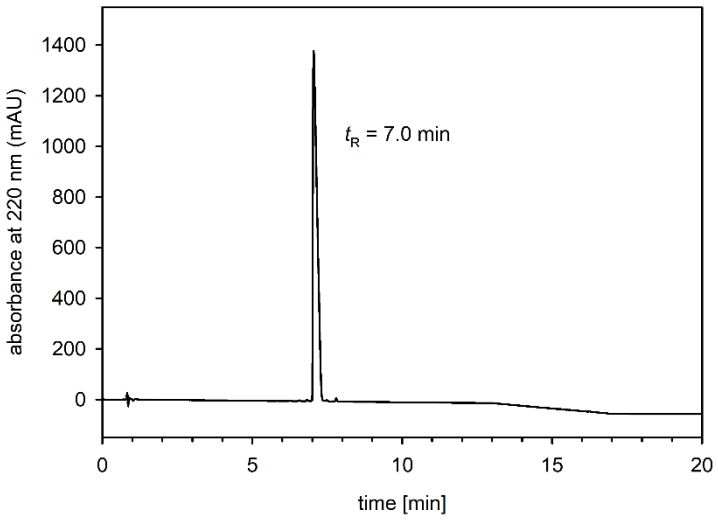

RP-HPLC analysis (purity control) of compound **5.17**

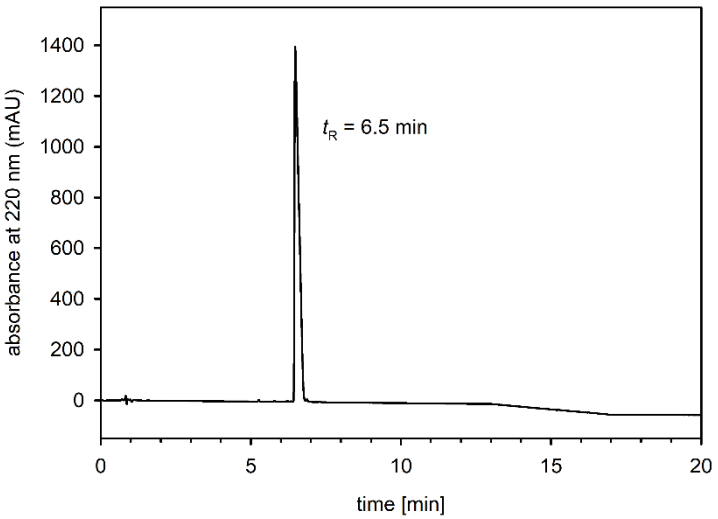

RP-HPLC analysis (purity control) of compound **5.18**

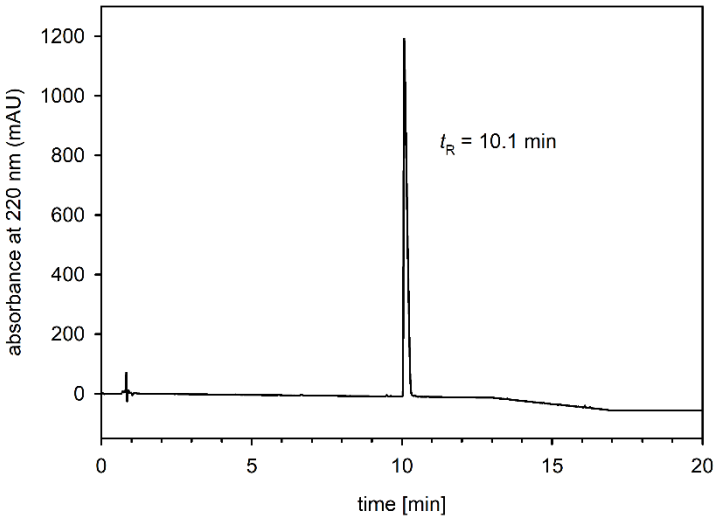

RP-HPLC analysis (purity control) of compound **5.19**

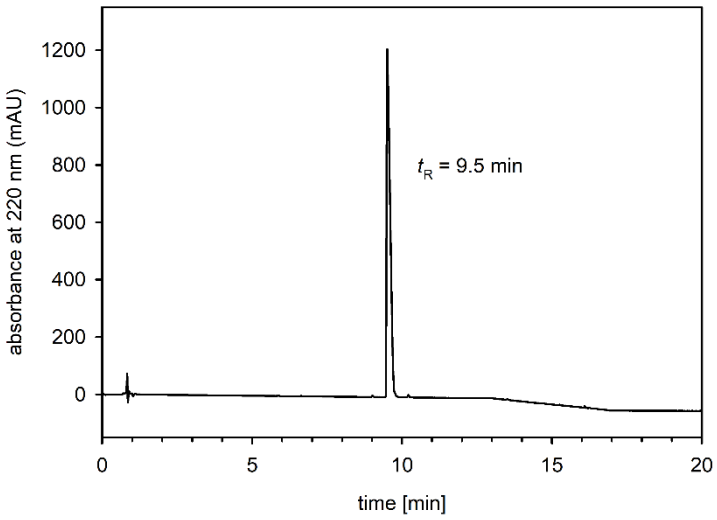

RP-HPLC analysis (purity control) of compound **5.20**

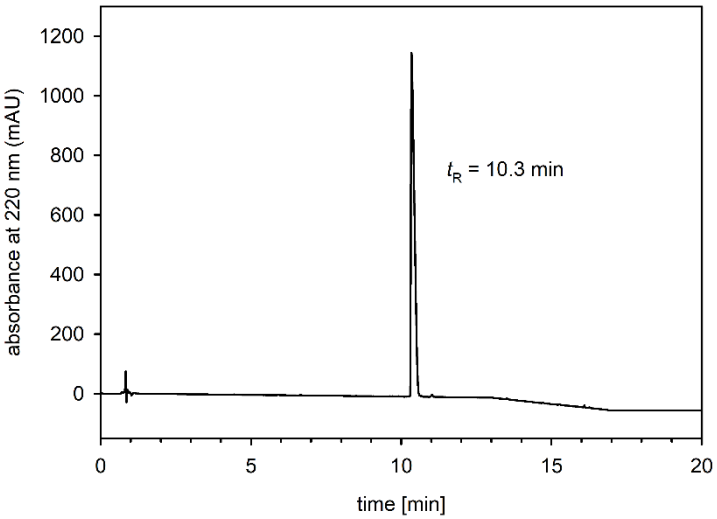

RP-HPLC analysis (purity control) of compound **5.21**

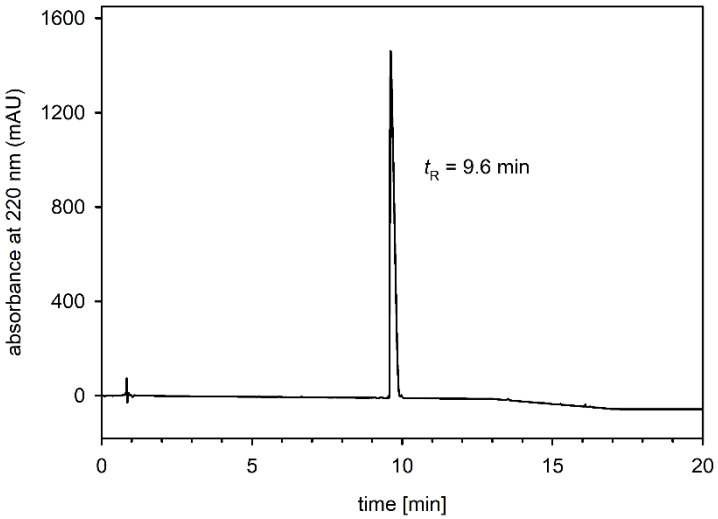

RP-HPLC analysis (purity control) of compound **5.22**

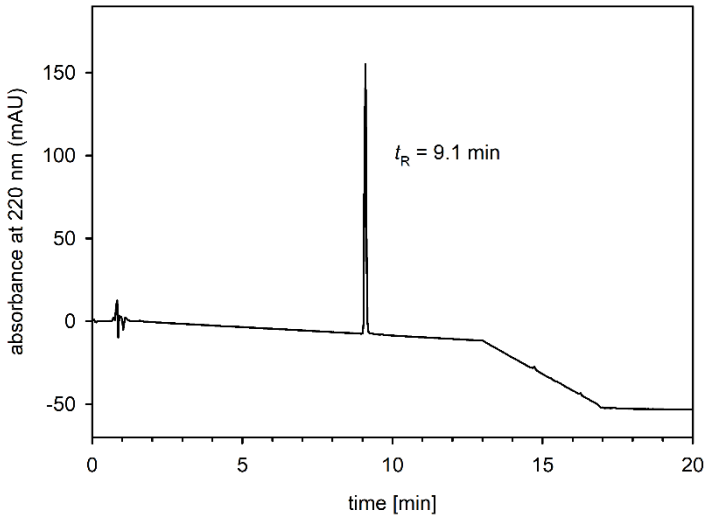

RP-HPLC analysis (purity control) of compound **5.23**

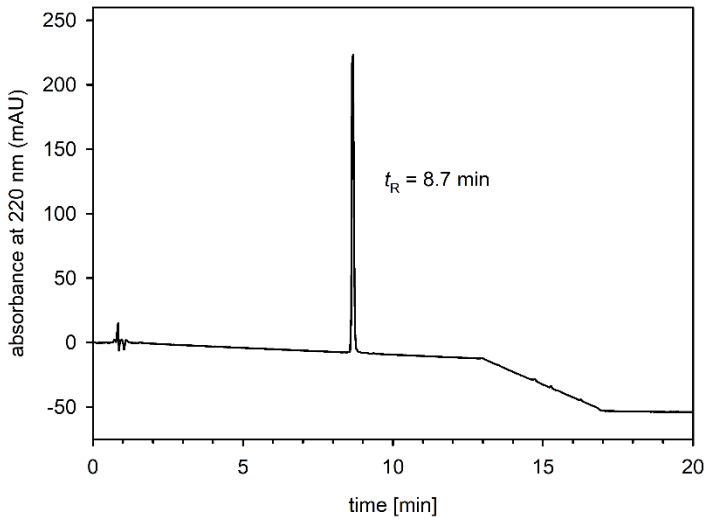

RP-HPLC analysis (purity control) of compound **5.24**

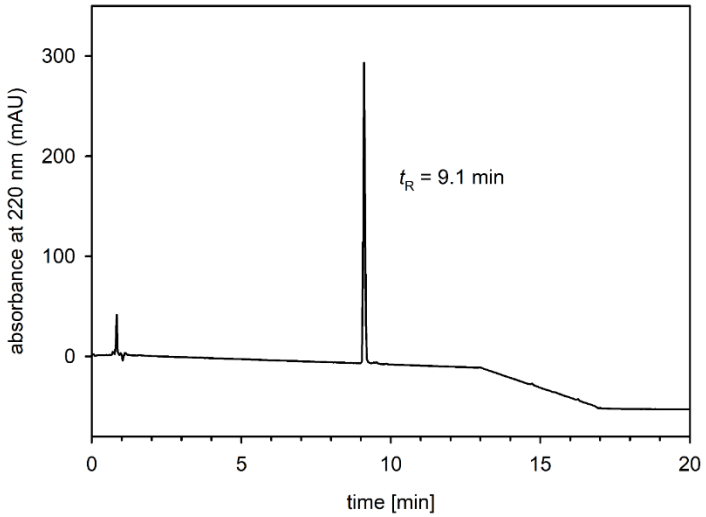

RP-HPLC analysis (purity control) of compound **5.25**

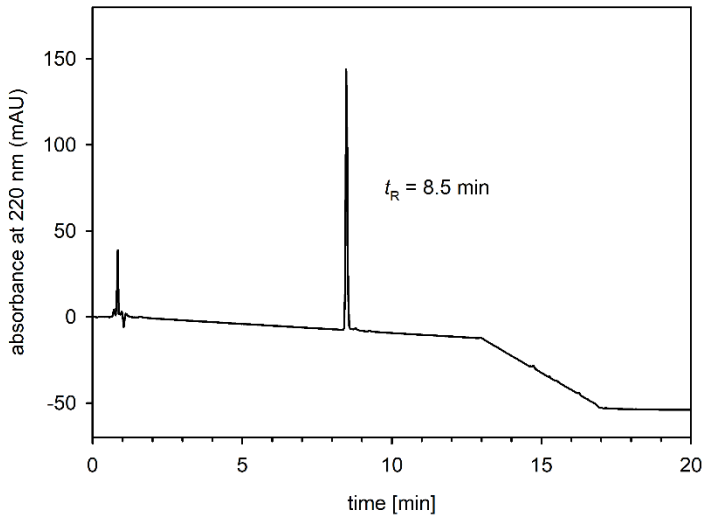

RP-HPLC analysis (purity control) of compound **5.26**

5.6.2 ^{1}H-NMR spectra of compounds 5.03, 5.04 and 5.15-5.22, and ^{13}C-NMR spectra of compounds 5.15-5.18

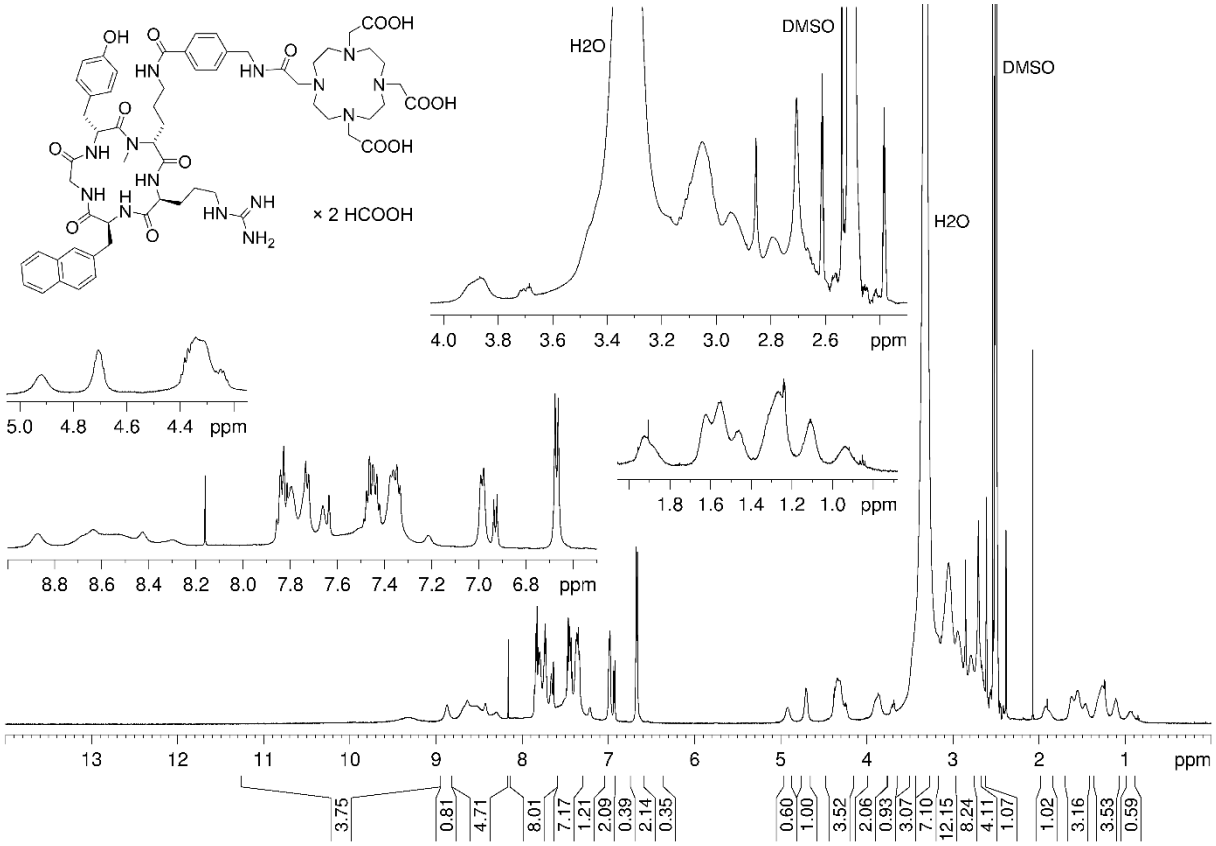

^{1}H-NMR spectrum (600 MHz, DMSO-d_6) of compound **5.03**

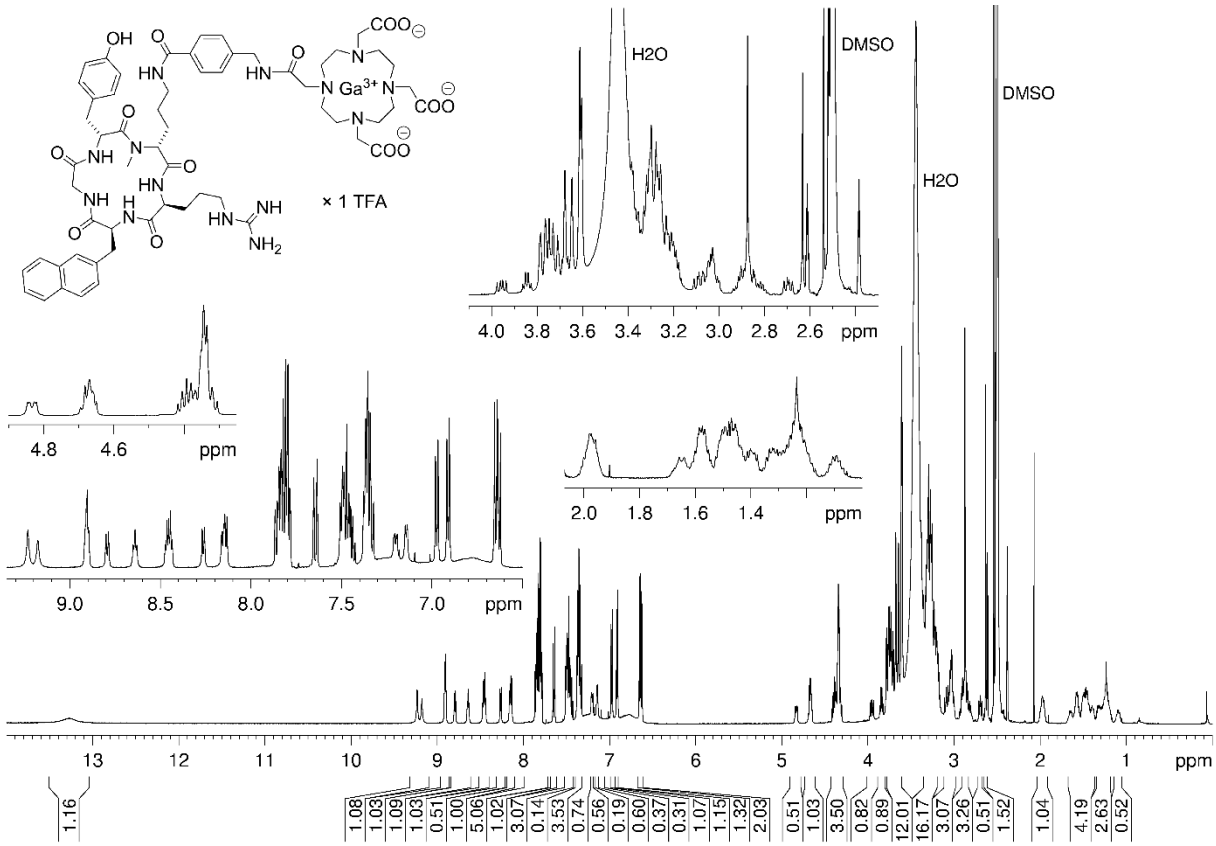

^{1}H-NMR spectrum (600 MHz, DMSO-d_6) of compound **5.04**

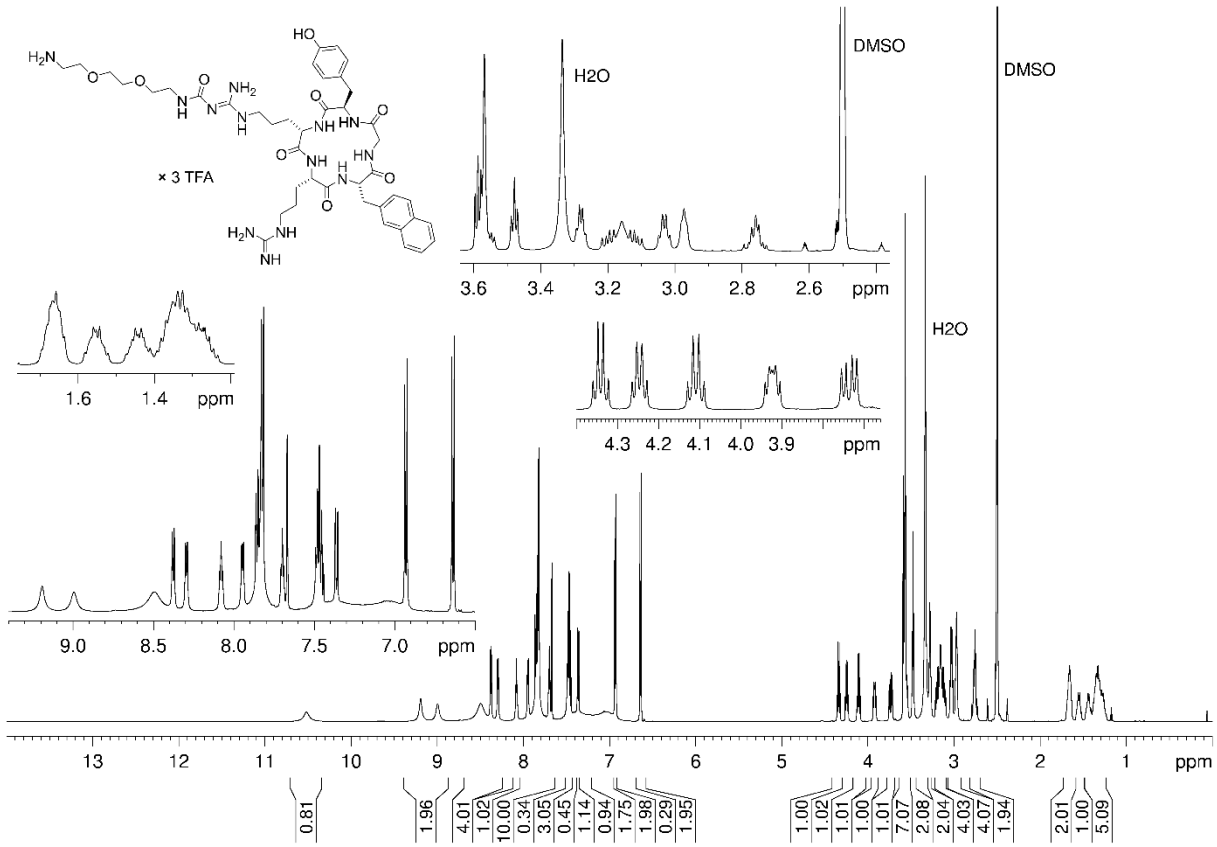

^{1}H-NMR spectrum (600 MHz, DMSO-d_6) of compound **5.15**

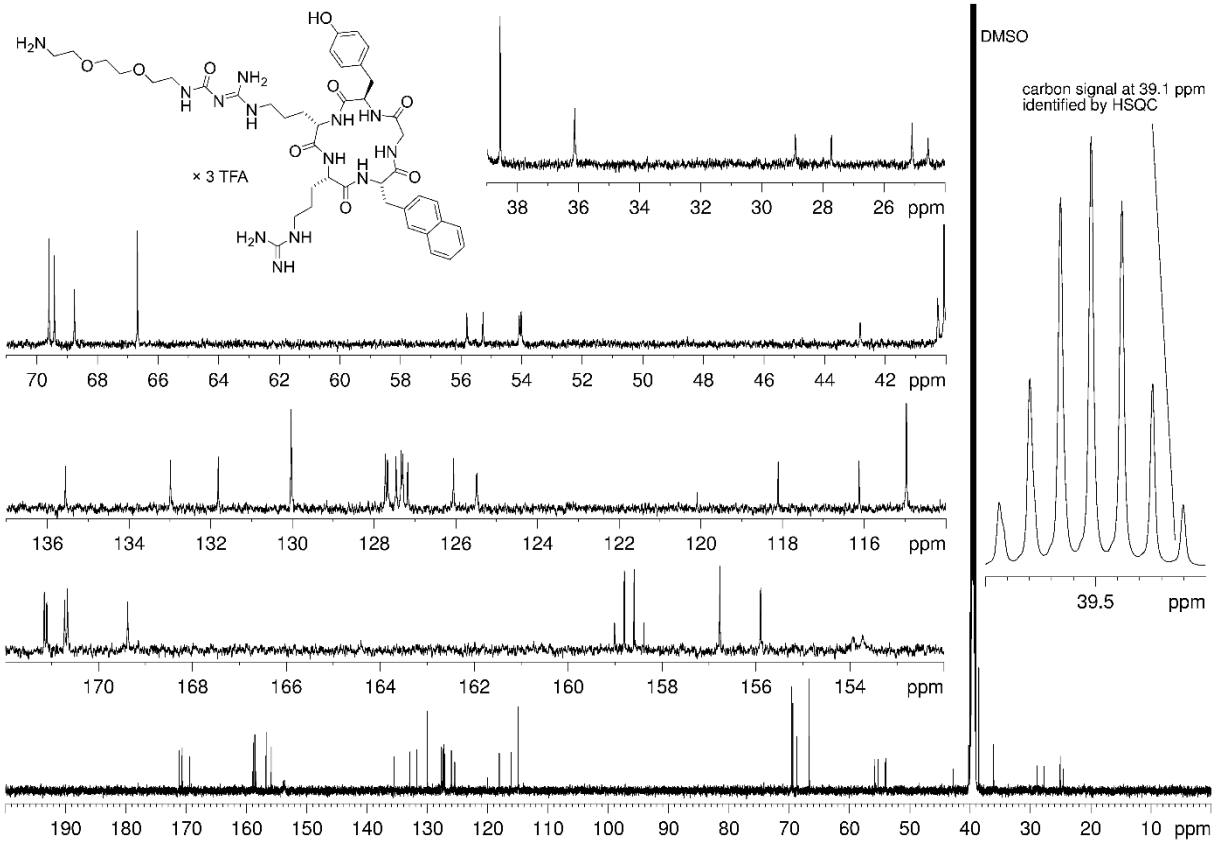

^{13}C-NMR spectrum (151 MHz, DMSO-d_6) of compound **5.15**

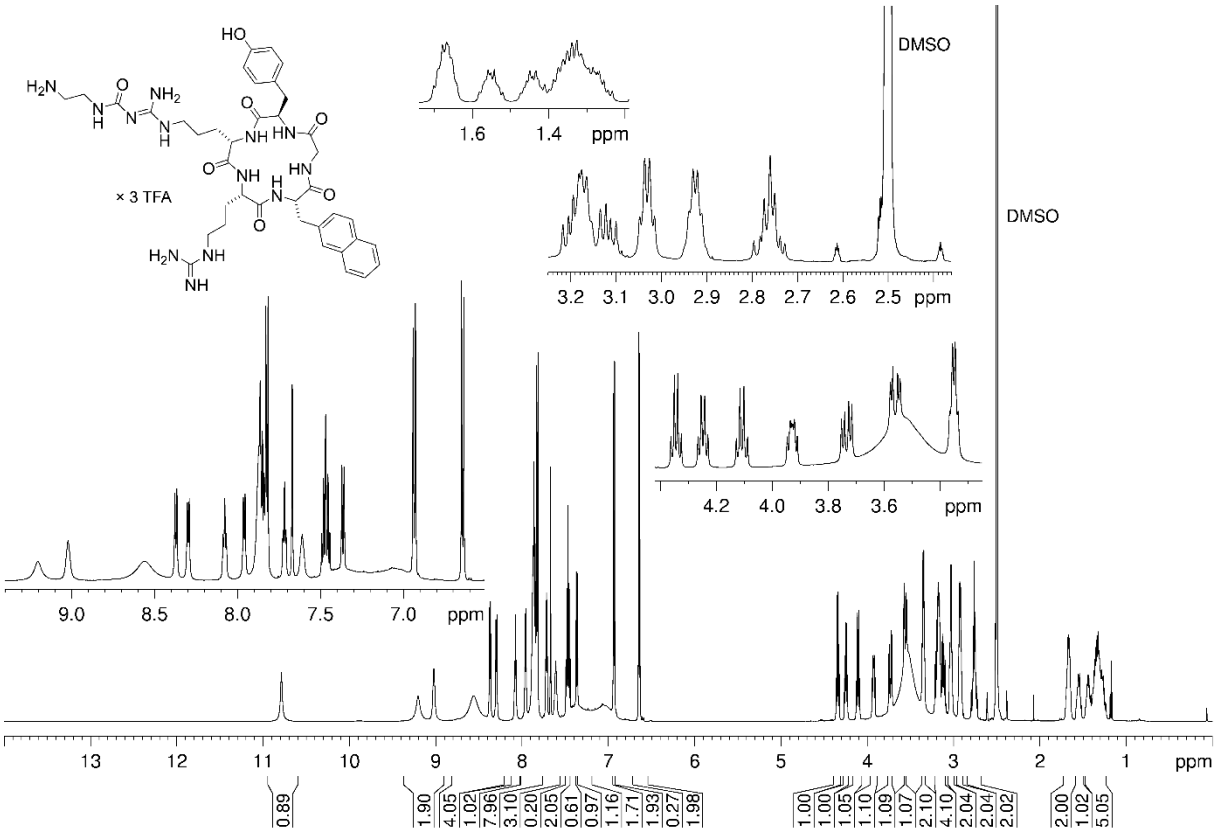

^{1}H-NMR spectrum (600 MHz, DMSO-d_6) of compound **5.16**

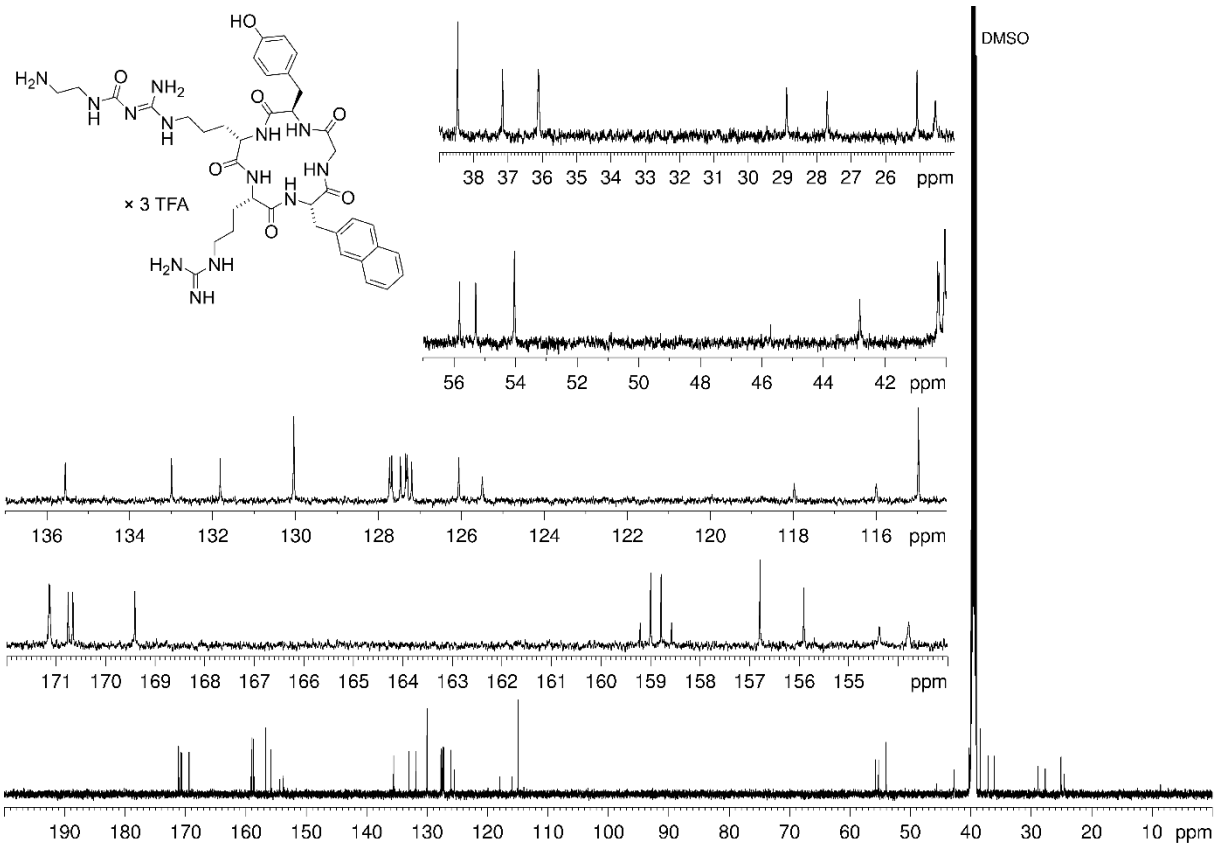

^{13}C-NMR spectrum (151 MHz, DMSO-d_6) of compound **5.16**

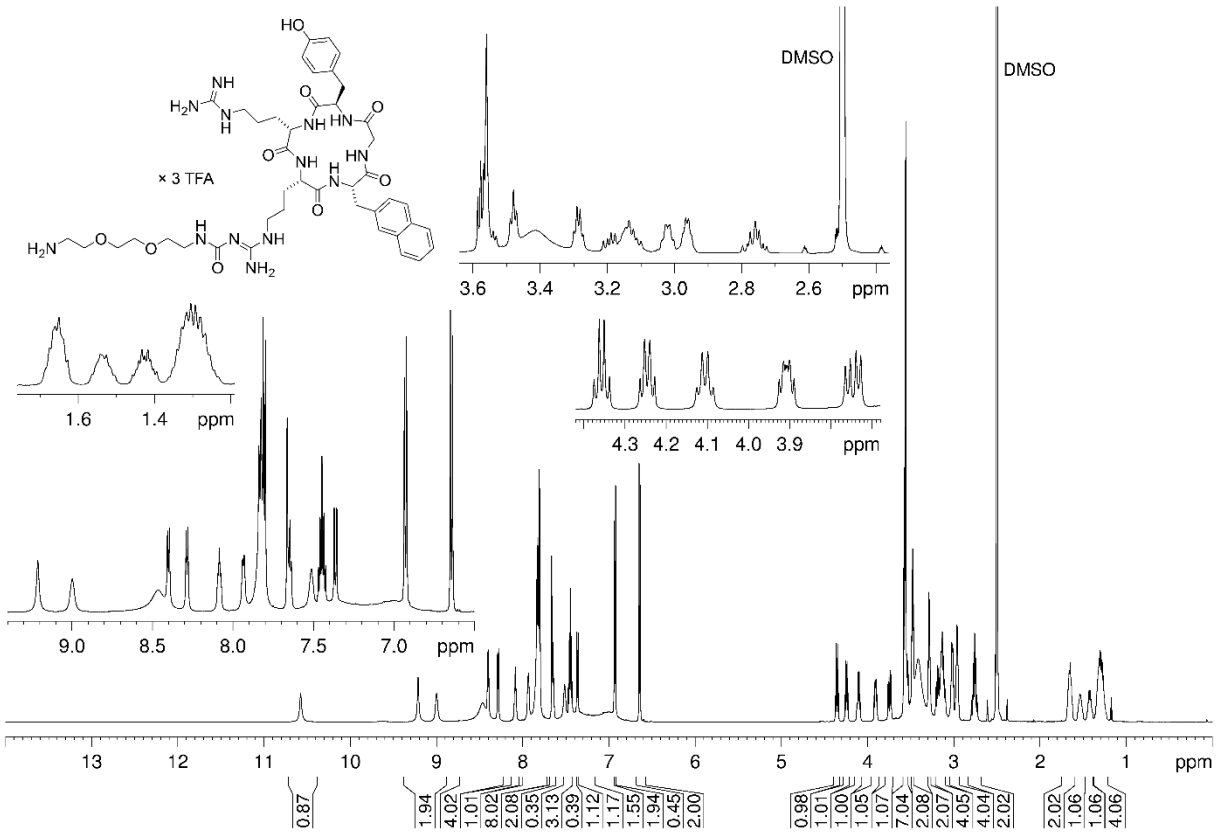

^{1}H-NMR spectrum (600 MHz, DMSO-d_6) of compound **5.17**

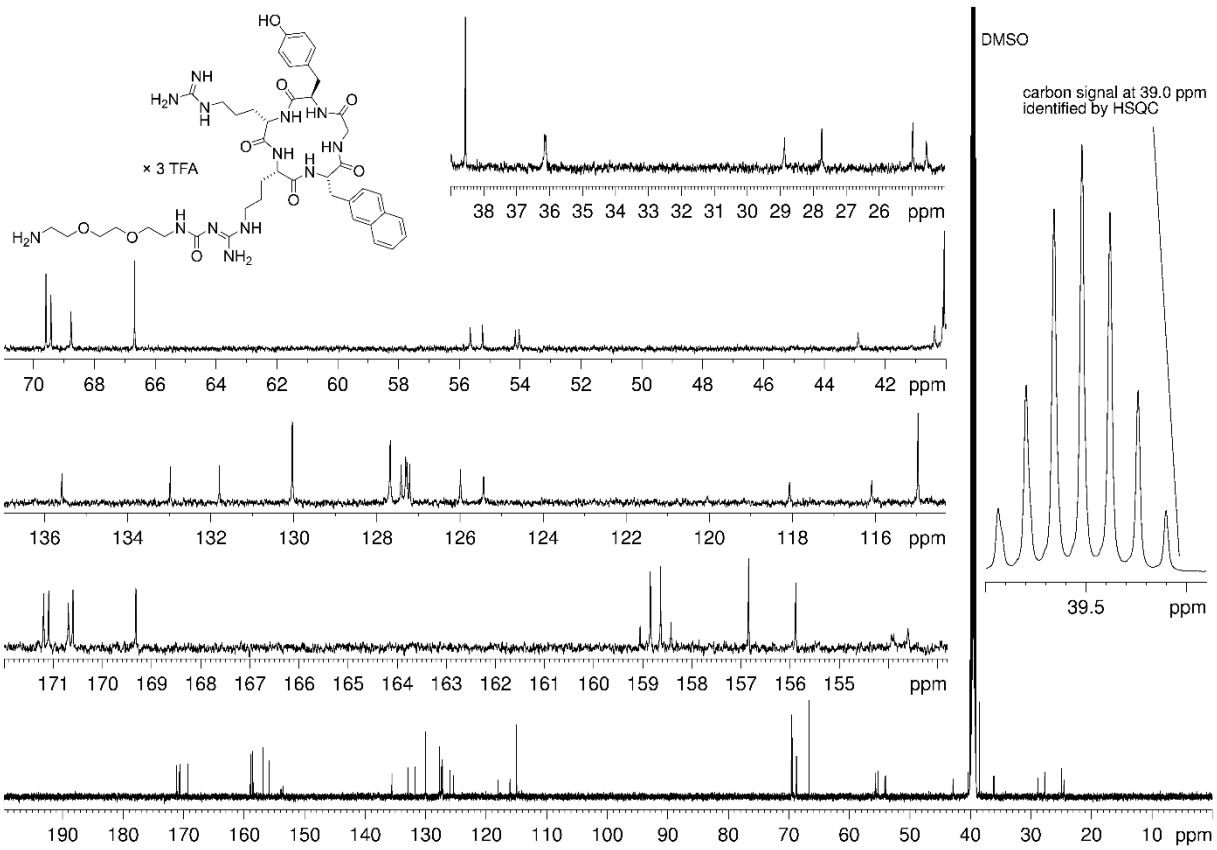

^{13}C-NMR spectrum (151 MHz, DMSO-d_6) of compound **5.17**

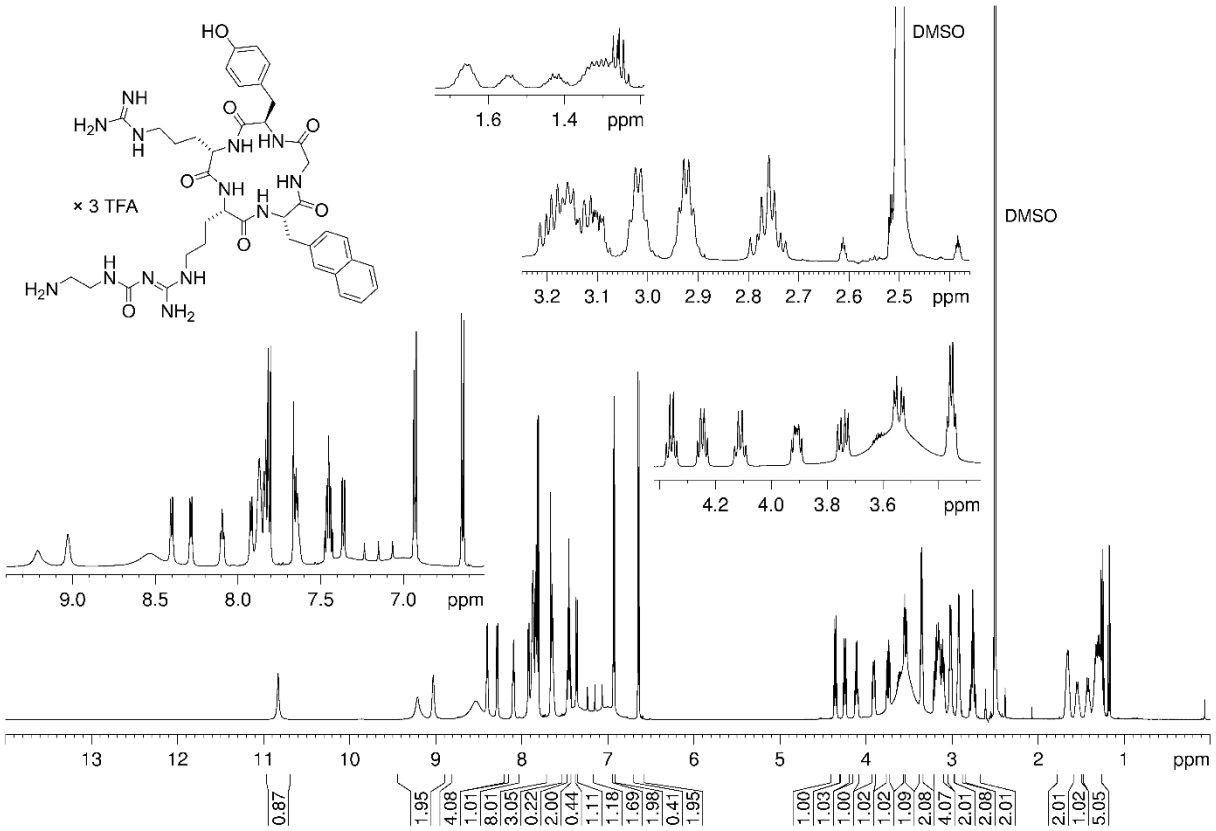

^{1}H-NMR spectrum (600 MHz, DMSO-d_6) of compound **5.18**

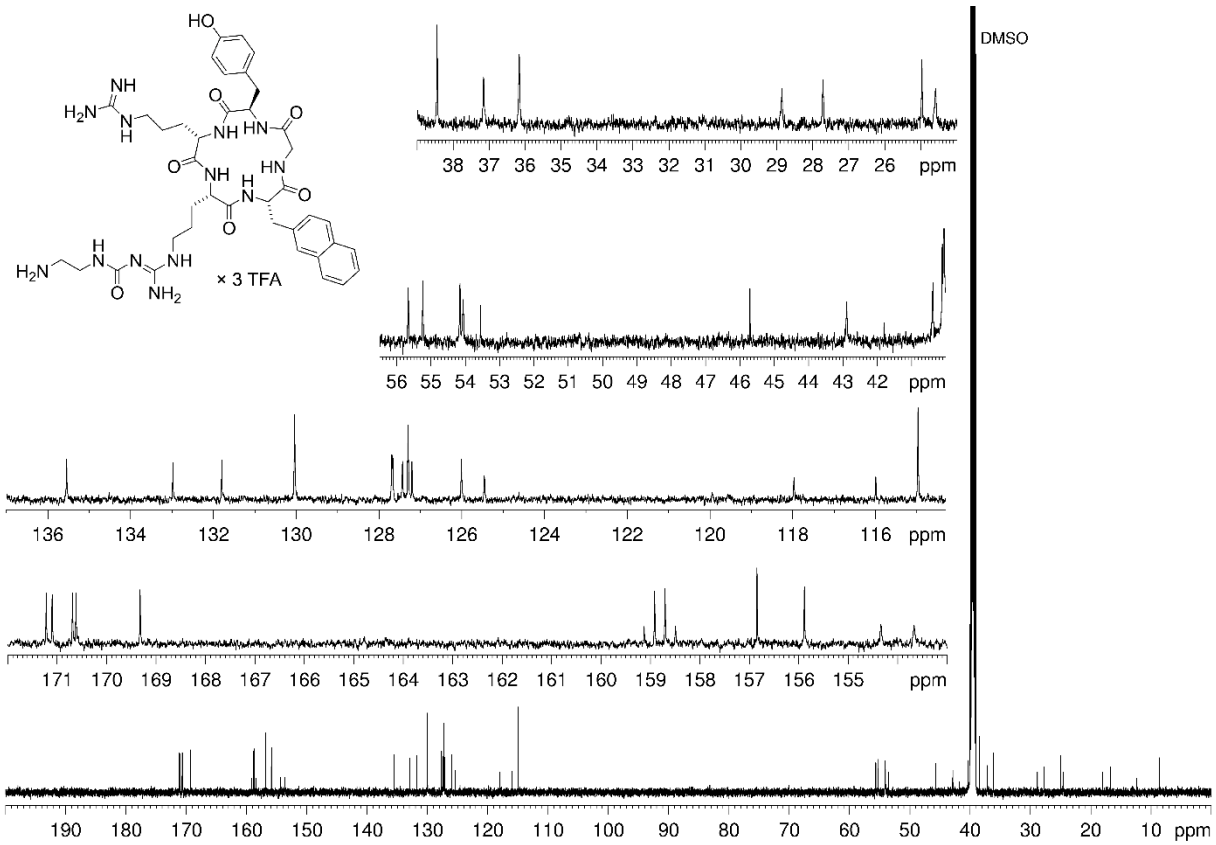

^{13}C-NMR spectrum (151 MHz, DMSO-d_6) of compound **5.18**

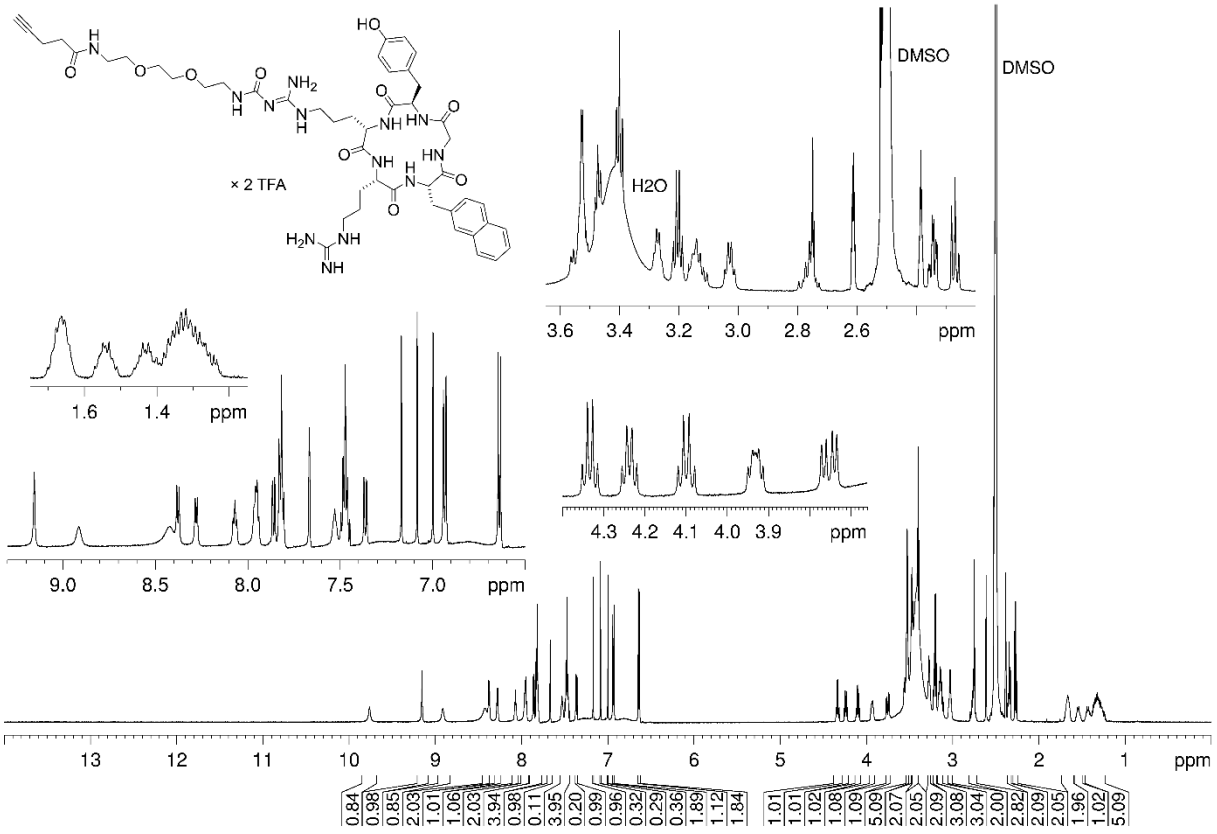

^{1}H-NMR spectrum (600 MHz, DMSO-d_6) of compound **5.19**

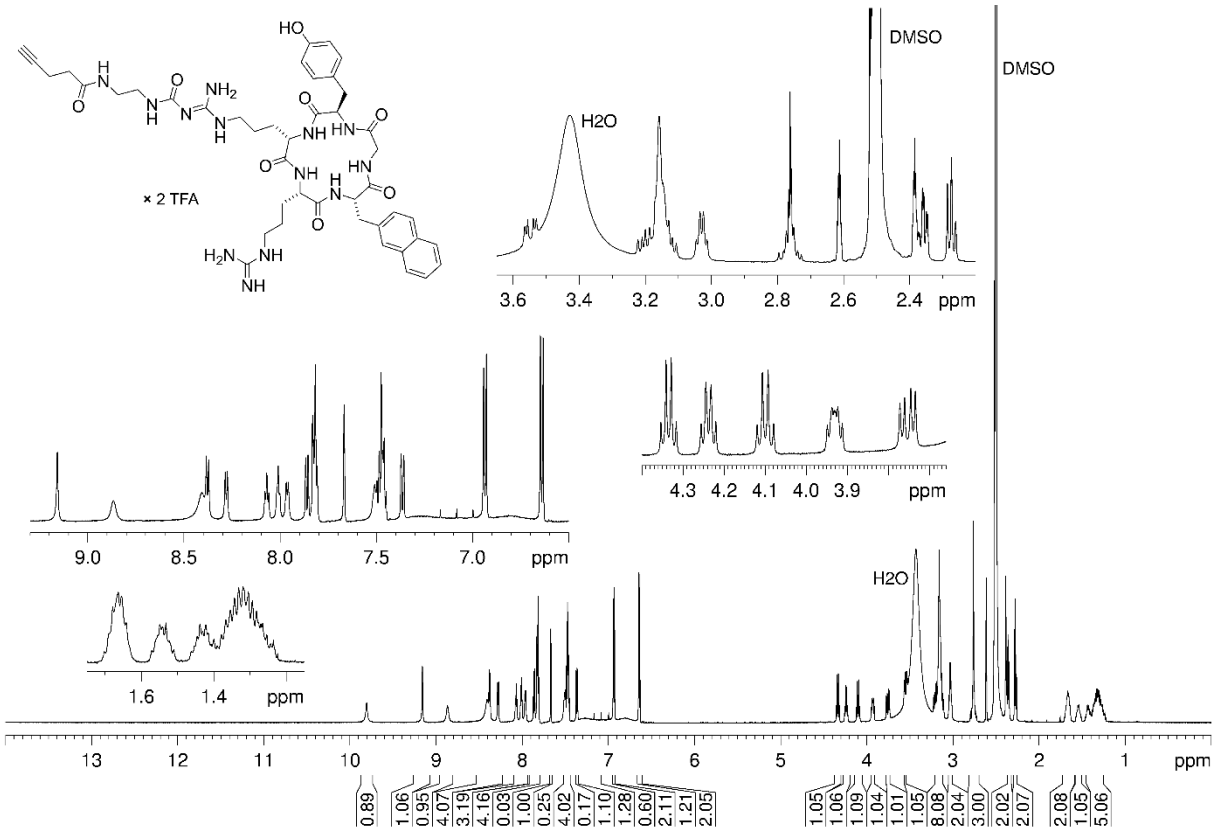

^{1}H-NMR spectrum (600 MHz, DMSO-d_6) of compound **5.20**

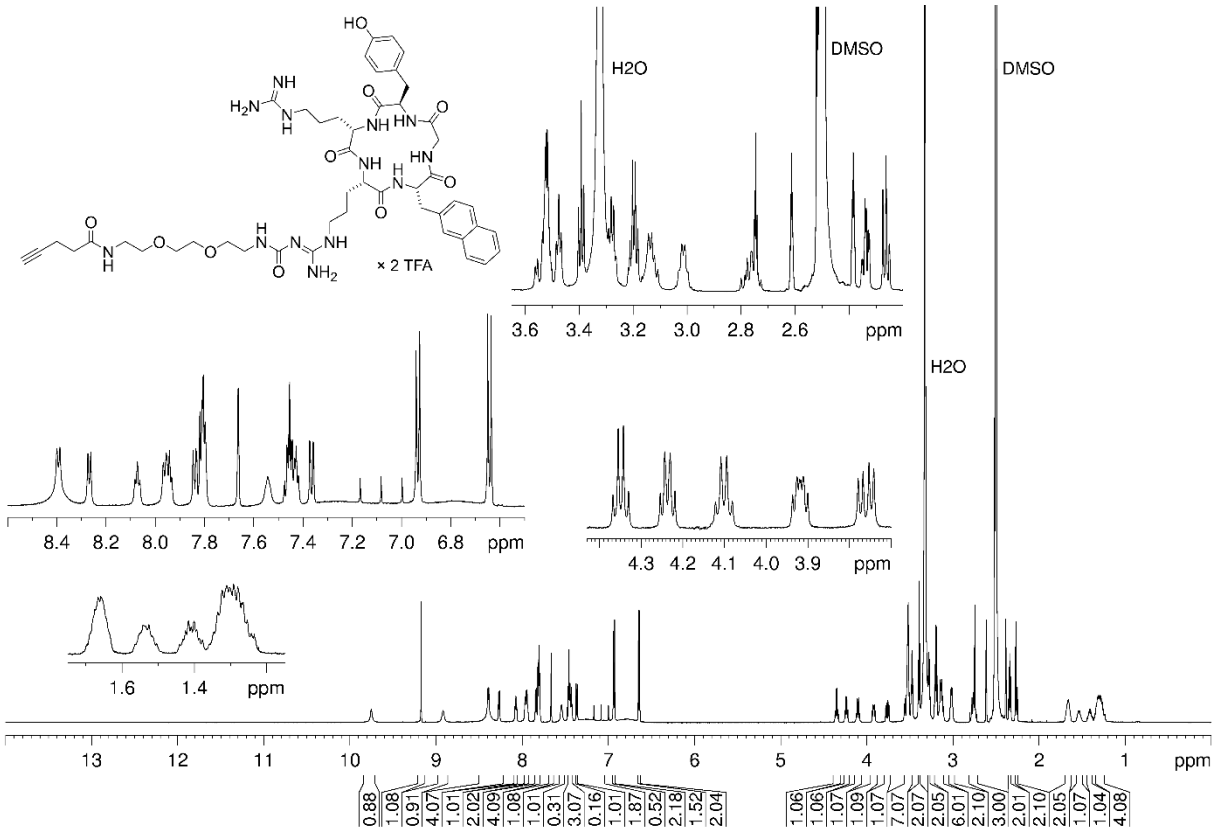

^{1}H-NMR spectrum (600 MHz, DMSO-d_6) of compound **5.21**

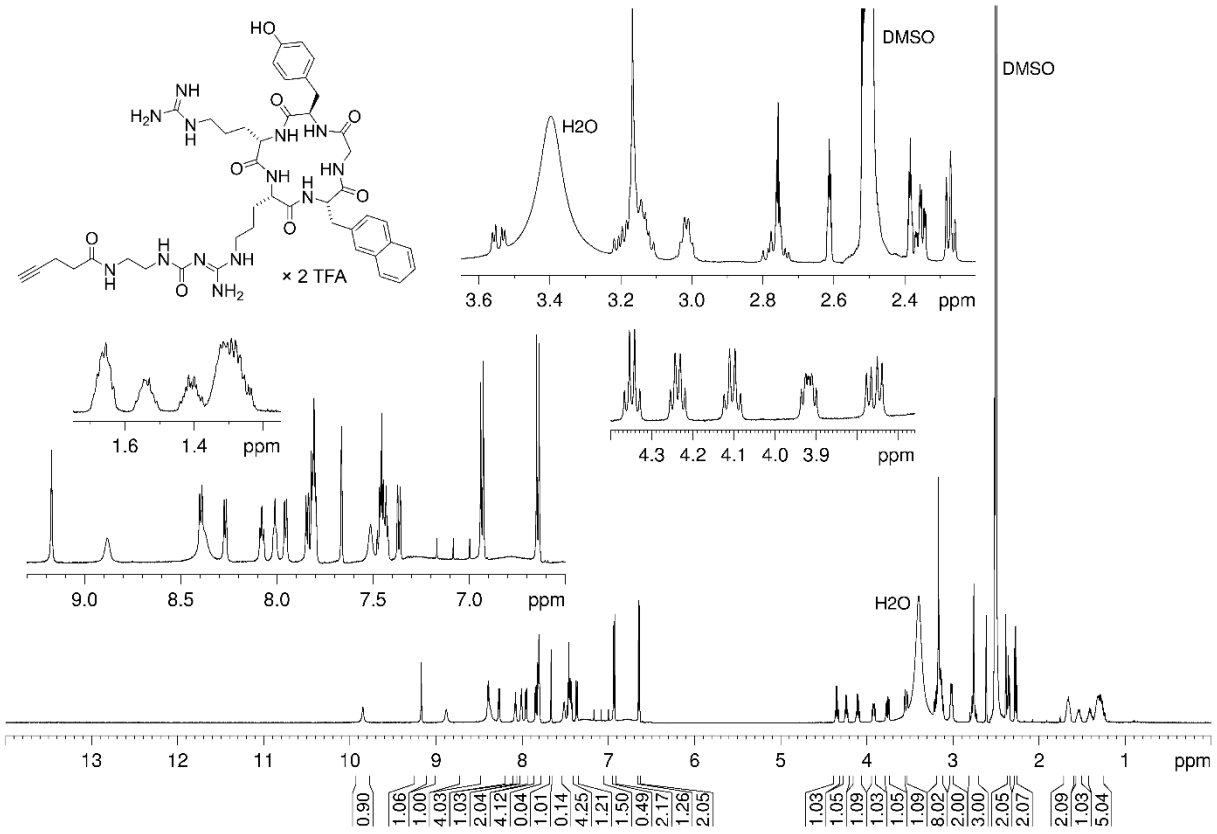

^{1}H-NMR spectrum (600 MHz, DMSO-d_6) of compound **5.22**

Chapter 6

Miscellaneous peptidic NTS_1R ligands with hydrophobic spacers or various metal ion chelators, and investigations on the insertion of AlF^{2+} into the NOTA chelator

6.1 Introduction

Principles of stabilizing peptidic NTS_1R ligands alongside with the preservation of their receptor affinity were described in Chapter 2, Chapter 3 and Chapter 4. The subsequent development of stabilized DOTA-conjugated NTS_1R ligands as precursors for labeling with $^{68}Ga^{3+}$ was subject of Chapter 4. This chapter comprises compounds which were prepared within the context of these investigations, but proved to be disadvantageous with respect to their syntheses, plasma stability or receptor affinity, and were therefore only incompletely characterized.

Furthermore, this chapter states different approaches towards the synthesis of peptidic NTS_1R ligands conjugated to metal ion chelators other than DOTA. In general, attachment of a chelator to a receptor ligand of choice enables the simple and fast preparation of its radiolabeled analog by complex formation of the chelator with a radionuclide metal ion. Depending on the kind of nuclide (e.g., oxidation state, ionic radius, preferred geometric nature of the coordination complex (i.e., tetrahedral, octahedral etc.)) and the site for conjugation at the ligand core structure, a suitable chelator has to be chosen in order to achieve high radiochemical yields for the labeling reaction. Concerning the requirements on a radionuclide for its applicability in positron emission tomography (PET) imaging, ^{18}F, a non-metal, exhibits almost ideal properties like a convenient half-life of 110 min and a low positron energy, resulting in higher spatial resolution in PET diagnostics compared to, e.g., PET tracers labeled with ^{68}Ga, emitting high-energy positrons[1,2]. The intention to combine the advantages of ^{18}F as positron-emitting radionuclide with the timesaving, often one-step labeling procedure via metal ion chelation led to an attempt to insert a complex of $^{18}F^-$ with aluminum into a peptide-bound chelator[3]. Among sixty other metal ion species, Al^{3+} binds F^- most strongly[4-7], its complex with F^- is stronger than with any other halide[5] and the aluminum-fluoride bond was reported to be stable in vivo[6,8,9]. After the initially applied diethylenetriaminepentaacetic acid (DTPA, for structure see Figure 6.1) chelator, comprising an acyclic heptadentate structure, showed a release of the inserted $[^{18}F]AlF^{2+}$ in human serum in vitro[3], other multifunctional chelating agents were investigated with respect to a stable complexation of $[^{18}F]AlF^{2+}$ [3,10,11]. The macrocyclic chelator 1,4,7-triazacyclononane-1,4,7-triacetic acid (NOTA, for structure see Figure 6.1) and pentadentate analogs thereof turned out as the most promising candidates with respect to labeling yields and stability in serum[3,10-13]. In order to increase the radiochemical yield for the complexation, the labeling procedures have additionally been optimized regarding solvent composition and pH, incubation time and temperature as well as stoichiometry of the reactants[10-15]. The NOTA chelator has successfully been used for the preparation of a variety of $[^{18}F]AlF^{2+}$-labeled PET ligands evaluated in pre-clinical studies with respect to imaging of prostate cancer[16,17], somatostatin receptor type 2 (SSTR2)-positive neuroendocrine tumors[10,18], B-cell lymphoma[19] or integrin-expressing glioblastomas[20]. The first in human application of a NOTA-conjugated $[^{18}F]AlF^{2+}$-labeled peptidic tracer was reported in 2013, where PET imaging of integrin was successfully performed in patients suffering from lung cancer[21]. To date, several $[^{18}F]AlF^{2+}$-labeled PET tracers are under investigation in clinical trials targeting a range of biomarkers, e.g., the somatostatin receptor, integrins, prostate specific membrane antigen (PSMA) or the chemokine receptor CXCR4[22].

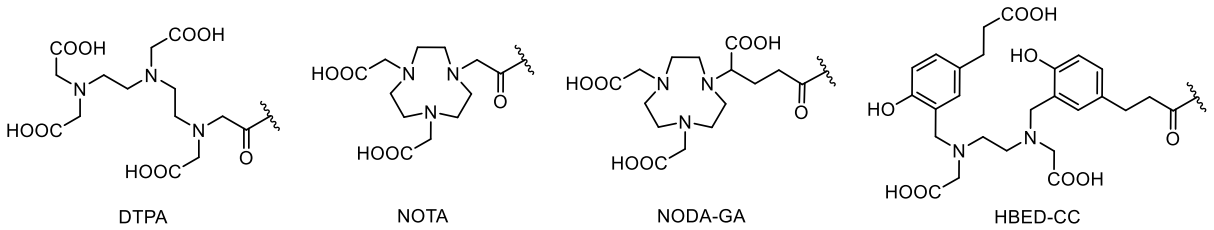

Figure 6.1. Structures of the multidentate chelating agents DTPA, NOTA, NODA-GA and HBED-CC, capable of forming complexes with ions that are relevant for clinical applications, e.g., $^{68}Ga^{3+}$, $^{64}Cu^{2+}$ and $[^{18}F]AlF^{2+}$ [3,10,11,23-26].

$[^{18}F]AlF^{2+}$-PET imaging of patients diagnosed with prostate cancer has lately been conducted using the PSMA ligand $[^{18}F]$AlF-PSMA-11[27-30] which was prepared using the identical labeling precursor as for the ^{68}Ga-labeled tracer $[^{68}Ga]$Ga-PSMA-11[31], a radioligand approved by the Food and Drug Administration (FDA) for PET imaging of PSMA-positive prostate cancer in 2020[32]. Notably, the targeting structure in PSMA-11, a peptidomimetic Glu-NH-CO-NH-Lys(Ahx) motif, is conjugated to the *N*,*N*′-bis[2-hydroxy-5(carboxyethyl)benzyl]ethylenediamine-*N*,*N*′-diacetic acid (HBED-CC, see Figure 6.1) chelator[27,28]. This acyclic hexadentate chelator was described to form strong complexes with Ga^{3+}-ions[23,31,33], but is technically assumed to be unfavorable for the chelation of AlF^{2+} considering reports on the preferred octahedral geometry of Al^{3+}-complexes which are best implemented by a pentadentate ligand, leaving one available binding site for the interaction of Al^{3+} with F^- [3,11,15,22]. Indeed, the stability of $[^{18}F]$AlF-PSMA-11 strongly depends on the formulation composition[28,34-36]; e.g., the radiochemical purity of a solution of $[^{18}F]$AlF-PSMA-11 in 1% EtOH in phosphate-buffered saline amounted to > 98% after 4 h, while the solution of $[^{18}F]$AlF-PSMA-11 in 1% EtOH in acetate buffer showed a radiochemical purity of 37% after 4 h[34]. The tracer proved to be stable in human plasma for only 1 h[35] and defluorination was observed in small animal PET studies[28,36] as well as during clinical tracer evaluation in prostate cancer patients[29,30]. Release of $^{18}F^-$ from the complex can lead to unspecific accumulation of activity in bones as previously observed for $[^{18}F]$AlF-PSMA-11[28,30,36,37], which could potentially hamper the visualization of bone lesions or result in false-positive metastasis identification. However, as comparative pre-clinical and clinical studies of $[^{68}Ga]$Ga-PSMA-11 and $[^{18}F]$AlF-PSMA-11 revealed an equal performance of the two tracers with respect to tumor uptake and visualization, cellular internalization, organ uptake and blood clearance, their diagnostic value and clinical relevance are considered to be similar[36,38,39]. Very recently, $[^{18}F]$AlF-PSMA-11 has been subject to a pre-clinical comparison with a different established ^{18}F-labeled PSMA PET tracer, again resulting in comparable performance regarding tumor uptake and tumor-to-organ ratios[40].

Labeling by chelation of $[^{18}F]AlF^{2+}$ was also described for a NODA-GA (1,4,7-triazacyclononane-1-glutaric acid-4,7-acetic acid)-conjugated compound (for structure of NODA-GA see Figure 6.1) despite the rather unfavorable configuration of NODA-GA for the complex formation[17,22]. This cyclic chelator is structurally closely related to NOTA and was initially reported to form stable complexes with Ga^{3+} and Cu^{2+} [24,41]. The more frequent and successful preparation of ^{68}Ga-labeled NODA-GA-conjugated PET tracers and their subsequent evaluation in small animal PET studies[42-44] indicates the more promising interaction of this chelator with Ga^{3+} (preferring octahedral complex geometry, i.e.,

hexadentate ligands[45,46]) compared to AlF^{2+} (preferring pentadentate ligands as mentioned above).

In this chapter, the use of NOTA, HBED-CC and NODA-GA as alternative chelating agents to DOTA for conjugation to peptidic NTS_1R ligands is addressed. As these conjugation reactions turned out to be challenging, different synthetic approaches are discussed and possible explanations for insufficient compound conversions are given as well as suggestions for improvement in future studies.

6.2 Results and discussion

6.2.1 Stabilized and less polar NTS_1R ligands for DOTA-conjugation

The hexapeptides **6.01**, **6.02** and **6.03** (*cf.* Scheme 6.1) were synthesized by manual solid-phase peptide synthesis (SPPS) within the context of investigations on modifications to NT(8-13) leading to enhanced proteolytic stability. Thus, in peptides **6.01** and **6.03** Ile in position 12 was exchanged by α-*tert*-butyl-Gly (Tle), and the α-nitrogen of Arg^9 (**6.01**, **6.02**) or Arg^8 (**6.03**) was additionally methylated, using a described procedure[47] in the case of **6.03**. To enable the conjugation of the peptides to the DOTA chelator, the lately reported approach of a bioisosteric exchange of arginine by an amino-functionalized N^{ω}-carbamoylated arginine was applied to all three compounds (position 8), using the Fmoc- and Boc-protected N^{ω}-carbamoylated arginine building blocks **3.06a**[47] (**6.01**, **6.02**) or **5.05** (see Chapter 5) (**6.03**) in SPPS. Notably, the complete peptide sequences, corresponding to **6.01** and **6.02**, turned out to be hardly accessible. The main product after cleavage of the peptide from the solid support represented the C-terminal pentapeptide Me-Arg^9-Pro^{10}-Tyr^{11}-Tle/Ile^{12}-Leu^{13} as confirmed by mass spectrometry (data not shown), whereas the intended hexapeptides **6.01** and **6.02** were obtained in minor amounts. As the coupling of an Fmoc-amino acid to an N^{α}-methylated N-terminal amino acid appeared to be the limiting step during these syntheses, the preparation of **6.01** and **6.02** was repeated by applying a described coupling procedure[48] for this critical amino acid coupling (synthesis not shown): the respective resin-bound side chain-protected pentapeptides were treated with a solution of triphosgene, collidine, **3.06a** and DIPEA in tetrahydrofuran (THF) at rt for 3 h followed by Fmoc-deprotection. However, only a minute fraction of the isolated products corresponded to the desired hexapeptides **6.01** and **6.02** (3% and 2%, respectively). Interestingly, application of the same procedure for the synthesis of NTS_1R ligand **4.11** (coupling of Fmoc-Arg(Pbf)-OH to the N^{α}-methylated N-terminal amino acid, *cf.* Chapter 4), gave the product in a much better yield of 23% (data not shown).

The amino-functionality of peptide **6.03**, which was obtained in good yield (63%), was used for the coupling to the DOTA chelator in analogy to the procedure described in Chapter 4 (*cf.* Scheme 6.1), giving the labeling precursor **6.04** after *t*Bu-deprotection. Insertion of $^{69}Ga^{3+}$ into the DOTA chelator of **6.04** afforded **6.05**, which represents the 'cold' analog of a NTS_1R PET ligand (see Scheme 6.1).

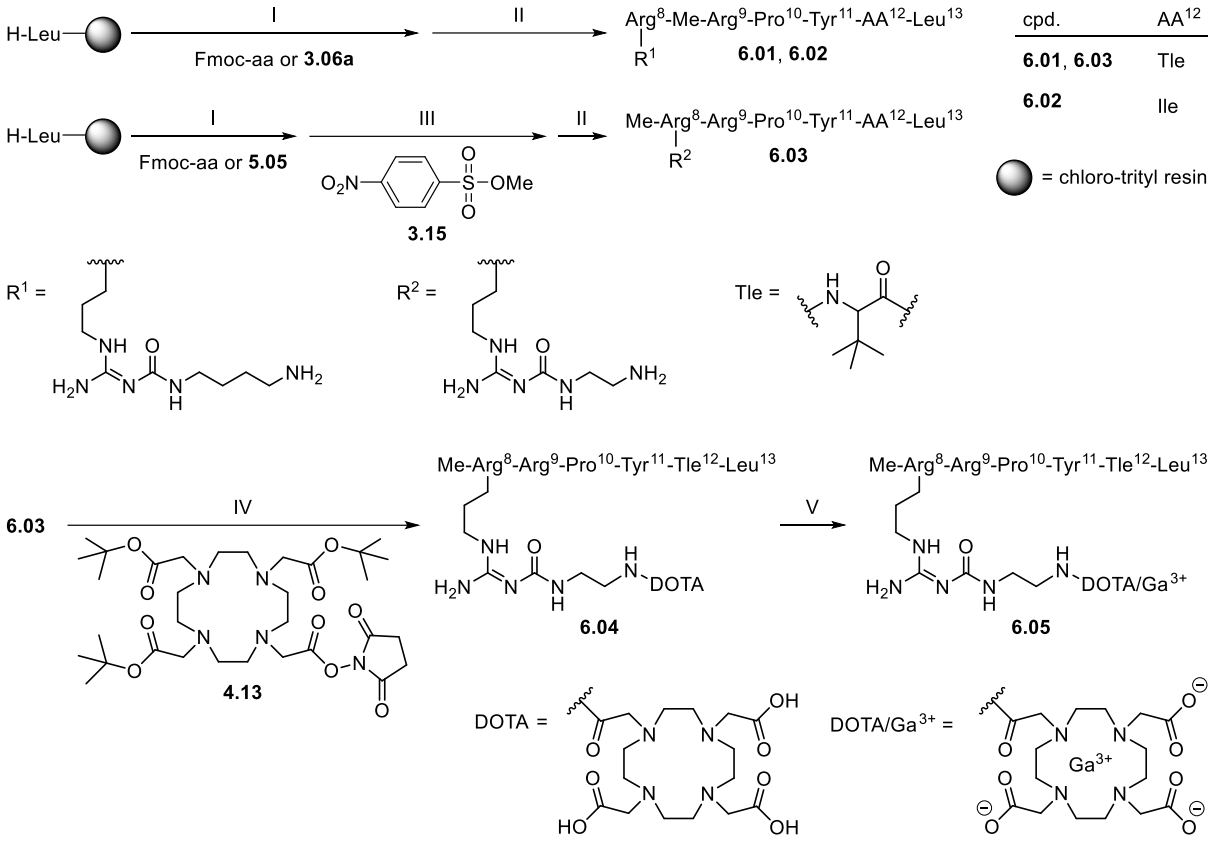

Scheme 6.1. Preparation of the amine-functionalized NT(8-13) derivatives **6.01**, **6.02** and **6.03**, labeling precursor **6.04** and the potential PET ligand **6.05**. Reagents and conditions: (I) Fmoc strategy SPPS using HBTU/HOBt and DIPEA, DMF/NMP (80:20 v/v), 35 °C, 2 × 1 h, 2 × 2 h or 1 × 16-19 h, Fmoc-deprotection: 20% piperidine in DMF/NMP (80:20 v/v), rt, 2 × 8-10 min; (II) (1) HFIP/CH_2Cl_2 (1:3 v/v), rt, 2 × 20 min, (2) TFA/H_2O (95:5 v/v), rt, 3 h; (III) (1) collidine, 2-nitrobenzenesulfonylchloride, CH_2Cl_2, rt, 2 h, (2) MTBD, DMF, rt, 30 min, (3) DBU, 2-mercaptoethanol, DMF, rt, 30 min; overall yields: 3% (**6.01**), 2% (**6.02**), 63% (**6.03**); (IV) (1) DIPEA, DMF/NMP 80:20 v/v, rt, 30 min, (2) TFA/H_2O 80:20 v/v, 50 °C, overnight, 76%; (V) $Ga(NO_3)_3 \times H_2O$, HEPES buffer (0.2 M, pH 4.2) or 10 mM HCl, 100 °C, 10 min, > 99%.

Alongside with the described less polar compounds **4.25**, **4.26**, **4.28**, **4.29** and **4.31** (*cf.* Chapter 4), additional peptidic NTS_1R ligands containing hydrophobic moieties were prepared starting from peptide **6.03** (Scheme 6.2). Conjugation of the N^{ω}-carbamoylated Arg^8 residue in **6.03** to the lipophilic building blocks **4.27** and **4.24** in analogy to a described procedure[49] (see Chapter 4) and subsequent Boc-deprotection gave the fluorinated compounds **6.06** and **6.07**, respectively (Scheme 6.2). The shift of polarity was assessed by changes in the RP-HPLC retention times using the HPLC system and conditions described for purity controls (see Experimental section). For comparison, stacked chromatograms of the RP-HPLC analyses are depicted in Figure A6.2 (Appendix). Compared to the parent compound **6.03** (t_R = 5.8 min), conjugation of the fluorinated aminomethyl-benzoyl spacer **4.27** (giving **6.06**, t_R = 6.5 min) had a much lesser effect on the compound's polarity than attachment of the fluorinated biphenyl-Ala spacer **4.24** (resulting in **6.07**, t_R = 11.4 min). Thus, conjugation to the DOTA chelator was only conducted with peptide **6.07**, giving compound **6.08** after removal of the *t*Bu-groups (*cf.* Scheme 6.2).

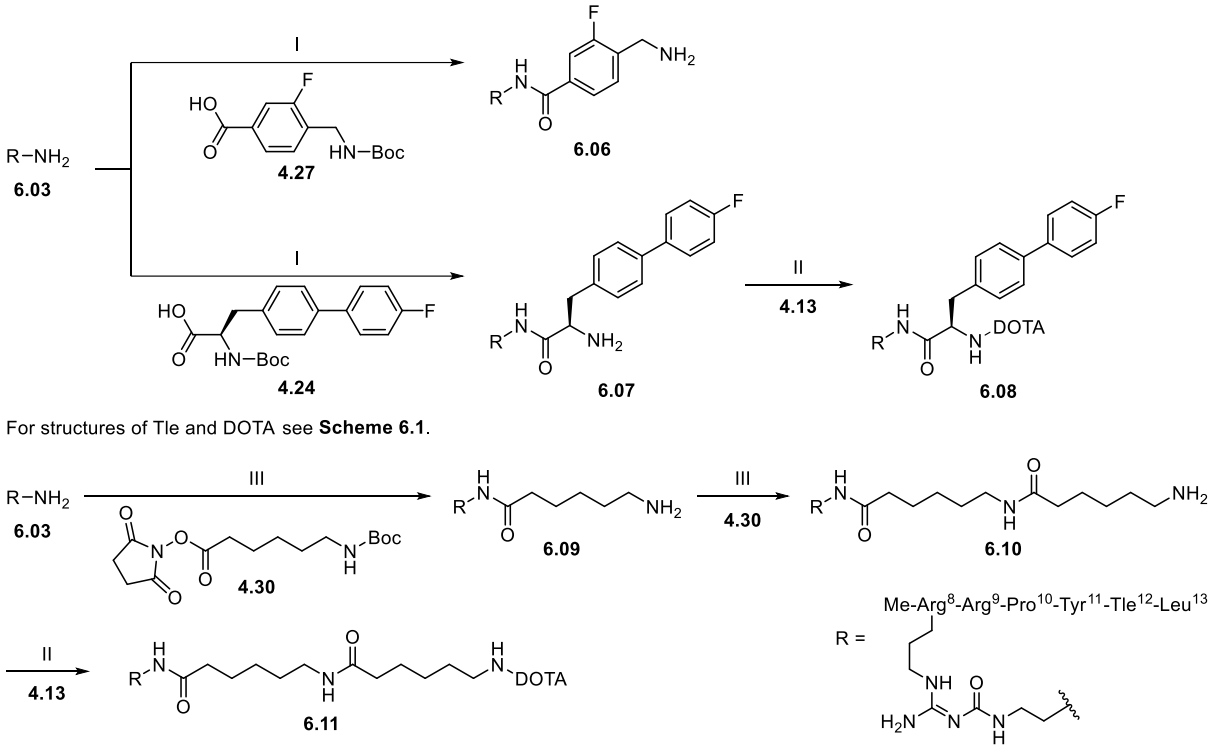

Scheme 6.2. Synthesis of the NTS_1R ligands **6.06**, **6.07**, **6.09** and **6.10** with enhanced lipophilicity, and preparation of the DOTA-conjugated peptides **6.08** and **6.11**. Reagents and conditions: (I) (1) DIPEA, HOBt, HBTU, DMF/NMP 80:20 v/v, rt, 60 min, (2) TFA/H_2O 95:5 v/v, rt, 3.5 h, 44% (**6.06**), 58% (**6.07**); (II) (1) DIPEA, DMF/NMP 80:20 v/v or 75:25 v/v, rt, 30 min, (2) TFA/H_2O 95:5 v/v, 50 °C, overnight, 45% (**6.08**), 64% (**6.11**); (III) (1) DIPEA, DMF/NMP 75:25 v/v, rt, 45 min, (2) TFA/H_2O 95:5 v/v, rt, 3.5 h, 82% (**6.09**), 93% (**6.10**).

6.03 was furthermore modified by conjugation to the aminohexanoyl spacer **4.30** via the N^{ω}-carbamoylated arginine side chain (*cf.* Scheme 6.2), giving derivatives **6.09** and **6.10** after a single and a twofold spacer elongation, respectively. Subsequent attachment of DOTA, resulting in compound **6.11** (see Scheme 6.2), was only performed starting from **6.10**, as the RP-HPLC analyses revealed a satisfactory drop of peptide polarity only after the second linker elongation step (t_R = 6.1 min (**6.09**) vs. t_R = 6.9 min (**6.10**); **6.03**: t_R = 5.8 min) (*cf.* Figure A6.2, Appendix).

NTS_1R binding of compounds **6.01**-**6.05** and **6.07**-**6.11** was determined in competition binding assays at intact $hNTS_1R$-expressing HT-29 colon carcinoma cells according to a described procedure[50] using the lately reported radioligand [^{3}H]UR-MK300 ([^{3}H]**2.13**)[50] (for structure see Chapter 2, Appendix). The obtained pK_i and K_i values are given in Table 6.1 and the resulting radioligand displacement curves are depicted in Figure A6.1 (Appendix). The described impairment of the NTS_1R affinity of NT(8-13) derivatives by the Ile^{12}/Tle^{12} exchange[49,51-56] was confirmed by the 14-fold decrease in the K_i value of **6.02** (Ile^{12}, K_i = 0.47 nM) compared to **6.01** (Tle^{12}, K_i = 6.6 nM). Similar to reported NTS_1R binding data for DOTA-conjugated ligands[49] (see Chapter 4), the presence of the DOTA-chelator in compounds **6.04**, **6.08** and **6.11** led to a slight decrease in receptor affinity compared to their amino-functionalized parent peptides **6.03**, **6.07** and **6.10**, respectively (*cf.* Table 6.1). In the case of **6.05**, the inserted Ga^{3+} ions provoked a shift to a lower K_i value compared to its precursor **6.04**, being in agreement with former findings on the effect of a compound's chelation state on the receptor affinity[44,49,57].

The stability against proteolytic degradation of compounds **6.01**, **6.02**, **6.03**, **6.04** and **6.05** was investigated by incubation in human plasma for up to 48 h according to a described procedure[56]; the amount of remaining intact peptide after different periods of incubation is given in Table 6.1. Comparison of the stability data of compounds **6.01** (Tle^{12}, > 99% after 48 h) and **6.02** (Ile^{12}, < 1% after 48 h) confirmed the reported stabilizing effect of the Ile^{12}/Tle^{12} exchange in NT(8-13) derivatives[44,49,51,53-55,57-69]. Interestingly, unlike described structurally closely related NT(8-13) analogs[49], insertion of Ga^{3+} into the DOTA chelator of **6.04** (resulting in **6.05**) did not cause a decrease in proteolytic stability (*cf.* Table 6.1).

Table 6.1. NTS_1R affinities of reference peptides **3.16**, **4.08** and **4.09** (for structures see Chapter 3 and Chapter 4) and compounds **6.01**-**6.05**, **6.07**-**6.11** and **6.13**, and in vitro plasma stabilities of **3.16**, **4.08**, **4.09**, **6.01**-**6.05** and **6.13**, determined at 37 °C.

cpd.	pK_i ± SEM / K_i [nM] NTS_1R[a]	% intact peptide in plasma after the given incubation time[b]			
		1 h	6 h	24 h	48 h
3.16	8.55 / 2.8[c]	> 99[c]	> 99[c]	> 99[c]	> 99[c]
4.08	8.28 / 5.3[d]	> 99[d]	> 99[d]	> 99[d]	> 99[d]
4.09	9.16 / 0.69[d]	99[d]	57[d]	3.0[d]	1.4[d]
6.01	8.18 ± 0.03 / 6.6	> 99	> 99	> 99	> 99
6.02	9.33 ± 0.02 / 0.47	78 ± 1	6.3 ± 0.2	< 1	< 1
6.03	8.73 ± 0.06 / 1.9	> 99	> 99	> 99	> 99
6.04	7.48 ± 0.03 / 34	98 ± 1	97 ± 1	92 ± 1	87 ± 1
6.05	8.12 ± 0.03 / 7.6	> 99	> 99	> 99	> 99
6.07	8.35 ± 0.11 / 4.7	n.d.	n.d.	n.d.	n.d.
6.08	7.82 ± 0.03 / 15	n.d.	n.d.	n.d.	n.d.
6.09	8.88 ± 0.08 / 1.4	n.d.	n.d.	n.d.	n.d.
6.10	8.57 ± 0.11 / 2.9	n.d.	n.d.	n.d.	n.d.
6.11	7.71 ± 0.12 / 20	n.d.	n.d.	n.d.	n.d.
6.13	7.83 ± 0.03 / 15	98 ± 1	96 ± 1	98 ± 1	97 ± 1

[a]Determined by radioligand competition binding with [^{3}H]**2.13** at HT-29 cells (K_d = 0.55 nM[56] or 0.41 nM[49], c = 1 nM); given are mean values ± SEM (pK_i) and mean values (K_i) from two (**6.01**, **6.11**) or three (**6.02**-**6.05**, **6.07**-**6.10**, **6.13**) independent experiments, each performed in triplicate. [b]The initial concentration of the peptide in human plasma/PBS (1:2 v/v) was 100 µM. Data represent means ± SEM from two or three independent experiments (SEM not given when no decomposition was observed). [c]Schindler et al.[47] [d]Schindler et al.[49] n.d. = not determined.

Taking into consideration the overall performance of the NT(8-13) derivatives **6.01**-**6.11** (synthetic accessibility, NTS_1R affinity, proteolytic stability), they proved to be inferior to their analogs described in Chapters 2, 3 and 4. Therefore, they were not considered for further in vitro and in vivo investigations.

6.2.2 NTS_1R ligands conjugated to the NOTA chelator for labeling with AlF^{2+}

In order to investigate the insertion reaction of AlF^{2+}-ions into a chelating moiety and thus prepare "cold" analogs of ^{18}F-labeled NTS_1R PET tracers, we aimed at the conjugation of the NOTA chelator to the amino-functionalized side chain of Arg^8 in **3.16**[47], resulting in compound **6.13** (as indicated in Figure 6.2A). However, as this reaction proved to be unsuccessful in the first approaches, additional NT(8-13) analogs were applied as starting material in order to optimize the route of synthesis for the NOTA-conjugation. The

structures of said hexapeptides **3.16**[47], **6.12**, **4.08**[49] and **4.11**[49] and their respective intended NOTA-conjugates **6.13**, **6.14**, **6.15** and **6.16** are depicted in Figure 6.2A, and the investigated synthetic routes and conditions **A1**-**B2** are summarized in Table 6.2.

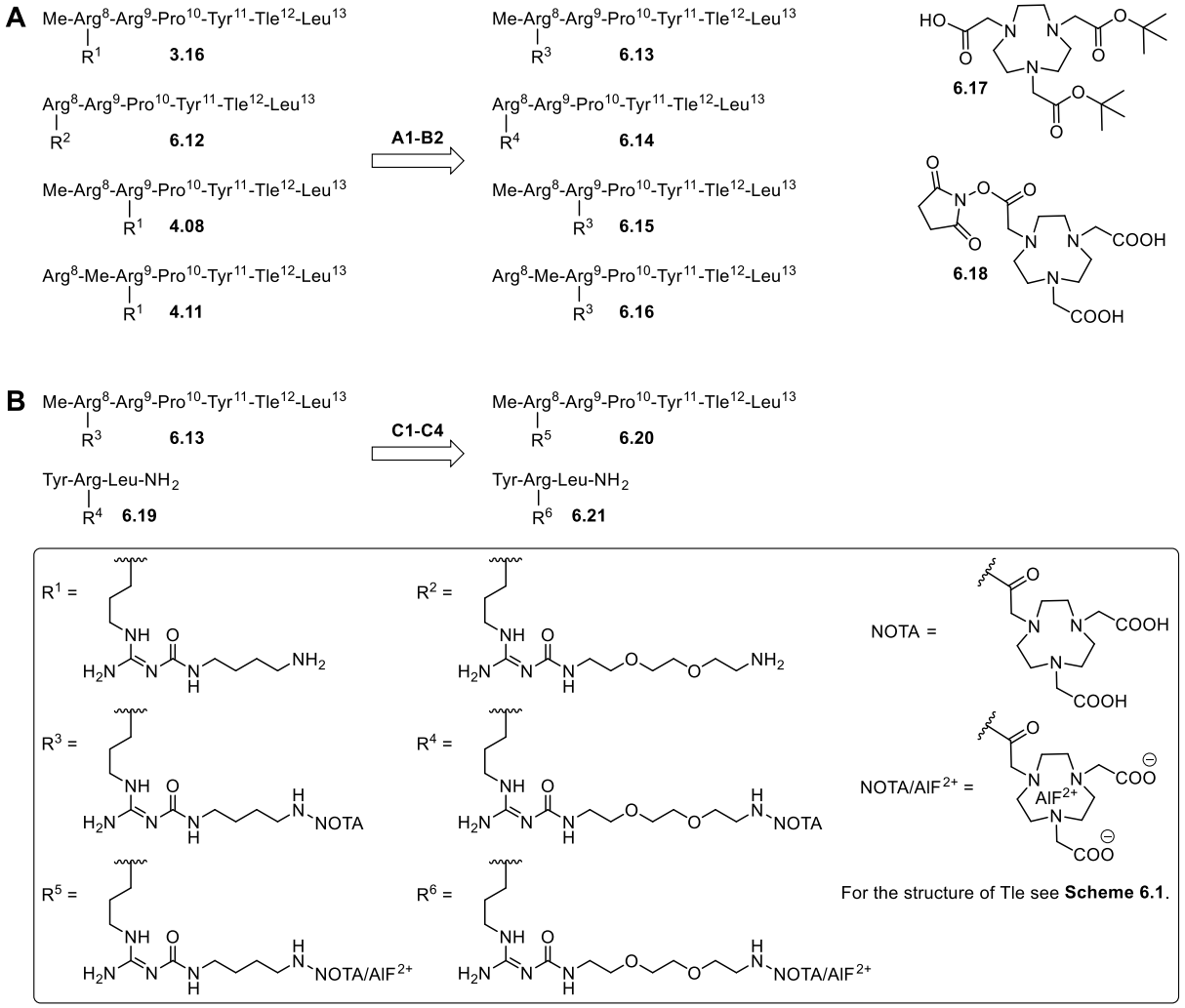

Figure 6.2. (A) Structures of the intended NOTA-conjugated peptides **6.13**, **6.14**, **6.15** and **6.16** originating from the amino-functionalized ligands **3.16**[47], **6.12**, **4.08**[49] and **4.11**[49], and structures of the NOTA derivatives **6.17** and **6.18** used for the conjugation reactions. Reagents and conditions **A1**-**B2** examined in the syntheses are given in Table 6.2 and the successfull preparation of **6.13**-**6.16** is depicted in Scheme 6.3. (B) Structures of the AlF^{2+}-complexes **6.20** and **6.21** aimed at by the insertion of AlF^{2+} into **6.13** and the dummy compound **6.19**, respectively. Reagents and conditions **C1**-**C4** examined in the syntheses are given in Table 6.3 and the eventual preparation of **6.20** and **6.21** is depicted in Scheme 6.3.

The use of a coupling reagent for the activation of a free carboxylic group as, e.g., in NOTA-bis(*t*Bu)ester **6.17** (for structure see Figure 6.2A), harbors the risk of an additional activation of the peptide C-terminus resulting in undesired side reactions (i.e., peptide cyclization instead of conjugation to the chelator). Nevertheless, in order to circumvent a possible separation problem of the remaining starting material from the respective conjugation product, the bis(*t*Bu)ester of NOTA (**6.17**) was initially applied for the syntheses using either HBTU/HOBt and DIPEA or oxyma and DIC as activation reagents (note: the succinimidyl ester of bis(*t*Bu)-protected NOTA was not commercially available and efforts to prepare it failed). Unfortunately, due to the emergence of numerous side products and no or only low product formation in small-scale reactions, an isolation of the

product was mostly unfeasible at first. This difficulty could be overcome by using the non-protected NOTA succinimidyl ester **6.18** (structure shown in Figure 6.2A), which led to the formation of the desired products **6.13**-**6.16** in good yields via approaches **B1** and **B2** using DIPEA as base (*cf.* Table 6.2).

Table 6.2. Explored synthetic conditions **A1**-**B2** for the conjugation of the NOTA chelator to the peptides **3.16**, **6.12**, **4.08** and **4.11** affording the labeling precursors **6.13**, **6.14**, **6.15** and **6.16** (*cf.* Figure 6.2A).

cond.[a]	NOTA derivative[b]	activation reagents	starting material	comments[c]
A1	**6.17** (1 equiv.)	HBTU (5 equiv.) HOBt (5 equiv.) DIPEA (10 equiv.)	**3.16** (1 equiv.)	isolation unfeasible
			4.11 (1 equiv.)	isolation unfeasible
A2	**6.17** (1 equiv.)	oxyma (5 equiv.) DIC (5 equiv.)	**3.16** (1 equiv.)	isolation unfeasible
			4.11 (1 equiv.)	no product formation
A3	**6.17** (1 equiv.)	HBTU (7.5 equiv.) HOBt (7.5 equiv.) DIPEA (15 equiv.)	**6.12** (1.5 equiv.)	isolation unfeasible; two fractions with same MW
			4.11 (1.5 equiv.)	isolation unfeasible
B1	**6.18** (1 equiv.)	DIPEA (12 equiv.)	**3.16** (1 equiv.)	two fractions with same MW
			6.12 (1 equiv.)	yield: 54%
			4.08 (1 equiv.)	yield: 76%
			4.11 (1 equiv.)	two fractions with same MW
B2	**6.18** (1 equiv.)	DIPEA (24 equiv.)	**3.16** (2 equiv.)	yield: 61-63%
			6.12 (2 equiv.)	yield: 53%
			4.08 (2 equiv.)	yield: 60%
			4.11 (2 equiv.)	two fractions with same MW

[a]For intended syntheses see Figure 6.2A; cond. = condition. [b]For structures of the NOTA derivatives **6.17** and **6.18** see Figure 6.2A. [c]MW = molecular weight.

However, the preparative work-up after conversion of the amino-functionalized peptides **3.16**[47] and **4.11**[49] by treatment with **6.18** each gave two product fractions, both corresponding to compounds exhibiting the molecular weight of the expected product (**6.13** and **6.16**, respectively) as confirmed by mass spectrometry (data not shown). To further investigate this issue, ^{1}H-NMR spectra of the two products corresponding to the correct mass of **6.16** were recorded. One possible explanation for the appearance of two constitutional isomers is the conjugation of the chelating moiety not only to the amino-functionality of the N^{ω}-carbamoylated Arg side chain (giving the desired product) but also to the N-terminus of the peptide, resulting in the identical chemical formula and molecular weight. The formation of this by-product could have been promoted by usage of insufficient amounts of base, as the N-terminal α-amino group is less basic than the amino group of the artificial Arg side chain and is thus deprotonated first. However, in the case of synthetic approaches **B1** and **B2**, comprising the use of 12 and 24 equiv. DIPEA, respectively (*cf.* Table 6.2), a selective deprotonation of the N-terminal α-amino group is considered unlikely. The high amount of base applied under conditions **B1** and **B2** could potentially lead to the deprotonation of the phenolic hydroxyl group of the Tyr residue, resulting in an (undesired) nucleophilic site for the conjugation to NOTA. However, the formation of such a by-product did most likely not take place during the synthesis of **6.16**, as the NMR spectra of both products displayed the typical singlet signal for the

unsubstituted tyrosine hydroxyl group (at ca. 9 ppm). Additionally, conjugation of NOTA via the Tyr residue would result in a loss of the compound's fluorescence emission at 305 nm, however, both products featured the typical tyrosine fluorescence (fluorescence spectra not shown). Deprotonation of only the guanidine moiety of Arg^8 in **6.16** and subsequent conjugation of the chelator onto the Arg^8 side chain is very unlikely due to the strong basicity of the monoalkylated guanidine group in this arginine, but the NMR spectrum of one of the investigated products did not show the typical two broad singlets at approximately 6.7-7.7 ppm for a protonated monoalkylated guanidine group (spectrum not shown). Therefore, and after comparison of both spectra with the spectra of the starting material **4.11** and the other NOTA-conjugated products (**6.13**-**6.15**), the product showing the typical two broad singlets at approximately 6.7-7.7 ppm in the ^{1}H-NMR spectrum is assumed to correspond to the desired product **6.16** (i.e., conjugation to NOTA via the amino-functionality of the N^{ω}-carbamoylated side chain). In future studies, a possible hint on the correct constitution could also be obtained by investigating the NTS_1R affinity of the different isomers, as the conjugation of the bulky chelator to the N-terminus is supposed to considerably impair the peptide's receptor binding properties.

The incorporation of AlF^{2+} into the NOTA chelator of **6.13**, resulting in the potential PET tracer **6.20** (for structure see Figure 6.2B) turned out to be challenging, as mass spectrometry revealed no product formation via the initial synthetic approach **C1** (*cf.* Figure 6.2B and Table 6.3). Thus, the NOTA-conjugated tripeptide **6.19** (*cf.* Figure 6.2B) served as 'dummy' starting material for exploring the synthetic conditions **C2**-**C4** for the insertion reaction of AlF^{2+} (for details on the synthetic pathways see Table 6.3), resulting in compound **6.21**. Note: dummy ligand **6.19** was prepared after optimization of the procedure for NOTA-conjugation, in analogy to compounds **6.13**-**6.16** (*cf.* Scheme 6.3).

AlF^{2+} ion formation occurred during a pre-incubation of $AlCl_3$ and NaF in sodium acetate buffer for 5 min (*cf.* Table 6.3). Unfortunately, only marginal amounts of the desired products **6.20** or **6.21** (for structure see Figure 6.2B) were detected by mass spectrometry, which could not be properly isolated by preparative HPLC due to interference with impurities (data not shown). Reports on higher product yields using a final reaction mixture containing 50% organic solvent[12,28] were confirmed via approaches **C3** and **C4**, where the use of a 1:1 (v/v) mixture of sodium acetate buffer and EtOH or MeCN, respectively, as solvent enabled the formation of the products **6.20** and **6.21** in isolatable amounts (Table 6.3, Scheme 6.3).

Table 6.3. Explored synthetic conditions **C1**-**C4** for the insertion of AlF^{2+} into the NOTA-conjugated NTS_1R ligand **6.13** and dummy compound **6.19**, aiming at the respective AlF^{2+}-containing peptides **6.20** and **6.21** (*cf*. Figure 6.2B).

cond.[a]	reagents	solvent	starting material	incubation at 100 °C	comments[b]
C1	$AlCl_3$ (1.3 equiv.) NaF (10 equiv.)	0.1 M NaOAc pH 4.4/ EtOH (1:1 v/v)	**6.13**	20 min	no product formation
C2	$AlCl_3$ (2.5 equiv.) NaF (5 equiv.)	2 mM NaOAc pH 4	**6.13**	20 min	isolation unfeasible
C3	$AlCl_3$ (2.5 equiv.) NaF (10 equiv.)	2 mM NaOAc pH 4/ EtOH (1:1 v/v)	**6.13**	20 min	isolation unfeasible
			6.13	10 min	yield: 12%; Zn^{2+}-containing bp
			6.19	60 min	isolation unfeasible
C4	$AlCl_3$ (2.5 equiv.) NaF (10 equiv.)	2 mM NaOAc pH 4/ MeCN (1:1 v/v)	**6.13**	30 min	yield: 2%; Zn^{2+}-containing bp
			6.19	60 min	isolation unfeasible
			6.19	30 min	yield: 48%

[a]For intended syntheses see Figure 6.2B; cond. = condition. [b]bp = by-product.

Using the crude reaction mixture of **6.21** (approach **C4**, 60 min of incubation at 100 °C, *cf*. Table 6.3), the solvents and gradient for product purification by preparative HPLC were optimized, enabling the isolation of **6.21** in a yield of 48%. Notably, using the conditions **C3** and **C4**, conversion of **6.13** resulted not only in recovery of the starting material and the formation of the desired peptide **6.20**, but also in the emergence of its Zn^{2+}-containing analog as a by-product (*cf*. Table 6.3), which could be separated by preparative RP-HPLC. The spontaneous insertion of Zn^{2+} into the empty NOTA chelator of a neuropeptide Y Y_1R ligand had been observed before within the scope of the Master Thesis of Diana Braun (Institute of Pharmacy, University of Regensburg, 2019), but did not markedly hamper the insertion of AlF^{2+} into the chelator. The stability constants of the NOTA complex with Al^{3+} and Zn^{2+} were reported to amount to logK = 17.9[70] and 18.3[71], respectively. As Zn^{2+}-ions occur as common impurities released from metal or glass materials during purification, analytic procedures and storage, the insertion of Zn^{2+} ions must always be considered as a potential side-reaction.

The eventual successful syntheses of the NOTA conjugated peptides **6.13**, **6.14**, **6.15** and **6.16**, which were conducted via synthetic pathway **B2** (*cf*. Table 6.2), are depicted in Scheme 6.3A. As mentioned above, the same strategy was used for the preparation of 'dummy' compound **6.19** from the described tripeptide **6.22**[50] (for structure see Scheme 6.3B). The successful insertion of AlF^{2+} into the chelator moiety of **6.13** and **6.19**, giving **6.20** and **6.21**, respectively, was eventually achieved via synthetic pathway **C4** (*cf*. Table 6.3) as depicted in Scheme 6.3C.

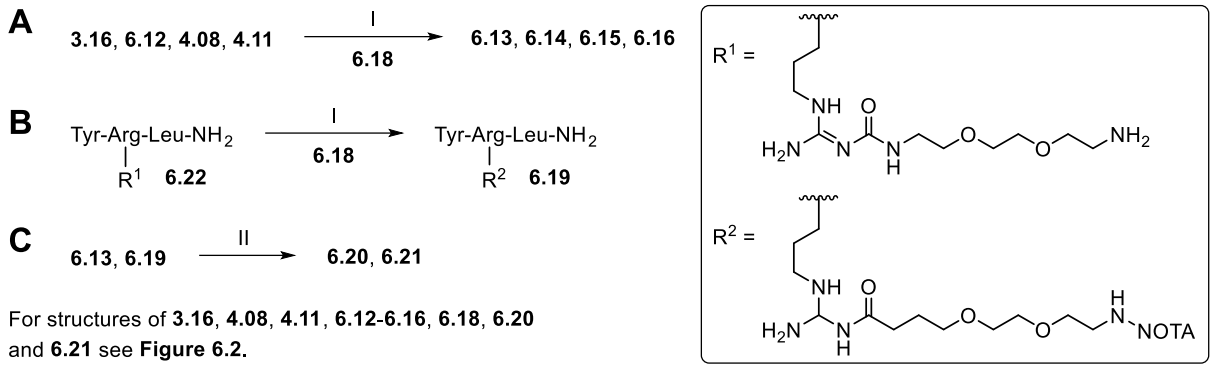

Scheme 6.3. (A) Successful syntheses of the NOTA-conjugated peptides **6.13**-**6.16** from the amino-functionalized compounds **3.16**[47], **6.12**, **4.08**[49] and **4.11**[49] by conjugation with **6.18**. (B) Preparation of the dummy compound **6.19** by conjugation of **6.18** to the described tripeptide **6.22**[50]. (C) Successful insertion reactions of AlF^{2+} into the NOTA chelator of **6.13** and **6.19**, giving the metal-complex compounds **6.20** and **6.21**. Reagents and conditions: (I) DIPEA, DMF/NMP 75:25 v/v or anhydrous DMF, rt, 60 min, 63% (**6.13**), 53% (**6.14**), 60% (**6.15**), 35% (**6.16**), 50% (**6.19**); (II) $AlCl_3$, NaF, sodium acetate buffer (2 mM, pH 4) and MeCN, 100 °C, 30 min, 2% (**6.20**), 48% (**6.21**).

Compound **6.13** was characterized with respect to NTS_1R affinity and plasma stability (*cf.* Table 6.1, Table A6.1 and Figure A6.1, Appendix), revealing a comparable receptor binding (K_i = 15 nM) and enzymatic degradation profile (97% intact peptide after 48 h of incubation) as its DOTA-conjugated analog **4.16**[49] (*cf.* Chapter 4, K_i = 33 nM, 84% intact peptide after 48 h of incubation). However, **6.13** and its AlF^{2+}-containing analog **6.20** were not subject of further in vitro and in vivo studies.

6.2.3 Other chelator-conjugated peptides intended for insertion of Ga^{3+}

The described hexapeptide **3.16**[47] (*cf.* Figure 6.2A) served as starting material for attempts to conjugate the acyclic HBED-CC chelator to its amino-functionalized N^{ω}-carbamoylated arginine side chain, theoretically resulting in compound **6.23** (*cf.* Figure 6.3). Furthermore, a conjugation of the cyclic NODA-GA chelator to the amino-functionality of the artificial arginine moieties in **4.08**[49] (*cf.* Figure 6.2A) and **3.16** was envisaged, in principle leading to compounds **6.24** and **6.25**, respectively (*cf.* Figure 6.3). The conditions of the synthetic approaches **D1** and **D2**, investigated for conjugation of HBED-CC-tris(*t*Bu)ester **6.26** (for structure see Figure 6.3), as well as the approaches **E1** and **E2**, explored for the conjugation of (*R*)-NODA-GA-tris(*t*Bu)ester **6.27** (for structure see Figure 6.3) are summarized in Table 6.4.

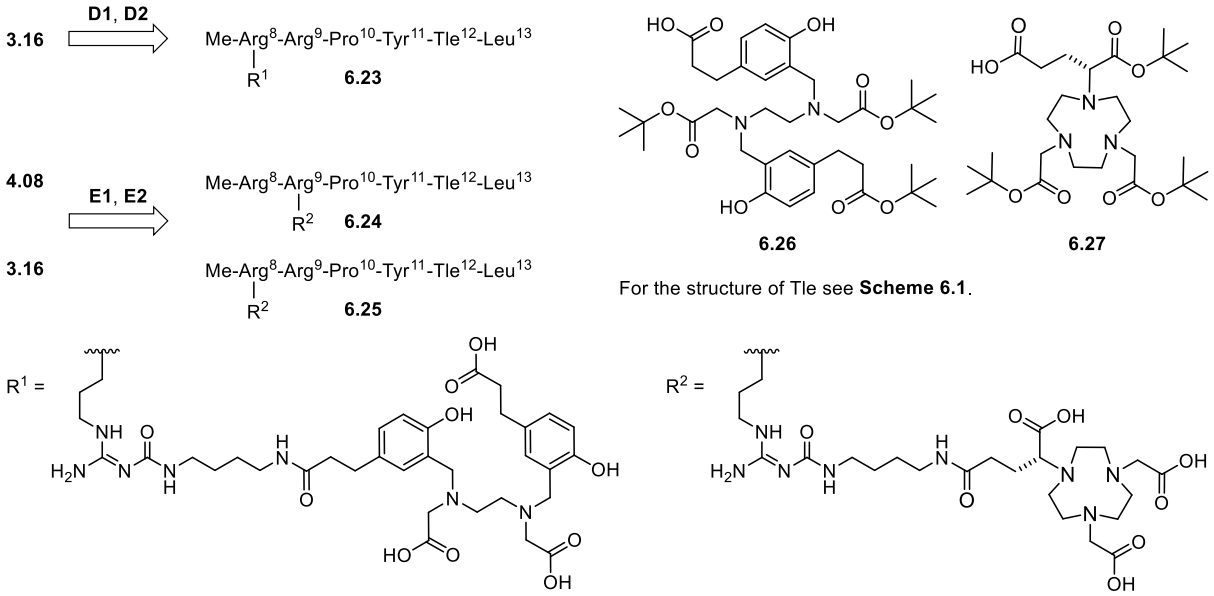

Figure 6.3. Structures of the chelator-conjugated compounds **6.23**, **6.24** and **6.25** aimed at by conjugation of the amino-functionalized ligands **3.16**[47] and **4.08**[49] to the protected chelators **6.26** or **6.27**. Reagents and conditions **D1**-**E2** used in the investigated syntheses are given in Table 6.4.

Notably, independent of the choice of activation reagents (HBTU/HOBt and DIPEA vs. oxyma and DIC, *cf.* Table 6.4), no formation of the desired product **6.23** was evident by mass spectrometry. Due to the limited commercial availability and high costs connected to the use of HBED-CC-tris(*t*Bu)ester this approach was not pursued any further.

Table 6.4. Synthetic conditions **D1**-**E2** pursued to prepare compounds **6.23**, **6.24** and **6.25** by conjugation of the HBED-CC- or the NODA-GA-chelator to the peptides **3.16** or **4.08** (*cf.* Figure 6.3).

cond.[a]	chelator (protected)[b]	activation reagents	starting material	comments[c]
D1	**6.26** (1 equiv.)	HBTU (10 equiv.) HOBt (10 equiv.) DIPEA (20 equiv.)	**3.16** (2 equiv.)	no product formation
D2	**6.26** (1 equiv.)	oxyma (10 equiv.) DIC (10 equiv.)	**3.16** (2 equiv.)	no product formation
E1	**6.27** (1 equiv.)	HBTU (8.3 equiv.) HOBt (8.3 equiv.) DIPEA (16.7 equiv.)	**4.08** (1.7 equiv.)	isolation unfeasible; several fractions with same MW
E2	**6.27** (1 equiv.)	oxyma (5 equiv.) DIC (5 equiv.) DIPEA (1.5 equiv.)	**3.16** (1 equiv.)	no product formation
			4.08 (1 equiv.)	isolation unfeasible

[a]For intended syntheses see Figure 6.3. [b]For structures of the protected chelators **6.26** and **6.27** see Figure 6.3. [c]MW = molecular weight.

Similar to the findings for the syntheses of **6.13** and **6.16**, the attempt to prepare and purify peptide **6.24** (via conditions **E1**, using HBTU/HOBt and DIPEA as activation reagents, *cf.* Table 6.4) resulted in several compounds displaying the same molecular weight, but only in non-isolatable amounts. Application of oxyma, DIC and DIPEA as activation reagents (approach **E2**, *cf.* Table 6.4) resulted in no conversion of **3.16** to **6.25** and gave only a marginal amount of **6.24** (starting from **4.08**), which could not be purified

due to a massive content of interfering impurities (chromatograms not shown). Therefore, the preparation of NODA-GA-conjugated NTS_1R ligands was not further attempted.

6.2.4 Chemical stability of the NOTA-AlF^{2+}-complex in 6.21 in aqueous solution

Similar to the results reported for [^{18}F]AlF-PSMA-11[28-30,36], a release of F^- from the AlF^{2+}-containing NOTA-chelator in a neuropeptide Y Y_1R ligand was observed within the Master Thesis of Diana Braun (Institute of Pharmacy, University of Regensburg, 2019), leading to the formation of increasing amounts of the Al^{3+}-NOTA complex immediately upon isolation by preparative HPLC. Stabilization of the intact complex could be achieved by the addition of NaF immediately after elution of the AlF^{2+}-containing product from the preparative HPLC column, indicating that the loss of F^- from the complex underlies an equilibrium. Therefore, the chemical stability of **6.21**, with regard to both a release of AlF^{2+} and a loss of F^-, was investigated. In a first approach, 400 µM, 200 µM, 100 µM and 50 µM dilutions of the crude product in 0.1% aq HCOOH immediately after synthesis were analyzed by analytical RP-HPLC, promptly and after incubation at rt overnight. For each concentration, the corresponding chromatograms are depicted as pairs (instant analysis vs. incubation overnight) in Figure 6.4A, revealing no noticeable change in the respective peak heights and retention times. LC-HRMS analysis of the 400 µM sample of **6.21** confirmed the identity of the species corresponding to the two main peaks in the chromatograms: the first peak (t_R = 4.2-4.6 min) arises from the intact AlF^{2+}-containing product **6.21**, while the second peak (t_R = 5.2-5.5 min) arises from the remaining starting material **6.19** (*cf.* Figure 6.4A). The marked difference in the retention times of **6.19** and **6.21** should enable the detection of a change of the compound ratio in case of a potential release of AlF^{2+} from the NOTA chelator (i.e., re-conversion to the starting material **6.19**). It should be noted that analytical studies required to assess a potential release of F^- from **6.21**, which includes the identification of the retention time of the corresponding decomposition product (Al^{3+}-complex), were not performed.

In a second approach, the stability of the AlF^{2+}-complex in **6.21** was assessed by comparing the RP-HPLC analyses of 100 µM eluate samples of purified **6.21** supplemented and not supplemented with NaF. Stackplots of the chromatograms of the analyses after incubation at rt for 0 min, 50 min and 100 min are given in Figure 6.4B. Comparable to the results from the analysis of the crude peptide samples, the chromatograms from the analyses of purified **6.21** revealed no changes in the peak pattern or height during the time of incubation. HRMS analysis of the solutions of purified **6.21** with and without additional NaF, notably more than two years after the above-mentioned investigations (during which the solutions had been stored at −80 °C), revealed that in both samples, the only detected peptide species was the intact, AlF^{2+}-containing product (m/z [M+H]$^+$ calcd. for [$C_{40}H_{67}AlFN_{12}O_{12}$]$^+$ 953.4795, found 953.4798 (with additional NaF) or 953.4800 (without additional NaF)). Thus, **6.21** proved to be stable in aqueous solution with respect to both defluorination and de-chelation (i.e., loss of the complete AlF^{2+}-ion). For future studies of AlF^{2+}-containing compounds, the additional preparation of the fluoride-free Al^{3+}-complex as a reference compound should support the investigation of the stability under various conditions.

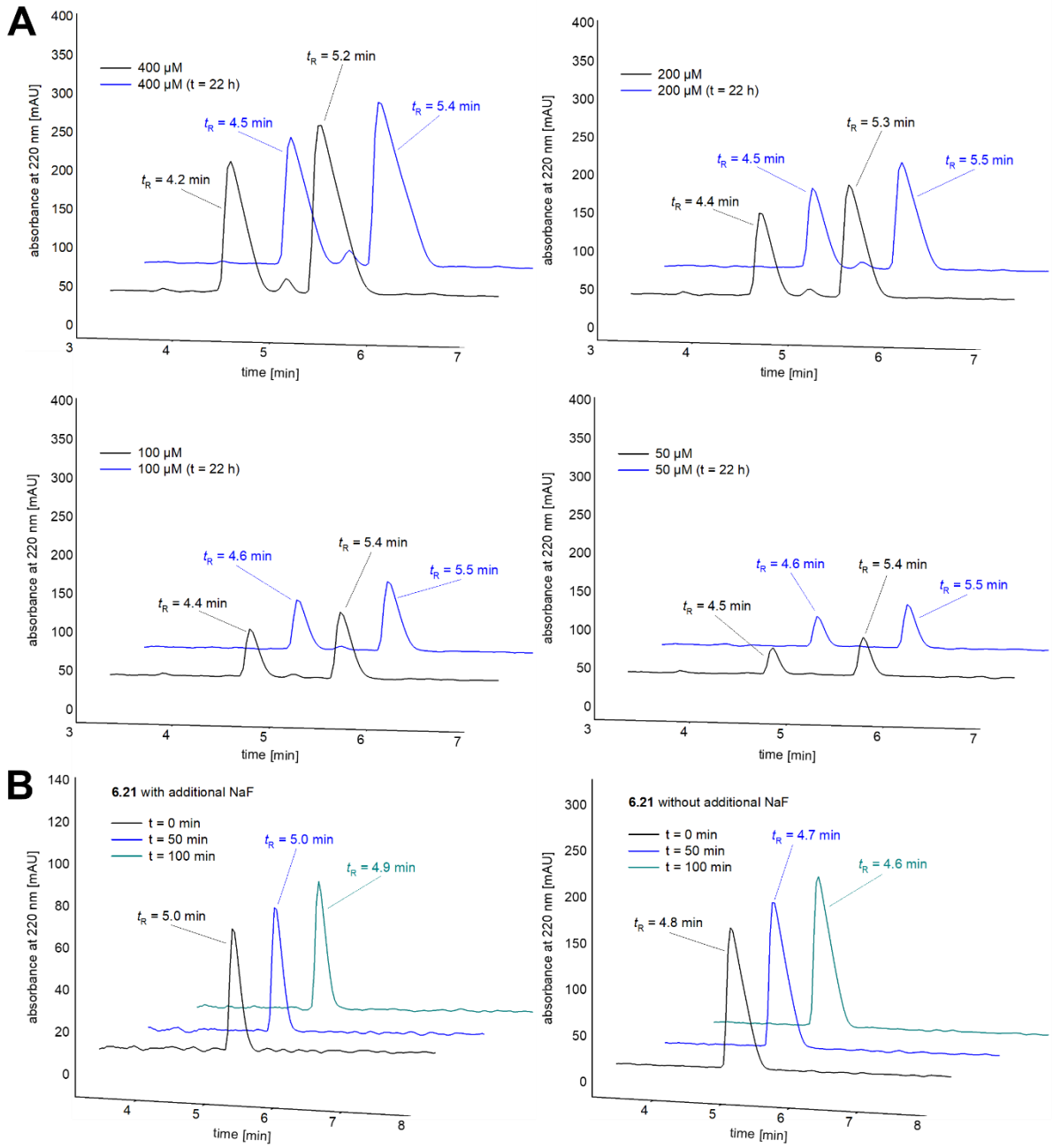

Figure 6.4. (A) Chromatograms (relevant region) of the RP-HPLC analyses of the crude reaction mixture after the synthesis of **6.21**, diluted with 0.1% aq HCOOH to a final sample concentration of 400 µM, 200 µM, 100 µM and 50 µM. The black line represents the analysis directly after the synthesis, the blue line represents the analysis after incubation of the diluted samples at rt overnight. (B) Chromatograms (relevant region) of the RP-HPLC analyses of the diluted stock solution of **6.21**, with or without additional NaF, after the given incubation times.

6.3 Conclusion

Aiming at radiolabeled receptor ligands suitable for tumor diagnosis by PET imaging, insertion of [^{18}F]AlF^{2+} into a chelator-conjugated ligand represents a reasonable alternative to the use of ^{68}Ga for tracer labeling[2,9,72]. Nevertheless, the application of [^{18}F]AlF^{2+} in complex with a chelating moiety for clinical PET imaging can be considered controversial: on the one hand, clinical investigations with a HBED-CC-conjugated PSMA ligand were pursued despite reports on its in vitro and in vivo instability[28-30,35,36,39]; on the other hand, the NOTA-conjugated [^{18}F]AlF^{2+}-labeled SSTR2 ligand [^{18}F]AlF-NOTA-octreotide, which showed no in vitro and in vivo decomposition[10,18], is currently subject to clinical studies and reveals comparable performance as the standard SSTR2 PET tracer [^{68}Ga]Ga-DOTA-TATE[73-76]. These contradictory observations emphasize that (aside from the structure of the PET ligand) the choice of an appropriate type of chelator is crucial in order to avoid defluorination or loss of the complete AlF^{2+}-ion under physiologic conditions. Following the objective of developing [^{18}F]AlF^{2+}-labeled NTS_1R PET ligands, this aspect has to be considered in future studies.

6.4 Experimental section

6.4.1 General experimental conditions

Solvents and buffer components, purchased from commercial suppliers, were of analytical grade. Gradient grade MeOH for HPLC was obtained from Merck Chemicals (Darmstadt, Germany) and gradient grade MeCN for HPLC was from Sigma-Aldrich (Taufkirchen, Germany) or Merck. *N*,*N*-Diisopropylethylamine (DIPEA, 99%) and (*R*)-2-(Boc-amino)-3-(4'-fluoro-[1,1'-biphenyl]-4-yl)propanoic acid (**4.24**) were obtained from ABCR (Karlsruhe, Germany). HCOOH and K_2CO_3 were from Roth (Karlsruhe, Germany) and 1 M HCl was from VWR Chemicals (Fontenay-sous-Bois, France). Anhydrous *N*,*N*-dimethylformamide (DMF) (99.8%), 1,1,1,3,3,3-hexafluoro-2-propanol (HFIP), $Ga(NO_3)_3$ hydrate, 7-methyl-1,5,7-triazabicyclo[4.4.0]dec-5-ene (MTBD), methyl-4-nitrobenzenesulfonate (**3.15**), 2-mercaptoethanol and 1-methyl-D-Trp were purchased from Sigma-Aldrich. Sodium acetate was from Merck Chemicals. DMF (for peptide synthesis, packed under nitrogen, code D/3848/PB17), 1-methylpyrrolidin-2-one (NMP) (for peptide synthesis, nitrogen flushed), anhydrous NMP (99.5%), CH_2Cl_2 and 1-hydroxy-1*H*-benzotriazole (HOBt) hydrate were obtained from Acros Organics/Fisher Scientific (Nidderau, Germany). When used for the coupling of non-standard Fmoc-amino acids (SPPS), HOBt hydrate, containing up to 3% water, was dried using a lyophilizer. Anhydrous $AlCl_3$ (98%) was from Merck (Hohenbrunn, Germany), and NaF was from Fluka/Sigma Aldrich (Steinheim, Germany). 4-[(Boc-amino)methyl]-3-fluoro-benzoic acid (> 95%) (**4.27**) was purchased from Activate Scientific (Prien am Chiemsee, Germany) and Boc-ε-aminocaproic acid succinimidyl ester (**4.30**) was purchased from Bachem (Bubendorf, Switzerland). DOTA-tris(*t*Bu)ester succinimidyl ester (**4.13**), NOTA-bis(*t*Bu)ester (**6.17**), NOTA succinimidyl ester (**6.18**) and (*R*)-NODA-GA-tris(*t*Bu)ester (**6.27**) were from CheMatech (Dijon, France), and HBED-CC-tris(*t*Bu)ester (**6.26**) was from ABX (Radeberg, Germany). Trifluoroacetic acid (TFA) and absolute EtOH were obtained from Honeywell (Seelze, Germany). Collidine, 2-nitrobenzenesulfonylchloride and 1,8-diazabicyclo[5.4.0]undec-7-ene (DBU) were from Alfa Aesar/ThermoFisher (Heysham, UK). Piperidine and *N*,*N*,*N*',*N*'-tetramethyl-*O*-(1*H*-benzotriazole-1-yl)-uronium hexafluorophosphate (HBTU) were purchased from Iris Biotech (Marktredwitz, Germany). Deuterated solvents were obtained from Deutero (Kastellaun, Germany). Bovine serum albumin (BSA) was purchased from Serva (Heidelberg, Germany). Oxyma pure, *N,N'*-diisopropylcarbodiimide (DIC), H-Leu-2-ClTrt resin (loading: 0.79 mmol/g), Fmoc-N-Me-Arg(Pbf)-OH, Fmoc-Pro-OH, Fmoc-Ile-OH and Fmoc-Tle-OH (Fmoc-L-α-*tert*-butylglycine) were from Merck Biosciences (Schwalbach am Taunus, Germany). Fmoc-Arg(Pbf)-OH and Fmoc-Tyr(*t*Bu)-OH were from Iris Biotech or Carbolution (St. Ingbert, Germany). Ultrapure 4-(2-hydroxyethyl)-1-piperazineethanesulfonic acid (HEPES) was from Gerbu (Heidelberg, Germany). The syntheses of the arginine building block **3.06a**[50], peptide **6.22**[50] and radioligand [^{3}H]UR-MK300 ([^{3}H]**2.13**)[50] were described elsewhere. The synthesis of arginine building block **5.05** was performed in analogy to building block **3.06a**[50] and will be described elsewhere. **6.12** was synthesized within the scope of the Master Thesis of Lisa Schindler (Institute of Pharmacy, University of Regensburg, 2016). Millipore water was used throughout for the preparation of buffers, stock solutions and HPLC eluents. 1.5- and 2-mL polypropylene reaction vessels with screw cap (in the following referred to as "reaction vessel with screw cap") from Süd-Laborbedarf (Gauting, Germany) were used for the preparation and

storage of stock solutions, and for small-scale reactions. 1.5- or 2-mL polypropylene reaction vessels (in the following referred to as "reaction vessel") from Sarstedt (Nümbrecht, Germany) were used for the preparation of serial dilutions and for the determination of stabilities in plasma. For the evaporation of solvents in 1.5- or 2-mL reaction vessels, a Savant Speed-Vac Plus SC110A vacuum concentrator (Thermo Fisher Scientific, Waltham, MA) was used. NMR spectra were recorded on a Bruker Avance 600 instrument (^{1}H: 600 MHz) (Bruker, Karlsruhe, Germany) at 300 K. The spectra were calibrated based on the solvent residual peaks (^{1}H-NMR: DMSO-d_6: δ = 2.50 ppm). ^{1}H-NMR data are reported as follows: chemical shift δ in ppm (multiplicity (s = singlet, d = doublet, t = triplet, m = multiplet, br s = broad singlet), integral, coupling constant J in Hz). High resolution mass spectra (HRMS) were acquired with an Agilent 6540 UHD Accurate-Mass Q-TOF LC/MS system coupled to an Agilent 1290 HPLC system (Agilent Technologies, Santa Clara, CA), using an ESI source. Analyses were performed using the following LC method: column: Luna Omega C18, 1.6 µm, 50 × 2.1 mm (Phenomenex, Aschaffenburg, Germany), column temperature: 40 °C, flow: 0.6 mL/min, solvent/linear gradient: 0-4 min: 0.1% aqueous HCOOH/0.1% HCOOH in MeCN 95:5-2:98, 4-5 min: 2:98. Preparative HPLC was performed with a system from Knauer (Berlin, Germany) consisting of two K-1800 pumps and a K-2001 detector. A Kinetex-XB C18, 5 µm, 250 mm × 21 mm (Phenomenex) or a Gemini-NX C18, 5 µm, 250 mm × 21 mm (Phenomenex) served as RP-columns at a flow rate of 20 mL/min. Mixtures of 0.2% aqueous TFA (A1) and MeCN (B1), 0.1% aq TFA (A2) and B1 or 0.1% aq HCOOH (A3) and 0.1% HCOOH in MeCN (B2) were used as mobile phase. A detection wavelength of 220 nm was used throughout. Collected fractions were lyophilized using an Alpha 2-4 LD apparatus (Martin Christ, Osterode am Harz, Germany) or a Scanvac CoolSafe 100-9 freeze-dryer (Labogene, Allerød, Denmark) both equipped with a vacuubrand RZ 6 rotary vane vacuum pump. Analytical HPLC analysis of compounds **6.01**-**6.11**, **6.13**-**6.16** and **6.19**-**6.21** was performed with a system from Agilent Technologies consisting of a 1290 Infinity binary pump equipped with a degasser, a 1290 Infinity Autosampler, a 1290 Infinity Thermostated Column Compartment, a 1260 Infinity Diode Array Detector and a 1260 Infinity Fluorescence Detector. A Kinetex-XB C18, 2.6 µm, 100 × 3 mm (Phenomenex) or a Gemini-NX C18, 3 µm, 150 × 3 mm (Phenomenex) served as stationary phase at a flow rate of 0.5 mL/min, 0.6 mL/min or 0.8 mL/min. The oven temperature was set to 25 °C. UV detection was performed at 220 nm and fluorescence detection at 275/305 nm. The injection volume was 20 µL. Mixtures of A3, 0.04% aq TFA (A4) or 0.05% aq HCOOH (A5) and B1, B2 or MeOH (B3) were used as mobile phase. The following linear gradients were applied for purity controls: compounds **6.01**-**6.04**, **6.06**-**6.11**, **6.13**-**6.16**, **6.19** and **6.20** (column: Kinetex-XB C18, flow rate: 0.6 mL/min): 0-12 min: A4/B1 90:10-70:30, 12-16 min: 70:30-5:95, 16-20 min: 5:95; compound **6.05** (column: Kinetex-XB C18, flow rate: 0.5 mL/min): 0-12 min: A5/B3 95:5-70:30, 12-16 min: 70:30-5:95, 16-20 min: 5:95. The following linear gradient was used for investigating the purity and the chemical stability of **6.21** (column: Gemini-NX C18, flow rate: 0.8 mL/min): 0-12 min: A3/B2 93:7-88:12, 12-16 min: 88:12-5:95, 16-20 min: 5:95. The following linear gradient was used for the analysis of plasma stability samples (column: Kinetex-XB C18, flow rate: 0.6 mL/min): 0-12 min: A4/B1 90:10-73:27, 12-16 min: 73:27-5:95, 16-20 min: 5:95. Retention (capacity) factors k were calculated from the retention times t_R according to $k = (t_R - t_0)/t_0$ (t_0 = dead time). Peptides were characterized by HRMS and RP-HPLC analysis. Additionally, ^{1}H- and ^{1}H-COSY NMR spectra were acquired of **6.01**-**6.05**, **6.13**-**6.16** and **6.19**.

Annotation concerning the ^{1}H-NMR spectra (solvent: DMSO-d_6): in order to allow an integration of the signals interfering with the broad water signal at ca 3.5 ppm, ^{1}H-NMR spectra were additionally recorded in DMSO-d_6/D_2O (9:1 v/v (**6.01**, **6.02**) or 5:1 v/v (**6.03**-**6.05**, **6.13**-**6.16** and **6.19**)) (spectra and data not shown).

Additional analytical data of compounds (HPLC analyses and ^{1}H-NMR spectra) are provided in the Appendix.

6.4.2 General procedure for solid-phase peptide synthesis (SPPS)

Peptides were synthesized by manual SPPS according to a reported procedure[50] with minor modifications. The resin was allowed to swell in the solvent for 45 min before the beginning of the synthesis. Protected standard amino acids (Fmoc-Arg(Pbf)-OH, Fmoc-Pro-OH, Fmoc-Ile-OH, Fmoc-Tyr(*t*Bu)-OH) were used in 5-fold excess, Fmoc-N-Me-Arg(Pbf)-OH was used in 3.5-fold excess, and Fmoc-Tle-OH was used in 4-fold excess (**6.01**) or 4.4-fold excess (**6.03**). The arginine building blocks **3.06a** and **5.05** were used in 3-fold excess. Amino acid coupling was performed with HBTU/HOBt/DIPEA (Fmoc-Arg(Pbf)-OH, Fmoc-Pro-OH, Fmoc-Ile-OH, Fmoc-Tyr(*t*Bu)-OH: 4.9/5/10 equiv., Fmoc-N-Me-Arg(Pbf)-OH: 3.45/3.5/7 equiv., Fmoc-Tle-OH: 3.95/4/8 (**6.01**) or 4.35/4.4/8.8 (**6.03**) equiv., **3.06a**, **5.05**: 3/3/6 equiv.). For the coupling of Fmoc-N-Me-Arg(Pbf)-OH and the arginine building blocks **3.06a** and **5.05**, anhydrous solvents (DMF, NMP) were used. Except for the arginine building blocks **3.06a** and **5.05**, "double coupling" was performed (2 × 60 min or 2 × 120 min at 35 °C). In the case of the arginine derivatives **3.06a** and **5.05**, "single coupling" was performed with a longer reaction time (16-19 h at 35 °C).

6.4.3 General procedure for the conjugation of the DOTA chelator to peptides

The reaction was performed in a 2-mL reaction vessel with screw cap, equipped with a magnetic micro stirrer. DIPEA (17 equiv. (**6.08**) or 13 equiv. (**6.04**, **6.11**)) was added to a solution of the peptide (1.4 equiv. (**6.08**) or 1.1 equiv. (**6.04**, **6.11**)) in DMF/NMP (75:25 v/v) or DMF/NMP (80:20 v/v) (20-65 µL), followed by the addition of DOTA tris(*tert*-butyl) succinimidyl ester **4.13** (1 equiv.) dissolved in DMF/NMP (75:25 v/v) or DMF/NMP (80:20 v/v) (10-18 µL). After stirring at rt for 30 min, 10% aq TFA (corresponding to 11.5 equiv. TFA (**6.08**) or 9 equiv. TFA (**6.04**, **6.11**)) was added. The protected intermediate was isolated by preparative HPLC. After lyophilization of the eluate, TFA/H_2O (80:20 v/v) (2 mL, **6.04**) or TFA/H_2O (95:5 v/v) (1.2-1.5 mL, **6.08**, **6.11**) was added, and the mixture was stirred at 50 °C overnight. H_2O (25-60 mL) was added and the mixture was subjected to lyophilization. The DOTA-conjugated peptide was purified by preparative HPLC.

6.4.4 General procedure for the conjugation of the NOTA chelator to peptides

The reaction was performed in a 2-mL reaction vessel with screw cap, equipped with a magnetic micro stirrer. DIPEA (24 equiv. (**6.13**-**6.16**) or 12 equiv. (**6.19**)) was added to a solution of the peptide (2 equiv. (**6.13**-**6.16**) or 1 equiv. (**6.19**)) in DMF/NMP (75:25 v/v) (125-320 µL), followed by the addition of NOTA succinimidyl ester **6.18** (1 equiv.) dissolved in anhydrous DMF (30-235 µL). After shaking at rt for 60 min, 10% aq TFA (corresponding

to 24 equiv. TFA (**6.13**-**6.16**) or 12 equiv. TFA (**6.19**)) was added. The NOTA-conjugated peptide was purified by preparative HPLC.

6.4.5 Synthesis protocols and analytical data of compounds 6.01-6.11, 6.13-6.16 and 6.19-6.21

***N*$^{\alpha}$-{*N*$^{\omega}$-[(4-Aminobutyl)aminocarbonyl]arginyl}-*N*$^{\alpha}$-methyl-Arg-Pro-Tyr-2-*tert*-butyl-Gly-Leu tetrakis(hydrotrifluoroacetate) (6.01).** Peptide **6.01** was synthesized according to the general procedure for SPPS using a H-Leu-2-ClTrt resin (loading 0.79 mmol/g) (202 mg, 0.16 mmol). Purification by preparative RP-HPLC (column: Kinetex-XB C18, gradient: 0-35 min: A1/B1 92:8-57:43, t_R = 18 min) afforded **6.01** as white fluffy solid (7.1 mg, 3%). ^{1}H-NMR (600 MHz, DMSO-d_6): δ 0.82-0.92 (m, 15H), 1.39-1.55 (m, 8H), 1.55-1.78 (m, 10H), 1.93-2.01 (m, 1H), 2.64-2.76 (m, 1H), 2.76-2.81 (m, 2H), 2.84-2.99 (m, 4H), 3.06-3.15 (m, 4H), 3.22-3.29 (m, 3H), 3.42-3.55 (m, 1H), 4.17-4.24 (m, 1H), 4.24-4.33 (m, 2H), 4.33-4.41 (m, 1H), 4.41-4.48 (m, 1H), 5.06-5.20 (m, 1H), 6.58-6.66 (m, 2H), 6.66-7.11 (br s, 2H, interfering with the next listed signal), 6.99-7.03 (m, 2H), 7.11-7.48 (br s, 2H), 7.48-7.86 (m, 6H), 7.97 (d, 1H, *J* 7.8 Hz), 8.00-8.32 (m, 4H), 8.32-8.70 (m, 2H), 8.89-9.28 (m, 2H), 10.54 (br s, 1H), 12.46 (br s, 1H). HRMS: *m/z* [*M*+2H]$^{2+}$ calcd. for [$C_{44}H_{78}N_{14}O_9$]$^{2+}$ 473.3033, found 473.3044. RP-HPLC (220 nm): 96% (t_R = 5.9 min, *k* = 6.8). $C_{44}H_{76}N_{14}O_9$ · $C_8H_4F_{12}O_8$ (945.18 + 456.09).

***N*$^{\alpha}$-{*N*$^{\omega}$-[(4-Aminobutyl)aminocarbonyl]arginyl}-*N*$^{\alpha}$-methyl-Arg-Pro-Tyr-Ile-Leu tetrakis(hydrotrifluoroacetate) (6.02).** Peptide **6.02** was synthesized according to the general procedure for SPPS using a H-Leu-2-ClTrt resin (loading 0.79 mmol/g) (120 mg, 0.095 mmol). Purification by preparative RP-HPLC (column: Kinetex-XB C18, gradient: 0-35 min: A1/B1 92:8-57:43, t_R = 19 min) afforded **6.02** as white fluffy solid (2.5 mg, 2%). ^{1}H-NMR (600 MHz, DMSO-d_6): δ 0.78-0.86 (m, 9H), 0.88-0.92 (m, 3H), 1.02-1.10 (m, 1H), 1.38-1.67 (m, 14H), 1.67-1.80 (m, 6H), 1.93-2.01 (m, 1H), 2.63-2.72 (m, 1H), 2.72-2.82 (m, 2H), 2.82-2.99 (m, 4H), 3.05-3.16 (m, 4H), 3.25-3.30 (m, 3H), 3.45-3.56 (m, 1H), 4.12-4.24 (m, 2H), 4.24-4.33 (m, 1H), 4.33-4.54 (m, 2H), 5.08-5.19 (m, 1H), 6.58-6.65 (m, 2H), 6.65-7.10 (br s, 2H, interfering with the next listed signal), 6.99-7.02 (m, 2H), 7.10-7.45 (br s, 2H), 7.45-7.87 (m, 6H), 7.90 (d, 1H, *J* 7.9 Hz), 7.94-8.35 (m, 4H), 8.35-8.84 (m, 2H), 8.96-9.28 (m, 2H), 10.50 (br s, 1H), 12.48 (br s, 1H). HRMS: *m/z* [*M*+2H]$^{2+}$ calcd. for [$C_{44}H_{78}N_{14}O_9$]$^{2+}$ 473.3033, found 473.3044. RP-HPLC (220 nm): 95% (t_R = 6.2 min, *k* = 7.2). $C_{44}H_{76}N_{14}O_9$ · $C_8H_4F_{12}O_8$ (945.18 + 456.09).

***N*$^{\alpha}$-Methyl-*N*$^{\omega}$-[(2-aminoethyl)aminocarbonyl]Arg-Arg-Pro-Tyr-2-*tert*-butyl-Gly-Leu tetrakis(hydrotrifluoroacetate) (6.03).** Peptide **6.03** was synthesized according to the general procedure for SPPS using a H-Leu-2-ClTrt resin (loading 0.79 mmol/g) (100 mg, 0.079 mmol) with the following modification: after coupling of arginine building block **5.05** and Fmoc-deprotection, the resin was washed with CH_2Cl_2 (5 ×), a solution of 2-nitrobenzenesulfonylchloride (52.5 mg, 0.237 mmol) and collidine (52.4 µL, 0.395 mmol) in CH_2Cl_2 (1.5 mL) was added and the mixture was shaken at rt for 2 h. The resin was washed with DMF (5 ×), and a solution of MTBD (45.4 µL, 0.316 mmol) and **3.15** (85.8 mg, 0.395 mmol) in DMF (1.8 mL) was added. After shaking at rt for 30 min, the resin was washed with DMF (3 ×) followed by the addition of a solution of DBU (59.0 µL, 0.395 mmol) and 2-mercaptoethanol (55.1 µL, 0.790 mmol) in DMF (1.5 mL) and shaking at rt for 30 min. The resin was washed with DMF (5 ×) followed by cleavage from the resin as

described in the general procedure for SPPS. Purification by preparative RP-HPLC (column: Gemini-NX C18, gradient: 0-30 min: A1/B1 92:8-60:40, t_R = 14 min) afforded **6.03** as white fluffy solid (68.3 mg, 63%). ^{1}H-NMR (600 MHz, DMSO-d_6): δ 0.79-0.96 (m, 15H), 1.44-1.88 (m, 14H), 1.91-2.05 (m, 1H), 2.45-2.48 (m, 3H), 2.64-2.71 (m, 1H), 2.82-2.96 (m, 3H), 3.05-3.14 (m, 2H), 3.23-3.31 (m, 4H), 3.52-3.64 (m, 2H), 3.74-3.88 (m, 1H), 4.16-4.25 (m, 1H), 4.26-4.30 (m, 1H), 4.31-4.39 (m, 1H), 4.42-4.61 (m, 2H), 6.58-6.63 (m, 2H), 6.63-7.09 (br s, 2H, interfering with the next listed signal), 6.97-7.00 (m, 2H), 7.09-7.51 (br s, 2H), 7.51-7.71 (m, 3H), 7.71-7.91 (m, 3H), 7.96 (d, 1H, *J* 7.9 Hz), 8.22 (d, 1H, *J* 7.5 Hz), 8.36-8.73 (m, 2H), 8.73-9.29 (m, 5H), 10.54-10.83 (m, 1H), 12.49 (br s, 1H). HRMS: *m/z* [*M*+3H]$^{3+}$ calcd. for $[C_{42}H_{75}N_{14}O_9]^{3+}$ 306.5275, found 306.5283. RP-HPLC (220 nm): 91% (t_R = 5.8 min, *k* = 6.6). $C_{42}H_{72}N_{14}O_9$ · $C_8H_4F_{12}O_8$ (917.13 + 456.09).

***N*$^{\alpha}$-Methyl-*N*$^{\omega}$-{[2-(N-{2-[4,7,10-tris(carboxymethyl)-1,4,7,10-tetraazacyclododecan-1-yl]acetyl})aminoethyl]aminocarbonyl}Arg-Arg-Pro-Tyr-2-*tert*-butyl-Gly-Leu tetrakis(hydrotrifluoroacetate) (6.04).** Compound **6.04** was prepared from **6.03** (9.7 mg, 7.06 µmol) and **4.13** (5.19 mg, 6.36 µmol) according to the general procedure for DOTA-conjugation. Isolation of the protected intermediate: column: Gemini-NX C18, gradient: 0-6 min: A1/B1 85:15-79:21, 6-28 min: 79:21-40:60, t_R = 18 min. Purification of the product by preparative RP-HPLC (column: Gemini-NX C18, gradient: 0-35 min: A1/B1 97:3-60:40, t_R = 21 min) afforded **6.04** as white fluffy solid (8.5 mg, 76%). ^{1}H-NMR (600 MHz, DMSO-d_6): δ 0.79-0.95 (m, 15H), 1.46-1.87 (m, 14H), 1.95-2.05 (m, 1H), 2.45-2.48 (m, 3H), 2.65-2.71 (m, 1H), 2.87-2.91 (m, 1H), 3.05-3.36 (m, 28H), 3.61-3.69 (m, 4H), 3.76-3.87 (m, 3H), 4.19-4.24 (m, 1H), 4.26-4.30 (m, 1H), 4.34-4.39 (m, 1H), 4.43-4.58 (m, 2H), 6.58-6.62 (m, 2H), 6.62-7.14 (br s, 2H, interfering with the next listed signal), 6.97-7.00 (m, 2H), 7.14-7.54 (br s, 2H), 7.54-7.68 (m, 2H), 7.68-8.00 (m, 2H), 8.00-8.65 (br s, 3H, interfering with the next listed signal), 8.21-8.24 (m, 1H), 8.65-9.57 (m, 5H), 11.78-12.98 (m, 2H). 4 exchangeable protons (NH, OH) of the presumably 4-fold protonated molecule could not be identified. HRMS: *m/z* [*M*+2H]$^{2+}$ calcd. for $[C_{58}H_{100}N_{18}O_{16}]^{2+}$ 652.3777, found 652.3785. RP-HPLC (220 nm): 99% (t_R = 6.0 min, *k* = 6.9). $C_{58}H_{98}N_{18}O_{16}$ · $C_8H_4F_{12}O_8$ (1303.53 + 456.09).

***N*$^{\alpha}$-Methyl-*N*$^{\omega}$-{[2-(N-{2-[gallium(III)-4,7,10-tris(carboxymethyl)-1,4,7,10-tetraazacyclododecan-1-yl]acetyl})aminoethyl]aminocarbonyl}Arg-Arg-Pro-Tyr-2-*tert*-butyl-Gly-Leu tris(hydrotrifluoroacetate) (6.05).** The incorporation reaction was performed in a 2-mL reaction vessel with screw cap. A solution of $Ga(NO_3)_3 \times H_2O$ (1.35 mg, 4.94 µmol, 0.4 M) in aqueous HCl (10 mM) was added to a solution of **6.04** (2.9 mg, 1.65 µmol, 4 mM) in HEPES buffer (0.2 M, pH 4.2) and the mixture was shaken at 100 °C for 10 min using a Thermocell mixing block from Bioer (Hangzhou, China). Purification by preparative RP-HPLC (column: Gemini-NX C18, gradient: 0-35 min: A2/B1 97:3-60:40, t_R = 21 min) yielded **6.05** as white fluffy solid (3.0 mg, > 99%). ^{1}H-NMR (600 MHz, DMSO-d_6): δ 0.80-0.95 (m, 15H), 1.37-1.90 (m, 14H), 1.93-2.04 (m, 1H), 2.47-2.49 (m, 3H), 2.63-2.74 (m, 1H), 2.84-2.92 (m, 1H), 3.07-3.31 (m, 20H), 3.45-3.49 (m, 2H), 3.49-3.92 (m, 13H), 4.18-4.25 (m, 1H), 4.25-4.31 (m, 1H), 4.31-4.41 (m, 1H), 4.42-4.60 (m, 2H), 6.58-6.63 (m, 2H), 6.63-7.14 (br s, 2H, interfering with the next listed signal), 6.98-7.01 (m, 2H), 7.14-7.54 (br s, 2H), 7.54-7.80 (m, 3H), 7.98 (d, 1H, *J* 7.7 Hz), 8.14-8.64 (m, 4H), 8.78-9.21 (m, 4H), 10.10-10.45 (m, 1H), 12.48 (br s, 1H), 13.29 (br s, 1H). HRMS: *m/z* [*M*+3H]$^{3+}$

calcd. for $[C_{58}H_{98}GaN_{18}O_{16}]^{3+}$ 457.2216, found 457.2223. RP-HPLC (220 nm): > 99% (t_R = 8.6 min, k = 10.3). $C_{58}H_{95}GaN_{18}O_{16}$ · $C_6H_3F_9O_6$ (1370.23 + 342.07).

N^{α}-Methyl-N^{ω}-{[2-N-(3-fluoro-4-aminomethyl-benzoyl)aminoethyl]aminocarbonyl}Arg-Arg-Pro-Tyr-2-*tert*-butyl-Gly-Leu tetrakis(hydrotrifluoroacetate) (6.06). HBTU (1.6 mg, 4.2 µmol) and DIPEA (1.5 µL, 8.4 µmol) were added to a solution of HOBt (0.6 mg, 4.2 µmol) and **4.27** (1.6 mg, 6.0 µmol) in DMF/NMP (80:20 v/v) (10 µL) in a 2-mL reaction vessel. The mixture was vortexed, incubated for 5 min at rt and added to a solution of **6.03** (11.7 mg, 8.5 µmol) and DIPEA (5.9 µL, 34.1 µmol) in DMF/NMP (80:20 v/v) (10 µL) in a 2-mL reaction vessel with screw cap equipped with a magnetic micro stirrer. After stirring at rt for 60 min, 10% aq TFA (42.4 µL, 42.4 µmol) was added. The protected intermediate was isolated by preparative HPLC (column: Gemini-NX C18, gradient: 0-6 min: A1/B1 85:15-82:18, 6-15 min: 82:18-70:30, 15-25 min: 70:30-60:40, t_R = 22 min). After lyophilization of the eluate, TFA/H_2O (95:5 v/v) (1 mL) was added, and the mixture was stirred at rt for 2.5 h. Additional TFA (300 µL) was added and stirring was continued for 1 h. H_2O (30 mL) was added and the mixture was subjected to lyophilization. Purification of the product by preparative RP-HPLC (column: Gemini-NX C18, gradient: 0-5 min: A1/B1 85:15-80:20, 5-15 min: 80:20-60:40, t_R = 11 min) afforded **6.06** as white fluffy solid (2.8 mg, 44%). ^{1}H-NMR (600 MHz, DMSO-d_6): δ 0.80-0.93 (m, 15H), 1.46-1.87 (m, 14H), 1.94-2.05 (m, 1H), 2.46-2.48 (m, 3H), 2.64-2.71 (m, 1H), 2.85-2.92 (m, 1H), 3.07-3.14 (m, 2H), 3.29-3.37 (m, 6H), 3.56-3.61 (m, 2H), 3.76-3.83 (m, 1H), 4.11-4.17 (m, 2H), 4.18-4.24 (m, 1H), 4.26-4.30 (m, 1H), 4.31-4.40 (m, 1H), 4.43-4.59 (m, 2H), 6.55-6.63 (m, 2H), 6.63-7.13 (br s, 2H, interfering with the next listed signal), 6.97-7.00 (m, 2H), 7.13-7.59 (br s, 2H), 7.59-7.76 (m, 6H), 7.97 (d, 1H, J 7.9 Hz), 8.12-8.63 (m, 6H), 8.63-9.31 (m, 6H), 10.23-10.56 (m, 1H), 12.49 (br s, 1H). HRMS: m/z $[M+H]^+$ calcd. for $[C_{50}H_{79}FN_{15}O_{10}]^+$ 1068.6113, found 1068.6112. RP-HPLC (220 nm): 98% (t_R = 6.5 min, k = 7.6). $C_{50}H_{78}FN_{15}O_{10}$ · $C_8H_4F_{12}O_8$ (1068.27 + 456.09).

N^{α}-Methyl-N^{ω}-({2-N-[4-(4-fluorophenyl)-phenylalanyl]aminoethyl}aminocarbonyl)Arg-Arg-Pro-Tyr-2-*tert*-butyl-Gly-Leu tetrakis(hydrotrifluoroacetate) (6.07). Compound **6.07** was prepared from **6.03** (11.6 mg, 8.4 µmol) and **4.24** (2.1 mg, 5.9 µmol) according to the procedure for the synthesis of **6.06**. Isolation of the protected intermediate: column: Gemini-NX C18, gradient: 0-6 min: A1/B1 85:15-82:18, 6-15 min: 82:18-70:30, 15-25 min: 70:30-60:40, 25-30 min: 60:40-40:60, t_R = 28 min. Purification of the product by preparative RP-HPLC (column: Gemini-NX C18, gradient: 0-5 min: A1/B1 85:15-70:30, 5-15 min: 70:30-50:50, t_R = 10 min) afforded **6.07** as white fluffy solid (3.9 mg, 58%). ^{1}H-NMR (600 MHz, DMSO-d_6): δ 0.80-0.94 (m, 15H), 1.44-1.86 (m, 14H), 1.94-2.03 (m, 1H), 2.42-2.47 (m, 3H), 2.64-2.72 (m, 1H), 2.86-2.92 (m, 1H), 2.96-3.01 (m, 1H), 3.03-3.17 (m, 6H), 3.20-3.28 (m, 3H), 3.49-3.65 (m, 2H), 3.69-3.88 (m, 1H), 3.90-3.99 (m, 1H), 4.17-4.25 (m, 1H), 4.25-4.31 (m, 1H), 4.32-4.38 (m, 1H), 4.41-4.60 (m, 2H), 6.57-6.62 (m, 2H), 6.62-7.09 (br s, 2H, interfering with the next listed signal), 6.97-7.00 (m, 2H), 7.09-7.51 (br s, 2H, interfering with the next listed signal), 7.27-7.33 (m, 4H), 7.51-7.75 (m, 7H), 7.97 (d, 1H, J 7.5 Hz), 8.06-8.73 (m, 7H), 8.73-9.29 (m, 4H), 10.29-10.72 (m, 1H), 12.49 (br s, 1H). 1 exchangeable proton (NH, OH) of the presumably 4-fold protonated molecule could not be identified. HRMS: m/z $[M+H]^+$ calcd. for $[C_{57}H_{85}FN_{15}O_{10}]^+$ 1158.6582, found 1158.6578. RP-HPLC (220 nm): > 99% (t_R = 11.4 min, k = 14.0). $C_{57}H_{84}FN_{15}O_{10}$ · $C_8H_4F_{12}O_8$ (1158.39 + 456.09).

***N*$^{\alpha}$-Methyl-*N*$^{\omega}$-[(2-N-{*N*$^{\alpha}$-[4,7,10-tris(carboxymethyl)-1,4,7,10-tetraazacyclododecan-1-yl]acetyl-4-(4-fluorophenyl)-phenylalanyl}aminoethyl)aminocarbonyl]Arg-Arg-Pro-Tyr-2-*tert*-butyl-Gly-Leu tetrakis(hydrotrifluoroacetate) (6.08).** Compound **6.08** was prepared from **6.07** (2.8 mg, 1.73 µmol) and **4.13** (0.99 mg, 1.21 µmol) according to the general procedure for DOTA-conjugation. Isolation of the protected intermediate: column: Gemini-NX C18, gradient: 0-5 min: A1/B1 85:15-70:30, 5-15 min: 70:30-50:50, t_R = 13 min. Purification of the product by preparative RP-HPLC (column: Gemini-NX C18, gradient: 0-5 min: A1/B1 85:15-70:30, 5-15 min: 70:30-50:50, t_R = 10 min) afforded **6.08** as white fluffy solid (1.1 mg, 45%). HRMS: *m/z* [*M*+2H]$^{2+}$ calcd. for $[C_{73}H_{112}FN_{19}O_{17}]^{2+}$ 772.9228, found 772.9240. RP-HPLC (220 nm): > 99% (t_R = 12.0 min, *k* = 14.8). $C_{73}H_{110}FN_{19}O_{17} \cdot C_8H_4F_{12}O_8$ (1544.80 + 456.09).

***N*$^{\alpha}$-Methyl-*N*$^{\omega}$-{[N-(6-aminohexanoyl)-2-aminoethyl]aminocarbonyl}Arg-Arg-Pro-Tyr-2-*tert*-butyl-Gly-Leu tetrakis(hydrotrifluoroacetate) (6.09).** The reaction was performed in a 2-mL reaction vessel with screw cap, equipped with a magnetic micro stirrer. DIPEA (8.8 µL, 50.7 µmol) and a solution of **4.30** (3.3 mg, 10.1 µmol) in anhydrous DMF/NMP (75:25 v/v) (11 µL) were added to a solution of **6.03** (17.4 mg, 12.7 µmol) in anhydrous DMF/NMP (75:25 v/v) (116 µL). The mixture was shaken at rt for 45 min followed by the addition of 10% aq TFA (50.7 µL, 50.7 µmol). The protected intermediate was isolated by preparative HPLC (column: Gemini-NX C18, gradient: 0-5 min: A1/B1 92:8-90:10, 5-18 min: 90:10-70:30, 18-25 min: 10:90 (isocratic), t_R = 22 min) and the eluate was subjected to lyophilization. TFA/H_2O (95:5 v/v) (2 mL) was added, and the mixture was stirred at rt for 3 h. Additional TFA (1 mL) was added and stirring was continued for 30 min. H_2O (40 mL) was added and the mixture was subjected to lyophilization. Purification of the product by preparative RP-HPLC (column: Gemini-NX C18, gradient: 0-5 min: A1/B1 92:8-85:15, 5-20 min: 85:15-70:30, t_R = 17 min) afforded **6.09** as white fluffy solid (12.4 mg, 82%). ^{1}H-NMR (600 MHz, DMSO-d_6): δ 0.79-0.98 (m, 15H), 1.23-1.29 (m, 2H), 1.45-1.88 (m, 18H), 1.96-2.08 (m, 3H), 2.45-2.49 (m, 3H), 2.64-2.72 (m, 1H), 2.72-2.79 (m, 2H), 2.84-2.93 (m, 1H), 3.05-3.18 (m, 6H), 3.24-3.28 (m, 2H), 3.50-3.66 (m, 2H), 3.72-3.89 (m, 1H), 4.18-4.26 (m, 1H), 4.26-4.31 (m, 1H), 4.32-4.40 (m, 1H), 4.42-4.59 (m, 2H), 6.57-6.62 (m, 2H), 6.62-7.10 (br s, 2H, interfering with the next listed signal), 6.97-7.00 (m, 2H), 7.10-7.47 (br s, 2H), 7.47-7.83 (m, 6H), 7.83-8.03 (m, 2H), 8.12-8.62 (m, 3H), 8.65-9.13 (m, 4H), 9.13-9.26 (m, 1H), 10.13-10.46 (m, 1H), 12.48 (br s, 1H). HRMS: *m/z* [*M*+2H]$^{2+}$ calcd. for $[C_{48}H_{85}N_{15}O_{10}]^{2+}$ 515.8296, found 515.8303. RP-HPLC (220 nm): 99% (t_R = 6.1 min, *k* = 7.0). $C_{48}H_{83}N_{15}O_{10} \cdot C_8H_4F_{12}O_8$ (1030.29 + 456.09).

***N*$^{\alpha}$-Methyl-*N*$^{\omega}$-({N-[N-(6-aminohexanoyl)-6-aminohexanoyl]-2-aminoethyl}aminocarbonyl)Arg-Arg-Pro-Tyr-2-*tert*-butyl-Gly-Leu tetrakis(hydrotrifluoroacetate) (6.10).** Compound **6.10** was prepared from **6.09** (9.5 mg, 6.4 µmol) and **4.30** (1.7 mg, 5.1 µmol) according to the procedure for the synthesis of **6.09**. Isolation of the protected intermediate: column: Gemini-NX C18, gradient: 0-5 min: A1/B1 90:10-82:18, 5-12 min: 82:18-70:30, 12-20 min: 70:30-55:45, t_R = 18 min. Purification of the product by preparative RP-HPLC (column: Gemini-NX C18, gradient: 0-5 min: A1/B1 92:8-85:15, 5-20 min: 85:15-70:30, t_R = 18 min) afforded **6.10** as white fluffy solid (7.6 mg, 93%). ^{1}H-NMR (600 MHz, DMSO-d_6): δ 0.80-0.94 (m, 15H), 1.18-1.28 (m, 4H), 1.33-1.38 (m, 2H), 1.43-1.88 (m, 20H), 1.93-2.07 (m, 5H), 2.45-2.48 (m, 3H), 2.64-2.72

(m, 1H), 2.72-2.79 (m, 2H), 2.85-2.92 (m, 1H), 2.97-3.02 (m, 2H), 3.06-3.15 (m, 6H), 3.24-3.27 (m, 2H), 3.54-3.62 (m, 2H), 3.77-3.87 (m, 1H), 4.18-4.25 (m, 1H), 4.26-4.30 (m, 1H), 4.32-4.39 (m, 1H), 4.44-4.59 (m, 2H), 6.58-6.62 (m, 2H), 6.62-7.11 (br s, 2H, interfering with the next listed signal), 6.98-7.00 (m, 2H), 7.11-7.48 (br s, 2H), 7.48-7.80 (m, 7H), 7.80-8.03 (m, 2H), 8.23 (d, 1H, *J* 7.6 Hz), 8.29-8.61 (m, 2H), 8.64-9.30 (m, 5H), 10.06-10.36 (m, 1H), 12.37 (br s, 1H). HRMS: *m/z* $[M+2H]^{2+}$ calcd. for $[C_{54}H_{96}N_{16}O_{11}]^{2+}$ 572.3717, found 572.3726. RP-HPLC (220 nm): 99% (t_R = 6.9 min, *k* = 8.1). $C_{54}H_{94}N_{16}O_{11}$ · $C_8H_4F_{12}O_8$ (1143.45 + 456.09).

N^{α}-Methyl-N^{ω}-[(N-{N-[6-(N-{2-[4,7,10-tris(carboxymethyl)-1,4,7,10-tetraazacyclododecan-1-yl]acetyl})aminohexanoyl]-6-aminohexanoyl}-2-aminoethyl)aminocarbonyl]Arg-Arg-Pro-Tyr-2-*tert*-butyl-Gly-Leu tetrakis(hydrotrifluoroacetate) (6.11). Compound **6.11** was prepared from **6.10** (6.3 mg, 3.9 µmol) and **4.13** (2.9 mg, 3.5 µmol) according to the general procedure for DOTA-conjugation. Isolation of the protected intermediate: column: Gemini-NX C18, gradient: 0-6 min: A1/B1 85:15-80:20, 6-20 min: 80:20-30:70, t_R = 15 min. Purification of the product by preparative RP-HPLC (column: Gemini-NX C18, gradient: 0-6 min: A1/B1 85:15-75:25, 6-20 min: 75:25-55:45, t_R = 9 min) afforded **6.11** as white fluffy solid (4.5 mg, 64%). HRMS: *m/z* $[M+2H]^{2+}$ calcd. for $[C_{70}H_{122}N_{20}O_{18}]^{2+}$ 765.4618, found 765.4631. RP-HPLC (220 nm): 98% (t_R = 7.2 min, *k* = 8.5). $C_{70}H_{120}N_{20}O_{18}$ · $C_8H_4F_{12}O_8$ (1529.85 + 456.09).

N^{α}-Methyl-N^{ω}-{[4-(N-{2-[4,7-bis(carboxymethyl)-1,4,7-triazacyclononan-1-yl]acetyl})aminobutyl]aminocarbonyl}Arg-Arg-Pro-Tyr-2-*tert*-butyl-Gly-Leu tetrakis(hydrotrifluoroacetate) (6.13). Compound **6.13** was prepared from **3.16** (18.4 mg, 13.1 µmol) and **6.18** (4.3 mg, 6.6 µmol) according to the general procedure for NOTA-conjugation. Purification of the product by preparative RP-HPLC (column: Gemini-NX C18, gradient: 0-20 min: A2/B1 85:15-75:25, t_R = 13 min) afforded **6.13** as white fluffy solid (7.0 mg, 63%). ^{1}H-NMR (600 MHz, DMSO-d_6): δ 0.78-0.95 (m, 15H), 1.42-1.88 (m, 18H), 1.94-2.04 (m, 1H), 2.46-2.48 (m, 3H), 2.62-2.79 (m, 4H), 2.84-3.06 (m, 7H), 3.06-3.23 (m, 9H), 3.25-3.30 (m, 4H), 3.51-3.72 (m, 6H), 3.74-4.82 (m, 1H), 4.17-4.25 (m, 1H), 4.25-4.31 (m, 1H), 4.32-4.40 (m, 1H), 4.43-4.59 (m, 2H), 6.58-6.62 (m, 2H), 6.62-7.13 (br s, 2H, interfering with the next listed signal), 6.97-7.01 (m, 2H), 7.13-7.45 (br s, 2H), 7.45-7.73 (m, 3H), 7.81-8.37 (m, 4H), 8.37-8.75 (m, 1H), 8.79-9.08 (m, 3H), 9.09-9.34 (m, 1H), 10.35-13.26 (m, 2H). 4 exchangeable protons (NH, OH) of the presumably 4-fold protonated molecule could not be identified. HRMS: *m/z* $[M+2H]^{2+}$ calcd. for $[C_{56}H_{97}N_{17}O_{14}]^{2+}$ 615.8695, found 615.8707. RP-HPLC (220 nm): 99% (t_R = 7.1 min, *k* = 8.3). $C_{56}H_{95}N_{17}O_{14}$ · $C_8H_4F_{12}O_8$ (1230.48 + 456.09).

N^{ω}-{[8-(N-{2-[4,7-bis(carboxymethyl)-1,4,7-triazacyclononan-1-yl]acetyl})amino-3,6-dioxaoctyl]aminocarbonyl}Arg-Arg-Pro-Tyr-2-*tert*-butyl-Gly-Leu tetrakis(hydrotrifluoroacetate) (6.14). Compound **6.14** was prepared from **6.12** (7.5 mg, 5.2 µmol) and **6.18** (1.7 mg, 2.6 µmol) according to the general procedure for NOTA-conjugation. Purification of the product by preparative RP-HPLC (column: Gemini-NX C18, gradient: 0-20 min: A2/B1 85:15-75:25, t_R = 14 min) afforded **6.14** as white fluffy solid (2.4 mg, 53%). ^{1}H-NMR (600 MHz, DMSO-d_6): δ 0.79-0.95 (m, 15H), 1.45-1.89 (m, 14H), 1.92-2.03 (m, 1H), 2.64-2.90 (m, 5H), 2.90-3.18 (m, 11H), 3.22-3.28 (m, 6H), 3.39-3.42 (m, 1H), 3.42-3.65 (m, 15H), 3.78-3.90 (m, 1H), 4.16-4.25 (m, 1H), 4.25-4.31 (m, 1H), 4.31-4.39 (m, 1H), 4.39-4.59 (m, 2H), 6.52-6.63 (m, 2H), 6.63-7.11 (br s, 2H, interfering with the

next listed signal), 6.96-7.01 (m, 2H), 7.11-7.47 (br s, 2H), 7.47-7.73 (m, 3H), 7.73-8.02 (m, 2H), 8.02-8.95 (m, 7H), 8.95-9.47 (m, 2H), 9.95-13.34 (m, 2H). 3 exchangeable protons (NH, OH) of the presumably 4-fold protonated molecule could not be identified. HRMS: *m/z* $[M+2H]^{2+}$ calcd. for $[C_{57}H_{99}N_{17}O_{16}]^{2+}$ 638.8722, found 638.8727. RP-HPLC (220 nm): 99% (t_R = 7.1 min, k = 8.3). $C_{57}H_{97}N_{17}O_{16}$ · $C_8H_4F_{12}O_8$ (1276.51 + 456.09).

N^{α}-(N^{α}-Methylarginyl)-N^{ω}-{[4-(N-{2-[4,7-bis(carboxymethyl)-1,4,7-triazacyclononan-1-yl]acetyl})aminobutyl]aminocarbonyl}Arg-Pro-Tyr-2-*tert*-butyl-Gly-Leu tetrakis(hydrotrifluoroacetate) (6.15). Compound **6.15** was prepared from **4.08** (7.5 mg, 5.4 µmol) and **6.18** (1.8 mg, 2.7 µmol) according to the general procedure for NOTA-conjugation. Purification of the product by preparative RP-HPLC (column: Gemini-NX C18, gradient: 0-20 min: A2/B1 85:15-75:25, t_R = 14 min) afforded **6.15** as white fluffy solid (2.7 mg, 60%). ^{1}H-NMR (600 MHz, DMSO-d_6): δ 0.79-0.93 (m, 15H), 1.42-1.64 (m, 12H), 1.64-1.87 (m, 6H), 1.95-2.04 (m, 1H), 2.47-2.48 (m, 3H), 2.65-2.90 (m, 5H), 2.93-3.20 (m, 14H), 3.20-3.30 (m, 5H), 3.51-3.72 (m, 6H), 3.74-3.83 (m, 1H), 4.14-4.25 (m, 1H), 4.25-4.39 (m, 2H), 4.42-4.62 (m, 2H), 6.55-6.62 (m, 2H), 6.62-7.13 (br s, 2H, interfering with the next listed signal), 6.97-7.00 (m, 2H), 7.13-7.46 (br s, 2H), 7.46-7.80 (m, 3H), 7.80-8.68 (m, 5H), 8.68-9.66 (m, 5H), 9.66-13.46 (m, 3H). 2 exchangeable protons (NH, OH) of the presumably 4-fold protonated molecule could not be identified. HRMS: *m/z* $[M+2H]^{2+}$ calcd. for $[C_{56}H_{97}N_{17}O_{14}]^{2+}$ 615.8695, found 615.8706. RP-HPLC (220 nm): 99% (t_R = 7.3 min, k = 8.6). $C_{56}H_{95}N_{17}O_{14}$ · $C_8H_4F_{12}O_8$ (1230.48 + 456.09).

N^{α}-Arginyl-N^{α}-methyl-N^{ω}-{[4-(N-{2-[4,7-bis(carboxymethyl)-1,4,7-triazacyclononan-1-yl]acetyl})aminobutyl]aminocarbonyl}Arg-Pro-Tyr-2-*tert*-butyl-Gly-Leu tetrakis(hydrotrifluoroacetate) (6.16). Compound **6.16** was prepared from **4.11** (17.9 mg, 12.8 µmol) and **6.18** (4.2 mg, 6.4 µmol) according to the general procedure for NOTA-conjugation. Purification of the product by preparative RP-HPLC (column: Gemini-NX C18, gradient: 0-30 min: A2/B1 85:15-70:30, t_R = 13 min) afforded **6.16** as white fluffy solid (3.8 mg, 35%). ^{1}H-NMR (600 MHz, DMSO-d_6): δ 0.79-0.95 (m, 15H), 1.42-1.80 (m, 18H), 1.93-2.00 (m, 1H), 2.62-2.75 (m, 4H), 2.81-3.07 (m, 10H), 3.07-3.21 (m, 8H), 3.21-3.30 (m, 6H), 3.48-3.55 (m, 1H), 3.55-3.73 (m, 4H), 4.16-4.25 (m, 1H), 4.25-4.32 (m, 2H), 4.32-4.39 (m, 1H), 4.42-4.50 (m, 1H), 5.11-5.19 (m, 1H), 6.56-6.69 (m, 2H), 6.71-7.17 (br s, 2H, interfering with the next listed signal), 6.98-7.03 (m, 2H), 7.17-7.45 (br s, 2H), 7.45-7.62 (m, 2H), 7.69-7.82 (m, 1H), 7.82-8.38 (m, 7H), 8.38-8.93 (m, 2H), 9.18 (s, 1H), 10.65-13.38 (m, 3H). 2 exchangeable protons (NH, OH) of the presumably 4-fold protonated molecule could not be identified. HRMS: *m/z* $[M+2H]^{2+}$ calcd. for $[C_{56}H_{97}N_{17}O_{14}]^{2+}$ 615.8695, found 615.8704. RP-HPLC (220 nm): > 99% (t_R = 7.2 min, k = 8.5). $C_{56}H_{95}N_{17}O_{14}$ · $C_8H_4F_{12}O_8$ (1230.48 + 456.09).

Tyr-(N^{ω}-{N-[8-(N-{2-[4,7-bis(carboxymethyl)-1,4,7-triazacyclononan-1-yl]acetyl})amino-3,6-dioxaoctyl]aminocarbonyl})Arg-Leu-amide tris(hydrotrifluoroacetate) (6.19). Compound **6.19** was prepared from **6.22** (19.3 mg, 20.0 µmol) and **6.18** (13.2 mg, 20.0 µmol) according to the general procedure for NOTA-conjugation. Purification of the product by preparative RP-HPLC (column: Gemini-NX C18, gradient: 0-25 min: A1/B1 92:8-71:29, t_R = 15 min) afforded **6.19** as white fluffy solid (12.4 mg, 50%). ^{1}H-NMR (600 MHz, DMSO-d_6): δ 0.80-0.94 (m, 6H), 1.39-1.65 (m, 6H), 1.65-1.77 (m, 1H), 2.77-3.09 (m, 14H), 3.22-3.29 (m, 6H), 3.43-3.47 (m, 4H), 3.56-3.60 (m, 6H), 3.66-3.70 (m, 4H), 3.96-4.00 (m, 1H), 4.25-4.31 (m, 1H), 4.36-4.43 (m, 1H), 6.64-6.71

(m, 2H), 6.94-7.05 (m, 3H), 7.34-7.60 (m, 2H), 7.86-8.31 (m, 5H), 8.31-8.64 (m, 2H), 8.68 (d, 1H, *J* 8.0 Hz), 8.85-9.58 (m, 2H), 10.26 (br s, 1H), 11.81 (br s, 2H). 1 exchangeable proton (NH, OH) of the presumably 3-fold protonated molecule could not be identified. HRMS: *m/z* $[M+2H]^{2+}$ calcd. for $[C_{40}H_{70}N_{12}O_{12}]^{2+}$ 455.2613, found 455.2621. RP-HPLC (220 nm): 85% (t_R = 4.3 min, *k* = 4.7). $C_{40}H_{68}N_{12}O_{12} \cdot C_6H_3F_9O_6$ (909.06 + 342.07).

N^{α}-Methyl-N^{ω}-{[4-(N-{2-[aluminum (III) fluoride-4,7-bis(carboxymethyl)-1,4,7-triazacyclononan-1-yl]acetyl})aminobutyl]aminocarbonyl}Arg-Arg-Pro-Tyr-2-*tert*-butyl-Gly-Leu tetrakis(hydrotrifluoroacetate) (6.20). Compound **6.20** was prepared from **6.13** (6.3 mg, 3.7 µmol) dissolved in 2 mM sodium acetate buffer (pH 4, 93 µL), $AlCl_3$ (1.2 mg, 9.3 µmol) and NaF (1.6 mg, 37.1 µmol) according to the procedure for the synthesis of **6.21**. Purification of the product by preparative RP-HPLC (column: Gemini-NX C18, gradient: 0-20 min: A3/B2 93:7-88:12, t_R = 13 min) afforded **6.20** as white fluffy solid (0.12 mg, 2%). The eluate of the preparative work-up was not split up. HRMS: *m/z* $[M+2H]^{2+}$ calcd. for $[C_{56}H_{95}AlFN_{17}O_{14}]^{2+}$ 637.8516, found 637.8522. RP-HPLC (220 nm): 98% (t_R = 6.6 min, *k* = 7.7). $C_{56}H_{93}AlFN_{17}O_{14} \cdot C_3H_6O_6$ (1274.44 + 138.08).

Tyr-(N^{ω}-{N-[8-(N-{2-[aluminum (III) fluoride-4,7-bis(carboxymethyl)-1,4,7-triazacyclononan-1-yl]acetyl})amino-3,6-dioxaoctyl]aminocarbonyl})Arg-Leu-amide bis(hydroacetate) (6.21). The reaction was performed in a 2-mL reaction vessel with screw cap, equipped with a magnetic micro stirrer. A solution of $AlCl_3$ (0.53 mg, 4.0 µmol) in 2 mM sodium acetate buffer (pH 4, 10 µL) and a solution of NaF (0.67 mg, 16.0 µmol) in 2 mM sodium acetate buffer (pH 4, 40 µL) were combined and shaken at rt for 5 min. MeCN (450 µL) was added to a solution of peptide **6.19** (2.0 mg, 1.6 µmol) in 2 mM sodium acetate buffer (pH 4, 400 µL) (final amount of MeCN in the reaction mixture = 50%), and the mixture was transferred to the $AlCl_3$/NaF-mixture, followed by shaking at 100 °C für 30 min. The reaction was stopped by cooling at −20 °C, and purification of the crude product by preparative HPLC (column: Gemini-NX C18, gradient: 0-20 min: A3/B2 93:7-88:12, t_R = 8 min) afforded **6.21** as white fluffy solid (0.80 mg, 48%). The eluate of the preparative work-up was split up in two fractions. A solution of NaF (8 µmol, corresponding to an approximately 10-fold excess relative to **6.21**) in 2 mM sodium acetate buffer pH 4 (2 mL) was added to one fraction. HRMS: *m/z* $[M+2H]^{2+}$ calcd. for $[C_{40}H_{68}AlFN_{12}O_{12}]^{2+}$ 477.2434, found 477.2446. RP-HPLC (220 nm): 93% (t_R = 3.7 min, *k* = 2.6). $C_{40}H_{66}AlFN_{12}O_{12} \cdot C_2H_4O_4$ (953.02 + 92.05).

6.4.6 Radiochemical binding assay (NTS_1R)

Radioligand competition binding experiments using [^{3}H]**2.13** (specific activity: 47.0 Ci/mmol[50] or 65.0 Ci/mmol[49], for structure see Chapter 2, Appendix) at $hNTS_1R$-expressing intact human HT-29 colon carcinoma cells were performed at 23 ± 1 °C according to a described procedure[50]. Two different batches of the radioligand [^{3}H]**2.13** were used. The K_d values of [^{3}H]**2.13** amounted to 0.55 nM (mean value from two independent saturation binding experiments, each performed in triplicate)[56] and 0.41 nM (mean value from two independent saturation binding experiments, each performed in triplicate)[49]. Specific binding data were obtained by subtracting unspecific binding from total binding and were normalized (100% = specifically bound radioligand in the absence of competitor) and plotted over log(concentration of competitor) followed by a four-parameter logistic fit (SigmaPlot 12.5, Systat Software). Resulting pIC_{50} values were

converted to IC_{50} values and K_i values were calculated from the IC_{50} values according to the Cheng-Prusoff equation[77] using a K_d value of 0.55 nM (**6.01**, **6.02** and **6.13**) or 0.41 nM (**6.03**-**6.05** and **6.07**-**6.11**). The K_i values from individual experiments were transformed to pK_i values, followed by the calculation of mean pK_i values ± SEM. The results of competition binding experiments are given in Table 6.1 and Figure A6.1 (Appendix).

6.4.7 Investigation of the stability of 6.01-6.05 and 6.13 in human plasma

The stabilities of **6.01**-**6.05** and **6.13** against enzymatic degradation were investigated in human blood plasma/PBS (136.9 mM NaCl, 2.68 mM KCl, 5.62 mM Na_2HPO_4, 1.09 mM NaH_2PO_4 and 1.47 mM KH_2PO_4) pH 7.4 (1:2 v/v) according to a described procedure[56], but using 5 mM stock solutions in MeCN/0.04% aq TFA (30:70 v/v) throughout for the addition of the peptides to plasma/PBS (1:2 v/v). As the RP-HPLC purity of 1-methyl-D-Trp (**2.14**), used as internal standard, was < 95% (data not shown), the compound was purified by preparative HPLC to give a purity of > 99%. The concentration of the peptides in plasma/PBS (1:2 v/v) was 80 µM and 4 µM (recovery determination) or 100 µM (stability tests). Data analysis was based on UV detection at 220 nm (**6.01**, **6.03-6.05** and **6.13**) or fluorescence detection at 275/305 nm (**6.02**). Reference samples, representing 100% recovery, were prepared in duplicate (**6.01**, **6.02**) or quadruplicate (**6.03**-**6.05** and **6.13**). Recovery ratios were obtained by dividing the recovery of the peptide by the recovery of **2.14** for each individual sample (n = 3-5). The obtained recoveries and the recovery ratios are summarized in Table A6.1, Appendix.

6.4.8 Investigation of the chemical stability of 6.21 in aqueous solvent

The stability of the AlF^{2+}-complex **6.21** was investigated immediately after the incorporation reaction of AlF^{2+} into the NOTA-conjugated dummy compound **6.19**. A fraction of the reaction mixture (concentration of **6.21** approximately 1.8 mM) was diluted with 0.1% aq HCOOH to give sample concentrations of 400 µM, 200 µM, 100 µM and 50 µM. The samples were filtrated through a 0.2 µm RC-membrane filter (Phenomenex, Aschaffenburg, Germany) and analyzed by RP-HPLC using the analytical HPLC system and conditions as described under the general experimental conditions. Note: the time span between the preparation of the dilutions of the reaction mixture and their injection into the RP-HPLC was 20 min throughout. A second set of the above-mentioned samples was prepared equally and incubated at rt overnight, followed by filtration and HPLC analysis as described above. Stackplots of the RP-HPLC chromatograms (relevant regions) of the samples analyzed immediately after the synthesis as well as after incubation overnight are given in Figure 6.4A. In order to confirm the identity of the species corresponding to the peaks in the HPLC chromatograms of crude **6.21**, a HRMS analysis was performed with the 400 µM-sample of **6.21** using the HRMS system described in the general experimental conditions, but with the following modified settings: column: Gemini-NX C18, 3 µm, 150 × 3 mm (Phenomenex), column temperature: 25 °C, flow: 0.8 mL/min, solvent/linear gradient: 0-12 min: A3/B2 93:7-88:12, 12-16 min: 88:12-5:95, 16-20 min: 5:95.

After preparative HPLC, the eluate of **6.21** was split up in two fractions and additional NaF was added to one fraction (see synthetic protocol). In order to compare the chemical stability of the AlF^{2+}-complex of **6.21** in the presence or absence of NaF in the solvent, 100 µM dilutions of both fractions in 0.1% aq HCOOH/MeCN (93:7 v/v) were prepared and

used as injection solutions (20 µL) for analytical RP-HPLC after incubation at rt for 0 min, 50 min and 100 min using the same HPLC system and conditions as for the analyses of the dilutions of crude **6.21**. Stackplots of the RP-HPLC chromatograms (relevant regions) of the samples with or without additional NaF after the respective incubation times are given in Figure 6.4B.

6.5 References

1. George, G.P.C.; Pisaneschi, F.; Nguyen, Q.D.; Aboagye, E.O. Positron emission tomographic imaging of CXCR4 in cancer: Challenges and promises. *Mol Imaging* **2015**, *14*, 1-19, doi:10.2310/7290.2014.00041.

2. Fersing, C.; Bouhlel, A.; Cantelli, C.; Garrigue, P.; Lisowski, V.; Guillet, B. A comprehensive review of non-covalent radiofluorination approaches using aluminum [^{18}F]fluoride: Will [^{18}F]AlF replace ^{68}Ga for metal chelate labeling? *Molecules* **2019**, *24*, 2866, doi:10.3390/molecules24162866.

3. McBride, W.J.; Sharkey, R.M.; Karacay, H.; D'Souza, C.A.; Rossi, E.A.; Laverman, P.; Chang, C.H.; Boerman, O.C.; Goldenberg, D.M. A novel method of ^{18}F radiolabeling for PET. *J Nucl Med* **2009**, *50*, 991-998, doi:10.2967/jnumed.108.060418.

4. Martin, R.B. Ternary hydroxide complexes in neutral solutions of Al^{3+} and F^{-}. *Biochem Bioph Res Co* **1988**, *155*, 1194-1200.

5. Martin, R.B. Ternary complexes of Al^{3+} and F^{-} with a third ligand. *Coordin Chem Rev* **1996**, *149*, 23-32, doi:Doi 10.1016/0010-8545(95)01170-6.

6. Li, L. The biochemistry and physiology of metallic fluoride: Action, mechanism, and implications. *Crit Rev Oral Biol M* **2003**, *14*, 100-114, doi:Doi 10.1177/154411130301400204.

7. Smith, G.E.; Sladen, H.L.; Biagini, S.C.G.; Blower, P.J. Inorganic approaches for radiolabelling biomolecules with fluorine-18 for imaging with positron emission tomography. *Dalton Trans* **2011**, *40*, 6196-6205, doi:10.1039/c0dt01594f.

8. Antonny, B.; Chabre, M. Characterization of the aluminum and beryllium fluoride species which activate transducin - Analysis of the binding and dissociation kinetics. *J Biol Chem* **1992**, *267*, 6710-6718.

9. Kumar, K.; Ghosh, A. ^{18}F-AlF Labeled peptide and protein conjugates as positron emission tomography imaging pharmaceuticals. *Bioconjug Chem* **2018**, *29*, 953-975, doi:10.1021/acs.bioconjchem.7b00817.

10. Laverman, P.; McBride, W.J.; Sharkey, R.M.; Eek, A.; Joosten, L.; Oyen, W.J.; Goldenberg, D.M.; Boerman, O.C. A novel facile method of labeling octreotide with ^{18}F-fluorine. *J Nucl Med* **2010**, *51*, 454-461, doi:10.2967/jnumed.109.066902.

11. McBride, W.J.; D'Souza, C.A.; Sharkey, R.M.; Karacay, H.; Rossi, E.A.; Chang, C.H.; Goldenberg, D.M. Improved ^{18}F labeling of peptides with a fluoride-aluminum-chelate complex. *Bioconjug Chem* **2010**, *21*, 1331-1340, doi:10.1021/bc100137x.

12. D'Souza, C.A.; McBride, W.J.; Sharkey, R.M.; Todaro, L.J.; Goldenberg, D.M. High-yielding aqueous ^{18}F-labeling of peptides via Al^{18}F chelation. *Bioconjug Chem* **2011**, *22*, 1793-1803, doi:10.1021/bc200175c.

13. Shetty, D.; Choi, S.Y.; Jeong, J.M.; Lee, J.Y.; Hoigebazar, L.; Lee, Y.S.; Lee, D.S.; Chung, J.K.; Lee, M.C.; Chung, Y.K. Stable aluminium fluoride chelates with

triazacyclononane derivatives proved by X-ray crystallography and ^{18}F-labeling study. *Chem Commun (Camb)* **2011**, *47*, 9732-9734, doi:10.1039/c1cc13151f.

14. Cleeren, F.; Lecina, J.; Billaud, E.M.; Ahamed, M.; Verbruggen, A.; Bormans, G.M. New chelators for low temperature Al^{18}F-labeling of biomolecules. *Bioconjug Chem* **2016**, *27*, 790-798, doi:10.1021/acs.bioconjchem.6b00012.

15. Russelli, L.; Martinelli, J.; De Rose, F.; Reder, S.; Herz, M.; Schwaiger, M.; Weber, W.; Tei, L.; D'Alessandria, C. Room temperature Al^{18}F labeling of 2-aminomethylpiperidine-based chelators for PET imaging. *ChemMedChem* **2020**, *15*, 284-292, doi:10.1002/cmdc.201900652.

16. Malik, N.; Zlatopolskiy, B.; Machulla, H.J.; Reske, S.N.; Solbach, C. One pot radiofluorination of a new potential PSMA ligand [Al^{18}F]NOTA-DUPA-Pep. *J Labelled Compd Rad* **2012**, *55*, 320-325, doi:10.1002/jlcr.2944.

17. Liu, T.L.; Liu, C.; Xu, X.X.; Liu, F.; Guo, X.Y.; Li, N.; Wang, X.J.; Yang, J.H.; Yang, X.; Zhu, H.; et al. Preclinical evaluation and pilot clinical study of Al^{18}F-PSMA-BCH for prostate cancer PET imaging. *J Nucl Med* **2019**, *60*, 1284-1292, doi:10.2967/jnumed.118.221671.

18. Laverman, P.; D'Souza, C.A.; Eek, A.; McBride, W.J.; Sharkey, R.M.; Oyen, W.J.G.; Goldenberg, D.M.; Boerman, O.C. Optimized labeling of NOTA-conjugated octreotide with F-18. *Tumor Biol* **2012**, *33*, 427-434, doi:10.1007/s13277-011-0250-x.

19. Poschenrieder, A.; Osl, T.; Schottelius, M.; Hoffmann, F.; Wirtz, M.; Schwaiger, M.; Wester, H.J. First ^{18}F-labeled Pentixafor-based imaging agent for PET imaging of CXCR4 expression in vivo. *Tomography* **2016**, *2*, 85-93, doi:10.18383/j.tom.2016.00130.

20. Lang, L.; Li, W.; Guo, N.; Ma, Y.; Zhu, L.; Kiesewetter, D.O.; Shen, B.; Niu, G.; Chen, X. Comparison study of [^{18}F]FAl-NOTA-PRGD2, [^{18}F]FPPRGD2, and [^{68}Ga]Ga-NOTA-PRGD2 for PET imaging of U87MG tumors in mice. *Bioconjug Chem* **2011**, *22*, 2415-2422, doi:10.1021/bc200197h.

21. Wan, W.; Guo, N.; Pan, D.; Yu, C.; Weng, Y.; Luo, S.; Ding, H.; Xu, Y.; Wang, L.; Lang, L.; et al. First experience of ^{18}F-alfatide in lung cancer patients using a new lyophilized kit for rapid radiofluorination. *J Nucl Med* **2013**, *54*, 691-698, doi:10.2967/jnumed.112.113563.

22. Archibald, S.J.; Allott, L. The aluminium-[^{18}F]fluoride revolution: Simple radiochemistry with a big impact for radiolabelled biomolecules. *EJNMMI Radiopharm Chem* **2021**, *6*, 30, doi:10.1186/s41181-021-00141-0.

23. Eder, M.; Wängler, B.; Knackmuss, S.; Le Gall, F.; Little, M.; Haberkorn, U.; Mier, W.; Eisenhut, M. Tetrafluorophenolate of HBED-CC: A versatile conjugation agent for ^{68}Ga-labeled small recombinant antibodies. *Eur J Nucl Med Mol Imaging* **2008**, *35*, 1878-1886, doi:10.1007/s00259-008-0816-z.

24. Fani, M.; Maecke, H.R. Radiopharmaceutical development of radiolabelled peptides. *Eur J Nucl Med Mol Imaging* **2012**, *39 Suppl 1*, 11-30, doi:10.1007/s00259-011-2001-z.

25. Deng, H.; Wang, H.; Zhang, H.; Wang, M.; Giglio, B.; Ma, X.; Jiang, G.; Yuan, H.; Wu, Z.; Li, Z. Imaging neurotensin receptor in prostate cancer with ^{64}Cu-labeled neurotensin analogs. *Mol Imaging* **2017**, *16*, 1-11, doi:10.1177/1536012117711369.

26. Hennrich, U.; Eder, M. [^{68}Ga]Ga-PSMA-11: The first FDA-approved ^{68}Ga-radiopharmaceutical for PET imaging of prostate cancer. *Pharmaceuticals (Basel)* **2021**, *14*, 713, doi:10.3390/ph14080713.

27. Malik, N.; Baur, B.; Winter, G.; Reske, S.N.; Beer, A.J.; Solbach, C. Radiofluorination of PSMA-HBED *via* Al^{18}F^{2+} chelation and biological evaluations in vitro. *Mol Imaging Biol* **2015**, *17*, 777-785, doi:10.1007/s11307-015-0844-6.

28. Boschi, S.; Lee, J.T.; Beykan, S.; Slavik, R.; Wei, L.; Spick, C.; Eberlein, U.; Buck, A.K.; Lodi, F.; Cicoria, G.; et al. Synthesis and preclinical evaluation of an Al^{18}F radiofluorinated GLU-UREA-LYS(AHX)-HBED-CC PSMA ligand. *Eur J Nucl Med Mol Imaging* **2016**, *43*, 2122-2130, doi:10.1007/s00259-016-3437-y.

29. Piron, S.; De Man, K.; Van Laeken, N.; D'Asseler, Y.; Bacher, K.; Kersemans, K.; Ost, P.; Decaestecker, K.; Deseyne, P.; Fonteyne, V.; et al. Radiation dosimetry and biodistribution of ^{18}F-PSMA-11 for PET imaging of prostate cancer. *J Nucl Med* **2019**, *60*, 1736-1742, doi:10.2967/jnumed.118.225250.

30. Piron, S.; De Man, K.; Schelfhout, V.; Van Laeken, N.; Kersemans, K.; Achten, E.; De Vos, F.; Ost, P. Optimization of PET protocol and interrater reliability of ^{18}F-PSMA-11 imaging of prostate cancer. *EJNMMI Res* **2020**, *10*, 14, doi:10.1186/s13550-020-0593-7.

31. Eder, M.; Schäfer, M.; Bauder-Wüst, U.; Hull, W.E.; Wängler, C.; Mier, W.; Haberkorn, U.; Eisenhut, M. ^{68}Ga-complex lipophilicity and the targeting property of a urea-based PSMA inhibitor for PET imaging. *Bioconjug Chem* **2012**, *23*, 688-697, doi:10.1021/bc200279b.

32. FDA approval letter for Gallium Ga 68 PSMA-11. Application number: 212642Orig1s000. December 1, 2020. Available online: https://www.accessdata.fda.gov/drugsatfda_docs/nda/2020/212642Orig1s000TOC.cfm (accessed on November 1, 2022).

33. Eder, M.; Knackmuss, S.; Le Gall, F.; Reusch, U.; Rybin, V.; Little, M.; Haberkorn, U.; Mier, W.; Eisenhut, M. ^{68}Ga-labelled recombinant antibody variants for immuno-PET imaging of solid tumours. *Eur J Nucl Med Mol Imaging* **2010**, *37*, 1397-1407, doi:10.1007/s00259-010-1392-6.

34. Al-Momani, E.; Israel, I.; Samnick, S. Validation of a [Al^{18}F]PSMA-11 preparation for clinical applications. *Appl Radiat Isot* **2017**, *130*, 102-108, doi:10.1016/j.apradiso.2017.09.003.

35. Giglio, J.; Zeni, M.; Savio, E.; Engler, H. Synthesis of an Al^{18}F radiofluorinated GLU-UREA-LYS(AHX)-HBED-CC PSMA ligand in an automated synthesis platform. *EJNMMI Radiopharm Chem* **2018**, *3*, 4, doi:10.1186/s41181-018-0039-y.

36. Lütje, S.; Franssen, G.M.; Herrmann, K.; Boerman, O.C.; Rijpkema, M.; Gotthardt, M.; Heskamp, S. In vitro and in vivo characterization of an ^{18}F-AlF-labeled PSMA

ligand for imaging of PSMA-expressing xenografts. *J Nucl Med* **2019**, *60*, 1017-1022, doi:10.2967/jnumed.118.218941.

37. Ioppolo, J.A.; Nezich, R.A.; Richardson, K.L.; Morandeau, L.; Leedman, P.J.; Price, R.I. Direct *in vivo* comparison of [^{18}F]PSMA-1007 with [^{68}Ga]Ga-PSMA-11 and [^{18}F]AlF-PSMA-11 in mice bearing PSMA-expressing xenografts. *Appl Radiat Isot* **2020**, *161*, 109164, doi:10.1016/j.apradiso.2020.109164.

38. Piron, S.; Verhoeven, J.; Descamps, B.; Kersemans, K.; De Man, K.; Van Laeken, N.; Pieters, L.; Vral, A.; Vanhove, C.; De Vos, F. Intra-individual dynamic comparison of ^{18}F-PSMA-11 and ^{68}Ga-PSMA-11 in LNCaP xenograft bearing mice. *Sci Rep* **2020**, *10*, 21068, doi:10.1038/s41598-020-78273-7.

39. dos Santos, G.; Taroco, M.R.; Giglio, J.; Savio, E.; Alonso, O. Al^{18}F-PSMA-HBED-CC as a novel tracer for the evaluation of prostate cancer patients with biochemical relapse: Intraindividual comparison with ^{68}Ga-PSMA-HBED-CC. *J Nucl Med* **2020**, *61*, 1268.

40. Piron, S.; Verhoeven, J.; Courtyn, J.; Kersemans, K.; Descamps, B.; Pieters, L.; Vral, A.; Vanhove, C.; De Vos, F. Preclinical comparative study of [^{18}F]AlF-PSMA-11 and [^{18}F]PSMA-1007 in varying PSMA expressing tumors. *Sci Rep* **2022**, *12*, 15744, doi:10.1038/s41598-022-20060-7.

41. Eisenwiener, K.P.; Prata, M.I.; Buschmann, I.; Zhang, H.W.; Santos, A.C.; Wenger, S.; Reubi, J.C.; Maecke, H.R. NODAGATOC, a new chelator-coupled somatostatin analogue labeled with [$^{67/68}$Ga] and [^{111}In] for SPECT, PET, and targeted therapeutic applications of somatostatin receptor (hsst2) expressing tumors. *Bioconjug Chem* **2002**, *13*, 530-541, doi:10.1021/bc010074f.

42. Fani, M.; Del Pozzo, L.; Abiraj, K.; Mansi, R.; Tamma, M.L.; Cescato, R.; Waser, B.; Weber, W.A.; Reubi, J.C.; Maecke, H.R. PET of somatostatin receptor-positive tumors using ^{64}Cu- and ^{68}Ga-somatostatin antagonists: The chelate makes the difference. *J Nucl Med* **2011**, *52*, 1110-1118, doi:10.2967/jnumed.111.087999.

43. Fani, M.; Braun, F.; Waser, B.; Beetschen, K.; Cescato, R.; Erchegyi, J.; Rivier, J.E.; Weber, W.A.; Maecke, H.R.; Reubi, J.C. Unexpected sensitivity of sst2 antagonists to N-terminal radiometal modifications. *J Nucl Med* **2012**, *53*, 1481-1489, doi:10.2967/jnumed.112.102764.

44. Maschauer, S.; Einsiedel, J.; Hübner, H.; Gmeiner, P.; Prante, O. ^{18}F- and ^{68}Ga-labeled neurotensin peptides for PET imaging of neurotensin receptor 1. *J Med Chem* **2016**, *59*, 6480-6492, doi:10.1021/acs.jmedchem.6b00675.

45. Kubíček, V.; Havlíčková, J.; Kotek, J.; Tircsó, G.; Hermann, P.; Tóth, E.; Lukeš, I. Gallium(III) complexes of DOTA and DOTA-monoamide: Kinetic and thermodynamic studies. *Inorg Chem* **2010**, *49*, 10960-10969, doi:10.1021/ic101378s.

46. Hennrich, U.; Benešová, M. [^{68}Ga]Ga-DOTA-TOC: The first FDA-approved ^{68}Ga-radiopharmaceutical for PET imaging. *Pharmaceuticals (Basel)* **2020**, *13*, 38, doi:10.3390/ph13030038.

47. Schindler, L.; Wohlfahrt, K.; Gluhacevic von Krüchten, L.; Prante, O.; Keller, M.; Maschauer, S. Neurotensin analogs by fluoroglycosylation at N^{ω}-carbamoylated arginines for PET imaging of NTS1-positive tumors. *Sci Rep* **2022**, *12*, 15028, doi:10.1038/s41598-022-19296-0.

48. Thern, B.; Rudolph, J.; Jung, G. Total synthesis of the nematicidal cyclododecapeptide omphalotin A by using racemization-free triphosgene-mediated couplings in the solid phase. *Angew Chem Int Edit* **2002**, *41*, 2307-2309, doi:Doi 10.1002/1521-3773(20020703)41:13<2307::Aid-Anie2307>3.0.Co;2-Y.

49. Schindler, L.; Moosbauer, J.; Schmidt, D.; Spruss, T.; Grätz, L.; Lüdeke, S.; Hofheinz, F.; Meister, S.; Echtenacher, B.; Bernhardt, G.; et al. Development of a neurotensin-derived ^{68}Ga-labeled PET ligand with high in vivo stability for imaging of NTS_1 receptor-expressing tumors. *Cancers (Basel)* **2022**, *14*, 4922, doi:10.3390/cancers14194922.

50. Keller, M.; Kuhn, K.K.; Einsiedel, J.; Hübner, H.; Biselli, S.; Mollereau, C.; Wifling, D.; Svobodová, J.; Bernhardt, G.; Cabrele, C.; et al. Mimicking of arginine by functionalized N^{ω}-carbamoylated arginine as a new broadly applicable approach to labeled bioactive peptides: High affinity angiotensin, neuropeptide Y, neuropeptide FF, and neurotensin receptor ligands as examples. *J Med Chem* **2016**, *59*, 1925-1945, doi:10.1021/acs.jmedchem.5b01495.

51. Bergmann, R.; Scheunemann, M.; Heichert, C.; Mäding, P.; Wittrisch, H.; Kretzschmar, M.; Rodig, H.; Tourwé, D.; Iterbeke, K.; Chavatte, K.; et al. Biodistribution and catabolism of ^{18}F-labeled neurotensin(8-13) analogs. *Nucl Med Biol* **2002**, *29*, 61-72, doi:10.1016/s0969-8051(01)00284-0.

52. Kokko, K.P.; Hadden, M.K.; Orwig, K.S.; Mazella, J.; Dix, T.A. In vitro analysis of stable, receptor-selective neurotensin[8-13] analogues. *J Med Chem* **2003**, *46*, 4141-4148, doi:10.1021/jm0300633.

53. Nock, B.A.; Nikolopoulou, A.; Reubi, J.C.; Maes, V.; Conrath, P.; Tourwé, D.; Maina, T. Toward stable N_4-modified neurotensins for NTS1-receptor-targeted tumor imaging with ^{99m}Tc. *J Med Chem* **2006**, *49*, 4767-4776, doi:10.1021/jm060415g.

54. Alshoukr, F.; Rosant, C.; Maes, V.; Abdelhak, J.; Raguin, O.; Burg, S.; Sarda, L.; Barbet, J.; Tourwé, D.; Pelaprat, D.; et al. Novel neurotensin analogues for radioisotope targeting to neurotensin receptor-positive tumors. *Bioconjug Chem* **2009**, *20*, 1602-1610, doi:10.1021/bc900151z.

55. Mascarin, A.; Valverde, I.E.; Mindt, T.L. Structure-activity relationship studies of amino acid substitutions in radiolabeled neurotensin conjugates. *ChemMedChem* **2016**, *11*, 102-107, doi:10.1002/cmdc.201500468.

56. Schindler, L.; Bernhardt, G.; Keller, M. Modifications at Arg and Ile give neurotensin(8-13) derivatives with high stability and retained NTS_1 receptor affinity. *ACS Med Chem Lett* **2019**, *10*, 960-965, doi:10.1021/acsmedchemlett.9b00122.

57. Maschauer, S.; Einsiedel, J.; Hocke, C.; Hübner, H.; Kuwert, T.; Gmeiner, P.; Prante, O. Synthesis of a ^{68}Ga-labeled peptoid-peptide hybrid for imaging of

neurotensin receptor expression in vivo. *ACS Med Chem Lett* **2010**, *1*, 224-228, doi:10.1021/ml1000728.

58. Tyler-McMahon, B.M.; Stewart, J.A.; Farinas, F.; McCormick, D.J.; Richelson, E. Highly potent neurotensin analog that causes hypothermia and antinociception. *Eur J Pharmacol* **2000**, *390*, 107-111, doi:10.1016/s0014-2999(99)00877-8.

59. Bruehlmeier, M.; García-Garayoa, E.; Blanc, A.; Holzer, B.; Gergely, S.; Tourwé, D.; Schubiger, P.A.; Bläuenstein, P. Stabilization of neurotensin analogues: Effect on peptide catabolism, biodistribution and tumor binding. *Nucl Med Biol* **2002**, *29*, 321-327, doi:10.1016/s0969-8051(01)00304-3.

60. García-Garayoa, E.; Bläuenstein, P.; Bruehlmeier, M.; Blanc, A.; Iterbeke, K.; Conrath, P.; Tourwé, D.; Schubiger, P.A. Preclinical evaluation of a new, stabilized neurotensin(8-13) pseudopeptide radiolabeled with ^{99m}Tc. *J Nucl Med* **2002**, *43*, 374-383.

61. Bläuenstein, P.; García-Garayoa, E.; Rüegg, D.; Blanc, A.; Tourwé, D.; Beck-Sickinger, A.; Schubiger, P.A. Improving the tumor uptake of ^{99m}Tc-labeled neuropeptides using stabilized peptide analogues. *Cancer Biother Radiopharm* **2004**, *19*, 181-188, doi:10.1089/108497804323071959.

62. Maes, V.; García-Garayoa, E.; Bläuenstein, P.; Tourwé, D. Novel ^{99m}Tc-labeled neurotensin analogues with optimized biodistribution properties. *J Med Chem* **2006**, *49*, 1833-1836, doi:10.1021/jm051172f.

63. Maina, T.; Nikolopoulou, A.; Stathopoulou, E.; Galanis, A.S.; Cordopatis, P.; Nock, B.A. [^{99m}Tc]Demotensin 5 and 6 in the NTS1-R-targeted imaging of tumours: Synthesis and preclinical results. *Eur J Nucl Med Mol Imaging* **2007**, *34*, 1804-1814, doi:10.1007/s00259-007-0489-z.

64. García-Garayoa, E.; Bläuenstein, P.; Blanc, A.; Maes, V.; Tourwé, D.; Schubiger, P.A. A stable neurotensin-based radiopharmaceutical for targeted imaging and therapy of neurotensin receptor-positive tumours. *Eur J Nucl Med Mol Imaging* **2009**, *36*, 37-47, doi:10.1007/s00259-008-0894-y.

65. Boules, M.; Liang, Y.; Briody, S.; Miura, T.; Fauq, I.; Oliveros, A.; Wilson, M.; Khaniyev, S.; Williams, K.; Li, Z.; et al. NT79: A novel neurotensin analog with selective behavioral effects. *Brain Res* **2010**, *1308*, 35-46, doi:10.1016/j.brainres.2009.10.050.

66. Maschauer, S.; Einsiedel, J.; Haubner, R.; Hocke, C.; Ocker, M.; Hübner, H.; Kuwert, T.; Gmeiner, P.; Prante, O. Labeling and glycosylation of peptides using click chemistry: A general approach to ^{18}F-glycopeptides as effective imaging probes for positron emission tomography. *Angew Chem Int Ed Engl* **2010**, *49*, 976-979, doi:10.1002/anie.200904137.

67. Alshoukr, F.; Prignon, A.; Brans, L.; Jallane, A.; Mendes, S.; Talbot, J.N.; Tourwé, D.; Barbet, J.; Gruaz-Guyon, A. Novel DOTA-neurotensin analogues for ^{111}In scintigraphy and ^{68}Ga PET imaging of neurotensin receptor-positive tumors. *Bioconjug Chem* **2011**, *22*, 1374-1385, doi:10.1021/bc200078p.

68. Maschauer, S.; Ruckdeschel, T.; Tripal, P.; Haubner, R.; Einsiedel, J.; Hübner, H.; Gmeiner, P.; Kuwert, T.; Prante, O. *In vivo* monitoring of the antiangiogenic effect of neurotensin receptor-mediated radiotherapy by small-animal positron emission tomography: A pilot study. *Pharmaceuticals (Basel)* **2014**, *7*, 464-481, doi:10.3390/ph7040464.

69. Jia, Y.; Shi, W.; Zhou, Z.; Wagh, N.K.; Fan, W.; Brusnahan, S.K.; Garrison, J.C. Evaluation of DOTA-chelated neurotensin analogs with spacer-enhanced biological performance for neurotensin-receptor-1-positive tumor targeting. *Nucl Med Biol* **2015**, *42*, 816-823, doi:10.1016/j.nucmedbio.2015.07.010.

70. Farkas, E.; Fodor, T.; Kálmán, F.K.; Tircsó, G.; Tóth, I. Equilibrium and dissociation kinetics of the [Al(NOTA)] complex (NOTA=1,4,7-triazacyclononane-1,4,7-triacetate). *React Kinet Mech Cat* **2015**, *116*, 19-33, doi:10.1007/s11144-015-0892-6.

71. Martell, A.E.; Motekaitis, R.J.; Clarke, E.T.; Delgado, R.; Sun, Y.Z.; Ma, R. Stability constants of metal complexes of macrocyclic ligands with pendant donor groups. *Supramol Chem* **1996**, *6*, 353-363, doi:Doi 10.1080/10610279608032555.

72. Pauwels, E.; Cleeren, F.; Bormans, G.; Deroose, C.M. Somatostatin receptor PET ligands - The next generation for clinical practice. *Am J Nucl Med Mol Imaging* **2018**, *8*, 311-331.

73. Hou, J.L.; Long, T.T.; Hu, S. Head-to-head comparison of the ^{18}F-AlF-NOTA-octreotide and ^{68}Ga-DOTATATE PET/CT within patients with neuroendocrine neoplasms. *J Nucl Med* **2020**, *61*, 59.

74. Pauwels, E.; Cleeren, F.; Tshibangu, T.; Koole, M.; Serdons, K.; Dekervel, J.; Van Cutsem, E.; Verslype, C.; Van Laere, K.; Bormans, G.; et al. [^{18}F]AlF-NOTA-octreotide PET imaging: Biodistribution, dosimetry and first comparison with [^{68}Ga]Ga-DOTATATE in neuroendocrine tumour patients. *Eur J Nucl Med Mol Imaging* **2020**, *47*, 3033-3046, doi:10.1007/s00259-020-04918-4.

75. Tshibangu, T.; Cawthorne, C.; Serdons, K.; Pauwels, E.; Gsell, W.; Bormans, G.; Deroose, C.M.; Cleeren, F. Automated GMP compliant production of [^{18}F]AlF-NOTA-octreotide. *EJNMMI Radiopharm Chem* **2020**, *5*, 4, doi:10.1186/s41181-019-0084-1.

76. Hou, J.L.; Long, T.T.; He, Z.Y.; Zhou, M.; Yang, N.A.; Chen, D.M.; Zeng, S.; Hu, S. Evaluation of ^{18}F-AlF-NOTA-octreotide for imaging neuroendocrine neoplasms: Comparison with ^{68}Ga-DOTATATE PET/CT. *Ejnmmi Res* **2021**, *11*, 55, doi:10.1186/s13550-021-00797-4.

77. Cheng, Y.; Prusoff, W.H. Relationship between the inhibition constant (K_I) and the concentration of inhibitor which causes 50 per cent inhibition (I_{50}) of an enzymatic reaction. *Biochem Pharmacol* **1973**, *22*, 3099-3108, doi:10.1016/0006-2952(73)90196-2.

6.6 Appendix

6.6.1 Figures A6.1 and A6.2 and Table A6.1

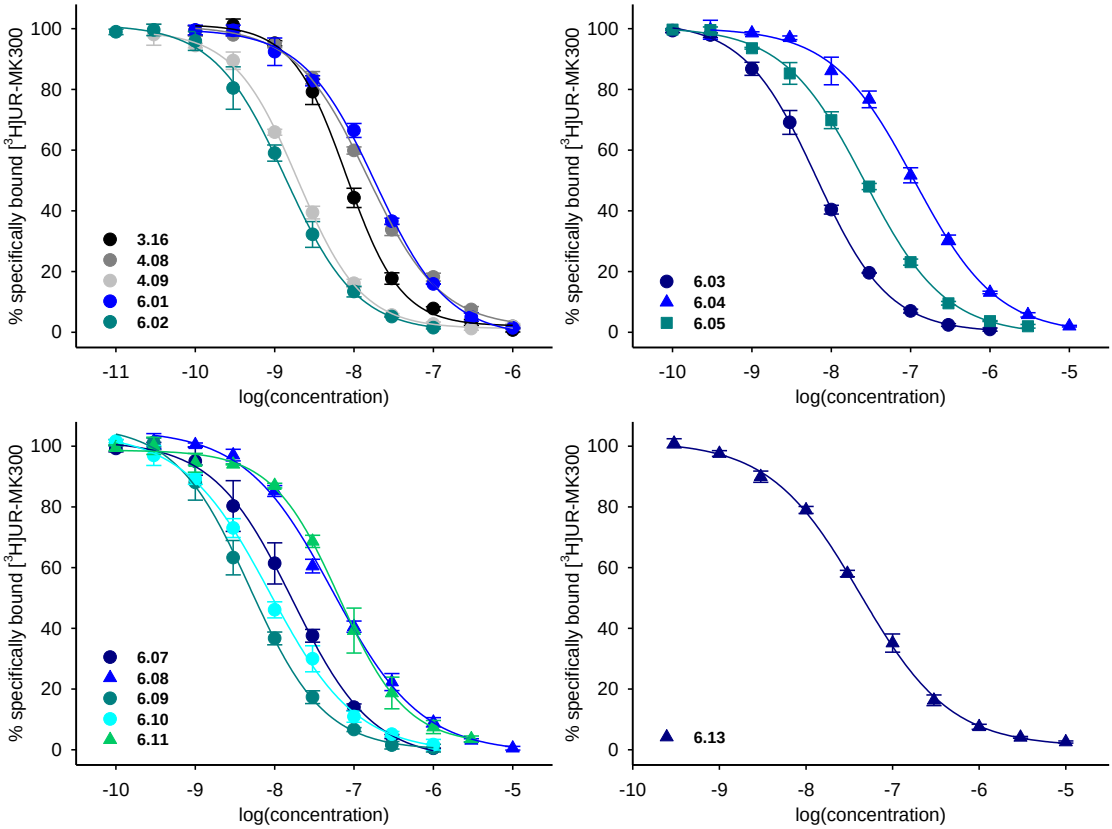

Figure A6.1. Radioligand displacement curves from competition binding experiments with [^{3}H]**2.13** (K_d = 0.55 nM or 0.41 nM, c = 1 nM) and reference compounds **3.16**[1], **4.08**[2], **4.09**[2] as well as compounds **6.01**-**6.05**, **6.07**-**6.11** and **6.13**, performed at intact $hNTS_1R$-expressing HT-29 cells. Amino-functionalized precursor peptides are represented by circles, DOTA- or NOTA-conjugated compounds are represented by triangles, and Ga^{3+}-containing peptides are represented by squares. Data represent mean values ± SEM from at least two independent experiments (performed in triplicate).

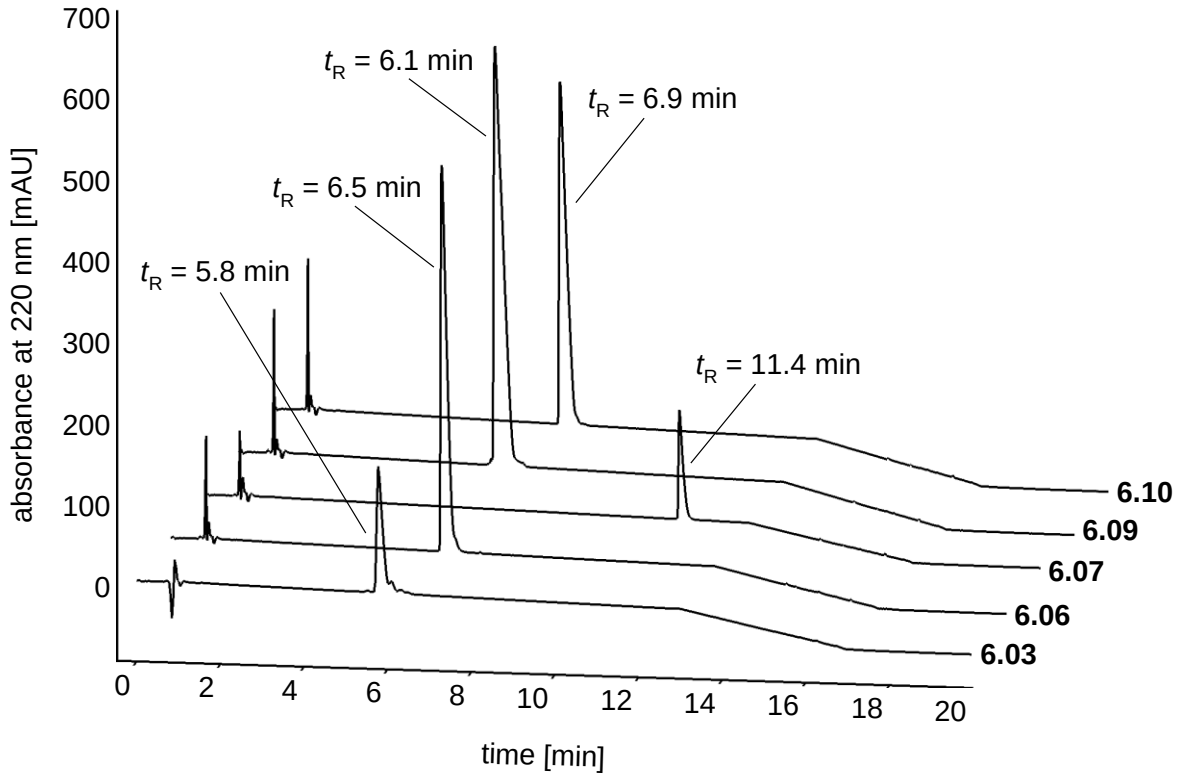

Figure A6.2. Chromatograms of the RP-HPLC analyses (purity controls) of peptides **6.03**, **6.06**, **6.07**, **6.09** and **6.10**.

Table A6.1. Recoveries of peptides **6.01**-**6.05** and **6.13** from human plasma/PBS (1:2 v/v) and ratios of peptide-recovery over recovery of **2.14**.

Compd.	Peptide concentration 80 μM			Peptide concentration 4 μM		
	recovery peptide (%)[a]	recovery **2.14** (%)[a]	ratio[b]	recovery peptide (%)[a]	recovery **2.14** (%)[a]	ratio[b]
6.01	78	100	0.78	87	94	0.92
	76	99	0.77	84	96	0.87
	76	97	0.78	94	100	0.94
	78	100	0.78	93	92	1.01
			(0.78 ± 0.01)			(0.94 ± 0.03)
6.02	95	118	0.81	93	111	0.83
	93	111	0.83	95	124	0.77
	93	119	0.79	103	128	0.81
	94	117	0.80			
	91	112	0.81			
			(0.81 ± 0.01)			(0.80 ± 0.02)
6.03	85	100	0.85	113	117	0.97
	84	101	0.83	103	109	0.95
	85	99	0.86	98	103	0.94
	89	100	0.89	99	102	0.97
	92	112	0.82			
			(0.85 ± 0.01)			(0.96 ± 0.21)
6.04	97	103	0.94	103	104	1.00
	94	102	0.93	107	109	0.98
	100	108	0.93	114	115	0.99
	98	101	0.97	104	107	0.98
				92	95	0.97
			(0.94 ± 0.01)			(0.98 ± 0.01)
6.05	98	110	0.89	103	104	0.99
	95	104	0.91	109	111	0.98
	93	104	0.90	100	101	0.99
	102	112	0.91	97	101	0.96
				105	109	0.97
			(0.90 ± 0.01)			(0.98 ± 0.01)
6.13	96	100	0.96	130	101	1.29
	95	100	0.95	137	105	1.30
	87	93	0.93	145	111	1.30
	89	93	0.95	143	111	1.28
	89	93	0.96			
			(0.95 ± 0.01)			(1.30 ± 0.01)

[a]Recoveries of the peptides and of **2.14** from human plasma/PBS (1:2 v/v) using a peptide concentration of 80 μM or 4 μM and a concentration of **2.14** of 10 μM (three, four or five independent experiments). [b]Ratios of peptide recovery over recovery of **2.14** calculated for individual experiments, as well as mean recovery ratios ± SEM (given in parenthesis). Note: When the remaining intact peptide concentration in plasma was > 20 μM, recovery ratios based on the 80 μM peptide concentrations were used to calculate peptide recoveries of the plasma stability samples. When the remaining intact peptide concentration was < 20 μM, recovery ratios based on the 4 μM peptide concentrations were used to calculate peptide recoveries of the plasma stability samples.

6.6.2 RP-HPLC chromatograms of compounds 6.01-6.11, 6.13-6.16 and 6.19-6.21

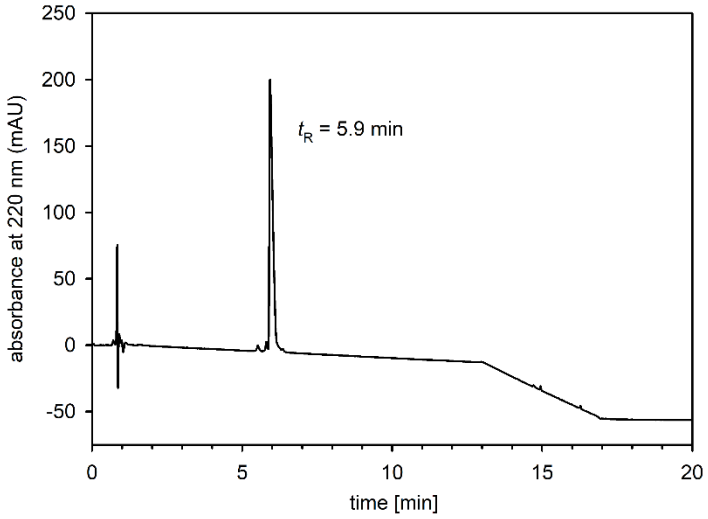

RP-HPLC analysis (purity control) of compound **6.01**

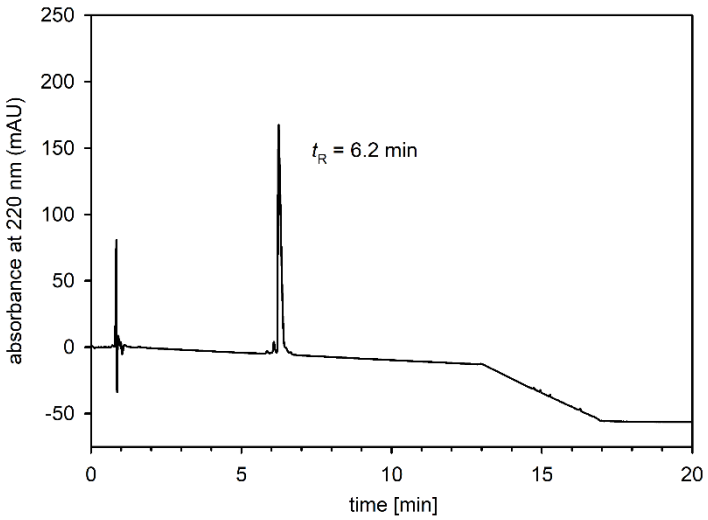

RP-HPLC analysis (purity control) of compound **6.02**

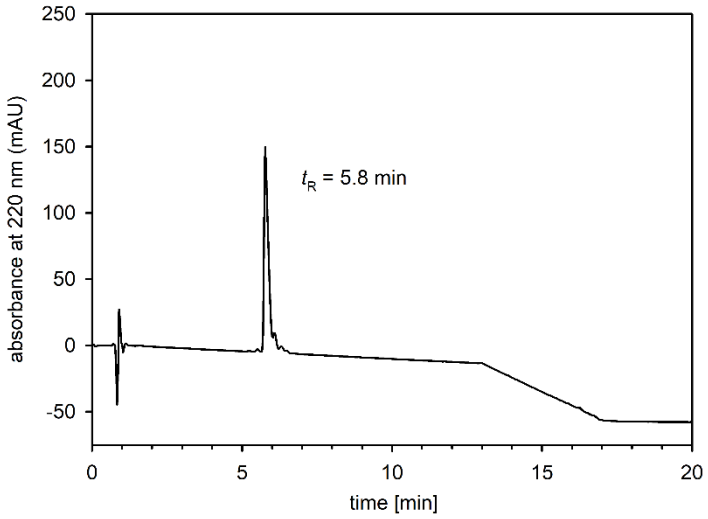

RP-HPLC analysis (purity control) of compound **6.03**

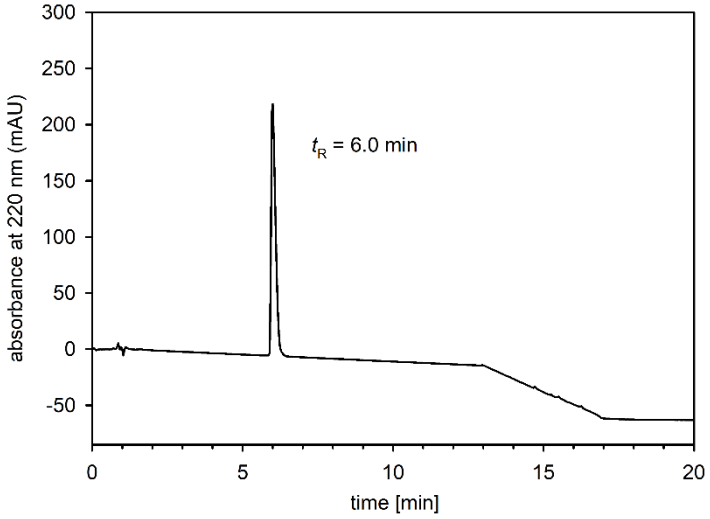

RP-HPLC analysis (purity control) of compound **6.04**

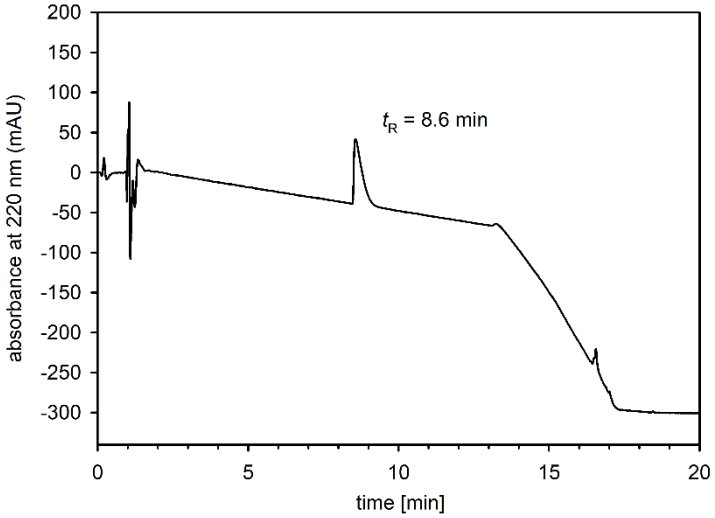

RP-HPLC analysis (purity control) of compound **6.05**

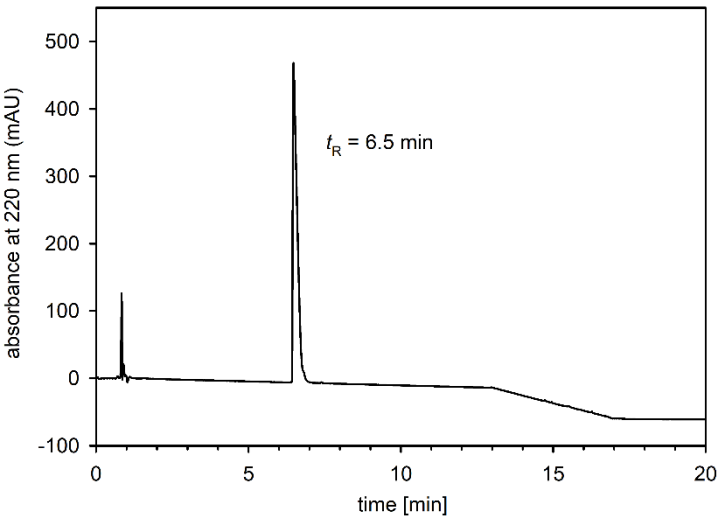

RP-HPLC analysis (purity control) of compound **6.06**

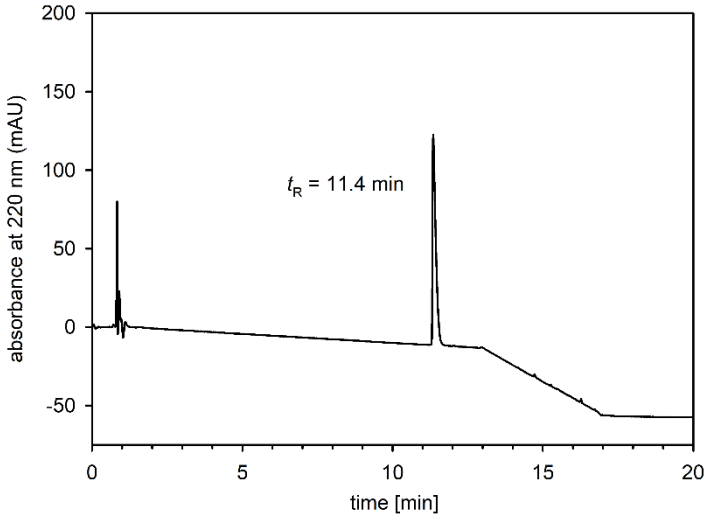

RP-HPLC analysis (purity control) of compound **6.07**

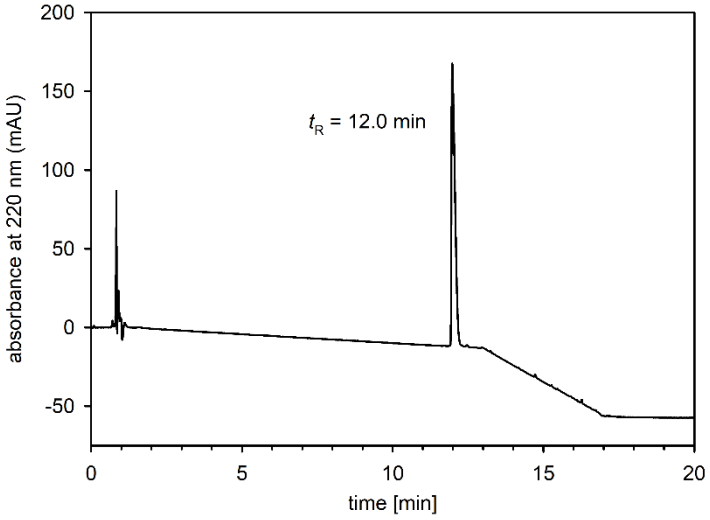

RP-HPLC analysis (purity control) of compound **6.08**

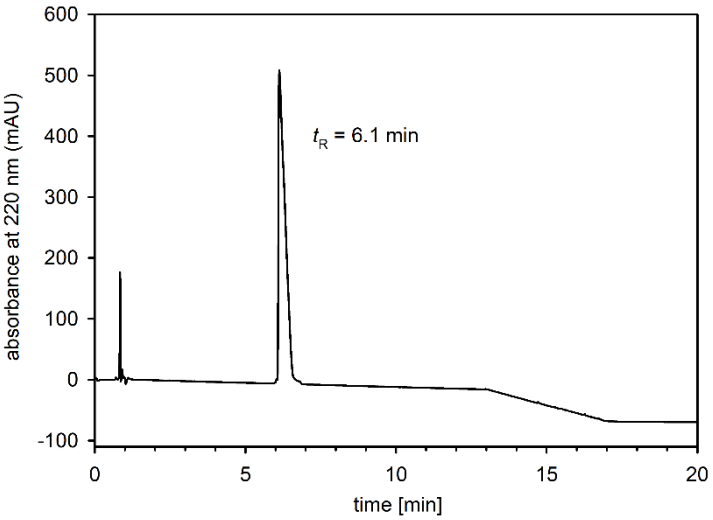

RP-HPLC analysis (purity control) of compound **6.09**

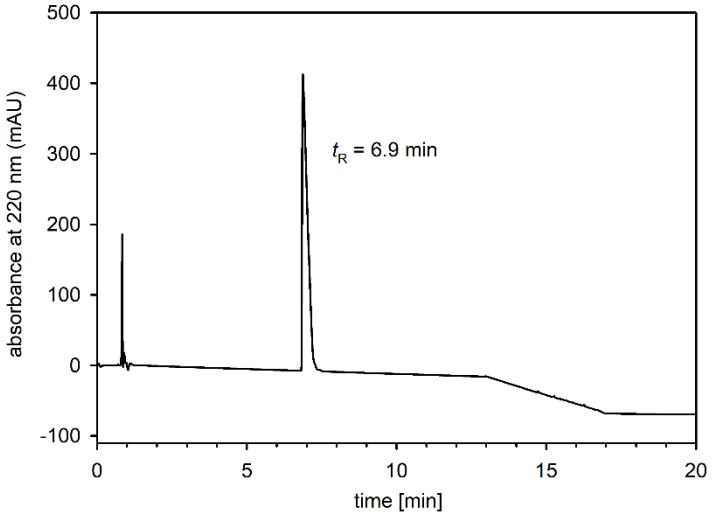

RP-HPLC analysis (purity control) of compound **6.10**

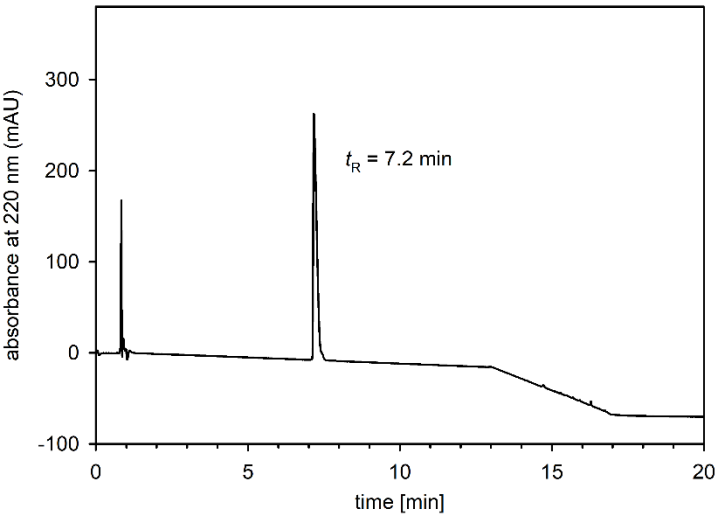

RP-HPLC analysis (purity control) of compound **6.11**

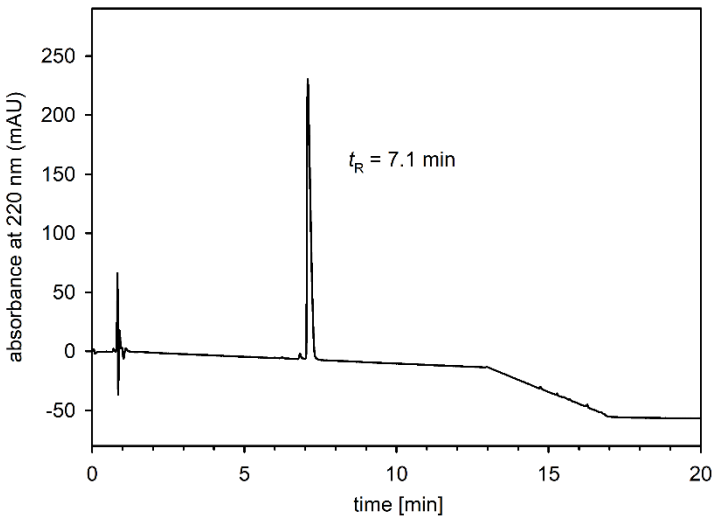

RP-HPLC analysis (purity control) of compound **6.13**

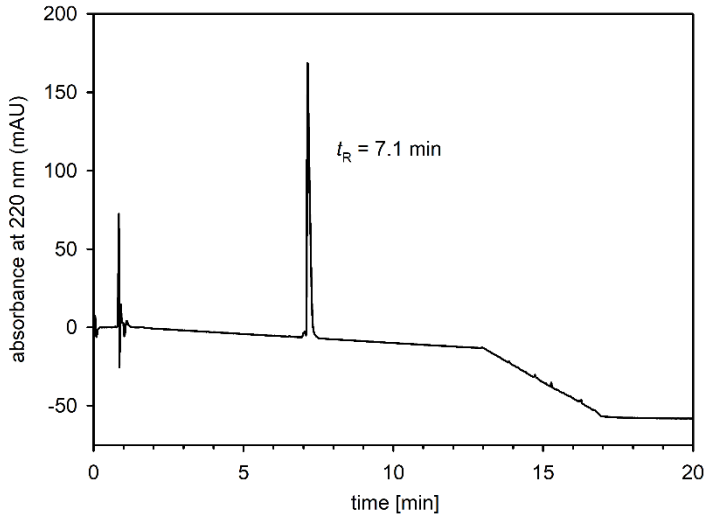

RP-HPLC analysis (purity control) of compound **6.14**

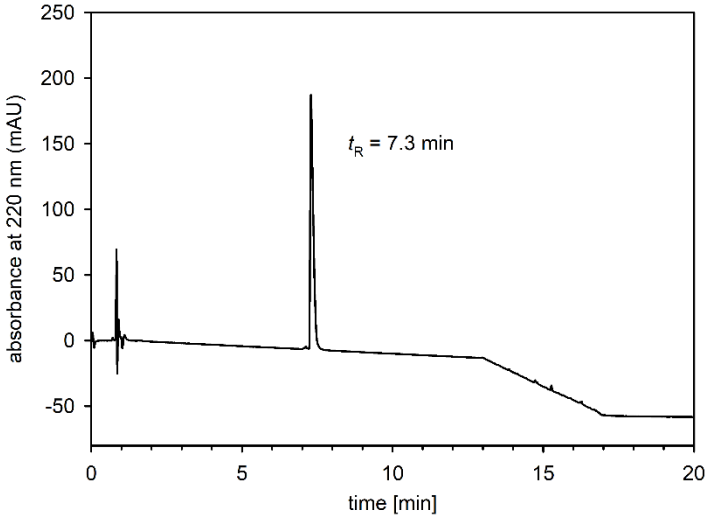

RP-HPLC analysis (purity control) of compound **6.15**

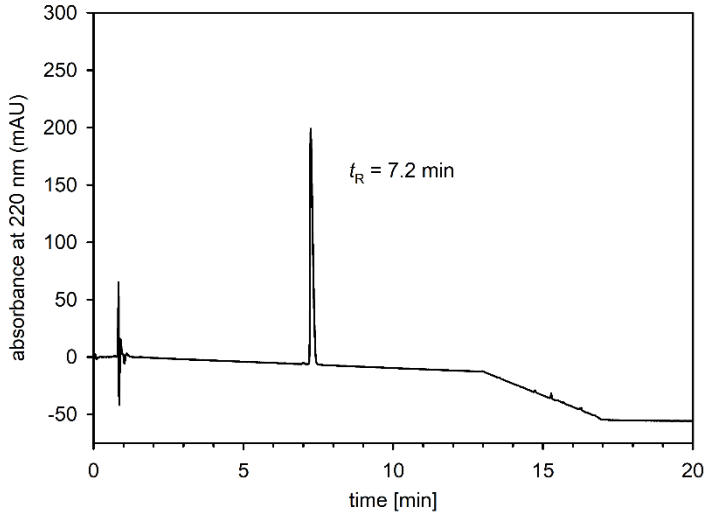

RP-HPLC analysis (purity control) of compound **6.16**

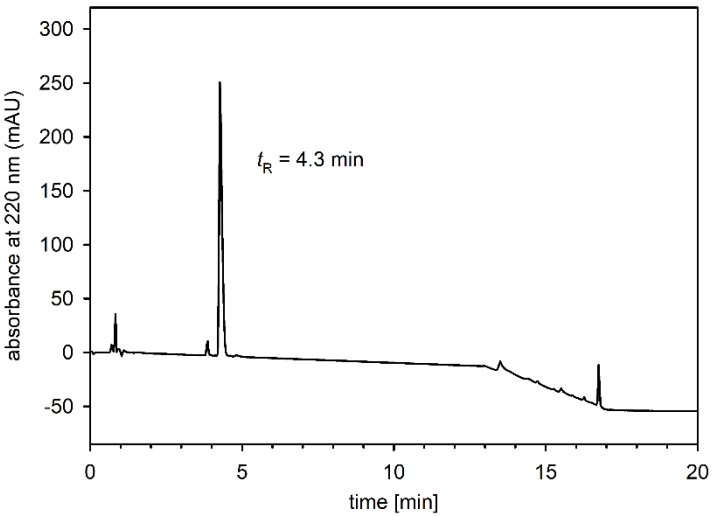

RP-HPLC analysis (purity control) of compound **6.19**

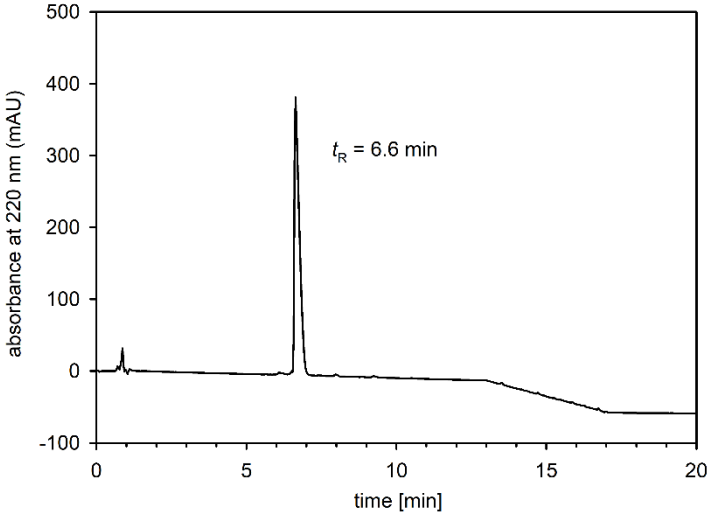

RP-HPLC analysis (purity control) of compound **6.20**

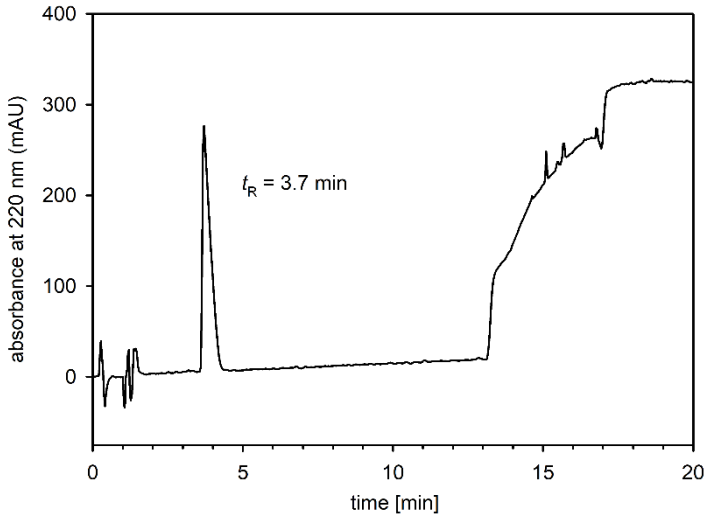

RP-HPLC analysis (purity control) of compound **6.21**

6.6.3 ^{1}H-NMR spectra of compounds 6.01-6.07, 6.09, 6.10, 6.13-6.16 and 6.19

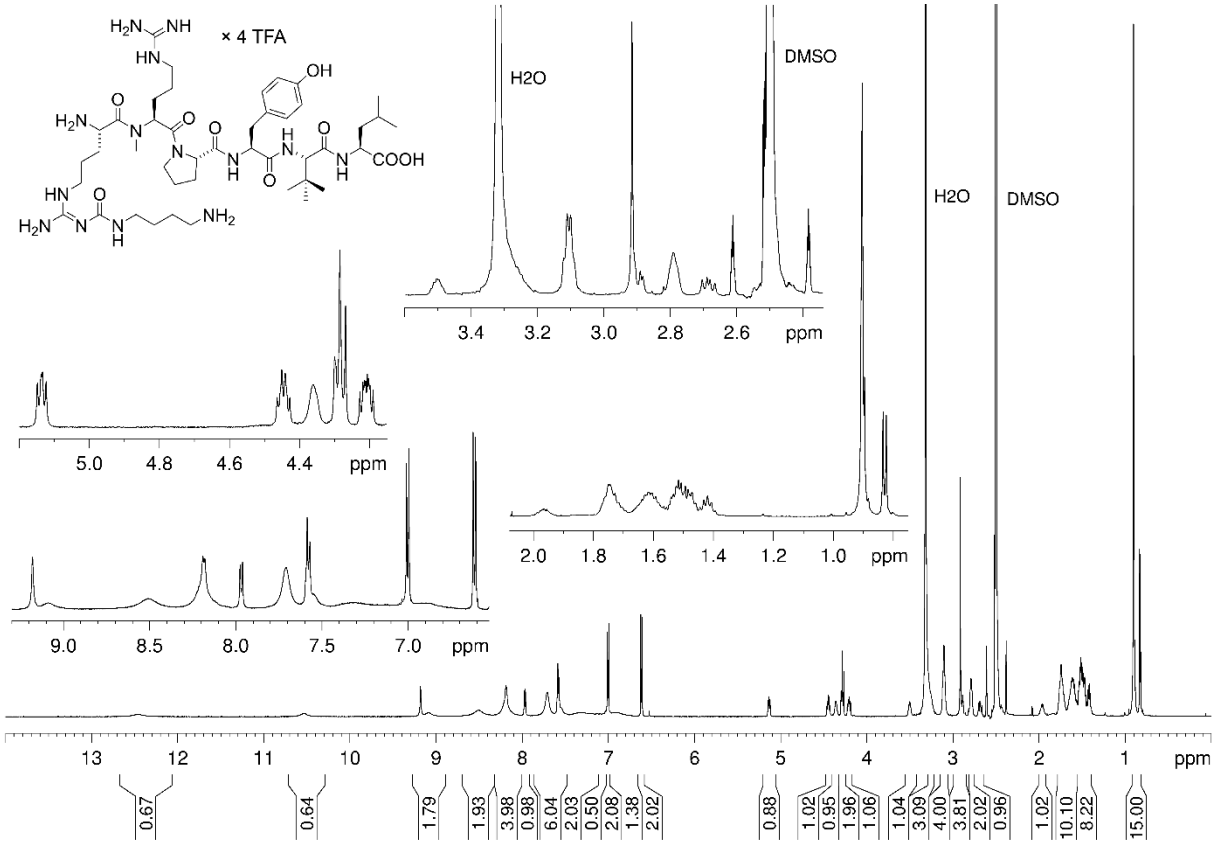

^{1}H-NMR spectrum (600 MHz, DMSO-d_6) of compound **6.01**

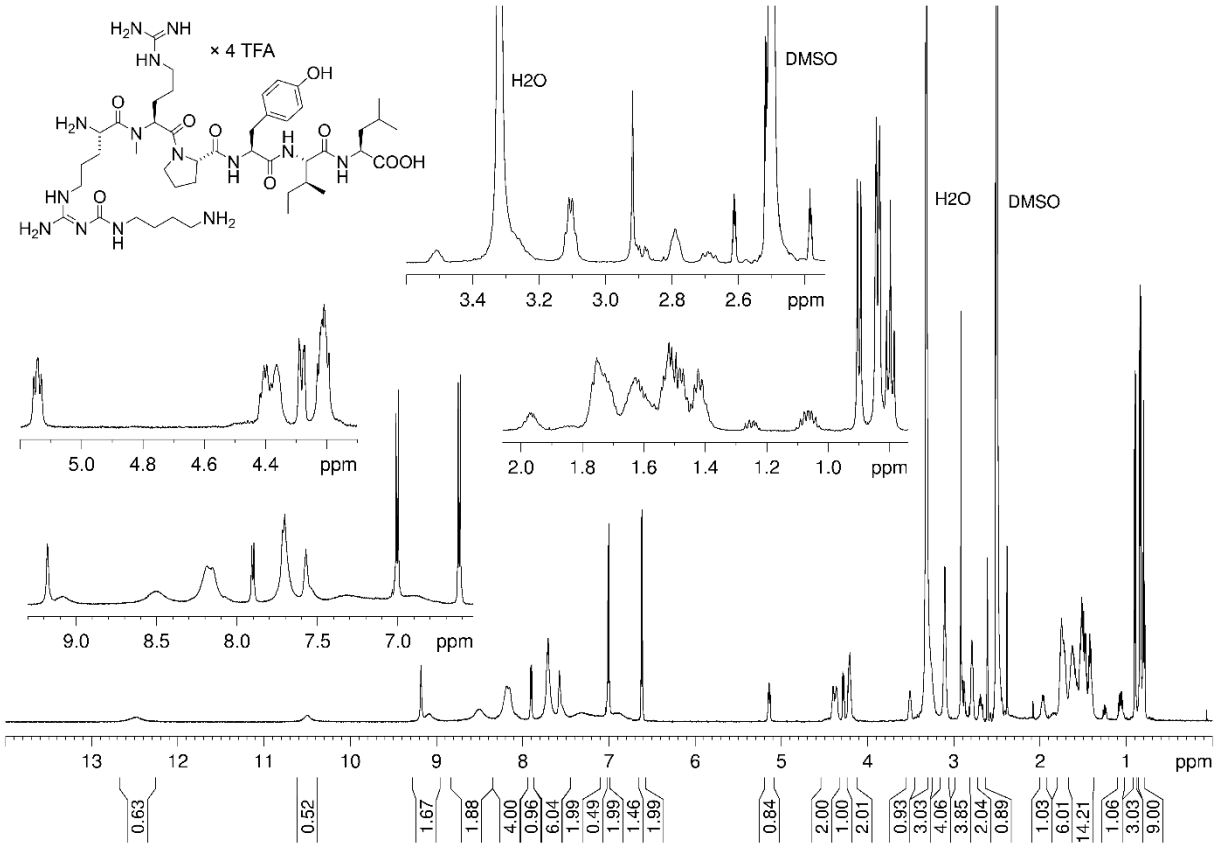

^{1}H-NMR spectrum (600 MHz, DMSO-d_6) of compound **6.02**

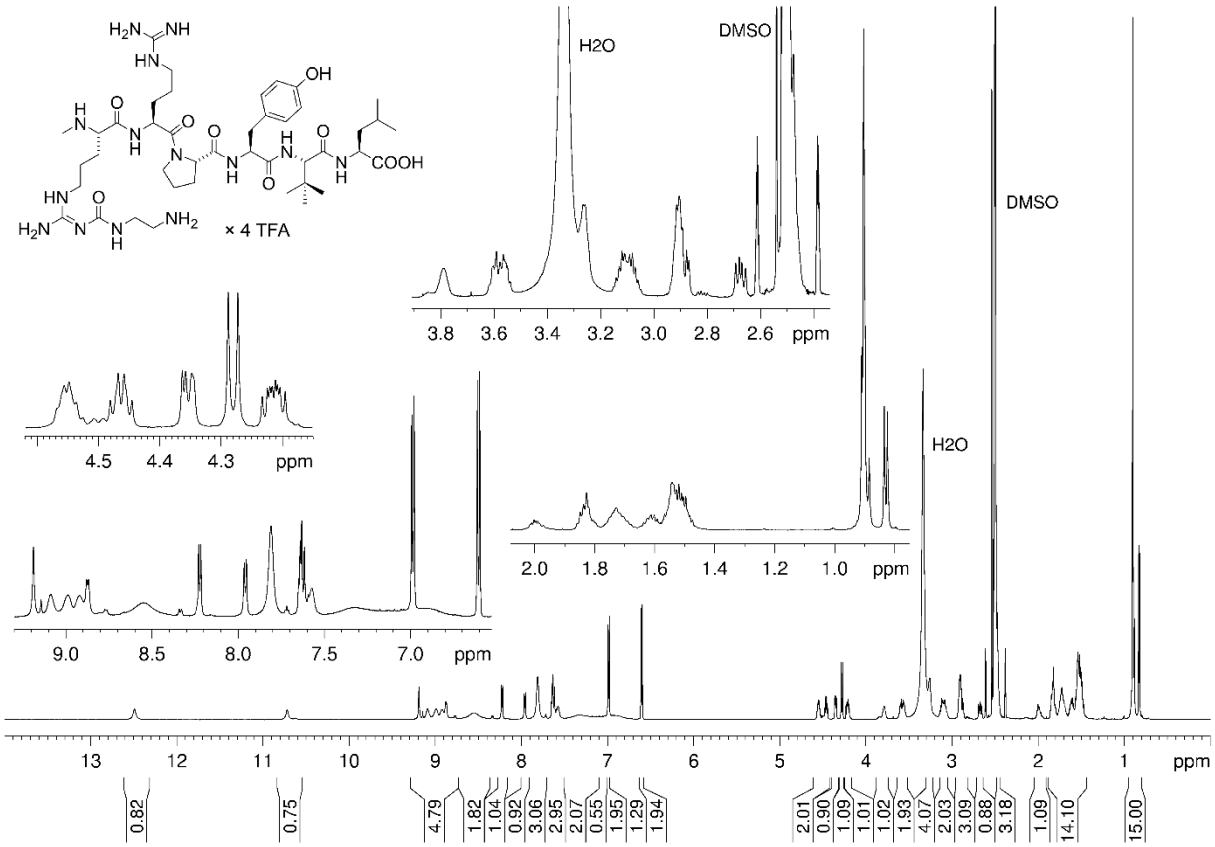

^{1}H-NMR spectrum (600 MHz, DMSO-d_6) of compound **6.03**

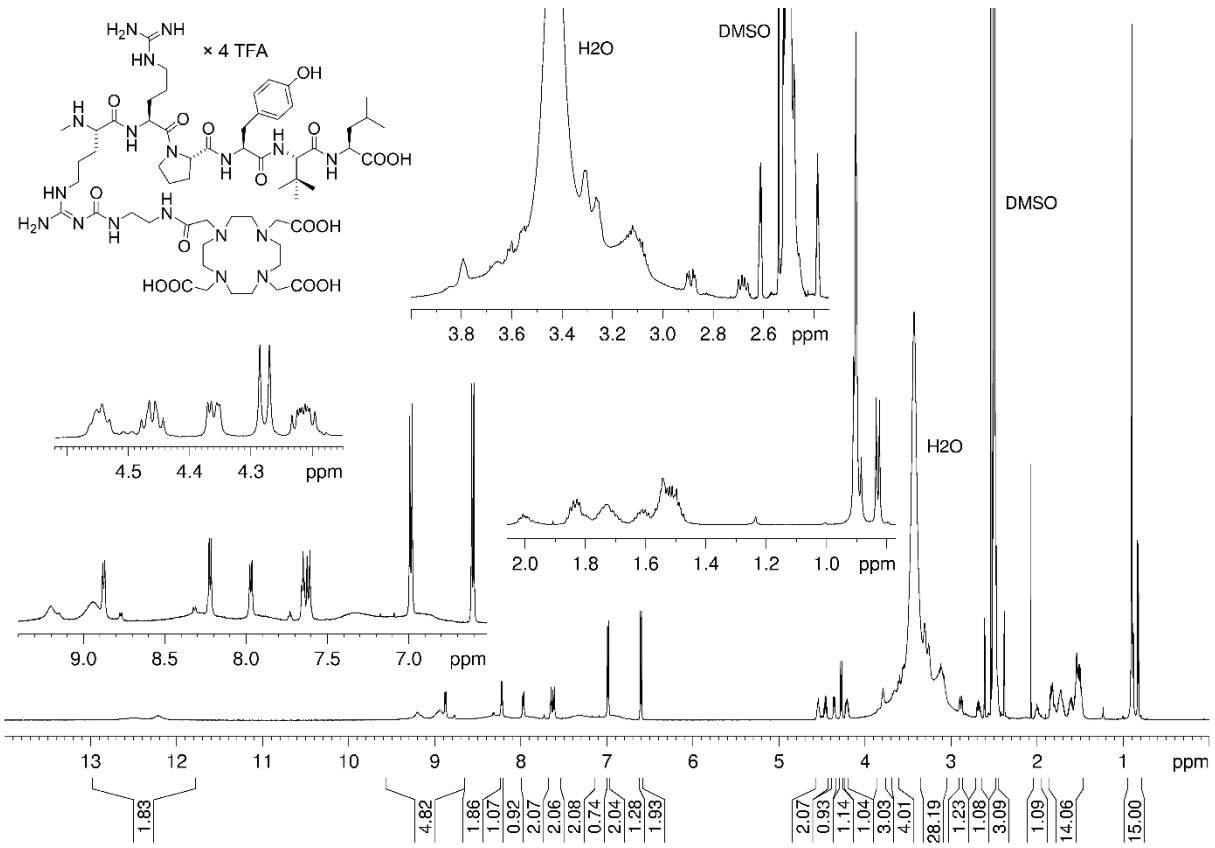

^{1}H-NMR spectrum (600 MHz, DMSO-d_6) of compound **6.04**

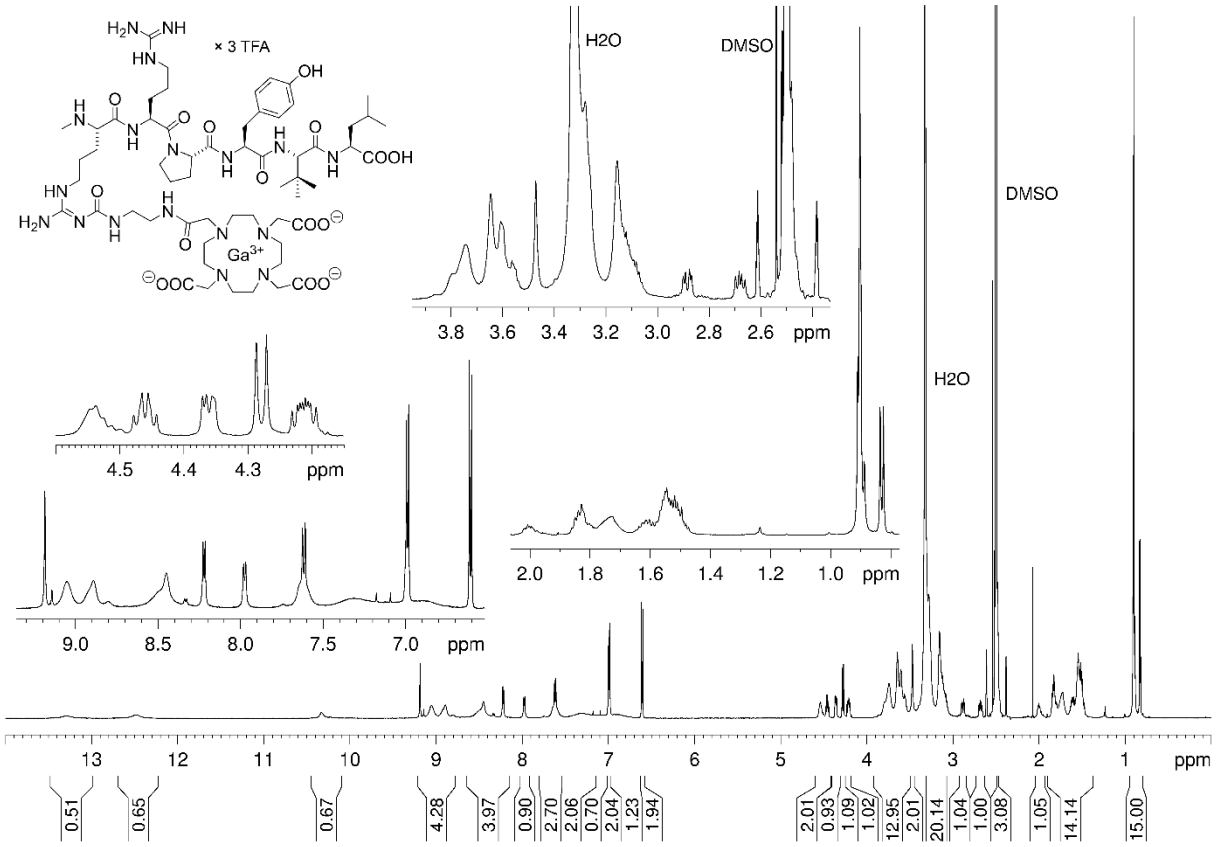

^{1}H-NMR spectrum (600 MHz, DMSO-d_6) of compound **6.05**

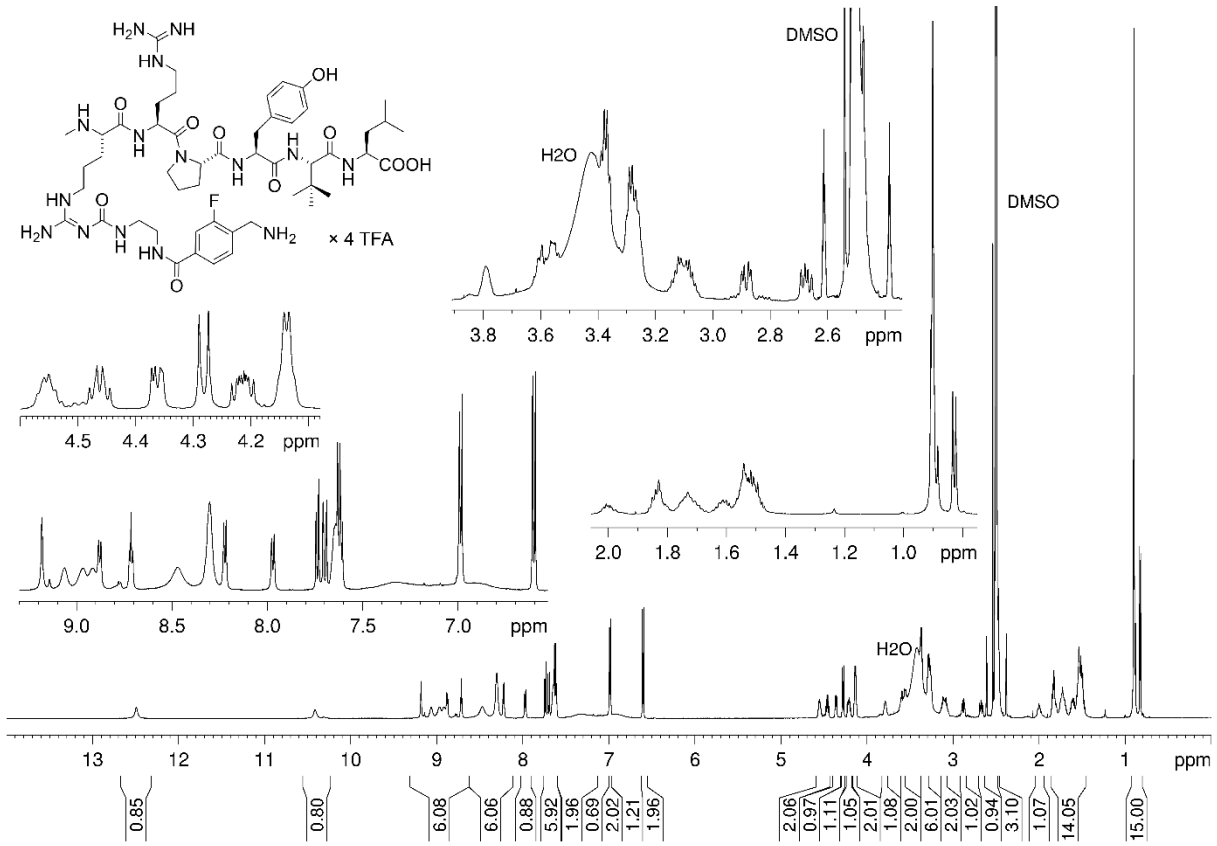

^{1}H-NMR spectrum (600 MHz, DMSO-d_6) of compound **6.06**

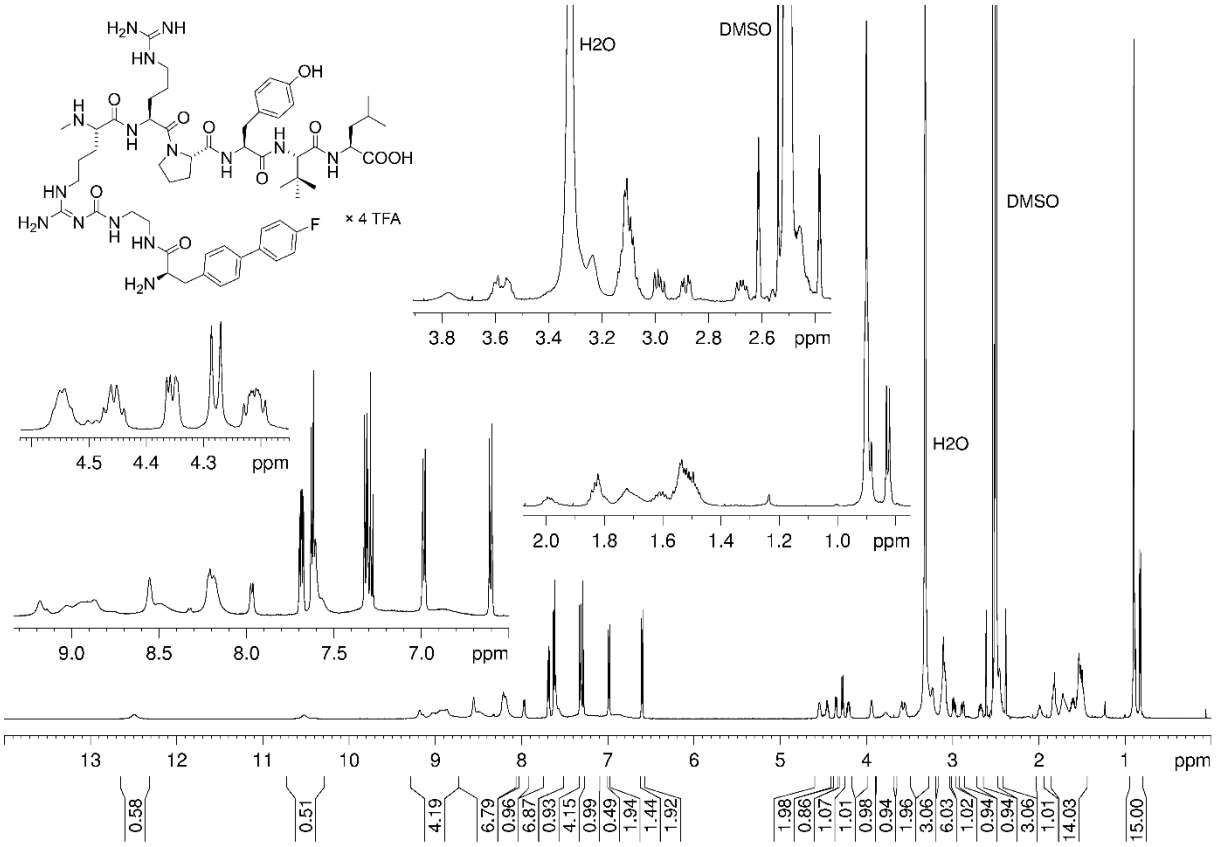

^{1}H-NMR spectrum (600 MHz, DMSO-d_6) of compound **6.07**

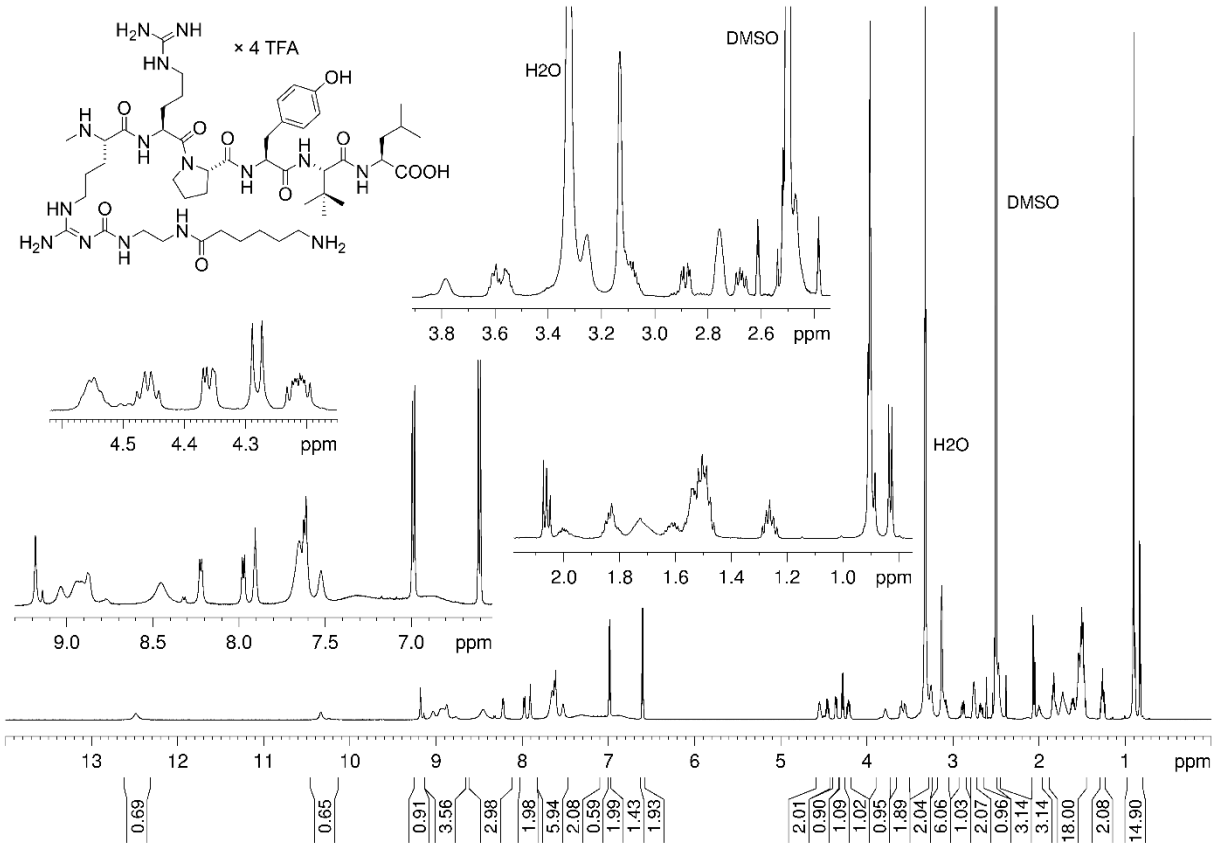

^{1}H-NMR spectrum (600 MHz, DMSO-d_6) of compound **6.09**

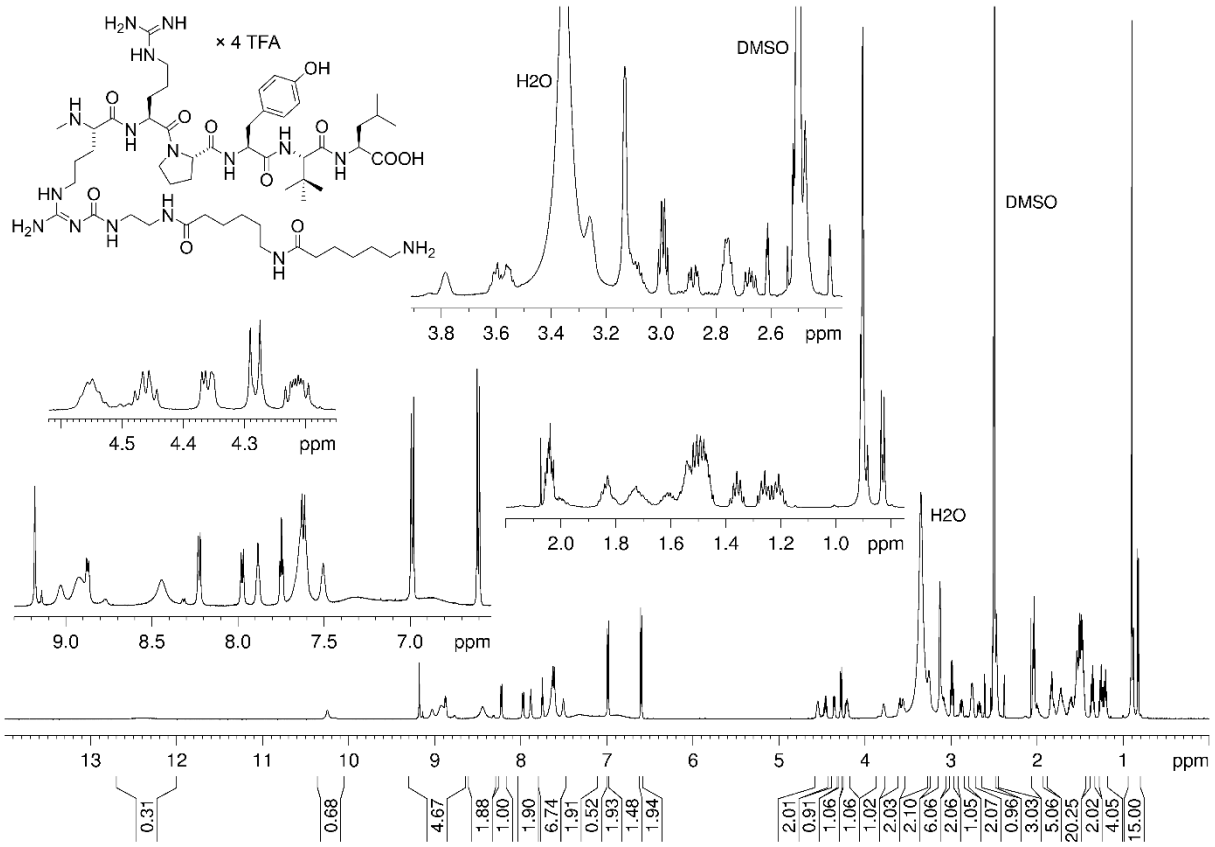

^{1}H-NMR spectrum (600 MHz, DMSO-d_6) of compound **6.10**

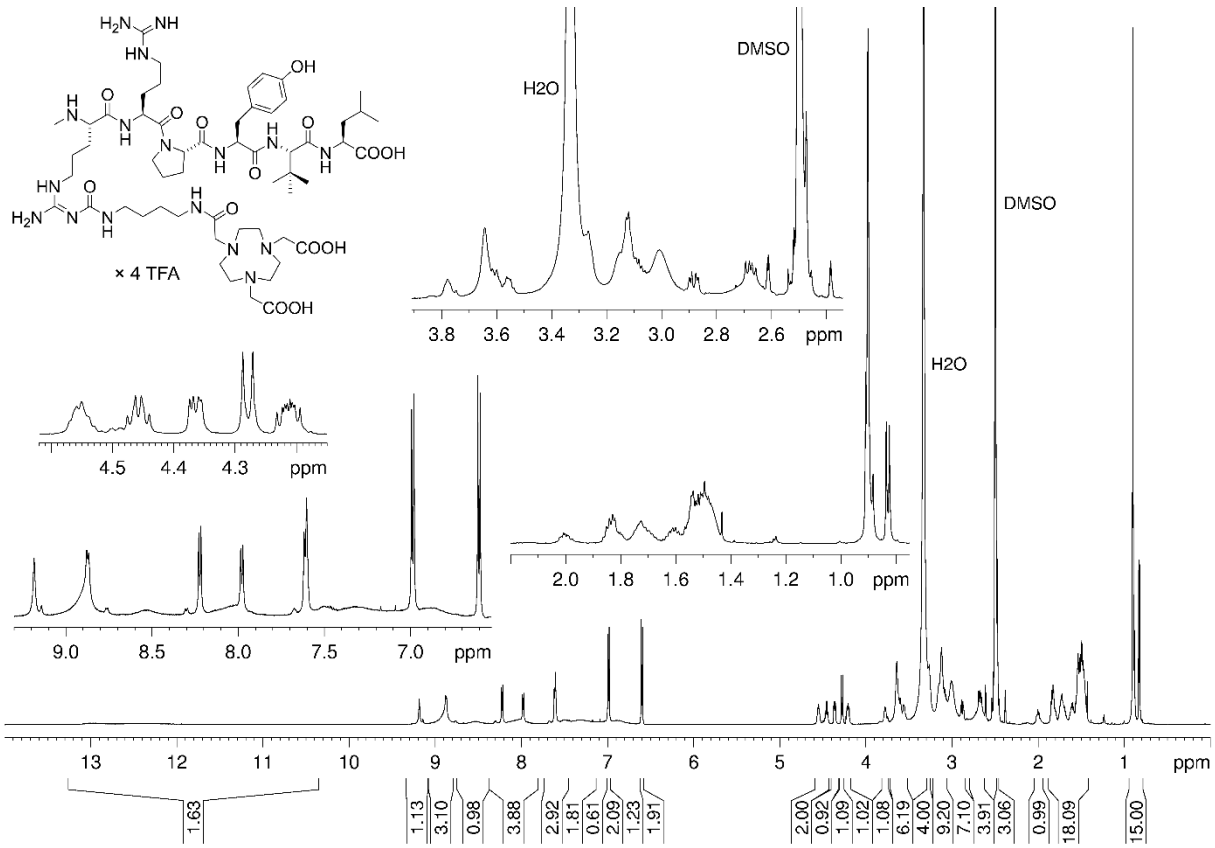

^{1}H-NMR spectrum (600 MHz, DMSO-d_6) of compound **6.13**

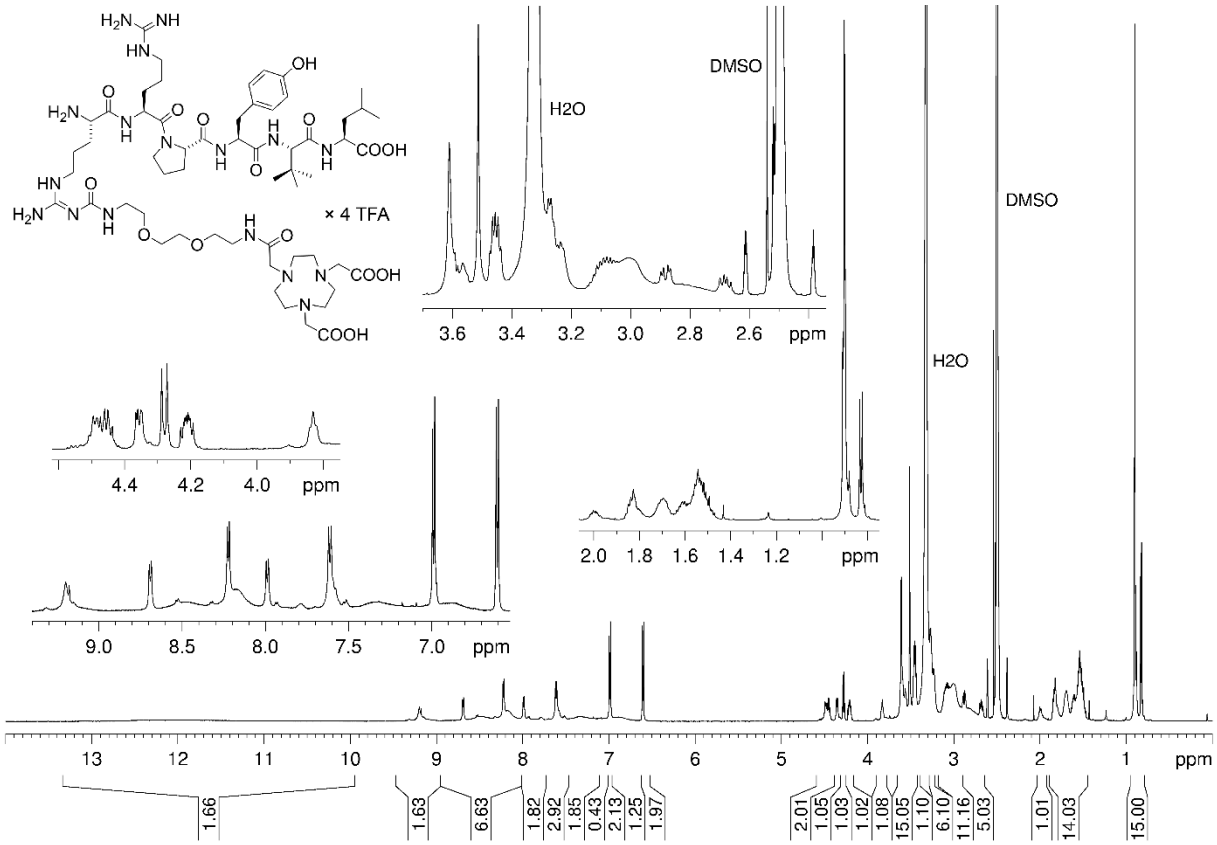

^{1}H-NMR spectrum (600 MHz, DMSO-d_6) of compound **6.14**

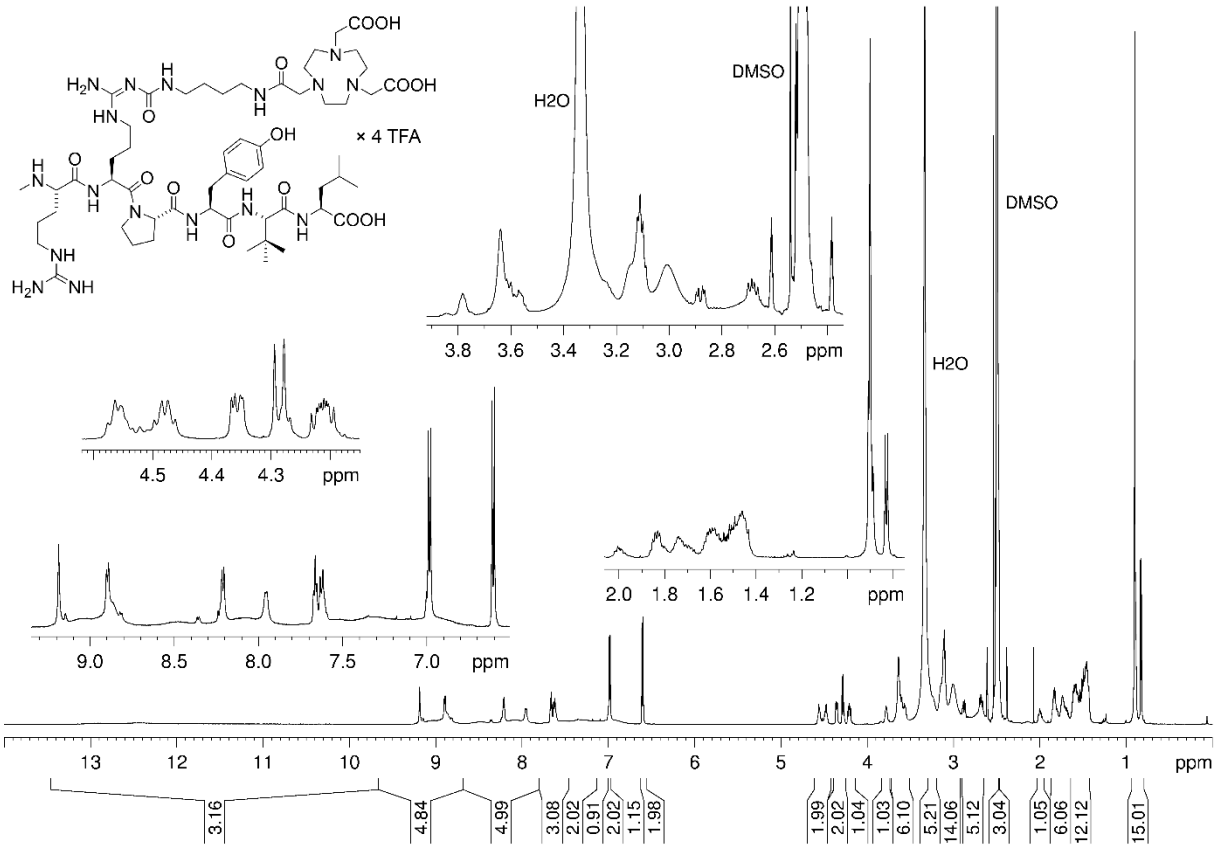

^{1}H-NMR spectrum (600 MHz, DMSO-d_6) of compound **6.15**

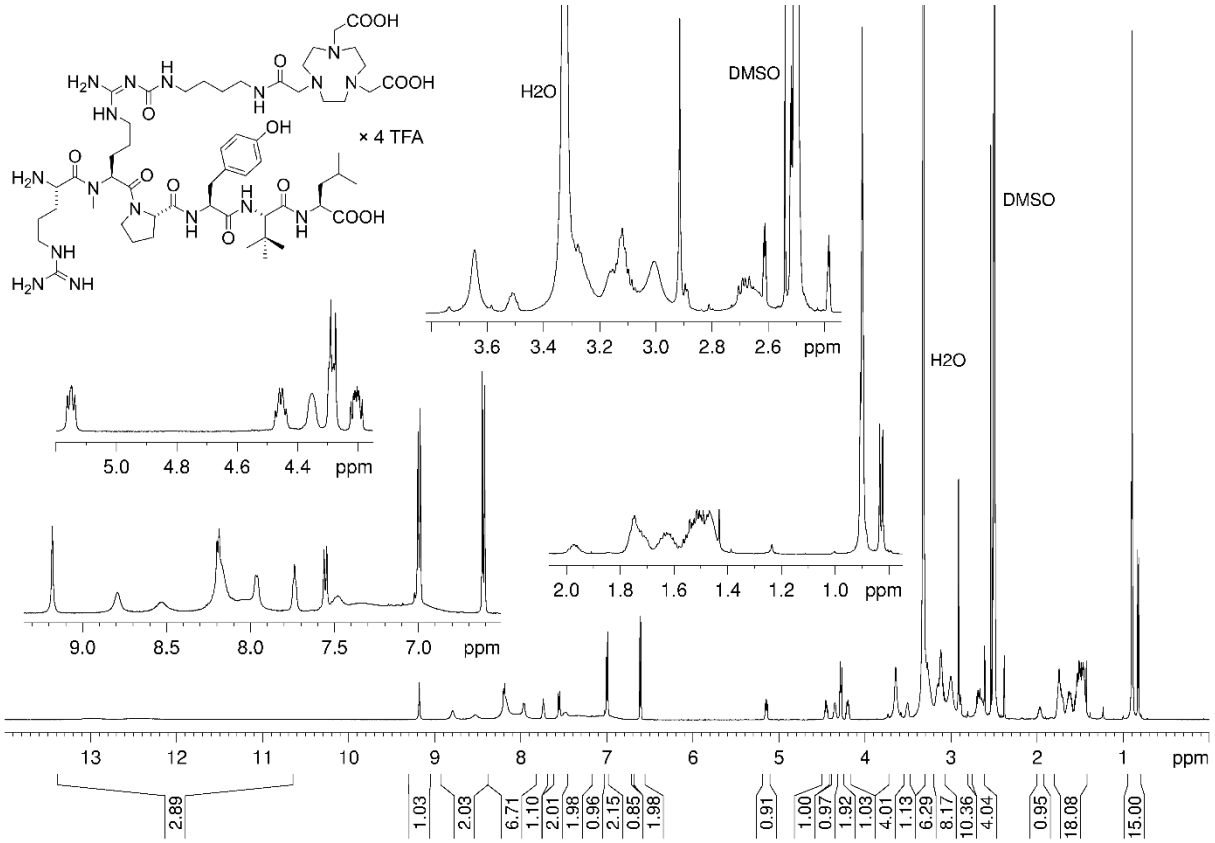

^{1}H-NMR spectrum (600 MHz, DMSO-d_6) of compound **6.16**

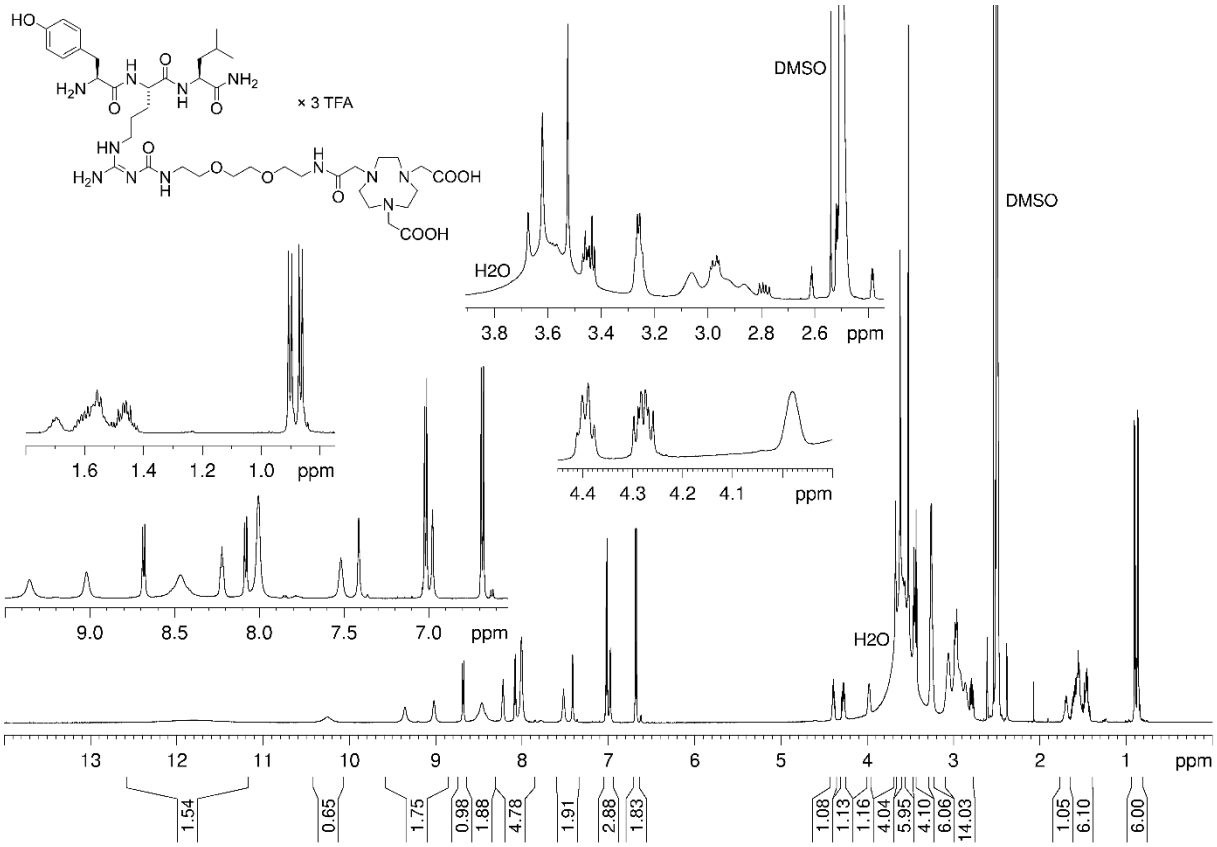

^{1}H-NMR spectrum (600 MHz, DMSO-d_6) of compound **6.19**

6.6.4 References

1. Schindler, L.; Wohlfahrt, K.; Gluhacevic von Krüchten, L.; Prante, O.; Keller, M.; Maschauer, S. Neurotensin analogs by fluoroglycosylation at N^{ω}-carbamoylated arginines for PET imaging of NTS1-positive tumors. *Sci Rep* **2022**, *12*, 15028, doi:10.1038/s41598-022-19296-0.

2. Schindler, L.; Moosbauer, J.; Schmidt, D.; Spruss, T.; Grätz, L.; Lüdeke, S.; Hofheinz, F.; Meister, S.; Echtenacher, B.; Bernhardt, G.; et al. Development of a neurotensin-derived ^{68}Ga-labeled PET ligand with high in vivo stability for imaging of NTS_1 receptor-expressing tumors. *Cancers (Basel)* **2022**, *14*, 4922, doi:10.3390/cancers14194922.

Chapter 7

Summary

The neuropeptide neurotensin (NT), mainly expressed in the CNS and the gastrointestinal tract, is involved in, e.g., the regulation of feeding, body temperature and nociception. One of the NT receptors, the G-protein coupled neurotensin receptor 1 (NTS_1R), represents an interesting target concerning tumor diagnosis and therapy, as its overexpression was reported for a variety of tumors such as breast cancer and pancreatic adenocarcinoma. The bioactive fragment of NT, NT(8-13), has served as a lead structure for the preparation of molecular tools useful for investigations at the NTS_1R. However, the development of radiolabeled NTS_1R ligands for in vivo applications such as tumor imaging by positron emission tomography (PET), is challenging due to proteolytic degradation of the peptidic compounds by peptidases. Therefore, appropriate structural modifications of NT(8-13) derivatives are necessary to enable an application as PET tracers.

The aim of this work was the development of stabilized analogs of NT(8-13) with high NTS_1R affinity including compounds useful for PET imaging, i.e., ^{18}F- or ^{68}Ga-labeled derivatives. Therefore, a series of NT(8-13) analogs was prepared by SPPS, applying modifications such as N^{α}-methylation or the replacement of amino acids by non-natural amino acids. The synthesized peptides were investigated with respect to in vitro plasma stability and NTS_1R affinity.

The incorporation of amino-functionalized N^{ω}-carbamoylated arginines instead of natural Arg enabled the conjugation of the respective NT(8-13) congeners to a prosthetic group of choice. After acylation of the amino group with 4-pentynoic acid, "cold" analogs of ^{18}F-labeled PET tracers were prepared by click chemistry-based attachment of a fluorinated glycosyl azide onto the modified arginine side chain. Using the corresponding [^{18}F]fluorinated azido sugar, the precursor of the most promising candidate (**3.21**), which showed an excellent half-life of > 24 h in vitro in human and mouse plasma and a K_i value of 4.3 nM at the NTS_1R, was used for ^{18}F-labeling in cooperation with the Department of Nuclear Medicine, Molecular Imaging and Radiochemistry at the Friedrich-Alexander-University Erlangen-Nürnberg. Biodistribution and PET imaging studies with [^{18}F]**3.21** in tumor-bearing mice revealed a high tumor-to-muscle ratio of 30 at 90 min p.i. and a specific accumulation of the tracer in subcutaneous NTS_1R-expressing HT-29 tumors. However, fast in vivo degradation of [^{18}F]**3.21** (70% degradation after 10 min p.i.) necessitates further improvement of the tracer.

Likewise, the amino-functionality of the carbamoylated arginines was used for the conjugation to chelators such as DOTA, suitable for the insertion of Ga^{3+}. Considering the overall performance of the "cold" forms of these NTS_1R PET ligands (receptor affinity, plasma stability, synthetic accessibility), ^{68}Ga-labeled analogs of the most promising candidates were prepared in cooperation with the Department of Nuclear Medicine at the University Hospital Regensburg. UR-LS130 (compound **4.56**) displayed high NTS_1R affinity (K_i = 1.2 nM) combined with excellent in vitro stability in human plasma ($t_{1/2}$ > 24 h), and its radiolabeled congener [^{68}Ga]**4.56** showed high specific accumulation in HT-29 tumors with a tumor-to-muscle ratio of 16 at 45 min p.i. in biodistribution and PET imaging studies performed with tumor-bearing mice. Notably, [^{68}Ga]**4.56** exhibited high in vivo stability, which can be attributed to the replacement of Tyr^{11} by ß,ß-dimethyl-tyrosine.

Taken together, two high-affinity NTS_1R PET ligands for tumor imaging with promising in vivo performance were developed. The identified stabilizing effect of ß,ß-dimethyl-tyrosine in position 11 of the peptide core structure, not affecting NTS_1R binding, will support the future development of NT(8-13)-derived tumor imaging probes.

A second project of this work aimed at fluorinated potential PET ligands for the CXCR4. This G-protein coupled chemokine receptor is overexpressed in different types of cancer, such as prostate or breast cancer. The "cold" forms of CXCR4 PET ligands derived from the reported peptidic CXCR4 antagonist FC131 were prepared by application of the replacement of Arg by an amino-functionalized N^{ω}-carbamoylated arginine, subsequent alkyne-functionalization and coupling to the aforementioned fluoroglycosyl azide. Investigations regarding their antagonistic activities at the CXCR4 and in vitro plasma stabilities revealed that compound **5.24**, displaying a pK_b value of 7.15 and a half-life of > 24h, may serve as a lead structure for the development of optimized fluorinated CXCR4 PET ligands in future studies.

Chapter 8

Glossary

8.1 Abbreviations

%ID/g	percentage of injected dose per gram tissue
[*I]SIB	*N*-succinimidyl-3-[*I]iodobenzoate
[^{18}F]SFB	*N*-succinimidyl-4-[^{18}F]fluorobenzoate
AA = aa	amino acid(s)
Ac	acetyl
ACE	angiotensin converting enzyme
Ahx	6-aminohexanoyl
allo-Ile	2-((1*R*)-1-methylpropyl)-glycine
aq	aqueous
Arg(carb)	N^{ω}-carbamoylated arginine
AsPC-1	human pancreatic adenocarcinoma cell line established from ascites
AU	absorbance unit
AY	activity yield
Boc	*tert*-butyloxycarbonyl
bp	by-product
Bq	Becquerel
br s	broad singlet (to describe the multiplicity of ^{1}H-NMR signals)
BSA	bovine serum albumin
c	concentration, or: speed of light
ca.	circa
calcd.	calculated
cAMP	3'-5'-cyclic adenosine monophosphate
CD	circular dichroism
CD4	cluster of differentiation 4
$CDCl_3$	deuterated chloroform
cDNA	complementary DNA
cf.	confer
CHO	Chinese hamster ovary cells
Ci	Curie
CNS	central nervous system
compd. (= cpd.)	compound
cond.	condition
COS-7	monkey kidney fibroblast-like cell line
COSY	correlated spectroscopy
COVID-19	coronavirus disease 2019
CPCR4-2	Pentixafor; CXCR4 ligand
cpd. (= compd.)	compound
cpm	counts per minute
cPrGly	α-cyclopropyl-glycine
CuAAC	copper(I)-catalyzed azide-alkyne cycloaddition
CXCL12 (= SDF-1α)	stromal cell derived factor 1α
CXCR4	CXC-motif chemokine receptor 4
d	doublet (to describe the multiplicity of ^{1}H-NMR signals)
D_2O	deuterated water

DAG	diacylglycerol
DBU	1,8-diazabicyclo[5.4.0]undec-7-ene
DCC	*N,N'*-dicyclohexylcarbodiimide
Deg	α,α-diethyl-glycine
DIC	*N,N'*-diisopropylcarbodiimide
DIPEA	diisopropylethylamine
DMF	*N,N*-dimethylformamide
DMSO	dimethylsulfoxide
DMSO-d_6	deuterated dimethylsulfoxide
DOTA	1,4,7,10-tetraazacyclododecane-1,4,7,10-tetraacetic acid
DOTA-TATE	DOTA-(Tyr^3,Thr^8)-octreotate
DOTA-TOC	DOTA-(Tyr^3)-octreotide
D-PBS	Dulbecco's phosphate-buffered saline
DTPA	diethylenetriaminepentaacetic acid
e^-	electron
e.g.	exempli gratia
EC	electron capture
EC_{50}	agonist concentration which induces 50% of the maximal effect
EC_{80}	agonist concentration which induces 80% of the maximal effect
EDTA	ethylenediamine-tetraacetic acid
EMA	European Medicines Agency
E_{max}	maximum energy
equiv.	equivalent(s)
ESI	electrospray ionisation
EtOAc	ethyl acetate
EtOH	ethanol
eV	electron-volt
FBS	fetal bovine serum
FCS	fetal calf serum
FDA	Food and Drug Administration
FGlc	fluoroglycosyl
Fmoc	9-fluorenylmethoxycarbonyl
FoV	field of view
FWHM	full width at half maximum
G418	geneticin
GPCR	G-protein coupled receptor
HBED-CC	*N,N'*-bis[2-hydroxy-5(carboxyethyl)benzyl]ethylenediamine-*N,N'*-diacetic acid
HBTU	*O*-(1*H*-benzotriazol-1-yl)-*N,N,N',N'*-tetramethyluronium hexafluorophosphate
HEK293 / HEK293T	human embryonic kidney cells
HEPES	4-(2-hydroxyethyl)-1-piperazineethanesulfonic acid
HFIP	1,1,1,3,3,3-hexafluoro-2-propanol
HIV	human immunodeficiency virus
HMBC	heteronuclear multiple bond correlation
$hNTS_1R$	human neurotensin receptor 1

$hNTS_2R$	human neurotensin receptor 2
HOBt	1-hydroxy-1*H*-benzotriazole
HPLC	high performance liquid chromatography
HRMS	high resolution mass spectrometry
HSQC	heteronuclear single quantum coherence
HT-29	human colorectal adenocarcinoma cell line
i.e.	id est
I.E. (= IU)	international unit, refering to an enzyme's catalytic activity
i.p.	intraperitoneal
i.v.	intravenous
IC_{50}	inhibitor/antagonist concentration which suppresses 50% of an agonist induced effect, or displaces 50% of a labelled ligand from the binding site
IP_3	inositol trisphosphate
IS	internal standard
IT	isomeric transition
IU (= I.E.)	international unit, refering to an enzyme's catalytic activity
IVC	individually ventilated cage(s)
J	coupling constant
k	retention (capacity) factor
K	association constant
K_b	dissociation constant derived from a functional assay
K_d	dissociation constant derived from a saturation experiment
K_i	dissociation constant derived from a competition binding assay
L-15	Leibovitz' L-15 medium
LC	liquid chromatography
lit.	literature data
$logD_{7.4}$	logarithm of the n-octanol/water distribution coefficient
m	mass, or: multiplet (to describe the multiplicity of ^{1}H-NMR signals)
m/z	mass-to-charge ratio
Me	methyl
MeCN	acetonitrile
MeOH	methanol
mG = mini-G	minimalized G-protein
mini-G = mG	minimalized G-protein
MRI	magnetic resonance imaging
MTBD	7-methyl-1,5,7-triazabicyclo[4.4.0]dec-5-en
MW	molecular weight
n	neutron
n.d.	not determined
n.r.	not reported
N_4	6-carboxy-1,4,8,11-tetraazaundecane
Nal	2-naphthylalanine
NanoLuc = Nluc	Nanoluciferase
n-hex	n-hexane

NHS	*N*-hydroxy-succinimide
Nluc = NanoLuc	Nanoluciferase
Nlys	peptoid-like lysine
NMP	1-methylpyrrolidin-2-one
NMR	nuclear magnetic resonance
NMRI	Naval Medical Research Institute
NODA-GA	1,4,7-triazacyclononane-1-glutaric acid-4,7-acetic acid
NOTA	1,4,7-triazacyclononane-1,4,7-triacetic acid
NT	Neurotensin
NTS_3R	neurotensin receptor 3
Orn	ornithine
p	proton
p.i.	post injection
Panc-1	human epithelioid carcinoma cell line from the pancreas
Pbf	2,2,4,6,7-pentamethyldihydrobenzofuran-5-sulfonyl
PBS	phosphate-buffered saline
PET-CT	positron emission tomography coupled with computed tomography
PKC	protein kinase C
PLC	phospholipase C
ppm	parts per million
Pra	propargylglycin
Prop	propionyl
PSMA	prostate specific membrane antigen
PyBOP	benzotriazol-1-yl-oxytripyrrolidinophosphonium hexafluorophosphate
q	quartet (to describe the multiplicity of ^{1}H-NMR signals)
rac	racemic
RC	regenerated cellulose
RCY	radiochemical yield
R_f	retardation factor
RLU	relative luminescence units
ROI	region of interest
RP	reversed phase
rt	room temperature
s	singlet (to describe the multiplicity of ^{1}H-NMR signals)
SD	standard deviation
SDF-1α (= CXCL12)	stromal cell derived factor 1α
SEM	standard error of the mean
SGLT	sodium-dependent glucose transporter
SPE	solid phase extraction
SPECT	single-photon emission computed tomography
SPF	specified pathogen free
SPPS	solid-phase peptide synthesis
SSTR2	somatostatin receptor type 2
SUV_{mean}	mean standardized uptake value
SVD	singular-value decomposition

t	time, or: triplet (to describe the multiplicity of ^{1}H-NMR signals)
t_0	dead time
$t_{1/2}$	half-life
TAC	time-activity-curve
*t*Bu	*tert*-butyl
TC	tissue culture
TFA	trifluoroacetic acid
THF	tetrahydrofuran
THPTA	tris(3-hydroxypropyltriazolyl)methylamine
TLC	thin-layer chromatography
Tle	α-*tert*-butylglycine, *tert*-leucine
TM	trans-membrane
TMS	trimethylsilyl
TOCSY	total correlated spectroscopy
t_R	retention time
Trt	trityl, triphenylmethyl
UV	ultraviolet
Vis	visible
vs.	versus
Y_1R	neuropeptide Y Y_1 receptor
ß,ß-diMe-Tyr	ß,ß-dimethyl-tyrosine
$ß^+$	positron
δ	chemical shift
v	neutrino

8.2 Overview of bold compound numerals and lab codes

cpd.	lab code	cpd.	lab code	cpd.	lab code
2.02	ls005	**4.22**	ls052	**5.12**	ls033
2.03	ls014	**4.23**	ls085	**5.13**	ls034
2.04	ls015	**4.25**	ls095	**5.14**	ls035
2.05	ls016	**4.26**	ls103	**5.15**	ks023
2.06	ls017	**4.28**	ls091	**5.16**	ls036
2.07	ls043	**4.29**	ls099	**5.17**	ls037
2.08	ls044	**4.31**	ls106	**5.18**	ls038
2.09	ls018	**4.32**	ls108	**5.19**	ls039
2.10	CM041 = MC029	**4.33**	ls109	**5.20**	ls040
2.11	ls019	**4.34**	ls096	**5.21**	ls041
2.12	ls045	**4.35**	ls104	**5.22**	ls042
2.13	mk300	**4.36**	ls097	**5.23**	ls053
3.06a	mk134	**4.37**	ls105	**5.24**	ls054
3.06b	ks009	**4.38**	ls114	**5.25**	ls055
3.07	ks014	**4.39**	ls115	**5.26**	ls056
3.08	ks033	**4.40**	ls116	**6.01**	ls022
3.09	lvk20b	**4.41**	ls117	**6.02**	ls024
3.11	ks030	**4.42**	ls118	**6.03**	ls082
3.12	ks034	**4.43**	ls119	**6.04**	ls084
3.13	lvk26	**4.44**	ls120	**6.05**	ls086
3.14	ls001	**4.45**	ls121	**6.06**	ls107
3.16	ls047	**4.46**	ls122	**6.07**	ls111
3.17	ks015	**4.47**	ls123	**6.08**	ls112
3.18	ks017	**4.48**	ls124-I	**6.09**	ls087
3.19	ls057	**4.49**	ls124-II	**6.10**	ls088
3.20	ks027	**4.50**	ls128-I	**6.11**	ls089
3.21	ls058	**4.51**	ls128-II	**6.12**	ls002
4.07	mk290	**4.52**	ls131-I	**6.13**	ls060
4.08	ls021	**4.53**	ls131-II	**6.14**	ls068
4.09	ls023	**4.54**	ls129	**6.15**	ls069
4.11	ls048	**4.55**	ls132	**6.16**	ls070
4.12	ls081	**4.56**	ls130	**6.19**	ls066
4.14	ls025	**4.57**	ls133	**6.20**	ls064
4.15	ls027	**5.03**	ls062	**6.21**	ls067
4.16	ls049	**5.04**	ls063	**6.22**	mk291
4.17	ls050	**5.05**	lvk17	**6.23**	ls074
4.18	ls083	**5.06**	ls062cd-linear	**6.24**	ls077
4.19	ls029	**5.07**	ls062cd-SK-E	**6.25**	ls078
4.20	ls031	**5.09**	ls062cd-AMBS-E		
4.21	ls051	**5.11**	ks021		

lab code	cpd.	lab code	cpd.	lab code	cpd.
CM041 = MC029	**2.10**	ls045	**2.12**	ls097	**4.36**
ks009	**3.06b**	ls047	**3.16**	ls099	**4.29**
ks014	**3.07**	ls048	**4.11**	ls103	**4.26**
ks015	**3.17**	ls049	**4.16**	ls104	**4.35**
ks017	**3.18**	ls050	**4.17**	ls105	**4.37**
ks021	**5.11**	ls051	**4.21**	ls106	**4.31**
ks023	**5.15**	ls052	**4.22**	ls107	**6.06**
ks027	**3.20**	ls053	**5.23**	ls108	**4.32**
ks030	**3.11**	ls054	**5.24**	ls109	**4.33**
ks033	**3.08**	ls055	**5.25**	ls111	**6.07**
ks034	**3.12**	ls056	**5.26**	ls112	**6.08**
ls001	**3.14**	ls057	**3.19**	ls114	**4.38**
ls002	**6.12**	ls058	**3.21**	ls115	**4.39**
ls005	**2.02**	ls060	**6.13**	ls116	**4.40**
ls014	**2.03**	ls062	**5.03**	ls117	**4.41**
ls015	**2.04**	ls062cd-AMBS-E	**5.09**	ls118	**4.42**
ls016	**2.05**	ls062cd-linear	**5.06**	ls119	**4.43**
ls017	**2.06**	ls062cd-SK-E	**5.07**	ls120	**4.44**
ls018	**2.09**	ls063	**5.04**	ls121	**4.45**
ls019	**2.11**	ls064	**6.20**	ls122	**4.46**
ls021	**4.08**	ls066	**6.19**	ls123	**4.47**
ls022	**6.01**	ls067	**6.21**	ls124-I	**4.48**
ls023	**4.09**	ls068	**6.14**	ls124-II	**4.49**
ls024	**6.02**	ls069	**6.15**	ls128-I	**4.50**
ls025	**4.14**	ls070	**6.16**	ls128-II	**4.51**
ls027	**4.15**	ls074	**6.23**	ls129	**4.54**
ls029	**4.19**	ls077	**6.24**	ls130	**4.56**
ls031	**4.20**	ls078	**6.25**	ls131-I	**4.52**
ls033	**5.12**	ls081	**4.12**	ls131-II	**4.53**
ls034	**5.13**	ls082	**6.03**	ls132	**4.55**
ls035	**5.14**	ls083	**4.18**	ls133	**4.57**
ls036	**5.16**	ls084	**6.04**	lvk17	**5.05**
ls037	**5.17**	ls085	**4.23**	lvk20b	**3.09**
ls038	**5.18**	ls086	**6.05**	lvk26	**3.13**
ls039	**5.19**	ls087	**6.09**	mk134	**3.06a**
ls040	**5.20**	ls088	**6.10**	mk290	**4.07**
ls041	**5.21**	ls089	**6.11**	mk291	**6.22**
ls042	**5.22**	ls091	**4.28**	mk300	**2.13**
ls043	**2.07**	ls095	**4.25**		
ls044	**2.08**	ls096	**4.34**		

Ich erkläre hiermit an Eides statt, dass ich die vorliegende Arbeit ohne unzulässige Hilfe Dritter und ohne Benutzung anderer als der angegebenen Hilfsmittel angefertigt habe; die aus anderen Quellen direkt oder indirekt übernommenen Daten und Konzepte sind unter Angabe des Literaturzitats gekennzeichnet.

Teile der experimentellen Arbeiten wurden in Zusammenarbeit mit anderen Institutionen und Personen durchgeführt. Entsprechende Vermerke zu den Beiträgen der betreffenden Personen finden sich jeweils zu Beginn des entsprechenden Kapitels und unter „Acknowledgments“.

Weitere Personen waren an der inhaltlich-materiellen Herstellung der vorliegenden Arbeit nicht beteiligt. Insbesondere habe ich hierfür nicht die entgeltliche Hilfe eines Promotionsberaters oder anderer Personen in Anspruch genommen. Niemand hat von mir weder unmittelbar noch mittelbar geldwerte Leistungen für Arbeiten erhalten, die im Zusammenhang mit dem Inhalt der vorgelegten Dissertation stehen.

Die vorliegende Arbeit wurde bisher weder im In- noch im Ausland in gleicher oder ähnlicher Form einer anderen Prüfungsbehörde vorgelegt.

Regensburg, den _____

Lisa Schindler